STIMULANT USE AND ADDICTIVE DISORDER

EDITED BY: Qi Wang, Di Wen, Yixiao Luo, Fanglin Guan, Jianfeng Liu and Zeng Xiao Feng

PUBLISHED IN: Frontiers in Pharmacology and Frontiers in Neuroscience

frontiers Research Topics

ISSN 1664-8714
ISBN 978-2-88974-259-2
DOI 10.3389/978-2-88974-259-2

About Frontiers

Frontiers is more than just an open-access publisher of scholarly articles: it is a pioneering approach to the world of academia, radically improving the way scholarly research is managed. The grand vision of Frontiers is a world where all people have an equal opportunity to seek, share and generate knowledge. Frontiers provides immediate and permanent online open access to all its publications, but this alone is not enough to realize our grand goals.

Frontiers Journal Series

The Frontiers Journal Series is a multi-tier and interdisciplinary set of open-access, online journals, promising a paradigm shift from the current review, selection and dissemination processes in academic publishing. All Frontiers journals are driven by researchers for researchers; therefore, they constitute a service to the scholarly community. At the same time, the Frontiers Journal Series operates on a revolutionary invention, the tiered publishing system, initially addressing specific communities of scholars, and gradually climbing up to broader public understanding, thus serving the interests of the lay society, too.

Dedication to Quality

Each Frontiers article is a landmark of the highest quality, thanks to genuinely collaborative interactions between authors and review editors, who include some of the world's best academicians. Research must be certified by peers before entering a stream of knowledge that may eventually reach the public - and shape society; therefore, Frontiers only applies the most rigorous and unbiased reviews.
Frontiers revolutionizes research publishing by freely delivering the most outstanding research, evaluated with no bias from both the academic and social point of view. By applying the most advanced information technologies, Frontiers is catapulting scholarly publishing into a new generation.

What are Frontiers Research Topics?

Frontiers Research Topics are very popular trademarks of the Frontiers Journals Series: they are collections of at least ten articles, all centered on a particular subject. With their unique mix of varied contributions from Original Research to Review Articles, Frontiers Research Topics unify the most influential researchers, the latest key findings and historical advances in a hot research area! Find out more on how to host your own Frontiers Research Topic or contribute to one as an author by contacting the Frontiers Editorial Office: frontiersin.org/about/contact

STIMULANT USE AND ADDICTIVE DISORDER

Topic Editors:
Qi Wang, Southern Medical University, China
Di Wen, Hebei Medical University, China
Yixiao Luo, Hunan Normal University, China
Fanglin Guan, Xi'an Jiaotong University Health Science Center, China
Jianfeng Liu, Texas A&M University, United States
Zeng Xiao Feng, Kunming Medical University, China

Citation: Wang, Q., Wen, D., Luo, Y., Guan, F., Liu, J., Feng, Z. X., eds. (2022). Stimulant Use and Addictive Disorder. Lausanne: Frontiers Media SA.
doi: 10.3389/978-2-88974-259-2

Table of Contents

frontiers in Pharmacology

REVIEW
published: 24 November 2020
doi: 10.3389/fphar.2020.603445

Toll-Like Receptor 4 Signaling and Drug Addiction

Ruyan Wu[1,2]* *and Jun-Xu Li*[2]

[1]School of Medicine, Yangzhou University, Yangzhou, China, [2]Department of Pharmacology and Toxicology, University at Buffalo, Buffalo, NY, United States

The emphasis of neuronal alterations and adaptations have long been the main focus of the studies of the mechanistic underpinnings of drug addiction. Recent studies have begun to appreciate the role of innate immune system, especially toll-like receptor 4 (TLR4) signaling in drug reward-associated behaviors and physiology. Drugs like opioids, alcohol and psychostimulants activate TLR4 signaling and subsequently induce proinflammatory responses, which in turn contributes to the development of drug addiction. Inhibition of TLR4 or its downstream effectors attenuated the reinforcing effects of opioids, alcohol and psychostimulants, and this effect is also involved in the withdrawal and relapse-like behaviors of different drug classes. However, conflicting results also argue that TLR4-related immune response may play a minimal part in drug addiction. This review discussed the preclinical evidence that whether TLR4 signaling is involved in multiple drug classes action and the possible mechanisms underlying this effect. Moreover, clinical studies which examined the potential efficacy of immune-base pharmacotherapies in treating drug addiction are also discussed.

Keywords: toll-like receptor 4, opioids, alcohol, psychostimulants, drug reward, reinstatement, withdrawal

OPEN ACCESS

Edited by:
Qi Wang,
Southern Medical University, China

Reviewed by:
Wu Xu,
China Medical University, China
Qiu Pingming,
Southern Medical University, China
Chunling Ma,
Hebei Medical University, China

***Correspondence:**
Ruyan Wu
ruyanwu0908@gmail.com

Received: *06 September 2020*
Accepted: *22 October 2020*
Published: *24 November 2020*

Citation:
Wu R and Li J-X (2020) Toll-Like Receptor 4 Signaling and Drug Addiction. Front. Pharmacol. 11:603445. doi: 10.3389/fphar.2020.603445

INTRODUCTION

Neuronal alterations and adaptations have long been the main focus of the studies of the mechanistic underpinnings of drug addiction (Kalivas and O'Brien, 2008; Otis and Mueller, 2017). The emphasis of dopaminergic and glutamatergic signaling in brain reward circuits yield extensive important progress in the study of drug addiction (Sesack and Grace, 2010; Lee et al., 2013; Ma et al., 2014; Zhang et al., 2016). However, they ignore the potential contributions of non-neuronal cells (e.g., microglia and astrocytes) to the synaptic and behavioral adaptations underlying addiction-like behaviors (Kashima and Grueter, 2017). Recent studies have begun to illustrate the role of innate immune system, especially toll-like receptor 4 (TLR4) in drug reward associated behaviors and physiology (Hutchinson et al., 2012; June et al., 2015; Northcutt et al., 2015). This review will briefly discuss the innate immune system and TLR4 signaling. Different classes of drugs including opioids, alcohol and psychostimulants will be reviewed to discuss whether TLR4 signaling can be used as a potential therapeutic target for the treatment of drug addiction. Furthermore, clinical studies which examined the potential efficacy of immune-base pharmacotherapies in treating drug addiction are also discussed.

THE TOLL-LIKE RECEPTOR 4-RELATED IMMUNE SYSTEM AND NEURONAL DISORDERS

The innate immune system, an evolutionary defense strategy, has been well characterized (Chaplin, 2010; Yu et al., 2018). TLRs are a group of pattern recognition receptors (PRRs) in the innate immune system which detect and respond not only to exogenous pathogen associated molecular patterns (PAMPs), but also to endogenous danger associated molecular patterns (DAMPs) (Koropatnick et al., 2004; Hennessy et al., 2010; Dunne et al., 2011). Activation of TLRs promotes the maturation of antigen presenting cells, like dendritic cells (DC), which subsequently directs the induction of adaptive immunity (Apetoh et al., 2007; Liu et al., 2010; Gaudino and Kumar, 2019). In this regard, TLR agonists have been studied as vaccine adjuvants for cancer or infectious disease (Caron et al., 2005; Sfondrini et al., 2006; Kronenberger and Zeuzem, 2009). However, considering the fact that activation of TLRs leads to the promotion of inflammatory cytokine production, the inhibitors of TLRs also have significant potential as therapeutic agents for inflammatory disorders, such as rheumatoid arthritis (Klareskog et al., 2004; Feldmann, 2009). As a result, the exploitation of TLRs-based therapeutics may be promising for the treatment of multiple infectious and inflammatory diseases.

Apart from their crucial roles in immune system-related diseases, recent studies also suggest that TLRs, especially TLR4, was widely involved in drug addiction-related behaviors (Hennessy et al., 2010; Crews et al., 2017b; Kashima and Grueter, 2017). We will discuss this topic later in detail. In response to pathogen and danger signals, TLR4 and its co-receptor MD-2 can signal through two different pathways, the myeloid differentiation primary response protein 88 (MyD88)-dependent and MyD88-independent pathway (Takeda and Akira, 2004) (**Figure 1**). In MyD88-dependent pathway, the signal transduces through Interleukin 1 receptor associated kinase 4 and 1 (IRAK4 and IRAK1) and the following TNF receptor associated factor 6 (TRAF6). The activation of TRAF6 leads to phosphorylation of inhibitors of nuclear factor κB Kinases (IKKs), which in turn activates the IκB. The activation of IκB leads to its degradation and the initiation of activation of NFκB and the production of proinflammatory cytokines, for example, Tumor Necrosis Factor (TNF), IL-1β, and IL-6 (Kawai and Akira, 2007). In contrast, MyD88-independent pathway adopts the adaptor protein TRIF and transduces the signal through TRAF3, TBK1, and IKKε, which then phosphorylates interferon regulatory factor 3 (IRF3). IRF3 then translocates to the nucleus and promotes the transcription of type 1 interferons (Takeda and Akira, 2005).

The involvement of TLR4 signaling has been suggested in several neuronal disorders, including neurodegenerative disorders, depression, impulsive behaviors and addiction (Landreth and Reed-Geaghan, 2009; Gesuete et al., 2014; Aurelian et al., 2016; Garcia Bueno et al., 2016; Crews et al., 2017b; Gasiorowski et al., 2018; Nie et al., 2018; Liu et al., 2019). TLR4 is mainly expressed in cells of innate immune system, including microglia and astrocytes (Vaure and Liu, 2014). Consistent to this, several microglia inhibitors attenuated some drug addiction-related behaviors in animal studies. In this review, we will focus on the role of TLR4 in regulating addiction-related behaviors from different drug classes.

ROLE OF TOLL-LIKE RECEPTOR 4 IN DIFFERENT CLASSES OF DRUG ADDICTION

Opioids

Evidence of a Role of Toll-Like Receptor 4 in Opioid Addiction

It is reported that opioids such as morphine can induce neuroinflammation in the central nervous system (Narita et al., 2006; Yang et al., 2010). Furthermore, this neuroinflammation has been associated with morphine analgesia, dependence, tolerance and withdrawal effects (Eidson and Murphy, 2013; Jacobsen et al., 2014; Mattioli et al., 2014; Eidson et al., 2017; Shah and Choi, 2017). It has been shown that morphine can directly bind to myeloid differentiation protein 2 (MD-2), the accessory receptor of TLR4, and activate TLR4 signaling by inducing the oligomerization of TLR4/MD-2. TLR4/MD-2 knockout animals showed enhanced morphine-induced analgesia, suggesting that blockade of TLR4/MD-2 inhibited morphine-induced proinflammatory responses (Wang et al., 2012b). Inhibition of TLR4 by the levo-isomer of naloxone, (+)-naloxone, attenuated morphine-induced conditioned place preference (CPP). This isomer of naloxone (26.3 mg/kg), which is inactive at opioid receptors, also reduced remifentanil self-administration. Furthermore, genetic knockout of TLR4 or MyD88 decreased oxycodone-induced CPP (Wang et al., 2012b). These results suggest that activation of TLR4 is involved in the rewarding effect of opioids. In addition, *in vivo* microdialysis study showed that (+)-naloxone decreased morphine-induced elevation of dopamine concentration in the shell region of nucleus accumbens (NAc) (Hutchinson et al., 2012). Together, they suggested that the TLR4/MD-2 signaling, along with classic opioid receptors, mediates opioid reward-related behaviors.

However, recent studies which contradict the role of TLR4 in opioid addiction add more complexity to this hypothesis. For example, Phil et al. reported that neither (+)-naloxone nor (+)-naltrexone (3 and 100 μM) inhibit LPS induced TLR4 activation *in vitro* (Skolnick et al., 2014). Stevens et al. also reported that morphine inhibits LPS-induced activation of TLR4 in a concentration-dependent manner, furthermore, this effect was not affected by naltrexone (Stevens et al., 2013). In correspondence of this discrepancy, Watkins lab pointed out the lack of translational potential of (+)-naloxone and (+)-naltrexone from *in vivo* studies considering the lack of biotransformation in in vitro systems (Watkins et al., 2014). In addition, apart from the difference in methodology, they also mentioned that not all agonist-antagonist relationships are equal under different conditions (Watkins et al., 2014). This explanation somewhat makes sense since antagonists could not bind to the receptors if they are fully occupied by respective agonists. Another

explanation is that there might be different signaling pathways involved in these interactions thus much effort should be spent to determine the exact signaling underlying the test agents (Watkins et al., 2014). Moreover, mixed results from *in vivo* studies need further consideration. The most intriguing finding is that TLR4 mutant and null mice maintained opioid induced tolerance, hyperalgesia and physical dependence, suggesting a minimal role of TLR4 in opioid actions (Mattioli et al., 2014). Additionally, acute injection of (+)-naltrexone immediately before extinction test had no effect in opioid-seeking behaviors. Meanwhile, acute or chronic delivery of (+)-naltrexone did not affect the extended access heroin self-administration behavior either (Theberge et al., 2013). More importantly, it was found that (+)-naltrexone or (+)-naloxone also reduced food self-administration (Tanda et al., 2016; Yue et al., 2020), suggesting a lack of behavioral specificity of TLR4 antagonists on drug-maintained operant behaviors (Tanda et al., 2016). These results question the validity of TLR4 hypothesis and should be further addressed before it is translated to the clinic. One possible explanation is the selectivity of TLR4 (+)-isomer ligands. Studies have identified non-stereoselective actions of naloxone at sites other than TLR4 (Wang and Burns, 2009; Burns and Wang, 2010; Wang et al., 2012a). Future studies that carefully examine how (+)-isomers act on non-TLR4 are needed to dissect the exact role of TLR4 in opioid addiction.

Possible Mechanisms Underlying the Role of Toll-Like Receptor 4 in Opioid Action

Neuronal mechanism of opioid addiction involves the inhibition of GABAergic tone on the mesolimbic dopaminergic reward pathway from ventral tegmental area (VTA) to nucleus accumbens (NAc), resulting in an increase in dopamine release in the NAc (Coller and Hutchinson, 2012; Fields and Margolis, 2015; Volkow and Morales, 2015). Meanwhile, opioids induced glia activation was thought to contribute to their reinforcing and rewarding-like effects, which is achieved possibly through the modulation of TLR4 (Jacobsen et al., 2014). A recent study showed that opioids, like morphine, interacts with MD2 and this binding is TLR4 dependent (Shah et al., 2016). Once activated by opioids, TLR4 increases the levels of pro-inflammatory cytokines and chemokines, which subsequently affect the neuronal transmission and plasticity that is associated with opioid-induced reward (Langlois and Nugent, 2017; Zhang et al., 2020). Therefore, immune factors like TNFα or IL-1β that can modulate synaptic functions may participate in opioid reward. TNFα is a downstream effector of TLR4 signaling and inhibition of TNFα blocked TLR4-mediated morphine-induced neuroinflammation (Kawai and Akira, 2010; Eidson et al., 2017). TNFα is shown to regulate synaptic transmission by affecting the activity of $GABA_A$ receptors, AMPA receptors and presynaptic metabotropic glutamate receptors (Bezzi et al., 2001; Stellwagen et al., 2005; Domercq et al., 2006; Stellwagen and Malenka, 2006; Pascual et al., 2012; Lewitus et al., 2014). It may also contribute to opioid reward by altering the opioid sensitivity as shown by a genetic human study (Reyes-Gibby et al., 2008). Like TNFα, activation of TLR4 also leads to an increase in IL-1β expression (Latz et al., 2013). IL-1β mediates long-term potentiation (LTP) which is important to learning and memory (Rizzo et al., 2018). As addiction can be viewed as a type of aberrant reward memory, IL-1β may play a role in the perception of opioid reward (Song et al., 2006). On the other hand, it has been shown that IL-1β suppresses postsynaptic GABA receptor activities through the activation of protein kinase C (PKC) in neurons. Meanwhile, IL-1β inhibits glial glutamate transporter activity, resulting in a deficiency in glutamate supply. This shortage in turn leads to the attenuation of glutamate-glutamine cycle-dependent GABA synthesis. These processes are widely involved in synaptic plasticity which may underlie TLR4-related drug actions (Wang et al., 2000). Though the exact role of TLR4 signaling in mediating opioid addiction remains unclear, it should be noted that activation of TLR4 mediated central immune response by drug of abuse can only work in concert with the well-established neuronal mechanisms of reward, as the central immune signaling alone cannot produce related behavioral effects (Coller and Hutchinson, 2012).

Clinical Implications for Toll-Like Receptor 4-Related Innate Immune Modulation in Opioid Addiction

With the knowledge that TLR4-related glial activity may play a role in opioid addiction preclinically, exploration of novel pharmacological treatments for opioid addiction by targeting the glial activity remains a promising choice (Zhang et al., 2020). One of the most studied existing medication is ibudilast, which is a non-selective phosphodiesterase inhibitor and TLR4 antagonist (Ruiz-Perez et al., 2016). Ibudilast is widely used in Asia for the treatment of asthma and post-stroke dizziness (Gibson et al., 2006), which showed a well safety and tolerability of a single dose (30 mg) and a 30-mg twice daily 2-week regimen in healthy subjects (Rolan et al., 2008). Recently, Comer lab has carefully examined the potential of ibudilast on opioid-induced analgesia, subjective and withdrawal symptoms in opioid-dependent volunteers. They found that ibudilast (40 mg, bid, 1 week) enhanced the oxycodone-induced analgesia as measured by subjective pain ratings (Cooper et al., 2017). Moreover, volunteers who received ibudilast (20 and 40 mg, bid, 2 weeks) also had lower ratings of withdrawal symptoms (Cooper et al., 2016). However, ibudilast did not affect oxycodone-induced subjective drug effect ratings (e.g., "high, good effect, I would pay") (Cooper et al., 2017). In contrary, another study by Metz et al. reported that ibudilast decreased the rating of drug like following 15 mg oxycodone in opioid-dependent volunteers (Metz et al., 2017). Ibudilast also significantly decreased the drug breakpoint value under 15 mg oxycodone condition, but not under 30 mg oxycodone condition. They also observed similar results that craving for heroin, cocaine and tobacco was also reduced under active ibudilast compared with placebo (Metz et al., 2017). It seems contradicting on whether ibudilast could decrease the subjective and reinforcing effects based on these results. However, they may reconcile at some point since Metz et al. found ibudilast reduced the craving following 15 mg, but not 30 mg oxycodone, while Comer lab examined higher doses of opioid (e.g., 30 mg morphine or 25, 50 mg/70 kg oxycodone). The discrepancy may also attribute to the limited sample volume and too few trails (Zhang et al., 2020). Meanwhile,

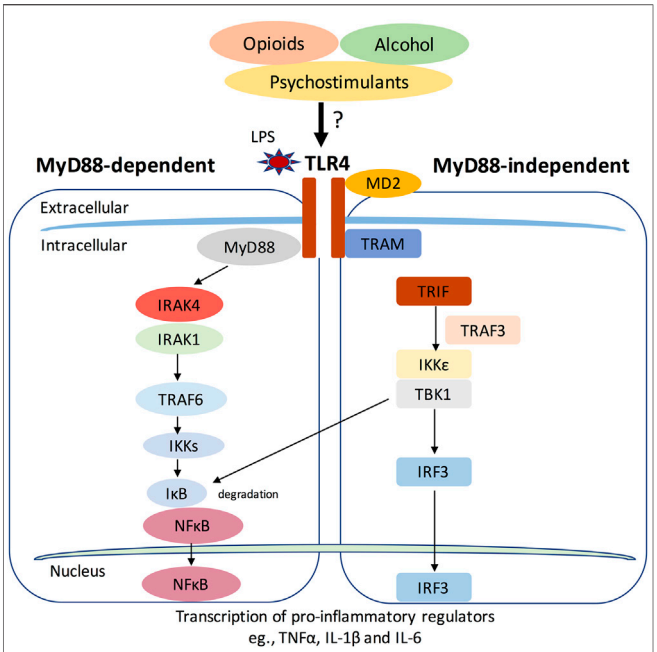

FIGURE 1 | The Toll-like receptor 4 (TLR4) signaling pathway. TLR4 and its co-receptor MD-2 can signal through two different pathways, the myeloid differentiation primary response protein 88 (MyD88)-dependent and MyD88-independent pathway. In MyD88-dependent pathway, the signal transduces through Interleukin 1 receptor associated kinase 4 and 1 (IRAK4 and IRAK1) and the following TNF receptor associated factor 6 (TRAF6). The activation of TRAF6 leads to phosphorylation of inhibitors of nuclear factor κB Kinases (IKKs), which in turn activates the IκB. The activation of IκB leads to its degradation and the initiation of activation of NFκB and the production of proinflammatory cytokines, for example, Tumor Necrosis Factor (TNF), IL-1β and IL-6 (Kawai and Akira, 2007). In contrast, MyD88-independent pathway adopts the adaptor protein TRIF and transduces the signal through TRAF3, TBK1 and IKKε, which then phosphorylates interferon regulatory factor 3 (IRF3). IRF3 then translocates to the nucleus and promotes the transcription of type 1 interferons. Drugs of abuse like opioids, alcohol and psychostimulants may activate TLR4 signaling and induce pro-inflammatory responses.

considerable individual variability may also add up to weaken the power of these studies. Therefore, future investigations with increased sample size are urgently needed to verify the clinical potential of glia modulators on opioid addiction.

Despite the clinical results of ibudilast are conflicting, the therapeutic potential of glial modulators in preventing opioid abuse should not be underestimated. Currently, other glial modulators are being examined for their ability in treating opioid use disorders as well. For example, minocycline increased accuracy on a cognition task in individuals with opioid use disorder, suggesting an effect like cognition enhancement. However, the pain threshold or tolerance, opioid craving and withdrawal weren't changed by minocycline treatment (Arout et al., 2019). Another glial modulator, cannabidiol, was shown to decrease opioid-induced craving and anxiety in drug-abstinent individuals with opioid use disorder (Hurd et al., 2015; Hurd et al., 2019). These results, albeit complex, suggesting a promising role of glial modulators in treating opioid addiction. Further studies with more dose regimen, greater sample size and prolonged trials are needed to figure out their exact roles.

Alcohol

Evidence of a Role of Toll-Like Receptor 4 in Alcohol Addiction

Studies have suggested that TLR4 affects some behavioral effects of ethanol (Pandey, 2012; Wu et al., 2012; Pascual et al., 2015; Blednov et al., 2017a). Both pharmacological inhibition of TLR4 and genetic deficiency of TLR4 or MyD88 significantly decreased the duration of loss of righting reflex (LORR) and reduced recovery time in motor impairment (rotarod test). Importantly, these effects were not due to changes of ethanol pharmacokinetics (Wu et al., 2012; Blednov et al., 2017a). In addition, TLR4-deficient mice showed lower sensitivity to pentobarbital-induced sedative effect and faster recovery from diazepam-induced motor impairment, suggesting a crosstalk between TLR4 and GABAergic functions (Blednov et al., 2017a). Chronic exposure of ethanol increases the expression of many cytokines (TNF-α, IL-1β) and chemokines (CX_3CL1, MCP-1) in the mice striatum and serum (Pascual et al., 2015). Interestingly, mice lacking TLR4 or TLR2 receptors are protected against ethanol-induced cytokine release (Pascual et al., 2015). These mice also showed less ethanol abstinence-induced behavioral changes such as increased anxiety (Pascual et al., 2015). Combined, these results suggest a clear involvement of TLR4 signaling in some acute and chronic effects of ethanol.

Binge drinking represents the initial stage of alcohol addiction, which has a link with anxiety (Chikritzhs et al., 2001; Naimi et al., 2003; Edenberg et al., 2004; Ducci et al., 2007). It is also suggested that TLR4-GABAA α2 subunit pathway regulates alcohol binge drinking in rodents (Spanagel et al., 1995; Roberts et al., 1996; Foster et al., 2004). By infusing a GABAA α2 siRNA vector in central nucleus of amygdala (CeA) of alcohol-preferring rats (P rats), Juan et al. reported a significant and specific reduction of alcohol binge drinking, reduced α2 subtype GABAA receptor expression, decreased GABAA receptor density and inhibition of TLR4(Liu et al., 2011). Moreover, TLR4 siRNA infusion to the CeA also decreased binge drinking behaviors without affecting sucrose intake, suggesting a specificity on alcohol-related behaviors (Liu et al., 2011). Similarly, another study showed that TLR4 or MCP-1 siRNA in CeA or VTA of P rats decreased the corresponding gene expression and binge drinking behavior (June et al., 2015). A further study also showed that α2 subtype of GABAA receptor activates TLR4 signals in neurons in VTA (Balan et al., 2018). Studies from inhibitors also support the central role of TLR4 in binge drinking as TLR4 inhibitor T5342126 decreased ethanol drinking (Bajo et al., 2016).

However, a recent comprehensive study has shown that manipulations of TLR4 may have minimal impact on excessive ethanol drinking behavior (Harris et al., 2017). By using the multiple models: TLR4-KO rats, selective Tlr4 knockdown in mouse NAc and inhibitor (+)-naloxone in different species, Harris et al. demonstrated that either genetic deletion of TLR4 or pharmacological inhibition of TLR4 or Tlr4 knockdown did not affect alcohol intake using two-bottle choice procedure and

drinking-in-the-dark assay (Harris et al., 2017). Meanwhile, specific Tlr4 knockdown in mouse NAc did not alter ethanol intake and preference for ethanol in the 24 h continuous access two-bottle test. These results suggest that TLR4 was not important to the excessive drinking behavior and subsequently question the hypothesis that TLR4 is a critical component in mediating alcohol response. One explanation is that Harris et al. examined a Tlr4 knockdown in the NAc while previous studies tested in the CeA or VTA. The difference in brain regions tested may lead to discrepancy in findings. In addition, while Harris used two-bottle and drinking-in-the dark tests, previous studies adopted binge-drinking model in P rats. It seems reasonable that increased GABAergic responses in P rats contribute to their altered binge-drinking behaviors. Nevertheless, they also reported consistent results that TLR4-KO rats had reduced duration of LORR, and CeA deletion of Tlr4 changed $GABA_A$ α2 subtype receptor function (Harris et al., 2017). These results at least suggest essential role of TLR4 signaling in mediating acute behavioral effects of ethanol (Alfonso-Loeches et al., 2010; Pascual et al., 2015; Blednov et al., 2017b). More studies are needed to disentangle the exact role of TLR4 signaling in alcohol addiction-related effects.

Possible Mechanisms Underlying the Role of Toll-Like Receptor 4 in Alcohol Action

Alcohol intake increases gut permeability, allowing translocation of bacterial toxins like LPS through the intestines into blood stream (Parlesak et al., 2000; Leclercq et al., 2012; Leclercq et al., 2014). LPS in the bloodstream reaches the liver and stimulate TLR4 in liver Kupffer cells, resulting in an increase in pro-inflammatory cytokines and chemokines (Roh and Seki, 2013) which can cross the blood-brain barrier and activate the glia cells in the brain (Montesinos et al., 2016). On the other hand, alcohol can activate glial TLR4 (Blanco et al., 2005; Fernandez-Lizarbe et al., 2009) and induce translocation to the lipid raft and promoting the activation of downstream effectors (Blanco et al., 2005; Blanco et al., 2008; Fernandez-Lizarbe et al., 2009). This activation contributes to ethanol-induced neuroinflammation and neurodegeneration (Alfonso-Loeches et al., 2010; Pascual et al., 2011; Alfonso-Loeches et al., 2012). Both chronic and acute exposure to ethanol cause TLR4-associated signaling response *in vivo* and *in vitro* (Blanco et al., 2004; Valles et al., 2004; Blanco et al., 2005; Blanco and Guerri, 2007). Conversely, inhibition of TLR4 blocks the proinflammatory responses and prevents cell damage (Blanco et al., 2005).

Indeed, the activation of innate immunity and TLR4 signaling appear to be essential for alcohol addiction-like behaviors (Pascual et al., 2011). The persistent activation of neuroinflammation exacerbates the neurodegeneration of key brain regions involved with excessive alcohol consumption, thus underlying at least partly the mechanisms that regulate the development of alcohol addiction (Crews et al., 2015; Flores-Bastias and Karahanian, 2018). Alcohol consumption promotes innate immune activation that are linked to alterations in executive function, reward and negative affect-craving-anxiety that contribute to alcohol use disorders (Vetreno and Crews, 2014; Crews et al., 2017a). Alcohol-induced cell damage in brain regions like prefrontal cortex may cause an executive dysfunction over behavioral inhibition (like binge drinking) and also a lack of inhibition in mesolimbic areas, which is turn increase drinking motivation (Crews et al., 2011; Crews et al., 2015). The loss of control over progression from initial intoxication and binge drinking stage to compulsive drinking stage may lead to the development of alcohol addiction.

Clinical Implications for Toll-Like Receptor 4-Related Innate Immune Modulation in Alcohol Addiction

Most recent studies have examined the potential of ibudilast in treating alcohol use disorders (AUD). In a recent randomized, double-blinded and placebo-control study, ibudilast was tested for its safety, tolerability and initial efficacy in mild-severe AUD outpatients (Ray et al., 2017). Ibudilast (50 mg, bid) was well-tolerated with no severe adverse events in the trial. However, ibudilast was not able to affect subjective response to alcohol as shown by craving, stimulation, sedation, positive or negative mood, "like" or "wanting" alcohol (Ray et al., 2017). Nevertheless, ibudilast was associated with mood improvements and decreased tonic level of craving after stress and alcohol cue exposure (Ray et al., 2017). Further analysis revealed that ibudilast attenuated the stimulating and mood-altering effects of alcohol among individuals with higher depressive ratings (Ray et al., 2017). This study suggested a possible mood-modulating effect of ibudilast in treating AUD and which may contribute to the reduced alcohol craving after stress or cue exposure. A more recent study further examined whether ibudilast affect other appetitive behavior, like food craving in AUD participants (Cummings et al., 2018). They found that ibudilast did not affect tonic high-fat/high-sugar food craving, indicating a specificity of modulating drinking behaviors (Cummings et al., 2018). These results provide the first evidence of whether ibudilast could be used for the treatment of alcohol addiction. However, it is still unclear whether ibudilast could decrease the subjective effect or alcohol intake since only few studies have examined this effect with limited participants and trails. More extensive studies are warranted to examine the potential of ibudilast on alcohol intake, withdrawal and relapse. Meanwhile, other neuroimmune modulators, like minocycline, PDE-4 inhibitor apremilast or selective PPARα agonist fenofibrate are undergoing clinical trials to determine their efficacy in reducing alcohol use, craving and related neuroinflammation (Erickson et al., 2019). More importantly, future studies that determine the effect of combination of neuroimmune pharmacotherapies with established medications for alcohol addiction are also warranted (Stopponi et al., 2013).

Psychostimulants

Evidence of a Role of Toll-Like Receptor 4 in Psychostimulants Addiction

There is a large body of literature that psychostimulants like cocaine and methamphetamine can activate and modulate neuroimmune responses (Loftis and Janowsky, 2014; Lacagnina et al., 2017). *In vitro* studies suggest that psychostimulants directly modulate the TLR4 signaling

activity. For example, cocaine exposure increases the expression of TLR4 in BV-2 cells in a dose-dependent manner (Periyasamy et al., 2018), and brain TLR4 expression was higher in mice self-administering cocaine than in those self-administering saline (Northcutt et al., 2015; Brown et al., 2018; Periyasamy et al., 2018), indicating an upregulation of TLR4 signaling by cocaine exposure. Similarly, methamphetamine treatment increases the expression of TLR4 in cultured astrocytes (Du et al., 2017) while silencing TLR4 expression using siRNA abolishes methamphetamine-induced expression of IL-1β and IL-18 (Du et al., 2017). *In vivo* evidence are consistent with these findings in that mice pretreated with the TLR4 inhibitor TAK-242 showed significantly decreased expression of IL-1β and IL-18 in striatum induced by methamphetamine (Du et al., 2017). All these results suggest that psychostimulants can activate TLR4 which may contribute to the behavioral effects of the drug.

Pharmacological antagonism of TLR4 also showed consistent results. Indeed, (+)-naloxone blocked cocaine-induced proinflammatory signaling both *in vitro* and *in vivo* (Northcutt et al., 2015). More importantly, evidence showed that TLR4 signaling at least partially contributed to cocaine-induced elevation of NAc dopamine (Northcutt et al., 2015). (+)-Naloxone ameliorated the robust increase in NAc dopamine induced by cocaine while it alone did not produce any effect (Ducci et al., 2007). Conversely, activation of TLR4 in the VTA by local LPS injection was sufficient to produce an elevation of dopamine in the NAc (Nie et al., 2018), suggesting a mediating role of TLR4 in cocaine-induced dopamine release. Behavioral studies further strengthened this notion as pretreatment of (+)-naloxone blocked the development of cocaine CPP and responding for cocaine injection (Northcutt et al., 2015). However, (+)-naloxone did not decrease the responding for food, which suggests that general operant behaviors are intact (Northcutt et al., 2015). In addition, a recent study has shown that TLR4 contributes to the drug-induced reinstatement of cocaine seeking (Brown et al., 2018). Local antagonism of TLR4 in the VTA decreased cocaine-seeking but not sucrose-seeking behavior (Brown et al., 2018). Collectively, these results showed that psychostimulant drugs activate TLR4 signaling which in turn contributes to the reinforcing and relapse-related effects of the drugs.

However, inconsistent evidence exists that pharmacological blockade of TLR4 by (+)-naloxone and (+)-naltrexone which attenuated cocaine self-administration also decreased food-maintained responding, suggesting a non-specific effect (Tanda et al., 2016). Meanwhile, pretreatment with (+)-naloxone and (+)-naltrexone did not affect the increased dopamine levels induced by cocaine (Tanda et al., 2016). Furthermore, a more recent study shows that TNF-α, an inflammatory cytokine downstream TLR4, suppresses cocaine-induced behavioral sensitization by depressing cocaine-induced synaptic changes in NAc core (Lewitus et al., 2016). Indeed, activation of microglia by cocaine increases TNF-α production, which subsequently limits the cocaine-induced changes to NAc circuity, and finally restrains the development of cocaine-induced behavioral sensitization. More importantly, after a period of abstinence, mild activation of TLR4 can reactivate microglia and reduce both synaptic strength in the NAc and locomotor activity to cocaine (Lewitus et al., 2016). Thus, it suggests that augmenting microglia responses through TLR4 or others might be a reasonable approach to treat addiction. Nonetheless, another study showed that TLR4 knockout (KO) mice had a deficit in low-frequency stimulation-induced NMDAR-dependent long-term depression (LTD) in NAc core, which contributed to an attenuation in drug reward learning (Kashima and Grueter, 2017). These mixed results about the role of TLR4 in psychostimulants action make it difficult to draw specific conclusions here. Explanations for this discrepancy may involve differences in addiction-related behaviors and stages of addiction studied. These differences promote continued examination of the effect of TLR4 in drug addiction.

Possible Mechanisms Underlying the Role of Toll-Like Receptor 4 in Psychostimulants Action

Studies have shown that cocaine and methamphetamine bind to the accessory receptor of TLR4, MD-2, which stabilizes the conformation of TLR4/MD-2 heterodimers. Methamphetamine binding activates TLR4 and NF-Kβ and upregulates the microglia activation marker CD11b and IL-6 in the VTA, which can be abolished by TLR4 antagonists LPS-RS and TAK-242 (Bachtell et al., 2015; Wang et al., 2019). Meanwhile, the TLR4 antagonist (+)-naloxone or (+)-naltrexone docked to the same pocket of MD-2, competing with other molecules, suggesting a potential modulatory role of TLR4 antagonist in psychostimulants-induced TLR4 activation (Northcutt et al., 2015). TLR4 activation by cocaine or methamphetamine leads to the increased levels of proinflammatory cytokines or chemokines, which subsequently contributes to abnormal neuronal excitatory and toxicity. This non-neuronal mechanism is believed to work in combination with the well-known neuronal circuity, such as psychostimulants-induced alterations of dopamine transporters functions (Hall et al., 2004), to achieve the associated development of drug addiction. It remains unclear how these two mechanisms synergize and result in addiction-like behaviors. However, alterations in synaptic plasticity and neuronal transmission induced by immune response are believed to play a part.

Clinical Implications for Toll-Like Receptor 4-Related Innate Immune Modulation in Psychostimulants Addiction

Currently, there are no FDA-approved medications for the treatment of psychostimulants addiction. However, accumulating evidence suggests that targeting neuroinflammation might be a promising strategy for developing a potential pharmacotherapy to treat stimulants addiction. In 2010, a case study reported that minocycline improved the psychotic symptoms in a female patient who had methamphetamine use disorder, suggesting a promising role of minocycline in treating methamphetamine addiction (Tanibuchi et al., 2010). However, there were no follow-up clinical studies which further examined the potential of minocycline in methamphetamine use disorders since then. On the other hand, ibudilast, which has been shown to reduce

methamphetamine self-administration and reinstatement in animals, was examined for its efficacy clinically. Ibudilast was able to reduce several methamphetamine–related subjective effects (Worley et al., 2016). Further study also demonstrated that ibudilast may improve attention during early abstinence from methamphetamine dependence (Birath et al., 2017). Despite the limitations of these early-stage studies, they provide first evidence that ibudilast might serve as a potential pharmacotherapy for methamphetamine use disorders. However, a most recent study showed that ibudilast did not affect methamphetamine abstinence (Heinzerling et al., 2020). This randomize trials included 64 participants for ibudilast group and 61 for placebo. Urine specimens for drug screens were collected twice a week. Nonetheless, there was no correlation between serum ibudilast levels and methamphetamine use during treatment. This study suggests that ibudilast might not be able to affect methamphetamine abstinence, yet it's hard to conclude that ibudilast has no effect on methamphetamine action since no further evidence reported whether ibudilast could affect methamphetamine intake or craving. Actually, a pilot randomized clinical research demonstrated that ibudilast reduced the increased levels of peripheral markers of inflammation induced by methamphetamine treatment in patients, which have implications for the development of treatment for psychostimulants addiction (Li et al., 2020). These results are encouraging, though more studies are needed to examine the long-term effect of ibudilast on both peripheral and central neuroinflammation markers and how these modulations link to clinical outcomes.

FUTURE DIRECTIONS

While significant effort has been made to illustrate the role of TLR4-related immune response in drug addiction, it is early to reach a solid conclusion. Since debates are remained about whether TLR4 is essential to drugs of abuse, further studies should further examine the link between TLR4-related immune activation and different stages of drug addiction. Meanwhile, it is generally believed that TLR4-related immune response activated by drugs of abuse work in concert with established neuronal mechanisms, which contribute to the rewarding and reinforcing effects. However, it remains elusive how non-neuronal activation communicates with the mesocorticolimbic reward system which underlies drug addiction-related behaviors. Thus, examinations of the interactions between these two systems would add valuable information to the knowledge of the mechanism underlying drug addiction. More importantly, these studies would further suggest the potential and novel therapeutic targets for the treatments of drug addiction. Moreover, randomized clinical trial which examines the potential efficacy of immune-based pharmacotherapies in drug addiction is in its infancy as conflicting results from clinical data weakens the translational value of the immune-based therapies. Current clinical trials have limited sample size and test restricted time window, dosage effects and drug actions. Consequently, future clinical studies including more participants, examining long-term efficacy and multiple dose-effects of immune-based pharmacotherapies for different stages of drug addiction are warranted.

SUMMARY

Emerging evidence suggest an important role of the neuroimmune system, especially TLR4, in addiction-related effects of different classes of drugs such as opioids, alcohol and psychostimulants. Drugs of abuse activate TLR4 signaling and the modulation of TLR4 signaling has been shown to be involved in different stages of drug addiction (binge or intoxication, withdrawal and relapse). Accordingly, pharmacological strategies such as non-specific microglia inhibition is a potentially promising approach to treat drug abuse. This is a burgeoning field that requires more mechanistically based studies for target validation and future clinical trials with clinically approved drugs to repurpose for the treatment of drug addiction.

AUTHOR CONTRIBUTIONS

RW: conception, design, gathering, interpretation of data and writing; JL: conception, interpretation of data and writing.

FUNDING

RW was partially supported by the National Natural Science Foundation of China (Grant 81701340) and Natural Science Foundation of Jiangsu Province (Grant BK 20170517).

REFERENCES

Alfonso-Loeches, S., Pascual, M., Gomez-Pinedo, U., Pascual-Lucas, M., Renau-Piqueras, J., and Guerri, C. (2012). Toll-like receptor 4 participates in the myelin disruptions associated with chronic alcohol abuse. *Glia* 60, 948–964. doi:10.1002/glia.22327

Alfonso-Loeches, S., Pascual-Lucas, M., Blanco, A. M., Sanchez-Vera, I., and Guerri, C. (2010). Pivotal role of TLR4 receptors in alcohol-induced neuroinflammation and brain damage. *J. Neurosci.* 30, 8285–8295. doi:10.1523/JNEUROSCI.0976-10.2010

Apetoh, L., Ghiringhelli, F., Tesniere, A., Obeid, M., Ortiz, C., Criollo, A., et al. (2007). Toll-like receptor 4-dependent contribution of the immune system to anticancer chemotherapy and radiotherapy. *Nat. Med.* 13, 1050–1059. doi:10.1038/nm1622

Arout, C. A., Waters, A. J., Maclean, R. R., Compton, P., and Sofuoglu, M. (2019). Minocycline does not affect experimental pain or addiction-related outcomes in opioid maintained patients. *Psychopharmacology (Berl)* 236, 2857–2866. doi:10.1007/s00213-018-5146-7

Aurelian, L., Warnock, K. T., Balan, I., Puche, A., and June, H. (2016). TLR4 signaling in VTA dopaminergic neurons regulates impulsivity through tyrosine hydroxylase modulation. *Transl. Psychiatry* 6, e815.

Bachtell, R., Hutchinson, M. R., Wang, X., Rice, K. C., Maier, S. F., and Watkins, L. R. (2015). Targeting the toll of drug abuse: the translational potential of toll-like receptor 4. *CNS Neurol. Disord. Drug Targets* 14, 692–699. doi:10.2174/1871527314666150529132503

Bajo, M., Montgomery, S. E., Cates, L. N., Nadav, T., Delucchi, A. M., Cheng, K., et al. (2016). Evaluation of TLR4 inhibitor, T5342126, in modulation of ethanol-drinking behavior in alcohol-dependent mice. *Alcohol Alcohol.* 51, 541–548. doi:10.1093/alcalc/agw026

Balan, I., Warnock, K. T., Puche, A., Gondre-Lewis, M. C., June, H., and Aurelian, L. (2018). The $GABA_A$ receptor alpha2 subunit activates a neuronal TLR4 signal in the ventral tegmental area that regulates alcohol and nicotine abuse. *Brain Sci.* 8, 72. doi:10.3390/brainsci8040072

Bezzi, P., Domercq, M., Brambilla, L., Galli, R., Schols, D., De Clercq, E., et al. (2001). CXCR4-activated astrocyte glutamate release via TNFalpha: amplification by microglia triggers neurotoxicity. *Nat. Neurosci.* 4, 702–710. doi:10.1038/89490

Birath, J. B., Briones, M., Amaya, S., Shoptaw, S., Swanson, A. N., Tsuang, J., et al. (2017). Ibudilast may improve attention during early abstinence from methamphetamine. *Drug Alcohol Depend.* 178, 386–390. doi:10.1016/j.drugalcdep.2017.05.016

Blanco, A. M., and Guerri, C. (2007). Ethanol intake enhances inflammatory mediators in brain: role of glial cells and TLR4/IL-1RI receptors. *Front. Biosci.* 12, 2616–2630. doi:10.2741/2259

Blanco, A. M., Pascual, M., Valles, S. L., and Guerri, C. (2004). Ethanol-induced iNOS and COX-2 expression in cultured astrocytes via NF-kappa B. *Neuroreport* 15, 681–685. doi:10.1097/00001756-200403220-00021

Blanco, A. M., Perez-Arago, A., Fernandez-Lizarbe, S., and Guerri, C. (2008). Ethanol mimics ligand-mediated activation and endocytosis of IL-1RI/TLR4 receptors via lipid rafts caveolae in astroglial cells. *J. Neurochem.* 106, 625–639. doi:10.1111/j.1471-4159.2008.05425.x

Blanco, A. M., Valles, S. L., Pascual, M., and Guerri, C. (2005). Involvement of TLR4/type I IL-1 receptor signaling in the induction of inflammatory mediators and cell death induced by ethanol in cultured astrocytes. *J. Immunol.* 175, 6893–6899. doi:10.4049/jimmunol.175.10.6893

Blednov, Y. A., Black, M., Benavidez, J. M., Da Costa, A., Mayfield, J., and Harris, R. A. (2017a). Sedative and motor incoordination effects of ethanol in mice lacking CD14, TLR2, TLR4, or MyD88. *Alcohol Clin. Exp. Res.* 41, 531–540. doi:10.1111/acer.13314

Blednov, Y. A., Black, M., Chernis, J., Da Costa, A., Mayfield, J., and Harris, R. A. (2017b). Ethanol consumption in mice lacking CD14, TLR2, TLR4, or MyD88. *Alcohol Clin. Exp. Res.* 41, 516–530. doi:10.1111/acer.13316

Brown, K. T., Levis, S. C., O'neill, C. E., Northcutt, A. L., Fabisiak, T. J., Watkins, L. R., et al. (2018). Innate immune signaling in the ventral tegmental area contributes to drug-primed reinstatement of cocaine seeking. *Brain Behav. Immun.* 67, 130–138. doi:10.1016/j.bbi.2017.08.012

Burns, L. H., and Wang, H. Y. (2010). PTI-609: a novel analgesic that binds filamin A to control opioid signaling. *Recent Pat. CNS Drug Discov.* 5, 210–220. doi:10.2174/157488910793362386

Caron, G., Duluc, D., Fremaux, I., Jeannin, P., David, C., Gascan, H., et al. (2005). Direct stimulation of human T cells via TLR5 and TLR7/8: flagellin and R-848 up-regulate proliferation and IFN-gamma production by memory CD4+ T cells. *J. Immunol.* 175, 1551–1557. doi:10.4049/jimmunol.175.3.1551

Chaplin, D. D. (2010). Overview of the immune response. *J. Allergy Clin. Immunol.* 125, S3–S23. doi:10.1016/j.jaci.2009.12.980

Chikritzhs, T. N., Jonas, H. A., Stockwell, T. R., Heale, P. F., and Dietze, P. M. (2001). Mortality and life-years lost due to alcohol: a comparison of acute and chronic causes. *Med. J. Aust.* 174, 281–284. doi:10.5694/j.1326-5377.2001.tb143269.x

Coller, J. K., and Hutchinson, M. R. (2012). Implications of central immune signaling caused by drugs of abuse: mechanisms, mediators and new therapeutic approaches for prediction and treatment of drug dependence. *Pharmacol. Ther.* 134, 219–245. doi:10.1016/j.pharmthera.2012.01.008

Cooper, Z. D., Johnson, K. W., Pavlicova, M., Glass, A., Vosburg, S. K., Sullivan, M. A., et al. (2016). The effects of ibudilast, a glial activation inhibitor, on opioid withdrawal symptoms in opioid-dependent volunteers. *Addict. Biol.* 21, 895–903. doi:10.1111/adb.12261

Cooper, Z. D., Johnson, K. W., Vosburg, S. K., Sullivan, M. A., Manubay, J., Martinez, D., et al. (2017). Effects of ibudilast on oxycodone-induced analgesia and subjective effects in opioid-dependent volunteers. *Drug Alcohol Depend.* 178, 340–347. doi:10.1016/j.drugalcdep.2017.04.029

Crews, F. T., Lawrimore, C. J., Walter, T. J., and Coleman, L. G., Jr (2017a). The role of neuroimmune signaling in alcoholism. *Neuropharmacology* 122, 56–73. doi:10.1016/j.neuropharm.2017.01.031

Crews, F. T., Sarkar, D. K., Qin, L., Zou, J., Boyadjieva, N., and Vetreno, R. P. (2015). Neuroimmune function and the consequences of alcohol exposure. *Alcohol Res.* 37, 331–341, 344–351.

Crews, F. T., Walter, T. J., Coleman, L. G., Jr, and Vetreno, R. P. (2017b). Toll-like receptor signaling and stages of addiction. *Psychopharmacology (Berl)* 234, 1483–1498. doi:10.1007/s00213-017-4560-6

Crews, F. T., Zou, J., and Qin, L. (2011). Induction of innate immune genes in brain create the neurobiology of addiction. *Brain Behav. Immun.* 25 (Suppl. 1), S4–S12. doi:10.1016/j.bbi.2011.03.003

Cummings, J. R., Tomiyama, A. J., and Ray, L. A. (2018). Does the neuroimmune modulator ibudilast alter food craving? Results in a sample with alcohol use disorder. *J Addict. Med.* 12, 410–417. doi:10.1097/ADM.0000000000000416

Domercq, M., Brambilla, L., Pilati, E., Marchaland, J., Volterra, A., and Bezzi, P. (2006). P2Y1 receptor-evoked glutamate exocytosis from astrocytes: control by tumor necrosis factor-alpha and prostaglandins. *J. Biol. Chem.* 281, 30684–30696. doi:10.1074/jbc.M606429200

Du, S. H., Qiao, D. F., Chen, C. X., Chen, S., Liu, C., Lin, Z., et al. (2017). Toll-like receptor 4 mediates methamphetamine-induced neuroinflammation through caspase-11 signaling pathway in astrocytes. *Front. Mol. Neurosci.* 10, 409. doi:10.3389/fnmol.2017.00409

Ducci, F., Enoch, M. A., Funt, S., Virkkunen, M., Albaugh, B., and Goldman, D. (2007). Increased anxiety and other similarities in temperament of alcoholics with and without antisocial personality disorder across three diverse populations. *Alcohol* 41, 3–12. doi:10.1016/j.alcohol.2007.02.005

Dunne, A., Marshall, N. A., and Mills, K. H. (2011). TLR based therapeutics. *Curr. Opin. Pharmacol.* 11, 404–411. doi:10.1016/j.coph.2011.03.004

Edenberg, H. J., Dick, D. M., Xuei, X., Tian, H., Almasy, L., Bauer, L. O., et al. (2004). Variations in GABRA2, encoding the alpha 2 subunit of the GABA(A) receptor, are associated with alcohol dependence and with brain oscillations. *Am. J. Hum. Genet.* 74, 705–714. doi:10.1086/383283

Eidson, L. N., Inoue, K., Young, L. J., Tansey, M. G., and Murphy, A. Z. (2017). Toll-like receptor 4 mediates morphine-induced neuroinflammation and tolerance via soluble tumor necrosis factor signaling. *Neuropsychopharmacology* 42, 661–670. doi:10.1038/npp.2016.131

Eidson, L. N., and Murphy, A. Z. (2013). Blockade of toll-like receptor 4 attenuates morphine tolerance and facilitates the pain relieving properties of morphine. *J. Neurosci.* 33, 15952–15963. doi:10.1523/JNEUROSCI.1609-13.2013

Erickson, E. K., Grantham, E. K., Warden, A. S., and Harris, R. A. (2019). Neuroimmune signaling in alcohol use disorder. *Pharmacol. Biochem. Behav.* 177, 34–60. doi:10.1016/j.pbb.2018.12.007

Feldmann, M. (2009). Translating molecular insights in autoimmunity into effective therapy. *Annu. Rev. Immunol.* 27, 1–27. doi:10.1146/annurev-immunol-082708-100732

Fernandez-Lizarbe, S., Pascual, M., and Guerri, C. (2009). Critical role of TLR4 response in the activation of microglia induced by ethanol. *J. Immunol.* 183, 4733–4744. doi:10.4049/jimmunol.0803590

Fields, H. L., and Margolis, E. B. (2015). Understanding opioid reward. *Trends Neurosci.* 38, 217–225. doi:10.1016/j.tins.2015.01.002

Flores-Bastias, O., and Karahanian, E. (2018). Neuroinflammation produced by heavy alcohol intake is due to loops of interactions between toll-like 4 and TNF receptors, peroxisome proliferator-activated receptors and the central melanocortin system: a novel hypothesis and new therapeutic avenues. *Neuropharmacology* 128, 401–407. doi:10.1016/j.neuropharm.2017.11.003

Foster, K. L., Mckay, P. F., Seyoum, R., Milbourne, D., Yin, W., Sarma, P. V., et al. (2004). GABA(A) and opioid receptors of the central nucleus of the amygdala selectively regulate ethanol-maintained behaviors. *Neuropsychopharmacology* 29, 269–284. doi:10.1038/sj.npp.1300306

Garcia Bueno, B., Caso, J. R., Madrigal, J. L., and Leza, J. C. (2016). Innate immune receptor toll-like receptor 4 signalling in neuropsychiatric diseases. *Neurosci. Biobehav. Rev.* 64, 134–147. doi:10.1016/j.neubiorev.2016.02.013

Gasiorowski, K., Brokos, B., Echeverria, V., Barreto, G. E., and Leszek, J. (2018). RAGE-TLR crosstalk sustains chronic inflammation in neurodegeneration. *Mol. Neurobiol.* 55, 1463–1476. doi:10.1007/s12035-017-0419-4

Gaudino, S. J., and Kumar, P. (2019). Cross-talk between antigen presenting cells and T cells impacts intestinal homeostasis, bacterial infections, and tumorigenesis. *Front. Immunol.* 10, 360. doi:10.3389/fimmu.2019.00360

Gesuete, R., Kohama, S. G., and Stenzel-Poore, M. P. (2014). Toll-like receptors and ischemic brain injury. *J. Neuropathol. Exp. Neurol.* 73, 378–386. doi:10.1097/NEN.0000000000000068

Gibson, L. C., Hastings, S. F., Mcphee, I., Clayton, R. A., Darroch, C. E., Mackenzie, A., et al. (2006). The inhibitory profile of Ibudilast against the human phosphodiesterase enzyme family. *Eur. J. Pharmacol.* 538, 39–42. doi:10.1016/j.ejphar.2006.02.053

Hall, F. S., Sora, I., Drgonova, J., Li, X. F., Goeb, M., and Uhl, G. R. (2004). Molecular mechanisms underlying the rewarding effects of cocaine. *Ann. N. Y. Acad. Sci.* 1025, 47–56. doi:10.1196/annals.1316.006

Harris, R. A., Bajo, M., Bell, R. L., Blednov, Y. A., Varodayan, F. P., Truitt, J. M., et al. (2017). Genetic and pharmacologic manipulation of TLR4 has minimal impact on ethanol consumption in rodents. *J. Neurosci.* 37, 1139–1155. doi:10.1523/JNEUROSCI.2002-16.2016

Heinzerling, K. G., Briones, M., Thames, A. D., Hinkin, C. H., Zhu, T., Wu, Y. N., et al. (2020). Randomized, placebo-controlled trial of targeting neuroinflammation with ibudilast to treat methamphetamine use disorder. *J. Neuroimmune Pharmacol.* 15, 238–248. doi:10.1007/s11481-019-09883-w

Hennessy, E. J., Parker, A. E., and O'neill, L. A. (2010). Targeting toll-like receptors: emerging therapeutics? *Nat. Rev. Drug Discov.* 9, 293–307. doi:10.1038/nrd3203

Hurd, Y. L., Spriggs, S., Alishayev, J., Winkel, G., Gurgov, K., Kudrich, C., et al. (2019). Cannabidiol for the reduction of cue-induced craving and anxiety in drug-abstinent individuals with heroin use disorder: a double-blind randomized placebo-controlled trial. *Am. J. Psychiatry* 176, 911–922. doi:10.1176/appi.ajp.2019.18101191

Hurd, Y. L., Yoon, M., Manini, A. F., Hernandez, S., Olmedo, R., Ostman, M., et al. (2015). Early phase in the development of cannabidiol as a treatment for addiction: opioid relapse takes initial center stage. *Neurotherapeutics* 12, 807–815. doi:10.1007/s13311-015-0373-7

Hutchinson, M. R., Northcutt, A. L., Hiranita, T., Wang, X., Lewis, S. S., Thomas, J., et al. (2012). Opioid activation of toll-like receptor 4 contributes to drug reinforcement. *J. Neurosci.* 32, 11187–11200. doi:10.1523/JNEUROSCI.0684-12.2012

Jacobsen, J. H., Watkins, L. R., and Hutchinson, M. R. (2014). Discovery of a novel site of opioid action at the innate immune pattern-recognition receptor TLR4 and its role in addiction. *Int. Rev. Neurobiol.* 118, 129–163. doi:10.1016/B978-0-12-801284-0.00006-3

June, H. L., Liu, J., Warnock, K. T., Bell, K. A., Balan, I., et al. (2015). CRF-amplified neuronal TLR4/MCP-1 signaling regulates alcohol self-administration. *Neuropsychopharmacology* 40, 1549–1559. doi:10.1038/npp.2015.4

Kalivas, P. W., and O'brien, C. (2008). Drug addiction as a pathology of staged neuroplasticity. *Neuropsychopharmacology* 33, 166–180. doi:10.1038/sj.npp.1301564

Kashima, D. T., and Grueter, B. A. (2017). Toll-like receptor 4 deficiency alters nucleus accumbens synaptic physiology and drug reward behavior. *Proc. Natl. Acad. Sci. U. S. A.* 114, 8865–8870. doi:10.1073/pnas.1705974114

Kawai, T., and Akira, S. (2007). Signaling to NF-kappaB by toll-like receptors. *Trends Mol. Med.* 13, 460–469. doi:10.1016/j.molmed.2007.09.002

Kawai, T., and Akira, S. (2010). The role of pattern-recognition receptors in innate immunity: update on Toll-like receptors. *Nat. Immunol.* 11, 373–384. doi:10.1038/ni.1863

Klareskog, L., Van Der Heijde, D., De Jager, J. P., Gough, A., Kalden, J., Malaise, M., et al. (2004). Therapeutic effect of the combination of etanercept and methotrexate compared with each treatment alone in patients with rheumatoid arthritis: double-blind randomised controlled trial. *Lancet* 363, 675–681. doi:10.1016/S0140-6736(04)15640-7

Koropatnick, T. A., Engle, J. T., Apicella, M. A., Stabb, E. V., Goldman, W. E., and Mcfall-Ngai, M. J. (2004). Microbial factor-mediated development in a host-bacterial mutualism. *Science* 306, 1186–1188. doi:10.1126/science.1102218

Kronenberger, B., and Zeuzem, S. (2009). Current and future treatment options for HCV. *Ann. Hepatol.* 8, 103–112. doi:10.1016/S1665-2681(19)31786-7

Lacagnina, M. J., Rivera, P. D., and Bilbo, S. D. (2017). Glial and neuroimmune mechanisms as critical modulators of drug use and abuse. *Neuropsychopharmacology* 42, 156–177. doi:10.1038/npp.2016.121

Landreth, G. E., and Reed-Geaghan, E. G. (2009). Toll-like receptors in Alzheimer's disease. *Curr. Top. Microbiol. Immunol.* 336, 137–153. doi:10.1007/978-3-642-00549-7_8

Langlois, L. D., and Nugent, F. S. (2017). Opiates and plasticity in the ventral tegmental area. *ACS Chem. Neurosci.* 8, 1830–1838. doi:10.1021/acschemneuro.7b00281

Latz, E., Xiao, T. S., and Stutz, A. (2013). Activation and regulation of the inflammasomes. *Nat. Rev. Immunol.* 13, 397–411. doi:10.1038/nri3452

Leclercq, S., Cani, P. D., Neyrinck, A. M., Starkel, P., Jamar, F., Mikolajczak, M., et al. (2012). Role of intestinal permeability and inflammation in the biological and behavioral control of alcohol-dependent subjects. *Brain Behav. Immun.* 26, 911–918. doi:10.1016/j.bbi.2012.04.001

Leclercq, S., Matamoros, S., Cani, P. D., Neyrinck, A. M., Jamar, F., Starkel, P., et al. (2014). Intestinal permeability, gut-bacterial dysbiosis, and behavioral markers of alcohol-dependence severity. *Proc. Natl. Acad. Sci. U. S. A.* 111, E4485–E4493. doi:10.1073/pnas.1415174111

Lee, B. R., Ma, Y. Y., Huang, Y. H., Wang, X., Otaka, M., Ishikawa, M., et al. (2013). Maturation of silent synapses in amygdala-accumbens projection contributes to incubation of cocaine craving. *Nat. Neurosci.* 16, 1644–1651. doi:10.1038/nn.3533

Lewitus, G. M., Konefal, S. C., Greenhalgh, A. D., Pribiag, H., Augereau, K., and Stellwagen, D. (2016). Microglial TNF-alpha suppresses cocaine-induced plasticity and behavioral sensitization. *Neuron* 90, 483–491. doi:10.1016/j.neuron.2016.03.030

Lewitus, G. M., Pribiag, H., Duseja, R., St-Hilaire, M., and Stellwagen, D. (2014). An adaptive role of TNFalpha in the regulation of striatal synapses. *J. Neurosci.* 34, 6146–6155. doi:10.1523/JNEUROSCI.3481-13.2014

Li, M. J., Briones, M. S., Heinzerling, K. G., Kalmin, M. M., and Shoptaw, S. J. (2020). Ibudilast attenuates peripheral inflammatory effects of methamphetamine in patients with methamphetamine use disorder. *Drug Alcohol Depend.* 206, 107776. doi:10.1016/j.drugalcdep.2019.107776

Liu, G., Zhang, L., and Zhao, Y. (2010). Modulation of immune responses through direct activation of toll-like receptors to T cells. *Clin. Exp. Immunol.* 160, 168–175. doi:10.1111/j.1365-2249.2010.04091.x

Liu, J. F., Wu, R., and Li, J. X. (2019). Toll of mental disorders: TLR-mediated function of the innate immune system. *Neurosci. Bull.* 35, 771–774. doi:10.1007/s12264-018-00335-8

Liu, J., Yang, A. R., Kelly, T., Puche, A., Esoga, C., June, H. L., Jr, et al. (2011). Binge alcohol drinking is associated with GABAA alpha2-regulated toll-like receptor 4 (TLR4) expression in the central amygdala. *Proc. Natl. Acad. Sci. U. S. A.* 108, 4465–4470. doi:10.1073/pnas.1019020108

Loftis, J. M., and Janowsky, A. (2014). Neuroimmune basis of methamphetamine toxicity. *Int. Rev. Neurobiol.* 118, 165–197. doi:10.1016/B978-0-12-801284-0.00007-5

Ma, Y. Y., Lee, B. R., Wang, X., Guo, C., Liu, L., Cui, R., et al. (2014). Bidirectional modulation of incubation of cocaine craving by silent synapse-based remodeling of prefrontal cortex to accumbens projections. *Neuron* 83, 1453–1467. doi:10.1016/j.neuron.2014.08.023

Mattioli, T. A., Leduc-Pessah, H., Skelhorne-Gross, G., Nicol, C. J., Milne, B., Trang, T., et al. (2014). Toll-like receptor 4 mutant and null mice retain morphine-induced tolerance, hyperalgesia, and physical dependence. *PloS One* 9, e97361. doi:10.1371/journal.pone.0097361

Metz, V. E., Jones, J. D., Manubay, J., Sullivan, M. A., Mogali, S., Segoshi, A., et al. (2017). Effects of ibudilast on the subjective, reinforcing, and analgesic effects of oxycodone in recently detoxified adults with opioid dependence. *Neuropsychopharmacology* 42, 1825–1832. doi:10.1038/npp.2017.70

Montesinos, J., Alfonso-Loeches, S., and Guerri, C. (2016). Impact of the innate immune response in the actions of ethanol on the central nervous system. *Alcohol Clin. Exp. Res.* 40, 2260–2270. doi:10.1111/acer.13208

Naimi, T. S., Brewer, R. D., Mokdad, A., Denny, C., Serdula, M. K., and Marks, J. S. (2003). Binge drinking among US adults. *J. Am. Med. Assoc.* 289, 70–75. doi:10.1001/jama.289.1.70

Narita, M., Miyatake, M., Narita, M., Shibasaki, M., Shindo, K., Nakamura, A., et al. (2006). Direct evidence of astrocytic modulation in the development of rewarding effects induced by drugs of abuse. *Neuropsychopharmacology* 31, 2476–2488. doi:10.1038/sj.npp.1301007

Nie, X., Kitaoka, S., Tanaka, K., Segi-Nishida, E., Imoto, Y., Ogawa, A., et al. (2018). The innate immune receptors TLR2/4 mediate repeated social defeat stress-

induced social avoidance through prefrontal microglial activation. *Neuron* 99, 464–479.e7. doi:10.1016/j.neuron.2018.06.035

Northcutt, A. L., Hutchinson, M. R., Wang, X., Baratta, M. V., Hiranita, T., Cochran, T. A., et al. (2015). DAT isn't all that: cocaine reward and reinforcement require toll-like receptor 4 signaling. *Mol Psychiatry* 20, 1525–1537. doi:10.1038/mp.2014.177

Otis, J. M., and Mueller, D. (2017). Reversal of cocaine-associated synaptic plasticity in medial prefrontal cortex parallels elimination of memory retrieval. *Neuropsychopharmacology* 42, 2000–2010. doi:10.1038/npp.2017.90

Pandey, S. C. (2012). TLR4-MyD88 signalling: a molecular target for alcohol actions. *Br. J. Pharmacol.* 165, 1316–1318. doi:10.1111/j.1476-5381.2011.01695.x

Parlesak, A., Schafer, C., Schutz, T., Bode, J. C., and Bode, C. (2000). Increased intestinal permeability to macromolecules and endotoxemia in patients with chronic alcohol abuse in different stages of alcohol-induced liver disease. *J. Hepatol.* 32, 742–747. doi:10.1016/s0168-8278(00)80242-1

Pascual, M., Balino, P., Alfonso-Loeches, S., Aragon, C. M., and Guerri, C. (2011). Impact of TLR4 on behavioral and cognitive dysfunctions associated with alcohol-induced neuroinflammatory damage. *Brain Behav. Immun.* 25 (Suppl. 1), S80–S91. doi:10.1016/j.bbi.2011.02.012

Pascual, M., Balino, P., Aragon, C. M., and Guerri, C. (2015). Cytokines and chemokines as biomarkers of ethanol-induced neuroinflammation and anxiety-related behavior: role of TLR4 and TLR2. *Neuropharmacology* 89, 352–359. doi:10.1016/j.neuropharm.2014.10.014

Pascual, O., Ben Achour, S., Rostaing, P., Triller, A., and Bessis, A. (2012). Microglia activation triggers astrocyte-mediated modulation of excitatory neurotransmission. *Proc. Natl. Acad. Sci. U. S. A.* 109, E197–E205. doi:10.1073/pnas.1111098109

Periyasamy, P., Liao, K., Kook, Y. H., Niu, F., Callen, S. E., Guo, M. L., et al. (2018). Cocaine-mediated downregulation of miR-124 activates microglia by targeting KLF4 and TLR4 signaling. *Mol. Neurobiol.* 55, 3196–3210. doi:10.1007/s12035-017-0584-5

Ray, L. A., Bujarski, S., Shoptaw, S., Roche, D. J., Heinzerling, K., and Miotto, K. (2017). Development of the neuroimmune modulator ibudilast for the treatment of alcoholism: a randomized, placebo-controlled, human laboratory trial. *Neuropsychopharmacology* 42, 1776–1788. doi:10.1038/npp.2017.10

Reyes-Gibby, C. C., El Osta, B., Spitz, M. R., Parsons, H., Kurzrock, R., Wu, X., et al. (2008). The influence of tumor necrosis factor-alpha -308 G/A and IL-6 -174 G/C on pain and analgesia response in lung cancer patients receiving supportive care. *Cancer Epidemiol. Biomarkers Prev.* 17, 3262–3267. doi:10.1158/1055-9965.EPI-08-0125

Rizzo, F. R., Musella, A., De Vito, F., Fresegna, D., Bullitta, S., Vanni, V., et al. (2018). Tumor necrosis factor and interleukin-1beta modulate synaptic plasticity during neuroinflammation. *Neural Plast.* 2018, 8430123. doi:10.1155/2018/8430123

Roberts, A. J., Cole, M., and Koob, G. F. (1996). Intra-amygdala muscimol decreases operant ethanol self-administration in dependent rats. *Alcohol Clin. Exp. Res.* 20, 1289–1298. doi:10.1111/j.1530-0277.1996.tb01125.x

Roh, Y. S., and Seki, E. (2013). Toll-like receptors in alcoholic liver disease, non-alcoholic steatohepatitis and carcinogenesis. *J. Gastroenterol. Hepatol.* 28 (Suppl. 1), 38–42. doi:10.1111/jgh.12019

Rolan, P., Gibbons, J. A., He, L., Chang, E., Jones, D., Gross, M. I., et al. (2008). Ibudilast in healthy volunteers: safety, tolerability and pharmacokinetics with single and multiple doses. *Br. J. Clin. Pharmacol.* 66, 792–801. doi:10.1111/j.1365-2125.2008.03270.x

Ruiz-Perez, D., Benito, J., Polo, G., Largo, C., Aguado, D., Sanz, L., et al. (2016). The effects of the toll-like receptor 4 antagonist, ibudilast, on sevoflurane's minimum alveolar concentration and the delayed remifentanil-induced increase in the minimum alveolar concentration in rats. *Anesth. Analg.* 122, 1370–1376. doi:10.1213/ANE.0000000000001171

Sesack, S. R., and Grace, A. A. (2010). Cortico-Basal Ganglia reward network: microcircuitry. *Neuropsychopharmacology* 35, 27–47. doi:10.1038/npp.2009.93

Sfondrini, L., Rossini, A., Besusso, D., Merlo, A., Tagliabue, E., Menard, S., et al. (2006). Antitumor activity of the TLR-5 ligand flagellin in mouse models of cancer. *J. Immunol.* 176, 6624–6630. doi:10.4049/jimmunol.176.11.6624

Shah, M., Anwar, M. A., Yesudhas, D., Krishnan, J., and Choi, S. (2016). A structural insight into the negative effects of opioids in analgesia by modulating the TLR4 signaling: an in silico approach. *Sci. Rep.* 6, 39271. doi:10.1038/srep39271

Shah, M., and Choi, S. (2017). Toll-like receptor-dependent negative effects of opioids: a battle between analgesia and hyperalgesia. *Front. Immunol.* 8, 642. doi:10.3389/fimmu.2017.00642

Skolnick, P., Davis, H., Arnelle, D., and Deaver, D. (2014). Translational potential of naloxone and naltrexone as TLR4 antagonists. *Trends Pharmacol. Sci.* 35, 431–432. doi:10.1016/j.tips.2014.06.008

Song, C., Horrobin, D. F., and Leonard, B. E. (2006). The comparison of changes in behavior, neurochemistry, endocrine, and immune functions after different routes, doses and durations of administrations of IL-1beta in rats. *Pharmacopsychiatry* 39, 88–99. doi:10.1055/s-2006-941557

Spanagel, R., Montkowski, A., Allingham, K., Stohr, T., Shoaib, M., Holsboer, F., et al. (1995). Anxiety: a potential predictor of vulnerability to the initiation of ethanol self-administration in rats. *Psychopharmacology (Berl)* 122, 369–373. doi:10.1007/BF02246268

Stellwagen, D., Beattie, E. C., Seo, J. Y., and Malenka, R. C. (2005). Differential regulation of AMPA receptor and GABA receptor trafficking by tumor necrosis factor-alpha. *J. Neurosci.* 25, 3219–3228. doi:10.1523/JNEUROSCI.4486-04.2005

Stellwagen, D., and Malenka, R. C. (2006). Synaptic scaling mediated by glial TNF-alpha. *Nature* 440, 1054–1059. doi:10.1038/nature04671

Stevens, C. W., Aravind, S., Das, S., and Davis, R. L. (2013). Pharmacological characterization of LPS and opioid interactions at the toll-like receptor 4. *Br. J. Pharmacol.* 168, 1421–1429. doi:10.1111/bph.12028

Stopponi, S., De Guglielmo, G., Somaini, L., Cippitelli, A., Cannella, N., Kallupi, M., et al. (2013). Activation of PPARgamma by pioglitazone potentiates the effects of naltrexone on alcohol drinking and relapse in msP rats. *Alcohol Clin. Exp. Res.* 37, 1351–1360. doi:10.1111/acer.12091

Takeda, K., and Akira, S. (2004). TLR signaling pathways. *Semin. Immunol.* 16, 3–9.

Takeda, K., and Akira, S. (2005). Toll-like receptors in innate immunity. *Int. Immunol.* 17, 1–14. doi:10.1093/intimm/dxh186

Tanda, G., Mereu, M., Hiranita, T., Quarterman, J. C., Coggiano, M., and Katz, J. L. (2016). Lack of specific involvement of (+)-Naloxone and (+)-Naltrexone on the reinforcing and neurochemical effects of cocaine and opioids. *Neuropsychopharmacology* 41, 2772–2781. doi:10.1038/npp.2016.91

Tanibuchi, Y., Shimagami, M., Fukami, G., Sekine, Y., Iyo, M., and Hashimoto, K. (2010). A case of methamphetamine use disorder treated with the antibiotic drug minocycline. *Gen. Hosp. Psychiatry* 32, 559.e1-3. doi:10.1016/j.genhosppsych.2009.12.005

Theberge, F. R., Li, X., Kambhampati, S., Pickens, C. L., St Laurent, R., Bossert, J. M., et al. (2013). Effect of chronic delivery of the toll-like receptor 4 antagonist (+)-naltrexone on incubation of heroin craving. *Biol. Psychiatry* 73, 729–737. doi:10.1016/j.biopsych.2012.12.019

Valles, S. L., Blanco, A. M., Pascual, M., and Guerri, C. (2004). Chronic ethanol treatment enhances inflammatory mediators and cell death in the brain and in astrocytes. *Brain Pathol.* 14, 365–371. doi:10.1111/j.1750-3639.2004.tb00079.x

Vaure, C., and Liu, Y. (2014). A comparative review of toll-like receptor 4 expression and functionality in different animal species. *Front Immunol.* 5, 316. doi:10.3389/fimmu.2014.00316

Vetreno, R. P., and Crews, F. T. (2014). Current hypotheses on the mechanisms of alcoholism. *Handb. Clin. Neurol.* 125, 477–497. doi:10.1016/B978-0-444-62619-6.00027-6

Volkow, N. D., and Morales, M. (2015). The brain on drugs: from reward to addiction. *Cell* 162, 712–725. doi:10.1016/j.cell.2015.07.046

Wang, H. Y., and Burns, L. H. (2009). Naloxone's pentapeptide binding site on filamin A blocks Mu opioid receptor-Gs coupling and CREB activation of acute morphine. *PloS One* 4, e4282. doi:10.1371/journal.pone.0004282

Wang, Q., Zhou, H., Gao, H., Chen, S. H., Chu, C. H., Wilson, B., et al. (2012a). Naloxone inhibits immune cell function by suppressing superoxide production through a direct interaction with gp91phox subunit of NADPH oxidase. *J. Neuroinflammation* 9, 32. doi:10.1186/1742-2094-9-32

Wang, S., Cheng, Q., Malik, S., and Yang, J. (2000). Interleukin-1beta inhibits gamma-aminobutyric acid type A (GABA(A)) receptor current in cultured hippocampal neurons. *J. Pharmacol. Exp. Ther.* 292, 497–504.

Wang, X., Loram, L. C., Ramos, K., De Jesus, A. J., Thomas, J., Cheng, K., et al. (2012b). Morphine activates neuroinflammation in a manner parallel to endotoxin. *Proc. Natl. Acad. Sci. U. S. A.* 109, 6325–6330. doi:10.1073/pnas.1200130109

Wang, X., Northcutt, A. L., Cochran, T. A., Zhang, X., Fabisiak, T. J., Haas, M. E., et al. (2019). Methamphetamine activates toll-like receptor 4 to induce central immune signaling within the ventral tegmental area and contributes to extracellular dopamine increase in the nucleus accumbens shell. *ACS Chem. Neurosci.* 10, 3622–3634. doi:10.1021/acschemneuro.9b00225

Watkins, L. R., Wang, X., Mustafa, S., and Hutchinson, M. R. (2014). *In vivo* veritas: (+)-Naltrexone's actions define translational importance: a letter in response to Skolnick et al. 'Translational potential of naloxone and naltrexone as TLR4 antagonists.' *Trends Pharmacol. Sci.* 35, 432–433. doi:10.1016/j.tips.2014.07.002

Worley, M. J., Swanson, A. N., Heinzerling, K. G., Roche, D. J., and Shoptaw, S. (2016). Ibudilast attenuates subjective effects of methamphetamine in a placebo-controlled inpatient study. *Drug Alcohol Depend.* 162, 245–250. doi:10.1016/j.drugalcdep.2016.02.036

Wu, Y., Lousberg, E. L., Moldenhauer, L. M., Hayball, J. D., Coller, J. K., Rice, K. C., et al. (2012). Inhibiting the TLR4-MyD88 signalling cascade by genetic or pharmacological strategies reduces acute alcohol-induced sedation and motor impairment in mice. *Br. J. Pharmacol.* 165, 1319–1329. doi:10.1111/j.1476-5381.2011.01572.x

Yang, H., Hreggvidsdottir, H. S., Palmblad, K., Wang, H., Ochani, M., Li, J., et al. (2010). A critical cysteine is required for HMGB1 binding to toll-like receptor 4 and activation of macrophage cytokine release. *Proc. Natl. Acad. Sci. U. S. A.* 107, 11942–11947. doi:10.1073/pnas.1003893107

Yu, J. C., Khodadadi, H., Malik, A., Davidson, B., Salles, E., Bhatia, J., et al. (2018). Innate immunity of neonates and infants. *Front. Immunol.* 9, 1759. doi:10.3389/fimmu.2018.01759

Yue, K., Tanda, G., Katz, J. L., and Zanettini, C. (2020). A further assessment of a role for toll-like receptor 4 in the reinforcing and reinstating effects of opioids. *Behav. Pharmacol.* 31, 186–195. doi:10.1097/FBP.0000000000000474

Zhang, H., Largent-Milnes, T. M., and Vanderah, T. W. (2020). Glial neuroimmune signaling in opioid reward. *Brain Res. Bull.* 155, 102–111. doi:10.1016/j.brainresbull.2019.11.012

Zhang, S., Hu, S., Sinha, R., Potenza, M. N., Malison, R. T., and Li, C. S. (2016). Cocaine dependence and thalamic functional connectivity: a multivariate pattern analysis. *Neuroimage Clin.* 12, 348–358. doi:10.1016/j.nicl.2016.08.006

Conflict of Interest: The authors declare that the research was conducted in the absence of any commercial or financial relationships that could be construed as a potential conflict of interest.

frontiers in Neuroscience

ORIGINAL RESEARCH
published: 27 November 2020
doi: 10.3389/fnins.2020.608349

Identification and Characterization of Biomarkers and Their Role in Opioid Addiction by Integrated Bioinformatics Analysis

*Xiuning Zhang[1,2,3], Hailei Yu[1,2], Rui Bai[1,2] and Chunling Ma[1,2]**

[1] *Hebei Key Laboratory of Forensic Medicine, Collaborative Innovation Center of Forensic Medical Molecular Identification, College of Forensic Medicine, Hebei Medical University, Shijiazhuang, China,* [2] *Research Unit of Digestive Tract Microecosystem Pharmacology and Toxicology, Chinese Academy of Medical Sciences, Shijiazhuang, China,* [3] *Department of Anesthesiology, The Third Hospital of Hebei Medical University, Shijiazhuang, China*

Although numerous studies have confirmed that the mechanisms of opiate addiction include genetic and epigenetic aspects, the results of such studies are inconsistent. Here, we downloaded gene expression profiling information, GSE87823, from the Gene Expression Omnibus database. Samples from males between ages 19 and 35 were selected for analysis of differentially expressed genes (DEGs). Kyoto Encyclopedia of Genes and Genomes (KEGG) pathway and Gene Ontology (GO) enrichment analyses were used to analyze the pathways associated with the DEGs. We further constructed protein-protein interaction (PPI) networks using the STRING database and used 10 different calculation methods to validate the hub genes. Finally, we utilized the Basic Local Alignment Search Tool (BLAST) to identify the DEG with the highest sequence similarity in mouse and detected the change in expression of the hub genes in this animal model using RT-qPCR. We identified three key genes, *ADCY9*, *PECAM1*, and *IL4*. *ADCY9* expression decreased in the nucleus accumbens of opioid-addicted mice compared with control mice, which was consistent with the change seen in humans. The importance and originality of this study are provided by two aspects. Firstly, we used a variety of calculation methods to obtain hub genes; secondly, we exploited homology analysis to solve the difficult challenge that addiction-related experiments cannot be carried out in patients or healthy individuals. In short, this study not only explores potential biomarkers and therapeutic targets of opioid addiction but also provides new ideas for subsequent research on opioid addiction.

Keywords: opioid addiction, biomarker, nucleus accumbens, ADCY9, conditioned place preference

OPEN ACCESS

Edited by:
Qi Wang,
Southern Medical University, China

Reviewed by:
Feng Chen,
Augusta University, United States
Chunxia Yan,
Xi'an Jiaotong University, China
Rui Zhao,
China Medical University, China

***Correspondence:**
Chunling Ma
chunlingma@126.com

Specialty section:
This article was submitted to Neuropharmacology, a section of the journal Frontiers in Neuroscience

Received: *20 September 2020*
Accepted: *04 November 2020*
Published: *27 November 2020*

Citation:
Zhang X, Yu H, Bai R and Ma C (2020) Identification and Characterization of Biomarkers and Their Role in Opioid Addiction by Integrated Bioinformatics Analysis. Front. Neurosci. 14:608349. doi: 10.3389/fnins.2020.608349

INTRODUCTION

Opioid abuse is currently a severe global epidemic problem for public health (Rudd et al., 2016; Roxburgh et al., 2017). In 2015, data from the WHO database revealed 450,000 deaths due to drug misuse globally. Among these deaths, 168,000 were due to opioid overdose. Indeed, from 2000 to 2015, the mortality rates related to opioid overdose increased by 500%. Opioid overdose-related deaths increased by 11% between 2014 and 2015 alone (Frauger et al., 2017;

Schifano et al., 2019), posing massive public health costs. It is therefore urgent to explore the mechanism of opioid addiction.

The impact of opioid abuse on the human body is a continuous process. Drug addiction has been recognized as a chronic relapsing disease of the brain, as drug abuse-induced addiction has a significant impact on the central nervous system. Constant exposure of the human brain to opioids results in changes at the epigenetic, mRNA, neuropeptide, and protein levels (Kendler et al., 2003; Agrawal and Lynskey, 2008; Nelson et al., 2013). Furthermore, these factors can affect the next generation through maternal drug abuse during pregnancy (Desai et al., 2015). Although there is no specific gene that can be used as a biomarker for an opioid use disorder, most current studies suggest that opioid-induced gene changes play roles at many different levels, directly affecting reward effects or drug metabolic pathways or by affecting the body's negative emotions. For example, OPRM1, an essential nucleus in opioid addiction, can trigger opioid addiction by participating in the orchestration of rewarding effects and the desire to avoid withdrawal symptoms (Hearing et al., 2018). The core and shell of the Nucleus accumbens (NAc), respectively, create complex neuroprotection loops by communicating with brain regions such as the prefrontal cortex, hippocampus, and thalamus. A large number of studies have proved that NAc is closely related to drug-induced reward, psychological craving, reinforcement, and other effects (Cooper et al., 2017; De Jong et al., 2019). Therefore, based on the morphine-related conditioned reward memory animal model, this study took the NAc brain region as the research object, focusing on the regulation mechanism of the changes in the expression level of related genes during the formation of morphine addiction.

There are many risk factors for genetic and epigenetic changes leading to the formation of opioid addiction, including gender and age (Gwira Baumblatt et al., 2014; Kolodny et al., 2015; Chartoff and Mchugh, 2016; Webster, 2017; Blanco and Volkow, 2019). Although addiction can start at any age, adolescents and young people in their developmental stages are more likely to try new things, which is one of the reasons why young people, especially men, account for the majority of drug addicts (Santiago Rivera et al., 2018). Few studies have focused on a specific age-group or a single-sex group. Therefore, we hope that re-screening addiction-related factors identified in relevant studies from the existing community according to age and gender stratification will reveal new insights. To identify transcriptome changes caused by opioid addiction in the young male population and to determine the mechanism of opioid addiction, we analyzed their transcriptomes.

Up until now, most studies at the animal level have been aimed at a specific age group or a single-sex animal group. Due to ethical issues and the limitation of population differences, it is challenging to study the mechanisms of drug-use disorders in humans. Whether the results of animal studies can be applied to humans is also a key question worth considering. If the target molecules identified in animal studies are also highly conserved in humans, then we will be more confident that the results obtained from animals can more likely be applied to human diseases.

Therefore, this study not only analyzed highly correlated transcriptome changes in the young male population but also established an opioid addiction model at the animal level through homology analysis to validate these changes, providing a new way of studying the mechanism of differentially expressed genes (DEGs) in opioid addiction. Strategies that target specific genetic and epigenetic factors and novel non-opioid medications hold promise as future therapeutic interventions of opioid abuse. We hope that successfully increasing treatment options in the clinical toolbox will help break the historical pattern of recurring opioid epidemics.

MATERIALS AND METHODS

Microarray Data and Groups

The gene expression profiling information GSE87823 was collected from the Gene Expression Omnibus (GEO)[1] database. Samples derived from 22 heroin addicts and five control subjects were examined in this array (Platform: GPL96). There were two additional conditions for enrollment: male; 15–35 years old.

Data Retrieval and Preparation

The GEO2R tool[2] was used to identify DEGs online. The GEOquery and Limma packages of the R language were used to control the high-latitude characteristics of the datasets according to the false positive rate control method proposed by Benjamini and Hochberg. For this process, raw datasets were filtered to meet the cut-off criteria of $|\ FC|\ > 2$ and $p < 0.01$. Altered genes were analyzed using the heat map tool utilizing the online platform OmicShare[3].

Processing of DEGs on the KEGG Pathway and GO Platforms

Functional analyses of specific genes are often performed using the Database for Annotation, Visualization, and Integrated Discovery (DAVID)[4]. The DAVID platform was therefore exploited to perform Gene Ontology (GO) analysis and KEGG pathway enrichment analyses; $p < 0.05$ represented statistical significance. These analyses revealed downregulated and upregulated genes.

Design of a Protein-Protein Interaction Network (PPI) and Performance of Module Analyses for DEGs

Understanding the molecular and metabolic mechanisms of addiction development requires knowledge regarding the functional interactions among proteins involved in such processes. The Search Tool for the Retrieval of Interacting Genes (STRING)[5] is an essential platform used to investigate the

[1]https://www.ncbi.nlm.nih.gov/geo/

[2]https://www.ncbi.nlm.nih.gov/geo/geo2r/

[3]http://www.omicshare.com/tools

[4]https://david.ncifcrf.gov/

[5]https://string-db.org/

interaction among known and unknown (predicted) proteins of multiple organisms. In this study, DEGs were analyzed using this software and a PPI network was constructed to visualize the results. An interaction score of 0.4 was set as the threshold. Finally, the top 30 hub genes in the PPI network were identified using 10 different calculation methods in the Cytoscape software (Cytoscape_v3.7.1). Genes that overlapped in the calculations using all 10 algorithms were considered for downstream analysis.

Sequence Similarity Analysis of Key Genes Among Different Species

Sequence similarity analysis was carried out with the Basic Local Alignment Search Tool (BLAST)[6], searching the nucleotide collection (nr/nt) in the database using Megablast (optimized for highly similar sequences). Key genes with percentage identity (Per. Ident) $>$ 85% and query cover $=$ 100% were selected for detecting their expression changes in the NAc of opioid-addicted mice.

Morphine-Induced Conditioned Place Preference

The unbiased conditioned place preference (CPP) paradigm was conducted as reported in a previous study (Golden et al., 2016). Each mouse was handled for 15 min by the investigator before the start of CPP. The experimental apparatus was made of different floor textures (rough or smooth surface) and two conditioning chambers (20 $\times$ 20 $\times$ 40 cm each) with different stripes (horizontal or vertical), which provided two distinct conditioning environments. On day 1 (Pre-test), mice moved freely and explored the entire equipment for 15 min. During this time, the duration of time the mice spent in each conditioning chamber was recorded. Subsequently, the mice were assigned into groups of approximately equal initial bias for the drug-paired chambers based on the time spent in each chamber. The conditioning test covered the period from 2 to 7 days. For this experiment, mice of the control group were given saline (i.h.) in both chambers while mice in the morphine group were given saline in one chamber and morphine (10 mg/kg, i.h.) in the other for 45 min. Each session was performed 6 h after the previous one and was performed by the same experimenter. We used subcutaneous administration due to morphine intraperitoneal administration of morphine reduced the bioavailability compared to subcutaneous administration (Handal et al., 2002). At the end of the test on day 8, the mice were allowed to move freely in the chamber, and the duration spent in each chamber was recorded. Preference scores (sec) were determined as the difference in time spent in the drug-paired chamber (**Figure 6H**).

Measurement of *ADCY9* Expression Using RT-PCR

Harvested NAc tissues were treated with RNAiso Plus (TAKARA BIO INC) to isolate total RNA following the manufacturer's instructions. ABI Prism 7500 sequence detection system software was used for data analysis. mRNA levels of the *ADCY9* gene were normalized to those of *GAPDH*. 5′–3′ nucleotide sequences of primers are CCCTGCCCACCGTCCCTTC (ADCY9 Reverse) and CGAGCCTAAGACCAGCACCAAG (ADCY9 Forward). The GAPDH forward primer sequence was AGCTGAACGGGAAGCTCACT, while the reverse primer sequence was CAACGTAGGTCCACCACTGACACGTTG.

Data Analysis

All data are shown as means $\pm$ SEM. The *t*-test was used to compare qPCR results between morphine-treated mice and control mice for data with normally distributed data. $p < 0.05$ was considered to be significant. All statistical analyses were performed using SPSS.

RESULTS

Identification of DEGs

The research flow chart is illustrated in **Figure 1**. The age difference between the two groups was not statistically significant (**Supplementary Table 6**, $F = 0.067$, $p = 0.799$). We identified 289 DEGs in the nucleus accumbens (NAc) of heroin addicts compared with normal control NAc, including 166 downregulated and 123 upregulated DEGs (**Figure 2**).

GO and KEGG Pathway Analysis

To reveal the roles of the DEGs, GO function enrichment was analyzed using the DAVID database. The top 10 cellular component, biological process, and molecular function (CC, BP, and MF) terms are shown in **Supplementary Table S1** and **Figure 3A**. In the BP group, the upregulated DEGs were associated with phagosome acidification and maturation, cellular response to organonitrogen and nitrogen compounds, and transferrin transport. The downregulated DEGs were enriched in smooth muscle cell chemotaxis positive and negative regulation, fibroblast growth factor production, and regulation (**Figure 3B**). In the CC group, the upregulated DEGs were enriched in the terms vacuolar proton-transporting V-type ATPase complex, and cytoplasm, and the downregulated DEGs were enriched in the terms phagocytic cup and intracellular organelle (**Figure 3C**). Moreover, in the MF group, the upregulated DEGs were enriched in ATPase activity and the downregulated DEGs were enriched in actin filament and chemokine binding (**Figure 3D**). Pathway analysis revealed that upregulated DEGs were enriched in morphine addiction, nicotine addiction, endocannabinoid signaling, and GABAergic synapse pathways (**Figure 4A**) and downregulated DEGs were enriched in protein absorption and digestion, cell cycle, and cytokine-cytokine receptor interaction Alzheimer disease pathways (**Figure 4B**). Details are shown in **Supplementary Table S2**.

PPI Network Analysis and Screening for Hub Genes

Network analysis using Cytoscape software and the STRING database yielded 156 nodes, among which 90 represented DEGs

[6]https://blast.ncbi.nlm.nih.gov/Blast.cgi

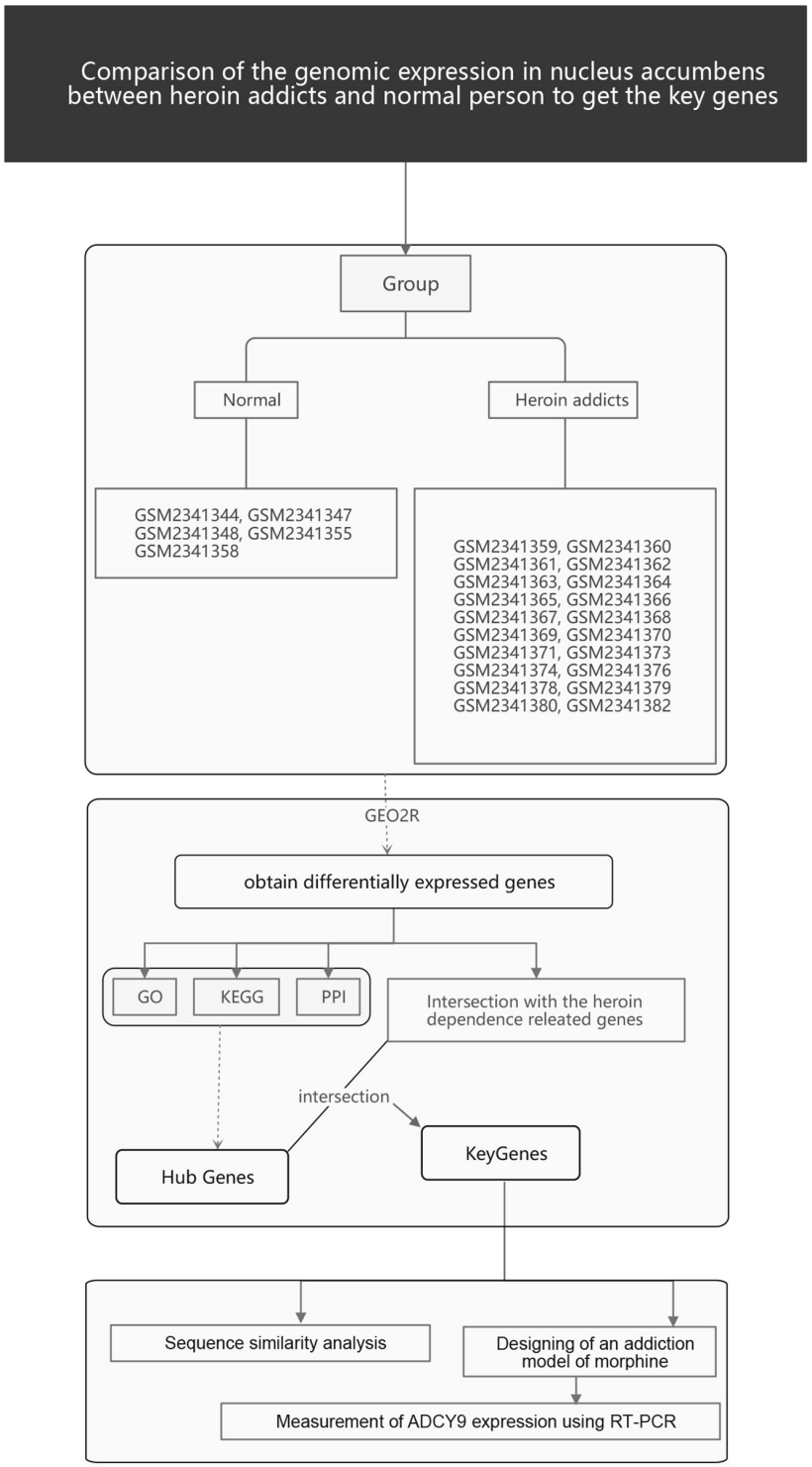

FIGURE 1 | The flowchart of the bioinformatics analysis.

downregulated and 66 represented DEGs upregulated in heroin addicts compared with control individuals (**Figure 5A**). Using the plug-in CytoHubba in Cytoscape software, we determined scores based on 10 methods to screen for hub genes in the PPI network (**Supplementary Table S3**). We looked at the top 30 genes overlapping in each calculation and determined six key genes: *ADCY9*, *IL4*, *PECAM1*, *PRKAR2B*, *BUB1*, and *NDE1* (**Figures 5B,C** and **Supplementary Table S4**).

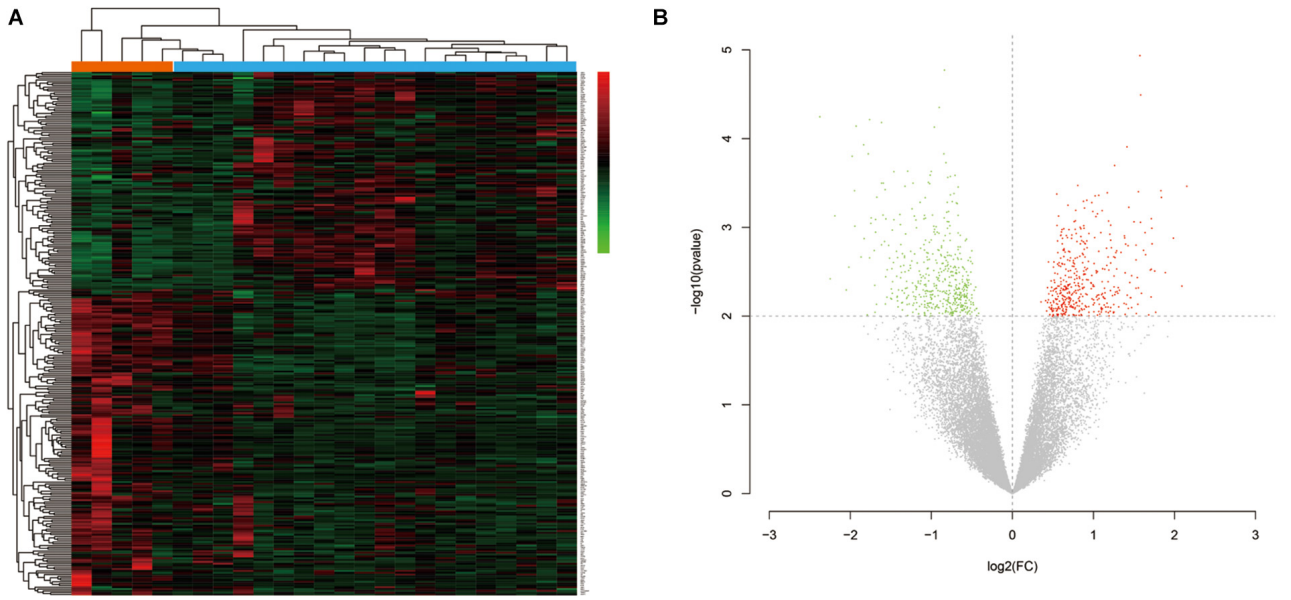

FIGURE 2 | (A) Hierarchical-clustering heat map of the 269 differentially expressed genes. Red indicates upregulation, and green indicates downregulation. **(B)** Volcano plot of the identified differentially expressed genes (DEGs) distribution in GSE87823. Red indicates DEGS with $\log_2FC \geq 2$, and green indicates DEGs with $\log_2FC \leq -2$.

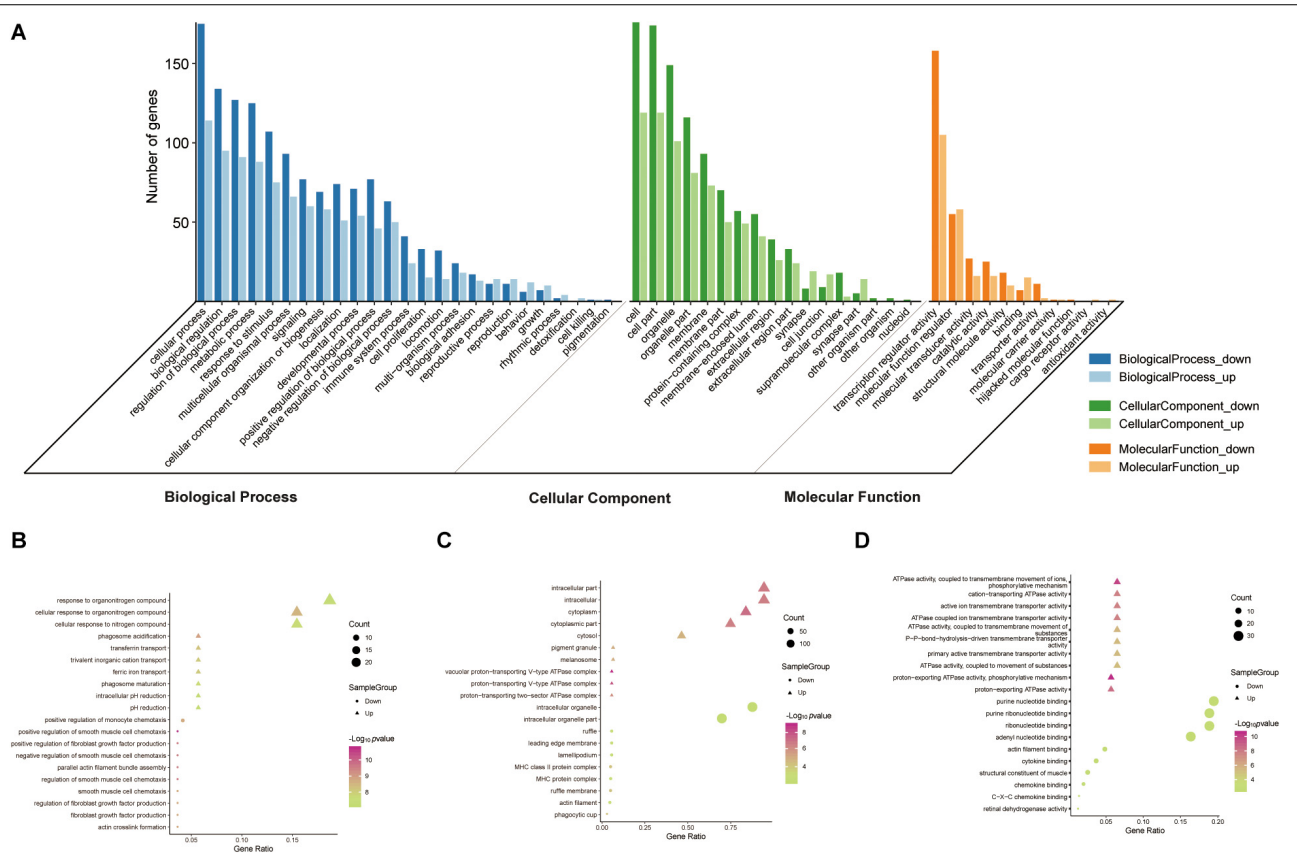

FIGURE 3 | GO functional enrichment analysis of up- and downregulated DEGs. The genes were ordered according to their logFC values setting gene **(A)**. The top 10 terms of BP **(B)**, CC **(C)**, MF **(D)** by *p*-value. The gradual color represents the z-score.

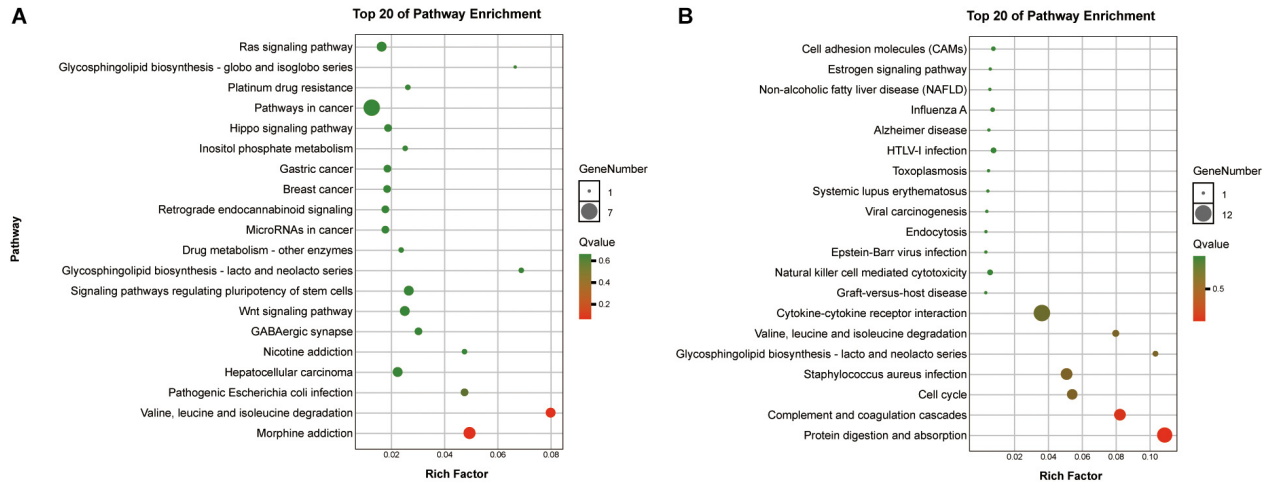

FIGURE 4 | KEGG enrichment analysis of the top 20 up-DEGs **(A)** and down-DEGs **(B)** pathways: the gradual color represents the *p*-value, the size of the spots represents the gene numbers.

Validation of Key Genes in NAc of Morphine-Addicted Mice

We determined integrated gene-disease, chemical-disease, and chemical-gene interactions using the comparative toxicogenomics database[7] to predict novel associations and create expanded networks (Davis et al., 2017). Using these data, we analyzed the relationships between DEGs and opioid addiction-related diseases. Our DEGs included one confirmed opioid addiction gene marker, *GABRA2* (**Figure 6A**), as well as the genes *ADCY9*, *IL4*, and *PECAM1*, which we determined to be "key genes" (**Figure 6B**). We used BLAST to calculate the sequence similarity of six key genes between human and mouse (**Figures 6D,F**) or human and other organisms (**Figures 6C,E,G**). The plots are shown in **Figures 6C–F** were created using Circoletto (Darzentas, 2010). Among these key genes, the human *ADCY9* sequence and the mouse *ADCY9* sequence had the highest similarity (**Figure 6D**).

To examine whether the expression of *ADCY9* would correlate with morphine addiction in mice, we conducted morphine-induced CPP, a wildly used morphine addiction model. Mice developed a significant place preference after morphine injection and these mice spent more time in the chamber where they were administered compared to mice that received saline after the conditioning phase. By contrast, the saline injection did not induce this effect (**Figure 6I**). Morphine also increased *ADCY9* mRNA expression in the mouse NAc, which was consistent with our previous results in human NAc (**Figure 6J**).

DISCUSSION

The pathogenesis of opioid abuse, a complex and chronic relapsing disease of the brain, remains unclear. Although numerous studies have confirmed that the mechanisms of opiate addiction include genetic and epigenetic aspects, the results of such studies are inconsistent (Skupio et al., 2017; Zhang et al., 2018). To our knowledge, our work is the first to use 10 different calculation methods, compared with the typical three methods, to calculate the association score among the DEGs for exploring novel hub genes. A recent study, GSE87823, detected the expression of genes in heroin abusers and healthy subjects. To minimize variability, we only enrolled samples from this dataset corresponding to males between the ages of 19 and 35 years, and genes exhibiting significant differential expression were identified using a variety of calculation methods. Our study provides evidence for the association of *ADCY9*, *PECAM1*, and *IL4* with heroin addiction through stringent bioinformatics analysis. The data presented here extend the previously reported association of *ADCY9*, *PECAM1*, and *IL4* with nicotine or alcohol addiction and psychiatric disorders. It is well known that the pharmacodynamically active metabolites of heroin include morphine, 6-diacetylmorphine, morphine 3-glucuronide, and morphine 6-glucuronide (Rook et al., 2006). In one study, five opioids were injected into heroin abusers, and morphine was found to make them feel as though they had received heroin (Comer et al., 2008). Moreover, there is some direct evidence that there are genes related to both heroin dependence and morphine dependence, such as *OPRM1* (Davis et al., 2019). Thus, we validated the transcriptional changes of *ADCY9* in a morphine addiction model in mice and found that these were consistent with those in humans. This study also provides evidence for the suitability of animal-level research in this regard, bypassing the difficulties in establishing human addiction models.

Our gene expression profiling identified pathways and key genes related to opioid addiction, which may potentially be therapeutic targets. Increased expression of *ADCY9* transcription is not only involved in the formation of a psycho-stimulant habit (Sokolov et al., 2003) but also found in the frontal pole brain of D2 mice after ethanol exposure (O'brien et al., 2018). A neuron

[7]http://ctdbase.org/

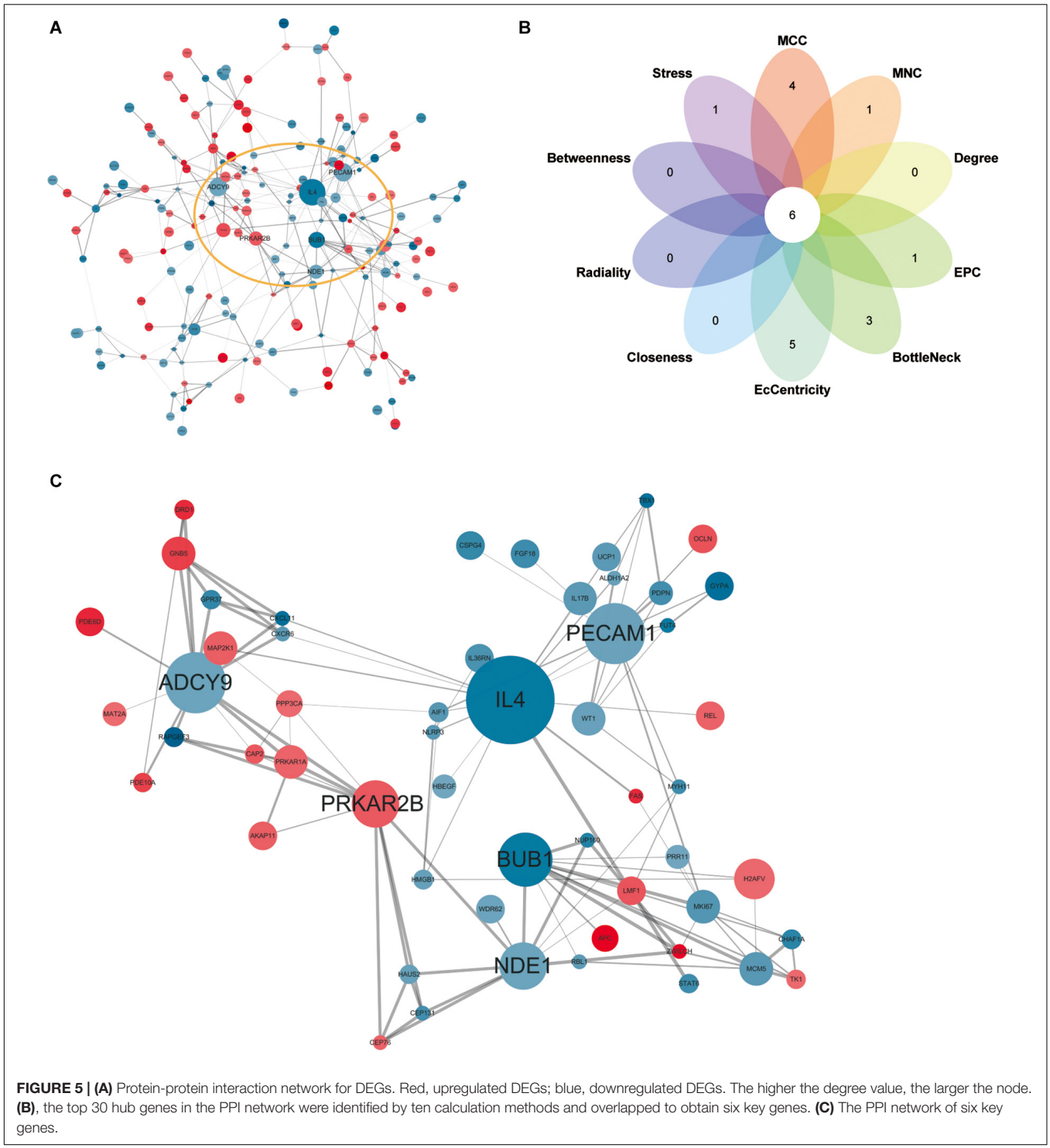

FIGURE 5 | (A) Protein-protein interaction network for DEGs. Red, upregulated DEGs; blue, downregulated DEGs. The higher the degree value, the larger the node. **(B)**, the top 30 hub genes in the PPI network were identified by ten calculation methods and overlapped to obtain six key genes. **(C)** The PPI network of six key genes.

is a special polarized cell type containing several synapses that respond to various stimuli (Wallace et al., 1998; Guzowski et al., 2001; Jones et al., 2001). The translation and transport of specific mRNA species regulate activity-dependent synaptic plasticity by modulating proteins that fine-tune neuronal responses to particular stimuli (Sutton and Schuman, 2006; Hoogenraad et al., 2007; Huang et al., 2017). We speculate that chronic opioid exposure causes changes in the synaptic plasticity of neurons by changing the transcription level of *ADCY9* in the NAc, thereby causing behavioral sensitization, which affects addictive behaviors. Opioid exposure also results in prolonged activation of N-methyl-D-aspartate (NMDA) receptors. NMDA inhibitor is linked to enhanced neuronal apoptosis in the developing rodent brain, and ADCY9 is involved in neuronal apoptosis

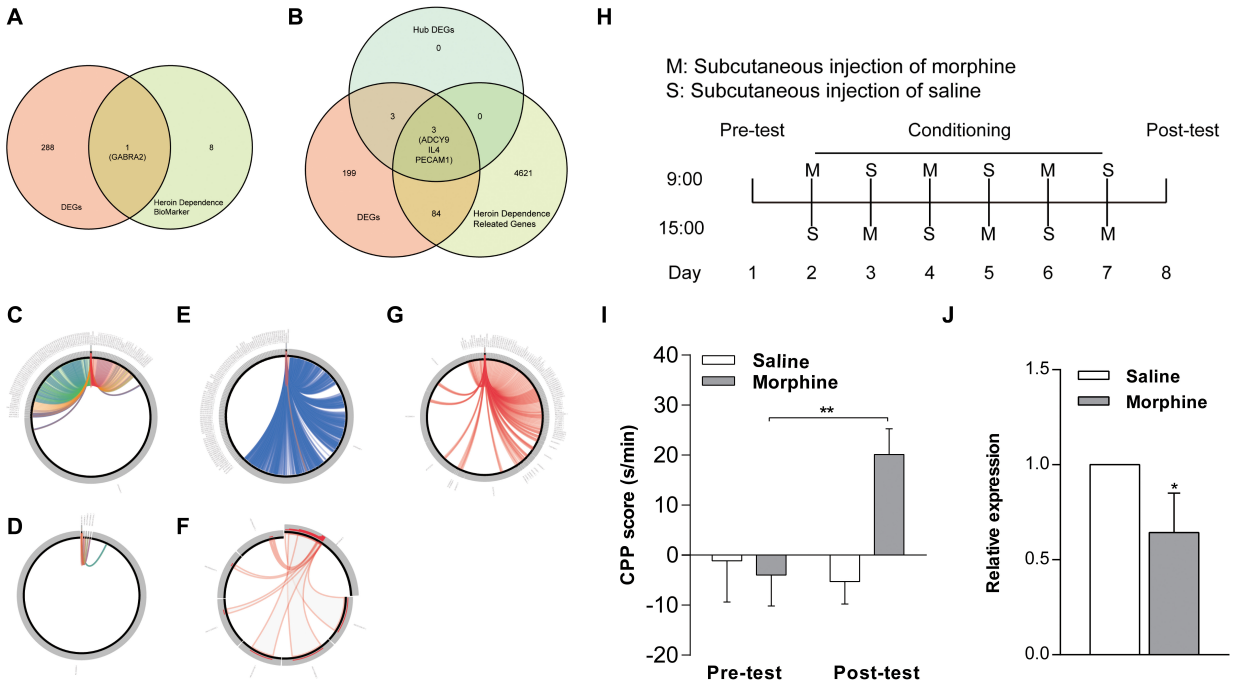

FIGURE 6 | Validation of key genes in NAc of morphine-addicted mice. We found our DEGs by including one confirmed opioid addiction gene marker, GABRA2 **(A)**, and the results also included the genes ADCY9, IL4, and PECAM1, which we determined to be "key genes" **(B)**. We used BLAST to calculate the sequence similarity of 6 key genes between human and mouse **(D,F)** or human and other biological sequences **(C,E,G)**. **(H)** The timeline about the establishment of morphine addicted mice. **(I)** CPP induced by 10 mg/kg of morphine. The CPP score of **(J)**, mRNA levels of the ADCY9 gene in morphine addicted mouse's NAc. $^{*}p < 0.05$, $^{**}p < 0.01$ significant difference.

induced by NMDA receptor blockade in neonatal rats (Sutton and Schuman, 2006; Hoogenraad et al., 2007; Huang et al., 2017). Of particular interest, immunoblotting data reveals a marked increase in GluN1 and GluN2B expression in three regions (medial prefrontal cortex mPFC, Lateral prefrontal cortex LPFC, and orbitofrontal cortex OFC) in men suffering from opioid addiction (Daneshparvar et al., 2019), suggesting that ADCY9 may also be involved in changes to NMDA receptors in opioid addiction. These changes may lead to behavioral sensitization and the formation of addictive memory. Due to ethical limitations, we cannot establish an opioid addiction model in humans to study the mechanism of ADCY9. However, we found that the similarity of the *ADCY9* gene sequence between mice and humans was more than 80%. By establishing a morphine addiction model in mice and detecting the expression level of *ADCY9* in the NAc, we found that the expression of *ADCY9* decreased. The expression of *ADCY9* in human opioid addiction showed the same trend. Therefore, we have reason to believe that it is beneficial to study the mechanism of ADCY9 in an opioid addiction mouse model.

IL4, an inflammatory factor, and PECAM1, platelet/endothelial cell adhesion molecule 1, both participate in the inflammatory reaction process of the body. Chronic morphine treatment induces an increase of IL4 in spleen cells (Greeneltch et al., 2005), and serum IL4 levels are also elevated in heroin and cocaine addicts (Ríos-Olivares et al., 2006). We know that the damage caused by opioid addiction is mostly related to the immune response, and previous studies have confirmed that an increase of PECAM1 in the blood-brain barrier of cocaine-addicted rats causes an immune response in endothelial cells, immune cells, and neuroendocrine cells, thus impairing the function of the blood-brain barrier (Fiala et al., 1998). In mice, IL4 and PECAM1 also cause neuroinflammation by recruiting mast cells and upregulating the release of various mediators, which may be involved in the formation of Parkinson's disease (Hong et al., 2018). In addition, changes in serum PECAM1 levels contribute to the occurrence and development of autism and depression (Serebruany et al., 2005; Tsuchiya et al., 2007). IL4 and PECAM1 might serve as the molecular and cellular basis of neurological damage by opioid addiction.

In summary, investigating the specific genes regulating the development of opioid addiction is an essential component of early treatment of the disease. We provide evidence that ADCY9 may lead to behavioral sensitization and addictive memory formation by altering the synaptic plasticity of NAc neurons, while IL4 and PEAM1 may participate in neuroinflammation caused by opioid addiction through immune responses. To apply our research results to clinical treatment, we need further research to verify this mechanism. We will focus on validating the usefulness of these DEGs as diagnostic and/or prognostic markers in a subsequent study. Our research expands our understanding of the mechanism of opioid addiction and proposes possible targets for addressing the symptoms of opioid addiction. These results lay the foundation for further development of treatments and related research.

DATA AVAILABILITY STATEMENT

The datasets presented in this study can be found in online repositories. The names of the repository/repositories and accession number(s) can be found below: https://www.ncbi.nlm.nih.gov/geo/, GSE87823.

ETHICS STATEMENT

The animal study was reviewed and approved by the Animal Care and Use Committee of Hebei medical University.

AUTHOR CONTRIBUTIONS

XZ conceived, designed, performed the experiments, analyzed the data, and wrote the manuscript. HY and RB performed the experiments and analyzed the data. CM conceived, designed and revised the manuscript. All authors contributed to the article and approved the submitted version.

FUNDING

This study was supported by the National Natural Science Foundation of China (No. 81871524 and 81971785), the Natural Science Foundation of Hebei Province (No. H2018206166).

SUPPLEMENTARY MATERIAL

The Supplementary Material for this article can be found online at: https://www.frontiersin.org/articles/10.3389/fnins.2020.608349/full#supplementary-material

Supplementary Table 1 | GO terms enrichment for DEGs.

Supplementary Table 2 | KEGG pathway analysis data of DEGs.

Supplementary Tables 3 and 4 | 10 methods to screen for hub genes.

Supplementary Table 5 | Results of the 269 differentially expressed genes, and marked the key genes in the file with red font.

Supplementary Table 6 | The demographic information of the normal people and addicts.

REFERENCES

Agrawal, A., and Lynskey, M. T. (2008). Are there genetic influences on addiction: evidence from family, adoption and twin studies. *Addiction* 103, 1069–1081. doi: 10.1111/j.1360-0443.2008.02213.x

Blanco, C., and Volkow, N. D. (2019). Management of opioid use disorder in the USA: present status and future directions. *Lancet* 393, 1760–1772. doi: 10.1016/s0140-6736(18)33078-2

Chartoff, E. H., and Mchugh, R. K. (2016). Translational studies of sex differences in sensitivity to opioid addiction. *Neuropsychopharmacology* 41, 383–384. doi: 10.1038/npp.2015.272

Comer, S. D., Sullivan, M. A., Whittington, R. A., Vosburg, S. K., and Kowalczyk, W. J. (2008). Abuse liability of prescription opioids compared to heroin in morphine-maintained heroin abusers. *Neuropsychopharmacology* 33, 1179–1191. doi: 10.1038/sj.npp.1301479

Cooper, S., Robison, A. J., and Mazei-Robison, M. S. (2017). Reward circuitry in addiction. *Neurotherapeutics* 14, 687–697. doi: 10.1007/s13311-017-0525-z

Daneshparvar, H., Sadat-Shirazi, M. S., Fekri, M., Khalifeh, S., Ziaie, A., Esfahanizadeh, N., et al. (2019). NMDA receptor subunits change in the prefrontal cortex of pure-opioid and multi-drug abusers: a post-mortem study. *Eur. Arch. Psychiatry Clin. Neurosci.* 269, 309–315. doi: 10.1007/s00406-018-0900-8

Darzentas, N. (2010). Circoletto: visualizing sequence similarity with Circos. *Bioinformatics* 26, 2620–2621. doi: 10.1093/bioinformatics/btq484

Davis, A. P., Grondin, C. J., Johnson, R. J., Sciaky, D., King, B. L., Mcmorran, R., et al. (2017). The comparative toxicogenomics database: update 2017. *Nucleic Acids Res.* 45, D972–D978. doi: 10.1093/nar/gkw838

Davis, A. P., Grondin, C. J., Johnson, R. J., Sciaky, D., Mcmorran, R., Wiegers, J., et al. (2019). The comparative toxicogenomics database: update 2019. *Nucleic Acids Res.* 47, D948–D954. doi: 10.1093/nar/gky868

De Jong, J. W., Afjei, S. A., Pollak Dorocic, I., Peck, J. R., Liu, C., Kim, C. K., et al. (2019). A neural circuit mechanism for encoding aversive stimuli in the mesolimbic dopamine system. *Neuron* 101, 133.e7–151.e7. doi: 10.1016/j.neuron.2018.11.005

Desai, R. J., Huybrechts, K. F., Hernandez-Diaz, S., Mogun, H., Patorno, E., Kaltenbach, K., et al. (2015). Exposure to prescription opioid analgesics in utero and risk of neonatal abstinence syndrome: population based cohort study. *BMJ* 350:h2102. doi: 10.1136/bmj.h2102

Fiala, M., Gan, X. H., Zhang, L., House, S. D., Newton, T., Graves, M. C., et al. (1998). Cocaine enhances monocyte migration across the blood-brain barrier. Cocaine's connection to AIDS dementia and vasculitis? *Adv. Exp. Med. Biol.* 437, 199–205. doi: 10.1007/978-1-4615-5347-2_22

Frauger, E., Pochard, L., Boucherie, Q., Giocanti, A., Chevallier, C., Daveluy, A., et al. (2017). [Surveillance system on drug abuse: interest of the French national OPPIDUM program of French addictovigilance network]. *Therapie* 72, 491–501. doi: 10.1016/j.therap.2017.01.010

Golden, S. A., Heshmati, M., Flanigan, M., Christoffel, D. J., Guise, K., Pfau, M. L., et al. (2016). Basal forebrain projections to the lateral habenula modulate aggression reward. *Nature* 534, 688–692. doi: 10.1038/nature18601

Greeneltch, K. M., Kelly-Welch, A. E., Shi, Y., and Keegan, A. D. (2005). Chronic morphine treatment promotes specific Th2 cytokine production by murine T cells in vitro via a Fas/Fas ligand-dependent mechanism. *J. Immunol.* 175, 4999–5005. doi: 10.4049/jimmunol.175.8.4999

Guzowski, J. F., Setlow, B., Wagner, E. K., and Mcgaugh, J. L. (2001). Experience-dependent gene expression in the rat hippocampus after spatial learning: a comparison of the immediate-early genes Arc, c-fos, and zif268. *J. Neurosci.* 21, 5089–5098. doi: 10.1523/jneurosci.21-14-05089.2001

Gwira Baumblatt, J. A., Wiedeman, C., Dunn, J. R., Schaffner, W., Paulozzi, L. J., and Jones, T. F. (2014). High-risk use by patients prescribed opioids for pain and its role in overdose deaths. *JAMA Intern. Med.* 174, 796–801. doi: 10.1001/jamainternmed.2013.12711

Handal, M., Grung, M., Skurtveit, S., Ripel, A., and Morland, J. (2002). Pharmacokinetic differences of morphine and morphine-glucuronides are reflected in locomotor activity. *Pharmacol. Biochem. Behav.* 73, 883–892. doi: 10.1016/s0091-3057(02)00925-5

Hearing, M., Graziane, N., Dong, Y., and Thomas, M. J. (2018). Opioid and psychostimulant plasticity: targeting overlap in nucleus accumbens glutamate signaling. *Trends Pharmacol. Sci.* 39, 276–294. doi: 10.1016/j.tips.2017.12.004

Hong, G. U., Cho, J. W., Kim, S. Y., Shin, J. H., and Ro, J. Y. (2018). Inflammatory mediators resulting from transglutaminase 2 expressed in mast cells contribute to the development of Parkinson's disease in a mouse model. *Toxicol. Appl. Pharmacol.* 358, 10–22. doi: 10.1016/j.taap.2018.09.003

Hoogenraad, C. C., Feliu-Mojer, M. I., Spangler, S. A., Milstein, A. D., Dunah, A. W., Hung, A. Y., et al. (2007). Liprinalpha1 degradation by calcium/calmodulin-dependent protein kinase II regulates LAR receptor tyrosine phosphatase distribution and dendrite development. *Dev. Cell* 12, 587–602. doi: 10.1016/j.devcel.2007.02.006

Huang, H., Lin, X., Liang, Z., Zhao, T., Du, S., Loy, M. M. T., et al. (2017). Cdk5-dependent phosphorylation of liprinalpha1 mediates neuronal activity-dependent synapse development. *Proc. Natl. Acad. Sci. U.S.A.* 114, E6992–E7001. doi: 10.1073/pnas.1708240114

Jones, M. W., Errington, M. L., French, P. J., Fine, A., Bliss, T. V., Garel, S., et al. (2001). A requirement for the immediate early gene Zif268 in the expression of late LTP and long-term memories. *Nat. Neurosci.* 4, 289–296. doi: 10.1038/85138

Kendler, K. S., Jacobson, K. C., Prescott, C. A., and Neale, M. C. (2003). Specificity of genetic and environmental risk factors for use and abuse/dependence of cannabis, cocaine, hallucinogens, sedatives, stimulants, and opiates in male twins. *Am. J. Psychiatry* 160, 687–695. doi: 10.1176/appi.ajp.160.4.687

Kolodny, A., Courtwright, D. T., Hwang, C. S., Kreiner, P., Eadie, J. L., Clark, T. W., et al. (2015). The prescription opioid and heroin crisis: a public health approach to an epidemic of addiction. *Annu. Rev. Public Health* 36, 559–574. doi: 10.1146/annurev-publhealth-031914-122957

Nelson, E. C., Lynskey, M. T., Heath, A. C., Wray, N., Agrawal, A., Shand, F. L., et al. (2013). ANKK1, TTC12, and NCAM1 polymorphisms and heroin dependence: importance of considering drug exposure. *JAMA Psychiatry* 70, 325–333. doi: 10.1001/jamapsychiatry.2013.282

O'brien, M. A., Weston, R. M., Sheth, N. U., Bradley, S., Bigbee, J., Pandey, A., et al. (2018). Ethanol-induced behavioral sensitization alters the synaptic transcriptome and exon utilization in DBA/2J Mice. *Front. Genet.* 9:402. doi: 10.3389/fgene.2018.00402

Ríos-Olivares, E., Vilá, L. M., Reyes, J. C., Rodríguez, J. W., Colón, J. H., Pagán, N. O., et al. (2006). Impaired cytokine production and suppressed lymphocyte proliferation activity in HCV-infected cocaine and heroin ("speedball") users. *Drug Alcohol Depend.* 85, 236–243. doi: 10.1016/j.drugalcdep.2006.05.013

Rook, E. J., Huitema, A. D., Van Den Brink, W., Van Ree, J. M., and Beijnen, J. H. (2006). Population pharmacokinetics of heroin and its major metabolites. *Clin. Pharmacokinet.* 45, 401–417. doi: 10.2165/00003088-200645040-00005

Roxburgh, A., Hall, W. D., Dobbins, T., Gisev, N., Burns, L., Pearson, S., et al. (2017). Trends in heroin and pharmaceutical opioid overdose deaths in Australia. *Drug Alcohol. Depend.* 179, 291–298. doi: 10.1016/j.drugalcdep.2017.07.018

Rudd, R. A., Aleshire, N., Zibbell, J. E., and Gladden, R. M. (2016). Increases in drug and opioid overdose deaths–United States, 2000-2014. *MMWR Morb. Mortal. Wkly. Rep.* 64, 1378–1382. doi: 10.15585/mmwr.mm6450a3

Santiago Rivera, O. J., Havens, J. R., Parker, M. A., and Anthony, J. C. (2018). Risk of heroin dependence in newly incident heroin users. *JAMA Psychiatry* 75, 863–864. doi: 10.1001/jamapsychiatry.2018.1214

Schifano, F., Chiappini, S., Corkery, J. M., and Guirguis, A. (2019). Assessing the 2004-2018 Fentanyl misusing issues reported to an international range of adverse reporting systems. *Front. Pharmacol.* 10:46. doi: 10.3389/fphar.2019.00046

Serebruany, V. L., Suckow, R. F., Cooper, T. B., O'connor, C. M., Malinin, A. I., Krishnan, K. R., et al. (2005). Relationship between release of platelet/endothelial biomarkers and plasma levels of sertraline and N-desmethylsertraline in acute coronary syndrome patients receiving SSRI treatment for depression. *Am. J. Psychiatry* 162, 1165–1170. doi: 10.1176/appi.ajp.162.6.1165

Skupio, U., Sikora, M., Korostynski, M., Wawrzczak-Bargiela, A., Piechota, M., Ficek, J., et al. (2017). Behavioral and transcriptional patterns of protracted opioid self-administration in mice. *Addict. Biol.* 22, 1802–1816. doi: 10.1111/adb.12449

Sokolov, B. P., Polesskaya, O. O., and Uhl, G. R. (2003). Mouse brain gene expression changes after acute and chronic amphetamine. *J. Neurochem.* 84, 244–252. doi: 10.1046/j.1471-4159.2003.01523.x

Sutton, M. A., and Schuman, E. M. (2006). Dendritic protein synthesis, synaptic plasticity, and memory. *Cell* 127, 49–58. doi: 10.1016/j.cell.2006.09.014

Tsuchiya, K. J., Hashimoto, K., Iwata, Y., Tsujii, M., Sekine, Y., Sugihara, G., et al. (2007). Decreased serum levels of platelet-endothelial adhesion molecule (PECAM-1) in subjects with high-functioning autism: a negative correlation with head circumference at birth. *Biol. Psychiatry* 62, 1056–1058. doi: 10.1016/j.biopsych.2006.12.018

Wallace, C. S., Lyford, G. L., Worley, P. F., and Steward, O. (1998). Differential intracellular sorting of immediate early gene mRNAs depends on signals in the mRNA sequence. *J. Neurosci.* 18, 26–35. doi: 10.1523/jneurosci.18-01-00026.1998

Webster, L. R. (2017). Risk factors for opioid-use disorder and overdose. *Anesth. Analg.* 125, 1741–1748. doi: 10.1213/ANE.0000000000002496

Zhang, Y., Liang, Y., Randesi, M., Yuferov, V., Zhao, C., and Kreek, M. J. (2018). Chronic oxycodone self-administration altered reward-related genes in the ventral and dorsal striatum of C57BL/6J mice: an RNA-seq analysis. *Neuroscience* 393, 333–349. doi: 10.1016/j.neuroscience.2018.07.032

Conflict of Interest: The authors declare that the research was conducted in the absence of any commercial or financial relationships that could be construed as a potential conflict of interest.

frontiers in Neuroscience

ORIGINAL RESEARCH
published: 14 January 2021
doi: 10.3389/fnins.2020.630713

Methamphetamine Inhibits Long-Term Memory Acquisition and Synaptic Plasticity by Evoking Endoplasmic Reticulum Stress

Guang Chen[1], Xiaoning Wei[2], Xiang Xu[3], Gang Yu[4], Zheng Yong[4], Ruibin Su[4] and Luyang Tao[1]**

[1] Department of Forensic Medicine, Medical School of Soochow University, Suzhou, China, [2] Becton, Dickinson and Company, Guangzhou, China, [3] School of Forensic Medicine, Wannan Medical College, Wuhu, China, [4] State Key Laboratory of Toxicology and Medical Countermeasures, Beijing Institute of Pharmacology and Toxicology, Beijing, China

Methamphetamine (MA), an illicit drug abused worldwide, leads to cognitive impairment and memory loss. However, the detailed mechanisms of MA-induced neurologic impairment are still unclear. The present study aimed to investigate the mechanisms of MA-induced inhibition of memory acquisition from the perspective of endoplasmic reticulum (ER) stress. ER stress, caused by the accumulation of wrongly folded proteins in the ER, is important for new protein synthesis, which further influence the formation of long-term memory. A subacute MA poisoning model of mice was established and several behavioral experiments were performed, including elevated plus maze, Morris water maze, electro-stimulus Y-maze, and novel object recognition tasks. The present results suggested that 4 days exposure to MA induced significant memory loss. Whereas, this damage to memory formation could be protected when mice were pre-treated with ER stress inhibitor, tauroursodeoxycholic acid (TUDCA). The results of Western blotting showed that subacute exposure to MA increased the expression levels of ER stress marker proteins, such as binding immunoglobulin protein, phosphorylated eukaryotic translation initiation factor 2α, cyclic AMP-dependent transcription factor (ATF)-4, ATF-6, and CCAAT-enhancer binding protein homologous protein. Meanwhile, the enhanced expression levels of these proteins were reversed by TUDCA, indicating that MA administration induced memory loss by evoking ER stress in the hippocampus. We also found that MA inhibited the induction of long-term potentiation (LTP) in the hippocampus. Nevertheless, LTP could be induced when mice were pre-treated with TUDCA. In conclusion, MA inhibited long-term memory acquisition and synaptic plasticity via ER stress.

Keywords: methamphetamine, neurotoxicity, endoplasmic reticulum stress, memory, tauroursodeoxycholic acid

OPEN ACCESS

Edited by:
Qi Wang,
Southern Medical University, China

Reviewed by:
Keiichi Kadoyama,
Himeji Dokkyo University, Japan
Yingmin Li,
Hebei Medical University, China

****Correspondence:***
Ruibin Su
ruibinsu@126.com
Luyang Tao
taoluyang@suda.edu.cn

Specialty section:
This article was submitted to Neuropharmacology, a section of the journal Frontiers in Neuroscience

Received: *18 November 2020*
Accepted: *14 December 2020*
Published: *14 January 2021*

Citation:
Chen G, Wei X, Xu X, Yu G, Yong Z, Su R and Tao L (2021) Methamphetamine Inhibits Long-Term Memory Acquisition and Synaptic Plasticity by Evoking Endoplasmic Reticulum Stress. Front. Neurosci. 14:630713. doi: 10.3389/fnins.2020.630713

INTRODUCTION

Methamphetamine (MA), an amphetamine-type stimulant, has been abused worldwide and its use has increased the heath and economic burden to individuals and society (Courtney and Ray, 2014; Xu et al., 2019). Acting mainly on the dopaminergic, noradrenergic, and serotonergic pathways of the central nervous system (Cruickshank and Dyer, 2009), MA induces significant

neurotoxicity (Shaerzadeh et al., 2018), one of which is cognitive impairment. Clinical researchers have found that chronic MA abuse leads to cognitive dysfunction (Scott et al., 2007), which is related to attention, psychomotor speed, and executive function in addition to memory loss. It is also suggested by previous studies that MA-treated rodents exhibit deficits in spatial and recognition memory (Belcher et al., 2008; North et al., 2013). In contrast, MA-induced memory enhancement has also been detected in rodents (Cao et al., 2013). Collectively, the differing effects of MA on memory may be attributed to different models of MA administration and behavioral tasks carried out in different studies.

Oxidative stress is considered as one important mechanism of MA-induced neurotoxicity that causes nerve cell death by disrupting cellular organelle function, including that of the endoplasmic reticulum (ER) (Krasnova and Cadet, 2009; Yu et al., 2015). Induced by the accumulation of unfolded proteins and protein aggregation, ER stress is initiated by phosphorylated inositol requiring kinase 1α (p-IRE1α), PKR-like ER kinase (PERK) or cyclic AMP-dependent transcription factor-6 (ATF-6). ER stress is mainly mediated by three pathways (Kim et al., 2008) and the role of ER stress is to reduce the protein load of the ER and promote the degradation or reassembly of misfolded proteins. However, if ER stress is too severe or lasts too long, it can lead to cell death (Sano and Reed, 2013). Recent studies have found that ER stress is involved in the pathophysiology of several diseases, including neurodegeneration, cancer, diabetes, stroke, and inflammation (Oyadomari and Mori, 2004). MA can also induce ER stress and lead to cell death via ER stress-associated autophagy and apoptosis (Jayanthi et al., 2004). However, it is still unclear whether ER stress is involved in MA-induced memory loss. As protein synthesis is essential for long-term memory induction, it can be postulated that ER stress may be involved in MA-induced long-term memory impairment.

In the present study, a subacute administration method of MA, which has been found to induce ER stress and neurotoxicity in mice (Cai et al., 2016), was used and different behavioral experiments, including elevated plus maze, Morris water maze, electro-stimulus Y-maze, and novel object recognition tasks, were conducted to investigate the impairment of memory caused by MA. Next, tauroursodeoxycholic acid (TUDCA), a general inhibitor for ER stress, was used to inhibit ER stress and the effect of TUDCA pre-treatment on MA-induced memory loss was evaluated. TUDCA, the taurine-conjugated derivative of ursodeoxycholic acid (UDCA) is a bile acid synthesized by intestinal bacteria, and used for the treatment of cholestatic liver diseases, diabetes, and atherosclerosis (Lebensztejn, 2000; Ozcan et al., 2006). Recent studies have found that TUDCA alleviates ER stress by enhancing ER folding ability and preventing protein aggregation (Liu et al., 2015). Meanwhile, we investigated the effect of ER stress on the synaptic plasticity by evaluating the role of ER stress in the induction of long-term potentiation (LTP) in the hippocampus, which is closely associated with memory formation and storage. LTP is defined as a long-term increase in synaptic response following a high frequency stimulation (HFS) (Baltaci et al., 2019). It has been suggested that LTP is not only a laboratory phenomenon, but also involved in the information storage (Pastalkova et al., 2006).

MATERIALS AND METHODS

Drugs

MA was obtained from the Beijing Institute of Pharmacology and Toxicology. TUDCA was purchased from Shanghai Aladdin Bio-Chem Technology Co., Ltd. (cat. no. S101371). All drugs were dissolved in the saline (0.9% NaCl solution) and prepared to a specified concentration. The mice were divided into four groups: (i) Saline, (ii) TUDCA, (iii) MA, and (iv) TUDCA + MA. In the MA group, mice were administered intraperitoneal (i.p.) injections of 15 mg/kg MA (twice a day) for 4 days. In the TUDCA + MA group, mice received i.p. injections of 200 mg/kg TUDCA 60 min before receiving MA injections every time. In the Saline and TUDCA groups, mice were administered i.p. injections of the saline and 200 mg/kg TUDCA, respectively.

Animals and Housing

Male C57BL/6 mice aged 6–8 weeks were obtained from SPF (Beijing) Biotechnology Co., Ltd. Mice had free access to water and food in standard experimental housing with a constant temperature range (25°C) and a 12 h light/dark cycle. All experimental animal procedures were conducted in accordance with the National Institutes of Health (NIH) and were approved by the Animal Care and Use Committee of the Beijing Institute of Pharmacology and Toxicology. Different mice were used in each of the following experiments.

Elevated Plus Maze

Elevated plus maze (EPM) task was initially performed (n = 8 per group) to evaluate whether drug administration had an effect on animal anxiety-like behavior, using a standard experimental apparatus manufactured by Shanghai Jiliang Software Technology Co., Ltd. The apparatus consisted of two open arms (30 × 5 cm, length × width) and two closed arms (30 × 5 × 15 cm, length × width × height) elevated 50 cm above the floor. The EPM testing was conducted as previously described (Psotta et al., 2015). At the beginning of the experiment, mice were placed in the central zone of the maze facing an open arm and were allowed to freely explore the maze for 5 min. The maze was carefully cleaned after each trial to remove odor cues. EPM testing was performed 24 h after the final injection of drugs (**Figure 1A**). Increased anxiety-like behavior was indicated by a lower percent time in the open arms.

Morris Water Maze

The Morris water maze (MWM) task was performed (n = 10 per group) to evaluate the effect drug administration on the spatial memory formation of mice. The apparatus, which was manufactured by Shanghai Jiliang Software Technology Co., Ltd., consisted of a stainless-steel circular tank (120 cm diameter, 60 cm height) filled with 23 ± 1°C water to a depth of 40 cm. A Plexiglas platform (10 cm diameter) was submerged 1.5 cm below the surface of the water during the training session and

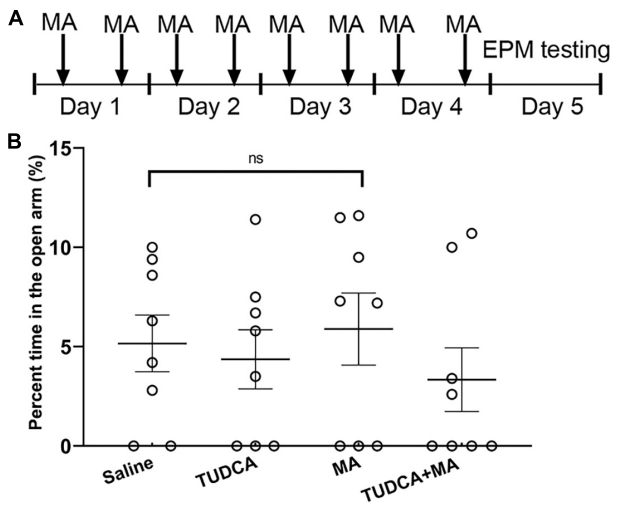

FIGURE 1 | MA administration has no effect on the anxiety-like behavior of mice. **(A)** The experimental flow diagram of elevated plus maze task. **(B)** There was no significant difference in the percent time spent in the open arms between the four groups. Data was presented as the mean ± SEM, $n = 8$ per group, ns indicated $p > 0.05$.

distal cues were placed within the experimental room. The protocol of MWM task was according to the previous reports (Vorhees and Williams, 2006; Cao et al., 2013) with some modifications. Mice were administered i.p. injections of drugs for 4 days followed by 4 days training with testing conducted 24 h after the last training session (**Figure 2A**). During the training session, mice were held facing the tank wall and randomly placed into the pool from one of four fixed entry points and allowed to swim freely for 90 s. A trial ended when the mouse climbed onto the platform and stopped for 5 s or when the 90 s time limit had elapsed. Mice were given a 15 min rest between two consecutive trials. A 60 s probe testing was performed 24 h after the last day of training with the platform removed. Swimming tracks were recorded and analyzed. Escaped latency (i.e., the interval between the start of the experiment and when mice climbed onto the platform) was used to evaluate spatial learning during the training stage. During the testing, platform site crossings and crossing latency (i.e., the interval between the start of the test and when mice swam across the site of the platform) were used to evaluate spatial memory retrieval.

Electro-Stimulus Y-Maze

Electro-stimulus Y-maze task was performed ($n = 8$ per group) to evaluate the effect of drug administration on the formation of recognition memory. The apparatus was manufactured by Zhangjiagang Biomedical Equipment Manufacturing Co., Ltd, and consisted of 3 arms with equal dimensions (65 × 15 × 15 cm, length × width × height), two of which were arranged at 120° angles. At the bottom of each arm, there were conductive gratings that were 0.5 cm in diameter and 0.5 cm in space. Each arm contained a light source. Three seconds after a light was turned on in one arm, an electrical stimulation lasting 10 s was given in the other two arms as well as the junctional zone. The task was performed as previously reported (Yu et al., 2003) with the procedure modified according to our experimental design. Mice were initially administered i.p. injections of drugs for 4 days, followed by 4 days training with 20 trials each day (**Figure 3A**). When performing the trials, electrical stimulation was given at random in the three arms and the junctional zone to help mice learn and remember that the arm in which the light was on was a safe area. If a mouse escaped into the safe arm within 10 s following electrical stimulation, the response would be recognized as correct. The testing, which consisted of 20 trials of electrical stimulation, was performed 24 h after the 4 days of training. For each mouse, 18 or more correct responses within 20 trials indicated learnt. Indices to evaluate the recognition memory included the percentages of correct trials and mice exhibiting learnt.

Novel Object Recognition

Novel object recognition (NOR) task was performed using a Plexiglas box (40 × 40 × 40 cm, length × width × height), manufactured by Shanghai Jiliang Software Technology Co., Ltd. The task consisted of three processes: habituation, training and testing. During the habituation (day 5), there was no object in the arena and mice were allowed to move freely for 20 min to become familiar with the environment. During the training (day 6), two identical objects were placed in the arena and mice were allowed to explore the objects for 10 min. During the testing, one of the objects was replaced with a novel object and mice were placed in the arena for 7 min to explore the two objects. In the present study, Test 1 and Test 2 were performed 30 min and 24 h post the training, respectively (**Figure 4A**). Novel object index (NOI), which is the time spent exploring the novel object divided by the time spent exploring the two objects, was used to evaluate the formation of recognition memory.

Western Blotting

Mice were killed by an overdose of isoflurane 24 h after the last ingestion of MA and the hippocampal tissue was dissected on ice to extract the whole protein fraction. Western blotting was performed as previously reported (Cai et al., 2016) to examine the expression of ER stress marker proteins, including binding immunoglobulin protein (Bip) (Abcam, ab21685), cyclic AMP–dependent transcription factor (ATF)-4 (Abclonal, A8687), phosphorylated eukaryotic translation initiation factor 2α (p-eIF2α) (CST, 3398s), ATF-6 (Abclonal, A0202) and CCAAT-enhancer binding protein homologous protein (Chop) (Abclonal, A0221). Values of these proteins were normalized to that of actin (Applygen, C1313). Bands were semi-quantified using Image J software (NIH).

Electrophysiology

The effect of MA on the induction of LTP *in vivo* of the perforant path (PP)–dentate gyrus (DG) pathway in the hippocampus was investigated as previously described (Gureviciene et al., 2004). Mice ($n = 5$ per group) were anesthetized with urethane (1.5 g/kg, i.p.) and then a pair of stimulating electrodes were implanted into the perforant path of the left hemisphere at A/P: −3.8 mm,

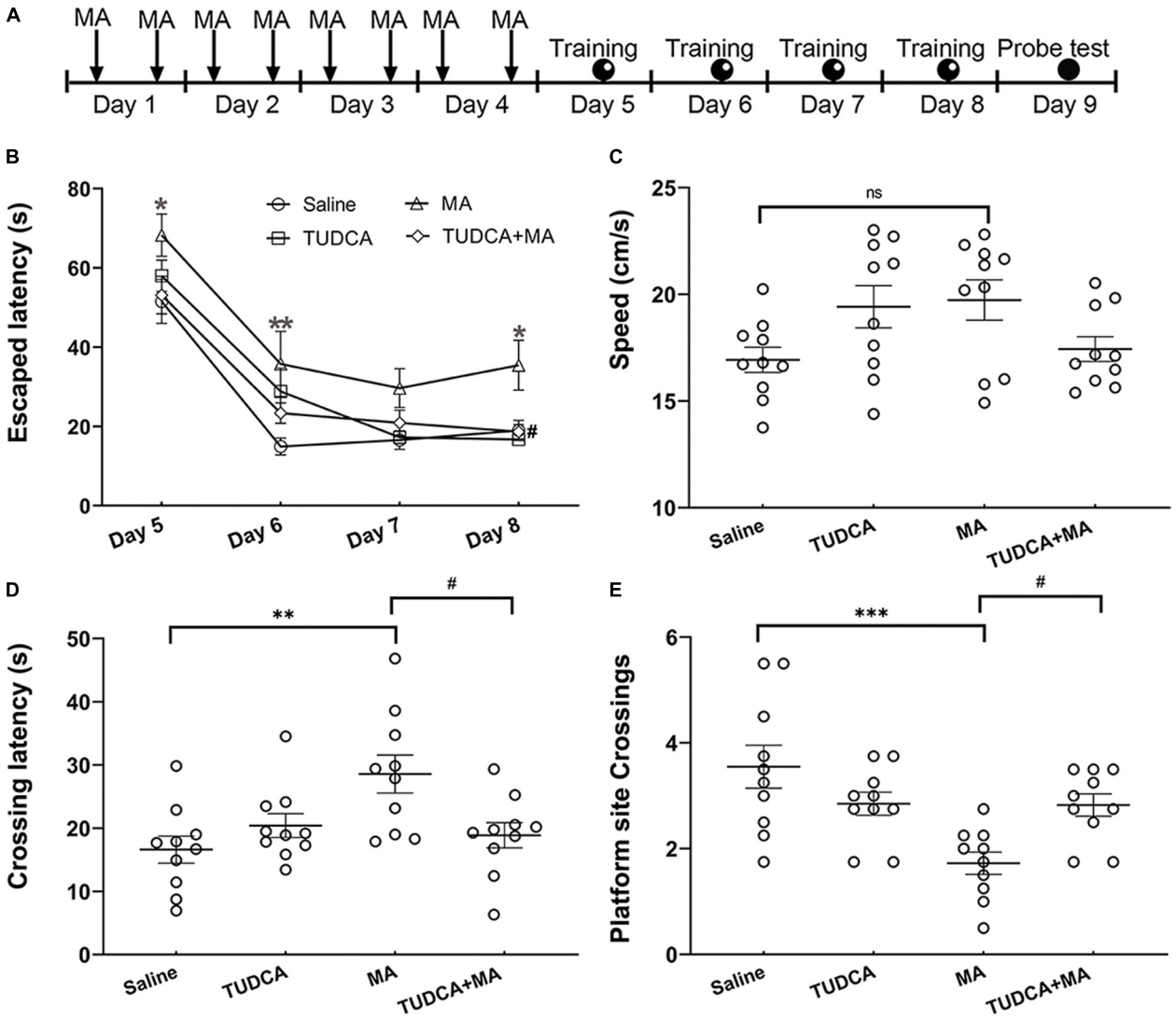

FIGURE 2 | MA-induced deficits of spatial memory are protected by TUDCA. **(A)** The experimental flow diagram of Morris water maze task. **(B)** MA-treated mice exhibited increased escaped latencies on days 1, 2, and 4 during the training session, in comparison with that of saline-treated mice. The escaped latency of TUDCA + MA-treated mice was less than that of MA-treated mice on day 4. **(C)** There was no difference in swimming speed between the four groups in the probe test. (**D**) MA-treated mice exhibited increased crossing latency, compared with that of saline-treated mice in the probe test, whereas mice of the TUDCA + MA group exhibited decreased latency, compared with that of MA-treated mice. **(E)** The platform site crossings of MA group were less than the Saline group, while mice of the TUDCA + MA group exhibited more platform position crossings than the MA group. $^{*}p < 0.05$, $^{**}p < 0.01$, $^{***}p < 0.001$ vs. the Saline group. $^{\#}p < 0.05$ vs. the MA group, ns indicated $p > 0.05$. Data was presented as the mean ± SEM, $n = 10$ per group.

M/L: −3.0 mm, D/V: −1.5 mm (from the dura). Meanwhile, a pair of recording electrodes were implanted into the dentate gyrus of the left hemisphere at A/P: −2.0 mm, M/L: −1.4 mm, D/V: −1.5 mm (from the dura, **Figure 6A**). The population spike (PS) was induced using monopolar pulses (duration, 400 μs; frequency, 1/30 Hz) using an Isolated Pulse Stimulator (A-M SYSTEMS Co., Ltd.) The PS was reported using a Differential AC Amplifier (A-M SYSTEMS Co., Ltd.) and Axon Digidata 1550A Data Acquisition System (Molecular Devices Co., Ltd.). When the stabilized PS (**Figure 6B**) lasted at least 30 min, we regulated the stimulating current to yield a PS that was 30–50% of the maximum amplitude. The PS was recorded for 30 min and the amplitude of PS was homogenized as the baseline. Then the HFS, consisting of three trains of 10 bursts (duration, 400 μs; frequency, 300 Hz) with an interval of 10 s between each train, was used to induce LTP *in vivo*. Next, the PS was yielded using formerly single monopolar pulses and recorded for 60 min. The amplitude of PS was calculated using pClamp10.0 software (Molecular Devices Co., Ltd.; **Figure 6C**).

Statistical Analysis

All experiments were randomized and performed in a blinded manner. Data was presented as the mean ± SEM. Statistical analysis was performed using GraphPad Prism 8.0 (GraphPad

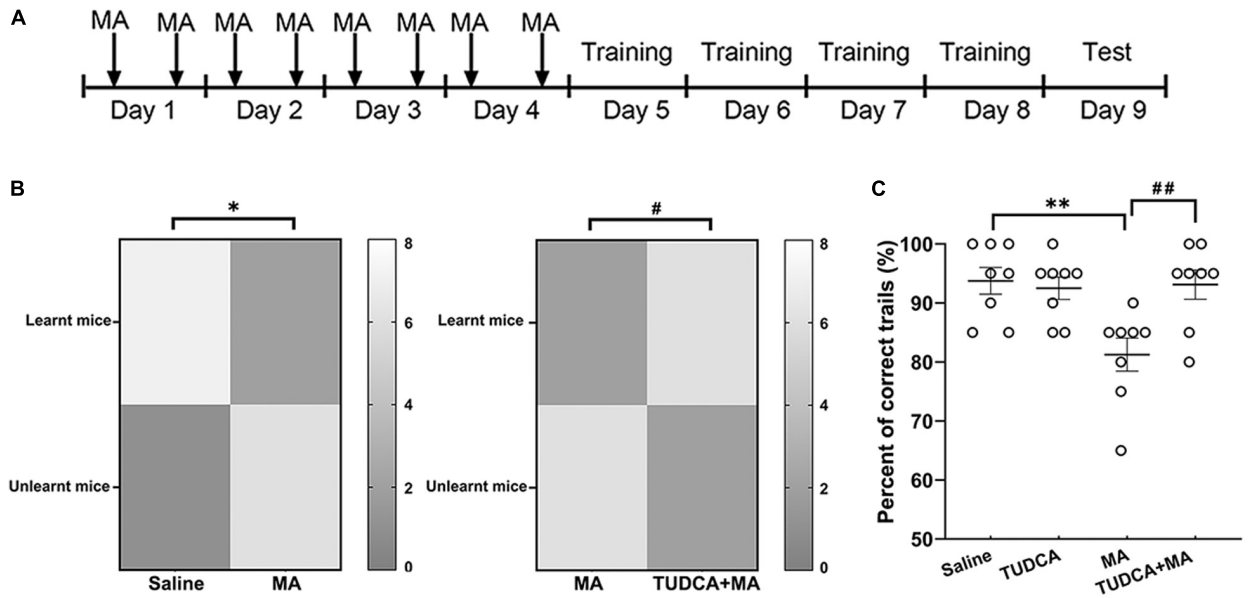

FIGURE 3 | MA-induced impairment of recognition memory is protected by TUDCA in electro-stimulus Y-maze. **(A)** The experimental flow diagram of electro-stimulus Y-maze task. **(B)** The number of mice exhibiting learnt and unlearnt in different groups. The present results indicated that a lower percent of MA-treated mice exhibited learnt in comparison with the saline group, whereas the percentage of mice exhibiting learnt in the TUDCA + MA group was higher than that of the MA group. **(C)** The percentage of correct trials in MA group was lower than that of the Saline group, while mice of the TUDCA + MA group represented a higher percent of correct trials in comparison with the MA group. $^{*}p < 0.05$, $^{**}p < 0.01$ vs. the Saline group. $^{\#}p < 0.05$, $^{\#\#}p < 0.01$ vs. the MA group. Data was presented as the mean ± SEM, $n = 8$ per group.

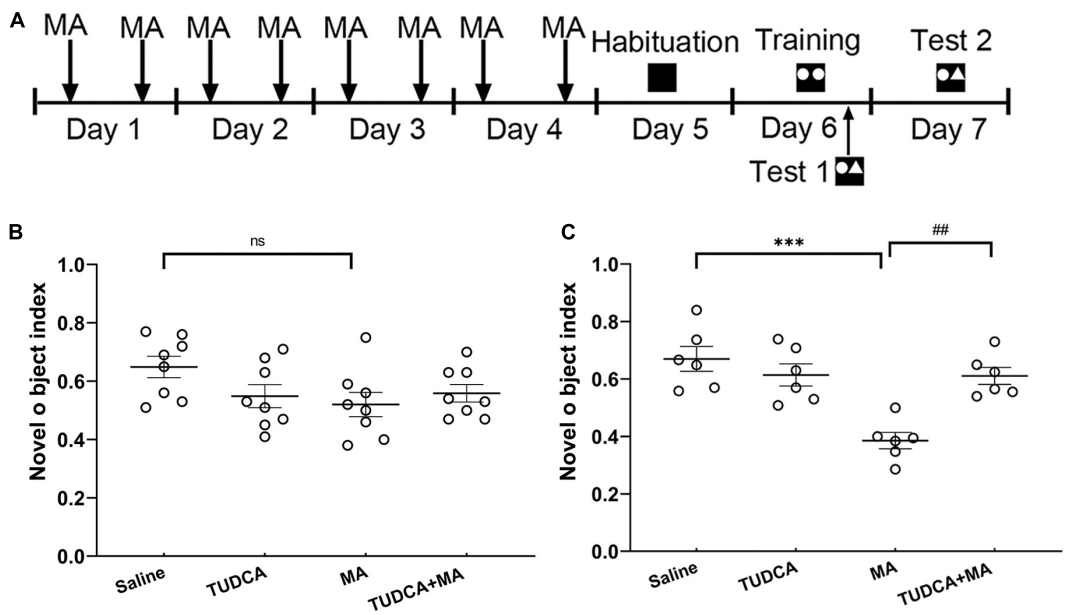

FIGURE 4 | MA-induced long-term recognition memory loss in novel object recognition task is avoided by TUDCA. **(A)** The experimental flow diagram of NOR task. **(B)** In Test 1, there was no difference in the novel object index (NOI) between the four groups. **(C)** In Test 2, MA-treated mice exhibited a lower NOI, compared with that of the Saline group, TUDCA + MA-treated mice exhibited a higher NOI in comparison with that of the MA group. $^{***}p < 0.001$ vs. the Saline group. $^{\#\#}p < 0.01$ vs. the MA group, ns indicated $p > 0.05$. Data was expressed as the mean ± SEM, $n = 8$ per group.

Software, Inc.). For EPM testing, a one-way ANOVA was used to analyze the difference in the percent time spent in the open arms. For MWM testing, a two-way repeated-measures ANOVA followed by Bonferroni's multiple comparison test was used to analyze the difference in escaped latency and a one-way ANOVA followed by Bonferroni's multiple comparison test was used

to analyze the difference in crossing latency and platform site crossings. For electro-stimulus Y-maze testing, a chi-square test was used to analyze the difference in the percentage of mice exhibiting learnt; a one-way ANOVA followed by Bonferroni's multiple comparison test was used to analyze the percentage of correct trials. For NOR testing, a one-way ANOVA followed by Bonferroni's multiple comparison test was used to analyze the difference in NOI. For electrophysiological experiments, a paired *t*-test was used to determine the difference in PS amplitude before and post HFS between different groups. The level of statistical significance was set at $p < 0.05$.

RESULTS

MA Administration Has No Effect on the Anxiety-Like Behavior of Mice

The present results showed that there was no significant difference ($p > 0.05$) in the percent time spent in the open arms between the four groups (**Figure 1B**). Therefore, 4 days i.p. injections of MA had no effect on the tension and anxiety of mice.

TUDCA Pre-treatment Ameliorates the Impairment of Spatial Memory Caused by MA

In the MWM testing, a two-way repeated-measures ANOVA of escaped latency revealed significant effects of time [$F_{(3,36)} = 74.38$, $p < 0.001$] and groups [$F_{(3,36)} = 7.848$, $p < 0.001$], but not their interaction [$F_{(9,108)} = 0.684$, $p > 0.05$]. MA-treated mice exhibited increased escaped latencies on day 1 ($p < 0.05$), day 2 ($p < 0.01$), and day 4 ($p < 0.05$) of the training session, compared with that of saline-treated mice; however, there was no difference in the escaped latency between the TUDCA + MA and Saline groups. Moreover, the escaped latency of TUDCA + MA-treated mice was less than that of MA group on the fourth day of training ($p < 0.05$; **Figure 2B**). In the probe test, MA-treated mice exhibited an increased crossing latency ($p < 0.01$) and decreased platform site crossings ($p < 0.001$) in comparison with saline-treated mice, whereas mice of the TUDCA + MA group exhibited a decreased crossing latency ($p < 0.05$) and increased platform site crossings ($p < 0.05$), compared with MA-treated mice (**Figures 2D,E**). Meanwhile, no difference in the swimming speed was found between the four groups ($p > 0.05$) in the probe test (**Figure 2C**).

MA-Induced Recognition Memory Defects Are Rescued by TUDCA Pre-treatment

In the electro-stimulus Y-maze testing, it was found that the percentage of mice exhibiting learnt in the MA group was lower than that of the Saline group ($p < 0.05$), meanwhile, the percentage of correct trials in the MA group was lower than that of the Saline group ($p < 0.01$). An increased percentage of TUDCA + MA-treated mice exhibited learnt ($p < 0.05$), compared with the MA group. The percentage of correct trials in the TUDCA + MA group was also higher than that of the MA group ($p < 0.01$; **Figures 3B,C**). In the NOR testing, no significant difference in NOI was found between the four groups in Test 1 ($p > 0.05$; **Figure 4B**). However, in Test 2, the NOI of the MA group was lower than that of the Saline group ($p < 0.001$). Mice of the TUDCA + MA group exhibited an increased NOI, compared with the MA group ($p < 0.01$; **Figure 4C**).

MA-Induced ER Stress Is Inhibited by TUDCA Pre-treatment

The results of the Western blotting suggested that the administration of MA in the present study increased the expression levels of ER stress marker proteins, including Bip ($p < 0.01$), ATF-6 ($p < 0.05$), ATF-4 ($p < 0.01$), *p*-eIF2α ($p < 0.05$), and Chop ($p < 0.01$), all of which were reversed by TUDCA (**Figures 5A,B**).

MA-Induced Inhibition of LTP *in vivo* Is Reversed by TUDCA Pre-treatment

The obtained data indicated that the HFS used in the present study induced LTP *in vivo* in the hippocampus, evidenced by the PS amplitude of saline-treated mice was enhanced to 132.00 ± 3.43% of the baseline ($p < 0.001$) post-HFS (**Figures 6D,E**). After the mice were administered i.p. injections of MA, however, the amplitude of PS could not be enhanced by the HFS ($p > 0.05$; **Figures 6F,G**). When mice were pre-treated with TUDCA, the PS amplitude was increased to 143.30 ± 6.56% of the baseline ($p < 0.01$) (**Figures 6H,I**).

DISCUSSION

MA is a worldwide abused illicit drug (Centazzo et al., 2019; Xu and Liu, 2019) and MA-induced cognitive impairment has been of increasing concern to the public (Morgan et al., 2012). Recently, several potential mechanisms underlying MA-induced neural damage have been proposed, including hyperthermia, excitotoxicity, inflammation, mitochondrial dysfunction, and oxidative stress (Yamamoto et al., 2010; Moszczynska and Callan, 2017). ER stress, which is involved in a variety of diseases, has been given much attention and considered as one mechanism mediating MA-induced neurotoxicity. Nevertheless, studies regarding the association between ER stress and MA-induced neural damage have largely focused on molecular mechanisms rather than behavioral manifestation. According to the molecular toxicology studies in our laboratory and other laboratories, it is postulated that ER stress may be one mechanism underlying the cognitive dysfunction caused by MA. To verify this hypothesis, the influence of MA administration on the memory formation was studied using different behavioral tests, including the MWM, electro-stimulus Y-maze, and NOR tasks. EPM testing was first performed to evaluate the effect of MA on anxiety-like behavior in mice. Compared with saline-treated mice, mice administered i.p. injections of MA exhibited no difference in the percentage of time spent in open arms, indicating that MA ingestion did not affect anxiety-like behavior of mice. MWM task was performed to investigate whether ER stress was involved in MA-induced spatial memory impairment.

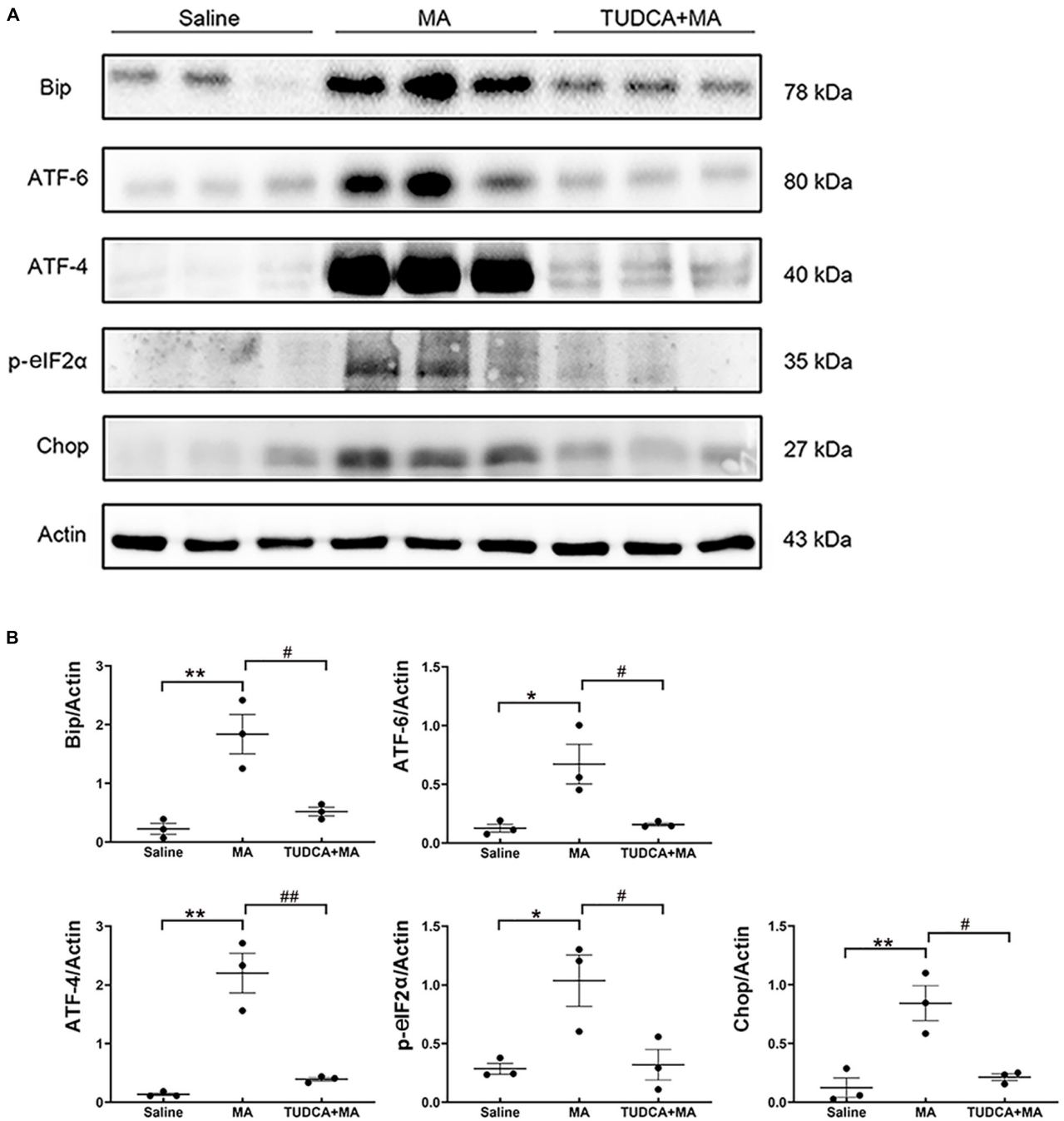

FIGURE 5 | MA-induced ER stress is reversed by TUDCA pre-treatment. **(A,B)** Four-day injections of MA increased the expression levels of Bip, ATF-4, ATF-6, p-eIF2α, and Chop, all of which were reversed by TUDCA pre-treatment. $^{*}p < 0.05$, $^{**}p < 0.01$ vs. the Saline group. $^{\#}p < 0.05$, $^{\#\#}p < 0.01$ vs. the MA group. Data was presented as the mean ± SEM, $n = 3$ per group.

Consistent with the findings of previous reports (Vorhees and Williams, 2006; Heysieattalab et al., 2016), MA induced spatial memory impairment, as indicated by the increased escaped latencies during the training stage, crossing latency as well as fewer platform site crossings in the probe test. Compared with MA-treated mice, TUDCA + MA-treated mice exhibited decreased escaped latency, crossing latency as well as more platform site crossings, demonstrating that inhibiting ER stress rescued MA-induced impairment of spatial memory. Besides spatial memory, we also evaluated the effect of MA exposure on recognition memory by conducting electro-stimulus Y-maze and NOR tasks. The present results of these two experiments suggested that MA-induced inhibition of recognition memory could also be protected by TUDCA pre-treatment. Meanwhile,

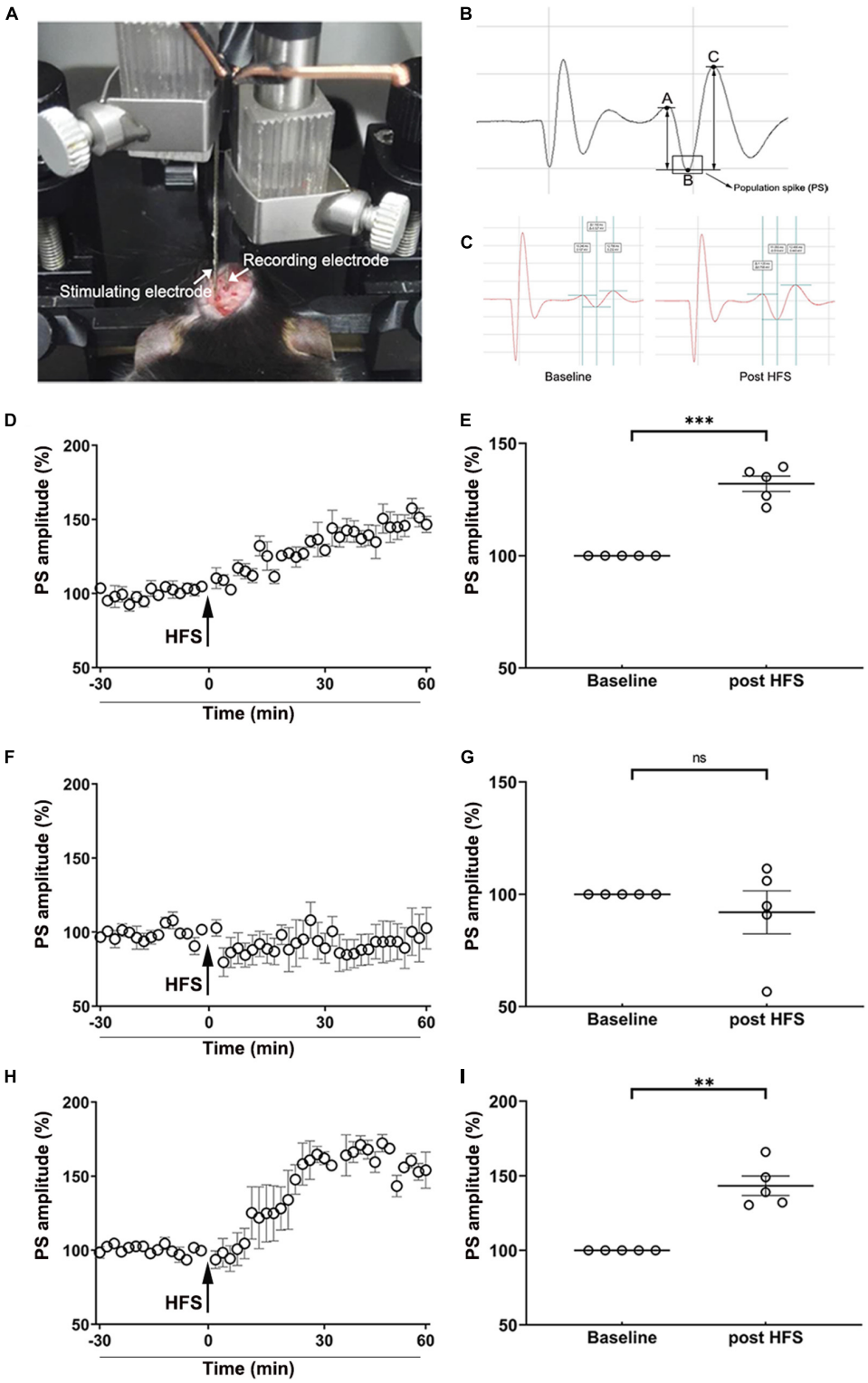

FIGURE 6 | MA-induced inhibition of LTP *in vivo* is reversed by TUDCA pre-treatment. **(A)** The position of stimulating electrodes and recording electrodes in the electrophysiological experiments. **(B)** A typical form of the population spike (PS) was consisted of a descending branch (AB) and an ascending branch (BC). The amplitude of PS was calculated by the average of the potential difference of AB and BC. **(C)** A typical enhancement of PS amplitude post-HFS, compared with the baseline. **(D,E)** The HFS induced a significant increase of the PS amplitude in the Saline group. **(F,G)** When mice were treated with MA, there was no difference in the PS amplitude post-HFS in comparison with the baseline. **(H,I)** When mice were pretreated with TUDCA, the HFS induced a prominent enhancement of the PS amplitude. $^{**}p < 0.01$, $^{***}p < 0.001$ vs. the baseline, ns indicated $p > 0.05$. Data was presented as the mean ± SEM, $n = 5$ per group.

we evaluated the effect of MA administration on the expression levels of ER stress marker proteins in the hippocampus, such as Bip, ATF-6, ATF-4, p-eIF2α, and Chop. The results showed that MA increased the expression levels of these proteins, while TUDCA pre-treatment reversed the effect of MA, confirming that the subacute administration of MA induced cognitive impairment via ER stress in the present study.

In the NOR tasks, two different tests were conducted to distinguish the effect of MA ingestion on working memory and long-term memory. In Test 1, MA-treated mice did not show a decreased NOI, while MA-treated mice had a lower NOI in Test 2, indicating 4 days injections of MA impaired long-term recognition memory, but had no effect on short-term recognition memory. It has been generally accepted that memory can be divided into two different forms, short-term memory (STM) and long-term memory (LTM) (Scoville and Milner, 1957), which have different duration as well as molecular mechanisms. Previous studies have suggested that newly synthesized proteins are essential for the formation of LTM rather than STM (Davis and Squire, 1984). Recently, researchers have further found that increased expression level of p-eIF2α impairs the induction of long-lasting LTP (L-LTP) and consolidation of spatial memory, indicating that translational control of gene expression by eIF2α signaling pathway may be a molecular switch for LTM formation (Costa-Mattioli and Sonenberg, 2008). Enhanced phosphorylation of eIF2α serves a negative control of the gene expression and protein synthesis (Dever, 2002) and p-eIF2α is also involved in the ER stress. In the present study, MA administration increased the phosphorylation of eIF2α and the expression level of ATF-4, which is a downstream of p-eIF2α. It was speculated that the inhibition of gene translation caused by p-eIF2α may be the reason why MA ingestion disturbed the formation of LTM, but not STM.

At last, the effect of MA poisoning on synaptic plasticity in the PP-DG pathway of the hippocampus was investigated to study the underlying mechanisms for MA-induced memory loss. We selected LTP *in vivo*, an intensively studied cellular model of the memory, to further study the role of MA-induced ER stress in the disruption of memory acquisition. LTP, referring to a sustained increase in efficiency of synaptic transmission caused by trains of high-frequency stimulation, was first fully described by Bliss and Lomo (1973). A great deal of research has revealed that LTP may be a biological substrate for at least some forms of memory (Lynch, 2004). In the present study, we found that MA-induced inhibitory of LTP in the hippocampus could also be reversed by ER stress inhibitor, TUDCA, indicating that ER stress may be a reason why LTP induction was inhibited by MA ingestion. However, the detailed mechanism for MA restraining LTP *in vivo* through ER stress needs further investigation in the future studies. In conclusion, MA inhibited long-term memory acquisition and synaptic plasticity by evoking ER stress.

DATA AVAILABILITY STATEMENT

The raw data supporting the conclusions of this article will be made available by the authors, without undue reservation, to any qualified researcher.

ETHICS STATEMENT

The animal study was reviewed and approved by the Animal Care and Use Committee of the Beijing Institute of Pharmacology and Toxicology.

AUTHOR CONTRIBUTIONS

GC conducted all of the experiments with the help of GY and ZY and wrote the manuscript with the help of XW. LT and RS designed the research. XX analyzed the results. All authors contributed to the article and approved the submitted version.

ACKNOWLEDGMENTS

We thank all the members of our laboratory for their helpful assistance.

REFERENCES

Baltaci, S., Mogulkoc, R., and Baltaci, A. (2019). Molecular Mechanisms of Early and Late LTP. *Neurochem. Res.* 44, 281–296. doi: 10.1007/s11064-018-2695-4

Belcher, A., Feinstein, E., O'dell, S., and Marshall, J. (2008). Methamphetamine influences on recognition memory: comparison of escalating and single-day dosing regimens. *Neuropsychopharmacology* 33, 1453–1463. doi: 10.1038/sj.npp.1301510

Bliss, T., and Lomo, T. (1973). Long-lasting potentiation of synaptic transmission in the dentate area of the anaesthetized rabbit following stimulation of the perforant path. *J. Physiol.* 232, 331–356. doi: 10.1113/jphysiol.1973.sp010273

Cai, D., Huang, E., Luo, B., Yang, Y., Zhang, F., Liu, C., et al. (2016). Nupr1/Chop signal axis is involved in mitochondrion-related endothelial cell apoptosis induced by methamphetamine. *Cell Death Dis.* 7:e2161. doi: 10.1038/cddis.2016.67

Cao, G., Zhu, J., Zhong, Q., Shi, C., Dang, Y., Han, W., et al. (2013). Distinct roles of methamphetamine in modulating spatial memory consolidation, retrieval, reconsolidation and the accompanying changes of ERK and CREB activation in hippocampus and prefrontal cortex. *Neuropharmacology* 67, 144–154. doi: 10.1016/j.neuropharm.2012.10.020

Centazzo, N., Frederick, B., Jacox, A., Cheng, S., and Concheiro-Guisan, M. (2019). Wastewater analysis for nicotine, cocaine, amphetamines, opioids and cannabis in New York City. *Forensic. Sci. Res.* 4, 152–167. doi: 10.1080/20961790.2019.1609388

Costa-Mattioli, M., and Sonenberg, N. (2008). Translational control of gene expression: a molecular switch for memory storage. *Progr. Brain Res.* 169, 81–95. doi: 10.1016/s0079-6123(07)00005-2

Courtney, K. E., and Ray, L. A. (2014). Methamphetamine: an update on epidemiology, pharmacology, clinical phenomenology, and treatment literature. *Drug Alcohol Depend* 143, 11–21. doi: 10.1016/j.drugalcdep.2014.08.003

Cruickshank, C., and Dyer, K. (2009). A review of the clinical pharmacology of methamphetamine. *Addiction* 104, 1085–1099. doi: 10.1111/j.1360-0443.2009.02564.x

Davis, H. P., and Squire, L. R. (1984). Protein synthesis and memory: a review. *Psychol. Bull.* 96, 518–559. doi: 10.1037/0033-2909.96.3.518

Dever, T. E. (2002). Gene-specific regulation by general translation factors. *Cell* 108, 545–556. doi: 10.1016/s0092-8674(02)00642-6

Gureviciene, I., Ikonen, S., Gurevicius, K., Sarkaki, A., Van Groen, T., Pussinen, R., et al. (2004). Normal induction but accelerated decay of LTP in APP + PS1 transgenic mice. *Neurobiol. Dis.* 15, 188–195. doi: 10.1016/j.nbd.2003.11.011

Heysieattalab, S., Naghdi, N., Zarrindast, M., Haghparast, A., Mehr, S., and Khoshbouei, H. (2016). The effects of GABAA and NMDA receptors in the shell-accumbens on spatial memory of METH-treated rats. *Pharmacol. Biochem. Behav.* 142, 23–35. doi: 10.1016/j.pbb.2015.12.008

Jayanthi, S., Deng, X., Noailles, P., Ladenheim, B., and Cadet, J. (2004). Methamphetamine induces neuronal apoptosis via cross-talks between endoplasmic reticulum and mitochondria-dependent death cascades. *FASEB J.* 18, 238–251. doi: 10.1096/fj.03-0295com

Kim, I., Xu, W., and Reed, J. (2008). Cell death and endoplasmic reticulum stress: disease relevance and therapeutic opportunities. *Nat. Rev. Drug Discov.* 7, 1013–1030. doi: 10.1038/nrd2755

Krasnova, I., and Cadet, J. (2009). Methamphetamine toxicity and messengers of death. *Brain Res. Rev.* 60, 379–407. doi: 10.1016/j.brainresrev.2009.03.002

Lebensztejn, D. (2000). Application of ursodeoxycholic acid (UDCA) in the therapy of liver and biliary duct diseases in children. *Med. Sci. Monit.* 6, 632–636.

Liu, F., Cui, Y., Ge, P., Luan, J., Zhou, X., and Han, J. (2015). Tauroursodeoxycholic acid attenuates inorganic phosphate-induced osteoblastic differentiation and mineralization in NIH3T3 fibroblasts by inhibiting the ER stress response PERK-eIF2alpha-ATF4 pathway. *Drug Discov. Ther.* 9, 38–44. doi: 10.5582/ddt.2015.01008

Lynch, M. (2004). Long-term potentiation and memory. *Physiological. Rev.* 84, 87–136.

Morgan, E., Woods, S., Poquette, A., Vigil, O., Heaton, R., and Grant, I. (2012). Visual memory in methamphetamine-dependent individuals: deficient strategic control of encoding and retrieval. *Austr. N. Zeal. J. Psych.* 46, 141–152. doi: 10.1177/0004867411433212

Moszczynska, A., and Callan, S. (2017). Molecular, Behavioral, and Physiological Consequences of Methamphetamine Neurotoxicity: Implications for Treatment. *J. Pharmacol. Exp. Ther.* 362, 474–488. doi: 10.1124/jpet.116.238501

North, A., Swant, J., Salvatore, M., Gamble-George, J., Prins, P., Butler, B., et al. (2013). Chronic methamphetamine exposure produces a delayed, long-lasting memory deficit. *Synapse* 67, 245–257. doi: 10.1002/syn.21635

Oyadomari, S., and Mori, M. (2004). Roles of CHOP/GADD153 in endoplasmic reticulum stress. *Cell Death Differ.* 11, 381–389. doi: 10.1038/sj.cdd.4401373

Ozcan, U., Yilmaz, E., Ozcan, L., Furuhashi, M., Vaillancourt, E., Smith, R., et al. (2006). Chemical chaperones reduce ER stress and restore glucose homeostasis in a mouse model of type 2 diabetes. *Science* 313, 1137–1140. doi: 10.1126/science.1128294

Pastalkova, E., Serrano, P., Pinkhasova, D., Wallace, E., Fenton, A., and Sacktor, T. (2006). Storage of spatial information by the maintenance mechanism of LTP. *Science* 313, 1141–1144. doi: 10.1126/science.1128657

Psotta, L., Rockahr, C., Gruss, M., Kirches, E., Braun, K., Lessmann, V., et al. (2015). Impact of an additional chronic BDNF reduction on learning performance in an Alzheimer mouse model. *Front. Behav. Neurosci.* 9:58.

Sano, R., and Reed, J. C. (2013). ER stress-induced cell death mechanisms. *Biochim. Biophys. Acta* 1833, 3460–3470.

Scott, J. C., Woods, S. P., Matt, G. E., Meyer, R. A., Heaton, R. K., Atkinson, J. H., et al. (2007). Neurocognitive effects of methamphetamine: a critical review and meta-analysis. *Neuropsychol. Rev.* 17, 275–297. doi: 10.1007/s11065-007-9031-0

Scoville, W. B., and Milner, B. (1957). Loss of recent memory after bilateral hippocampal lesions. *J. Neurol. Neurosurg. Psychiatry* 20, 11–21. doi: 10.1136/jnnp.20.1.11

Shaerzadeh, F., Streit, W., Heysieattalab, S., and Khoshbouei, H. (2018). Methamphetamine neurotoxicity, microglia, and neuroinflammation. *J. Neuroinflamm.* 15:341.

Vorhees, C., and Williams, M. (2006). Morris water maze: procedures for assessing spatial and related forms of learning and memory. *Nat. Protoc.* 1, 848–858. doi: 10.1038/nprot.2006.116

Xu, B., Ye, Y., and Liao, L. (2019). Rapid and simple analysis of amphetamine-type illegal drugs using excitation-emission matrix fluorescence coupled with parallel factor analysis. *Forensic. Sci. Res.* 4, 179–187. doi: 10.1080/20961790.2017.1349600

Xu, F., and Liu, L. (2019). Simultaneous determination of free methamphetamine, pethidine, ketamine and tramadol in urine by dispersive liquid-liquid microextraction combined with GC-MS. *Forensic. Sci. Res.* 4, 188–194. doi: 10.1080/20961790.2017.1377386

Yamamoto, B., Moszczynska, A., and Gudelsky, G. (2010). Amphetamine toxicities: classical and emerging mechanisms. *Ann. N. Y. Acad. Sci.* 1187, 101–121. doi: 10.1111/j.1749-6632.2009.05141.x

Yu, J., Huang, Y. W., and Chen, Z. (2003). [Improved alternative electro-stimulus Y-maze for evaluating the spatial memory of rats]. *Zhejiang Da Xue Xue Bao Yi Xue Ban* 32:140.

Yu, S., Zhu, L., Shen, Q., Bai, X., and Di, X. (2015). Recent advances in methamphetamine neurotoxicity mechanisms and its molecular pathophysiology. *Behav. Neurol.* 2015:103969.

Conflict of Interest: XW was employed by Becton, Dickinson and Company, Guangzhou, China.

The remaining authors declare that the research was conducted in the absence of any commercial or financial relationships that could be construed as a potential conflict of interest.

frontiers in Neuroscience

HYPOTHESIS AND THEORY
published: 22 January 2021
doi: 10.3389/fnins.2020.589897

Single Low Dose of Cocaine–Structural Brain Injury Without Metabolic and Behavioral Changes

*Camilla Nicolucci[1], Mariana Lapo Pais[2,3,4], A. C. Santos[3,4,5], Fabiana M. Ribeiro[6], Pedro M. C. C. Encarnação[6], Ana L. M. Silva[6,7], I. F. Castro[7], Pedro M. M. Correia[6,7], João F. C. A. Veloso[6], Julie Reis[4], Marina Z. Lopes[8], Maria F. Botelho[3,4], Frederico C. Pereira[4,5,9] and Denise G. Priolli[1]**

[1] Multidisciplinary Research Laboratory, São Francisco University Post-graduation Stricto Sensu Programme, Bragança Paulista, Brazil, [2] Faculty of Sciences and Technology, University of Coimbra, Coimbra, Portugal, [3] Faculty of Medicine, Institute of Biophysics, University of Coimbra, Coimbra, Portugal, [4] Faculty of Medicine, Coimbra Institute for Clinical and Biomedical Research, University of Coimbra, Coimbra, Portugal, [5] Center for Innovative Biomedicine and Biotechnology, Coimbra, Portugal, [6] Department of Physics, Institute for Nanostructures, Nanomodelling and Nanofabrication (i3N), University of Aveiro, Aveiro, Portugal, [7] Radiation Imaging Technologies Lda, Ílhavo, Portugal, [8] Multidisciplinary Research Laboratory, São Francisco University Scientific Initiation Programme, Bragança Paulista, Brazil, [9] Faculty of Medicine, Institute of Pharmacology and Experimental Therapeutics, University of Coimbra, Coimbra, Portugal

OPEN ACCESS

Edited by:
Yixiao Luo,
Hunan Normal University, China

Reviewed by:
Ying Han,
Peking University, China
Robert Warren Gould,
Wake Forest School of Medicine, United States
Yan-Xue Xue,
Peking University, China

***Correspondence:**
Denise G. Priolli
depriolli@terra.com.br;
denise.priolli@usf.edu.br

Specialty section:
This article was submitted to Neuropharmacology, a section of the journal Frontiers in Neuroscience

Received: 31 July 2020
Accepted: 15 December 2020
Published: 22 January 2021

Citation:
Nicolucci C, Pais ML, Santos AC, Ribeiro FM, Encarnação PMCC, Silva ALM, Castro IF, Correia PMM, Veloso JFCA, Reis J, Lopes MZ, Botelho MF, Pereira FC and Priolli DG (2021) Single Low Dose of Cocaine–Structural Brain Injury Without Metabolic and Behavioral Changes. Front. Neurosci. 14:589897. doi: 10.3389/fnins.2020.589897

Chronic cocaine use has been shown to lead to neurotoxicity in rodents and humans, being associated with high morbidity and mortality rates. However, recreational use, which may lead to addictive behavior, is often neglected. This occurs, in part, due to the belief that exposure to low doses of cocaine comes with no brain damage risk. Cocaine addicts have shown glucose metabolism changes related to dopamine brain activity and reduced volume of striatal gray matter. This work aims to evaluate the morphological brain changes underlying metabolic and locomotor behavioral outcome, in response to a single low dose of cocaine in a pre-clinical study. In this context, a Balb-c mouse model has been chosen, and animals were injected with a single dose of cocaine (0.5 mg/kg). Control animals were injected with saline. A behavioral test, positron emission tomography (PET) imaging, and anatomopathological studies were conducted with this low dose of cocaine, to study functional, metabolic, and morphological brain changes, respectively. Animals exposed to this cocaine dose showed similar open field activity and brain metabolic activity as compared with controls. However, histological analysis showed alterations in the prefrontal cortex and *hippocampus* of mice exposed to cocaine. For the first time, it has been demonstrated that a single low dose of cocaine, which can cause no locomotor behavioral and brain metabolic changes, can induce structural damage. These brain changes must always be considered regardless of the dosage used. It is essential to alert the population even against the consumption of low doses of cocaine.

Keywords: cocaine, brain damage, metabolic imaging, histological change, behavior

INTRODUCTION

Drug dependency is considered a physical and psychological condition that induces chronic and recurrent diseases. The continued use of psychoactive substances can cause functional changes in the brain (Dias et al., 2008). Cocaine is one of the most widely used drugs in the world. The European Drug Report of 2020 showed that about 4.3 million people between 15 and 64 years old used cocaine in 2018, and 17.9 million had used it at least once (European Drug Report, 2020). In 2016, the number of young people who have already had any contact with illicit drugs was 236,800 (European Drug Report, 2016). Its consumption reaches about 0.4% of the world population, and most users (70%) are concentrated in the American continent (Gootenberg, 2019).

It is well-established that cocaine is a psychostimulant (Kalivas, 2007). This drug inhibits the reuptake of monoamine neurotransmitters, including dopamine (DA) and noradrenaline (NA). The DA increase occurs in the mesocorticolimbic system (the brain reward system), which is responsible for the well-being sensation and euphoria, thus playing a major role in the addiction process (Planeta et al., 2013). DA auto-oxidation can lead to oxidative stress and apoptosis (Dias et al., 2008; Planeta et al., 2013). There is evidence that oxidative stress contributes to cocaine neurotoxicity (Dietrich et al., 2005; Pereira et al., 2015). Changes in brain circulation triggered by cocaine use led to additional brain injury risk (Niu et al., 2019). Browndyke et al. (2004) demonstrated that these blood flow abnormalities might be related to cognitive impairments reported in cocaine-dependent populations (Browndyke et al., 2004). Moreover, cerebrovascular accidents rank amongst the most severe adverse events from cocaine abuse (Sordo et al., 2014).

Pre-clinical neuroimaging studies aiming to model human diseases and traits have been increasing in the last decade (Volkow et al., 1997; Moreno-López et al., 2012; Caprioli et al., 2013; Hanlon et al., 2013; Cannella et al., 2017; Nicolas et al., 2017). In an animal model, individuals can be followed up longitudinally over time, allowing the study of disease progression, development of compensatory changes, and long-term evaluation of the safety and efficacy of interventions (Zaidi, 2014; Cannella et al., 2017; Nicolas et al., 2017). In particular, pre-clinical positron emission tomography (PET) plays a fundamental role, not only in the validation of animal models of human brain disease but also in the quantitative measurement of regional changes in brain activity. These regional alterations in cerebral sub-regions are affected by diseases or psychoactive agents such as drugs of abuse. There is also evidence that repeated administration of a psychostimulant drug in laboratory animals may cause a change of different parameters, including cerebral glucose metabolism, in opposition to the one caused by an acute administration (Hammer and Cooke, 1994; Zocchi et al., 2001). The selectivity of glucose metabolism changes in the basal ganglia and prefrontal cortex (PFC) suggests that regional metabolic changes, observed in cocaine users during detoxification, are related to changes in the DA activity in the brain (Volkow et al., 1997). Several studies used brain imaging techniques to investigate the changes in brain activity induced by drugs (Hammer et al., 1993; Gould et al., 2009; Caprioli et al., 2013; Hanlon et al., 2013). Particularly, PET studies using 2-deoxy-2-[^{18}F]fluoro-D-glucose (^{18}F-FDG) have demonstrated abnormal brain glucose metabolism connected to cocaine addiction and withdrawal. The ^{18}F-FDG is a widely used radiotracer in PET due to its convenient half-life (110 min) and its well-established role in glycolytic metabolism (Alavi and Reivich, 2002; Caprioli et al., 2013; Hanlon et al., 2013; Cannella et al., 2017; Nicolas et al., 2017). Acute withdrawal in cocaine addicts is associated with a glucose metabolic rate higher than drug-naïve controls or cocaine abusers tested in late withdrawal (Volkow et al., 1991). Other researchers discovered a negative correlation between the severity of cocaine use and the glucose metabolic rate (Moreno-López et al., 2012). Regarding pre-clinical models, some authors evaluated the metabolic activity changes after short (1 week) and long (4 weeks) periods of cocaine abstinence in rats with a history of cocaine self-administration, using the escalation model (Nicolas et al., 2017). They showed that escalation of cocaine self-administration produced cerebral changes that are quantitatively and qualitatively different from those found after short access to cocaine self-administration; i.e., the changes in basal brain metabolic activity depend on the intensity of cocaine self-administration and the duration of abstinence (Nicolas et al., 2017). Although there are a growing number of neuroimaging studies in cocaine addiction settings, there are no neuroimaging studies in the context of a single low dose of cocaine. Additionally, data on the potential for brain injury induced by the consumption of low doses of cocaine remain scarce (Volkow et al., 1997; Heard et al., 2008).

The present work puts forward the hypothesis that even a single low dose of cocaine can cause deleterious brain changes. Therefore, this work aims to evaluate locomotor behavioral, metabolic, and morphological brain data of mice exposed to a single low dose of cocaine.

MATERIALS AND METHODS

Subjects and Housing Conditions

Male Balb-c mice, with a mean age of 6 weeks and an average weight between 20 and 30 g, were used in this study. The Multidisciplinary Research Laboratory of the University of São Francisco, Bragança Paulista (Brazil), in collaboration with both the Biophysics and Pharmacology and Experimental Therapeutics Institutes of the Faculty of Medicine of University of Coimbra (Portugal), developed the research. All experiments were conducted following the European Union directives (86/609/EEC) for the care of laboratory animals and the iCBR *Vivarium* guidelines. The project is under the ORBEA 17/2015 and the DGAV authorization.

General Experimental Design

Our general experimental design is presented in **Figure 1**. A total of 18 animals were used, being randomly divided into two groups: mice *non-exposed* ($n = 8$) or mice *exposed* ($n = 10$) to a single low dose of cocaine (Merck, Darmstadt, Germany). The *non-exposed* animals represent the controls that were injected intraperitoneally (i.p.) with saline (0.9% NaCl,

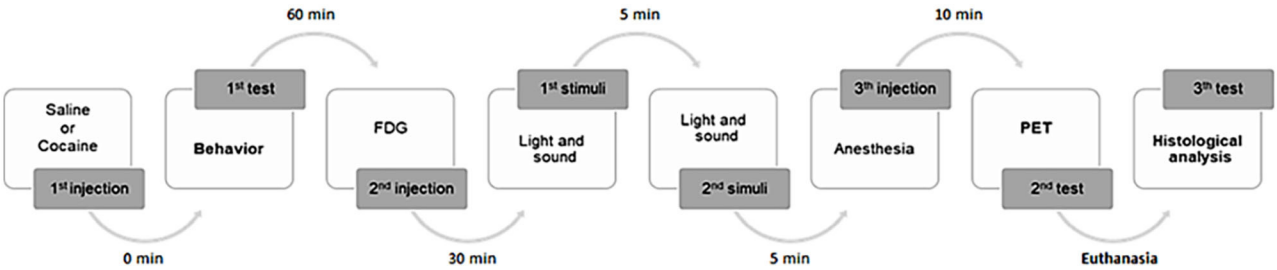

FIGURE 1 | General experimental design. A total of 18 animals were used, randomly divided into two groups: mice *non-exposed* ($n = 8$) or mice *exposed* ($n = 10$) to a single low dose of cocaine. Mice were submitted to a behavioral study. Five animals from each group were subsequently studied by PET imaging analysis. To histological analysis, six randomized mice brain samples were collected.

0.5 ml). The *exposed group* was injected (also i.p.) with cocaine (0.5 mg/kg, 0.5 ml). The dose was chosen based on the lowest dose having demonstrated dopaminergic visible action on PET imaging evaluation in human volunteers (Heard et al., 2008), although promoting changes in brain neurochemistry (Volkow et al., 1997).

Animals were submitted to a behavioral test followed by PET imaging; and brains were collected. Initially, saline or cocaine was administered to the animals, which subsequently underwent a behavioral test for 60 min. Afterwards, five randomized mice from each group were injected (i.p.) with ^{18}F-FDG. The radiotracer had an uptake period of 50 min post-injection. Subsequently, animals were anesthetized (i.p. injection) [0.2 ml of a mixture of ketamine (1.5 mg/mg weight) + chlorpromazine (0.05 mg/mg weight) (3:1):saline (1:1)] 10 min prior to the PET imaging acquisition (+/−30 min). For routine histological technique analysis, anesthesia (ketamine + chlorpromazine) overdose was induced in three randomized mice from each group for brain sample collection.

Behavioral Study

The open field maze (OFM) test has been used to assess general motor activity and anxiety (Gould et al., 2009; Kraeuter et al., 2019). The animals were allowed a habituation period of 45 min to the behavioral test room before the OFM test procedure. A soundproof test room was used. Moreover, the behavioral test was performed under a white noise (80 dB) stimulus to further attenuate sound interference (Henry et al., 2010). Additionally, the light level inside the OFM was maintained at 7–8 lux. Following saline or cocaine administration, animals were immediately placed in the middle [AS4] of the open field, and motor activity was monitored through a video camera positioned above the apparatus. The images were analyzed later with the ANY Maze video tracking (Stoelting Co., Wood Dale, IL, USA) by a researcher who was unaware to which experimental group the animals belonged to. The animals were allowed to move freely in the OFM for 60 min. The OFM evaluation was performed by analyzing the following parameters: (a) total walked distance; (b) mean speed; (c) maximum speed; (d) periphery distance; (e) time spent in the periphery; (f) latency time to center; g) the number of entrances in the center; (h) center distance; and (i) time spent in the center.

Positron Emission Tomography Imaging Study

A metabolic PET scan with ^{18}F-FDG was performed, under basal conditions in fasted animals (6–8 h), to study the cerebral metabolic rate of glucose consumption. The small animal PET scanner used herein was the *easy*PET.3D system. This is a cost-effective benchtop PET system with a simple and unique image acquisition method (Patent, Universidade de Aveiro: WO2016147130), based on the rotation of two detector modules with two degrees of freedom (https://www.ri-te.pt/). This innovative scanning method, in which the detector modules are always face to face, strongly reduces parallax errors, thus simultaneously achieving a great level of detail and spatial resolution. Detector arrays can have different geometries. Each scan can be performed using different parameters to achieve different sensitivity, level of desired detail/speed, or image-specific regions of interest within the field of view (FOV), which is also a unique feature of this technology. The *easy*PET.3D model used in this study has two arrays of ^{162}lutetium–yttrium oxyorthosilicate (LYSO) crystals with a size of 2,230 mm^3 coupled to corresponding arrays of silicon photomultipliers with a 1.3-mm^2 active area, covering an axial FOV of 3.4 cm (length) and a maximum radial FOV of 4.8 cm (diameter).

According to the experimental design (**Figure 1**), awake mice were i.p. injected with ^{18}F-FDG (7.5 MBq/0.4 ml 0.9% NaCl) and placed in their home cages, after the behavioral test. For optimal radiotracer distribution, mice were kept conscious during the uptake period (60 min). Fifty minutes post-radiotracer injection, the animals were anesthetized (i.p.) [0.2 ml of a mixture of ketamine (1.5 mg/mg weight) + chlorpromazine (0.05 mg/mg weight) (3:1):saline (1:1)]. The anesthetized animals were placed on the bed of the *easy*PET.3D scanner, centered in the FOV. The PET imaging acquisition started, taking place during 30 min. A heating apparatus (Heat Therapy Pump, Adroit Medical Systems, Loudon, TN 37774, USA) is connected to the scanner's bed to keep the animals warm.

The data were reconstructed using a dedicated 3D reconstruction method based on a GPU implementation of

the List-Mode Maximum-Likelihood Expectation-Maximization (LM-MLEM) algorithm, considering the original geometry of the *easy*PET.3D scanner and a high number of possible lines of response. The values of the PET image resulting from the reconstruction are expressed as a linear colormap (percent, %). Since cerebral metabolic rates of glucose consumption are reflected by local radiotracer uptake, a qualitative analysis of changes in brain metabolic activity of animals *non-exposed* or *exposed* to a single low dose of cocaine was done. In order to improve the image visualization, the hot metal scale was selected, and a threshold was applied. The Digimouse 3D mouse atlas (http://neuroimage.usc.edu) was applied for anatomical detail. Moreover, the volumes of interest (VOIs) were drawn from the same template co-registered with the PET data using AMIDE software (http://amide.sourceforge.net/). Semi-quantitative measurements of glucose metabolism were obtained using the standardized uptake value (SUV), which is a normalized target-to-background measure. SUV is defined as the regional tissue activity concentration (kBq/ml) normalized for both the decay correction of the injected activity (kBq) and weight of the studied animal (g). Usually, a density equivalent to 1.0 g/ml in tissue is assumed, ensuring that the units effectively cancel and the resulting SUV number becomes dimensionless. In the present study, the mean SUV was obtained, with the respective mean standard error correlated with the VOI. Areas too small to be identified using a microPET system were not included in this analysis.

Histological Study

Macroscopy and microscopy analyses were done for the whole brain and different brain areas. The analyzed specimens were fixed in 10% neutral buffered formalin solution and processed for routine paraffin embedding. Three 4-μm sections were obtained from each block and stained with hematoxylin–eosin technique (H&E) for optical microscopy. The PFC pyramidal neurons, as well as the *hippocampus* (HC) and *cerebellum* (Cb) granular neurons, were counted by computerized image processing (NIS for Windows) (Martinez et al., 2011; Priolli et al., 2013). The number of neuronal cells was obtained as an average of three randomly selected fields of three sections from each animal.

Statistical Analysis

The analysis of the results was performed by adopting a $p < 5\%$ ($p < 0.05$) to reject the null hypothesis, using the following statistical tools: sample size; descriptive statistics; measures of central tendency; normality test; comparison test (*t*-test); and two-way repeated-measures ANOVA followed by Sidak's multiple comparison tests (OFM study). The statistical Package Bioestat version 5.0 for Windows (Brazilian Science and Technology Ministry) was used.

RESULTS

Behavioral Analysis

Exploratory and locomotor activities of mice injected with a low dose of cocaine in an open field apparatus were evaluated. The OFM analysis showed no differences in the behavior of neither group of mice (*non-exposed* or *exposed* to cocaine). All analyzed parameters (including the total, peripheral, and central distance traveled; mean and maximum speed; time spent in the periphery and in the center; and time latency to enter in the center) were not statistically different between groups ($p > 0.05$) (**Figure 2**).

Positron Emission Tomography Imaging Analysis

Figure 3 illustrates the metabolic activity in mice *non-exposed* (saline injection) compared with mice *exposed* to cocaine. Representative ^{18}F-FDG PET images were selected for each group (**Figure 3**). According to the intensity of the colormap selected (hot metal), the presence or absence of abnormal radiotracer accumulation was analyzed. The size and intensity of the uptake region, especially when the accumulation was focal, was also associated. The evaluation of the PET data (SUV) showed no significant differences between the groups (*non-exposed vs. exposed*) for any of the analyzed brain structures, which are typically affected by cocaine (**Figure 4**). Additionally, PET analysis of the entire brain showed no statistically significant alterations between groups (**Figure 4**).

Histological Analysis

Histological analysis of PFC, HC, and Cb were also performed in mice *non-exposed* and *exposed* to cocaine (**Figure 5**). No histological differences between groups were found for the Cb. On the contrary, morphological lesions were found in the PFC of mice *exposed* to cocaine, ranging from mild gliosis up to ischemic tissue necrosis. Additionally, histological analysis showed morphological deterioration and low neural count in PFC and HC in all animals exposed to cocaine. It is also noteworthy that the HC granular layer of the group *exposed* to a single low dose of cocaine was clearly distinct from that of controls.

DISCUSSION

Acute exposure to cocaine in humans includes euphoria, high self-confidence, motor arousal, restlessness, increased sensory perceptions, mood changes, irritability, impulsivity, anxiety, fear, paranoia, and avoidance (Silva et al., 2008). These symptoms are dependent upon the extension of cocaine impact to affected brain areas (Gallucci Neto et al., 2005). Although there is a robust body of literature regarding acute high doses of cocaine, as well as cocaine addiction scenarios, an integrated analysis of behavioral, metabolic, and structural brain changes associated with an acute low dose of cocaine is lacking.

Herein, the locomotor and exploratory behaviors associated with a low dose of cocaine using an OFM test were firstly analyzed. The presented behavioral data suggest that this cocaine dose (0.5 mg/kg) did not change either the locomotor or exploratory behaviors. It is well-known that this psychostimulant increase dose dependently the locomotor activity in different mice and rat strains (3–56 mg/kg) (Thomsen and Caine, 2011). For example, cocaine doses ranging from 1 to 20 mg/kg (Barr et al., 2020; Romero-Fernandez et al., 2020) have been shown to elicit psychomotor activating effects. da Silveira et al. (2018) also

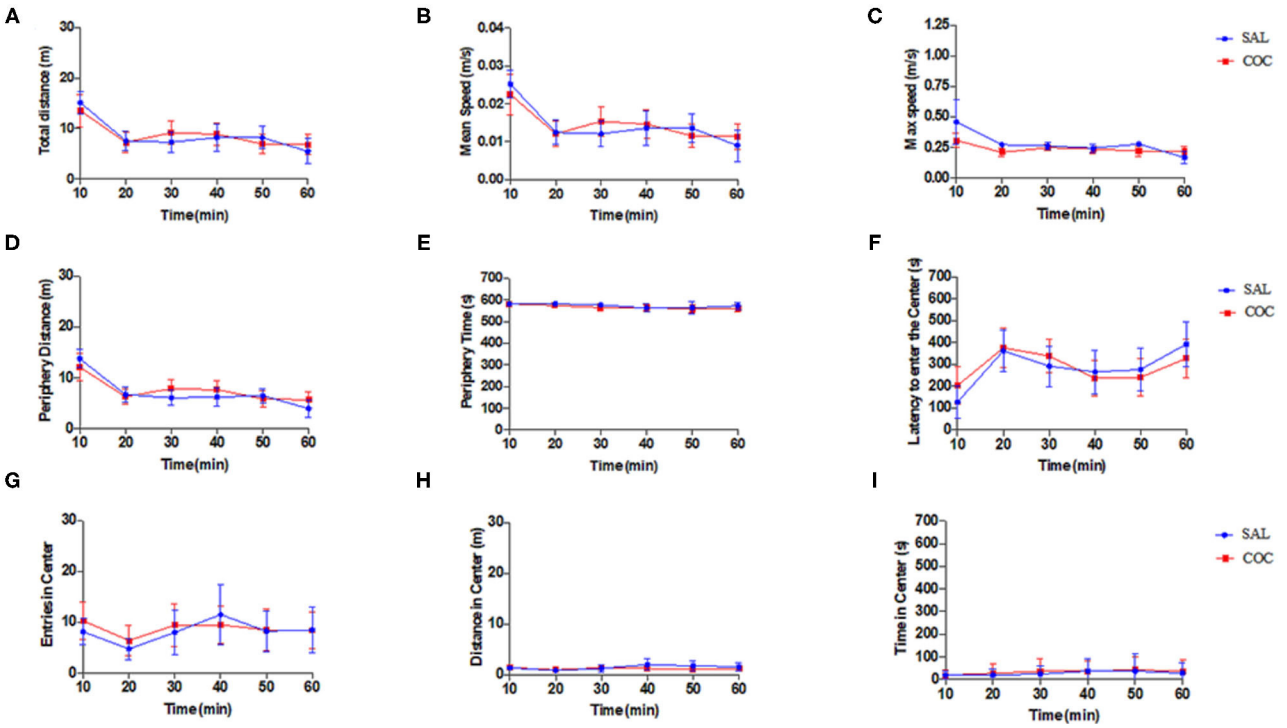

FIGURE 2 | Open field behavior study. Mice *non-exposed* (saline injection, $n = 8$) and mice *exposed* (cocaine injection, $n = 10$) had similar behavioral parameters (two-way repeated-measures ANOVA followed by Sidak's multiple comparison tests): **(A)** total distance (m); **(B)** mean speed (m/s); **(C)** maximum speed (m/s); **(D)** periphery distance (m); **(E)** periphery time (s); **(F)** latency to enter the center (s); **(G)** entries in center; **(H)** distance in center (m); and **(I)** time in center (s). Data represent mean ± standard error of the mean.

showed that 10 mg/kg of cocaine (but not lower doses including 2.5 and 5 mg/kg) increased the distance traveled by male Swiss mice in the open field (da Silveira et al., 2018). Moreover, it was further shown that the threshold dose of cocaine that significantly stimulated forward locomotion of rats in an open field arena was 10 mg/kg (Baumann et al., 2013). In the present study, 0.5 mg/kg was used (which is 20 times lower); therefore, it should not cause any locomotor or exploratory effect (the behavioral parameters evaluated in the open field arena). Thus, the absence of locomotor behavioral changes seen herein was expected. There is less information regarding the behavioral effects of cocaine in Balb-c mice, which is the strain used herein. It has been shown that 20 and 40 mg/kg of cocaine acutely induced locomotor activity in an open field arena for this mouse strain (Kosten et al., 2014; Murthy et al., 2014). However, the emotional and cognitive behaviors associated with cocaine for this mouse strain remain to be characterized. This should be done in future investigations.

The ^{18}F-FDG PET imaging study performed herein showed no significant differences between controls and mice *exposed* to a single low dose of cocaine. This could be explained by the very low cocaine dose used. The experimental design could also be responsible for the absence of alteration in the PET analysis. In fact, PET-FDG images were acquired 1 h 50 min post-cocaine injection. It is noteworthy that it has been demonstrated that after i.p. injection of either 10 or 25 mg/kg of cocaine to mice, cocaine disappeared from the plasma and brain with a half-life of 16 min (Benuck et al., 1987). Therefore, the lack of metabolic changes that are seen here may reflect cocaine pharmacokinetics. In fact, this PET analysis may have been performed at a time point where there were only vestigial plasmatic cocaine levels. There are only a few studies looking at acute pharmacological effects of cocaine on rodent brain glucose metabolism. An acute intravenous administration of cocaine (0.75 mg/kg) decreased metabolic glucose rates in discrete brain areas (cortical and basal ganglia regions) of C57Bl/6 and DBA/2 awake mice (Zocchi et al., 2001). Nonetheless, the distribution pattern of these changes is different between the two strains. Briefly, in the referred study, rodents were sequentially intravenously injected with cocaine and with 2-[^{14}C]deoxyglucose. Animals were sacrificed 40 min after the administration of the tracer, and brains were collected for glucose consumption assessment. These results are aligned with the findings in primates, also obtained using the quantitative 2-[^{14}C]deoxyglucose method (Lyons et al., 1996). In fact, intravenous infusion of 1 mg/kg of cocaine acutely decreased glucose consumption in discrete brain structures including the interconnected limbic regions, such as ventral prefrontal cortex and ventral striatal complex in awake *Cynomolgus* monkeys. More recently, a PET-[^{18}F]-FDG approach showed that cocaine (1 mg/kg) acutely increased metabolism in the prefrontal cortex, but not in the striatum of *Rhesus* monkeys in the cocaine-naïve

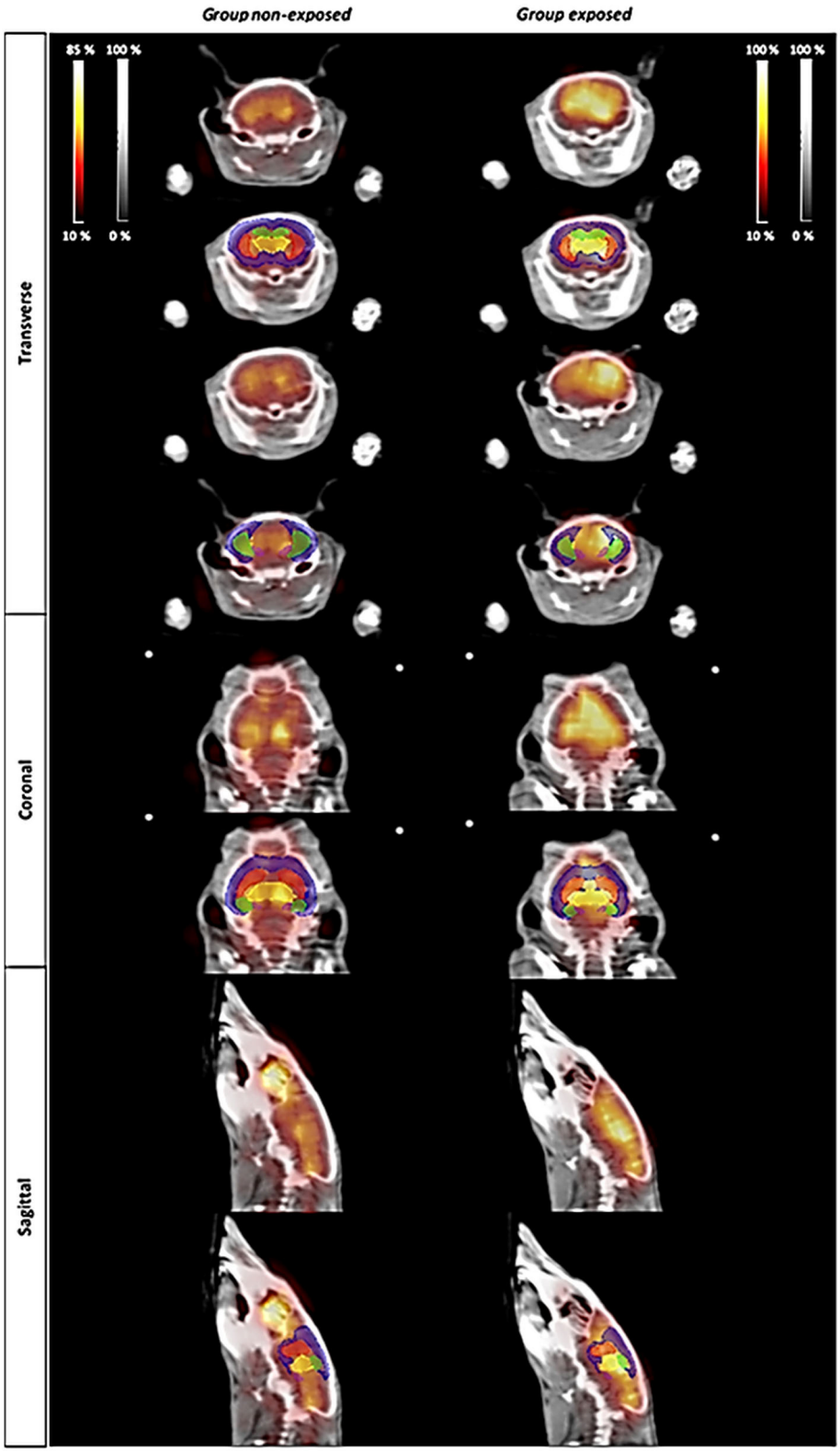

FIGURE 3 | PET imaging study. Changes in metabolic activity in animals *non-exposed* (controls) and *exposed* to a single dose of cocaine (0.5 mg/kg). The atlas-derived volumes of interest (VOIs) of the main areas commonly affected by cocaine are shown superimposed on transverse, coronal, and sagittal image slices of mice brain from both representative ^{18}F-FDG PET studies and CT derived from Digimouse 3D atlas. VOIs: prefrontal cortex (PFC, blue), *striatum* (St, red), *hippocampus* (HC, green), *thalamus* (TH, yellow), and *amygdala* (AMY, pink).

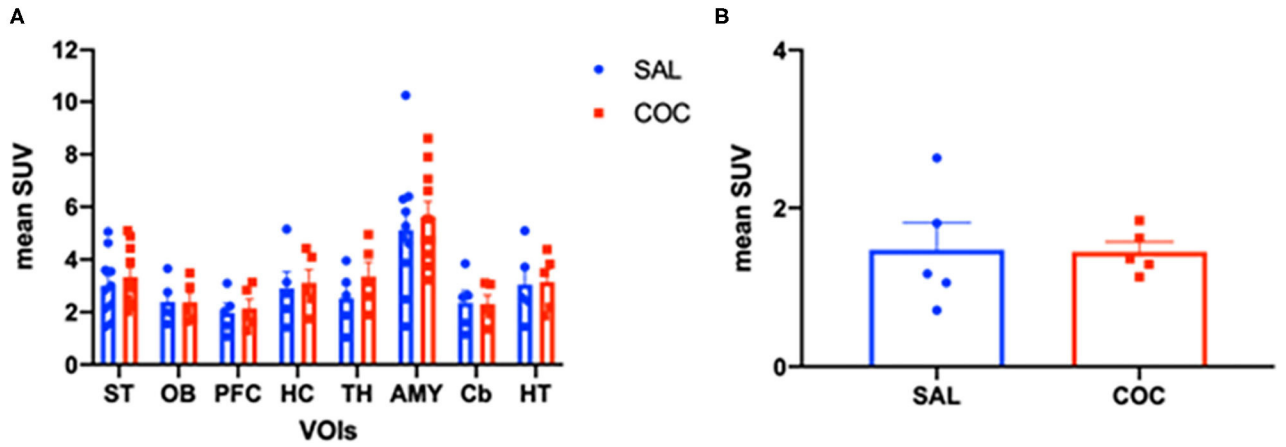

FIGURE 4 | Bar graph of the statistical analysis of standardized uptake value (SUV) in animals *non-exposed* and *exposed* to a single low dose of cocaine. **(A)** SUV analysis of the following brain regions: *striatum* (ST), olfactory bulb (OB), prefrontal cortex (PFC), *hippocampus* (HC), *amygdala* (AMY), *cerebellum* (Cb), and *hypothalamus* (HT). **(B)** Metabolic all-brain analysis. Note the absence of metabolic changes. Data represent mean ± standard error of the mean.

state (Henry et al., 2010). These authors co-injected cocaine and [^{18}F]-FDG and performed a static PET scan starting 40 min post-injection (image acquisition during 30 min). These apparently discrepant results may, however, highlight that cocaine acutely recruits cortical and subcortical regions and changes their metabolism in different species. Nonetheless, other studies are needed to see whether these metabolic alterations are long-lasting (e.g., 24, 48, 72 h, or 1 week later). Additionally, cocaine-induced activation was shown to be far less robust following withdrawal in a cocaine self-administration setting (Henry et al., 2010). This suggests that a history of cocaine use may impact the acute metabolic effects of cocaine. Finally, this absence of metabolic changes seems consistent with the lack of locomotor behavioral changes. In this context, the authors are already planning to perform PET scan analysis immediately after cocaine i.p. injection to examine its immediate pharmacological effects on glucose consumption.

Notably, cocaine induced histological alterations in PFC and HC, which are suggestive of mild gliosis up to ischemic tissue necrosis (**Figure 5**). Both PFC and HC have a crucial role in drug addiction processes, throughout the regulation of limbic reward regions and their involvement in higher-order executive and cognitive functions (e.g., self-control, salience attribution, and awareness; Goldstein and Volkow, 2011). The histological changes seen in this study raise concerns regarding episodic consumption of low doses of cocaine. Glutamate is the main excitatory neurotransmitter both in PFC and HC. A growing body of evidence suggests that cocaine indirectly influences glutamate transmission (Schmidt and Pierce, 2010). Therefore, one cannot rule out the role of glutamate in the cocaine-induced histological alterations reported here. Regarding the *hippocampus*, CA1 region is structured depthwise in defined layers: *oriens*, *pyramidale*, *radiatum*, and *lacunosum-moleculare.* The cell bodies of horizontal trilaminar cells and inhibitory basket cells are located in the *oriens*. *Pyramidale* layer contains the cell bodies of the pyramidal neurons, which are the main excitatory neurons of the *hippocampus.* This layer also contains the cell bodies of many interneurons, including axo-axonic cells, bistratified cells, and radial trilaminar cells. *Radiatum* layer contains commissural and septal fibers and Schaffer collateral fibers, which are projected to CA1. *Laconosum* is a thin layer and is often grouped with molecular stratum into a single layer named *lacunosum-moleculare layer*. Moreover, it contains Schaffer collateral fibers and perforant path fibers coming from the superficial layers of the entorhinal cortex. *Dentate gyrus* is part of the HC trisynaptic circuit and is thought to contribute to the formation of new episodic memories. This region promotes spontaneous exploration of novel environments, synaptic plasticity, rapid acquisition of spatial memory, and other functions (Saab et al., 2009; Lee et al., 2016). The CA1 and DG are the most sensitive regions to hypoxia, and their examination is mandatory to investigate possible acute neuronal necrosis and gliosis (Liu et al., 2004).

In fact, glial alterations were visible in the present study. The nuclei of glial cells are also recognizable in HE: the nuclei of astrocytes and oligodendrocytes are round, with the first being larger and more loose. The nuclei of the microglia are elongated, comma-shaped, and dense. When there is damage to the nervous tissue, the microglial cells lose their extensions and assume a rounded shape, constituting macrophages with phagocytic capacity. Histological analysis suggests that microglia in the cocaine group have fine foamy cytoplasm since they phagocytize lipids derived from degenerated nervous tissue. In *exposed* cocaine mice, histology showed gemistocytic astrocytes, characterized by abundant and pink cytoplasm and eccentric nuclei. A clear halo around oligodendrocyte nuclei can also be observed (**Figure 5**), suggesting the entry of water into the cells due to hypoxia.

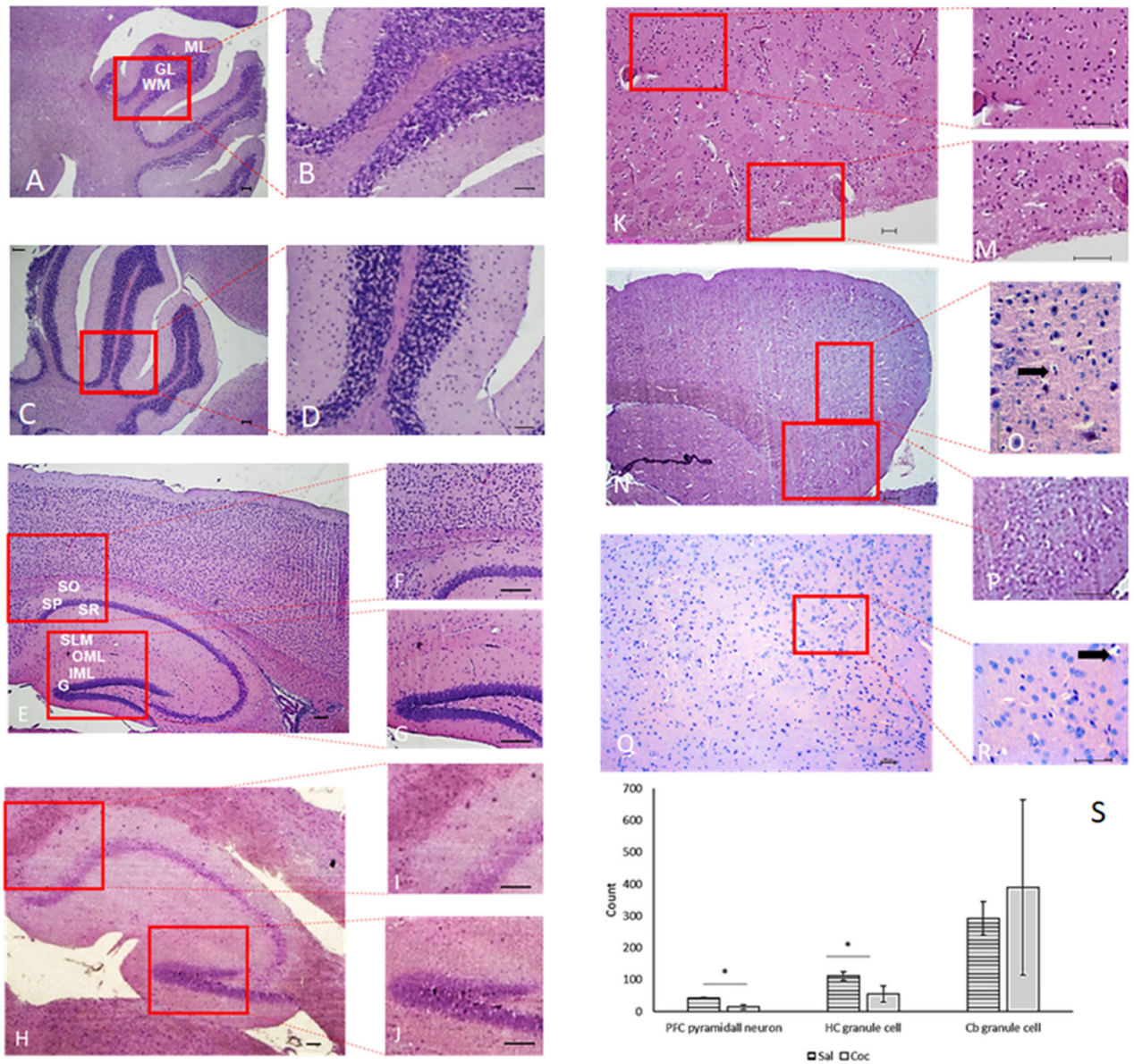

FIGURE 5 | Microphotographs of PFC, HC and Cb. Cb **(A–D)** of saline **(A,B)**, and cocaine **(C,D)** animals. ML, molecular layer; G, granular layers; WM, white matter. Cocaine did not trigger any histopathological changes. HC **(E–J)** of saline **(E–G)**, and cocaine **(H–J)** groups. CA1 region **(F,I)** dentate gyrus **(G,J)**. SO, oriens layer; SP, pyramidal layer; SR, radiatum layer; SLM, lacunosum-moleculare layer; OML, outer molecular layer; IML, inner molecular layer; G, granule cell layer. Animals *exposed* to cocaine show hippocampal histopathological changes in the pyramidal cell layer and granule cell layer in the CA1 region and *dentate gyrus*, respectively, with neuronal loss **(G,H)**. PFC **(K–R)** of saline **(K–M)** and cocaine **(N–R)** groups. Animals depthwise to cocaine present histological changes, including ischemic necrosis **(P,Q)**. Observe (arrow) the clear halo around oligodendrocyte nuclei **(O,R)**. These features demonstrate irreversible hypoxic lesions and the presence of granule-adipose cells **(O,P)**. HandE: **(A**,**C**,**E**,**H**,**K**,**N**,**Q)**, 40×; **(F,G,I,J,L,M,P,R)**, 100×; **(B,D,O)**, 400×. **(S)** The difference between cell numbers in PFC ($p = 0.008$) and HC (*t*-test, n = 6, $p = 0.05$). Data represent mean ± standard deviation of the mean. PFC, prefrontal cortex; HC, hippocampus; Cb, cerebellum. *Significant.

Although there are few experimental studies about the Cb relationship to addictive drug behavior, evidence suggests that cerebellar activation may be involved in functions such as cognition, prediction, learning, and memory, being associated with compulsive and perseverative behaviors (Carbo-Gas et al., 2014; López-Pedrajas et al., 2015; Moreno-Rius and Miquel, 2017). The alterations in Cb resulting from chronic cocaine use have been correlated with its relationship and the maintenance of drug memory. However, despite the evidence of higher cerebellar activation in studies with cocaine, this mechanism

is still unclear (Jiménez-Rivera et al., 2000; Nicastri, 2001; Carbo-Gas et al., 2014; López-Pedrajas et al., 2015; Vazquez-Sanroman et al., 2015). Cb neurons and glia are arranged in layers. The molecular layer is located at the surface and contains the dendrites of Purkinje neurons, axons of granule cells (parallel fibers), fibers of Bergmann glia, basket cells, and stellate cells. The granular cell layer contains granule cells, Golgi cells, Lugaro cells, and unipolar brush cells (Hashimoto and Hibi, 2012). In general, Cb has a characteristic dopaminergic distribution. Dopaminergic fibers, projecting from the ventral tegmental area to the cerebellar cortex, terminate mainly in the granular layer and additionally in the Purkinje cell layer, but not at all in the molecular layer (Ikai et al., 1992). This morphological characteristic can explain the absence of evident histological changes in animals exposed to cocaine. It may be consistent with findings suggesting a relationship between high doses of cocaine and gray matter volume reduction in the Cb (López-Pedrajas et al., 2015). One should stress that the histological alterations did not translate into locomotor and metabolic changes. This suggests that structural changes should be more profound and more widely spread across the brain to trigger functional brain changes. Nevertheless, the animal model presents some limitations, such as the inability to evaluate sociocultural and genetic factors, and personality and psychological traits, which are relevant issues to determine drug addiction development in humans (El Rawas et al., 2020). Future studies need to assess if these structural changes persist (e.g., 24, 48, 72 h, or 1 week later).

Overall, it is shown, for the first time, that a single low dose of cocaine, which did not change locomotor behavior and brain metabolism, has the potential to induce structural neurological damage. There is no safe dose for cocaine exposure. Brain structural changes must be considered regardless of the used dosage. It is essential to alert the population against any consumption, not underestimating acute and recreational dosage since the use, even in a low single dose, can generate structural tissue damage.

DATA AVAILABILITY STATEMENT

The raw data supporting the conclusions of this article will be made available by the authors, without undue reservation.

ETHICS STATEMENT

The animal study was reviewed and approved by the ORBEA (Órgãos Responsáveis pelo Bem-Estar dos Animais (#17/2015) and the DGAV (DIREÇÃO DE SERVIÇOS DE PROTEÇÃO ANIMAL) authorization.

AUTHOR CONTRIBUTIONS

CN and DP: conception of the presented idea. CN: experiment execution (histological analysis, OFM, and PET). MP: experiment execution (OFM and PET). ACS: experiment execution (histological analysis and PET). FR and MP: experiment execution (PET). JR: experiment execution (OFM). ML: experiment execution (histological analysis). CN, DP, and FR: wrote the manuscript. CN, FR, FP, ACS, and DP: interpretation of the results. FP and MB: helped supervise the project. JV, ACS, and DP: supervision of the project. All authors discussed the results and contributed to the final manuscript.

FUNDING

This work was supported by (A) the FAPESP (São Paulo Research Foundation) 2015/07981-2 and 2017/26010-3; (B) the CAPES (Coordenação de Aperfeiçoamento de Pessoal de Nível 327 Superior – Brasil) 88887.176059/2018-00; (C) the project iPET CENTRO-01-0247-FEDER-039880, co-financed by the EU through FEDER; (D) the project i3N, UIDB/50025/2020 and UIDP/50025/2020, financed by national funds through the FCT/MEC; and (E) a grant to FR (SFRH/BD/137800/2018) and PMMC Encarnação (SFRH/BD/143964/2019) through the FCT, Portugal.

REFERENCES

Alavi, A., and Reivich, M. (2002). Guest editorial: the conception of FDG-PET imaging. *Semin. Nucl. Med.* 32, 2–5. doi: 10.1053/snuc.2002.29269

Barr, J. L., Brailoiu, G. C., Abood, M. E., Rawls, S. M., Unterwald, E. M., and Brailoiu, E. (2020). Acute cocaine administration alters permeability of blood-brain barrier in freely-moving rats- Evidence using miniaturized fluorescence microscopy. *Drug Alcohol Depend.* 206:107637. doi: 10.1016/j.drugalcdep.2019.107637

Baumann, M. H., Partilla, J. S., Lehner, K. R., Thorndike, E. B., Hoffman, A. F., Holy, M., et al. (2013). Powerful cocaine-like actions of 3,4-methylenedioxypyrovalerone (MDPV), a principal constituent of psychoactive "bath salts" products. *Neuropsychopharmacology* 38, 552–562. doi: 10.1038/npp.2012.204

Benuck, M., Lajtha, A., and Reith, M. E. (1987). Pharmacokinetics of systemically administered cocaine and locomotor stimulation in mice. *J. Pharmacol. Exp. Ther.* 243, 144–149.

Browndyke, J. N., Tucker, K. A., Woods, S. P., Beauvais, J., Cohen, R. A., Gottschalk, P. C. H., et al. (2004). Examining the effect of cerebral perfusion abnormality magnitude on cognitive performance in recently abstinent chronic cocaine abusers. *J. Neuroimaging* 14, 162–169. doi: 10.1111/j.1552-6569.2004.tb00234.x

Cannella, N., Cosa-Linan, A., Roscher, M., Takahashi, T. T., Vogler, N., Wängler, B., et al. (2017). [^{18}F]-Fluorodeoxyglucose-positron emission tomography in rats with prolonged cocaine self-administration suggests potential brain biomarkers for addictive behavior. *Front. Psychiatry* 8:218. doi: 10.3389/fpsyt.2017.00218

Caprioli, D., Fryer, T. D., Sawiak, S. J., Aigbirhio, F. I., and Dalley, J. W. (2013). Translating positron emission tomography studies in animals to stimulant addiction: promises and pitfalls. *Curr. Opin. Neurobiol.* 23, 597–606. doi: 10.1016/j.conb.2013.04.003

Carbo-Gas, M., Vazquez-Sanroman, D., Gil-Miravet, I., De las Heras-Chanes, J., Coria-Avila, G. A., Manzo, J., et al. (2014). Cerebellar hallmarks of conditioned preference for cocaine. *Physiol. Behav.* 132, 24–35. doi: 10.1016/j.physbeh.2014.04.044

da Silveira, V. T., Röpke, J., Matosinhos, A. L., Issy, A. C., Del Bel, E. A., de Oliveira, A. C., et al. (2018). Effects of the monoamine stabilizer (-)-OSU6162 on locomotor and sensorimotor responses predictive of antipsychotic activity. *Naunyn Schmiedebergs. Arch. Pharmacol.* 391, 761–768. doi: 10.1007/s00210-018-1500-x

Dias, A. C., Ribeiro, M., Dunn, J., Sesso, R., and Laranjeira, R. (2008). Follow-up study of crack cocaine users: situation of the patients after 2, 5, and 12 years. *Subst. Abus.* 29, 71–79. doi: 10.1080/08897070802218125

Dietrich, J.-B., Mangeol, A., Revel, M.-O., Burgun, C., Aunis, D., and Zwiller, J. (2005). Acute or repeated cocaine administration generates reactive oxygen species and induces antioxidant enzyme activity in dopaminergic rat brain structures. *Neuropharmacology* 48, 965–974. doi: 10.1016/j.neuropharm.2005.01.018

El Rawas, R., Amaral, I. M., and Hofer, A. (2020). Social interaction reward: a resilience approach to overcome vulnerability to drugs of abuse. *Eur. Neuropsychopharmacol.* 37, 12–28. doi: 10.1016/j.euroneuro.2020.06.008

European Drug Report (2016). *European Drug Report*. Available online at: https://www.emcdda.europa.eu/edr2016_en (accessed November 15, 2020).

European Drug Report (2020). *European Drug Report 2020*. Available online at: https://www.emcdda.europa.eu/edr2020_en (accessed November 15, 2020).

Gallucci Neto, J., Tamelini, M. G., and Forlenza, O. V. (2005). Diagnóstico diferencial das demências. *Arch. Clin. Psychiatry* 32, 119–130. doi: 10.1590/S0101-60832005000300004

Goldstein, R. Z., and Volkow, N. D. (2011). Dysfunction of the prefrontal cortex in addiction: neuroimaging findings and clinical implications. *Nat. Rev. Neurosci.* 12, 652–669. doi: 10.1038/nrn3119

Gootenberg, P. (2019). *Coca and Cocaine in Latin American History*. Oxford Research Encyclopedia of Latin American History. Oxford: Oxford University Press. doi: 10.1093/acrefore/9780199366439.013.754

Gould, T. D., Dao, D. T., and Kovacsics, C. E. (2009). "The Open Field Test," in *Mood and Anxiety Related Phenotypes in Mice: Characterization Using Behavioral Tests*, ed T. D. Gould (Totowa, NJ: Humana Press), 1–20. doi: 10.1007/978-1-60761-303-9_1

Hammer, R. P., and Cooke, E. S. (1994). Gradual tolerance of metabolic activity is produced in mesolimbic regions by chronic cocaine treatment, while subsequent cocaine challenge activates extrapyramidal regions of rat brain. *J. Neurosci.* 14, 4289–4298. doi: 10.1523/JNEUROSCI.14-07-04289.1994

Hammer, R. P., Pires, W. S., Markou, A., and Koob, G. F. (1993). Withdrawal following cocaine self-administration decreases regional cerebral metabolic rate in critical brain reward regions. *Synapse* 14, 73–80. doi: 10.1002/syn.890140110

Hanlon, C. A., Beveridge, T. J. R., and Porrino, L. J. (2013). Recovering from cocaine: insights from clinical and preclinical investigations. *Neurosci. Biobehav. Rev.* 37, 2037–2046. doi: 10.1016/j.neubiorev.2013.04.007

Hashimoto, M., and Hibi, M. (2012). Development and evolution of cerebellar neural circuits. *Dev. Growth Differ.* 54, 373–389. doi: 10.1111/j.1440-169X.2012.01348.x

Heard, K., Palmer, R., and Zahniser, N. R. (2008). Mechanisms of acute cocaine toxicity. *Open Pharmacol. J.* 2, 70–78. doi: 10.2174/1874143600802010070

Henry, P. K., Murnane, K. S., Votaw, J. R., and Howell, L. L. (2010). Acute brain metabolic effects of cocaine in rhesus monkeys with a history of cocaine use. *Brain Imaging Behav.* 4, 212–219. doi: 10.1007/s11682-010-9100-5

Ikai, Y., Takada, M., Shinonaga, Y., and Mizuno, N. (1992). Dopaminergic and non-dopaminergic neurons in the ventral tegmental area of the rat project, respectively, to the cerebellar cortex and deep cerebellar nuclei. *Neuroscience* 51, 719–728. doi: 10.1016/0306-4522(92)90310-X

Jiménez-Rivera, C. A., Segarra, O., Jiménez, Z., and Waterhouse, B. D. (2000). Effects of intravenous cocaine administration on cerebellar purkinje cell activity. *Eur. J. Pharmacol.* 407, 91–100. doi: 10.1016/S0014-2999(00)00711-1

Kalivas, P. W. (2007). Cocaine and amphetamine-like psychostimulants: neurocircuitry and glutamate neuroplasticity. *Dialogues Clin. Neurosci.* 9, 389–397. Available online at: https://www.ncbi.nlm.nih.gov/pmc/articles/PMC3202508 (accessed November 15, 2020).

Kosten, T. A., Shen, X. Y., Kinsey, B. M., Kosten, T. R., and Orson, F. M. (2014). Attenuation of cocaine-induced locomotor activity in male and female mice by active immunization. *Am. J. Addict.* 23, 604–607. doi: 10.1111/j.1521-0391.2014.12152.x

Kraeuter, A. K., Guest, P. C., and Sarnyai, Z. (2019). The Y-Maze for assessment of spatial working and reference memory in mice. *Methods Mol. Biol.* 1916, 105–111. doi: 10.1007/978-1-4939-8994-2_10

Lee, C.-H., Ryu, J., Lee, S.-H., Kim, H., and Lee, I. (2016). Functional cross-hemispheric shift between object-place paired associate memory and spatial memory in the human hippocampus. *Hippocampus* 26, 1061–1077. doi: 10.1002/hipo.22587

Liu, C. L., Siesjö, B. K., and Hu, B. R. (2004). Pathogenesis of hippocampal neuronal death after hypoxia-ischemia changes during brain development. *Neuroscience* 127, 113–123. doi: 10.1016/j.neuroscience.2004.03.062

López-Pedrajas, R., Ramírez-Lamelas, D. T., Muriach, B., Sánchez-Villarejo, M. V., Almansa, I., Vidal-Gil, L., et al. (2015). Cocaine promotes oxidative stress and microglial-macrophage activation in rat cerebellum. *Front. Cell. Neurosci.* 9:279. doi: 10.3389/fncel.2015.00279

Lyons, D., Friedman, D. P., Nader, M. A., and Porrino, L. J. (1996). Cocaine alters cerebral metabolism within the ventral striatum and limbic cortex of monkeys. *J. Neurosci.* 16, 1230–1238. doi: 10.1523/JNEUROSCI.16-03-01230.1996

Martinez, N. P., Kanno, D. T., Pereira, J. A., Cardinalli, I. A., and Priollo, D. G. (2011). Beta-catenin and E-cadherin Tissue "content" as prognostic markers in left-side colorectal cancer. *Cancer Biomark.* 1, 129–135. doi: 10.3233/DMA-2011-0843

Moreno-López, L., Soriano-Mas, C., Delgado-Rico, E., Rio-Valle, J. S., and Verdejo-García, A. (2012). Brain structural correlates of reward sensitivity and impulsivity in adolescents with normal and excess weight. *PLoS ONE* 7:e49185. doi: 10.1371/journal.pone.0049185

Moreno-Rius, J., and Miquel, M. (2017). The cerebellum in drug craving. *Drug Alcohol Depend.* 173, 151–158. doi: 10.1016/j.drugalcdep.2016.12.028

Murthy, V., Gao, Y., Geng, L., LeBrasseur, N., White, T., and Brimijoin, S. (2014). Preclinical studies on neurobehavioral and neuromuscular effects of cocaine hydrolase gene therapy in mice. *J. Mol. Neurosci.* 53, 409–416. doi: 10.1007/s12031-013-0130-5

Nicastri, S. (2001). Métodos de neuroimagem e abuso de substâncias psicoativas. *Braz. J. Psychiatry* 23, 28–31. doi: 10.1590/S1516-44462001000500009

Nicolas, C., Tauber, C., Lepelletier, F.-X., Chalon, S., Belujon, P., Galineau, L., et al. (2017). Longitudinal changes in brain metabolic activity after withdrawal from escalation of cocaine self-administration. *Neuropsychopharmacology* 42, 1981–1990. doi: 10.1038/npp.2017.109

Niu, F., Liao, K., Hu, G., Sil, S., Callen, S., Guo, M.-L., et al. (2019). Cocaine-induced release of CXCL10 from pericytes regulates monocyte transmigration into the CNS. *J. Cell Biol.* 218, 700–721. doi: 10.1083/jcb.201712011

Pereira, R. B., Andrade, P. B., and Valentão, P. (2015). A comprehensive view of the neurotoxicity mechanisms of cocaine and ethanol. *Neurotox. Res.* 28, 253–267. doi: 10.1007/s12640-015-9536-x

Planeta, C. S., Lepsch, L. B., Alves, R., and Scavone, C. (2013). Influence of the dopaminergic system, CREB, and transcription factor-κB on cocaine neurotoxicity. *Braz. J. Med. Biol. Res.h* 46, 909–915. doi: 10.1590/1414-431X20133379

Priolli, D. G., Canelloi, T. P., Lopes, C. O., Valdívia, J. C., Martinez, N. P., Açari, D. P., et al. (2013). Oxidative DNA damage and β-catenin expression in colorectal cancer evolution. *Int. J. Colorectal. Dis.* 28, 713–722. doi: 10.1007/s00384-013-1688-7

Romero-Fernandez, W., Zhou, Z., Beggiato, S., Wydra, K., Filip, M., Tanganelli, S., et al. (2020). Acute cocaine treatment enhances the antagonistic allosteric adenosine A2A-dopamine D2 receptor-receptor interactions in rat dorsal striatum without increasing significantly extracellular dopamine levels. *Pharmacol. Rep.* 72, 332–339. doi: 10.1007/s43440-020-00069-3

Saab, B. J., Georgiou, J., Nath, A., Lee, F. J. S., Wang, M., Michalon, A., et al. (2009). NCS-1 in the dentate gyrus promotes exploration, synaptic plasticity, and rapid acquisition of spatial memory. *Neuron* 63, 643–656. doi: 10.1016/j.neuron.2009.08.014

Schmidt, H. D., and Pierce, R. C. (2010). Cocaine-induced neuroadaptations in glutamate transmission: potential therapeutic targets for craving and addiction. *Ann. N. Y. Acad. Sci.* 1187, 35–75. doi: 10.1111/j.1749-6632.2009.05144.x

Silva, M. A., Jocham, G., Barros, M., Tomaz, C., and Müller, C. P. (2008). Neurokinin receptor modulation of the behavioral and neurochemical effects of cocaine in rats and monkeys. *Rev. Neurosci.* 19, 101–111. doi: 10.1515/REVNEURO.2008.19.2-3.101

Sordo, L., Indave, B. I., Barrio, G., Degenhardt, L., de la Fuente, L., and Bravo, M. J. (2014). Cocaine use and risk of stroke: a systematic review. *Drug Alcohol Depend.* 142, 1–13. doi: 10.1016/j.drugalcdep.2014.06.041

Thomsen, M., and Caine, S. B. (2011). Psychomotor stimulant effects of cocaine in rats and 15 mouse strains. *Exp. Clin. Psychopharmacol.* 19, 321–341. doi: 10.1037/a0024798

Vazquez-Sanroman, D., Leto, K., Cerezo-Garcia, M., Carbo-Gas, M., Sanchis-Segura, C., Carulli, D., et al. (2015). The cerebellum on cocaine: plasticity and metaplasticity. *Addict. Biol.* 20, 941–955. doi: 10.1111/adb.12223

Volkow, N. D., Fowler, J. S., Wolf, A. P., Hitzemann, R., Dewey, S., Bendriem, B., et al. (1991). Changes in brain glucose metabolism in cocaine dependence and withdrawal. *Am. J. Psychiatry* 148, 621–626. doi: 10.1176/ajp.148.5.621

Volkow, N. D., Wang, G.-J., Fischman, M. W., Foltin, R. W., Fowler, J. S., Abumrad, N. N., et al. (1997). Relationship between subjective effects of cocaine and dopamine transporter occupancy. *Nature* 386, 827–830. doi: 10.1038/386827a0

Zaidi, H. (Ed.). (2014). *Molecular Imaging of Small Animals*. New York, NY: Springer New York. doi: 10.1007/978-1-4939-0894-3

Zocchi, A., Conti, G., and Orzi, F. (2001). Differential effects of cocaine on local cerebral glucose utilization in the mouse and in the rat. *Neurosci. Lett.* 306, 177–180. doi: 10.1016/S0304-3940(01)01898-5

Conflict of Interest: The authors declare that the research was conducted in the absence of any commercial or financial relationships that could be construed as a potential conflict of interest.

frontiers in Neuroscience

ORIGINAL RESEARCH
published: 28 January 2021
doi: 10.3389/fnins.2020.626348

Dynamic Changes of Cytoskeleton-Related Proteins Within Reward-Related Brain Regions in Morphine-Associated Memory

Xixi Yang[1,2†], Yichong Wen[1†], Yuxiang Zhang[1,2,3], Feifei Gao[1,2], Jingsi Yang[1,2], Zhuojin Yang[1,2] and Chunxia Yan[1,2*]*

[1] College of Forensic Medicine, Xi'an Jiaotong University Health Science Center, Xi'an, China, [2] Bio-Evidence Sciences Academy, Western China Science and Technology Innovation Harbor, Xi'an Jiaotong University, Xi'an, China, [3] NHC Key Laboratory of Drug Addiction Medicine, Kunming Medical University, Kunming, China

OPEN ACCESS

Edited by:
Qi Wang,
Southern Medical University, China

Reviewed by:
Luyang Tao,
Soochow University, China
Yan-Wei Shi,
Sun Yat-sen University, China

***Correspondence:**
Yuxiang Zhang
yuxiangzhang@mail.xjtu.edu.cn
Chunxia Yan
yanchunxia@mail.xjtu.edu.cn;
yanchunxia@xjtu.edu.cn

[†] These authors have contributed equally to this work

Specialty section:
This article was submitted to Neuropharmacology, a section of the journal Frontiers in Neuroscience

Received: 05 November 2020
Accepted: 28 December 2020
Published: 28 January 2021

Citation:
Yang X, Wen Y, Zhang Y, Gao F, Yang J, Yang Z and Yan C (2021) Dynamic Changes of Cytoskeleton-Related Proteins Within Reward-Related Brain Regions in Morphine-Associated Memory. Front. Neurosci. 14:626348. doi: 10.3389/fnins.2020.626348

Drug-induced memory engages complex and dynamic processes and is coordinated at multiple reward-related brain regions. The spatiotemporal molecular mechanisms underlying different addiction phases remain unknown. We investigated the role of β-actin, as well as its potential modulatory protein activity-regulated cytoskeletal-associated protein (Arc/Arg3.1) and extracellular signal-regulated kinase (ERK), in reward-related associative learning and memory using morphine-induced conditioned place preference (CPP) in mice. CPP was established by alternate morphine (10 mg/kg) injections and extinguished after a 10-day extinction training, while the withdrawal group failed to extinguish without training. In the nucleus accumbens (NAc), morphine enhanced the level of β-actin and Arc only during extinction, while p-ERK1/2 was increased during both CPP acquisition and extinction phases. In the dorsal hippocampus, morphine induced an upregulation of p-ERK only during extinction, while p-β-actin was elevated during both CPP establishment and extinction. In the dorsal hippocampus, Arc was elevated during CPP formation and suppressed during extinction. Compared with the NAc and dorsal hippocampus, dynamic changes in the medial prefrontal cortex (mPFC) and caudate putamen (CPu) were not very significant. These results suggested region-specific changes of p-β-actin, Arc/Arg3.1, and p-ERK1/2 protein during establishment and extinction phases of morphine-induced CPP. These findings unveiled a spatiotemporal molecular regulation in opiate-induced plasticity.

Keywords: morphine, extinction, β-actin, Arc/Arg31, ERK, NAc, dorsal hippocampus

INTRODUCTION

Drug addiction is a brain disease, defined as compulsive drug use, and characterized by stubborn persistence despite adverse consequences (Hyman, 2005; Zhang et al., 2018). Long-term alterations in brain neural circuits are well known to be responsible for normal appetitive learning and memory processes (Torregrossa et al., 2011). Drug-associated memory is an aberrant memory that shares the

same memory processes with other forms of memories (Liu et al., 2019). The medial prefrontal cortex (mPFC) and hippocampus are involved in memory encoding and storage. The striatum is a subcortical structure in the forebrain, which can be further subdivided into dorsal [caudate putamen (CPu)] and ventral [nucleus accumbens (NAc)], and is implicated in regulating responses to rewarding stimuli (Wang et al., 2019; Bang et al., 2020; Spechler et al., 2020). Exposure to addictive drugs has been shown to induce both structural and functional changes in these brain regions (Kai et al., 2018).

Drug addiction is associated with large mushroom-shaped changes in synaptic plasticity of spines (Rothenfluh and Cowan, 2013). In this regard, cytoskeletal actin is the major structural component of the dendritic spine and has been shown to play a role in synaptic plasticity by maintaining characteristically and highly dynamic transformation through actin rearrangement (Hou et al., 2009). It is thus meaningful that the drug abuse field has focused on drug-induced changes in cytoskeletal protein and its regulatory mechanisms. Recent studies found that the actin cytoskeleton has been shown to be involved in many key neuronal processes by subserving events related to memory at different stages of learning and memory (Lamprecht, 2016; Basu and Lamprecht, 2018; Henneberger et al., 2020; Suratkal et al., 2020). One of the cytoskeletal proteins, β-actin, has already been found to change drastically after morphine administration. Activity-regulated cytoskeletal-associated protein (Arc), or Arg3.1, is an important cytoskeletal protein (Bramham et al., 2010), which is able to maintain F-actin stability and contributes to its polarized elongation by binding to it. Activating the brain-derived neurotrophic factor (BDNF) TrkB receptor, group 1 metabotropic glutamate receptors (mGluR1s), and *N*-methyl-D-aspartate (NMDA) receptors dramatically upregulated Arc transcription. The extracellular signal-regulated kinase (ERK) is a central node of the signaling pathways downstream of these receptors and is required for Arc transcription (Korb and Finkbeiner, 2011). However, their intimate relationship in morphine-induced memory remained to be elucidated.

In the present study, using conditioned place preference (CPP) to measure drug-associated reward memory, we focused on the regulation of drug reward memories by modulating two phases of memory: acquisition and extinction. Besides, we also compared extinction training and withdrawal. Lastly, we explored the effects of actin-related protein expression in different phases of morphine-induced CPP in relevant brain regions.

MATERIALS AND METHODS

Animals and Drugs

Adult male C57BL/6J mice weighing 25–30 g were purchased from Xi'an Jiaotong University Animal Laboratory. Ninety-six mice were housed under constant temperature (22–24°C) and humidity (50–60%) and maintained on a 12-h light/dark cycle (lights on at 8 a.m.). Food and water were available *ad libitum*. All mice were handled individually with a sham intraperitoneal (i.p.) injection once daily for a week. The experimental procedures were approved by Xi'an Jiaotong University Laboratory Animal Administration Committee and conducted in accordance with the Xi'an Jiaotong University Guidelines for Animal Experimentation. Morphine hydrochloride was purchased from First Pharmaceutical Factory of Shenyang (China), dissolved in sterile 0.9% saline, and administered by i.p. injection at a volume of 10 mg/kg.

Behavioral Test

The CPP procedures were similar with previous study with some modifications, and detailed procedures were divided into two phases as shown in **Figure 1**. We focused on two phases of memory, i.e., acquisition and extinction.

Acquisition of Morphine Conditioned Place Preference

After 1 week of habituation, a total of 96 mice randomly divided into two equal groups (n = 48) were used for CPP. On day 1, all mice were placed separately into the apparatus for 15 min with free access to all the compartments, and the amount of time spent in each compartment was measured to assess unconditioned preference. The mice that spent more than 60% (>540 s) of the total time (900 s) for either of the compartments were eliminated from the study. During the conditioning phase (days 2–9), mice in the morphine treatment group were treated once daily from 8:00 a.m. for 8 consecutive days with four cycles of morphine (10 mg/kg, i.p.), then saline (10 ml/kg, i.p.) on alternating days. After the injection of morphine or saline, mice were immediately placed in the white compartment or black compartment for 40 min with sliding door. In the control group, saline was given in all training days with alternating compartment. On the 10th day, the sliding door was removed, and mice were allowed to move freely for 15 min. CPP score was determined by the time spent in morphine-paired compartment minus the time in saline-paired compartment. After the posttest, six mice were eliminated from the morphine group for the lack of formation CPP, while four mice were eliminated from the saline control group for the sharp variation from the baseline test. In addition, data about the moving distance, average velocity, and shuttle times were also collected.

Extinction of Morphine Conditioned Place Preference

In the extinction phase, mice in the morphine group (n = 42) were randomly divided into two groups and respectively underwent two extinction sessions, i.e., *Extinction 1* (days 11–14) and *Extinction 2* (days 16–19). Each session was followed by a test. For training extinction (Training Ext) groups (n = 21), mice were confined to each chamber for 40 min on alternate days with i.p. saline. For withdrawal groups (n = 21), mice were put in their homecage without any treatment. The remaining mice in the saline group (n = 44) were randomly divided into two groups (n = 22) as control of the above two experiment groups separately. Tests for CPP expression were performed after each extinction trial on days 15 and 20 for both groups. The success judgment of extinction training is based on the fact that CPP scores in 2 consecutive days during the extinction period became equal to those on the preconditioning test.

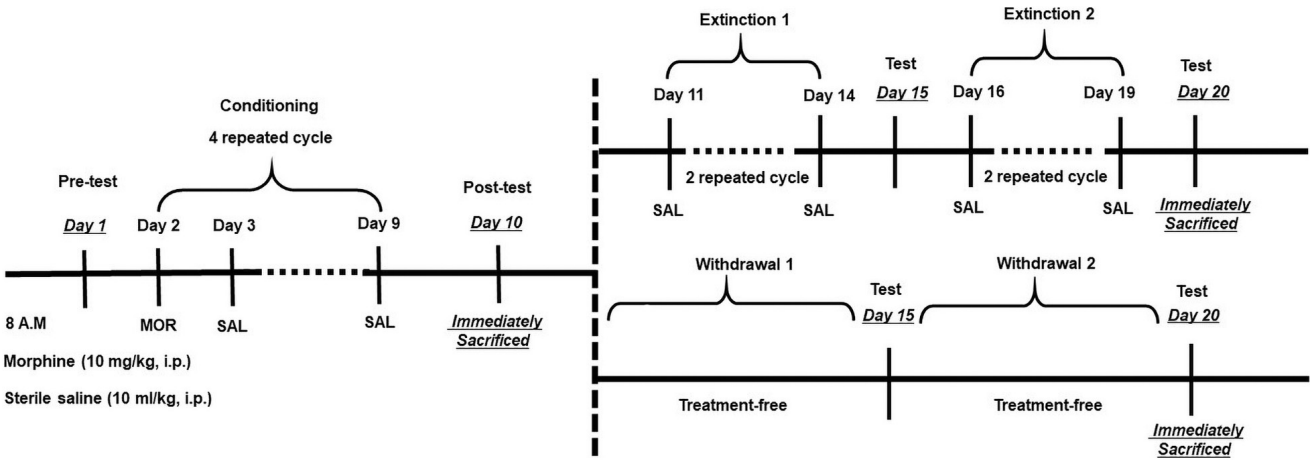

FIGURE 1 | Experimental design for morphine conditioned place preference (CPP) and extinction training. After habituation for 1 week, pretest was performed on Day 1 for an unconditioned place preference. Conditioning period consists of four repeated cycles (Days 2–9), followed by a posttest on Day 10. Then, mice were treated with two kinds of extinction. As for the training extinction group, mice were trained through two trials, Trial 1 (Days 11–14) and Trial 2 (Days 16–19); during extinction trials, mice were placed in one chamber and, on alternate days, the other chamber with both saline [intraperitoneal (i.p.)]. As for the withdrawal group, mice were put in their homecage without any treatment. Tests for CPP expression were performed after each extinction trial on Days 15 and 20. On posttest Day 10 and extinction Day 20, mice were sacrificed by decapitation immediately after the test for protein analysis.

Experimental Procedures for Western Blotting

Animals were divided into three main groups as morphine-induced CPP group (n = 16), training extinction group (n = 16), and withdrawal group (n = 16). Each group consists of CPP acquisition (n = 8) and saline control (n = 8). For saline and morphine-induced CPP groups, animals were sacrificed on day 10, and the training extinction and withdrawal groups were on day 20. Immediately after the test, the NAc, dorsal hippocampus, CPu, and mPFC were dissected out for Western blotting. Tissues were homogenized in an ice-cold radioimmunoprecipitation assay (RIPA) buffer (Pioneer) containing protease phosphatase inhibitor cocktail (Roche). Samples were centrifuged for 20 min at 12,000 rpm at 4°C. Protein concentrations were determined using the bicinchoninic acid (BCA) assay (Pioneer) and analyzed directly by sodium dodecyl sulfate-polyacrylamide gel electrophoresis (SDS-PAGE). Membrane homogenates (10 μg) were loaded in 12% SDS-PAGE gels, transferred onto polyvinylidene fluoride (PVDF) membranes. Membranes were blocked in TBST [Tris-buffered saline (TBS) containing 0.1% Tween 20] containing 5% non-fat dry milk for 2 h. Then, blots were incubated overnight at 4°C with specific antibodies against p-ERK1/2 (1:1,000; Cell Signaling Technology), total ERK1/2 (1:1,000; Cell Signaling Technology), p-Actin (p-Actin, 1:1,000; EMC Biosciences), total β-actin (1:1,000; Santa Cruz), and Arc/Arg3.1 (1:1,000; Proteintech). Then, the PVDF membrane was incubated with goat anti-rabbit or anti-mouse horseradish peroxidase-conjugated secondary antisera (1:10,000) for 120 min. Blots were developed with an enhanced chemiluminescence (ECL) plus detection kit (Millipore Corporation, Bedford, MA, United States). β-Actin was used as a loading control. The blot intensities were analyzed using ImageJ (NIH) to calculate the target protein.

Data Analysis

All behavioral and molecular data were expressed as the mean ± SEM. The data from CPP test were analyzed with Student's t-test, two-way ANOVA; the different protein expression levels were analyzed with one-way ANOVA followed by Bonferroni *post hoc* analysis for multiple comparisons. For results with significant interaction effects in two-way ANOVA, a simple effect test was performed for further analysis. For results without significant interaction effects, Bonferroni *post hoc* test or Student's t-test was further conducted as needed. The data analyses were performed using IBM SPSS statistics 24 and GraphPad Prism 7.0. Statistical significance was set at $p < 0.05$.

RESULTS

Behavioral Experiment

Acquisition of Conditioned Place Preference

As shown in **Figure 2**, two-way ANOVA revealed significant effects of interaction [$F_{(1,84)}$ = 10.66, p = 0.0016], time [$F_{(1,84)}$ = 7.805, p = 0.0065], and group [$F_{(1,84)}$ = 39.78, $p < 0.0001$]. Mice administered 10 mg/kg morphine had significantly higher CPP scores compared to saline-treated mice during posttest. We also measured the moving distance, average velocity, and shuttle times. We did not observe any difference in moving distance and average velocity, suggesting that morphine-induced memory did not influence explorative behavior of mice in the test apparatus. Two-way ANOVA on shuttle times indicated significant effect of time [$F_{(1,84)}$ = 20.11, $p < 0.0001$] but no significant effect of interaction [$F_{(1,84)}$ = 0.2481, p = 0.6197] or morphine [$F_{(1,84)}$ = 3.615, p = 0.0607]. T-test showed that shuttle times in the posttest were dramatically decreased in both saline–treated (t_{43} = 3.219, p = 0.0024) and

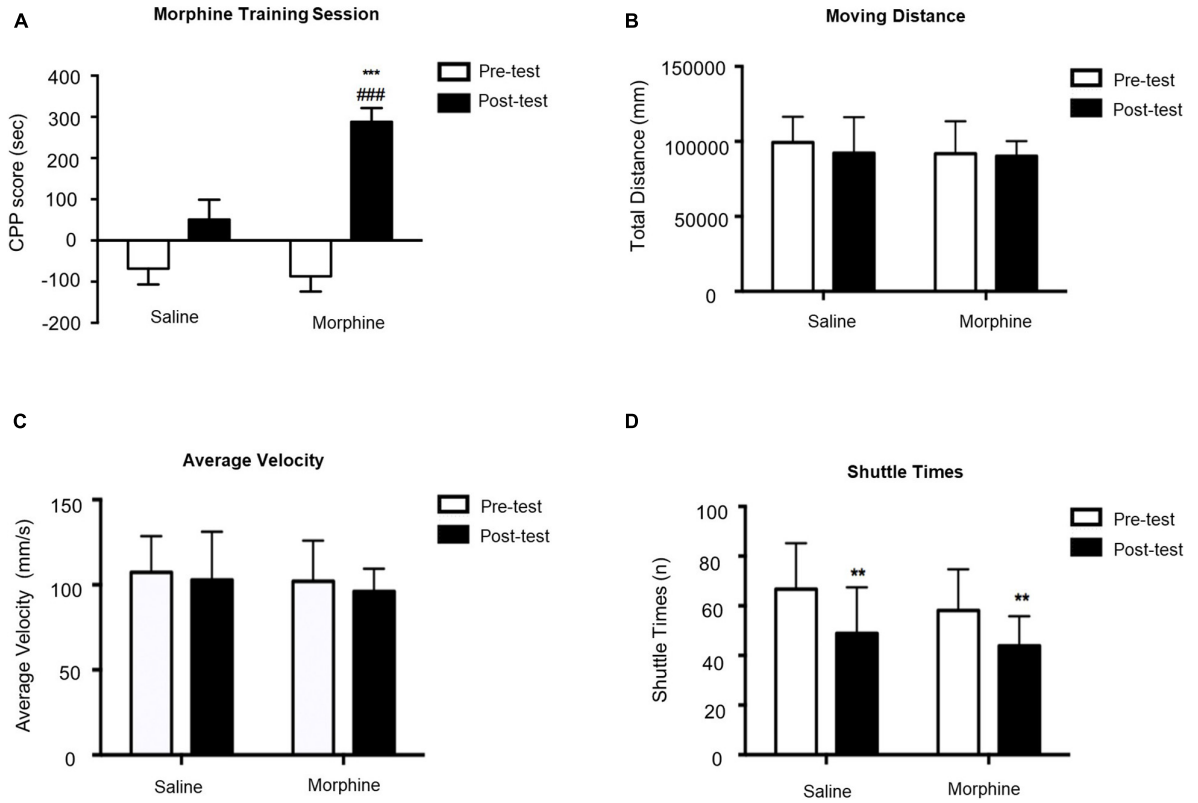

FIGURE 2 | Morphine-induced conditioned place preference (CPP) acquisition on Day 10. **(A)** CPP score of pretest (Day 1) and posttest (Day 10). **(B)** Moving distance of pretest and posttest. **(C)** Average velocity of pretest and posttest. **(D)** Shuttle times of pretest and posttest. $^{**}p < 0.01$ and $^{***}p < 0.001$ compared to the pretest; $^{###}p < 0.001$ compared to the posttest.

morphine-treated ($t_{41} = 3.193$, $p = 0.0027$) mice, suggesting their familiarity to the apparatus.

Extinction of Conditioned Place Preference

As shown in **Figure 3A**, mice with morphine-induced CPP went through the first extinction session with two different methods (training extinction vs. withdrawal extinction). No significant difference was observed between posttest and Extinction 1 in either training extinction groups ($p > 0.05$) or Withdrawal groups ($p > 0.05$), implying that the CPP still existed after the first extinction session. Additionally, the locomotion parameters were also monitored in all groups. As illustrated in **Figures 3B,C**, there were no significant differences in moving distance and average velocity, which revealed that the morphine-induced CPP and training extinction procedures did not affect the explorative behavior and general activity. Similar to CPP acquisition phase, two-way ANOVA on shuttle times, as shown in **Figure 3D**, revealed significant difference of time [$F_{(2,84)} = 17.46$, $p < 0.0001$] but non-significant effect of interaction [$F_{(6,84)} = 1.306$, $p = 0.2633$] or group [$F_{(3,84)} = 1.305$, $p = 0.2748$]. In the posttest, the decrease of shuttle times in the four groups revealed that the mice were more familiar with the test apparatus. In the first extinction session, the shuttle times in the training extinction group were basically unchanged, while those in the withdrawal group increased significantly with the constant total moving distance, indicating that morphine-induced memory was toward fading. Although the shuttle times may reveal a drug-related phenotype to some extent, it was not readout of drug-related memory. Therefore, there was a modest trending decrease of the CPP score during Extinction 1 in both groups.

As illustrated in **Figure 4**, mice with morphine-induced CPP went through the second extinction session in two different methods. CPP was extinguished in the training extinction group after two sessions of extinction, as *post hoc* test revealed a significant difference in CPP score between the second extinction and the posttest ($p < 0.001$). In contrast, withdrawal group showed no significant differences compared to the first extinction, implying that the CPP still existed by the end of the second extinction session ($p > 0.05$). In addition, the locomotion parameters did not change significantly in different phases of morphine-induced CPP of each group.

Western Blotting Analysis

We evaluated the p-β-actin/β-actin ratio, Arc expression level, and p-ERK/ERK ratio in different brain regions during the different phases of morphine CPP. We also compared protein expression after two different methods of extinction test. Since all the control groups in the three different experimental

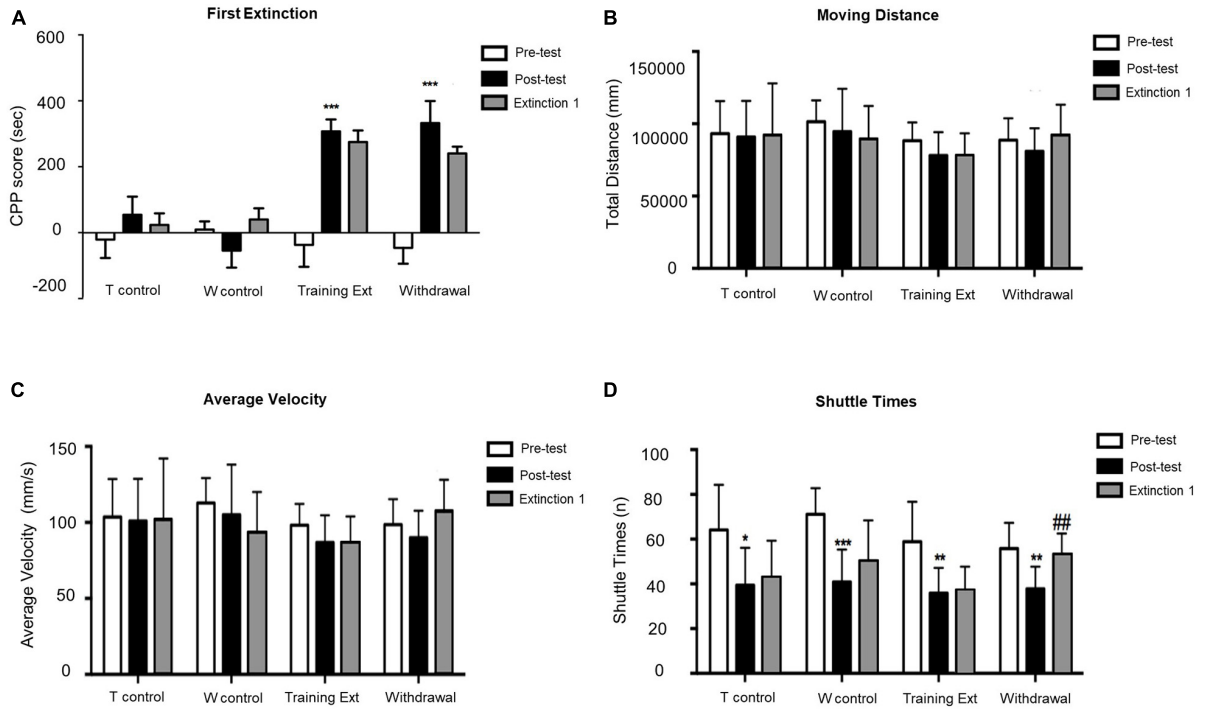

FIGURE 3 | Morphine-induced conditioned place preference (CPP) was not extinguished after the first extinction session (Extinction 1). **(A)** CPP score of pretest (Day 1), posttest (Day 10), and extinction 1 test (Day 15). **(B)** Moving distance of pretest (Day 1), posttest (Day 10), and extinction 1 test (Day 15). **(C)** Average velocity of pretest (Day 1), posttest (Day 10), and extinction 1 test (Day 15). **(D)** Shuttle times of pretest (Day 1), posttest (Day 10), and extinction 1 test (Day 15). The Training Control group (*T control*) went through the same procedures as the Training Extinction group (*Training Ext*) except that the *T control* only received saline without morphine during conditioning; the Withdrawal Control group (*W control*) went through the same procedures as the *Withdrawal* group except that the *W control* only received saline without morphine during conditioning. $^{*}p < 0.05$ compared to the pretest; $^{**}p < 0.01$ compared to the pretest; $^{***}p < 0.001$ compared to the pretest; $^{\#\#}p < 0.01$ compared to the posttest. n = 6–12 mice/group.

groups were essentially the same, we used the control of morphine-induced CPP group as a representative to simplify the data analysis.

Alterations of p-β-actin/β-actin Ratio, Arc Expression, and p-ERK/ERK Ratio in the Nucleus Accumbens at Different Phases of Morphine-Induced Conditioned Place Preference

Activation of striatal neurons critically contributes to drug-associated memories, so firstly, we examined the protein expression in NAc. The red dotted line shown in **Figure 5A** indicated the dissection of samples from the NAc. As shown in **Figure 5B**, one-way ANOVA followed by Bonferroni test showed that the increase of p-β-actin/β-actin ratio [$F_{(3,20)} = 22.05$, $p < 0.0001$] in the training extinction group ($p < 0.001$) was more considerable than that of the withdrawal group ($p < 0.01$) compared to the CPP group. As illustrated in **Figure 5C**, the expression of Arc level [$F_{(3,20)} = 9.270$, $p = 0.0005$] did not change significantly in morphine-induced CPP group ($p > 0.05$) compared to the saline control, while it was remarkably upregulated in both the training extinction group and withdrawal group ($p < 0.001$) compared to the CPP group. Notably, the Arc alteration level tended to be consistent between the training extinction group and withdrawal group. As shown in **Figure 5D**, compared to saline control ($p < 0.001$), the p-ERK/ERK ratio dramatically increased after morphine exposure [$F_{(3,20)} = 11.76$, $p = 0.0001$]. Furthermore, after extinction training, the p-ERK/ERK ratio was further upregulated ($p < 0.001$). Taken together, our data indicated that morphine strongly regulated specific protein in the NAc.

Alterations of p-β-actin/β-actin Ratio, Arc Expression Level, and p-ERK/ERK Ratio in the Dorsal Hippocampus at Different Phases of Morphine-Induced Conditioned Place Preference

The red dotted line shown in **Figure 6A** indicated the dorsal hippocampus region, where we extracted bilateral brain tissue for experiments. As illustrated in **Figure 6B**, one-way ANOVA [$F_{(3,20)} = 39.32$, $p < 0.0001$] followed by Bonferroni test showed that p-β-actin/β-actin ratio in the morphine-induced CPP group was remarkably increased ($p < 0.001$) compared to its control group. The increase in training extinction was also significant ($p < 0.001$) compared to the CPP group, while in the withdrawal group, the ratio showed no significant change ($p > 0.05$). One-way ANOVA comparing protein levels of Arc showed a significant effect [$F_{(3,20)} = 14.28$, $p < 0.0001$]. Bonferroni test revealed that the Arc protein in the CPP group showed a noteworthy increase ($p < 0.001$) than that in the control

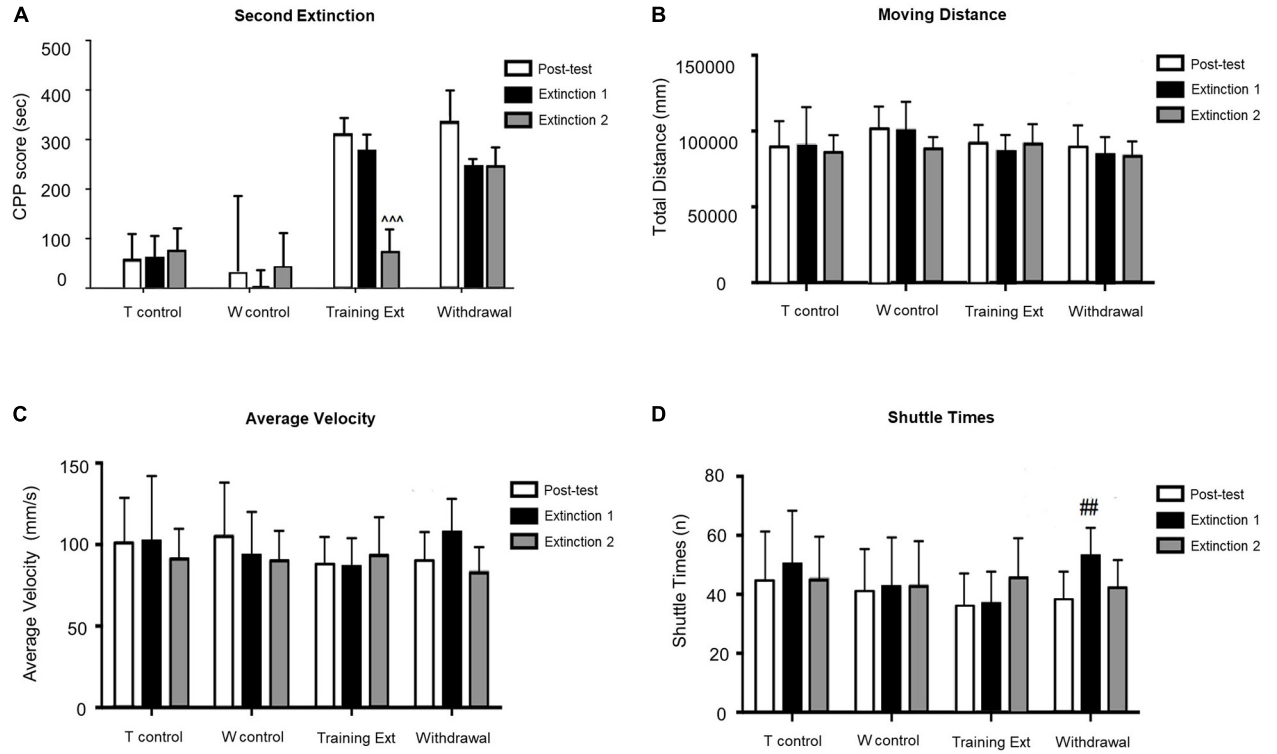

FIGURE 4 | Morphine-induced conditioned place preference (CPP) was extinguished after the second extinction session (Extinction 2) in the extinction training group, but not in the withdrawal group. **(A)** CPP score of posttest (Day 10), extinction 1 test (Day 15), and extinction 2 test (Day 20). **(B)** Moving distance of each test. **(C)** Average velocity of each test. **(D)** Shuttle times of each test. The Training Control group (*T control*) went through the same procedures as the Training Extinction group (*Training Ext*) except that the *T control* only received saline without morphine during conditioning; the Withdrawal Control group (*W control*) went through the same procedures as the *Withdrawal* group except that the *W control* only received saline without morphine during conditioning. $^{\wedge\wedge\wedge}p < 0.001$ compared to the posttest; $^{\#\#}p < 0.01$ compared to the posttest. n = 6–12 mice/group.

group. After two training extinction sessions, the protein level showed a remarkable decrease ($p < 0.05$) compared to the CPP phase. Besides, the protein level in the withdrawal group was significant higher ($p < 0.05$) than that in the training extinction group, as shown in **Figure 6C**. One-way ANOVA comparing protein levels of p-ERK/ERK ratio demonstrated a significant effect [$F_{(3,20)} = 43.78$, $p < 0.0001$], as shown in **Figure 6D**. The increase in both extinction groups showed a significant difference compared to that of the CPP group ($p < 0.001$).

Alterations of p-β-actin/β-actin Ratio, Arc Expression Level, and p-ERK/ERK Ratio in the Medial Prefrontal Cortex at Different Phases of Morphine-Induced Conditioned Place Preference

The red dotted line shown in **Figure 7A** indicated the dissection of samples from the mPFC. As demonstrated in **Figure 7B**, one-way ANOVA [$F_{(3,20)} = 45.32$, $p > 0.05$] followed by Bonferroni test showed that p-β-actin/β-actin ratio in four different groups had no significant effect in the mPFC, as well as Arc expression level [$F_{(3,20)} = 39.89$, $p > 0.05$] shown in **Figure 7C**. As for p-ERK/ERK ratio [$F_{(3,20)} = 16.15$, $p > 0.05$], only the withdrawal group showed a significant increase ($p < 0.05$) compared to the training extinction group, as shown in **Figure 7D**.

Alterations of p-β-actin/β-actin Ratio, Arc Expression Level, and p-ERK/ERK Ratio in the Caudate Putamen at Different Phases of Morphine-Induced Conditioned Place Preference

Lastly, we measured the protein expression in the CPu. **Figure 8A** indicated the range of brain tissue extracted. One-way ANOVA [$F_{(3,20)} = 22.16$, $p < 0.05$] followed by Bonferroni test indicated that the increase of p-β-actin/β-actin ratio in the training extinction showed a dramatic increase compared to the saline group in the CPu ($p < 0.05$), as shown in **Figure 8B**. As for Arc expression level [$F_{(3,20)} = 11.59$, $p > 0.05$] and p-ERK/ERK ratio [$F_{(3,20)} = 3.79$, $p > 0.05$], no significant difference was observed in the four groups, as shown in **Figures 8C,D**.

DISCUSSION

The striatum, which was commonly divided into the dorsal part (CPu) and ventral part (NAc) based on anatomical localization, receives a prominent source of glutamatergic innervation from mPFC and hippocampus (Gonzales and Smith, 2015). Mounting evidence has demonstrated that these brain regions have been implicated in drug-associated memory

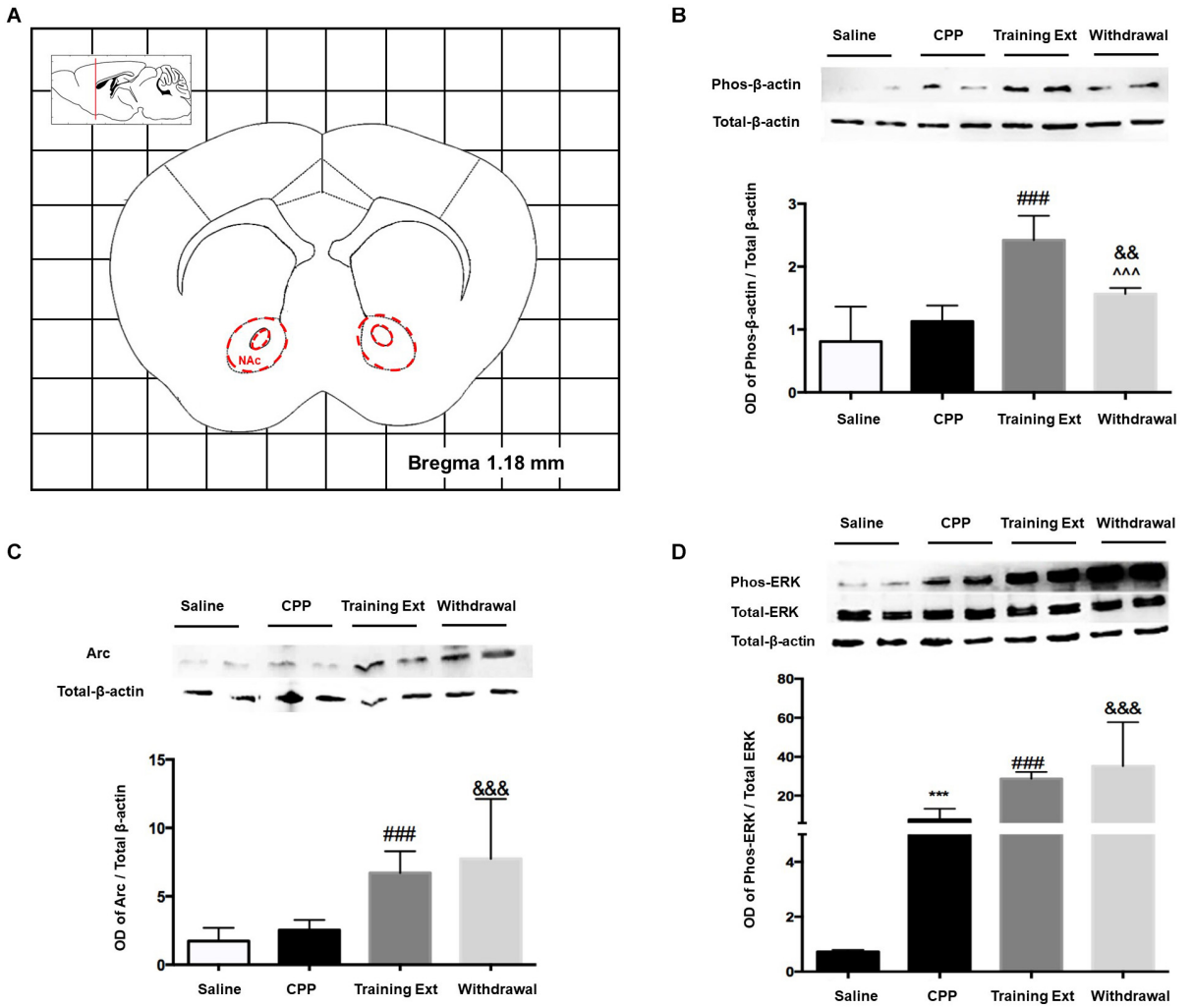

FIGURE 5 | Alterations of the p-β-actin/β-actin ratio, Arc expression level, and p-ERK/ERK ratio in the nucleus accumbens (NAc) at different phases of the morphine-induced conditioned place preference (CPP). **(A)** Red letters and red dotted line in the coronal section inset indicate the dissection of samples from the NAc. Effects of different morphine-induced CPP phases on the **(B)** p-β-actin/β-actin ratio, **(C)** Arc expression level, and **(D)** p-ERK/ERK ratio in the NAc. The animals in the *Saline* or *CPP* group were sacrificed on posttest Day 10, while those in the Training Extinction group (*Training Ext*) and *Withdrawal* groups were sacrificed on Day 20. The *Training Ext* went through CPP procedures followed by saline injections in the training extinction; the *Withdrawal* group went through the CPP procedures followed by spontaneous extinction without any injections. $^{***}p < 0.001$ compared to the saline group; $^{\#\#\#}p < 0.001$ compared to CPP acquisition group; $^{\wedge\wedge\wedge}p < 0.001$ compared to training extinction group; $^{\&\&}p < 0.01$ and $^{\&\&\&}p < 0.001$ compared to CPP acquisition group. n = 6–8 mice/group.

(Arias-Carrion et al., 2010; Torregrossa et al., 2011), and many agents in these regions elicit aberrant drug-associated memory.

Alteration in the Corticostriatal System

Most of the neurons within the striatum are medium spiny neurons. As previous studies have shown, drugs induced morphological changes of dendritic spines after withdrawal from chronic administration by means of modulating the actin cycle dynamic in the NAc (Zhao et al., 2019; Iino et al., 2020). Specifically, the underlying mechanisms are as follows. After withdrawal from repeated cocaine exposure, there was a reduction in the LIM kinase, which could inactivate cofilin, an actin-binding protein that controls the disassembly of actin filaments; alternatively, after chronic cocaine administration, cofilin is released from the inhibitory control of LIM kinase, potentiating the disassembly of actin filaments in individual monomers (Toda et al., 2006). Both pathways could result in an increasing amount of G-actin, specifically, β-actin.

There is, however, a paucity of studies directly investigating the role of β-actin in opiate extinction. Previous study examined dendritic morphology after extinction training in an opiate CPP model and demonstrated a reduction of dendritic complexity (Leite-Morris et al., 2014). These results may seem at odds with the present findings, and the discrepancy may be attributed to two reasons. It is known that cocaine and morphine induce changes in dendritic spine morphology *via* two phases. The first phase is characterized by an initial increase in spine head diameter and increases in AMPA receptor expression,

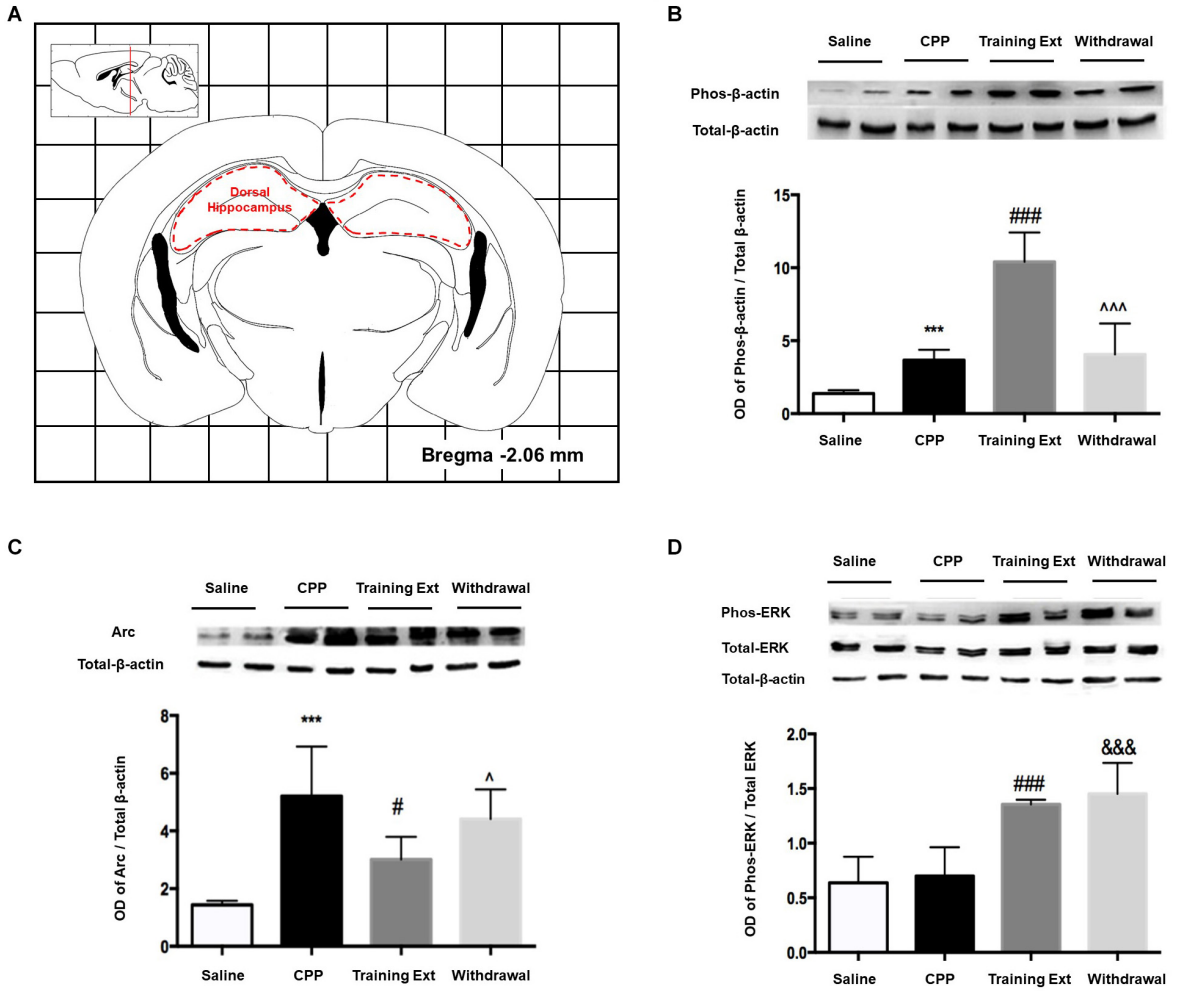

FIGURE 6 | Alterations of the p-β-actin/β-actin ratio, Arc expression level, and p-ERK/ERK ratio in the dorsal hippocampus at different phases of the morphine-induced conditioned place preference (CPP). **(A)** Red letters and red dotted line in the coronal section inset indicate the dissection of samples from the dorsal hippocampus. Effects of different morphine-induced CPP phases on the **(B)** p-β-actin/β-actin ratio, **(C)** Arc expression level, and **(D)** p-ERK/ERK ratio in the dorsal hippocampus. The animals in the *Saline* or *CPP* group were sacrificed on posttest Day 10, while those in the Training Extinction group (*Training Ext*) and *Withdrawal* groups were sacrificed on Day 20. The *Training Ext* went through CPP procedures followed by saline injections in the training extinction; the *Withdrawal* group went through CPP procedures followed by spontaneous extinction without any injections. $^{***}p < 0.001$ compared to the saline group; $^{\#}p < 0.05$ and $^{\#\#\#}p < 0.001$ compared to CPP acquisition group; $^{\wedge}p < 0.05$ and $^{\wedge\wedge\wedge}p < 0.001$ compared to training extinction group; $^{\&\&\&}p < 0.001$ compared to CPP acquisition group. n = 6–8 mice/group.

followed by a second stage of spine head diameter retraction and reduction of the AMPA receptor expression in spines (Quintero, 2013). Our extinction training went through just two trials, almost 10 days from posttest to tissue sampling, while Kimberly A performed three trials, 16 days in total before morphological detection. Thus, the contrasting findings just reflect dendritic spine morphology and actin dynamics at different time points. On the other hand, the reduction in dendritic complexity, characterized by a decreased number of dendritic intersections, shorter total dendritic length, as well as decreased c-Fos protein expression, appears to result primarily from depolymerization of F-actin into monomeric forms, resulting in a transient rise of β-actin, which was observed in our experiment. Hence, we postulated that the relationship between β-actin increase and F-actin formation might not be a simple linear positive correlation.

Previous study has demonstrated that Arc/Arg3.1 protein expression in the NAc core is critical for the acquisition, expression, and reinstatement of morphine CPP (Lv et al., 2011), as well as its role in the NAc shell during the reconsolidation (Lv et al., 2015). However, little is known about the function of this protein in the extinction period of drug-induced long-term memory. The results from our experiments revealed that, when re-exposed to the context after 8 days of extinction training, the significant place preference for the morphine-paired chamber disappeared in the training extinction group but not in the withdrawal group, both of which were accompanied by an increase in Arc/Arg3.1 protein expression in the NAc. The

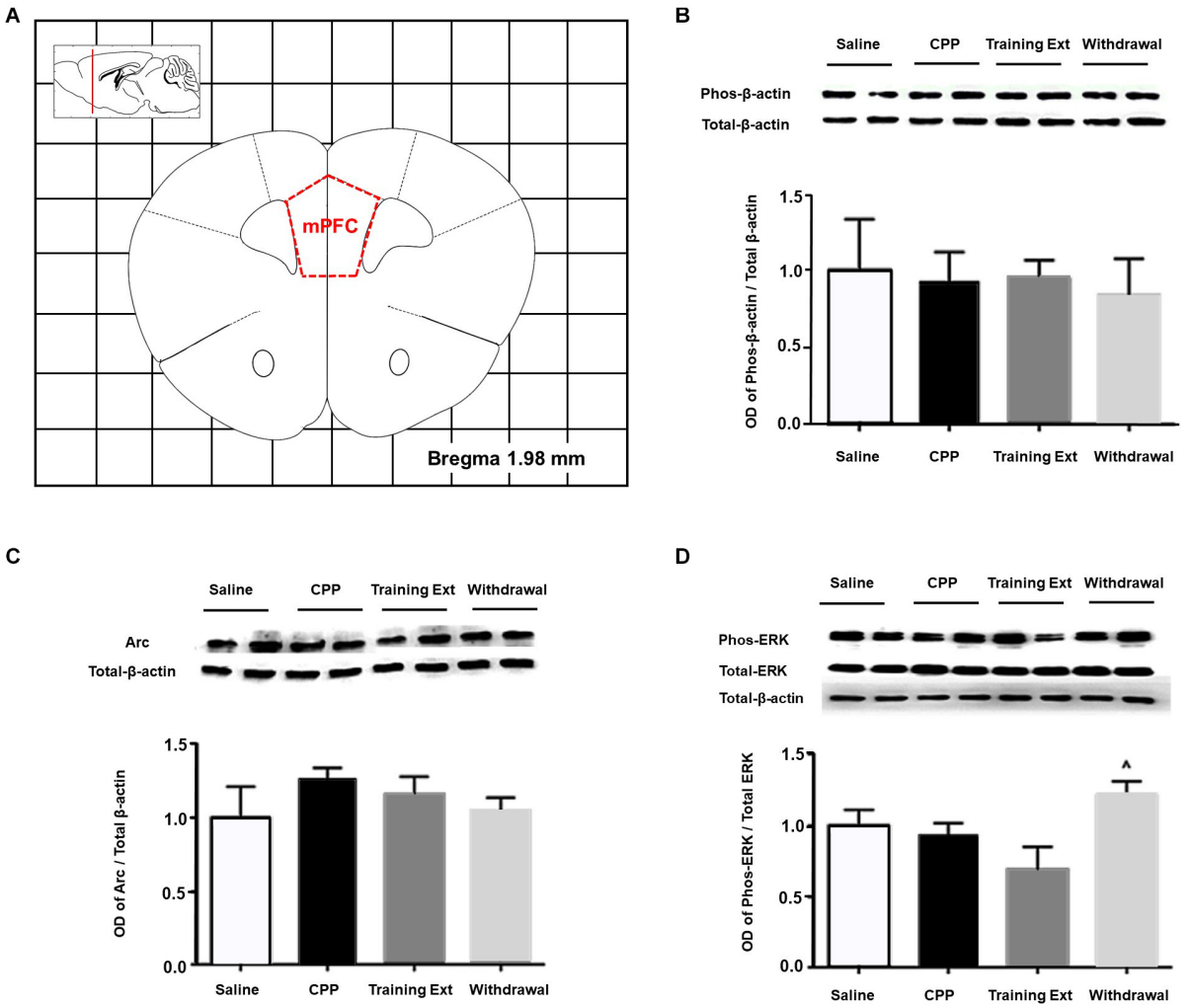

FIGURE 7 | Alterations of the p-βactin/β-actin ratio, Arc expression level, and p-ERK/ERK ratio in the medial prefrontal cortex (mPFC) at different phases of the morphine-induced conditioned place preference (CPP). **(A)** Red letters and red dotted line in the coronal section inset indicate the dissection of samples from the mPFC. Effects of different morphine-induced CPP phases on the **(B)** p-β-actin/β-actin ratio, **(C)** Arc expression level, and **(D)** p-ERK/ERK ratio in the mPFC. The animals in the *Saline* or *CPP* group were sacrificed on posttest Day 10, while those in the Training Extinction group (*Training Ext*) and *Withdrawal* groups were sacrificed on Day 20. The *Training Ext* went through CPP procedures followed by saline injections in the training extinction; the *Withdrawal* group went through CPP procedures followed by spontaneous extinction without any injections. $\hat{}p < 0.05$ compared to *Training Ext*. $n = 6$–8 mice/group.

elevation of Arc/Arg3.1 protein in both groups was in accordance with augmentation of β-actin. Based on these findings, we hypothesized that there might be a positive correlation between Arc/Arg3.1 protein expression and β-actin in the NAc. It is noteworthy that there is no significant increase in the expression of Arc/Arg3.1 after CPP acquisition, while a previous study revealed that reactivation of morphine context memory after the expression test dramatically enhanced the Arc/Arg3.1 protein level, accompanied by increases in p-ERK1/2, specifically in the NAc shell (Lv et al., 2011). This discrepancy is most likely due to the different harvest time points, i.e., immediately after CPP test in the current study vs. 2 h after the expression test in the previous study. The Arc gene belongs to immediate early gene (IEG) group (Fujiki et al., 2020). Similar to other IEGs, such as c-fos, the expression of Arc is temporally specific, as it demonstrated that a single dose of morphine increased Arc/Arg3.1 protein levels in the NAc core 2 h after morphine administration, rather than 1, 3, and 4 h (Lv et al., 2011). The 2-h interval is just for Arc mRNA to selectively target, translate, and be enriched at recently activated synaptic sites (Liu et al., 2012). Translation of the dendritically localized Arc mRNA is required for consolidation of long-term potentiation (LTP) and stabilization of nascent polymerized actin, which are believed to underlie synaptic plasticity in long-term memory (Bramham, 2008).

Abuse of drugs, including morphine and cocaine, increased ERK phosphorylation in the NAc (Valjent et al., 2004; Xu et al., 2012). Consistent with these reports, our results showed that an upregulation of p-ERK1/2 was observed during the establishment phase and extinction phase, including training extinction group and withdrawal group. Slightly different from the researches

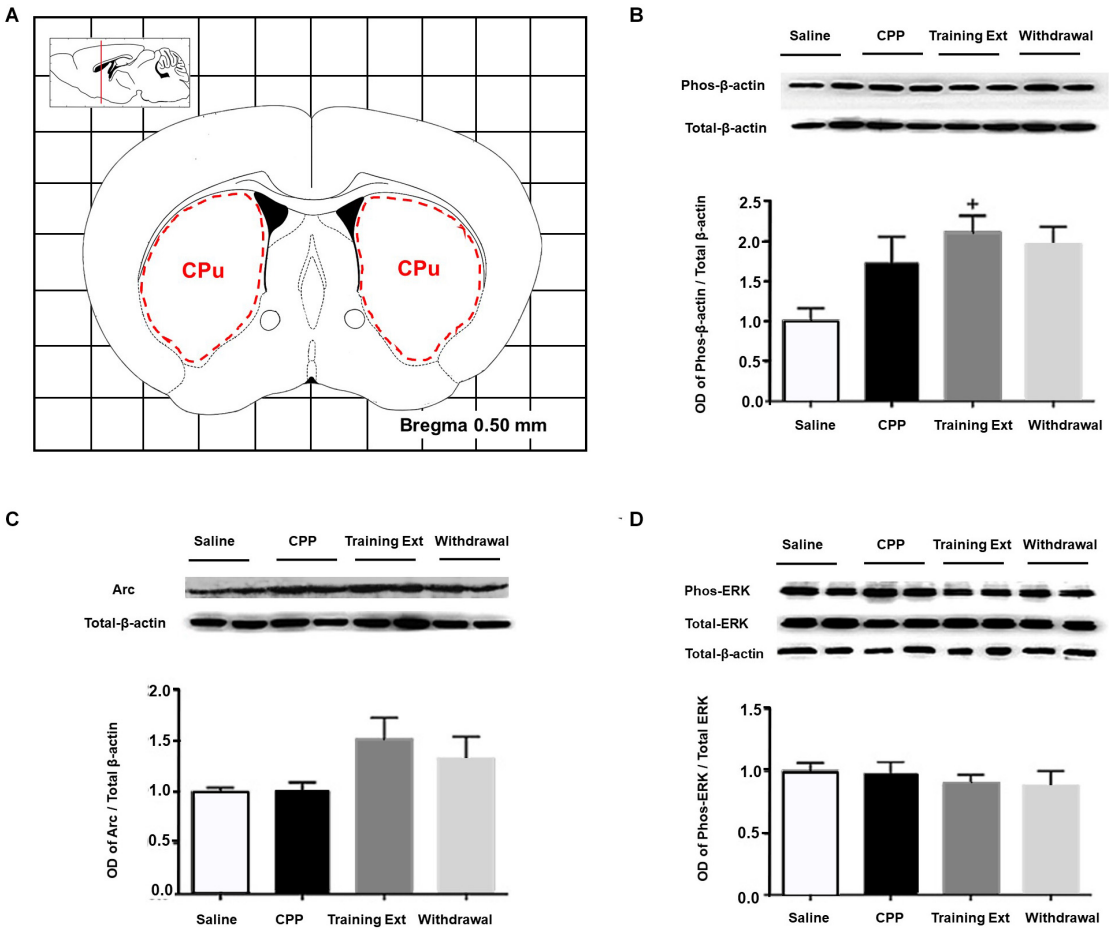

FIGURE 8 | Alterations of the p-βactin/β-actin ratio, Arc expression level, and p-ERK/ERK ratio in the caudate putamen (CPu) at different phases of the morphine-induced conditioned place preference (CPP). **(A)** Red letters and red dotted line in the coronal section inset indicate the dissection of samples from the CPu. Effects of different morphine-induced CPP phases on the **(B)** p-β-actin/β-actin ratio, **(C)** Arc expression level, and **(D)** p-ERK/ERK ratio in the CPu. The animals in the *Saline* or *CPP* group were sacrificed on posttest Day 10, while those in the Training Extinction group (*Training Ext*) and *Withdrawal* groups were sacrificed on Day 20. The *Training Ext* went through CPP procedures followed by saline injections in the training extinction; the *Withdrawal* group went through CPP procedures followed by spontaneous extinction without any injections. $^{+}p < 0.05$ compared to the saline group. n = 6–8 mice/group.

mentioned above, Yuan Ma et al. (2014) reported that morphine decreased the level of ERK1/2 mRNA during the establishment phase and increased during the extinction phase. Considering the structural and functional complexity of NAc, as well as testing approaches as Western blotting vs. RT-PCR, it is hard to reach a consensus on the overall effect of morphine in the NAc during CPP. Besides, the local activation of the ERK–CREB signal pathway, as an upstream mechanism of Arc/Arg3.1, is required for Arc/Arg3.1 in the NAc shell, mediating morphine-associated context memory (Lv et al., 2015).

In conclusion, β-actin in the NAc mediates morphine-associated context memory *via* upregulating the level of Arc/Arg3.1. In this process, the local activation of the ERK signal pathway, as an upstream mechanism of Arc/Arg3.1, is required.

Alteration in the Dorsal Hippocampus

Hippocampus activity is required for both learning to associate specific contexts with reinforcing availability and spatial learning (Li et al., 2020). Stabilization of LTP depends on multiple signaling cascades linked to actin polymerization (Fedulov et al., 2007). Hippocampal LTP is accompanied by enhanced F-actin content within the dendritic spine, which is essential for late LTP maintenance in unanesthetized freely moving rats (Fukazawa et al., 2003). Besides, actin assembly plays an essential role in the molecular process underlying hippocampal LTP. Moreover, actin turnover in dendritic spines influences spine development, morphology, and plasticity, with functional consequences on learning and memory formation.

The above findings suggested that β-actin, with its modulator, Arc/Arg3.1, might initiate changes in synaptic anatomy while maintaining LTP. An upregulation of β-actin was observed in both expression and extinction phases compared with saline group. As we all know, both development and extinction of CPP reflected formation of new memory, while the withdrawal group reflected that new memory had not been well established. In line with our behavioral data, β-actin was elevated in two relevant

groups and decreased in the withdrawal group. Since β-actin is sensitive to alterations in hippocampus, it may be regarded as a marker of neuronal activation in this brain region.

Previous studies have demonstrated that Arc controls LTP consolidation *via* regulating of local actin polymerization in the dentate gyrus *in vivo* and amygdala modulates inhibitory avoidance and contextual fear memories by regulating the expression of Arc gene and/or protein in the hippocampus (Hou et al., 2009). However, elevation of Arc was detected by neither immunohistochemistry nor Western blotting in the dorsal hippocampus, which suggested that the amygdala modulated aversive memory of morphine withdrawal *via* actin rearrangements but not Arc protein expression in the dorsal hippocampus (Hou et al., 2009). In parallel with these findings, our results revealed a lack of upregulation of Arc in the extinction phase despite a significant elevation in CPP expression phase, which is distinct from modulation of memories by the NAc.

It is also noticeable that there are challenging studies dealing with ERK activity within the hippocampus. In a previous study, Yuan Ma et al. (2014) showed that ERK1 and ERK2 mRNA levels were downregulated in the hippocampus during the three phases of CPP. Earlier study showed that chronic methamphetamine (METH) treatment did not alter ERK phosphorylation in mouse hippocampus (Su et al., 2013). Furthermore, another investigation indicated that there was no significant alteration of p-ERK in the hippocampus and PFC after CPP induced by chemical stimulation of the lateral hypothalamus (Haghparast et al., 2011). Concurrent with recent investigations, our results showed that morphine did not change the level of activated ERK1/2 during the establishment phase, but abruptly increased it in the extinction phase. Thus, it could be taken into consideration that ERK in the dorsal hippocampus is a crucial player for CPP extinction, but not for CPP development.

It also should be noted that actin rearrangements and its modulator Arc in the NAc were delayed than that in the hippocampus, as no fluctuations of their expression were observed during the CPP development period. This may suggest that the hippocampus may impose some regulation on NAc anatomically and functionally, which requires further investigation.

In summary, our work illustrated that morphine altered β-actin and Arc, ERK1/2 expression in brain regions during both CPP establishment phase and extinction phase, leading to brain region-specific changes. Those proteins were in a different level related to different behavioral stages in the NAc and dorsal hippocampus, respectively. Phosphorylation of β-actin and Arc contribute to memory formation, while p-ERK was affected by drug reward response from morphine and may affect the response in return. These findings contribute to a deeper understanding of the potential mechanisms of cytoskeletal protein in cellular and molecular processes underlying drug-seeking behaviors. Last but not least, F-actin and G-actin should also be detected in future studies to reflect actin rearrangement more directly. It is expected that the actin dynamics in the process of drug-induced behavior will provide more insights into the treatment of drug addiction.

DATA AVAILABILITY STATEMENT

The original contributions presented in the study are included in the article/supplementary material, further inquiries can be directed to the corresponding author/s.

ETHICS STATEMENT

The animal study was reviewed and approved by Xi'an Jiaotong University Laboratory Animal Administration Committee.

AUTHOR CONTRIBUTIONS

XY, YZ, and CY designed the research. XY, YW, and YZ performed the experiments. FG, JY, and ZY provided the technical support. XY and YW analyzed the data. XY and YZ wrote the manuscript. CY edited the manuscript. All the authors approved the manuscript for publication.

FUNDING

This study was supported by the National Natural Science Foundation of China (81971792 and 81901920) and the NHC Key Laboratory of Drug Addiction Medicine (2020DAMOP-007).

ACKNOWLEDGMENTS

We thank all the members of our laboratory for their kind help.

REFERENCES

Arias-Carrion, O., Stamelou, M., Murillo-Rodriguez, E., Menendez-Gonzalez, M., and Poppel, E. (2010). Dopaminergic reward system: a short integrative review. *Int. Arch. Med.* 3:24. doi: 10.1186/1755-7682-3-24

Bang, D., Kishida, K. T., Lohrenz, T., White, J. P., Laxton, A. W., Tatter, S. B., et al. (2020). Sub-second dopamine and serotonin signaling in human striatum during perceptual decision-making. *Neuron* 108, 999.e6–1010.e6.

Basu, S., and Lamprecht, R. (2018). The role of actin cytoskeleton in dendritic spines in the maintenance of long-term memory. *Front. Mol. Neurosci.* 11:143. doi: 10.3389/fnmol.2018.00143

Bramham, C. R. (2008). Local protein synthesis, actin dynamics, and LTP consolidation. *Curr. Opin. Neurobiol.* 18, 524–531. doi: 10.1016/j.conb.2008.09.013

Bramham, C. R., Alme, M. N., Bittins, M., Kuipers, S. D., Nair, R. R., Pai, B., et al. (2010). The Arc of synaptic memory. *Exp. Brain Res.* 200, 125–140.

Fedulov, V., Rex, C. S., Simmons, D. A., Palmer, L., Gall, C. M., and Lynch, G. (2007). Evidence that long-term potentiation occurs within individual hippocampal synapses during learning. *J. Neurosci.* 27, 8031–8039. doi: 10.1523/jneurosci.2003-07.2007

Fujiki, M., Yee, K. M., and Steward, O. (2020). Non-invasive high frequency repetitive transcranial magnetic stimulation (hfrTMS) robustly activates molecular pathways implicated in neuronal growth and synaptic plasticity in

select populations of neurons. *Front Neurosci* 14:558. doi: 10.3389/fnins.2020.00558

Fukazawa, Y., Saitoh, Y., Ozawa, F., Ohta, Y., Mizuno, K., and Inokuchi, K. (2003). Hippocampal LTP is accompanied by enhanced F-actin content within the dendritic spine that is essential for late LTP maintenance in vivo. *Neuron* 38, 447–460. doi: 10.1016/s0896-6273(03)00206-x

Gonzales, K. K., and Smith, Y. (2015). Cholinergic interneurons in the dorsal and ventral striatum: anatomical and functional considerations in normal and diseased conditions. *Ann. N. Y. Acad. Sci.* 1349, 1–45. doi: 10.1111/nyas.12762

Haghparast, A., Taslimi, Z., Ramin, M., Azizi, P., Khodagholi, F., and Hassanpour-Ezatti, M. (2011). Changes in phosphorylation of CREB, ERK, and c-fos induction in rat ventral tegmental area, hippocampus and prefrontal cortex after conditioned place preference induced by chemical stimulation of lateral hypothalamus. *Behav. Brain Res.* 220, 112–118. doi: 10.1016/j.bbr.2011.01.045

Henneberger, C., Bard, L., Panatier, A., Reynolds, J. P., Kopach, O., Medvedev, N. I., et al. (2020). LTP induction boosts glutamate spillover by driving withdrawal of perisynaptic astroglia. *Neuron* 108, 919.e11–936.e11.

Hou, Y. Y., Lu, B., Li, M., Liu, Y., Chen, J., Chi, Z. Q., et al. (2009). Involvement of actin rearrangements within the amygdala and the dorsal hippocampus in aversive memories of drug withdrawal in acute morphine-dependent rats. *J. Neurosci.* 29, 12244–12254. doi: 10.1523/jneurosci.1970-09.2009

Hyman, S. E. (2005). Addiction: a disease of learning and memory. *Am. J. Psychiatry* 162, 1414–1422. doi: 10.1176/appi.ajp.162.8.1414

Iino, Y., Sawada, T., Yamaguchi, K., Tajiri, M., Ishii, S., Kasai, H., et al. (2020). Dopamine D2 receptors in discrimination learning and spine enlargement. *Nature* 579, 555–560. doi: 10.1038/s41586-020-2115-1

Kai, Y., Li, Y., Sun, T., Yin, W., Mao, Y., Li, J., et al. (2018). A medial prefrontal cortex-nucleus acumens corticotropin-releasing factor circuitry for neuropathic pain-increased susceptibility to opioid reward. *Transl. Psychiatry* 8:100.

Korb, E., and Finkbeiner, S. (2011). Arc in synaptic plasticity: from gene to behavior. *Trends Neurosci.* 34, 591–598. doi: 10.1016/j.tins.2011.08.007

Lamprecht, R. (2016). The role of actin cytoskeleton in memory formation in amygdala. *Front. Mol. Neurosci.* 9:23. doi: 10.3389/fnmol.2016.00023

Leite-Morris, K. A., Kobrin, K. L., Guy, M. D., Young, A. J., Heinrichs, S. C., and Kaplan, G. B. (2014). Extinction of opiate reward reduces dendritic arborization and c-Fos expression in the nucleus accumbens core. *Behav. Brain Res.* 263, 51–59. doi: 10.1016/j.bbr.2013.12.041

Li, M., Xie, A. M., Liu, Y., Zeng, Q., Huang, S. C., Huang, Q. P., et al. (2020). Ketamine administration leads to learning-memory dysfunction and decreases serum brain-derived neurotrophic factor in rats. *Front. Psychiatry* 11:576135. doi: 10.3389/fpsyt.2020.576135

Liu, J. F., Tian, J., and Li, J. X. (2019). Modulating reconsolidation and extinction to regulate drug reward memory. *Eur. J. Neurosci.* 50, 2503–2512. doi: 10.1111/ejn.14072

Liu, Y., Zhou, Q. X., Hou, Y. Y., Lu, B., Yu, C., Chen, J., et al. (2012). Actin polymerization-dependent increase in synaptic Arc/Arg3.1 expression in the amygdala is crucial for the expression of aversive memory associated with drug withdrawal. *J. Neurosci.* 32, 12005–12017. doi: 10.1523/jneurosci.0871-12.2012

Lv, X. F., Sun, L. L., Cui, C. L., and Han, J. S. (2015). NAc shell Arc/Arg3.1 protein mediates reconsolidation of morphine CPP by increased GluR1 cell surface expression: activation of ERK-coupled CREB is required. *Int. J. Neuropsychopharmacol.* 18:yv030.

Lv, X. F., Xu, Y., Han, J. S., and Cui, C. L. (2011). Expression of activity-regulated cytoskeleton-associated protein (Arc/Arg3.1) in the nucleus accumbens is critical for the acquisition, expression and reinstatement of morphine-induced conditioned place preference. *Behav. Brain Res.* 223, 182–191. doi: 10.1016/j.bbr.2011.04.029

Quintero, G. C. (2013). Role of nucleus accumbens glutamatergic plasticity in drug addiction. *Neuropsychiatr. Dis. Treat* 9, 1499–1512. doi: 10.2147/ndt.s45963

Rothenfluh, A., and Cowan, C. W. (2013). Emerging roles of actin cytoskeleton regulating enzymes in drug addiction: actin or reactin'? *Curr. Opin. Neurobiol.* 23, 507–512. doi: 10.1016/j.conb.2013.01.027

Spechler, P. A., Stewart, J. L., Kuplicki, R., and Paulus, M. P. (2020). Attenuated reward activations associated with cannabis use in anxious/depressed individuals. *Transl. Psychiatry* 10:189.

Su, H. L., Zhu, J., Chen, Y. J., Zhao, N., Han, W., Dang, Y. H., et al. (2013). Roles of levo-tetrahydropalmatine in modulating methamphetamine reward behavior. *Physiol. Behav.* 118, 195–200. doi: 10.1016/j.physbeh.2013.05.034

Suratkal, S. S., Yen, Y. H., and Nishiyama, J. (2020). Imaging dendritic spines: molecular organization and signaling for plasticity. *Curr. Opin. Neurobiol.* 67, 66–74. doi: 10.1016/j.conb.2020.08.006

Toda, S., Shen, H. W., Peters, J., Cagle, S., and Kalivas, P. W. (2006). Cocaine increases actin cycling: effects in the reinstatement model of drug seeking. *J. Neurosci.* 26, 1579–1587. doi: 10.1523/jneurosci.4132-05.2006

Torregrossa, M. M., Corlett, P. R., and Taylor, J. R. (2011). Aberrant learning and memory in addiction. *Neurobiol. Learn. Mem.* 96, 609–623. doi: 10.1016/j.nlm.2011.02.014

Valjent, E., Pagès, C., Hervé, D., Girault, J. A., and Caboche, J. (2004). Addictive and non-addictive drugs induce distinct and specific patterns of ERK activation in mouse brain. *Eur. J. Neurosci.* 19, 1826–1836. doi: 10.1111/j.1460-9568.2004.03278.x

Wang, Y., Zhang, H., Cui, J., Zhang, J., Yin, F., Guo, H., et al. (2019). Opiate-associated contextual memory formation and retrieval are differentially modulated by dopamine D1 and D2 signaling in hippocampal-prefrontal connectivity. *Neuropsychopharmacology* 44, 334–343. doi: 10.1038/s41386-018-0068-y

Xu, Y., Lv, X. F., Cui, C. L., Ge, F. F., Li, Y. J., and Zhang, H. L. (2012). Essential role of NR2B-containing NMDA receptor-ERK pathway in nucleus accumbens shell in morphine-associated contextual memory. *Brain Res. Bull.* 89, 22–30. doi: 10.1016/j.brainresbull.2012.06.012

Yuan Ma, J., Zhi, Gu, S., Meng, M., Hui Dang, Y., Ya Huang, C., et al. (2014). Regional expression of extracellular signal-regulated kinase 1 and 2 mRNA in a morphine-induced conditioned place preference model. *Brain Res.* 1543, 191–199. doi: 10.1016/j.brainres.2013.11.022

Zhang, Y. X., Akumuo, R. C., España, R. A., Yan, C. X., Gao, W. J., and Li, Y. C. (2018). The histone demethylase KDM6B in the medial prefrontal cortex epigenetically regulates cocaine reward memory. *Neuropharmacology* 141, 113–125. doi: 10.1016/j.neuropharm.2018.08.030

Zhao, J., Ying, L., Liu, Y., Liu, N., Tu, G., Zhu, M., et al. (2019). Different roles of Rac1 in the acquisition and extinction of methamphetamine-associated contextual memory in the nucleus accumbens. *Theranostics* 9, 7051–7071. doi: 10.7150/thno.34655

Conflict of Interest: The authors declare that the research was conducted in the absence of any commercial or financial relationships that could be construed as a potential conflict of interest.

frontiers in Pharmacology

ORIGINAL RESEARCH
published: 08 February 2021
doi: 10.3389/fphar.2021.627307

Basolateral Amygdala Serotonin 2C Receptor Regulates Emotional Disorder-Related Symptoms Induced by Chronic Methamphetamine Administration

Zhuo Wang[1†], Chen Li[2†], Jiuyang Ding[3†], Yanning Li[2], Zhihua Zhou[4], Yanjun Huang[5], Xiaohan Wang[2], Haoliang Fan[2], Jian Huang[2], Yitong He[2], Jianwei Li[1], Jun Chen[1] and Pingming Qiu[2]**

[1]Department of Infertility and Sexual Medicine, The Third Affiliated Hospital of Sun Yat-sen University, Guangzhou, China, [2]School of Forensic Medicine, Southern Medical University, Guangzhou, China, [3]School of Forensic Medicine, Guizhou Medical University, Guiyang, China, [4]Department of Neurology, The First Affiliated Hospital, School of Clinical Medicine of Guangdong Pharmaceutical University, Guangzhou, China, [5]Department of Neurology, Zhujiang Hospital, Southern Medical University, Guangzhou, China

OPEN ACCESS

Edited by:
Fanglin Guan,
Xi'an Jiaotong University Health Science Center, China

Reviewed by:
Giuseppe Di Giovanni,
University of Malta, Malta
Luc Maroteaux,
INSERM U839 Institut du Fer à Moulin (IFM), France

***Correspondence:**
Jun Chen
jchen121121@hotmail.com
Pingming Qiu
qiupmfy@126.com

[†]These authors have contributed equally to this work

Specialty section:
This article was submitted to Neuropharmacology, a section of the journal Frontiers in Pharmacology

Received: 09 November 2020
Accepted: 06 January 2021
Published: 08 February 2021

Citation:
Wang Z, Li C, Ding J, Li Y, Zhou Z, Huang Y, Wang X, Fan H, Huang J, He Y, Li J, Chen J and Qiu P (2021) Basolateral Amygdala Serotonin 2C Receptor Regulates Emotional Disorder-Related Symptoms Induced by Chronic Methamphetamine Administration. Front. Pharmacol. 12:627307. doi: 10.3389/fphar.2021.627307

Globally, methamphetamine (MA) is the second most abused drug, with psychotic symptoms being one of the most common adverse effects. Emotional disorders induced by MA abuse have been widely reported both in human and animal models; however, the mechanisms underlying such disorders have not yet been fully elucidated. In this study, a chronic MA administration mouse model was utilized to elucidate the serotonergic pathway involved in MA-induced emotional disorders. After 4 weeks of MA administration, the animals exhibited significantly increased depressive and anxious symptoms. Molecular and morphological evidence showed that chronic MA administration reduced the expression of the 5-hydroxytryptamine (5-HT) rate-limiting enzyme, tryptophan hydroxylase 2, in the dorsal raphe and the concentrations of 5-HT and its metabolite 5-hydroxyindoleacetic acid in the basolateral amygdala (BLA) nuclei. Alterations in both 5-HT and 5-HT receptor levels occurred simultaneously in BLA; quantitative polymerase chain reaction, western blotting, and fluorescence analysis revealed that the expression of the 5-HT2C receptor (5-HT_{2C}R) increased. Neuropharmacology and virus-mediated silencing strategies confirmed that targeting 5-HT_{2C}R reversed the depressive and anxious behaviors induced by chronic MA administration. In the BLA, 5-HT_{2C}R-positive cells co-localized with GABAergic interneurons. The inactivation of 5-HT_{2C}R ameliorated impaired GABAergic inhibition and decreased BLA activation. Thus, herein, for the first time, we report that the abnormal regulation of 5-HT_{2C}R is involved in the manifestation of emotional disorder-like symptoms induced by chronic MA use. Our study suggests that 5-HT_{2C}R in the BLA is a promising clinical target for the treatment of MA-induced emotional disorders.

Keywords: methamphetamine, emotional disorder, basolateral amygdala, serotonin 2C receptor, 5-HT

INTRODUCTION

Methamphetamine (MA) is a highly addictive amphetamine-type stimulant (ATS) (Takayuki et al., 2018). According to the World Drug Report (United Nations, 2020), there are about 27 million global ATS abusers. In China, MA has replaced heroin as the most widely abused drug and it is also the most widely used ATS in Southeast Asia and North America. MA has a strong toxic effect on multiple organs—especially the brain—and strong withdrawal symptoms (Prakash et al., 2017; Voce et al., 2019). Chronic MA administration is accompanied by numerous emotional symptoms, such as depression, anxiety, and decreased will and activity (Bagheri et al., 2015), that increase the risk of impulsive drug use and relapse after withdrawal, thereby contributing to MA addiction. The underlying molecular mechanisms of emotional symptoms, including depression and anxiety, in chronic MA users are still unclear (Casaletto et al., 2015; Ru et al., 2019); however, revealing these could provide a theoretical basis and therapeutic targets for the reduction of and recovery from MA abuse.

The pathogenesis of depression is complicated and not yet fully understood (Gonda et al., 2019). The dysfunction of monoamine neurotransmitters—especially a decrease in the presence of 5-hydroxytryptamine (5-HT)—has been implicated in the occurrence of numerous emotional disorders, including depression (Cryan and Leonard, 2000). MA use has been shown to reduce the concentration of 5-HT in the brain (Althobaiti et al., 2016). The rate-limiting enzyme involved in brain 5-HT synthesis, tryptophan hydroxylase (TPH) 2, is mainly expressed in 5-HT neurons, originating from the raphe nucleus. The mRNA and protein expression of TPH2 is significantly decreased in the brain of a rat depression model (Angoa-Pérez et al., 2014; Chen et al., 2017). Similarly, acute and binge MA usage can affect 5-HT levels and TPH2 activity in the brain. The emotional symptoms caused by long-term drug use may be a secondary response to the changes in brain serotonergic activity.

As a neurotransmitter, 5-HT combines with the 5-HT receptor (5-HTR) to exert its regulatory function in the brain. The 5-HTR2 family is closely related to the regulation of emotion (Nic Dhonnchadha et al., 2003; Quesseveur et al., 2012). The 5-HT$_2$R receptors family have a high homology, overlapping pharmacological properties, and similar second messenger signaling systems, making them attractive candidates as pharmacotherapy targets in drug abuse (Bubar and Cunningham, 2008; Cunningham and Anastasio, 2014; Howell and Cunningham, 2015). MA administration induces alterations in the expression of 5-HTRs (Mcfadden et al., 2018); however, the brain area and subtype specificity of 5-HTR2 and the causes behind MA-associated emotional disorders require further investigation. Mcfadden et al. (2018).

The basal lateral amygdala (BLA) is an integral part of the limbic system, which is responsible for the regulation of emotion (Kedo et al., 2018). Numerous studies have shown that 5-HT neurons in the dorsal raphe nucleus (DRN) exert their effects on the BLA via serotonergic regulation. In female mice exposed to 4-vinylcyclohexene, the synthesis of 5-HT in the DRN and its afferents to BLA are decreased, thereby causing impaired long-term damage in the BLA and anxiety-associated behaviors (Wang et al., 2019a). The 5-HT pathway in the DRN-BLA is also involved in the formation and recovery of fear memory, with the involvement of 5-HT$_{1A/2A}$R signal transduction in BLA (Sengupta and Holmes, 2019). These studies suggest that the 5-HT system in the BLA plays an important role in the regulation of negative emotions.

These studies indicate that MA may affect the BLA 5-HT system. Herein, we established a chronic MA abuse model (10 mg/kg/day i. p., 4 weeks) to observe emotional symptoms and BLA serotonergic changes. The results of this study may elucidate the long-term effects of MA administration on the serotonergic system and how these contribute to the manifestation of emotional disorder-related symptoms.

MATERIALS AND METHODS

Animals

Male C57BL/6J mice (10–12 weeks, 20–22 g) were provided by the Experimental Animal Center of Southern Medical University. The mice in each group could drink and eat freely in a standard specific pathogen-free environment, with alternating 12 h light and dark cycles (lighting interval: 7:00–19:00). All animal procedures were performed according to the National Institutes of Health guide for the care and use of animals for scientific purposes and preapproved by the Institutional Animal Care and Use Committee of Southern Medical University. To simulate chronic MA consumption, MA (purity ≥99.1%, provided by the National Institute Control of Pharmaceutical and Biological Products, Beijing, China) was administered for 4 weeks as previously described (Keshavarzi et al., 2019) (10 mg/kg i. p. daily). Ethology tests were performed after MA administration. At the end of the experiment, mice were euthanized and their brain tissues were collected for analysis. Every effort was made to minimize animal pain, suffering, and distress and reduce the number of animals used.

Forced Swim Test

The FST was used to evaluate depressive-associated behavior in the animals (Cao et al., 2013). The experimental device was a transparent plexiglass hollow cylinder (25 cm high and 12 cm in diameter). The water level was at an approximate height of 20 cm and the water temperature was 25 ± 1 °C. During the experiment, the mice were placed gently into the water and allowed to swim freely for 6 min. Their cumulative immobility time was recorded for the last 4 min. After each experiment, the mice were removed, dried with a towel, and put back into the cage and the water in the device was changed.

Tail Suspension Test

The tail end of the mouse was fixed with tape and hung above the ground for 6 min to suspend the head downward. The body of the mice did not contact the tail suspension instrument, except for the tail. The immobility time of mice was recorded in the last 4 min.

Sucrose Preference Test

SPT was used to evaluate anhedonia during MA-induced depression in mice (Qin et al., 2019). In this experiment, the mice were fed in a single cage. Pure water was placed on one side of the cage and 1% sucrose solution was placed on the opposite side; the mice could freely choose between the pure water and sugar solution. The relative positions of each were randomly decided and we recorded the consumption of both. Sugar preference is expressed as a percentage of the total liquid consumption.

Elevated Plus Maze

The EPM consisted of an open arm and closed arm. The mice were gently placed in the central area with their back to the experimenter. Video was recorded for 5 min. After the test of each mouse was completed, the device was cleaned thoroughly with 75% alcohol. The total time of open arm entry and the number of open arm entries for each mouse were counted.

Immunohistochemistry

After anesthetization with 1% pentobarbital sodium (40 mg/kg), the heart was exposed through a thoracotomy, while the brain was extracted after perfusion. Brain tissue was immersed in 4% paraformaldehyde in saline for 24 h; subsequently, we performed gradient dehydration of the sucrose solution and immersed the brain tissue in a 30% sucrose solution. Then, we performed serial coronal sectioning (40 μm). The brain slices were rinsed with 0.1 M phosphate buffer saline (PBS) three times on a shaking table (5 min each time). A 3% bovine serum albumin (BSA) solution containing 0.5% Triton X-100 was added before drilling for 40 min. Primary antibodies (Mouse anti-GAD67, MAB5406, 1:1,000, Merck Millipore, Billerica, Mass., USA; rabbit anti-TPH2, ab184505, 1:1,000, Abcam, Cambridge, United Kingdom) were added after dilution with 0.1 M PBS containing 3% BSA and incubated in a shaker at 4 °C for 24 h. After rinsing three times with 0.1 M PBS, the corresponding fluorescent secondary antibody was added and incubated for 1 h in the dark at 25 °C. Then, the brain slices were sealed with a mounting medium (Vector Laboratories, Inc., Burlingame, CA), containing 4′,6-diamidino-2-phenylindole. Images were captured under a laser confocal microscope (LSM 710; Carl Zeiss Microscopy, Thornwood, NY, United States).

Quantitative Polymerase Chain Reaction

Total RNA was extracted from the tissue samples using TRIzol. The transcripts of the target genes in each sample were normalized with GAPDH/β-actin and expressed as a fold change using the $2^{-\Delta\Delta Ct}$ equation. The PCR primers used in this study are listed as follows:

TPH2, forward, 5′ AGCATTTGGACGGAGGAAGA 3′, reverse, 5′ TGTACTCGACCCTGGGAATG 3′;
5-HTR1A, forward, 5′CTTTCTACATCCCGCTGCTG 3′, reverse, 5′ CCCGACTCTCCATTCACACT 3′;
5-HTR2A, forward, 5′ CTCCTTCAGCTTCCTCCCTC 3′, reverse, 5′ GCAGGGCTCCAATGACATTT 3′;
5-HTR2C, forward, 5′ TCGTTCTCATCGGGTCCTTC 3′, reverse, 5′ CTCATCACCCTTCTTGCAGC 3′;
5-HTR3, forward, 5′ GGACTCCTGAGGACTTCGAC 3′, reverse, 5′ CTACAGGCGGTCACCAATTG 3′;
5-HTR4, forward, 5′ CTGGGCTTATGGGGAGATGT 3′, reverse, 5′ GCCACCAAAGGAGAAGTTGC 3′.

Western Blotting

All brain tissues were homogenized in a protein extraction buffer (Beyotime, Shanghai, China) containing protease and phosphatase inhibitors at 4 °C for 30 min. The supernatant was collected after the lysates were centrifuged. Protein concentrations were measured using the BCA Protein Assay Kit (Beyotime, Shanghai, China). The samples were separated by sodium dodecyl sulfate-polyacrylamide gel electrophoresis and transferred to polyvinylidene difluoride membranes (Millipore, Billerica, MA, United States). The membranes were blocked in a blocking buffer at room temperature for 1 h and incubated overnight at 4 °C with anti-TPH2 (1:1,000, ab184505, Abcam), anti-5-HTR2C (1:1,000, ab137529, Abcam), and anti-GAPDH (1:5,000, ab125247, Abcam). Furthermore, the membranes were washed with a Tris-buffered saline with 0.1% Tween 20 Detergent buffer and incubated with corresponding secondary antibodies at room temperature for 1 h. The membranes were detected using electrochemiluminescence reagents (Bio-Rad, Hercules, CA, United States) and visualized using a Tanon Imaging system (Tanon, Shanghai, China). Band densities were measured using the ImageJ software and normalized to GAPDH expression. This experiment was performed in triplicate, and the representative images are presented.

High-Performance Liquid Chromatographic With Electrochemical Detection

Monoamine transmitters in the brain homogenate were detected by HPLC. The HPLC system included a Sykam high-performance liquid chromatograph, C18 reverse-phase analytical column (DIAMONSIL, 2.1 × 100 mm, 2.5 μm), column temperature chamber, SenCell electronic flow cell (Antec, Netherlands), ADF filter (0.05 Hz), 25 μm electrode, *in situ* Ag/AgCl reference electrode, VT 03 glass carbon working electrode (3 mm), and pulse damper. The mobile phase consisted of a 15% methanol aqueous solution containing 0.74 mmol/L sodium octane sulfonate, 80 mmol/L sodium dihydrogen phosphate, 0.027 mmol/L disodium ethylenediaminetetraacetic acid, and 2 mmol/L potassium chloride adjusted to pH 3.0 with phosphoric acid. After all solutions were prepared, a 0.22-μm organic phase filter membrane was used to remove bacteria, followed by ultrasonic degassing for 30 min. The column temperature was maintained at 40 °C. Fresh standards were prepared before the experiment. The working voltage of the electrochemical detector electrode and its attenuation were 0.56 V and 200 nA, respectively.

Stereotactic Surgery

Stereotactic surgery was conducted as previously described (Wang et al., 2019b). Briefly, after mice were anesthetized using an intraperitoneal injection of 40 mg/kg pentobarbital sodium, erythromycin eye ointment was applied to their eyes, and the hair on the top of the skull was cut off using eye scissors. Following iodine disinfection, the scalp was cut, exposing the anterior fontanelle. The position of the mouse head was adjusted to have both the front and back as well as the right and left levels of the mouse brain in the same line. The location of the BLA was: AP = −1.5 mm, ML = ±2.7 mm, and DV = −4.5 mm. The skull was drilled with a dental drill, and the drug delivery cannula (purchased from RWD) was embedded and fixed on the top of the mouse head with dental cement. It was used for drug administration and related behavior tests after 1 week of recovery.

To inject the virus, the microinjection needle (Hamilton, 5 μL, 33 g) was used to puncture to the corresponding depth and 100 nL of adeno-associated virus (AAV) was injected into the bilateral brain regions at a speed of 50 nL/min. After 5 min, the microinjection needle was slowly withdrawn to ensure that the AAV solution was fully absorbed. After suturing, kanamycin lidocaine was applied to the wound to prevent infection.

Drug Administration

In the last week of MA administration, the relevant drug intervention experiments began. The catheter was inserted into the cannula and the infusion of the 5-HT$_{2A}$R receptor antagonist M100907 (0.1 μmol in 100 nL) (Adrielle and Helio, 2012) and the 5-HT$_{2C}$R antagonist sb242084 (10 nmol in 100 nL) (Ceglia et al., 2010) was performed using a microsyringe (701-RN, Hamilton, USA) connected to a microinfusion pump (KD Scientific, United Ststes) within 2 min. After the injection, the catheter was removed after 1 min. The related behavioral experiments were performed 30 min after the last administration.

Construction of AAV-5-HT$_{2C}$R-shRNA

Small hairpin RNA (shRNA) directed against 5-HT2CR was adapted from Anastasio et al. (2015) and verified by RT-qPCR. The shRNA sequence was synthesized and packed into rAAV-U6-shRNA (5-HT2CR)-CMV-EGFP (rAAV2) by BrainVTA (Wuhan, China). Using a similar process, rAAV-U6-shRNA (scramble)-CMV-EGFP was produced as a scrambled control. The virus (titer: 1×10^{13} vg/mL) was injected into the mice 2 weeks before the end of MA administration.

Electrophysiology

After decapitation, the brain tissue was quickly removed and placed in precooled artificial cerebrospinal fluid (ACSF). After soaking for 1 min, the brain slices containing BLA tissue were transferred to an incubator in a constantly warm ACSF bath and incubated for 1 h. A glass microelectrode was used, with a tip resistance of 3.5 MQ when filled with an internal solution. We adjusted the perfusion speed to 1.5 ml/min and circulated the ACSF (124 mmol/L NaCl, 24 mmol/L $NaHCO_3$, 5 mmol/L KCl, 2.4 mmol/L $CaCl_2$, 21.3 mmol/L $MgSO_4$, 1.2 mmol/L KH2PO_4, and 10 mmol/L glucose, pH 7.35–7.45), continuously saturating the solution with a mixture of 95% O_2 and 5% CO_2. The incubated brain slices were carefully transferred to the recording tank with a pipette and fixed with a cover net. The electrode tip was adjusted to the center of the field of vision under a low-power microscope, to slowly drop the solution onto the cell and form a high-resistance sealing state. The hold current was within 100 pA. Pyramidal neurons and interneurons are distinguished by morphology and action potential (AP), as previously described (Rainnie, 1999). The SF-77 multichannel perfusion system was used for fast liquid exchange (Warner Instrument Corporation). When miniature inhibitory postsynaptic currents (mIPSCs) were recorded, magnesium-free ACSF, TTX, DNQX, and APV were added to the perfusion system to block the action potentials produced by the Na^{2+} channel and the excitatory current mediated by the N-methyl-d-aspartate (NMDA)- and α-amino-3-hydroxy-5-methyl-4-isoxazolepropionic acid-type glutamate receptors. The frequency and amplitude of mIPSCs were recorded with the membrane potential held between −70 and −80 mV. When AP was recorded, the recording mode was adjusted to the current-clamp mode. APs were evoked by a 600-ms, 100 pA depolarizing current pulse. Signals were acquired using a Multiclamp 700 b amplifier (Cellular Devices, Sunnyvale, CA, United States) and pClamp 10 (Molecular Devices, Sunnyvale, CA, United States). The recorded data were analyzed using MiniAnal software.

Statistical Analysis

The data are expressed as mean ± standard error (SEM). SPSS (Released 2007. Version 16.0. Chicago, SPSS Inc.) was used for statistical analysis. Student's t-test and one-way analysis of variance were used to analyze the differences between groups. Differences with p values <0.05 were considered statistically significant.

RESULTS

Chronic MA Administration Leads to Emotional Disorder-Related Symptoms and DRN TPH2 Changes

After 4 weeks of administration, depression-like behaviors were measured using the FST, SPT, and TST. In the FST experiment, the immobility time in the MA group was significantly higher than that in the control group (**Figure 1A**). In the SPT, the sucrose preference of mice in the MA group was significantly lower than that in the control group (**Figure 1B**). In the TST, significantly higher mean immobility times were observed in the MA group than in the control group (**Figure 1C**). These three tests consistently showed the depression-like state of the animals in the MA group. To assess anxiety-like behavior, mice were placed in an EPM; those in the MA group spent significantly less time in the open arm (**Figure 1D**) and entered less frequently than those in the control group (**Figure 1E**), which indicated anxiety-like behavior. We then examined the biosynthesis of 5-HT in the DRN during the behavioral changes. The results of TPH immunofluorescence staining showed that the intensity of TPH2 immunoreactivity in the MA group was significantly lower than that in the control group (**Figure 1F**). The results from the qPCR and WB analysis of TPH2 showed the same tendency and verified this result (**Figures 1G,H**). The expression of TPH2 in the DRN was significantly lower in the MA group than in the control group and accompanied the occurrence of emotional disorder-related symptoms.

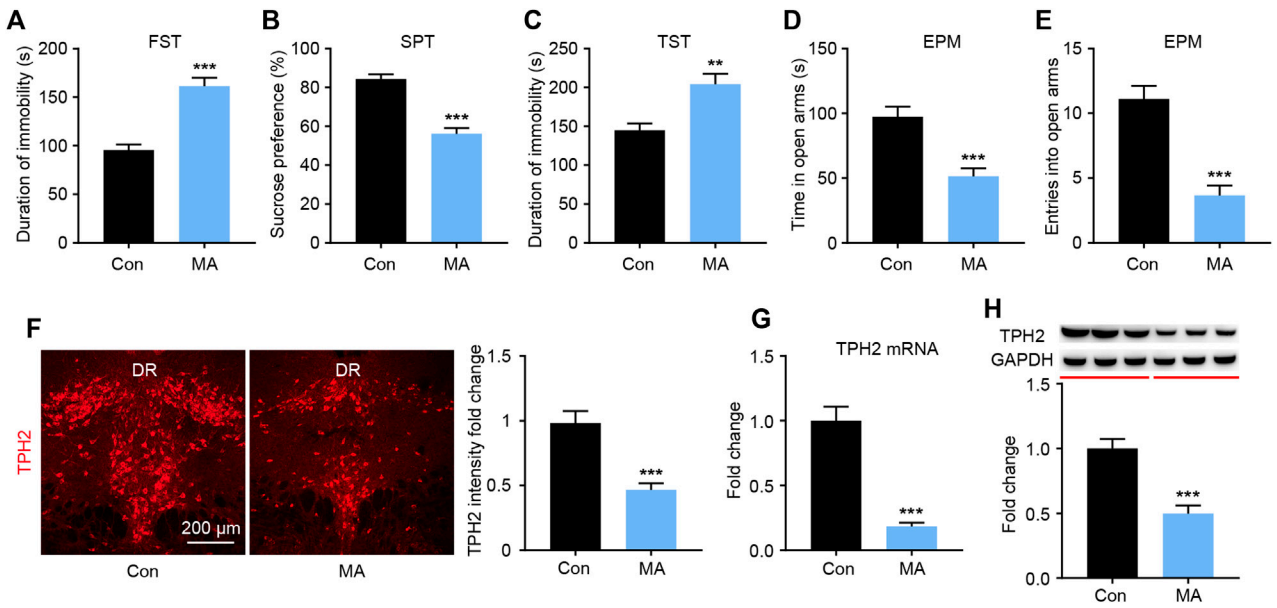

FIGURE 1 | Effects of chronic MA administration on depressive symptoms and DRN 5-HT synthesis. **(A)** Immobility time during the FST. **(B)** Sucrose preference in the SPT to illuminate anhedonia. **(C)** Immobility time in the TST. **(D)** Total time exploring the open arm of elevated plus maze. **(E)** Total entries into open arm of elevated plus maze. **(F)** TPH2 immunoreactivity in dorsal raphe (DR) of the mice brain, scale bar = 200 μm. **(G, H)** TPH2 expression was quantified by qPCR and WB. DRD; dorsal part of the DR, DRV; ventral part of the DR. Data are presented as the mean ± SEM. $^{**}p < 0.01$, $^{***}p < 0.001$.

Chronic MA Administration Affects 5-HT Metabolism in the BLA

It is known that DRN is the main area in the brain where 5-HT neurons are distributed. The 5-HT neurons of the DRN project to the BLA; the terminals of 5-HT neurons have been extensively marked in the BLA area (http://connectivity.brain-map.org/). BLA tissue was collected, and HPLC analyses were performed to assay serotonergic metabolism in the BLA regions of the mice. MA administration significantly decreased the levels of 5-HT and its metabolite 5-hydroxyindoleacetic acid (5-HIAA) in the BLA (**Figures 2A,B**). 5-HT exerts its role by binding with different receptor subtypes, so we examined the mRNA levels of the 5-HT receptors in the BLA. The qPCR results showed that the expression of 5-HT$_{1A}$R was significantly decreased, that of 2A and 2C was significantly, and that of 5-HT$_3$R and 5-HT$_4$R did not significantly change after MA administration (**Figure 2C**). The 5-HT$_{2C}$R immunofluorescence and WB analysis confirmed that the expression of 5-HT$_{2C}$R in the MA group was significantly higher than that in the control group (**Figures 2D,E**).

Pharmacological Inhibition of 5-HT$_{2C}$R Alleviates Emotional Disorder-Related Behavioral Changes After Chronic MA Administration

5-HTRs are potential therapeutic targets for the treatment of emotional disorders (Amidfar and Kim, 2018). We investigated how changes in 5-HTR affected behavioral changes using a neuropharmacological strategy. During MA administration, we implanted a drug delivery cannula on the bilateral BLA and either the 5-HT$_{2C}$R (sb242084) or the 5-HT$_{2A}$R (M100907) antagonist was infused (**Figure 3A**). After 1 week of antagonist administration, we performed the behavioral tests. In the FST experiment, the immobility time of the 5-HT$_{2C}$R antagonist group was significantly lower than that in the vehicle-treated group, whereas the 5-HT$_{2A}$R antagonist exerted little effect (**Figure 3B**). In the SPT, the 5-HT$_{2C}$R antagonist group showed higher sucrose preference than the vehicle-treated group (**Figure 3C**). The anxiety-like behavior was evaluated by EPM; the time spent investigating the open arm (**Figure 3D**) and number of entries into the open arm (**Figure 3E**) were significantly higher in the 5-HT$_{2C}$R antagonist group than in the vehicle-treated group, whereas the 5-HT$_{2A}$R antagonist treatment had little effect. These pharmacological blockade experiments show that BLA 5-HT$_{2C}$R is a valid target against emotional symptoms when ceasing chronic MA administration.

Effects of Virus-Mediated 5-HT$_{2C}$R Knockdown in BLA on Behavioral Changes After Chronic MA Administration

To confirm the role of 5-HT$_{2C}$R in the treatment of emotional symptoms, we packed recombinant AAV2 vector-expressing shRNA against 2C (5-HT$_{2C}$R-shRNA1/2) and nonsense shRNA as a negative control (Con-shRNA). The AAV contains a GFP tag to visualize *in vivo* expression. After AAV-5-HT$_{2C}$R-shRNA was injected into the BLA, the virus expressed its GFP in the BLA (**Figure 4A**), with WB results confirming its interference efficiency (**Figure 4B**). We then conducted depression-screening behavioral tests. In the FST experiment, the knockdown of 5-HT$_{2C}$R significantly increased immobility

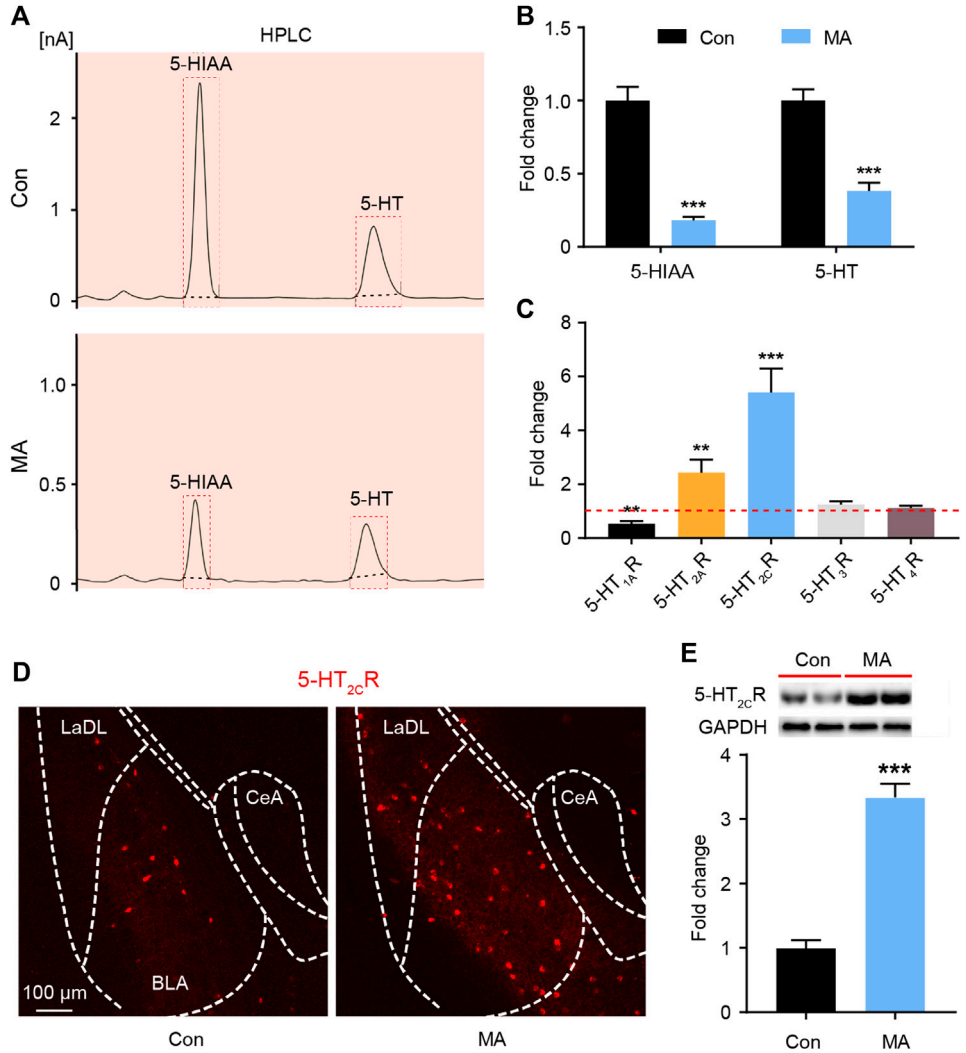

FIGURE 2 | Effects ofchronic MA administration on serotonergic changes in BLA. **(A)** HPLC results of 5-HIAA and 5-HT in BLA. **(B)** Relative concentrations of 5-HIAA and 5-HT in BLA. **(C)** Relative mRNA expression of 5-HT$_{1A}$R, 5-HT$_{2A}$R, 5-HT$_{2C}$R, 5-HT$_3$R, and 5-HT$_4$R in BLA. **(D)** 2C immunoreactivity in BLA of the mice brain, scale bar = 100 μm. **(E)** 5-HT2CR expression was quantified by WB. 5-HIAA; 5-hydroxyindole acetic acid. Data are presented as the mean ± SEM. $^{**}p < 0.01$, $^{***}p < 0.001$.

time (**Figure 4C**). In the SPT, the knockdown of 5-HT$_{2C}$R reversed the decreased sucrose preference compared with that in the Con-shRNA-transfected group (**Figure 4D**). In the EPM test, the knockdown of 5-HT$_{2C}$R resulted in anxiolytic-like effects on behavior in chronic MA administration mice, with significantly increased open arm stay time (**Figure 4E**) and number of entries (**Figure 4F**). These knockdown strategy results further show that BLA 5-HT$_{2C}$R is a valid target against the emotional symptoms caused by chronic MA administration.

5-HT$_{2C}$R Mediated Decreased GABA Inhibition and Increased BLA Activity During Chronic MA Administration

5-HT$_{2C}$R-positive neurons have been shown to be co-expressed with GABAergic interneurons in other brain areas (Liu et al., 2007). We performed immunofluorescent co-staining between 5-HT$_{2C}$R and GAD67 in the BLA and found that most 5-HT$_{2C}$R-positive neurons co-labeled with GAD67 (>93%, **Figure 5A**), suggesting that 5-HT$_{2C}$R-positive neurons in the BLA are GABAergic interneurons. 5-HT$_{2C}$R has also been found to be coupled with the GABA-A receptor (Burke et al., 2015). GABA-A is an ion channel with an inhibitory function, indicating that the function of interneurons in the local brain region of the BLA are inhibited during chronic MA administration. We detected mIPSCs in the BLA. The mIPSC frequency was lower in the MA group than in the control group; however, the amplitude remained unchanged (**Figures 5B,D**). After 5-HT$_{2C}$R interference, the function of mIPSCs was partially recovered—the frequency significantly increased, which implies that there is a disinhibitory mechanism in BLA pyramidal neurons. We speculated that 5-HT$_{2C}$R positive interneurons regulate the excitability of pyramidal neurons in the local BLA region, thereby affecting neuronal activity. Therefore, we

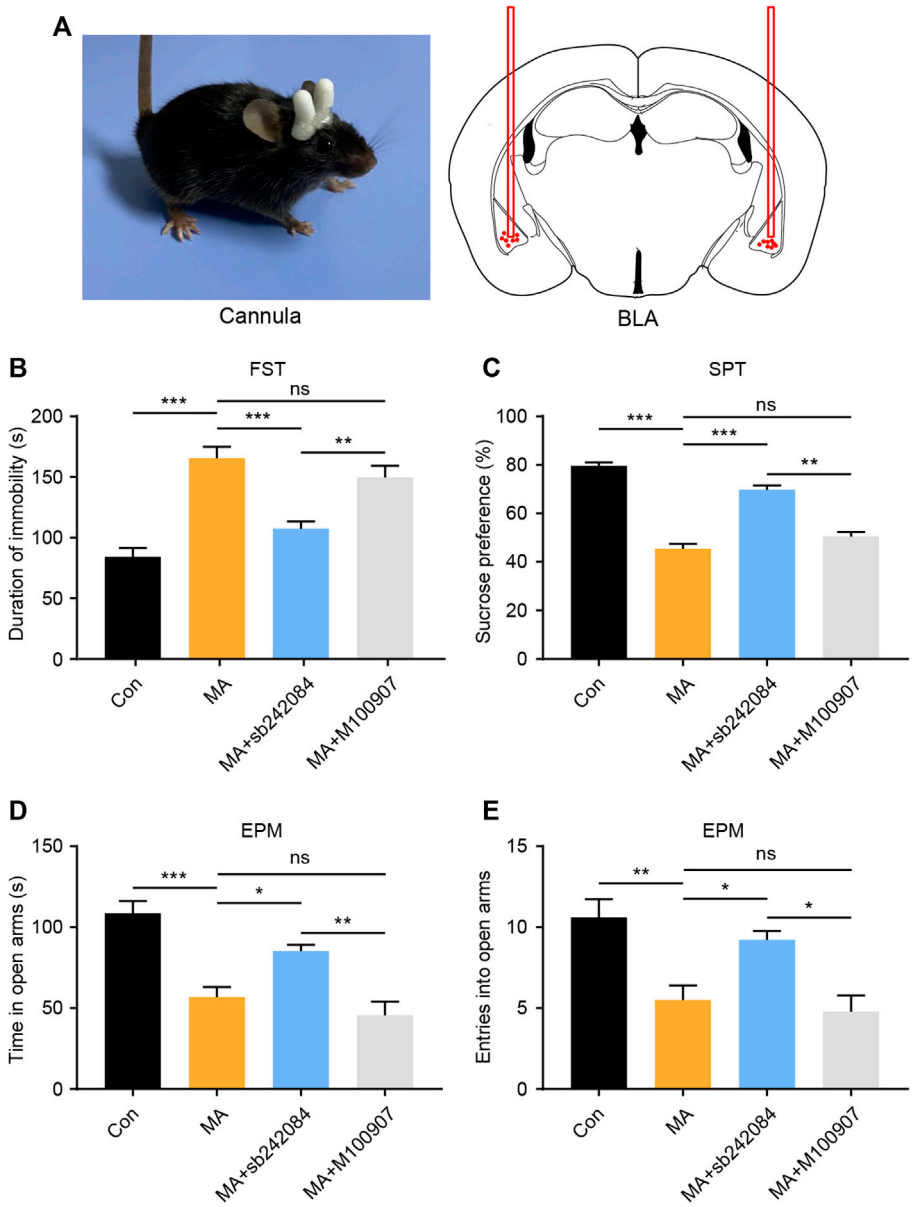

FIGURE 3 | Pharmacological inhibition of 5-HT$_{2C}$R reverses depressive and anxiety-like behaviors caused by chronic MA administration. **(A)** Schematic diagram of drug delivery strategy. **(B)** Immobility time during the FST after pharmacological intervention. **(C)** Sucrose preference in the SPT after pharmacological intervention. **(D)** Total time exploring the open arm of elevated plus maze. **(E)** Total entries into open arm of elevated plus maze. Data are presented as the mean ± SEM. $^{*}p < 0.05$, $^{**}p < 0.01$, $^{***}p < 0.001$.

recorded the AP of excitatory principal neurons in BLA; the frequency of BLA AP significantly increased in the MA group but decreased in the 5-HT$_{2C}$R knockdown group (**Figures 5C,E**). Thus, 5-HT$_{2C}$R-positive interneuron likely mediates neuronal activities in the BLA.

DISCUSSION

MA-induced emotional disorders have been widely reported in human and animal models (Glasner-Edwards and Mooney, 2014; Ru et al., 2019); however, their underlying mechanisms have not been fully elucidated. Here, we explored the potential underlying mechanisms. The results showed that chronic MA administration inhibited the expression of TPH2 in the raphe nucleus, reduced the secretion of 5-HT, and decreased the metabolism of 5-HT in the amygdala. Among the 5-HTRs, 5-HT$_{2C}$R was upregulated in the BLA and is a potential target for therapeutic interventions of emotional disorder-related symptoms. Mechanistically, 5-HT$_{2C}$R is mostly expressed in GABAergic neurons, exerts a disinhibitory role in BLA, inhibits the activity of GABAergic interneurons and

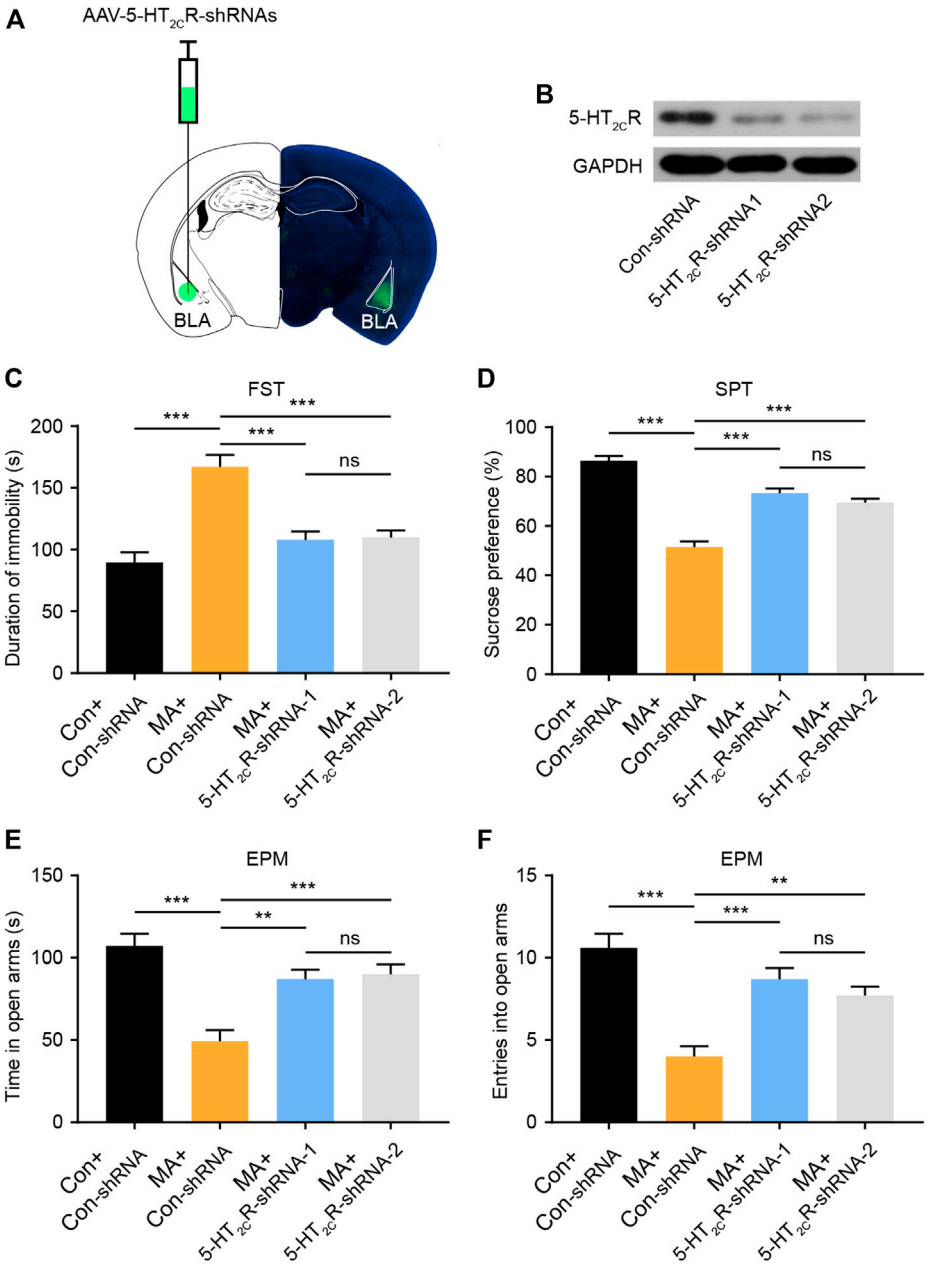

FIGURE 4 | Knockdown of 5-HT$_{2C}$R via AAV-shRNA injection reverses depressive-like behaviors caused by chronic MA administration. **(A)** Schematic of AAV vector-mediated 5-HT$_{2C}$R knockdown in BLA. **(B)** WB results show 5-HT$_{2C}$R expression after AAV-mediated knockdown. **(C)** Immobility time during the FST after AAV-mediated 5-HT$_{2C}$R knockdown. **(D)** Sucrose preference in the SPT after AAV-mediated 5-HT$_{2C}$R knockdown. **(E)** Total time exploring the open arm of elevated plus maze. **(F)** Total entries into open arm of elevated plus maze. Data are presented as the mean ± SEM. $^{**}p < 0.01$, $^{***}p < 0.001$.

causes an excitation imbalance of the amygdala to promote the manifestation of emotional disorder-related symptoms induced by MA administration. Here, we report, for the first time, the role of amygdala-related serotonin mechanisms in the pathogenesis of MA-induced emotional disorders.

In the brain, 5-HT regulates emotions, synaptic plasticity, learning, memory, and reward behavior (Ji and Suga, 2007; Hayes and Greenshaw, 2011; Meneses and Liy-Salmeron, 2012), as it is one of the most vital neurotransmitters. TPH2 is the rate-limiting enzyme for the synthesis of 5-HT in the brain (Al-Tikriti et al., 2012) and is essential for the biosynthesis of 5-HT in the central nervous system. MA enters the brain through the blood-brain barrier and inhibits TPH2 enzyme activity, even when exposure occurs just once (Haughey et al., 1999; Northrop and Nicole, 2015). Nevertheless, it remains unclear whether the effects of chronic MA use on 5-HT occur owing to changes in the biochemical properties of the TPH2 enzyme itself or the quantity of the enzyme. Here, we found that chronic MA

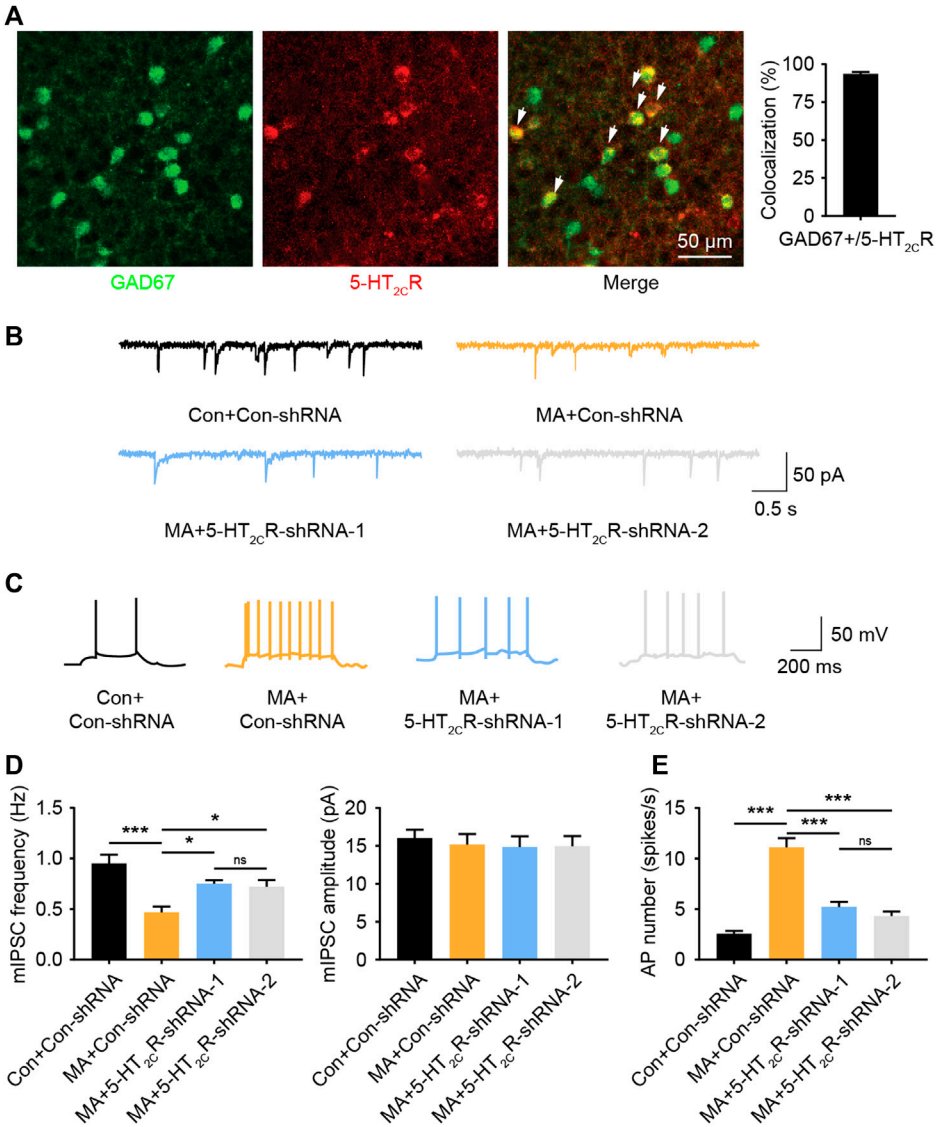

FIGURE 5 | MA decreases the inhibition of BLA 5-HT$_{2C}$R-positive interneurons and increases BLA activity. **(A)** Co-immunofluorescent staining of 5-HT$_{2C}$R (red) and GAD67 (green) was used to reveal their colocalization, 5-HT$_{2C}$R and GAD67 merged image is also shown (white arrow heads), scale bar = 50 μm. **(B)** Representative trace of mIPSC after AAV-mediated 5-HT$_{2C}$R knockdown in BLA. **(C)** Representative trace of action potential after AAV-mediated 5-HT$_{2C}$R knockdown in BLA. **(D)** Chronic MA decreased the frequency of mIPSCs; this was rescued by AAV-mediated 5-HT$_{2C}$R knockdown, while had little effect on the mIPSC amplitude. **(E)** Chronic MA increased the frequency of action potentials; this was reversed by AAV-mediated 5-HT$_{2C}$R knockdown. Data are presented as the mean ± SEM. *p < 0.05, ***p < 0.001.

administration directly inhibited the expression of TPH2 in DR-related brain regions and initiated different serotonergic molecular events related to synaptic plasticity, thereby causing subsequent behavioral changes. The DR projects onto and regulates other brain areas. In this study, we focused on the BLA, which plays a key role in the regulation of negative emotions (Kedo et al., 2018). The DR has extensive regulatory control over the BLA, suggesting that the changes in TPH2 observed in the DR could affect the metabolism of 5-HT in BLA. Previous studies have shown that this pathway participates in the regulation of multiple behaviors (Sengupta and Holmes, 2019) and is closely related to the regulation of negative emotion (Wang et al., 2019b). Therefore, we investigated local 5-HT-related metabolism in BLA. The HPLC results showed that 5-HT and 5-HIAA concentrations in the BLA were significantly decreased in MA group. The changes in the concentrations of neurotransmitters can also cause an alteration in the plasticity of the neurotransmitter-related receptors.

The interaction between 5-HT and its receptors in BLA is complex which exert diverse excitatory and inhibitory role in local microcircuit comprising multiple neuron populations (Sengupta et al., 2017). Among the receptors we tested, 5-HT$_{1A}$R is expressed in BLA and its activation mediates the anxiolytic effect (Strauss et al., 2013), whereas 5-HT$_{2A}$R is

located on multiple neuronal types and its activation in the BLA mediates emotional symptoms (McDonald and Mascagni, 2007; Clinard et al., 2015). The increased expression of 5-HT_{2C}R is associated with anxiogenic effects (Li et al., 2012), and a reduction in the expression of 5-HT_{2C}R is involved in the anxiolytic effect of antidepressant drugs (Vicente and Zangrossi, 2014). 5-HT_3R and 5-HT_4R are also distributed in BLA and regulate emotion (Mikics et al., 2009; Chegini et al., 2014). Chronic MA administration induced generalized BLA 5-HTR changes, with 5-HT_{2C}R the most affected. 5-HT_{2C}R has been found to be involved in the regulation of anxiety and depression (Greenwood et al., 2012). The qPCR, immunofluorescence, and western blot results consistently confirmed that the expression of 5-HT_{2C}R in the BLA was increased in the chronic MA model and that the change in the expression of 5-HT_{2C}R during the chronic administration of MA was accompanied by emotional disorder-related symptoms, suggesting that 5-HT_{2C}R may mediate such symptoms. Our neuropharmacological inhibition and virus-mediated knockdown strategy results confirmed 5-HT_{2C}R as an appropriate therapeutic target for the treatment of chronic MA-induced emotional symptoms. As for the alteration in the expression of 5-HT_{2A}R, although a previous study has suggested that targeting 5-HT_{2A}R may exert beneficial therapeutic effects (Sengupta et al., 2017), our neuropharmacological intervention experiments showed that it had no significant effect on the behavioral changes. Thus, it is suspected that the mechanisms underlying the treatment of emotional symptoms are complex and that the targets and pathways in the various brain regions and etiology differ.

The amygdala neurons are mainly composed of glutamatergic and GABAergic neurons. There are multiple type of GABAergic neurons in the amygdala, which produce inhibitory effects in the local brain regions, thereby regulating the neural activities. Consistent with previous findings that 5-HT_{2C}R-positive neurons are co-expressed with GABAergic inhibitory interneuron markers (Liu et al., 2007; Spoida et al., 2014), we also observed this colocalization in BLA regions. In the local brain area, 5-HT_{2C}R-positive inhibitory interneurons can regulate excitatory pyramidal neurons and exert influence on the output signal of the nucleus. The GABA-A receptor, which is an ion channel with inhibitory functions, has also been found to be coupled with 5-HT_{2C}R (Burke et al., 2015). The increase in 5-HT_{2C}R expression can also increase the inhibitory effect of GABAergic neurons, which was confirmed by our mIPSC results. The inhibition of GABAergic interneurons in the BLA nucleus disinhibited local pyramidal neurons and caused an imbalance between excitability and inhibitory signals in the BLA. We detected the local action potential of BLA and found that the knockdown treatment strategy targeting 5-HT_{2C}R successfully attenuated amygdala activation induced by chronic MA usage. This might explain the observed antidepressant effects of 5-HT_{2C}R-targeted therapy.

MA users account for more than half of the drug abusers and MA abuse has become the most serious challenge in drug control in China. A study in forensic psychiatry has found that MA abusers are widely affected by emotional symptoms, such as anxiety, depression, and even suicidal ideation (Kalechstein et al., 2000). In addition, depression is the leading withdrawal symptom among MA users, and relapse is significantly associated with depressive symptoms (Zhang et al., 2014). Exploring the related pathological mechanisms and potential therapeutic targets of these emotional symptoms will not only help to improve the emotional health of MA users but also contribute to the efficacy of drug withdrawal therapy. The present study extends our understanding of the etiology and identifies the molecular targets responsible for these symptoms. In conjunction with the plasticity of serotonergic pathways that have previously been reported to be regulated by MA in BLA, we elucidated the role of 5-HT_{2C}R plasticity in emotional disorders induced by chronic MA administration. Future more extensive experiments will further explore dose- and site-dependent effects of 5-HT_{2C}R-targeted therapy. Furthermore, it would be interesting to explore the possibility of using 5-HT_{2C}R as a treatment target in emotional disorder-related symptoms induced by chronic MA administration.

In summary, our model mimics the emotional disorder-related symptoms of chronic MA administration in MA abusers. Long-term MA administration upregulates the expression of 5-HT_{2C}R in BLA, inhibits the activity of GABAergic interneurons, disinhibits local pyramidal neurons and causes abnormal BLA activity, thereby inducing emotional disorder-related symptoms. This study expands the understanding of emotional disorders among MA abusers and elucidates the potential therapeutic effect of targeting 5-HT_{2C}R.

DATA AVAILABILITY STATEMENT

The raw data supporting the conclusions of this article will be made available by the authors, without undue reservation.

ETHICS STATEMENT

The animal study was reviewed and approved by Southern Medical University.

AUTHOR CONTRIBUTIONS

PQ and JC designed the research. ZW, CL, JD, ZZ, YL, YaH, XW, JH, HF, YiH, and JL performed experiments, analyzed the data, and drafted the paper. CL and ZW performed the illustrations of the data. All authors have read and approved the final manuscript.

FUNDING

This work was supported by China Postdoctoral Science Foundation (Grant Nos. 2020M672991) and the National Natural Science Foundation of China (No. 82001528, 81671865).

REFERENCES

Adrielle, V. M., and Helio, Z. (2012). Serotonin-2C receptors in the basolateral nucleus of the amygdala mediate the anxiogenic effect of acute imipramine and fluoxetine administration. *Int. J. Neuropsychopharmacol.* 15 (3), 389–400. doi:10.1017/S1461145711000873

Al-Tikriti, M. S., Khamas, W., Chebolu, S., and Darmani, N. A. (2012). Distribution of serotonin-immunoreactive enterochromaffin cells in the gastrointestinal tract of the least shrew (*Cryptotis parva*). *Int. J. Morphol.* 30 (3), 916–923. doi:10.4067/S0717-95022012000300025

Althobaiti, Y., Almalki, A., Das, S., Alshehri, F., and Sari, Y. (2016). Effects of repeated high-dose methamphetamine and ceftriaxone post-treatments on tissue content of dopamine and serotonin as well as glutamate and glutamine. *Neurosci. Lett.* 634, 25–31. doi:10.1016/j.neulet.2016.09.058

Amidfar, M., and Kim, Y. (2018). Recent developments on future antidepressant-related serotonin receptors. *Curr. Pharmaceut. Des.* 24 (22), 2541–2548. doi:10.2174/1381612824666180803111240

Anastasio, N., Stutz, S., Fink, L., Swinford-Jackson, S., Sears, R., DiLeone, R., et al. (2015). Serotonin (5-HT) 5-HT2A receptor (5-HT2AR):5-HT2CR imbalance in medial prefrontal cortex associates with motor impulsivity. *ACS Chem. Neurosci.* 6 (7), 1248–1258. doi:10.1021/acschemneuro.5b00094

Angoa-Pérez, M., Kane, M., Herrera-Mundo, N., Francescutti, D., and Kuhn, D. (2014). Effects of combined treatment with mephedrone and methamphetamine or 3,4-methylenedioxymethamphetamine on serotonin nerve endings of the hippocampus. *Life Sci.* 97 (1), 31–36. doi:10.1016/j.lfs.2013.07.015

Bagheri, M., Mokri, A., Khosravi, A., and Kabir, K. (2015). Effect of abstinence on depression, anxiety, and quality of life in chronic methamphetamine users in a therapeutic community. *Int. J. High Risk Behav. Addict.* 4 (3), e23903. doi:10.5812/ijhrba.23903

Bubar, M., and Cunningham, K. (2008). Prospects for serotonin 5-HT2R pharmacotherapy in psychostimulant abuse. *Prog. Brain Res.* 172, 319–346. doi:10.1016/s0079-6123(08)00916-3

Burke, M. V., Nocjar, C., Sonneborn, A. J., Mccreary, A. C., and Pehek, E. A. (2015). Striatal serotonin 2C receptors decrease nigrostriatal dopamine release by increasing GABA-A receptor tone in the substantia nigra. *J. Neurochem.* 131 (4), 432–443. doi:10.1111/jnc.12842

Cao, X., Li, L., Wang, Q., Wu, Q., Hu, H., Zhang, M., et al. (2013). Astrocyte-derived ATP modulates depressive-like behaviors. *Nat. Med.* 19 (6), 773–777. doi:10.1038/nm.3162

Casaletto, K., Obermeit, L., Morgan, E., Weber, E., Franklin, D., Grant, I., et al. (2015). Depression and executive dysfunction contribute to a metamemory deficit among individuals with methamphetamine use disorders. *Addict. Behav.* 40, 45–50. doi:10.1016/j.addbeh.2014.08.007

Ceglia, I., Carli, M., Baviera, M., Renoldi, G., Calcagno, E., and Invernizzi, R. W. (2010). The 5-HT receptor antagonist M100,907 prevents extracellular glutamate rising in response to NMDA receptor blockade in the mPFC. *J. Neurochem.* 91 (1), 189–199. doi:10.1111/j.1471-4159.2004.02704.x

Chegini, H., Nasehi, M., and Zarrindast, M. (2014). Differential role of the basolateral amygdala 5-HT3 and 5-HT4 serotonin receptors upon ACPA-induced anxiolytic-like behaviors and emotional memory deficit in mice. *Behav. Brain Res.* 261, 114–126. doi:10.1016/j.bbr.2013.12.007

Chen, Y., Xu, H., Zhu, M., Liu, K., Lin, B., Luo, R., et al. (2017). Stress inhibits tryptophan hydroxylase expression in a rat model of depression. *Oncotarget* 8 (38), 63247–63257. doi:10.18632/oncotarget.18780

Clinard, C., Bader, L., Sullivan, M., and Cooper, M. (2015). Activation of 5-HT2a receptors in the basolateral amygdala promotes defeat-induced anxiety and the acquisition of conditioned defeat in Syrian hamsters. *Neuropharmacology* 90, 102–112. doi:10.1016/j.neuropharm.2014.11.016

Cryan, J. F., and Leonard, B. E. (2000). 5-HT1A and beyond: the role of serotonin and its receptors in depression and the antidepressant response. *Hum. Psychopharmacol.* 15 (2), 113–135. doi:10.1002/(SICI)1099-1077(200003)15:2<113::AID-HUP150>3.0.CO;2-W

Cunningham, K., and Anastasio, N. (2014). Serotonin at the nexus of impulsivity and cue reactivity in cocaine addiction. *Neuropharmacology*, 76 Pt B, 460–478. doi:10.1016/j.neuropharm.2013.06.030

Glasner-Edwards, S., and Mooney, L. (2014). Methamphetamine psychosis: epidemiology and management. *CNS Drugs* 28 (12), 1115–1126. doi:10.1007/s40263-014-0209-8

Gonda, X., Petschner, P., Eszlari, N., Baksa, D., Edes, A., Antal, P., et al. (2019). Genetic variants in major depressive disorder: from pathophysiology to therapy. *Pharmacol. Ther.* 194, 22–43. doi:10.1016/j.pharmthera.2018.09.002

Greenwood, B. N., Strong, P. V., Loughridge, A. B., Day, H. E., Clark, P. J., Mika, A., et al. (2012). 5-HT2C receptors in the basolateral amygdala and dorsal striatum are a novel target for the anxiolytic and antidepressant effects of exercise. *PloS One* 7 (9), e46118. doi:10.1371/journal.pone.0046118

Haughey, H. M., Fleckenstein, A. E., and Hanson, G. R. (1999). Differential regional effects of methamphetamine on the activities of tryptophan and tyrosine hydroxylase. *J. Neurochem.* 72 (2), 661–668. doi:10.1046/j.1471-4159.1999.0720661.x

Hayes, D. J., and Greenshaw, A. J. (2011). 5-HT receptors and reward-related behaviour: a review. *Neurosci. Biobehav. Rev.* 35 (6), 1419–1449. doi:10.1016/j.neubiorev.2011.03.005

Howell, L., and Cunningham, K. (2015). Serotonin 5-HT2 receptor interactions with dopamine function: implications for therapeutics in cocaine use disorder. *Pharmacol. Rev.* 67 (1), 176–197. doi:10.1124/pr.114.009514

Ji, W., and Suga, N. (2007). Serotonergic modulation of plasticity of the auditory cortex elicited by fear conditioning. *J. Neurosci.* 27 (18), 4910–4918. doi:10.1523/JNEUROSCI.5528-06.2007

Kalechstein, A. D., Newton, T. F., Longshore, D., Anglin, M. D., Van Gorp, W. G., and Gawin, F. H. (2000). Psychiatric comorbidity of methamphetamine dependence in a forensic sample. *J. Neuropsychiatry Clin. Neurosci.* 12, 480–484. doi:10.1176/jnp.12.4.480

Kedo, O., Zilles, K., Palomero-Gallagher, N., Schleicher, A., Mohlberg, H., Bludau, S., et al. (2018). Receptor-driven, multimodal mapping of the human amygdala. *Brain Struct. Funct.* 223 (4), 1637–1666. doi:10.1007/s00429-017-1577-x

Keshavarzi, S., Kermanshahi, S., Karami, L., Motaghinejad, M., Motevalian, M., and Sadr, S. (2019). Protective role of metformin against methamphetamine induced anxiety, depression, cognition impairment and neurodegeneration in rat: the role of CREB/BDNF and Akt/GSK3 signaling pathways. *Neurotoxicology* 72, 74–84. doi:10.1016/j.neuro.2019.02.004

Li, Q., Luo, T., Jiang, X., and Wang, J. (2012). Anxiolytic effects of 5-HT$_1$A receptors and anxiogenic effects of 5-HT$_2$C receptors in the amygdala of mice. *Neuropharmacology* 62 (1), 474–484. doi:10.1016/j.neuropharm.2011.09.002

Liu, S., Bubar, M. J., Lanfranco, M. F., Hillman, G. R., and Cunningham, K. A. (2007). Serotonin2C receptor localization in GABA neurons of the rat medial prefrontal cortex: implications for understanding the neurobiology of addiction. *Neuroscience* 146 (4), 1677–1688. doi:10.1016/j.neuroscience.2007.02.064

McDonald, A., and Mascagni, F. (2007). Neuronal localization of 5-HT type 2A receptor immunoreactivity in the rat basolateral amygdala. *Neuroscience* 146 (1), 306–320. doi:10.1016/j.neuroscience.2007.01.047

Mcfadden, L. M., Cordie, R., Livermont, T., and Johansen, A. (2018). Behavioral and serotonergic changes in the frontal cortex following methamphetamine self-administration. *Int. J. Neuropsychopharmacol.* 21 (8), 758–763. doi:10.1093/ijnp/pyy044

Meneses, A., and Liy-Salmeron, G. (2012). Serotonin and emotion, learning and memory. *Rev. Neurosci.* 23 (5-6), 543–553. doi:10.1515/revneuro-2012-0060

Mikics, E., Vas, J., Aliczki, M., Halasz, J., and Haller, J. (2009). Interactions between the anxiogenic effects of CB1 gene disruption and 5-HT3 neurotransmission. *Behav. Pharmacol.* 20 (3), 265–272. doi:10.1097/FBP.0b013e32832c70b1

Nic Dhonnchadha, B., Bourin, M., and Hascoët, M. (2003). Anxiolytic-like effects of 5-HT2 ligands on three mouse models of anxiety. *Behav. Brain Res.* 140, 203–214. doi:10.1016/s0166-4328(02)00311-x

Northrop, N. A., and Yamamoto, B. K. (2015). Methamphetamine effects on blood-brain barrier structure and function. *Front. Neurosci.* 9, 69. doi:10.3389/fnins.2015.00069

Prakash, M., Tangalakis, K., Antonipillai, J., Stojanovska, L., Nurgali, K., and Apostolopoulos, V. (2017). Methamphetamine: effects on the brain, gut and immune system. *Pharmacol. Res.* 120, 60–67. doi:10.1016/j.phrs.2017.03.009

Qin, X., Wu, Z., Dong, J., Zeng, Y., Xiong, W., Liu, C., et al. (2019). Liver soluble epoxide hydrolase regulates behavioral and cellular effects of chronic stress. *Cell Rep.* 29 (10), 3223–3234.e6. doi:10.1016/j.celrep.2019.11.006

Quesseveur, G., Nguyen, H., Gardier, A., and Guiard, B. (2012). 5-HT2 ligands in the treatment of anxiety and depression. *Expet Opin. Invest. Drugs* 21 (11), 1701–1725. doi:10.1517/13543784.2012.719872

Rainnie, D. (1999). Serotonergic modulation of neurotransmission in the rat basolateral amygdala. *J. Neurophysiol.* 82 (1), 69–85. doi:10.1152/jn.1999.82.1.69

Ru, Q., Xiong, Q., Zhou, M., Chen, L., Tian, X., Xiao, H., et al. (2019). Withdrawal from chronic treatment with methamphetamine induces anxiety and depression-like behavior in mice. *Psychiatr. Res.* 271, 476–483. doi:10.1016/j.psychres.2018.11.072

Sengupta, A., Bocchio, M., Bannerman, D., Sharp, T., and Capogna, M. (2017). Control of amygdala circuits by 5-HT neurons via 5-HT and glutamate cotransmission. *J. Neurosci.* 37 (7), 1785–1796. doi:10.1523/jneurosci.2238-16.2016

Sengupta, A., and Holmes, A. (2019). A discrete dorsal raphe to basal amygdala 5-HT circuit calibrates aversive memory. *Neuron* 103 (3), 489–505.e7. doi:10.1016/j.neuron.2019.05.029

Spoida, K., Masseck, O. A., Deneris, E. S., and Herlitze, S. (2014). Gq/5-HT2c receptor signals activate a local GABAergic inhibitory feedback circuit to modulate serotonergic firing and anxiety in mice. *Proc. Natl. Acad. Sci. U.S.A.* 111 (17), 6479–6484. doi:10.1073/pnas.1321576111

Strauss, C., Vicente, M., and Zangrossi, H. (2013). Activation of 5-HT1A receptors in the rat basolateral amygdala induces both anxiolytic and antipanic-like effects. *Behav. Brain Res.* 246, 103–110. doi:10.1016/j.bbr.2013.03.005

Takayuki, H., Hiroshi, T., Rintaro, M., and Wilson, D. B. (2018). Cognitivebehavioural treatment for amphetamine-type stimulants (ATS)-use disorders. *Cochrane Database Syst. Rev.* 12, CD011315. doi:10.1002/14651858.CD011315.pub2

United Nations (2020). World drug report. Available at: https://wdr.unodc.org/wdr2020/ (Accessed October 27, 2020).

Vicente, M., and Zangrossi, H. (2014). Involvement of 5-HT2C and 5-HT1A receptors of the basolateral nucleus of the amygdala in the anxiolytic effect of chronic antidepressant treatment. *Neuropharmacology* 79, 127–135. doi:10.1016/j.neuropharm.2013.11.007

Voce, A., Calabria, B., Burns, R., Castle, D., and Mcketin, R. (2019). A systematic review of the symptom profile and course of methamphetamine-associated psychosis. *Subst. Use Misuse* 54 (4), 549–559. doi:10.1080/10826084.2018.1521430

Wang, Y., Liu, Y., Xiong, J., Di, T., Yuan, Z., Wu, J., et al. (2019a). Reduced serotonin impairs long-term depression in basolateral amygdala complex and causes anxiety-like behaviors in a mouse model of perimenopause. *Exp. Neurol.* 321, 113030. doi:10.1016/j.expneurol.2019.113030

Wang, Z., Zeng, Y. N., Yang, P., Jin, L. Q., and Zhu, X. H. (2019b). Axonal iron transport in the brain modulates anxiety-related behaviors. *Nat. Chem. Biol.* 15 (12), 1214–1222. doi:10.1038/s41589-019-0371-x

Zhang, J., Xie, Y., Su, H., Tao, J., Sun, Y., Li, L., et al. (2014). Prevalence and correlates of depressive symptoms during early methamphetamine withdrawal in Han Chinese population. *Drug Alcohol Depend.* 142, 191–196. doi:10.1016/j.drugalcdep.2014.06.021

Conflict of Interest: The authors declare that the research was conducted in the absence of any commercial or financial relationships that could be construed as a potential conflict of interest.

frontiers in Pharmacology

ORIGINAL RESEARCH
published: 18 February 2021
doi: 10.3389/fphar.2021.625610

Long-Term Outcomes of Patients With Cocaine Use Disorder: A 18-years Addiction Cohort Study

*Arantza Sanvisens[1], Anna Hernández-Rubio[1], Paola Zuluaga[1], Daniel Fuster[1], Esther Papaseit[2], Sara Galan[1], Magí Farré[2] and Robert Muga[1]**

[1]Department of Internal Medicine, Hospital Universitari Germans Trias i Pujol-IGTP, Universitat Autónoma de Barcelona, Department of Medicine, Badalona, Spain, [2]Department of Clinical Pharmacology, Hospital Universitari Germans Trias i Pujol-IGTP, Universitat Autònoma de Barcelona, Badalona, Spain

OPEN ACCESS

Edited by:
Qi Wang,
Southern Medical University, China

Reviewed by:
Yadong Guo,
Central South University, China
Sun Junhong,
Shanxi Medical University, China
Keiichi Kadoyama,
Himeji Dokkyo University, Japan

***Correspondence:**
Robert Muga
rmuga.germanstrias@gencat.cat

Specialty section:
This article was submitted to Neuropharmacology, a section of the journal Frontiers in Pharmacology

Received: 03 November 2020
Accepted: 14 January 2021
Published: 18 February 2021

Citation:
Sanvisens A, Hernández-Rubio A, Zuluaga P, Fuster D, Papaseit E, Galan S, Farré M and Muga R (2021) Long-Term Outcomes of Patients With Cocaine Use Disorder: A 18-years Addiction Cohort Study. Front. Pharmacol. 12:625610. doi: 10.3389/fphar.2021.625610

Objective: Cocaine Use Disorder (CUD) has been associated with multiple complications and premature death. The purpose of the present study was to analyze the relationship between baseline medical comorbidity and long-term medical outcomes (i.e., hospitalization, death) in a cohort of patients primarily admitted for detoxification. In addition, we aimed to analyze cause-specific mortality.

Methods: longitudinal study in CUD patients admitted for detoxification between 2001 and 2018. Substance use characteristics, laboratory parameters and medical comorbidity by VACS Index were assessed at admission. Follow-up and health-related outcomes were ascertained through visits and e-health records. Kaplan-Meier and Cox regression models were used to analyze survival and predictors of hospitalization and death.

Results: 175 patients (77.7% men) were included. Age at admission was 35 years [IQR: 30–41 years], 59.4% of the patients being intranasal users, 33.5% injectors, and 7.1% smokers. Almost 23% of patients had concomitant alcohol use disorder, 39% were cannabis users and 9% opiate users. The median VACS Index score on admission was 10 points [IQR: 0–22]. After 12 years [IQR: 8.6–15 years] of follow-up there were 1,292 (80.7%) ED admissions and 308 (19.3%) hospitalizations. The incidence rate of ED admission and hospitalization was 18.6 × 100 p-y (95% CI: 15.8–21.8 × 100 p-y). Mortality rate was 1.4 × 100 p-y (95% CI: 0.9–2.0 × 100 p-y) and, baseline comorbidity predicted hospitalization and mortality: those with VACS Index >40 were 3.5 times (HR:3.52, 95% CI: 1.19–10.4) more likely to dye with respect to patients with VACS < 20.

Conclusion: addiction care warrants optimal stratification of medical comorbidity to improve health outcomes and survival of CUD patients seeking treatment of the disorder.

Keywords: cocaine use disorder, VACS index, comorbidity, mortality, hospitalization

INTRODUCTION

Cocaine is the second most widely used illegal drug in Western Europe after cannabis. According to the European Monitoring Center for Drugs and Drug Addiction (EMCDDA), about four million people aged 15–64 have used cocaine in the last year, and the number of users has increased in recent years (European Monitoring Center for Drugs and Drug Addiction (EMCDDA), 2019).

According to the EDADES population survey on alcohol and drugs, 2% of the general population aged 15–64 in Spain uses cocaine (Observatorio Español de las Drogas y las Adicciones, 2019). Moreover, 54% of people who have used cocaine in the last year have used it in the last month (Observatorio Español de las Drogas y las Adicciones, 2019). In Catalonia (Spain), 24% of people who seek treatment for substance use disorder (SUD) have a cocaine use disorder (CUD), and this percentage has increased in recent years (Subdirecció General de Drogodependències, 2018).

CUD has been associated with serious systemic complications, frequent use of healthcare resources (i.e., emergency department (ED) admissions, hospitalization), and premature death (Degenhardt et al., 2011; Butler et al., 2017). In fact, cocaine use can aggravate inflammatory diseases and alter immune functions that favor the progression of cardiovascular, respiratory, or infectious diseases (Taylor et al., 2016; Bachi et al., 2017). In addition, it has been communicated that cocaine intoxication can cause acute kidney injury, hepatotoxicity, and disseminated intravascular coagulation (Vitcheva, 2012; Filho et al., 2019). On the other hand, cocaine use has been associated with an increased risk of HIV infection and hepatitis C virus (HCV) infection even in the absence of injecting drug use (Macías et al., 2008; Deiss et al., 2012).

In addition, patients with CUD show a high prevalence of psychiatric comorbidities, such as mood disorders (12–62%), anxiety disorders (21–45%) and suicidal tendencies, among others (Vergara-Moragues et al., 2012; Warden et al., 2016). Cocaine use has also been associated with traffic accidents and violence (Giovanardi et al., 2005; Pavarin et al., 2011).

Polysubstance use is common among cocaine users, especially alcohol consumption, but the concurrent use of marijuana and opiates is also prevalent, and has been associated with poor health outcomes (Stinson et al., 2005; Timko et al., 2018). In the US, the second wave of the National Epidemiologic Survey on Alcohol and Related Conditions (NESARC) estimated that 79% of people with CUD have a concomitant alcohol use disorder (AUD) (Stinson et al., 2005).

A recent systematic review and meta-analysis on healthcare utilization demonstrated that in SUD patients, hospitalization and ED admissions are 5 and 7 times more frequent, respectively, compared to the general population (Lewer et al., 2020). In addition, the death rate of patients with CUD ranges from 0.5 to 6.2 × 100 person-years (p-y) and is considered to be 4 to 8 times higher than the death rate of the general population (Arendt et al., 2011; Degenhardt et al., 2011).

Our hypothesis is that the chronicity of CUD is suggestive of the presence of multiple medical complications, which leads to the excessive use of healthcare resources (i.e., ED visits and hospitalization). We aimed to analyze the relationship between baseline medical comorbidity, use of health resources, and long-term health outcomes among those seeking treatment for CUD.

MATERIALS AND METHODS

This was a longitudinal study of patients admitted to the addiction treatment unit of a tertiary hospital (Germans Trias i Pujol University Hospital) between January 2001 and May 2018. The unit admits patients diagnosed with SUD in an area in the north of Barcelona (Spain) with 400,000 inhabitants. There were 837 admissions for addiction treatment between January 2001 and May 2018, of which 195 (23.3%) were due to CUD in 175 patients. In those who were admitted more than once, only the first admission was analyzed.

The patients came from local primary care centers and from two municipal outpatient addiction clinics, one in Badalona (250,000 inhabitants) and the other in Santa Coloma de Gramenet (150,000 inhabitants), both located in the metropolitan area of Barcelona (Spain). The main admission criteria for CUD treatment were as follows: failure in outpatient treatment, concurrent dependency on other addictive drugs or alcohol, serious concurrent medical problems, severe impairment of psychosocial functioning, lack of family and social support, and use of crack or freebase cocaine or intravenous cocaine abuse, among others.

All patients received a diagnosis of CUD according to the Diagnostic and Statistical Manual of Mental Disorders, fourth Ed (DSM-IV) and fifth Ed (DSM-5). Due to the transition from DSM-IV to DSM-5, not all participants were evaluated under the same DSM.

On admission, data on the use of cocaine and other substances (i.e., alcohol, cannabis, opiates) were collected, including age of onset, route of administration, and duration. DSM criteria were used to diagnose AUD. Cannabis and opiates use was ascertained through urinalysis at admission. For the purposes of this study, patients were classified according to the route of cocaine administration as either intranasal or non-intranasal users (i.e., injectors, smokers).

In all patients, blood samples were drawn for biochemical and hematological parameters, and for serologic testing for human immunodeficiency virus (HIV) infection and hepatitis C virus (HCV) infection. Anthropometric data (i.e., height and weight) were obtained as well.

Medical comorbidity on admission was analyzed using the VACS Index (Veterans Aging Cohorts Study Index). VACS Index assigns a score based on age and on blood parameters, such as hemoglobin, platelets, aspartate and alanine aminotransferase levels, creatinine, HIV infection, CD4 lymphocytes, HIV RNA, and HCV infection. The VACS Index ranges from 0 to 164 points, with a higher score indicating greater comorbidity. The VACS Index has been associated with an increased risk of hospitalization and death in patients with and without HIV infection (Blackstock et al., 2013; Justice et al., 2013; Tate et al., 2013). In HIV-negative patients, HIV RNA is considered undetectable.

Follow-Up, Comorbidity and Outcomes

The patients were followed up until September 30, 2018 through in-person visits and review of the ED visits and hospitalization

e-health records of the Catalan health department. The diagnoses made during the ED visits and hospitalization were coded according to the 10th revision of the International Classification of Diseases (ICD-10). The diagnostic coding was carried out by two members of the research team (AS and RM) independently; coding discrepancies were resolved by consensus.

Mortality was analyzed by cross-referencing the data with the National Death Index as of September 30, 2018. The causes of death were established by reviewing the medical history.

Ethics

All patients gave written informed consent, and the study design was approved by the Ethics Committee of the Germans Trias i Pujol University Hospital (approval number PI-13-082). The methods were in compliance with the ethical standards for medical research and the principles of good clinical practice in accordance with the World Medical Association's Declaration of Helsinki.

Statistical Analysis

Descriptive statistics were expressed as median and interquartile range (IQR) for quantitative variables and as absolute frequencies and percentages for qualitative variables.

We used the chi-square test to detect significant differences in qualitative variables and t-Student test for differences in quantitative variables. The Kruskal-Wallis equality-of-populations rank test and Mann-Whitney U test were used to analyze differences in the distribution of episodes during follow-up.

Rates were calculated in p-y by dividing the number of observed events during the study period by the sum of all individual follow-up times. The survival estimates were analyzed using the Kaplan-Meier curves. Cox regression models were used to analyze the risk factors of first hospitalization after discharge and mortality. The sex, variables related to substance use, and the VACS Index score were included in the analysis. All covariates that were statistically significant in the univariate analysis were included in the multivariate analysis. Prior to implementing the statistical models, we checked the proportional hazard assumptions using tests and graphs based on the Schoenfeld residuals.

p-values <0.05 were considered statistically significant. Statistical analysis was performed using Stata software (version 11.1, College Station, Texas, United States).

RESULTS

Patient Characteristics at Baseline

The study included 175 patients (77.7% men) aged 35 years [IQR: 30–41 years]. The age of onset of cocaine use was 22 years [IQR: 18–26 years], with 59.4% of the patients being intranasal users, 33.5% injectors, and 7.1% smokers. Moreover, 22.9% of the patients had concomitant AUD. According to the screening for illegal drugs in urine samples, 39.4% were cannabis users and 9% opiate users. Overall, 58.1% of the patients used alcohol or other substances in addition to cocaine. The most common combinations of substances were cocaine and cannabis (27.5%), cocaine and alcohol (14.4%), and cocaine, alcohol, and cannabis (7.5%).

TABLE 1 | Sociodemographic characteristics, alcohol and substance use, and clinical and blood parameters in 175 patients admitted for the treatment of CUD in metropolitan Barcelona, Spain.

	N = 175
Men, *n* (%)	136 (77.7)
Age, median [IQR]	35 [30–41]
BMI, (kg/m^2) (*n* = 144), median [IQR]	19.5 [16.4–23.0]
Drug related parameters	*n* (%)
Age at starting cocaine use, median [IQR]	22 [18–26]
Route of cocaine administration (*n* = 170)	
Injected	57 (33.5)
Intranasal	101 (59.4)
Smoked	12 (7.1)
Duration of CUD (months) (*n* = 164), median [IQR]	111 [36–180]
AUD	40 (22.9)
Urine screening at admission	
Opiates (*n* = 158)	14 (8.9)
Cannabis (*n* = 160)	63 (39.4)
Antecedent of injection drug use (*n* = 172)	82 (47.7)
Hematology parameters	Median [IQR]
Platelet count (x10^{9}L) (*n* = 174)	219 [184–270]
Hemoglobin (g/dL) (*n* = 174)	14.2 [12.9–15.3]
Biochemistry	Median [IQR]
Creatinine (mg (dL) (*n* = 173)	0.9 [0.78–0.99]
Glomerular filtration rate (*n* = 173)	97.6 [83.9–109]
Aspartate aminotransferase (U/L)	24 [18–40]
Alanine aminotransferase (U/L) (*n* = 173)	25 [16–46]
Comorbidity	n (%)
HIV Infection (*n* = 174)	43 (24.7)
CD4$^+$ T cell (x10^{9}L), median [IQR]	457 [214–730]
Viral load (copies/mL), median [IQR]	1,000 [49–22,000]
HCV Infection (*n* = 173)	82 (47.4)
FIB-4 (*n* = 173), median [IQR]	0.76 [0.54–1.28]
Advanced liver fibrosis (>3.25)	8 (4.6)
VACS index (*n* = 173), median [IQR]	10 [0–22]
<20	123 (71.1)
20–39	38 (22.0)
>40	12 (6.9)

AUD, alcohol use disorder; BMI, body mass index; CUD, cocaine use disorder; HCV, hepatitis C virus; HIV, human immunodeficiency virus; IQR, interquartile range.

The laboratory test results for hemoglobin, total cholesterol, and gamma-glutamyl transferase were 14.2 g/dl [IQR: 12.9–15.3 g/dl], 170 mg/dl [IQR: 147–201 mg/dl], and 28 U/L [IQR: 17–62 U/L], respectively. Moreover, 24.7% of the patients were HIV-positive and 47.4% were anti-HCV positive.

The body mass index (BMI) was 19.5 kg/m^2 [IQR: 16.4–23.0 kg/m^2]. The median VACS Index score on admission was 10 points [IQR: 0–22; range 0–69]. **Table 1** shows the sociodemographic characteristics, alcohol and substance use, and clinical and blood parameters.

Follow-Up, ED Visits, Hospitalizations and Comorbidity

Table 2 shows the socio-demographics, substance use characteristics, and clinical and blood parameters of CUD patients that were hospitalized during follow-up. Hospitalization was significantly more frequent in women (p = 0.049), in those with antecedent of injecting drug use (p = 0.028), and in HIV-positive and HCV-positive patients (p = 0.001 and p = 0.047, respectively).

TABLE 2 | Baseline characteristics of CUD patients according to hospitalization and death during follow-up.

	Hospitalization			Death		
	Yes	No	*p* value	Yes	No	*p* value
	N = 97	N = 78		N = 27	N = 148	
Men, *n* (%)	70 (72.2)	66 (84.6)	0.049	21 (77.8)	115 (77.7)	0.993
Age, median [IQR]	36 [31–41]	34.5 [30–40]	0.392	37 [32–42]	34.5 [30–40.5]	0.323
BMI, (kg/m^2) (*n* = 144), median [IQR]	18.5 [15.6–22.0]	21.0 [17.6–23.4]	0.030	19.4 [14.6–22.7]	19.6 [16.7–23.1]	0.334
Drug related parameters						
Age at starting cocaine use, median [IQR]	21 [17–26]	19.5 [18–25]	0.484	22 [18–24]	20 [17–26]	0.963
Route of cocaine administration (*n* = 170)						
Injected	33 (35.5)	24 (31.2)	0.509	17 (63.0)	40 (28.0)	0.001
Intranasal	52 (55.9)	49 (63.6)		10 (37.0)	91 (63.6)	
Smoked	8 (8.6)	4 (5.2)		0 (0)	12 (8.4)	
Duration of CUD (months) (*n* = 164), median [IQR]	120 [42–180]	96 [36–180]	0.968	96 [36–204]	114 [48–180]	0.604
AUD	25 (25.8)	15 (19.2)	0.306	4 (14.8)	36 (24.3)	0.279
Urine screening at admission						
Opiates (*n* = 158)	8 (9.1)	6 (8.6)	0.909	3 (13.0)	11 (8.1)	0.445
Cannabis (*n* = 160)	34 (37.8)	29 (41.4)	0.639	12 (50.0)	51 (37.5)	0.248
Antecedent of injection drug use (*n* = 172)	52 (55.3)	30 (38.5)	0.028	21 (80.8)	61 (41.8)	<0.001
*H*ematology parameters						
Platelet count (×10^{9}L) (*n* = 174)	226 [189–279]	210 [181–262]	0.148	193 [139–233]	224 [191–272]	0.005
Hemoglobin (g/dL) (*n* = 174)	14.2 [13–15.2]	14.1 [12.9–15.3]	0.861	14.7 [12.6–15.1]	14.1 [13.0–15.3]	0.973
Biochemistry						
Creatinine (mg (dL) (*n* = 173)	0.89 [0.78–0.99]	0.9 [0.78–0.97]	0.876	0.9 [0.74–1.01]	0.89 [0.79–0.99]	0.955
Glomerular filtrate rate (*n* = 173)	96.5 [82.8–107.5]	98.3 [85.7–112.4]	0.248	97.7 [83.7–112.4]	97.6 [84.1–108.4]	0.997
Aspartate aminotransferase (U/L)	25 [19–39]	23 [17–41]	0.429	38 [22–73]	23 [18–36.5]	0.006
Alanine aminotransferase (U/L) (*n* = 173)	25.5 [16–43.5]	22 [15–51]	0.877	42 [21–65]	23 [15–42]	0.109
Comorbidity						
HIV Infection (*n* = 174)	33 (34.4)	10 (12.8)	0.001	14 (51.8)	29 (19.7)	<0.001
CD4$^+$ T cell (x10^{9}L), median [IQR]	486 [242–771]	382 [202–562]	0.314	364 [202–457]	562 [242–792]	0.097
Viral load (copies/mL), median [IQR]	2,700 [49–22,000]	337 [49–8,100]	0.325	4,050 [49–15,000]	570 [49–22,000]	0.725
HCV Infection (*n* = 173)	52 (54.2)	30 (39.0)	0.047	21 (77.8)	61 (41.8)	0.001
FIB-4, median [IQR] (*n* = 173)	0.76 [0.54–1.30]	0.78 [0.53–1.26]	0.732	1.5 [0.8–2.2]	0.7 [0.5–1.1]	<0.001
Advanced liver fibrosis (>3.25)	3 (3.1)	5 (6.5)	0.294	4 (14.8)	4 (2.7)	0.006
VACS index, median [IQR] (*n* = 173)	10 [0–27]	10 [0–15]	0.110	21 [11–33]	10 [0–19]	0.001
<20	64 (66.7)	59 (76.6)	0.349	13 (48.1)	110 (75.3)	0.005
20–39	24 (25.0)	14 (18.2)		9 (33.3)	29 (19.9)	
>40	8 (8.3)	4 (5.2)		5 (18.5)	7 (4.8)	

AUD, alcohol use disorder; BMI, body mass index; CUD, cocaine use disorder; HCV, hepatitis C virus; HIV, human immunodeficiency virus; IQR, interquartile range.

The median follow-up time was 12.1 years [IQR: 8.6–15.1 years] with a total time of 1,973.2 p-y. At the end of the study, there were 1,292 (80.7%) ED admissions and 308 (19.3%) hospitalizations. The median number of ED admissions and hospitalizations per patient were 5 [IQR: 1–10] and 1 [IQR: 0–2], respectively. The vast majority (85.1%) of the patients presented at least one episode of ED admission or hospitalization. Statistically significant differences were observed in the distribution of episodes (either ED admission or hospitalization) according to gender and HIV status; specifically, women (z = −2.704, p = 0.007) and HIV-positive patients (z = −2.291, p = 0.022) had a greater number of episodes (**Figure 1**). The probability of having an ED admission or hospitalization was 50% after 2.5 years (95% CI: 1.9–3.7 years) (**Figure 2A**).

The incidence rate of ED admission or hospitalization was 18.6 × 100 p-y (95% CI: 15.8–21.8 × 100 p-y), which was significantly higher in women (rate ratio (RR): 1.8, 95% CI: 1.22–2.60, p = 0.002) and in patients with concomitant AUD (RR: 2.0, 95% CI: 1.3–2.9, p < 0.001). **Figure 3A** shows the incidence of episodes according to baseline medical comorbidity.

In terms of ED admissions, 19% were related to trauma/injuries (i.e., fractures, contusions, wounds), 19% to non-specific/unclassified symptoms, 10% to substance use, and 8.5% to mental disorder.

Regarding hospitalization, almost 40% of the episodes were related to mental health, 11% to the liver/digestive system, and 10.4% to respiratory conditions (i.e., pneumonia). **Figure 4** shows the distribution of ED admission and hospitalization episodes according to the main diagnosis.

Table 3 shows the risk factors for hospitalization. Specifically, being women (hazard ratio (HR): 1.61, 95% CI: 1.02–2.58), presenting concomitant AUD (HR: 1.42, 95% CI: 1.18–1.71), and having VACS Index >40 (HR: 2.59, 95% CI: 1.13–5.94) were significantly associated with a higher probability of hospitalization.

Mortality and Causes of Death

Of the patients included in the study, 15.4% (n = 27) died during the follow-up and the death rate was 1.4 × 100 p-y (95% CI: 0.9–2.0 × 100 p-y). **Table 2** shows the differences between those who died and those who survived; all-cause mortality was

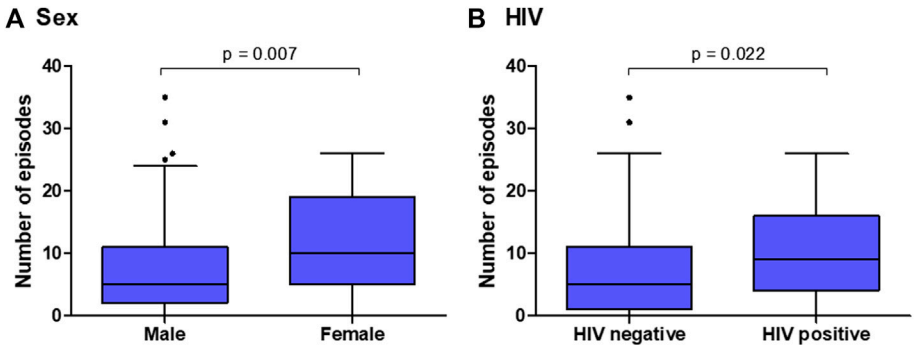

FIGURE 1 | ED admissions or hospitalizations by **(A)** sex and **(B)** HIV infection status in a cohort of 175 patients admitted for treatment of CUD in metropolitan Barcelona, Spain.

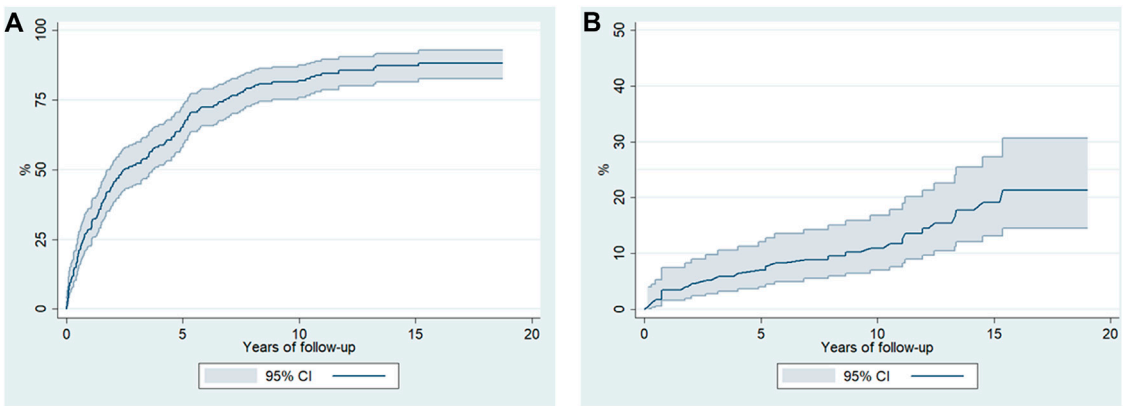

FIGURE 2 | Kaplan-Meier estimates (95% confidence intervals) for **(A)** ED visits or hospitalization episodes of 175 CUD patients and for **(B)** survival after being admitted for detoxification in metropolitan Barcelona, Spain.

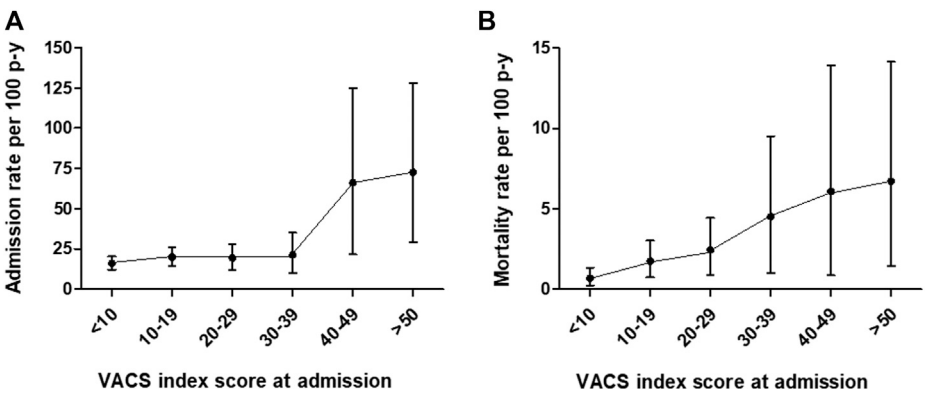

FIGURE 3 | Comorbidity (VACS Index)-adjusted incidence rates (95% confidence intervals) of **(A)** ED admission or hospitalization episodes and **(B)** mortality in a cohort of 175 patients seeking treatment of CUD in metropolitan Barcelona, Spain.

significantly associated with current or past injecting drug use ($p = 0.001$ and $p < 0.001$, respectively), HIV infection ($p < 0.001$), HCV infection ($p < 0.001$), advanced liver fibrosis ($p = 0.006$) and higher scores in VACS Index ($p = 0.005$).

Figure 2B shows the estimate (Kaplan-Meier) of survival after admission for CUD treatment. The multivariate analysis showed that medical comorbidity was the only predictor of death; patients with VACS >40 showed 3.5 times greater probability of death (HR 3.52,

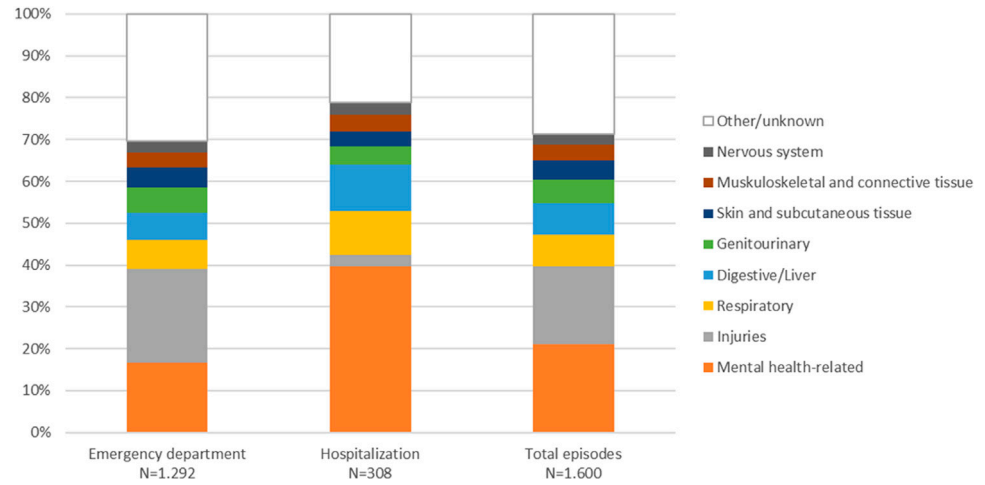

FIGURE 4 | Distribution of 1,292 ED admissions and 308 hospitalizations according to ICD-10 diagnostic codes.

TABLE 3 | Cox regression model for predictors of hospitalization and death in a cohort of 175 patients admitted for treatment of CUD in metropolitan Barcelona, Spain.

	Hospitalitzation		Death	
	Unadjusted HR (95% CI)	**Multivariate HR (95% CI)**	**Unadjusted HR (95% CI)**	**Multivariate HR (95% CI)**
Women	**1.89 (1.21–2.96)**	**1.61 (1.01–2.58)**	1.07 (0.43–2.65)	
Age at starting cocaine use: 5 years increase	1.15 (0.93–1.43)		0.93 (0.57–1.52)	
Non-intranasal cocaine	0.94 (0.62–1.41)		**2.30 (1.05–5.03)**	1.64 (0.69–3.92)
Duration of CUD	0.99 (0.99–1.00)		1.00 (0.99–1.01)	
AUD	**1.23 (1.05–1.44)**	**1.27 (1.08–1.48)**	0.96 (0.67–1.38)	
Urine screening at admission				
Opiates	0.72 (0.35–1.50)		1.28 (0.38–4.32)	
Cannabis	0.84 (0.55–1.29)		1.49 (0.67–3.32)	
VACS index				
<20	1	1	1	1
20–39	1.30 (0.81–2.08)	1.24 (0.77–2.02)	**2.39 (1.02–5.59)**	1.86 (0.73–4.72)
>40	**2.63 (1.25–5.52)**	**2.64 (1.20–5.83)**	**4.35 (1.55–12.2)**	**3.52 (1.19–10.4)**

Statistically significant differences are in bold. AUD, alcohol use disorder; CUD, cocaine use disorder; CI, confidence interval; HR: hazard ratio.

95% CI: 1.19–10.4) compared to patients with VACS Index <20 (**Table 3**). **Figure 3B** shows death rates according to VACS Index.

The cause of death was determined in 77.7% (21/27) of cases; the main causes were drug-related in 40% (n = 8; 5 overdoses, 3 unattended deaths in the context of current drug use), cancer in 19% (n = 4), infectious diseases in 9.5% (n = 2), cardiovascular diseases in 9.5% (n = 2), and liver cirrhosis in 9.5% (n = 2).

DISCUSSION

This longitudinal study in patients with CUD who were followed for 12 years confirms the prognostic value of a comorbidity index in predicting the risk of hospitalization and death in patients seeking treatment for the disorder. VACS is a multiorgan system injury index validated in 2013 for HIV-positive patients, although it has been described as a reliable index for HIV-negative patients as well and as a predictor of health outcomes such as hospitalization (Tate et al., 2013; Barakat et al., 2015; Hotton et al., 2017). To the best of our knowledge, this is the first time that VACS Index was analyzed in a cohort of HIV-positive and HIV-negative patients with CUD. Our results support the use of medical comorbidity rates in patients with SUD who start treatment, although more studies are required to confirm these findings.

In this study, VACS Index at baseline reflected moderate organ system damage, even though 47 and 25% of the patients had HCV and HIV infection, respectively. Despite moderate comorbidity, those with a VACS Index score over 40 were up to 2.6 times more likely to require hospitalization than those with a VACS score under 20. On the other hand, women with CUD and AUD were at a higher risk of hospitalization. Concomitant AUD is frequent in CUD and has been described as an indicator of poor health outcomes (Timko et al., 2018). Specifically, cocaethylene, the metabolite resulting from the concomitant use of alcohol and cocaine, has a known toxicity (Jones, 2019). This potent stimulant

is more toxic than cocaine itself and has a longer half-life. On the other hand, the increased risk of hospitalization for women with CUD requires an accurate evaluation of the continuum of care and care coordination after discharge.

It was interesting to confirm that medical comorbidity was the only predictor of death in this cohort with a high prevalence of polysubstance use. Some studies on CUD indicate that the risk of death is higher in men, in those with a history of injected drugs, in those with an early onset of use, in those who drink alcohol, or in those with psychiatric comorbidity (Arendt et al., 2011; de la Fuente et al., 2014). However, there are hardly any studies on the medical comorbidity of CUD other than HIV infection and HCV infection. VACS Index analyzes kidney and liver function in addition to age, hemoglobin and HIV and HCV infections, thus reflecting the general health status. The recent 2019 version includes albumin, blood cell count, and BMI (Tate et al., 2019), which may improve the prognostic value of VACS.

It was interesting to note that BMI was below 19.5 kg/m^2 in 50% of the patients in this study and below 16.4 kg/m^2 in 25%, which indicates that being underweight might be associated with CUD or an underlying disease. A population study in adults aged 18–45 years demonstrated that the BMI of cocaine users is lower than that of non-users, although those BMI values were much higher than those observed in this study (Qureshi et al., 2014).

On the other hand, death rates in this hospital-based cohort were higher than that reported by another Spanish study of patients recruited in outpatient clinics (de la Fuente et al., 2014), although clearly lower than that reported by our group in past decades (Sanvisens et al., 2014).

ED admissions for accidents/injuries and non-specific symptoms were the most frequent during follow-up, suggesting that they could be related to continued substance use or complications derived from such use. The first systematic review and meta-analysis on healthcare utilization in patients with SUD was published in 2019 and shows that hospitalization and ED admissions are 5 and 7 times more frequent, respectively, in this group than in the general population (Lewer et al., 2020). In Spain, 38.4% of drug-related ED admissions can be attributed to cocaine (Miró et al., 2019). Furthermore, a study reveals that 18% of those admitted to an ED for cocaine use are readmitted in the following year (Miro et al., 2010).

Mental health-related complications, accidents/injuries, respiratory/lung related conditions, and digestive/liver diseases were other diagnoses frequently observed during follow-up. About 40% of the episodes were related to SUD either due to an associated mental illness or to trauma/accidents associated with substance use. These results are consistent with those presented in individuals who use illicit drugs (Aitken et al., 2013; Kendall et al., 2017). The pulmonary complications resulting from cocaine use could be due to several reasons, although the route of administration is relevant (Mégarbane and Chevillard, 2013); cocaine's respiratory toxicity can be immediate (i.e., acute lung injury or hypersensitivity reaction) or delayed (i.e., chronic obstructive pulmonary disease, cancer) (Mégarbane and Chevillard, 2013). A recent study shows that cocaine users are at increased risk for pulmonary hypertension (Alzghoul et al., 2020).

In terms of digestive/liver comorbidity, our findings are consistent with those observed in other studies (Pavarin et al., 2011). Liver decompensation was another frequent reason for clinical attention; however, a study in patients coinfected with HIV and HCV was unable to demonstrate an association between cocaine/crack use and evolution of liver fibrosis (Martel-Laferrière et al., 2017). Therefore, it is likely that alcohol abuse in the patients could explain those findings.

Cardiovascular complications in this long-term followed-up cohort were less frequent than expected, despite the extensive scientific literature on CUD and acute coronary syndrome (Lippi et al., 2010; Carrillo et al., 2011). However, the results are consistent with those reported in other cohorts with low frequency of coronary ischemic complications (Qureshi et al., 2014).

This study has several limitations that should be mentioned. First, socioeconomic and baseline psychiatric comorbidity data were not available, which could have facilitated the interpretation of some findings during follow-up. Second, temporary changes in cocaine use (i.e., remission or exacerbation of use) were not analyzed. In this sense, retention in care is critical for achieving remission of CUD. The high rate of ED admissions of the patients in this study and the diagnoses of episodes related to continued substance use suggest low treatment retention. Third, patients from this study were evaluated with different DSM versions; however, criteria for admission were similar throughout the study period and mainly related to the severity of CUD. Fourth, this study had a limited number of patients, which impairs the interpretation of some associations due to lack of statistical power (i.e., route of cocaine administration). In addition, this study was carried out in a single unit which limits the generalization of the findings.

In contrast, the strength of this study among patients seeking treatment for CUD highlights the challenges in measuring medical comorbidity with an index that has proven to be useful in the context of SUD. Most studies on cocaine-related morbidity are conducted in EDs with patients with acute intoxication (Arendt et al., 2011; Qureshi et al., 2014; Miró et al., 2019; Santurtún et al., 2020), which prevents an accurate clinical assessment of comorbidity. Finally, understanding the risk factors for mortality allows us to target preventive interventions to increase retention in care among those seeking treatment for the disorder.

DATA AVAILABILITY STATEMENT

The datasets generated for this study are available on request to the corresponding author.

ETHICS STATEMENT

The studies involving human participants were reviewed and approved by the Ethics Committee of the Germans Trias i Pujol University Hospital (approval number PI-13-082). The patients/

participants provided their written informed consent to participate in this study.

AUTHOR CONTRIBUTIONS

AS and RM designed the study and wrote the first draft of the manuscript. AHR and SG reviewed e-health records and managed the databases. AS managed the literature searches and statistical analysis. RM, PZ and DF recruited the study population and took care of patients. AS and RM reviewed the literature and made contributions to the interpretation of data. AS, EP, MF, and RM contributed to the discussion section. All the authors revised and approved the final manuscript.

FUNDING

This work was funded by the Ministry of Science, Innovation and Universities, Carlos III Health Institute (ISCIII), Spain and European Fund for Regional Development (FEDER), (grant numbers RD16/0017/0003, PI17/00174, PI20/00883); the Ministry of Health, Social Services and Equality, National Plan on Drugs (PNSD), Spain (grant number 2018/020 and 2020/024); the Agency for Management of University and Research Grants, Government of Catalonia (grant number 2017SGR316). DF is attached to the Research Intensification Program of the Carlos III Health Institute (grant number INT19/00026). PZ is attached to the Joan Rodés Program of the Carlos III Health Institute (grant number JR20/00016).

REFERENCES

Aitken, C., Kerr, T., Hickman, M., Stoové, M., Higgs, P., and Dietze, P. (2013). A cross-sectional study of emergency department visits by people who inject drugs. *Emerg. Med. J.* 30, 421–422. doi:10.1136/emermed-2012-201170

Alzghoul, B. N., Abualsuod, A., Alqam, B., Innabi, A., Palagiri, D. R., Gheith, Z., et al. (2020). Cocaine use and pulmonary hypertension. *Am. J. Cardiol.* 125, 282–288. doi:10.1016/j.amjcard.2019.10.008

Arendt, M., Munk-Jørgensen, P., Sher, L., and Jensen, S. O. (2011). Mortality among individuals with cannabis, cocaine, amphetamine, MDMA, and opioid use disorders: a nationwide follow-up study of Danish substance users in treatment. *Drug Alcohol Depend.* 114, 134–139. doi:10.1016/j.drugalcdep.2010.09.013

Bachi, K., Mani, V., Jeyachandran, D., Fayad, Z. A., Goldstein, R. Z., and Alia-Klein, N. (2017). Vascular disease in cocaine addiction. *Atherosclerosis* 262, 154–162. doi:10.1016/j.atherosclerosis.2017.03.019

Barakat, L. A., Juthani-Mehta, M., Allore, H., Trentalange, M., Tate, J., Rimland, D., et al. (2015). Comparing clinical outcomes in HIV-infected and uninfected older men hospitalized with community-acquired pneumonia. *HIV Med.* 16, 421–430. doi:10.1111/hiv.12244

Blackstock, O. J., Tate, J. P., Akgün, K. M., Crystal, S., Duggal, M., Edelman, E. J., et al. (2013). Sex disparities in overall burden of disease among hiv-infected individuals in the veterans affairs healthcare system. *J. Gen. Intern. Med.* 28 Suppl 2, S577. doi:10.1007/s11606-013-2346-z

Butler, A. J., Rehm, J., and Fischer, B. (2017). Health outcomes associated with crack-cocaine use: systematic review and meta-analyses. *Drug Alcohol Depend.* 180, 401–416. doi:10.1016/j.drugalcdep.2017.08.036

Carrillo, X., Curós, A., Muga, R., Serra, J., Sanvisens, A., and Bayes-Genis, A. (2011). Acute coronary syndrome and cocaine use: 8-year prevalence and inhospital outcomes. *Eur. Heart J.* 32, 1244–1250. doi:10.1016/j.ycar.2012.01.08210.1093/eurheartj/ehq504

de la Fuente, L., Molist, G., Espelt, A., Barrio, G., Guitart, A., Bravo, M. J., et al. (2014). Mortality risk factors and excess mortality in a cohort of cocaine users admitted to drug treatment in Spain. *J. Subst. Abuse Treat.* 46, 219–226. doi:10.1016/j.jsat.2013.07.001

Degenhardt, L., Singleton, J., Calabria, B., McLaren, J., Kerr, T., Mehta, S., et al. (2011). Mortality among cocaine users: a systematic review of cohort studies. *Drug Alcohol Depend.* 113, 88–95. doi:10.1016/j.drugalcdep.2010.07.026

Deiss, R. G., Lozada, R. M., Burgos, J. L., Strathdee, S. A., Gallardo, M., Cuevas, J., et al. (2012). HIV prevalence and sexual risk behaviour among non-injection drug users in Tijuana, Mexico. *Global Publ. Health* 7, 175–183. doi:10.1080/17441692.2010.549141

European Monitoring Centre for Drugs and Drug Addiction (EMCDDA) (2019). *European monitoring Centre for drugs and drug addiction (2019), European drug report 2019: trends and developments*. Brussels, Belgium: Publications Office of the European Union.

Filho, J. C. C. L., Ogawa, M. Y., De Souza Andrade, T. H., De Andrade Cordeiro Gadelha, S., Fernandes, P. F. C. B. C., Queiroz, A. L., et al. (2019). Spectrum of acute kidney injury associated with cocaine use: report of three cases. *BMC Nephrol.* 20, 99. doi:10.1186/s12882-019-1279-0

Giovanardi, D., Castellana, C. N., Pisa, S., Poppi, B., Pinetti, D., Bertolini, A., et al. (2005). Prevalence of abuse of alcohol and other drugs among injured drivers presenting to the emergency department of the University Hospital of Modena, Italy. *Drug Alcohol Depend.* 80, 135–138. doi:10.1016/j.drugalcdep.2005.04.010

Hotton, A. L., Weber, K. M., Hershow, R. C., Anastos, K., Bacchetti, P., Golub, E. T., et al. (2017). Prevalence and predictors of hospitalizations among HIV-infected and at-risk HIV-uninfected women. *J. Acquir. Immune Defic. Syndr.* 75, e27–e35. doi:10.1097/QAI.0000000000001278

Jones, A. W. (2019). Forensic drug profile: cocaethylene. *J. Anal. Toxicol.* 43, 155–160. doi:10.1093/JAT/BKZ007

Justice, A. C., Modur, S. P., Tate, J. P., Althoff, K. N., Jacobson, L. P., Gebo, K. A., et al. (2013). Predictive accuracy of the veterans aging cohort study index for mortality with HIV infection: a north american cross cohort analysis. *J. Acquir. Immune Defic. Syndr.* 62, 149–163. doi:10.1097/QAI.0b013e31827df36c

Kendall, C. E., Boucher, L. M., Mark, A. E., Martin, A., Marshall, Z., Boyd, R., et al. (2017). Erratum to: a cohort study examining emergency department visits and hospital admissions among people who use drugs in Ottawa, Canada. *Harm Reduct. J.* 14, 42. doi:10.1186/s12954-017-0169-7

Lewer, D., Freer, J., King, E., Larney, S., Degenhardt, L., Tweed, E. J., et al. (2020). Frequency of health-care utilization by adults who use illicit drugs: a systematic review and meta-analysis. *Addiction* 115, 1011–1023. doi:10.1111/add.14892

Lippi, G., Plebani, M., and Cervellin, G. (2010). Cocaine in acute myocardial infarction. *Adv. Clin. Chem.* 51, 53–70. doi:10.1016/S0065-2423(10)51003-5

Macías, J., Palacios, R. B., Claro, E., Vargas, J., Vergara, S., Mira, J. A., et al. (2008). High prevalence of hepatitis C virus infection among noninjecting drug users: association with sharing the inhalation implements of crack. *Liver Int.* 28, 781–786. doi:10.1111/j.1478-3231.2008.01688.x

Martel-Laferrière, V., Nitulescu, R., Cox, J., Cooper, C., Tyndall, M., Rouleau, D., et al. (2017). Cocaine/crack use is not associated with fibrosis progression measured by AST-to-Platelet Ratio Index in HIV-HCV co-infected patients: a cohort study. *BMC Infect. Dis.* 17, 80. doi:10.1186/s12879-017-2196-0

Mégarbane, B., and Chevillard, L. (2013). The large spectrum of pulmonary complications following illicit drug use: features and mechanisms. *Chem. Biol. Interact.* 206, 444–451. doi:10.1016/j.cbi.2013.10.011

Miró, Ò., Dargan, P. I., Wood, D. M., Dines, A. M., Yates, C., Heyerdahl, F., et al. (2019). Epidemiology, clinical features and management of patients presenting to European emergency departments with acute cocaine toxicity: comparison between powder cocaine and crack cocaine cases. *Clin. Toxicol.* 57, 718–726. doi:10.1080/15563650.2018.1549735

Miro, O., Galicia, M., Sanchez, M., and Nogué, S. (2010). Factores que determinan la reconsulta a urgencias tras una atención urgente por consumo de cocaína. *Emergencias* 22, 408–414, http://emergencias.portalsemes.org/numeros-anteriores/volumen-22/numero-6/factores-que-determinan-la-reconsulta-a-urgencias-tras-una-atencion-urgente-por-consumo-de-cocaina/.

Observatorio Español de las Drogas y las Adicciones (2019). EDADES 2017—informe web actualizado marzo 2019 OEDA. Available at: moz-

extension://a8bef36a-8935-4d90-87ae-d41d2b63b348/enhanced-reader.html?openApp&pdf=http%3A%2F%2Fwww.pnsd.mscbs.gob.es%2Fprofesionales%2FsistemasInformacion%2FsistemaInformacion%2Fpdf%2FEDADES_2017_Informe.pdf (Accessed March 30, 2020).

Pavarin, R., Lugoboni, F., Mathewson, S., Ferrari, A. M., Guizzardi, G., and Quaglio, G. (2011). Cocaine-related medical and trauma problems: a consecutive series of 743 patients from a multicentre study in Italy. *Eur. J. Emerg. Med.* 18, 208–214. doi:10.1097/MEJ.0b013e3283440f25

Qureshi, A., Chaudhry, S., and Suri, M. (2014). Cocaine use and the likelihood of cardiovascular and all-cause mortality: data from the third national health and nutrition examination survey mortality follow-up study. *J. Vasc. Interv. Neurol.* 7, 76–82. doi:10.1212/wnl.78.1_meetingabstracts.p07.031

Santurtún, A., García Blanco, A., Fdez-Arroyabe, P., Santurtún, M., and Zarrabeitia, M. T. (2020). Cocaine in hospital admissions for diseases of the circulatory system and as the underlying cause of death: analysis and discussion. *Cardiovasc. Toxicol.* 20, 20–27. doi:10.1007/s12012-019-09537-6 (Accessed October 15, 2020)

Sanvisens, A., Vallecillo, G., Bolao, F., Rivas, I., Fonseca, F., Fuster, D., et al. (2014). Temporal trends in the survival of drug and alcohol abusers according to the primary drug of admission to treatment in Spain. *Drug Alcohol Depend.* 136, 115–120. doi:10.1016/j.drugalcdep.2013.12.022

Stinson, F. S., Grant, B. F., Dawson, D. A., Ruan, W. J., Huang, B., and Saha, T. (2005). Comorbidity between DSM-IV alcohol and specific drug use disorders in the United States: results from the national epidemiologic survey on alcohol and related conditions. *Drug Alcohol Depend.* 80, 105–116. doi:10.1016/j.drugalcdep.2005.03.009

Subdirecció General de Drogodependències (2018). Sistema d'Informació sobre Drogodependències de Catalunya. Available at: http://drogues.gencat.cat/ca/professionals/epidemiologia/sid/ (Accessed October 15, 2020).

Tate, J. P., Justice, A. C., Hughes, M. D., Bonnet, F., Reiss, P., Mocroft, A., et al. (2013). An internationally generalizable risk index for mortality after one year of antiretroviral therapy. *AIDS* 27, 563–572. doi:10.1097/QAD.0b013e32835b8c7f

Tate, J. P., Sterne, J. A. C., and Justice, A. C. (2019). Albumin, white blood cell count, and body mass index improve discrimination of mortality in HIV-positive individuals. *AIDS* 33, 903–912. doi:10.1097/QAD.0000000000002140

Taylor, A. L., Denniston, M. M., Klevens, R. M., McKnight-Eily, L. R., and Jiles, R. B. (2016). Association of hepatitis C virus with alcohol use among U.S. Adults: nhanes 2003–2010. *Am. J. Prev. Med.* 51, 206–215. doi:10.1016/j.amepre.2016.02.033

Timko, C., Han, X., Woodhead, E., Shelley, A., and Cucciare, M. A. (2018). Polysubstance use by stimulant users: health outcomes over 3 years. *J. Stud. Alcohol Drugs* 79, 799–807. doi:10.15288/jsad.2018.79.799

Vergara-Moragues, E., González-Saiz, F., Lozano, O. M. O., Betanzos Espinosa, P., Fernández Calderón, F., Bilbao-Acebos, I., et al. (2012). Psychiatric comorbidity in cocaine users treated in therapeutic community: substance-induced versus independent disorders. *Psychiatr. Res.* 200, 734–741. doi:10.1016/j.psychres.2012.07.043

Vitcheva, V. (2012). Cocaine toxicity and hepatic oxidative stress. *Curr. Med. Chem.* 19, 5677–5682. doi:10.2174/092986712803988929

Warden, D., Sanchez, K., Greer, T., Carmody, T., Walker, R., dela Cruz, A., et al. (2016). Demographic and clinical characteristics of current comorbid psychiatric disorders in a randomized clinical trial for adults with stimulant use disorders. *Psychiatr. Res.* 246, 136–141. doi:10.1016/j.psychres.2016.09.007

Conflict of Interest: The authors declare that the research was conducted in the absence of any commercial or financial relationships that could be construed as a potential conflict of interest.

frontiers in Neuroscience

ORIGINAL RESEARCH
published: 19 February 2021
doi: 10.3389/fnins.2021.618190

The Pathology of Morphine-Inhibited Nerve Repair and Morphine-Induced Nerve Damage Is Mediated via Endoplasmic Reticulum Stress

Jie Liu[1,2†], Shanyong Yi[1,3†], Weibo Shi[1], Guozhong Zhang[1], Songjun Wang[1], Qian Qi[1], Bin Cong[1] and Yingmin Li[1]**

[1] Hebei Key Laboratory of Forensic Medicine, Collaborative Innovation Center of Forensic Medical Molecular Identification, College of Forensic Medicine, Hebei Medical University, Shijiazhuang, China, [2] Research Center of Basic Medical Sciences, Department of Pathology, School of Basic Medical Sciences, Hubei University of Science and Technology, Xianning, China, [3] School of Forensic Medicine, Xinxiang Medical University, Xinxiang, China

OPEN ACCESS

Edited by:
Yixiao Luo,
Hunan Normal University, China

Reviewed by:
Tomohisa Mori,
Hoshi University, Japan
Chunxia Yan,
Xi'an Jiaotong University, China

***Correspondence:**
Bin Cong
cong6406@126.com
Yingmin Li
liyingmin888@126.com

[†] These authors have contributed equally to this work

Specialty section:
This article was submitted to Neuropharmacology, a section of the journal Frontiers in Neuroscience

Received: 16 October 2020
Accepted: 25 January 2021
Published: 19 February 2021

Citation:
Liu J, Yi S, Shi W, Zhang G, Wang S, Qi Q, Cong B and Li Y (2021) The Pathology of Morphine-Inhibited Nerve Repair and Morphine-Induced Nerve Damage Is Mediated via Endoplasmic Reticulum Stress. Front. Neurosci. 15:618190. doi: 10.3389/fnins.2021.618190

Objective: The aim of the present study was to observe the pathological damage in the cerebral cortex of rats under acute morphine exposure (AME) and different durations of morphine dependence (MD), explore whether endoplasmic reticulum stress (ERS) is involved in the damage process, and assess the effect of morphine exposure on the proliferation and differentiation of newborn neurons.

Methods: Rat models of AME and different durations of MD were established. Pathological changes in cortical neurons were assessed by hematoxylin and eosin (H&E) and thionine staining. The expression of nuclear receptor-related factor 1 (NURR1) and that of the ERS-related proteins glucose-regulated protein 78 (GRP78), p-eIF2α, activating transcription factor 6 (ATF6), and CHOP in cortical neurons was assessed by immunohistochemistry. Double immunofluorescence labeling was used to observe the expression of Ki-67.

Results: H&E and thionine staining revealed that AME resulted in pyknotic changes in cortical neurons. With prolonged morphine exposure, the number of pyknotic neurons was significantly increased, the protein expression of Ki-67 and NURR1 was significantly decreased, and the protein levels of GRP78, p-eIF2α, ATF6, and CHOP showed marked dynamic changes.

Conclusion: AME and different durations of MD caused varying degrees of pathological changes in the cortex. Furthermore, the dynamic changes observed in ERS-related protein expression suggested that ERS may be associated with cortical injury. Different durations of MD inhibited the proliferation, differentiation, and migration of newborn neurons, which may affect the nerve repair process after injury.

Keywords: morphine dependence, acute morphine exposure, cortex, ERS, Ki67, NURR1

INTRODUCTION

A report by the World Health Organization on the abuse of morphine indicated that the misuse of this drug had increased in recent years (Volkow and Skolnick, 2012). Morphine dependence (MD) refers to a chronic recurrent brain disease characterized by the loss of self-control and compulsive, continuous drug seeking (Lamb and Ginsburg, 2018). Several studies have shown that MD can inflict varying degrees of injury on different systems of the body, including damage to the heart and lungs, direct effects on the central nervous system, and inhibitory effects on the respiratory center. Moreover, these effects may lead to acute or chronic cerebral ischemia and hypoxia, which, in turn, may cause nerve damage (Brailoiu et al., 2004; Luo et al., 2013; Rohbani et al., 2019). MD involves a complex series of pathophysiological changes in multiple brain regions, including, importantly, the cerebral cortex (Katebi et al., 2013; Adedayo et al., 2018); however, little is known about the pathomorphological changes induced by the misuse of this substance.

The endoplasmic reticulum (ER) is the primary organelle for protein synthesis, glycosylation, folding, secretion, and nascent protein transport. Under normal conditions, the protein folding ability of the ER matches the body's protein synthesis requirements (Iurlaro and Muñoz-Pinedo, 2016; Kropski and Blackwell, 2018). However, when the body is stimulated by ischemia, hypoxia, injury, or other insults, the microenvironment of the ER changes, which can result in the accumulation of unfolded or misfolded proteins in the ER lumen and the subsequent induction of endoplasmic reticulum stress (ERS) (Xiang et al., 2017; Muneer and Shamsher Khan, 2019). Under ERS, the expression of glucose-regulated protein 78 (GRP78) increases, which can inhibit the synthesis of cellular proteins, accelerate the degradation of misfolded or unfolded proteins, and maintain ER homeostasis (Ibrahim et al., 2019). However, when ERS persists, protein kinase RNA (PKR)-like endoplasmic reticulum kinase (PERK), and activating transcription factor 6 (ATF6) can dissociate from GRP78, thereby activating downstream signaling pathways. Recent studies have shown that the activation of the ATF6 signaling pathway mainly exerts a cell-protective role (Hillary and FitzGerald, 2018), whereas the activation of the PERK/p-eIF2α signaling pathway can lead to the upregulation of CCAAT/-enhancer-binding protein homologous protein (CHOP) expression, and continuous CHOP expression can induce cell injury, or even cell death (Hu et al., 2019). Brain injury can induce the proliferation of endogenous neural stem cells (NSCs) and enable the newborn neurons to differentiate and migrate to the site of injury (Dai et al., 2019). Ki-67, a nuclear antigen, is often used as a marker for evaluating cell proliferation (Miller et al., 2018). Meanwhile, nuclear receptor-related factor 1 (NURR1), a member of the orphan nuclear receptor superfamily, is indispensable for neuronal differentiation, migration, maturation, and survival (Dong et al., 2016).

The activation status of ERS-related proteins and the proliferation and differentiation status of endogenous NSCs in acute morphine exposure (AME)- and chronic MD-induced cortical nerve damage remain unknown. In the present study, we first established rat models of AME as well as of different durations of MD. Subsequently, we investigated the pathological changes in cortical neurons, the alterations in the expression levels of ERS-related proteins, and changes in the proliferation, differentiation, and maturation status of newborn neurons aiming to provide pathomorphological evidence for the mechanisms underlying morphine-induced injury.

MATERIALS AND METHODS

Animals

Adult male Wistar rats (Experimental Animal Center, Hebei Medical University, China), weighing 250 ± 20 g, were maintained in a room with an ambient temperature of 22 ± 2°C and a 12/12-h light/dark cycle, and had *ad libitum* access to food and water. This study was approved by the Institutional Review Board for Animal Experiments at the Hebei Medical University. Every attempt was made to reduce the number of animals used and to minimize animal pain and suffering. The rats were randomly divided into the following groups: 1-week control (Con), 3-week control, 6-week control, 1-week MD, 3-week MD, 6-week MD, 2-h control, and AME groups ($n = 8$ per group).

Model of MD

As previously described (Shi et al., 2019), the model of MD was established through subcutaneous injections of morphine hydrochloride at increasing doses. Rats in the three morphine-dependence groups were subcutaneously injected in the back with morphine hydrochloride twice daily (08:00 and 20:00) for 5 days. The initial dose administered was 10 mg/kg and was increased by 10 mg/kg every other day until day 5 of treatment. The control rats received equal volumes of saline. The MD of model rats was confirmed after 5 days of morphine administration as described in Maldonado et al. (1992). Two rats were randomly selected from each control group and each morphine-dependent group and given a subcutaneous injection of naloxone hydrochloride (5 mg/kg) to induce withdrawal symptoms. Scoring involved observing signs of opiate withdrawal, including wet-dog shakes, stretching, cleaning fur, swallowing, standing, jumping, and teeth chattering. Following this assessment, 30 mg/kg morphine was administered twice daily (08:00 and 20:00) until 1-, 3-, or 6-weeks post-establishment of dependence.

Rats in the AME group were subcutaneously injected once in the back with morphine hydrochloride at a dose of 30 mg/kg. The control rats received an equal volume of saline.

Tissue Preparation

Two hours after the last morphine or saline injection, the rats were deeply anesthetized and euthanized. The tissue used for staining was harvested and immediately fixed in 10% formalin, subsequently dehydrated using a graded ethanol series, and embedded in paraffin. Brain slices were obtained using a stereotaxic atlas (Paxinos and Watson, 2007) and a rotary microtome (Leica RM2255, Shanghai, China). Sections (5 mm) were prepared for thionine, immunohistochemical,

and immunofluorescence staining and examined under a light microscope (Olympus IX71; Olympus, Tokyo, Japan).

Reagents

Rabbit polyclonal antibodies against GRP78 (ab188878), CHOP (ab179823), and NURR1 (ab176184); the mouse monoclonal antibody against MAP2 (ab11268); and the rabbit monoclonal antibody targeting Ki-67 (ab16667) were purchased from Abcam (United States). Rabbit polyclonal antibodies against p-eIF2α (AF3087) and ATF6 (DF6009) were purchased from Affinity (China). The Alexa Fluor 488 donkey anti-mouse IgG (H + L) (1975519) and the Alexa Fluor 594 donkey anti-rabbit IgG (H + L) (1827674) secondary antibodies were purchased from Invitrogen (United States). The immunohistochemistry kit (SP9001) was purchased from the Zhongshan Goldenbridge Biotech, China, and the morphine hydrochloride for injection was produced in the First Pharmaceutical Factory of Shenyang, China.

Body Weight Measurements

The body weight of the rats in all the groups was measured daily before treatment throughout the experiment.

Hematoxylin and Eosin Staining

Deparaffinized sections were stained with hematoxylin for 2 min, transferred to 1% hydrochloric acid alcohol differentiation solution, and then stained with eosin for 3 s.

Thionine Staining

Thionine staining was performed as previously described (Yi et al., 2019). Deparaffinized sections were stained with 4% thionine for 90 s at 60°C, dehydrated through a graded alcohol series, and mounted with neutral gum.

Immunohistochemistry

Immunohistochemistry was performed as previously described (Yi et al., 2019). Antigen retrieval of deparaffinized sections was performed using a microwave, followed by incubation in 3% H_2O_2 in cold methanol for 30 min and blocking for 30 min using goat serum. The tissues were then incubated overnight at 4°C with antibodies against GRP78 (1:200), p-eIF2α (1:100), CHOP (1:200), ATF6 (1:100), and NURR1 (1:100). The next day, the tissues were incubated for 1 h with biotinylated secondary antibody and subsequently with horseradish peroxidase (HRP)-conjugated biotin for 30 min. Finally, DAB or AP-red was used as the chromagen. The tissues were counterstained with hematoxylin to demarcate locations in the sections. The primary antibodies were replaced with 0.01 mmol/L PBS in the negative controls (data not shown).

Immunofluorescence Double Staining

Immunofluorescence was performed as previously described (Shi et al., 2019). The anti-Ki-67 antibody (1:100) was used as the first primary antibody and the anti-MAP2 antibody (1:150) as the second primary antibody. DyLight 594-conjugated AffiniPure goat anti-rabbit Ig (1:150) and DyLight 488-conjugated AffiniPure goat anti-mouse Ig (1:100) were used as the secondary antibodies.

Cell Counting

Six rats from each group were used for morphological observation. One out of every three serial sections were selected for cell counting. Following a comparison of the sections after immunohistochemical staining and double immunofluorescence staining, the numbers of positive cells were counted in a field of view at 100× magnification. Two independent observers who were blinded to the experimental conditions performed the counts and calculated the average number of positive cells.

Statistical Methods

The Kolmogorov–Smirnov test showed that the data were normally distributed in all groups ($P > 0.1$). The results are presented as mean ± SD. The data were analyzed by one-way ANOVA. Significance was defined as $P < 0.05$ for all statistical tests.

RESULTS

Weight Change

A change in body weight can be considered as a physiological indicator of morphine exposure. The weight of rats in the control group showed a marked increase after 1 week (297.78 ± 15.43), 3 weeks (327.08 ± 23.57), and 6 weeks (369.52 ± 28.81). In comparison, the weight of morphine-dependent rats was slightly decreased at 1 week (260.08 ± 8.18, $P < 0.01$), with slower increases being recorded at 3 weeks (280.18 ± 13.14, $P < 0.05$) and 6 weeks (305.64 ± 22.68, $P < 0.05$) after treatment (**Figure 1**).

Hematoxylin and Eosin Staining Showed Pathological Changes in the Cerebral Cortex

The cerebral cortices of rats in the control groups showed no pathological changes (data not shown), presenting a clear

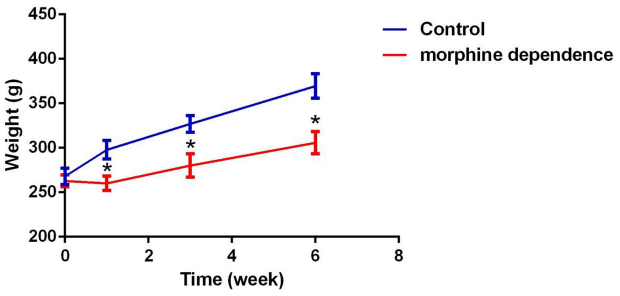

FIGURE 1 | Effect of different durations of morphine dependence on the body weight. Compared with the control group, morphine dependence significantly reduced the body weight gain of rats. The results are shown as mean ± SD, *$P < 0.05$ vs. control group.

structure and neatly arranged neurons. Compared with the control group, no obvious change was observed after 1 week of MD. However, after 3 weeks of MD, the gaps around the small blood vessels and neurons widened, and microglial hyperplasia could be seen. Additionally, after 6 weeks of MD, tissue and cellular damage was more extensive and neurons were pyknotic and dying. Some pyknotic cells also appeared in the cortices of rats of the AME group (**Figure 2**).

Thionine Staining Showed Pathological Changes in Cortical Neurons

In the control group, the neuronal structures were clear, and Nissl bodies were evenly distributed in the cytoplasm; a similar phenotype was observed after 1 week of MD. However, after 3 weeks of MD, a proportion of Nissl bodies had disappeared and pyknotic neurons were visible. Cellular damage was more extensive at 6 weeks. Meanwhile, some Nissl bodies had also disappeared in the AME group, and pyknotic neurons were also visible (**Figure 3**).

GRP78, p-eIF2α, CHOP, ATF6, and NURR1 Expression in the Cerebral Cortex

Immunohistochemical staining showed that GRP78, p-eIF2α, ATF6, and CHOP proteins were located in the cytoplasm and were stained brown, while NURR1 protein was localized to the nucleus and was stained red.

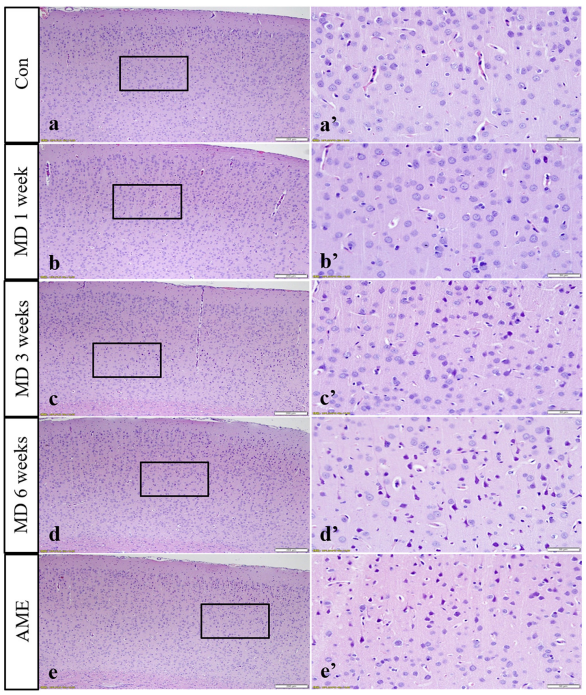

FIGURE 2 | Hematoxylin staining of the cortex. Panels **(a'–e')** are magnified areas of panels **(a–e)**, respectively. With increasing periods of morphine dependence, gaps around the small blood vessels and neurons widened, and microglia hyperplasia. Bars = 200 μm in panels **(a–e)**. Bars = 50 μm in panels **(a'–e')**; MD, morphine dependence; AME, acute morphine exposure.

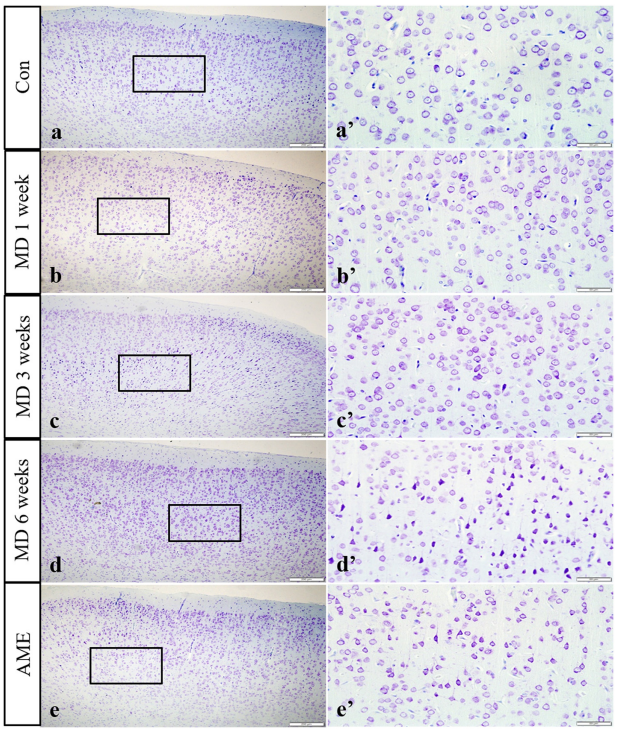

FIGURE 3 | Thionine staining of the cortex. Panels **(a'–e')** are magnified areas of panels **(a–e)**, respectively. With increasing periods of morphine dependence, Nissl body structures are not clear, and neurons are pyknotic and deeply stained. Bars = 200 μm in panels **(a–e)**. Bars = 50 μm in panels **(a'–e')**; MD, morphine dependence; AME, acute morphine exposure.

ANOVA for GRP78-positive cells in the cerebral cortex showed that there were significant differences among the groups (F [4, 25] = 687.7; $P < 0.0001$). Compared with the control group (5.24 ± 1.55, $n = 6$), GRP78 expression was significantly upregulated in the 1-week MD (38.63 ± 3.51, $P < 0.01$, $n = 6$), 3-week MD (90.74 ± 6.25, $P < 0.01$, $n = 6$), 6-week MD (77.52 ± 5.15, $P < 0.01$, $n = 6$), and AME (24.4 ± 2.46, $P < 0.01$, $n = 6$) groups (**Figure 4**).

ANOVA for p-eIF2α-positive cells in the cerebral cortex showed that there were significant differences among the groups (F [4, 25] = 99.58; $P < 0.0001$). Compared with the control group (1.12 ± 0.94, $n = 6$), p-eIF2α expression remained at a low level in the 6-week MD group (1.45 ± 1.34, $n = 6$), but was significantly upregulated in the 1-week MD (10.42 ± 2.41, $P < 0.01$, $n = 6$), 3-week MD (30.14 ± 3.03, $P < 0.01$, $n = 6$), and AME (11.62 ± 3.20, $P < 0.01$, $n = 6$) groups (**Figure 5**).

ANOVA for CHOP-positive cells in the cerebral cortex showed that there were significant differences among the groups (F [4, 25] = 1493; $P < 0.0001$). Compared with the control group (15.23 ± 1.55, $n = 6$), CHOP expression was significantly upregulated in the 1-week MD (54.72 ± 1.89, $P < 0.01$, $n = 6$), 3-week MD (114.12 ± 3.67, $P < 0.01$, $n = 6$), 6-week MD

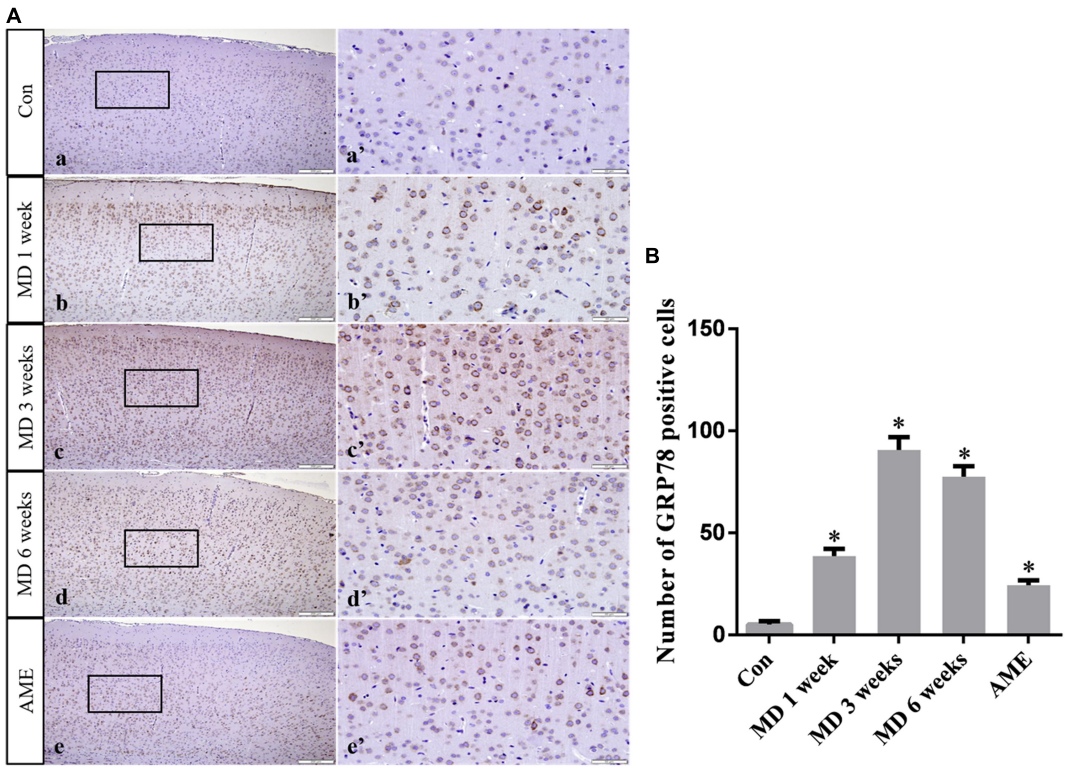

FIGURE 4 | (A) Representative images showing GRP78 immunohistochemistry in the cortex. Panels **(a'–e')** are magnified areas of panels **(a–e)**. Bars = 200 μm in panels **(a–e)**. Bars = 50 μm in panels **(a'–e')**. **(B)** Quantitative analysis of the number of GRP78 positive cells. The data are shown as mean ± SD, *$P < 0.05$ vs. control group ($n = 6$). MD, morphine dependence; AME, acute morphine exposure.

(56.46 ± 1.43, $P < 0.01$, $n = 6$), and AME (34.46 ± 1.55, $P < 0.01$, $n = 6$) groups (**Figure 6**).

ANOVA for ATF6-positive cells in the cerebral cortex showed that there were significant differences among the groups (F [4, 25] = 257.5; $P < 0.0001$). Compared with the control group (1.11 ± 1.14, $n = 6$), ATF6 expression was significantly upregulated in the 1-week MD (15.2 ± 2.22, $P < 0.01$, $n = 6$), 3-week MD (65.2 ± 5.07, $P < 0.01$, $n = 6$), 6-week MD (29.5 ± 6.74, $P < 0.01$, $n = 6$), and AME (38.34 ± 4.57, $P < 0.01$, $n = 6$) groups (**Figure 7**).

ANOVA for NURR1-positive cells in the cerebral cortex showed that there were significant differences among the groups (F [4, 25] = 8.613; $P = 0.0002$). Compared with the control group (9.12 ± 0.88, $n = 6$), NURR1 expression remained at a high level in the AME group (8.71 ± 1.25, $n = 6$), but was significantly downregulated in the 1-week MD (7.63 ± 0.84, $P < 0.01$, $n = 6$), 3-week MD (7.21 ± 0.92, $P < 0.01$, $n = 6$), and 6-week MD (6.94 ± 0.74, $P < 0.01$, $n = 6$) groups (**Figure 8**).

Ki-67 Expression Around the Ventricle

Double-labeling showed that Ki-67 mostly co-localized with the neuronal marker MAP2 around the ventricle. Ki-67 protein was located in the nucleus and was stained red, and MAP2 protein was located in the cytoplasm and was stained green. ANOVA for Ki-67-positive cells in the cerebral cortex showed that there were significant differences among the groups (F [4, 25] = 163.4; $P < 0.0001$). Compared with the control group (44.32 ± 3.81, $n = 6$), the number of Ki-67/MAP2-positive cells remained at a high level in the AME group (48.12 ± 5.04, $n = 6$), and was significantly downregulated in the 1-week MD (35.62 ± 2.95, $P < 0.01$, $n = 6$), 3-week MD (32.63 ± 3.17, $P < 0.01$, $n = 6$), and 6-week MD (9.32 ± 1.63, $P < 0.01$, $n = 6$) groups (**Figure 9**).

DISCUSSION

Several studies have shown that long-term MD can cause acute or chronic cerebral ischemia and hypoxia by directly affecting the central nervous system and inhibiting the respiratory center, which can lead to central nervous system damage (Brailoiu et al., 2004; Volkow and Skolnick, 2012). Animal models allow for the identification and investigation of mechanisms underlying the effects of MD. In the present study, we established rat models of AME and different durations of MD aiming to better understand the mechanisms involved in morphine exposure-induced injury on the body and provide treatment and prevention strategies.

The cerebral cortex comprises a layer of neurons and synapses located on the surface of the cerebral hemispheres. The cerebral cortex is folded into gyri, and approximately two-thirds of it is submerged inside brain fissures. The cortex is involved in higher mental functions, general movements, functions of the

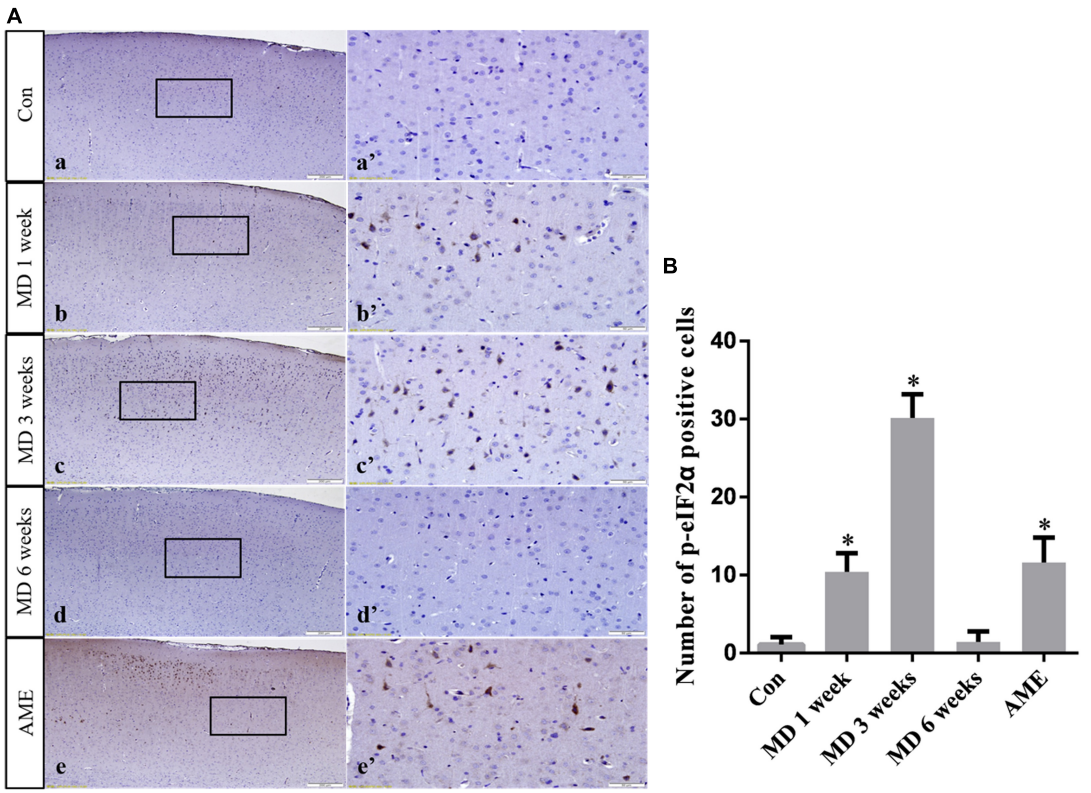

FIGURE 5 | (A) Representative images showing p-eIF2α immunohistochemistry in the cortex. Panels **(a'–e')** are magnified areas of panels **(a–e)**. Bars = 200 μm in panels **(a–e)**. Bars = 50 μm in panels **(a'–e')**. **(B)** Quantitative analysis of the number of p-eIF2α positive cells. The data are shown as mean ± SD, $^*P < 0.05$ vs. control group ($n = 6$). MD, morphine dependence; AME, acute morphine exposure.

viscera, perception, and behavioral reactions (Cadwell et al., 2019). However, the changes induced in cortical neurons by MD or AME remain poorly understood. In the present study, the results of hematoxylin and eosin (H&E) and thionine staining revealed that long-term MD and AME resulted in pyknotic neurons and a reduction in the number of Nissl bodies, which suggested that long-term MD and AME can cause nerve damage, and that, with increasing periods of morphine exposure, nerve damage can become more extensive.

There is an important link between ERS and body damage. Several studies have demonstrated that ERS not only participates in the occurrence and progression of a variety of neurodegenerative diseases, but also plays a critical role in the pathology of nerve cell dysfunction (Johnson et al., 2011; Xiang et al., 2017; Muneer and Shamsher Khan, 2019). Under ERS, the protective mechanisms of the cell are activated, namely, the unfolded protein response (UPR), which results in the upregulation of the expression of GRP78, a molecular chaperone. GRP78 can bind to misfolded or unfolded proteins, thereby reducing the burden of the ER and restoring its function (Ni et al., 2011). In the present study, the expression level of GRP78 in the AME group was significantly higher than that in the control group, and, with increasing periods of morphine exposure, the expression level of GRP78 showed a significantly increasing trend. This suggested that ERS occurred in the cortex of morphine-dependent rats, and that the body's protective mechanisms were activated.

When morphine exposure persists, signaling pathways downstream of ERS will be activated, which can result in cell damage, or even cell death (Omura et al., 2013; Zhang et al., 2017). This may explain the shrinkage, disappearance of Nissl bodies, and other increasingly serious pathological impairments observed in this study.

Activating transcription factor 6 is a type-II transmembrane glycoprotein that, under ERS, can be transferred from the ER to the Golgi apparatus, where it is cleaved by site-1 and site-2 proteases. The N-terminal fragment, containing the alkaline leucine zipper domain, translocates into the nucleus and acts as a transcription factor that can activate the expression of ERS-related genes by combining ERS response elements and UPR elements (Papaioannou et al., 2018). Because the ERS response triggered by the selective activation of ATF6 is conducive to virus replication and the maintenance of cell viability, it is currently believed that the primary role of the ATF6 signaling pathway is the promotion of cell survival (Hillary and FitzGerald, 2018). In the present study, the expression level of ATF6 in the AME group was significantly higher than that in the control group, and, with increasing periods of morphine exposure, the expression level of ATF6 increased in the initial stages of MD, and then decreased at 6 weeks. These results showed that the protective

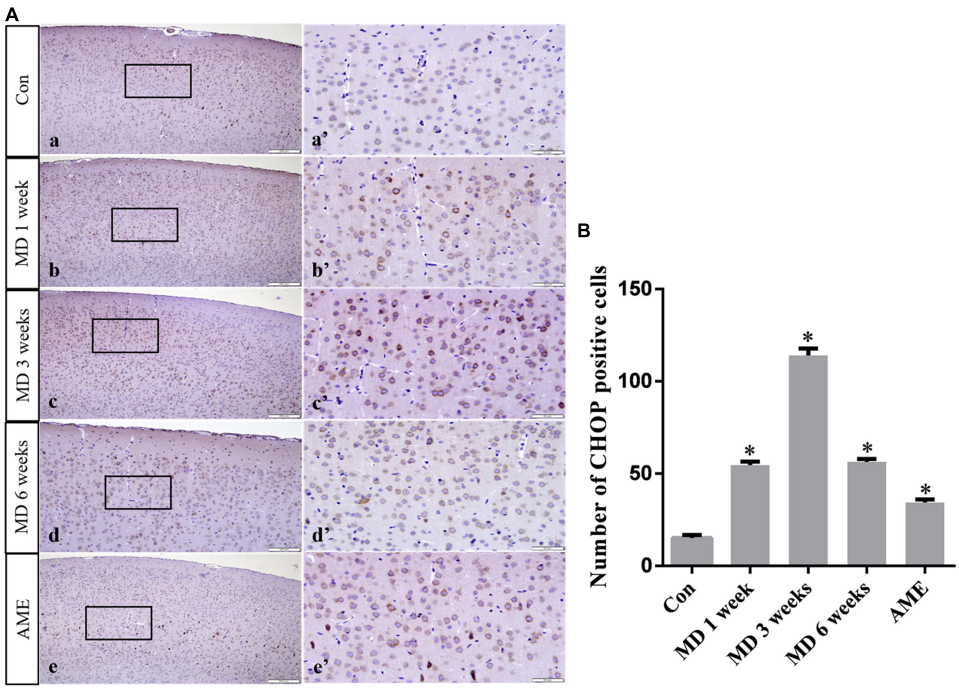

FIGURE 6 | (A) Representative images showing CHOP immunohistochemistry in the cortex. Panels **(a'–e')** are magnified areas of panels **(a–e)**. Bars = 200 μm in panels **(a–e)**. Bars = 50 μm panels in **(a'–e')**. **(B)** Quantitative analysis of the number of CHOP positive cells. The data are shown as mean ± SD, $^*P < 0.05$ vs. control group ($n = 6$). MD, morphine dependence; AME, acute morphine exposure.

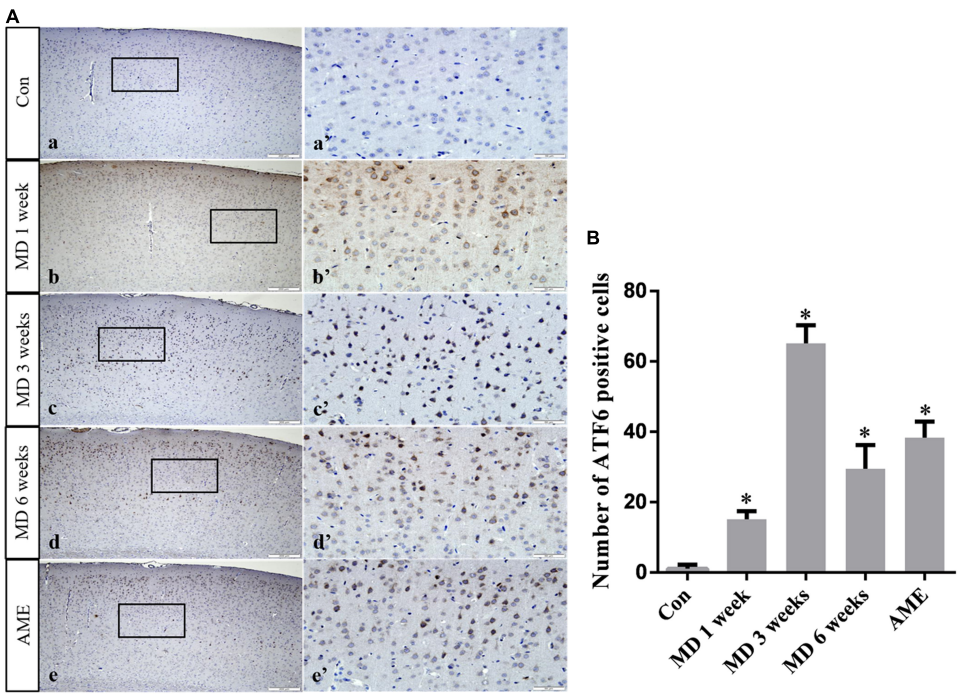

FIGURE 7 | (A) Representative images showing ATF6 immunohistochemistry in the cortex. Panels **(a'–e')** are magnified areas of panels **(a–e)**. Bars = 200 μm in panels **(a–e)**. Bars = 50 μm in panels **(a'–e')**. **(B)** Quantitative analysis of the number of ATF6 positive cells. The data are shown as mean ± SD, $^*P < 0.05$ vs. control group ($n = 6$). MD, morphine dependence; AME, acute morphine exposure.

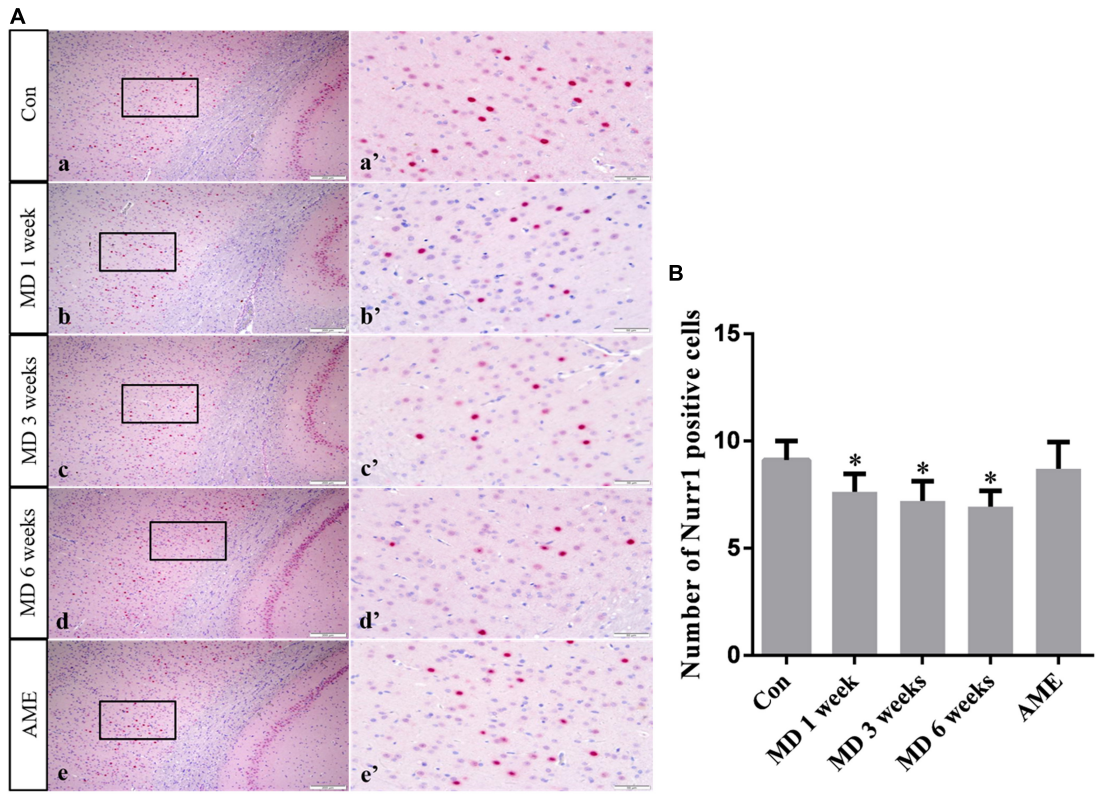

FIGURE 8 | (A) Representative images showing Nurr1 immunohistochemistry in the cortex. Panels **(a'–e')** are magnified areas of panels **(a–e)**. Bars = 200 μm in panels **(a–e)**. Bars = 50 μm in panels **(a'–e')**. **(B)** Quantitative analysis of the number of Nurr1 positive cells. The data are shown as mean ± SD, $^*P < 0.05$ vs. control group ($n = 6$). MD, morphine dependence; AME, acute morphine exposure.

effect of ATF6 on cortical neurons was significantly weakened with prolonged morphine exposure, leading to the activation of a series of downstream signaling pathways that induced cell injury and/or cell death.

CHOP, also known as growth arrest and DNA-damage inducible gene 153 (GADD153), is a key, ERS-specific proapoptotic transcription factor. Under normal physiological conditions, CHOP is expressed at a very low level (Yi et al., 2019). The PERK/eIF2α signaling pathway plays a dominant role in inducing CHOP expression (Rozpedek et al., 2016). PERK can inhibit the effect of eIF2B by promoting the phosphorylation of eIF2α, which can reduce protein translation and the amount of unfolded protein, thereby maintaining cell survival. When ERS is severe or prolonged, upstream open reading frame regulatory sequences present in the 5'-untranslated regions of mRNAs become activated, which inhibits eIF2α-dependent protein translation and activates the downstream ATF4/CHOP signaling pathway. Continuous expression of CHOP can cause cell damage, or even cell death (Cubillos-Ruiz et al., 2017; Wu et al., 2018; Lorenzon-Ojea et al., 2020). In this study, the expression levels of p-eIF2α and CHOP in the AME group were significantly higher than those of the control group. With increasing periods of morphine exposure, the expression level of p-eIF2α first increased, and then underwent a significant decline at 6 weeks, while CHOP showed sustained high levels of expression. These results suggested that the protective and damaging effects of ERS on neurons were in a state of mutual restraint in the 1- and 3-week MD groups. Subsequently, the high level of CHOP expression could lead to cell injury and death, which was consistent with our observations of pathological changes in cortical neurons after 6 weeks of MD. These data indicated that the PERK/p-eIF2α/CHOP pathway is associated with morphine exposure-induced cortical neuronal injury.

Ki-67 is a nuclear antigen specifically expressed by proliferating cells and is commonly used to evaluate tumor proliferative ability, malignancy, and prognosis (Scholzen and Gerdes, 2000; Miller et al., 2018). Under normal circumstances, Ki-67 is expressed in multiple brain regions, especially around the ventricle. Given that Ki-67-positive cells around the ventricle are NSCs and neural progenitor cells (NPCs), the expression of Ki-67 likely reflects the proliferation of nerve cells. In the present study, double immunofluorescence labeling of the neuron-specific marker MAP2 and Ki-67 were used as indicators of the proliferative status of NSCs and NPCs around the lateral ventricle after morphine exposure. No significant differences were observed between the AME and control groups, while the number of double-labeled Ki-67/MAP2-positive cells around the lateral ventricle showed a decreasing trend with increasing periods of morphine exposure. These results suggested that MD suppressed the proliferation of NSCs and NPCs around the

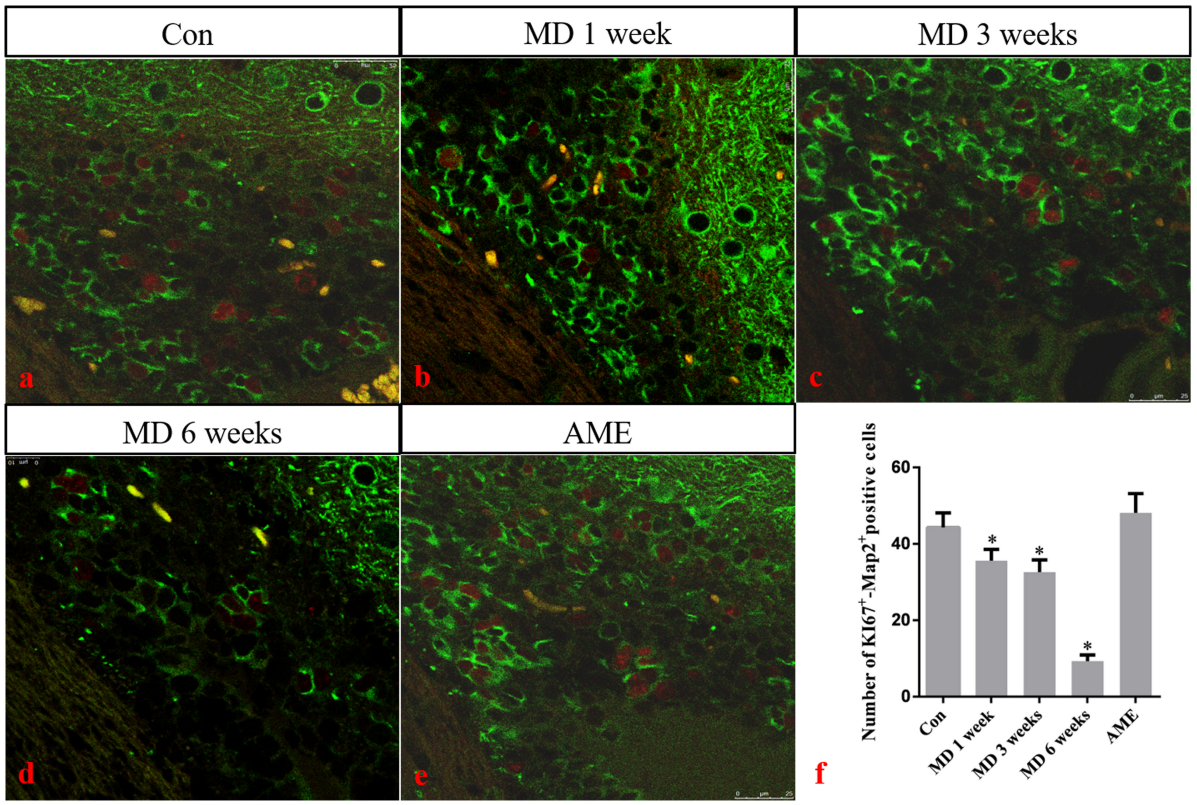

FIGURE 9 | (a–e) Immunofluorescence staining for Ki67 (red) and Map2 (green) in the cortex. Bars = 25 μm in panels **(a–e)**. **(f)** Quantitative analysis of the number of Ki67+ – Map2+ positive cells. The data are shown as mean ± SD, $^*P < 0.05$ vs. control group ($n = 6$). MD, morphine dependence; AME, acute morphine exposure.

lateral ventricle. We have previously shown that NURR1 plays an important role in the differentiation, migration, and maturation of atypical dopaminergic neurons outside the midbrain (Li et al., 2011, 2012). Although NURR1 is mainly expressed in dopaminergic neurons in the ventral side of the midbrain, it is also expressed in layers II–V of the cortex (Sano et al., 2008). In the present study, NURRl expression was significantly decreased in the morphine-dependent groups. These results suggested that MD inhibited the differentiation, migration, and maturation of cortical neurons, which may result in a decrease in the number of newborn neurons.

In conclusion, the results of this study demonstrated that ERS is involved in morphine exposure-induced injury. Moreover, morphine exposure inhibited the proliferation of endogenous NSCs and the differentiation and maturation of newborn neurons, thereby affecting nerve repair. We believe these findings provide morphological evidence for the mechanisms involved in morphine-induced cortical neuron injury and the repair process after brain injury.

DATA AVAILABILITY STATEMENT

The original contributions presented in the study are included in the article/supplementary material, further inquiries can be directed to the corresponding author/s.

ETHICS STATEMENT

The animal study was reviewed and approved by the Institutional Review Board for Animal Experiments at the Hebei Medical University.

AUTHOR CONTRIBUTIONS

JL and SY designed and performed the experiments. WS and GZ performed the statistical analysis and organized the data. SW and QQ created the figures. BC and YL supervised the research design and revised the manuscript. All the authors read and approved the final version of the manuscript.

FUNDING

This study was supported by the National Natural Science Foundation of China (81971787), the Key Projects of Basic Research in Hebei Province (189677108D), the Natural Science Foundation of Hebei Province (H2020206150), the Science and Technology Research Project of Hebei Higher Education Institutions (QN2019095), and the Spring Rain Project of Hebei Medical University (CYQD201905).

REFERENCES

Adedayo, A. D., Aderinola, A. A., Adekilekun, T. A., Olaolu, O. O., Olanike, A. M., and Olayemi, I. K. (2018). Morphine-alcohol treatment impairs cognitive functions and increases neuro-inflammatory responses in the medial prefrontal cortex of juvenile male rats. *Anat. Cell Biol.* 51, 41–51. doi: 10.5115/acb.2018.51.1.41

Brailoiu, E., Hoard, J., Brailoiu, G. C., Chi, M., Godbolde, R., and Dun, N. J. (2004). Ultra low concentrations of morphine increase neurite outgrowth in cultured rat spinal cord and cerebral cortical neurons. *Neurosci. Lett.* 365, 10–13. doi: 10.1016/j.neulet.2004.03.092

Cadwell, C. R., Bhaduri, A., Mostajo-Radji, M. A., Keefe, M. G., and Nowakowski, T. J. (2019). Development and arealization of the cerebral cortex. *Neuron* 103, 980–1004. doi: 10.1016/j.neuron.2019.07.009

Cubillos-Ruiz, J. R., Mohamed, E., and Rodriguez, P. C. (2017). Unfolding anti-tumor immunity: ER stress responses sculpt tolerogenic myeloid cells in cancer. *J Immunother. Cancer* 5:5. doi: 10.1186/s40425-016-0203-4

Dai, Y., Sun, F., Zhu, H., Liu, Q., Xu, X., Gong, P., et al. (2019). Effects and mechanism of action of neonatal versus adult astrocytes on neural stem cell proliferation after traumatic brain injury. *Stem Cells* 37, 1344–1356. doi: 10.1002/stem.3060

Dong, J., Li, S., Mo, J. L., Cai, H. B., and Le, W. D. (2016). Nurr1-based therapies for Parkinson's disease. *CNS Neurosci. Ther.* 22, 351–359. doi: 10.1111/cns.12536

Hillary, R. F., and FitzGerald, U. (2018). A lifetime of stress: ATF6 in development and homeostasis. *J. Biomed. Sci.* 25:48. doi: 10.1186/s12929-018-0453-1

Hu, H., Tian, M., Ding, C., and Yu, S. (2019). The C/EBP homologous protein (CHOP) transcription factor functions in endoplasmic reticulum stress-induced apoptosis and microbial infection. *Front. Immunol.* 9:3083. doi: 10.3389/fimmu.2018.03083

Ibrahim, I. M., Abdelmalek, D. H., and Elfiky, A. A. (2019). GRP78: a cell's response to stress. *Life Sci.* 226, 156–163. doi: 10.1016/j.lfs.2019.04.022

Iurlaro, R., and Muñoz-Pinedo, C. (2016). Cell death induced by endoplasmic reticulum stress. *FEBS J.* 283, 2640–2652. doi: 10.1111/febs.13598

Johnson, G. G., White, M. C., and Grimaldi, M. (2011). Stressed to death: targeting endoplasmic reticulum stress response induced apoptosis in gliomas. *Curr. Pharmac. Design* 17, 284–292. doi: 10.2174/138161211795049660

Katebi, S. N., Razavi, Y., Zeighamy Alamdary, S., Khodagholi, F., and Haghparast, A. (2013). Morphine could increase apoptotic factors in the nucleus accumbens and prefrontal cortex of rat brain's reward circuitry. *Brain Res.* 1540, 1–8. doi: 10.1016/j.brainres.2013.09.045

Kropski, J. A., and Blackwell, T. S. (2018). Endoplasmic reticulum stress in the pathogenesis of fibrotic disease. *J. Clin. Invest.* 128, 64–73. doi: 10.1172/JCI93560

Lamb, R. J., and Ginsburg, B. C. (2018). Addiction as a BAD, a behavioral allocation disorder. *Pharmacol. Biochem. Behav.* 164, 62–70. doi: 10.1016/j.pbb.2017.05.002

Li, Y., Cong, B., Ma, C., Qi, Q., Fu, L., Zhang, G., et al. (2011). Expression of Nurr1 during rat brain and spinal cord development. *Neurosci. Lett.* 488, 49–54. doi: 10.1016/j.neulet.2010.10.078

Li, Y., Qi, Q., Cong, B., Shi, W., Liu, X., Zhang, G., et al. (2012). Expression patterns of Nurr1 in rat retina development. *J. Mol. Histol* 43, 633–639. doi: 10.1007/s10735-012-9433-z

Lorenzon-Ojea, A. R., Yung, H. W., Burton, G. J., and Bevilacqua, E. (2020). The potential contribution of stromal cell-derived factor 2 (SDF2) in endoplasmic reticulum stress response in severe preeclampsia and labor-onset. *Biochim. Biophys. Acta Mol. Basis Dis.* 1866:165386. doi: 10.1016/j.bbadis.2019.01.012

Luo, F. C., Zhao, L., Deng, J., Liang, M., Zeng, X. S., Liu, H., et al. (2013). Geranylgeranylacetone protects against morphine-induced hepatic and renal damage in mice. *Mol. Med. Rep.* 7, 694–700. doi: 10.3892/mmr.2012.1217

Maldonado, R., Negus, S., and Koob, G. F. (1992). Precipitation of morphine withdrawal syndrome in rats by administration of mu-, delta- and kappa-selective opioid antagonists. *Neuropharmacology* 31, 1231–1241. doi: 10.1016/0028-3908(92)90051-p

Miller, I., Min, M., Yang, C., Tian, C., Gookin, S., Carter, D., et al. (2018). Ki67 is a Graded rather than a binary marker of proliferation versus quiescence. *Cell Rep.* 24, 1105–1112.e5. doi: 10.1016/j.celrep.2018.06.110

Muneer, A., and Shamsher Khan, R. M. (2019). Endoplasmic Reticulum stress: implications for neuropsychiatric disorders. *Chonnam. Med. J.* 55, 8–19. doi: 10.4068/cmj.2019.55.1.8

Ni, M., Zhang, Y., and Lee, A. S. (2011). Beyond the endoplasmic reticulum: atypical GRP78 in cell viability, signalling and therapeutic targeting. *Biochem. J.* 434, 181–188. doi: 10.1042/BJ20101569

Omura, T., Asari, M., Yamamoto, J., Oka, K., Hoshina, C., Maseda, C., et al. (2013). Sodium tauroursodeoxycholate prevents paraquat-induced cell death by suppressing endoplasmic reticulum stress responses in human lung epithelial A549 cells. *Biochem. Biophys. Res. Commun.* 432, 689–694. doi: 10.1016/j.bbrc.2013.01.131

Papaioannou, A., Higa, A., Jégou, G., Jouan, F., Pineau, R., Saas, L., et al. (2018). Alterations of EDEM1 functions enhance ATF6 pro-survival signaling. *FEBS J.* 285, 4146–4164. doi: 10.1111/febs.14669

Paxinos, G., and Watson, C. (2007). *The Rat Brain in Stereotaxic Coordinates*, 6 Edn. Amsterdam: Academic Press.

Rohbani, K., Sabzevari, S., Sadat-Shirazi, M. S., Nouri Zadeh-Tehrani, S., Ashabi, G., Khalifeh, S., et al. (2019). Parental morphine exposure affects repetitive grooming actions and marble burying behavior in the offspring: Potential relevance for obsessive-compulsive like behavior. *Eur. J. Pharmacol.* 865:172757. doi: 10.1016/j.ejphar.2019.172757

Rozpedek, W., Pytel, D., Mucha, B., Leszczynska, H., Diehl, J. A., and Majsterek, I. (2016). The role of the PERK/eIF2α/ATF4/CHOP Signaling pathway in tumor progression during endoplasmic reticulum stress. *Curr. Mol. Med.* 16, 533–544. doi: 10.2174/1566524016666160523143937

Sano, K., Miyaji-Yamaguchi, M., Tsutsui, K. M., and Tsutsui, K. (2008). Topoisomerase IIbeta activates a subset of neuronal genes that are repressed in AT-rich genomic environment. *PLoS One* 3:e4103. doi: 10.1371/journal.pone.0004103

Scholzen, T., and Gerdes, J. (2000). The Ki-67 protein: from the known and the unknown. *J. Cell Physiol.* 182, 311–322. doi: 10.1002/(SICI)1097-4652(200003)182:3<311::AID-JCP1<3.0.CO;2-9

Shi, W., Zhang, Y., Zhao, G., Wang, S., Zhang, G., Ma, C., et al. (2019). Dysregulation of dopaminergic regulatory factors TH, Nurr1, and Pitx3 in the ventral tegmental area associated with neuronal injury induced by chronic morphine dependence. *Int. J. Mol. Sci.* 20:250. doi: 10.3390/ijms20020250

Volkow, N. D., and Skolnick, P. (2012). New medications for substance use disorders: challenges and opportunities. *Neuropsychopharmacology* 37, 290–292. doi: 10.1038/npp.2011.84

Wu, F., Qiu, J., Fan, Y., Zhang, Q., Cheng, B., Wu, Y., et al. (2018). Apelin-13 attenuates ER stress-mediated neuronal apoptosis by activating Gαi/Gαq-CK2 signaling in ischemic stroke. *Exp. Neurol.* 302, 136–144. doi: 10.1016/j.expneurol.2018.01.006

Xiang, C., Wang, Y., Zhang, H., and Han, F. (2017). The role of endoplasmic reticulum stress in neurodegenerative disease. *Apoptosis* 22, 1–26. doi: 10.1007/s10495-016-1296-4

Yi, S., Chen, K., Zhang, L., Shi, W., Zhang, Y., Niu, S., et al. (2019). Endoplasmic reticulum stress is involved in stress-induced hypothalamic neuronal injury in rats via the PERK-ATF4-CHOP and IRE1-ASK1-JNK pathways. *Front. Cell Neurosci.* 13:190. doi: 10.3389/fncel.2019.00190

Zhang, M., Liu, X., Wang, Q., Ru, Y., Xiong, X., Wu, K., et al. (2017). NDRG2 acts as a PERK co-factor to facilitate PERK branch and ERS-induced cell death. *FEBS Lett.* 591, 3670–3681. doi: 10.1002/1873-3468.12861

Conflict of Interest: The authors declare that the research was conducted in the absence of any commercial or financial relationships that could be construed as a potential conflict of interest.

frontiers in Pharmacology

ORIGINAL RESEARCH
published: 19 February 2021
doi: 10.3389/fphar.2021.641917

Luteolin Alleviates Methamphetamine-Induced Hepatotoxicity by Suppressing the p53 Pathway-Mediated Apoptosis, Autophagy, and Inflammation in Rats

Kai-Kai Zhang[1†], Hui Wang[2†], Dong Qu[1], Li-Jian Chen[1], Li-Bin Wang[3], Jia-Hao Li[1], Jia-Li Liu[1], Ling-Ling Xu[3], Jamie Still Yoshida[4], Jing-Tao Xu[5,6], Xiao-Li Xie[3]* and Dong-Ri Li[7]**

[1]Department of Forensic Pathology, School of Forensic Medicine, Southern Medical University, Guangzhou, China, [2]Department of Pediatric Surgery, Guangzhou Institute of Pediatrics, Guangzhou Women and Children's Medical Center, Guangzhou Medical University, Guangzhou, China, [3]Department of Toxicology, School of Public Health, Southern Medical University, Guangzhou, China, [4]Faculty of Health Sciences, Butsuryo College of Osaka, Sakai, Japan, [5]Shanghai Key Laboratory of Forensic Medicine, Institute of Forensic Science, Ministry of Justice, Shanghai, China, [6]Department of Forensic Clinical Medicine, School of Forensic Medicine, Southern Medical University, Guangzhou, China, [7]Department of Forensic Evidence Science, School of Forensic Medicine, Southern Medical University, Guangzhou, China

OPEN ACCESS

Edited by:
Di Wen,
Hebei Medical University, China

Reviewed by:
Qian Ren,
Hebei Medical University, China
Tao Wang,
Soochow University, China

***Correspondence:**
Jing-Tao Xu
xjt3080@fimmu.com
Xiao-Li Xie
xiexiaoli1999@126.com
Dong-Ri Li
lidongri@smu.edu.cn

[†]These authors have contributed equally to this work

Specialty section:
This article was submitted to Experimental Pharmacology and Drug Discovery, a section of the journal Frontiers in Pharmacology

Received: 15 December 2020
Accepted: 19 January 2021
Published: 19 February 2021

Citation:
Zhang K-K, Wang H, Qu D, Chen L-J, Wang L-B, Li J-H, Liu J-L, Xu L-L, Yoshida JS, Xu J-T, Xie X-L and Li D-R (2021) Luteolin Alleviates Methamphetamine-Induced Hepatotoxicity by Suppressing the p53 Pathway-Mediated Apoptosis, Autophagy, and Inflammation in Rats. Front. Pharmacol. 12:641917. doi: 10.3389/fphar.2021.641917

Misuse of the psychostimulant methamphetamine (METH) could induce serious hepatotoxicity. Our previous study revealed the effects of luteolin on alleviating METH-induced hepatotoxicity, however, the detailed mechanisms have not been elucidated. In this study, rats were orally pretreated with 100 mg/kg luteolin or sodium dodecyl sulfate water, and then METH (15 mg/kg, intraperitoneal [i.p.]) or saline was administered. Histopathological and biochemical analyses were used to determine the alleviative effects of luteolin. Based on the RNA-sequencing data, METH induced 1859 differentially expressed genes (DEGs) in comparison with the control group, which were enriched into 11 signaling pathways. Among these DEGs, 497 DEGs could be regulated through luteolin treatment and enriched into 16 pathways. The p53 signaling pathway was enriched in both METH administered and luteolin pretreated rats. Meanwhile, luteolin significantly suppressed METH-induced elevation of p53, caspase9, caspase3, cleaved caspase3, the ratio of Bax/Beclin-2, as well as autophagy-related Beclin-1, Atg5, and LC3-II. Luteolin also relieved METH-induced hepatotoxicity by decreasing inflammation factors, including TNF-α, IL-1β, and IL-18. Moreover, the levels of PI3K, *p*-Akt, and the normalized ratio of *p*-Akt/Akt declined after METH administration, whereas luteolin pretreatment failed to reverse these effects. Our results suggest that luteolin alleviates METH-induced hepatic apoptosis, autophagy, and inflammation through repressing the p53 pathway. It further illustrates the protective mechanisms of luteolin on METH-induced hepatotoxicity and provides a research basis for clinical treatment.

Keywords: methamphetamine, luteolin, hepatotoxicity, protective effect, p53 signaling pathway

INTRODUCTION

Methamphetamine (METH), a highly addictive stimulant, has become a public health problem due to its abuse globally (Centazzo et al., 2019; Xu et al., 2019; Xu and Liu, 2019). METH could cause abnormal behavioral phenotypes and result in neurotoxicity, including mediating oxidative stress, promoting neuroinflammation, stimulating neural apoptosis, and autophagy (Yamamoto and Bankson, 2005; Park et al., 2017; Tan et al., 2020). Increasing evidence shows that METH could also cause multiple organs damage, including the liver (Qu et al., 2020). Complex mechanisms are involved in METH-induced hepatotoxicity, including mediating hepatic metabolic disorders, stimulating oxidative stress, promoting hyperthermia, and inducing mitochondrial impairment (Willson, 2019). Our previous study confirmed that METH-induced hepatic injury was related to the blocking of multiple cellular processes, such as cell division and cycle, which might accelerate hepatic apoptosis (Wang et al., 2017). However, there are limited effective treatments for METH-induced hepatotoxicity.

Luteolin (3,4,5,7-tetrahydroxy flavone), a type of flavonoid, is generally found richly in natural vegetables, fruits, and other plants (Seelinger et al., 2008). Luteolin is extensively utilized to treat multiple diseases in Chinese traditional medicine including tumor, allergy, oxidation, inflammation, apoptosis, and autophagy (Manzoor et al., 2019; Tan et al., 2020). Also, luteolin has been reported to alleviate multiple hepatic injuries. Luteolin protects against galactosamine/lipopolysaccharide-induced hepatic apoptosis, inflammation, and oxidative stress (Lee et al., 2011; Park and Song, 2019). Mercuric chloride-induced hepatotoxicity can also be ameliorated by luteolin through modulating the Nrf2/NF-κB/p53 signaling pathway (Zhang et al., 2017). Our previous study showed that luteolin effectively alleviated METH-induced hepatotoxicity. Multiple pathways could contribute to its protective effects, though the detailed mechanisms haven't been clarified (Qu et al., 2020).

The p53 signaling pathway has been recognized as a crucial regulator of multiple biological processes, including tumor growth, cell cycle arrest, DNA repair, cell metabolism, necrosis, and proliferation (Aubrey et al., 2018). The p53 signaling pathway is also a regulator of apoptosis and autophagy (Robin et al., 2019). Meanwhile, p53 shows a close association with PI3K/Akt signaling pathway (Grinkevich et al., 2017), and our previous study has confirmed its key role in luteolin's protective effects on METH-induced neurotoxicity (Tan et al., 2020). This study examined whether this pathway also participates in the hepatic protection by luteolin.

Rats were pretreated with luteolin, followed by the administration of METH. Histopathological and biochemical analyses were performed to determine the hepatic damages. The potential pathways involved in the protective effects of luteolin were enriched and the detailed mechanisms were investigated based on RNA-sequencing. These findings may lead to the development of therapeutic drugs for METH-induced hepatotoxicity.

MATERIALS AND METHODS

Chemicals and Drugs

METH was obtained from the National Institute for the Control of Pharmaceutical and Biological Products (Beijing, China) and the purity was >99%. The purity of luteolin was >96% (Push Bio-Technology Co., Ltd. (Chengdu, China)), whereas 0.5% Sodium dodecyl sulfate (SDS) water was utilized as its solvent.

Animals and Treatments

Sprague Dawley (SD) rats (6–8 weeks old, male, 200 ± 5 g) were purchased from the Experimental Animal Center of Southern Medical University. All rats were allowed to acclimatize in the SPF animal room for 1 week before the experiment (light/dark cycle, 12 h; room temperature, 22 ± 2°C). Food and water were freely available during this period. All experimental steps strictly followed the National Institute of Health Guide for the Care and Use of Laboratory Animals of the Southern Medical University. The number of the Ethical Committee Approval Code was L2018123.

All the rats were randomly assigned to three groups each having six rats: the Control, METH, and luteolin pretreated group (**Figure 1**) (Qu et al., 2020; Tan et al., 2020). In brief, rats were orally pretreated with luteolin (100 mg/kg) or 0.5% SDS water (once daily) for 3 days. Subsequently, 15 mg/kg METH or an equal volume of saline (i.p.) were intraperitoneally (i.p.) injected at 12 h intervals for four consecutive days. All rats were sacrificed under deep anesthesia (60 mg/kg i. p. pentobarbital sodium)12 h after the final injection (Xu et al., 2018).

Blood samples were centrifuged (3,000 r/mins, 10 min s) at room temperature to separate plasma, and then stored at −80°C for biochemical analysis. One-half of the liver tissues were fixed with 10% phosphate-buffered formalin, whereas the other tissues were rapidly frozen in liquid nitrogen and stored at −80°C for further detection.

Histopathology

After fixing for 24 h, liver tissues were embedded in paraffin and sectioned at a 3 μm thickness on a manual rotary microtome. Hematoxylin and eosin (HandE) staining was conducted for further histopathological examination (Xie et al., 2019).

Biochemical Analysis

An Enzyme-linked immunosorbent assay (CUSABIO Biotechnology, Wuhan, China) was performed to examine the degree of liver damage and evaluate the protective effects of luteolin. This was to determine the levels of aspartate transaminase (AST) and alanine aminotransferase (ALT) in plasma.

RNA-Seq Data Processing, Analysis and Result Reporting

Principal Component Analysis and Correlation Analysis of Samples

Based on our published RNA-seq data (Qu et al., 2020) [BioProject: PRJNA529763], principal component analysis (PCA) was performed to integrate the principal component and simplify the complexity of the sample reads (http://deweylab.biostat.wisc.edu/rsem/) (Giuliani, 2017). The high similarity samples and the outliers were filtered out according to the relationship and the size of variation among samples.

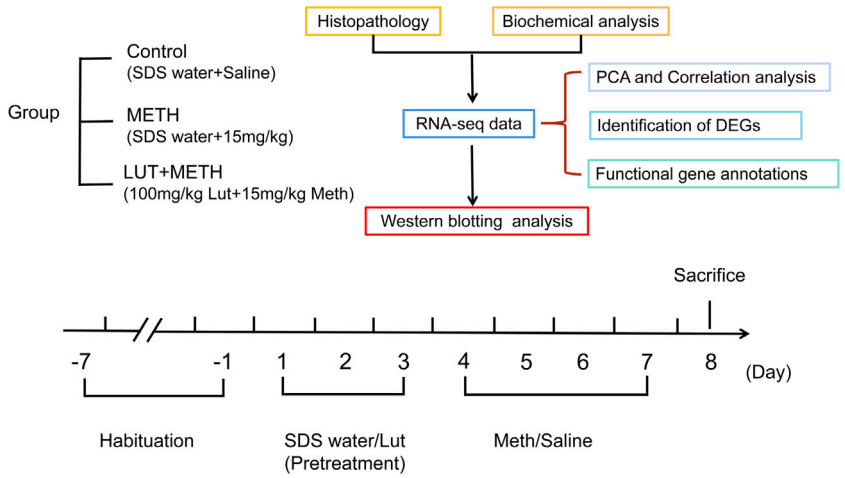

FIGURE 1 | Experimental design for METH exposure and luteolin pretreatment.

Similarly, Correlation analysis was conducted to determine the variation of repeat samples and evaluate the reliability of experimental treatment.

Identification of Differentially Expressed Genes

Fragments per Kilobases per Million reads (FPKM) method was performed to avoid the influence of length difference and compare the expression level of genes (Li and Dewey, 2011). The DESeq2 tool was utilized to assess the differential genes to accurately screen out DEGs. The screening parameters were set as: the fold change ≥2 or ≤0.5, p-value < 0.05.

Functional Gene Annotations

The Kyoto Encyclopedia of Genes and Genomes (KEGG) analysis (https://www.genome.jp/kegg/) and Protein-Protein Interaction (PPI) tools (https://string-db. org/and Cytoscape_ v3.6.1) were conducted for enrichment analysis and protein interactions respectively to analyze the potential function of the DEGs (Kanehisa et al., 2017; Szklarczyk et al., 2017). Annotations of the DEGs referred to the DAVID (http://david.ncifcrf.gov) and the STRING database (http://string.db.org).

Western Blotting Analysis

The isolated total protein was separated using SDS-PAGE gels (20 ug, per sample) and transferred to polyvinylidene difluoride (PVDF, 0.22uM) membranes (Qu et al., 2019; Zhao et al., 2020). The following steps were then conducted on the membranes orderly: Blocked in 5% skim milk for 2 h at room temperature, incubated with the primary antibodies overnight at 4°C and the secondary antibodies for 1 h at room temperature. Finally, the blots were visualized on the ECL System. The following primary antibodies were utilized: Anti-P53 (diluted 1:1,000; 4 A Biotech), anti-caspase9 (diluted 1:1,000, Proteintech), anti-caspase3 (diluted 1:1,000; ABclonal), anti-cleaved caspase3 (diluted 1:1,000; CST), anti-Bax (diluted 1:1,000; CST), anti-Beclin2 (diluted 1:1,000; Proteintech), anti-Beclin1 (diluted 1:1,000; CST), anti-ATG5 (diluted 1:1,000; HuaAn Biotechnology), anti-LC3 (diluted 1:1,000; Proteintech), anti-TNF-α (diluted 1:1,000, Proteintech), anti-IL-1β (diluted 1:1,000, Proteintech), anti-IL-18 (diluted 1:1,000, Proteintech), anti-PI3K p85 alpha(diluted 1:1,000; Proteintech), anti-AKT (diluted 1:1,000; Proteintech), anti-AKT-phospho-S473 (diluted 1:1,000; Proteintech) and anti-Beta-Actin (diluted 1:1,000; 4 A Biotech). The secondary antibodies (HRP-labeled goat anti-mouse IgG (H + L) or anti-rabbit IgG (H + L), Beijing Dingguo Changsheng Biotechnology) were diluted at the concentration of 1:5,000.

Statistical Analysis

All biochemical analysis and Western Blotting experiments were carried out in triplicate. All values were reported as mean ± SEM. The GraphPad Prism version 6.0 (San Diego, United States) was utilized for statistical analysis. One-way analysis of variance (ANOVA) followed by post-hoc Tukey tests, was used for comparisons of multiple groups. PCA analysis was performed on RSEM software (version 1.3.1) with TPM methods and the Pearson correlation analysis was employed to analyze the correlation among samples, while DESeq2 tool (version 1.24.0) was utilized to screen the DEGs. Values of p < 0.05 were considered statistically significant.

RESULTS

Luteolin Effectively Alleviated METH-Induced Hepatotoxicity

Histopathological analysis showed that 15 mg/kg METH significantly damaged the microstructure of hepatic cells by

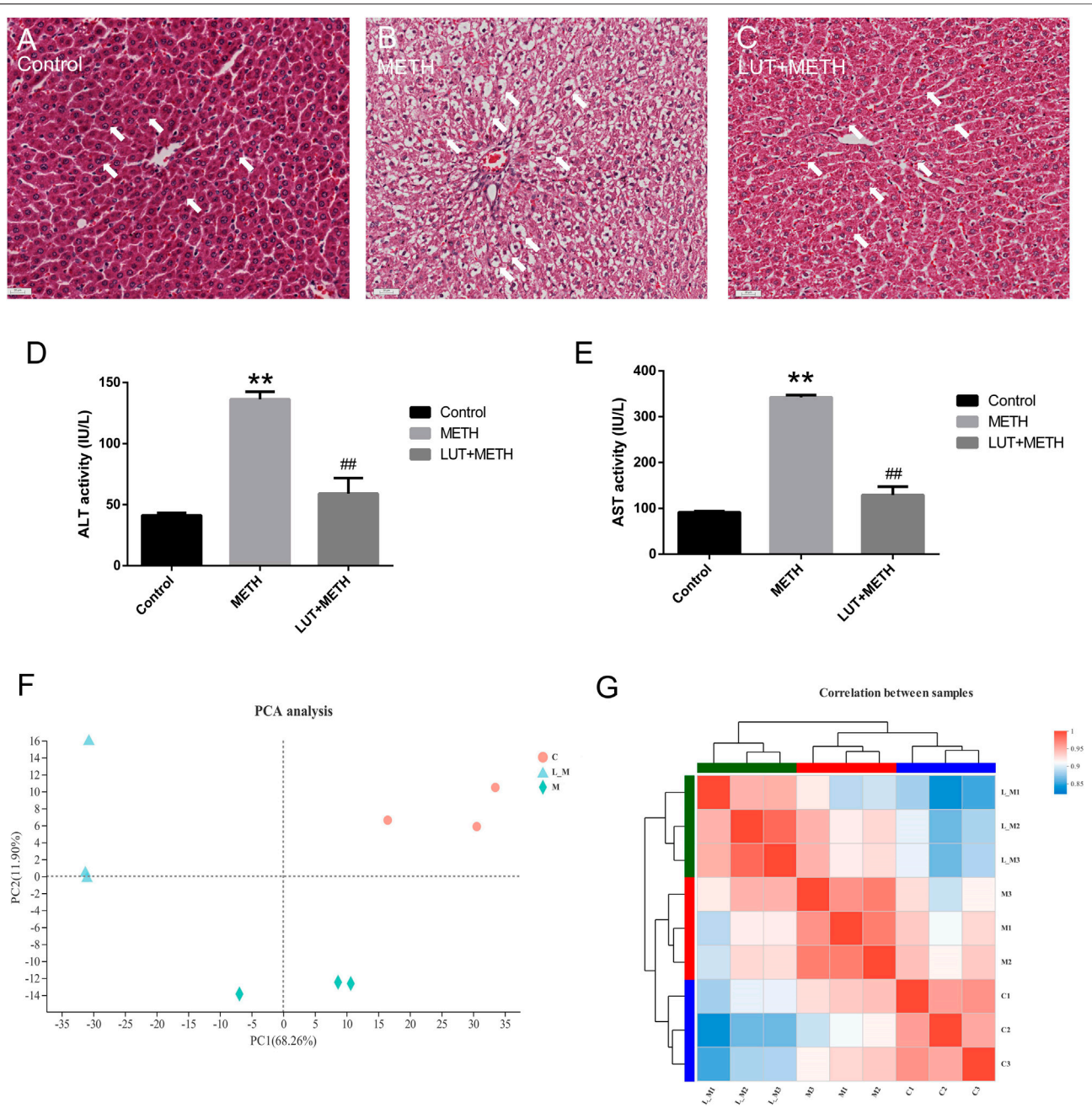

FIGURE 2 | Histopathological and biochemical assessment of liver injury. **(A–C)** Compared to the control group, METH-induced serious hepatocyte ballooning. Luteolin + METH group alleviated liver injury in comparison to the METH group. **(D, E)** METH significantly enhanced the level of ALT and AST in plasma relative to the control group. The increasing level was attenuated in the Luteolin + METH group.$^{**}p < 0.01$, compared with control group, $^{\#\#}p < 0.01$, compared with METH group (mean ± SEM). Principal correlation analysis and correlation analysis among groups. **(F)** According to the principal component, intra-group samples were clustered respectively, and then, three groups were separated distinctly. L_M, luteolin + METH. (G) Correlation analysis among samples. The tree presents the correlation among samples, whereas the color displays the coefficient of correlation.

mediating extensively hepatocyte ballooning in the test group compared to the control group (**Figures 2A,B**). Compared with the METH group, the pathological changes were alleviated by the pretreatment of luteolin (**Figure 2C**).

Biochemical indexes, ALT and AST, can mirror the function and the damage degree of the liver. Therefore, these indexes were also examined in this study. METH significantly elevated the plasma level of ALT and AST.

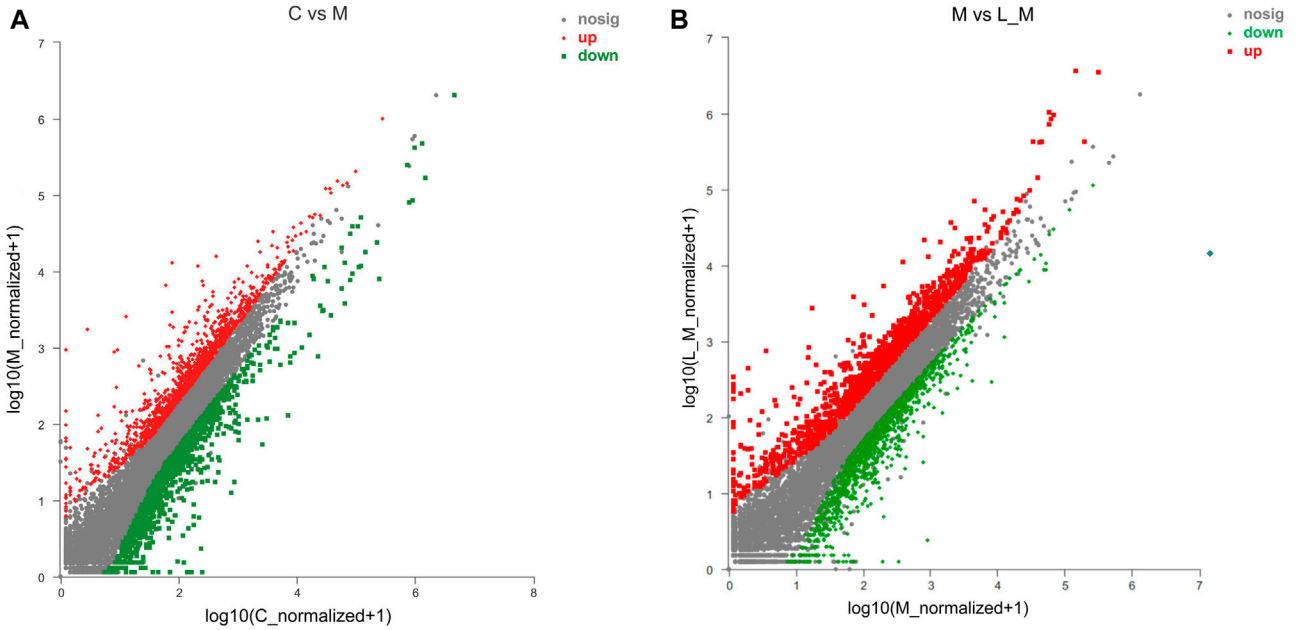

FIGURE 3 | Identification of DEGs using the Scatter plot method. **(A)** METH treatment induced the DEGs, relative to the control group; **(B)** compared to the METH group, luteolin pretreatment produced DEGs (the fold change ≥2 or ≤0.5, p-value < 0.05). The red plots represent the up-regulated DEGs, whereas the down-regulated DEGs are represented by green plots.

These increased indexes were attenuated by the pretreatment of luteolin (**Figures 2D,E**).

Screening of the Potentially Protective Mechanisms of Luteolin

Principal Component (PCA) and Correlation Analysis

The PCA analysis can simplify the RNA-seq reads and directly reflect the principal components. The distance of spots represented the similarity of principal components. Samples of the control group (red circles), METH group (green rhombuses), and luteolin pretreated group (blue triangles) were clustered separately (**Figure 2F**), which meant that the higher the difference between groups the lower variation intra-group. Correlation analysis produced similar results. Intra-group samples were clustered and shown a higher correlation compared to samples from other groups (**Figure 2G**).

Screening of DEGs

METH significantly up-regulated 873 DEGs and down-regulated 986 DEGs in comparison to the control group (**Figure 3A**). Luteolin pretreatment also induced 899 DEGs up-regulation and 978 DEGs down-regulation in the test group compared to the METH group (**Figure 3B**). Among the METH-induced DEGs, 497 DEGs could be regulated through luteolin treatment (314 up-regulated and 183 down-regulated DEGs).

Functional Annotation of DEGs

The interactions among these DEGs were analyzed through PPI analysis to investigate the underlying mechanisms of METH hepatotoxicity and luteolin's protective effects. Genes with direct or indirect connections were linked, whereas the unrelated or unrecognized genes were eliminated automatically. The more the connections between proteins, the closer they were to the center of the circle, which suggested the strong relationships among the identified DEGs (**Figures 4A,B**).

The KEGG analysis further provided the clues of the pathways involved. The METH-induced DEGs were mainly enriched into 11 pathways, whereas the DEGs which could be regulated by luteolin were enriched into 16 pathways (**Tables 1,2**). Interestingly, the p53 signaling pathway, which has been reported to mediate the toxicity of METH, was enriched in both groups. The DEGs from two groups were further annotated according to the classification of metabolism, genetic information processing, environmental information processing, cellular processes, organismal systems, and human diseases (**Figures 4C,D**).

Pretreatment of Luteolin Alleviates METH-Induced Apoptosis via Repressing p53 Pathway

Results from KEGG analysis show a significant alteration of the p53 pathway in both treatment groups. Therefore, the western blotting analysis was employed to study this pathway. For the test group compared to the control group, METH significantly increased the expression of p53 and its downstream apoptosis-related proteins, including caspase9, caspase3, cleaved caspase3, Bax, and the ratio of Bax/Beclin-2, whereas the up-regulation of these proteins were effectively repressed by luteolin pretreatment (**Figures 5A,B**).

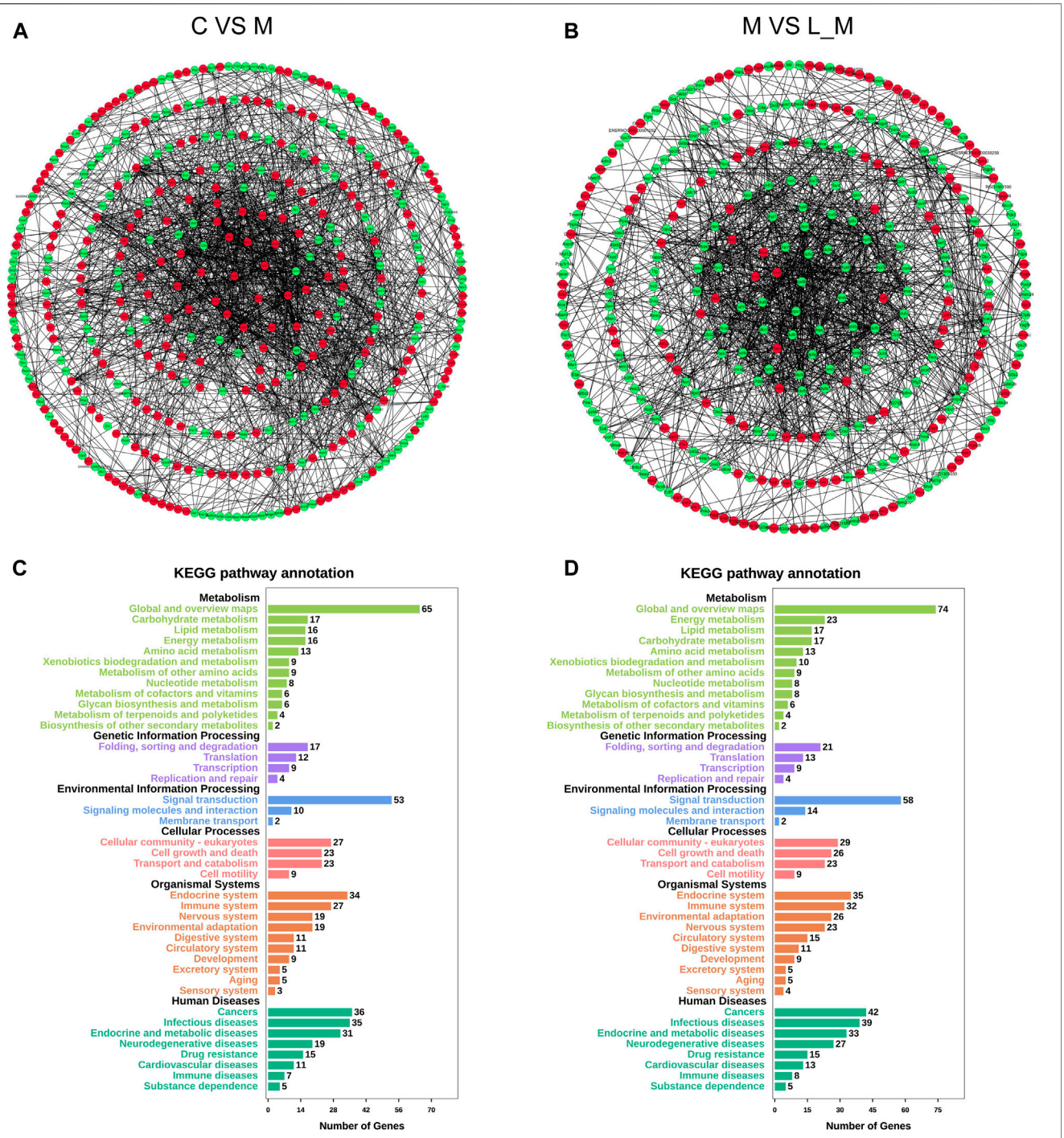

FIGURE 4 | PPI and KEGG analysis of DEGs in the METH and luteolin pretreated group **(A, B)** PPI analysis revealed the direct and indirect connections among DEGs. Up-regulated DEGs were represented by red, and down-regulated DEGs were remarked with green **(C, D)** *X*-axis; the number of the enriched DEGs, *Y*-axis; the second level term of gene ontology.

TABLE 1 | Pathway enrichment of the METH group.

Pathway enrichment					
No	**Pathway ID**	**Pathway**	**Count**	**%**	***p*-value**
1	rno04151	Metabolic pathways	54	0.070,537,522	0.001,386,404
2	rno00190	Oxidative phosphorylation	12	0.015,675,005	0.002,143,915
3	rno00510	N-Glycan biosynthesis	7	0.009,143,753	0.002,439,666
4	rno05012	Parkinson's disease	12	0.015,675,005	0.003,272,982
5	rno01130	Biosynthesis of antibiotics	14	0.018,287,506	0.00778,871
6	rno03050	Proteasome	6	0.007,837,502	0.009,337,467
7	rno05010	Alzheimer's disease	12	0.015,675,005	0.012,312,085
8	rno04152	AMPK signaling pathway	9	0.011,756,254	0.025,718,304
9	rno04540	Gap junction	7	0.009,143,753	0.035,091,577
10	rno04115	p53 signaling pathway	6	0.007,837,502	0.044,351,924
11	rno05206	MicroRNAs in cancer	9	0.011,756,254	0.045,162,063

Pretreatment of Luteolin Restrains METH-Induced Autophagy and Inflammation

The expression of autophagy-related proteins was also observed given the close relation between autophagy and the p53 signaling pathway. The expression levels of Beclin-1, Atg5, and LC3-II were increased following METH treatment. Luteolin restrained the up-regulation of these proteins (**Figures 6A,B**).

There was a significant elevation of inflammatory factors compared to the control group; TNF-α, IL-1β, and IL-18 after METH treatment. Luteolin pretreatment also significantly alleviated the METH-induced high expression of these proteins (**Figures 6C,D**).

Preatment With Luteolin Fails to Reverse METH-Induced Repression of PI3K/Akt Pathway

Luteolin alleviates METH-induced neurotoxicity by modulating PI3K/Akt pathway (Tan et al., 2020). Here, this pathway was studied. There was a significant decline of related proteins following METH treatment: PI3K, Akt phosphorylation (*p*-Akt), and the *p*-Akt/Akt ratio. Interestingly, these low expression proteins weren't reversed through luteolin pretreatment (**Figures 7A,B**).

DISCUSSION

In our previous study, luteolin showed protective effects on METH-induced hepatotoxicity (Qu et al., 2020), though the potential mechanisms were not clear. In this study, we confirmed that luteolin effectively alleviated METH-induced hepatic-pathological changes and decreased biochemical indexes of ALT and AST. The p53 pathway was enriched in both the METH and luteolin pretreated groups via KEGG analysis, based on the RNA-seq data. Downstream, the expression of apoptosis- and autophagy-related proteins were up-regulated following METH treatment, which was attenuated by luteolin pretreatment. Moreover, METH-induced inflammation was also repressed by luteolin. The PI3K/Akt pathway was suppressed after METH treatment, while this effect wasn't reversed by luteolin. These results suggested that luteolin could protect against METH mediated hepatic toxicity by repressing the p53 pathway.

RNA-sequencing data provided the detailed mechanisms of METH-induced hepatotoxicity and luteolin's protective effects. According to the KEGG analysis, eight pathways were both enriched into the METH group and luteolin pre-treated group. Among these pathways, metabolic pathways were the most enriched pathways. Conceivably, METH exposure has been reported to induce the serious disfunction of hepatic metabolism (Zhang et al., 2019). As a conserved master regulator of metabolism, the AMPK signaling pathway has been recognized as the potential therapeutic target of hepatic metabolic diseases (Smith et al., 2016; Garcia et al., 2019). In addition, oxidative phosphorylation provides the most ATP for higher animals and the damage of this pathway could induce the energy metabolism disorder (Wilson, 2017), suggesting the potential mechanism of hyperpyrexia after METH treatment (White, 2002). Interestingly, PD- and AD-related pathways were also enriched in liver tissue. This phenomenon strongly hints the pro-neurodegeneration effects of METH (Shin et al., 2017; Keshavarzi et al., 2019). The reverse regulation of these pathways could be involved in the protective effects of luteolin.

Increasing evidence shows that p53 plays a crucial role in METH-induced toxicity. Here, the p53 signaling pathway was also enriched in METH-induced hepatotoxicity. METH has been reported to mediate neural apoptosis by up-regulating p53 (Imam et al., 2001), whereas special deletion effectively alleviated METH-induced neurotoxicity (Hirata and Cadet, 1997; Lu et al., 2017). Meanwhile, Bax (a cell death effector) and the ratio of Bax/Beclin-2 (molecular markers of cell apoptosis) were also up-regulated after METH treatment, although its liberation regulator Beclin-2 wasn't altered (Ke et al., 2015; Ali et al., 2018). Activated Bax can mediate the apoptosis cascade of aspartate-specific cysteine proteases by increasing caspase9 (Li et al., 1997; Hakem et al., 1998). Consistently, METH-induced increase of Bax also showed the stimulating effects on apoptosis. METH increased the expression of caspase9 and then elevated the level of caspase3 and cleaved caspase3, which played a crucial role in apoptosis (Porter and Jänicke, 1999). Furthermore, the anti-apoptotic bioactivity of luteolin has been confirmed in multiple *in vivo*/*in vitro* models (Zhang et al., 2016; Liu and Meng, 2018). In the current study, luteolin pretreatment effectively repressed METH-mediated stimulation of the p53 pathway. These findings showed that luteolin significantly suppressed METH-induced overexpression of p53 and then, reduced the level of Bax, the ratio of Bax/Beclin-2, caspase9, caspase3, and cleaved caspase3, suggesting that the p53 pathway could play a key role in the protective effects of luteolin.

TABLE 2 | Pathway enrichment of luteolin pre-treated group.

Pathway enrichment					
NO	**Pathway ID**	**Pathway**	**Count**	**%**	***p*-value**
1	rno01100	Metabolic pathways	62	0.086,741,189	9.24344E-06
2	rno00190	Oxidative phosphorylation	16	0.022,384,823	1.03828E-05
3	rno05012	Parkinson's disease	16	0.022,384,823	1.99834E-05
4	rno05010	Alzheimer's disease	16	0.022,384,823	0.00016011
5	rno01130	Biosynthesis of antibiotics	17	0.023,783,875	0.000387,545
6	rno05016	Huntington's disease	15	0.020,985,772	0.001,562,905
7	rno04932	Non-alcoholic fatty liver disease (NAFLD)	13	0.018,187,669	0.001,843,786
8	rno03320	PPAR signaling pathway	7	0.00979,336	0.02,007,818
9	rno00480	Glutathione metabolism	6	0.008,394,309	0.022,249,139
10	rno00270	Cysteine and methionine metabolism	5	0.006,995,257	0.024,500,584
11	rno00900	Terpenoid backbone biosynthesis	4	0.005,596,206	0.025,077,535
12	rno04152	AMPK signaling pathway	9	0.012,591,463	0.026,348,516
13	rno04540	Gap junction	7	0.00979,336	0.035,775,325
14	rno03050	Proteasome	5	0.006,995,257	0.041,183,838
15	rno04115	p53 signaling pathway	6	0.008,394,309	0.045,094,341
16	rno05206	MicroRNAs in cancer	9	0.012,591,463	0.046,195,794

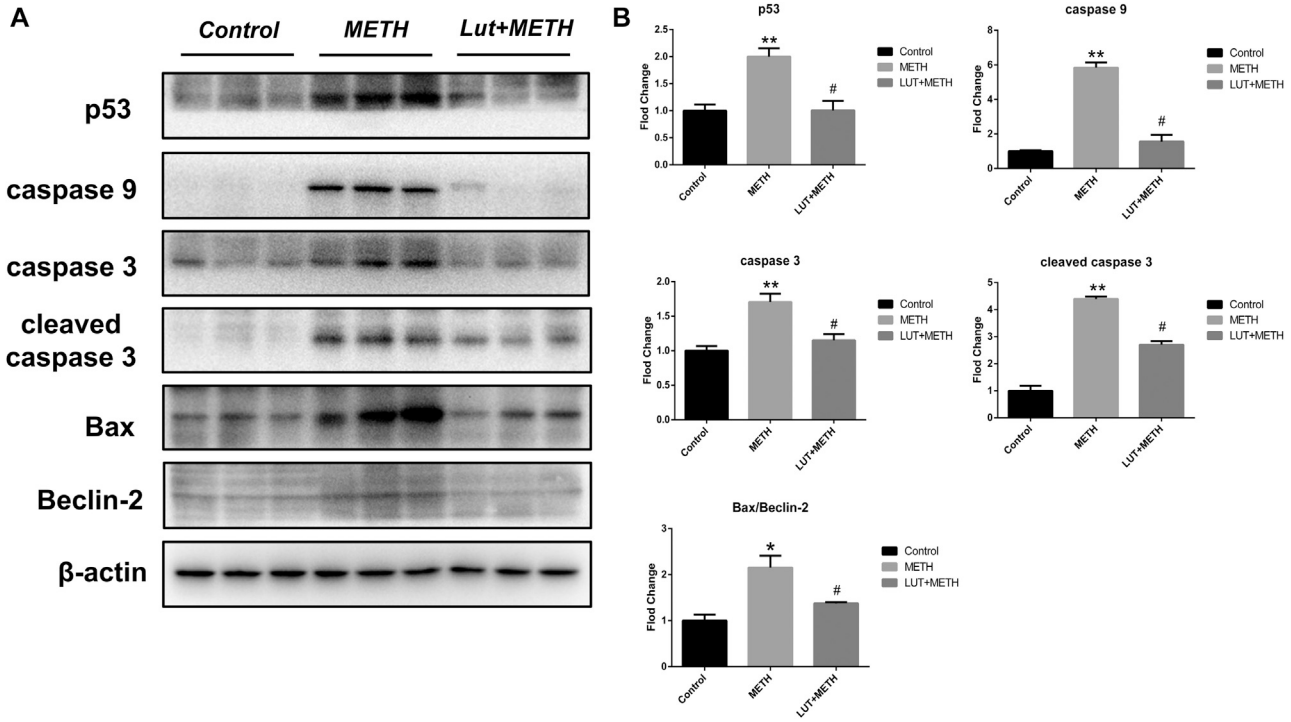

FIGURE 5 | Western blotting analysis for the expression of p53, caspase9, caspase3, cleaved caspase3, Bax, Beclin-2 **(A, B)** Compared to the control group, METH significantly increased the expression level of p53, caspase9, caspase3, cleaved caspase3, Bax, and the normalized ratio of Bax/Beclin-2. These alterations were eliminated by luteolin pretreatment. $^{*}p < 0.05$, $^{**}p < 0.01$, compared with control group, $^{\#}p < 0.05$, compared with METH group (mean ± SEM).

There is a complex interplay between autophagy and apoptosis. The activation of p53 functionally intertwines with the autophagic pathway (Baehrecke, 2005; Maiuri et al., 2007; White, 2016). In this study, the up-regulation of autophagy-related proteins following METH injections (Beclin-1, Atg5, and LC3-II) was investigated. Autophagy-related 5 (Atg5) is well-known for its proautophagic activation and can stimulate cell death, which is associated with the processing of microtubule-associated protein light chain 3 (LC3), a marker of autophagy (Tanida et al., 2008; Zheng et al., 2019). Activation of Beclin-1 initiates autophagosome formation and is required for Atg5-dependent autophagy (Kang et al., 2011). Luteolin pretreatment effectively alleviated the up-regulation of these proteins, suggesting that luteolin could resist METH-induced autophagy

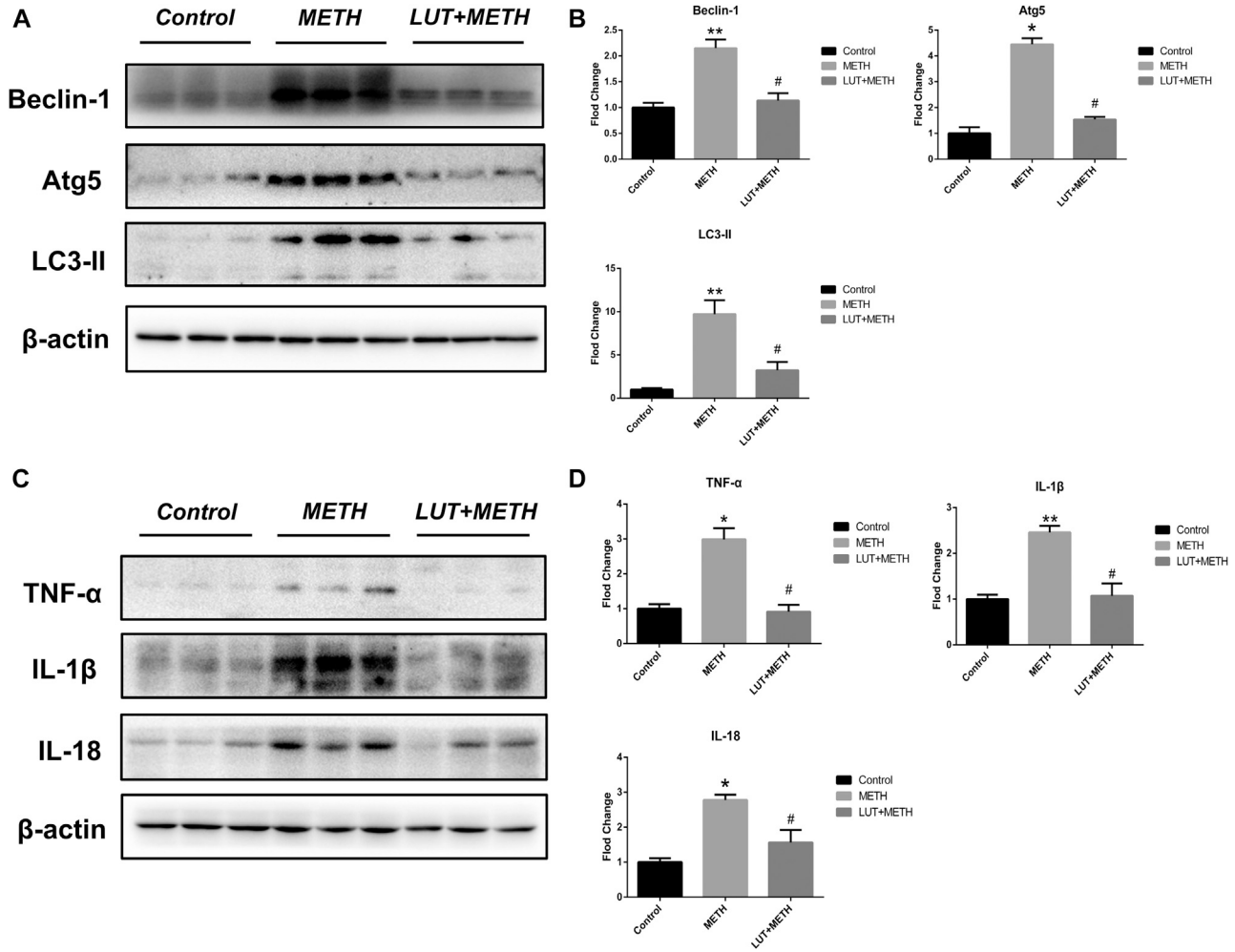

FIGURE 6 | Western blotting analysis for the expression of Beclin-1, Atg5, LC3-II, TNF-α, IL-1β, and IL-18 **(A, B)** Expression of Beclin-1, Atg5, and LC3-II were elevated after METH treatment in comparison with the control group, but these overexpressions were relieved by luteolin treatment **(C, D)** Similarly, METH also up-regulated the level of TNF-α, IL-1β, and IL-18, but these effects were diminished by luteolin. $^{*}p < 0.05$, $^{**}p < 0.01$, compared with control group, $^{\#}p < 0.05$, compared with METH group (mean ± SEM).

in rat liver, despite that the interaction between apoptosis and autophagy has not been fully illuminated.

Also, the increase of inflammatory factors, TNF-α, IL-1β, and IL-18, was observed after METH treatment, suggesting the activation of hepatic inflammation. Apoptosis/autophagy has a close association with inflammation and plays the role of checkpoint (Messer, 2017). Both apoptosis and autophagy can be triggered by inflammation and cause the process of interaction (Elmore, 2007; Levine and Kroemer, 2008). Interestingly, the findings showed that both apoptosis and autophagy were activated after METH treatment, implying that inflammation could be the origin of these consequences. Moreover, luteolin pretreatment restrained METH-induced hepatic inflammation by decreasing the high level of TNF-α, IL-1β, and IL-18, which was consistent with the anti-inflammatory effects of luteolin (Park and Song, 2019).

It has been confirmed that p53 can subdue the stimulation of the PI3K/Akt pathway, which represses mTOR (Moore et al., 2008; Grinkevich et al., 2017). This reduces mTOR's negative regulation to apoptosis and autophagy (Feng et al., 2018). Here, the findings also showed the deactivation of the PI3K/Akt pathway after METH administration. The decreasing level of PI3K and the lower *p*-Akt/Akt ratio implies that apoptosis and autophagy could be stimulated by the suppression of the PI3K/Akt pathway, whereas the overexpression of p53 could initiate it. The blocking effect of METH on the PI3K/AKT pathway was also observed in other *in vivo/in vitro* models, which mediated apoptosis and oxidative stress (Lee et al., 2020; Meng et al., 2020). Interestingly, luteolin pretreatment failed to reverse the deactivation of the PI3K/AKT pathway, indicating that the protection of luteolin on METH-induced hepatotoxicity was independent of PI3K/AKT pathway.

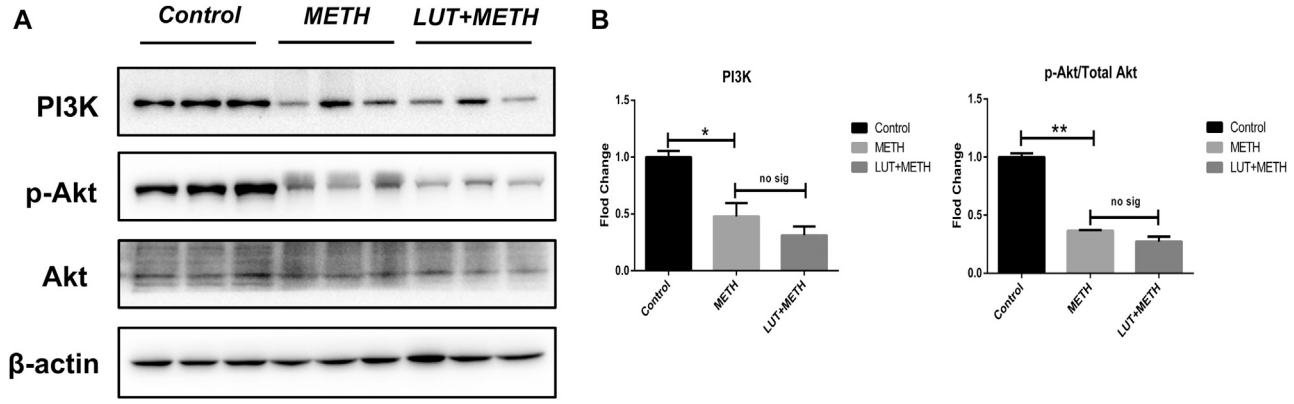

FIGURE 7 | Western blotting analysis for the expression of PI3K, *p*-Akt, and Akt **(A, B)** Relative to the control group, PI3K, *p*-Akt, and the normalized ratio of *p*-Akt/Akt were enhanced following METH treatment, while these effects weren't attenuated by luteolin pretreatment. $^{*}p < 0.05$, $^{**}p < 0.01$, compared with control group, no sig, there was no statistical significance, compared with METH group (mean ± SEM).

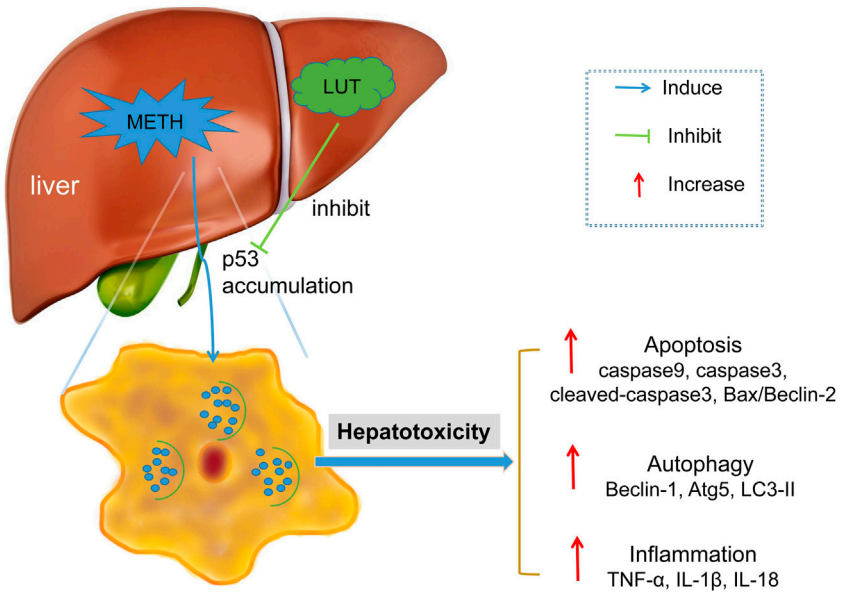

FIGURE 8 | METH stimulated the activation of p53 pathway in hepatic cell, which subsequently mediated apoptosis, autophagy and inflammation. These toxic effects could be attenuated through luteolin pre-treatment via suppressing p53 pathway.

In conclusion, this study showed that the p53 signaling pathway played a key role in METH-induced hepatotoxicity and the protective effects of luteolin. METH stimulates the activation of the p53 pathway, which triggers hepatic apoptosis, autophagy, and inflammation. Notably, these consequences were attenuated by the pretreatment of luteolin by suppressing the p53 pathway (**Figure 8**). The PI3K/Akt pathway was repressed by METH, though the protection of luteolin on METH-induced hepatotoxicity was independent of PI3K/AKT pathway. This study further investigates the protective mechanisms of luteolin on METH-induced hepatotoxicity, which could serve in the development of treatment drugs.

DATA AVAILABILITY STATEMENT

The datasets presented in this study can be found in online repositories. The names of the repository/repositories and accession number(s) can be found below: https://www.ncbi.nlm.nih.gov/, PRJNA529763.

ETHICS STATEMENT

The animal study was reviewed and approved by the National Institutes of Health Guide for the Care and Use of Laboratory Animals of the Southern Medical University.

AUTHOR CONTRIBUTIONS

J-TX, X-LX, and D-RL contributed to conception and design of the study. K-KZ and HW organized the database. DQ, L-JC, and L-BW performed the statistical analysis. K-KZ and J-LL wrote the first draft of the manuscript. J-HL, L-LX, and JSY wrote sections of the manuscript. All authors contributed to manuscript revision, read, and approved the submitted version.

FUNDING

This work was supported by the National Natural Science Foundation of China under Grant No. 81971802; Opening Foundation of Shanghai Key Laboratory of Forensic Medicine under Grant No. KF1407, and Natural Science Foundation of Guangdong Province under Grant No. 2018A0303130267.

REFERENCES

Ali, D., Tripathi, A., Al Ali, H., Shahi, Y., Mishra, K. K., Alarifi, S., et al. (2018). ROS-dependent Bax/Bcl2 and caspase 3 pathway-mediated apoptosis induced by zineb in human keratinocyte cells. *Onco. Targets Ther.* 11, 489–497. doi:10.2147/OTT.S140358

Aubrey, B. J., Kelly, G. L., Janic, A., Herold, M. J., and Strasser, A. (2018). How does p53 induce apoptosis and how does this relate to p53-mediated tumour suppression?. *Cell Death Differ.* 25 (1), 104–113. doi:10.1038/cdd.2017.169

Baehrecke, E. H. (2005). Autophagy: dual roles in life and death?. *Nat. Rev. Mol. Cell Biol.* 6 (6), 505–510. doi:10.1038/nrm1666

Centazzo, N., Frederick, B. M., Jacox, A., Cheng, S. Y., and Concheiro-Guisan, M. (2019). Wastewater analysis for nicotine, cocaine, amphetamines, opioids and cannabis in New York city. *Forensic Sci. Res.* 4 (2), 152–167. doi:10.1080/20961790.2019.1609388

Elmore, S. (2007). Apoptosis: a review of programmed cell death. *Toxicol. Pathol.* 35 (4), 495–516. doi:10.1080/01926230701320337

Feng, H., Cheng, X., Kuang, J., Chen, L., Yuen, S., Shi, M., et al. (2018). Apatinib-induced protective autophagy and apoptosis through the AKT-mTOR pathway in anaplastic thyroid cancer. *Cell Death Dis.* 9 (10), 1030. doi:10.1038/s41419-018-1054-3

Garcia, D., Hellberg, K., Chaix, A., Wallace, M., Herzig, S., Badur, M. G., et al. (2019). Genetic liver-specific AMPK activation protects against diet-induced obesity and NAFLD. *Cell Rep.* 26 (1), 192–e6. doi:10.1016/j.celrep.2018.12.036

Giuliani, A. (2017). The application of principal component analysis to drug discovery and biomedical data. *Drug Discov. Today* 22 (7), 1069–1076. doi:10.1016/j.drudis.2017.01.005

Grinkevich, V. V., Nikulenkov, F., Shi, Y., Enge, M., Bao, W., Maljukova, A., et al. (2017). Ablation of key oncogenic pathways by RITA-reactivated p53 is required for efficient apoptosis. *Cancer Cell* 31 (5), 724–726. doi:10.1016/j.ccell.2017.04.014

Hakem, R., Hakem, A., Duncan, G. S., Henderson, J. T., Woo, M., Soengas, M. S., et al. (1998). Differential requirement for caspase 9 in apoptotic pathways *in vivo*. *Cell* 94 (3), 339–352. doi:10.1016/s0092-8674(00)81477-4

Hirata, H., and Cadet, J. L. (1997). p53-knockout mice are protected against the long-term effects of methamphetamine on dopaminergic terminals and cell bodies. *J. Neurochem.* 69 (2), 780–790. doi:10.1046/j.1471-4159.1997.69020780.x

Imam, S. Z., Itzhak, Y., Cadet, J. L., Islam, F., Slikker, W., and Ali, S. F. (2001). Methamphetamine-induced alteration in striatal p53 and bcl-2 expressions in mice. *Brain Res. Mol. Brain Res.* 91 (1-2), 174–178. doi:10.1016/s0169-328x(01)00139-5

Kanehisa, M., Furumichi, M., Tanabe, M., Sato, Y., and Morishima, K. (2017). KEGG: new perspectives on genomes, pathways, diseases and drugs. *Nucleic Acids Res.* 45 (D1), D353–D361. doi:10.1093/nar/gkw1092

Kang, R., Zeh, H. J., Lotze, M. T., and Tang, D. (2011). The Beclin 1 network regulates autophagy and apoptosis. *Cell Death Differ.* 18 (4), 571–580. doi:10.1038/cdd.2010.191

Ke, F., Grabow, S., Kelly, G. L., Lin, A., O'Reilly, L. A., and Strasser, A. (2015). Impact of the combined loss of BOK, BAX and BAK on the hematopoietic system is slightly more severe than compound loss of BAX and BAK. *Cell Death Dis.* 6 (10), e1938. doi:10.1038/cddis.2015.304

Keshavarzi, S., Kermanshahi, S., Karami, L., Motaghinejad, M., Motevalian, M., and Sadr, S. (2019). Protective role of metformin against methamphetamine induced anxiety, depression, cognition impairment and neurodegeneration in rat: the role of CREB/BDNF and Akt/GSK3 signaling pathways. *Neurotoxicology* 72, 74–84. doi:10.1016/j.neuro.2019.02.004

Lee, H. S., Kim, E. N., and Jeong, G. S. (2020). Lupenone protects neuroblastoma SH-SY5y cells against methamphetamine-induced apoptotic cell death via PI3K/Akt/mTOR signaling pathway. *Int. J. Mol. Sci.* 21 (5), 1617. doi:10.3390/ijms21051617

Lee, W. C., Jung, H. A., Choi, J. S., Kim, Y. S., and Lee, S. M. (2011). Protective effects of luteolin against apoptotic liver damage induced by D-galactosamine/lipopolysaccharide in mice. *J. Nat. Prod.* 74 (9), 1916–1921. doi:10.1021/np2003935

Levine, B., and Kroemer, G. (2008). Autophagy in the pathogenesis of disease. *Cell* 132 (1), 27–42. doi:10.1016/j.cell.2007.12.018

Li, B., and Dewey, C. N. (2011). RSEM: accurate transcript quantification from RNA-Seq data with or without a reference genome. *Bmc. Bioinformatics* 12, 323. doi:10.1186/1471-2105-12-323

Li, P., Nijhawan, D., Budihardjo, I., Srinivasula, S. M., Ahmad, M., Alnemri, E. S., et al. (1997). Cytochrome c and dATP-dependent formation of Apaf-1/caspase-9 complex initiates an apoptotic protease cascade. *Cell* 91 (4), 479–489. doi:10.1016/s0092-8674(00)80434-1

Liu, X., and Meng, J. (2018). Luteolin alleviates LPS-induced bronchopneumonia injury *in vitro* and *in vivo* by down-regulating microRNA-132 expression. *Biomed. Pharmacother.* 106, 1641–1649. doi:10.1016/j.biopha.2018.07.094

Lu, T., Kim, P. P., Greig, N. H., and Luo, Y. (2017). Dopaminergic neuron-specific deletion of p53 gene attenuates methamphetamine neurotoxicity. *Neurotox. Res.* 32 (2), 218–230. doi:10.1007/s12640-017-9723-z

Maiuri, M. C., Zalckvar, E., Kimchi, A., and Kroemer, G. (2007). Self-eating and self-killing: crosstalk between autophagy and apoptosis. *Nat. Rev. Mol. Cell Biol.* 8 (9), 741–752. doi:10.1038/nrm2239

Manzoor, M. F., Ahmad, N., Ahmed, Z., Siddique, R., Zeng, X. A., Rahaman, A., et al. (2019). Novel extraction techniques and pharmaceutical activities of luteolin and its derivatives. *J. Food Biochem.* 43 (9), e12974. doi:10.1111/jfbc.12974

Meng, X., Zhang, C., Guo, Y., Han, Y., Wang, C., Chu, H., et al. (2020). TBHQ attenuates neurotoxicity induced by methamphetamine in the VTA through the Nrf2/HO-1 and PI3K/AKT signaling pathways. *Oxid. Med. Cell Longev.* 2020, 8787156. doi:10.1155/2020/8787156

Messer, J. S. (2017). The cellular autophagy/apoptosis checkpoint during inflammation. *Cell Mol. Life Sci.* 74 (7), 1281–1296. doi:10.1007/s00018-016-2403-y

Moore, T., Beltran, L., Carbajal, S., Strom, S., Traag, J., Hursting, S. D., et al. (2008). Dietary energy balance modulates signaling through the Akt/mammalian target of rapamycin pathways in multiple epithelial tissues. *Cancer Prev. Res. (Phila).* 1 (1), 65–76. doi:10.1158/1940-6207.CAPR-08-0022

Park, C. M., and Song, Y. S. (2019). Luteolin and luteolin-7-O-glucoside protect against acute liver injury through regulation of inflammatory mediators and antioxidative enzymes in GalN/LPS-induced hepatitic ICR mice. *Nutr. Res. Pract.* 13 (6), 473–479. doi:10.4162/nrp.2019.13.6.473

Park, J. H., Seo, Y. H., Jang, J. H., Jeong, C. H., Lee, S., and Park, B. (2017). Asiatic acid attenuates methamphetamine-induced neuroinflammation and neurotoxicity through blocking of NF-kB/STAT3/ERK and mitochondria-mediated apoptosis pathway. *J. Neuroinflammation* 14 (1), 240. doi:10.1186/s12974-017-1009-0

Porter, A. G., and Jänicke, R. U. (1999). Emerging roles of caspase-3 in apoptosis. *Cell Death Differ.* 6 (2), 99–104. doi:10.1038/sj.cdd.4400476

Qu, D., Tan, X. H., Zhang, K. K., Wang, Q., and Wang, H. J. (2019). ATF3 mRNA, but not BTG2, as a possible marker for vital reaction of skin contusion. *Forensic Sci Int* 303, 109937. doi:10.1016/j.forsciint.2019.109937

Qu, D., Zhang, K., Chen, L., Wang, Q., and Wang, H. (2020). RNA-sequencing analysis of the effect of luteolin on methamphetamine-induced hepatotoxicity in rats: a preliminary study. *Peerj* 8, e8529. doi:10.7717/peerj.8529

Robin, M., Issa, A. R., Santos, C. C., Napoletano, F., Petitgas, C., Chatelain, G., et al. (2019). *Drosophila* p53 integrates the antagonism between autophagy and apoptosis in response to stress. *Autophagy* 15 (5), 771–784. doi:10.1080/15548627.2018.1558001

Seelinger, G., Merfort, I., Wölfle, U., and Schempp, C. M. (2008). Anti-carcinogenic effects of the flavonoid luteolin. *Molecules* 13 (10), 2628–2651. doi:10.3390/molecules13102628

Shin, E. J., Dang, D. K., Tran, T. V., Tran, H. Q., Jeong, J. H., Nah, S. Y., et al. (2017). Current understanding of methamphetamine-associated dopaminergic neurodegeneration and psychotoxic behaviors. *Arch. Pharm. Res.* 40 (4), 403–428. doi:10.1007/s12272-017-0897-y

Smith, B. K., Marcinko, K., Desjardins, E. M., Lally, J. S., Ford, R. J., and Steinberg, G. R. (2016). Treatment of nonalcoholic fatty liver disease: role of AMPK. *Am. J. Physiol. Endocrinol. Metab.* 311 (4), E730–E740. doi:10.1152/ajpendo.00225.2016

Szklarczyk, D., Morris, J. H., Cook, H., Kuhn, M., Wyder, S., Simonovic, M., et al. (2017). The STRING database in 2017: quality-controlled protein-protein association networks, made broadly accessible. *Nucleic Acids Res.* 45 (D1), D362–D368. doi:10.1093/nar/gkw937

Tan, X. H., Zhang, K. K., Xu, J. T., Qu, D., Chen, L. J., Li, J. H., et al. (2020). Luteolin alleviates methamphetamine-induced neurotoxicity by suppressing PI3K/Akt pathway-modulated apoptosis and autophagy in rats. *Food Chem. Toxicol.* 137, 111179. doi:10.1016/j.fct.2020.111179

Tanida, I., Ueno, T., and Kominami, E. (2008). LC3 and autophagy. *Methods Mol. Biol.* 445, 77–88. doi:10.1007/978-1-59745-157-4_4

Wang, Q., Wei, L. W., Xiao, H. Q., Xue, Y., Du, S. H., Liu, Y. G., et al. (2017). Methamphetamine induces hepatotoxicity via inhibiting cell division, arresting cell cycle and activating apoptosis: in vivo and *in vitro* studies. *Food Chem. Toxicol.* 105, 61–72. doi:10.1016/j.fct.2017.03.030

White, E. (2016). Autophagy and p53. *Cold Spring Harb. Perspect Med.* 6 (4), a026120. doi:10.1101/cshperspect.a026120

White, S. R. (2002). Amphetamine toxicity. *Semin. Respir. Crit. Care Med.* 23 (1), 27–36. doi:10.1055/s-2002-20586

Willson, C. (2019). Sympathomimetic amine compounds and hepatotoxicity: not all are alike-Key distinctions noted in a short review. *Toxicol. Rep.* 6, 26–33. doi:10.1016/j.toxrep.2018.11.013

Wilson, D. F. (2017). Oxidative phosphorylation: regulation and role in cellular and tissue metabolism. *J. Physiol. (Lond).* 595 (23), 7023–7038. doi:10.1113/JP273839

Xie, X. L., Zhou, W. T., Zhang, K. K., Yuan, Y., Qiu, E. M., Shen, Y. W., et al. (2019). PCB52 induces hepatotoxicity in male offspring through aggravating loss of clearance capacity and activating the apoptosis: sex-biased effects on rats. *Chemosphere* 227, 389–400. doi:10.1016/j.chemosphere.2019.04.077

Xu, B., Ye, Y., and Liao, L. (2019). Rapid and simple analysis of amphetamine-type illegal drugs using excitation-emission matrix fluorescence coupled with parallel factor analysis. *Forensic Sci Res* 4 (2), 179–187. doi:10.1080/20961790.2017.1349600

Xu, F., and Liu, L. (2019). Simultaneous determination of free methamphetamine, pethidine, ketamine and tramadol in urine by dispersive liquid-liquid microextraction combined with GC-MS. *Forensic Sci. Res.* 4 (2), 188–194. doi:10.1080/20961790.2017.1377386

Xu, J., Zhao, R., Xue, Y., Xiao, H., Sheng, Y., Zhao, D., et al. (2018). RNA-seq profiling reveals differentially expressed genes as potential markers for vital reaction in skin contusion: a pilot study. *Forensic Sci. Res.* 3 (2), 153–160. doi:10.1080/20961790.2017.1349639

Yamamoto, B. K., and Bankson, M. G. (2005). Amphetamine neurotoxicity: cause and consequence of oxidative stress. *Crit. Rev. Neurobiol.* 17 (2), 87–117. doi:10.1615/critrevneurobiol.v17.i2.30

Zhang, B. C., Zhang, C. W., Wang, C., Pan, D. F., Xu, T. D., and Li, D. Y. (2016). Luteolin attenuates foam cell formation and apoptosis in ox-LDL-stimulated macrophages by enhancing autophagy. *Cell Physiol. Biochem.* 39 (5), 2065–2076. doi:10.1159/000447902

Zhang, H., Tan, X., Yang, D., Lu, J., Liu, B., Baiyun, R., et al. (2017). Dietary luteolin attenuates chronic liver injury induced by mercuric chloride via the Nrf2/NF-κB/P53 signaling pathway in rats. *Oncotarget* 8 (25), 40982–40993. doi:10.18632/oncotarget.17334

Zhang, Y., Li, L., Wang, Q., Shen, M., Han, W., Yang, X., et al. (2019). Simultaneous determination of metabolic and elemental markers in methamphetamine-induced hepatic injury to rats using LC-MS/MS and ICP-MS. *Anal Bioanal. Chem.* 411 (15), 3361–3372. doi:10.1007/s00216-019-01810-5

Zhao, D., Wang, Q., Zhou, W. T., Wang, L. B., Yu, H., Zhang, K. K., et al. (2020). PCB52 exposure alters the neurotransmission ligand-receptors in male offspring and contributes to sex-specific neurodevelopmental toxicity. *Environ. Pollut.* 264, 114715. doi:10.1016/j.envpol.2020.114715

Zheng, W., Xie, W., Yin, D., Luo, R., Liu, M., and Guo, F. (2019). ATG5 and ATG7 induced autophagy interplays with UPR via PERK signaling. *Cell Commun. Signal.* 17 (1), 42. doi:10.1186/s12964-019-0353-3

Conflict of Interest: The authors declare that the research was conducted in the absence of any commercial or financial relationships that could be construed as a potential conflict of interest.

frontiers in Pharmacology

ORIGINAL RESEARCH
published: 17 March 2021
doi: 10.3389/fphar.2021.619436

Methamphetamine and HIV-Tat Protein Synergistically Induce Oxidative Stress and Blood-Brain Barrier Damage via Transient Receptor Potential Melastatin 2 Channel

Jian Huang[1,2†], Ruilin Zhang[1,2†], Shangwen Wang[1,2†], Dongxian Zhang[1,2†], Chi-Kwan Leung[3,4], Genmeng Yang[1], Yuanyuan Li[1], Liu Liu[1], Yue Xu[1], Shucheng Lin[1], Chan Wang[1], Xiaofeng Zeng[1,2] and Juan Li[1,5]**

[1]NHC Key Laboratory of Drug Addiction Medicine, Kunming Medical University, Kunming, China, [2]School of Forensic Medicine, Kunming Medical University, Kunming, China, [3]School of Biomedical Sciences, The Chinese University of Hong Kong, Hong Kong, China, [4]CUHK-SDU Joint Laboratory of Reproductive Genetics, School of Biomedical Sciences, The Chinese University of Hong Kong, Hong Kong, China, [5]School of Basic Medicine, Kunming Medical University, Kunming, China

OPEN ACCESS

Edited by:
Maria Angela Sortino, University of Catania, Italy

Reviewed by:
Keith David Rochfort, Dublin City University, Ireland
Fruzsina R. Walter, Hungarian Academy of Sciences (MTA), Hungary

***Correspondence:**
Xiaofeng Zeng
zxf2004033@163.com
Juan Li
121093258@qq.com

†*These authors have contributed equally to this work*

Specialty section:
This article was submitted to Experimental Pharmacology and Drug Discovery, a section of the journal Frontiers in Pharmacology

Received: *27 October 2020*
Accepted: *25 January 2021*
Published: *17 March 2021*

Citation:
Huang J, Zhang R, Wang S, Zhang D, Leung C-K, Yang G, Li Y, Liu L, Xu Y, Lin S, Wang C, Zeng X and Li J (2021) Methamphetamine and HIV-Tat Protein Synergistically Induce Oxidative Stress and Blood-Brain Barrier Damage via Transient Receptor Potential Melastatin 2 Channel. Front. Pharmacol. 12:619436. doi: 10.3389/fphar.2021.619436

Synergistic impairment of the blood-brain barrier (BBB) induced by methamphetamine (METH) and HIV-Tat protein increases the risk of HIV-associated neurocognitive disorders (HAND) in HIV-positive METH abusers. Studies have shown that oxidative stress plays a vital role in METH- and HIV-Tat-induced damage to the BBB but have not clarified the mechanism. This study uses the human brain microvascular endothelial cell line hCMEC/D3 and tree shrews to investigate whether the transient receptor potential melastatin 2 (TRPM2) channel, a cellular effector of the oxidative stress, might regulate synergistic damage to the BBB caused by METH and HIV-Tat. We showed that METH and HIV-Tat damaged the BBB *in vitro*, producing abnormal cell morphology, increased apoptosis, reduced protein expression of the tight junctions (TJ) including Junctional adhesion molecule A (JAMA) and Occludin, and a junctional associated protein Zonula occludens 1 (ZO1), and increased the flux of sodium fluorescein (NaF) across the hCMEC/D3 cells monolayer. METH and HIV-Tat co-induced the oxidative stress response, reducing catalase (CAT), glutathione peroxidase (GSH-PX), and superoxide dismutase (SOD) activity, as well as increased reactive oxygen species (ROS) and malonaldehyde (MDA) level. Pretreatment with n-acetylcysteine amide (NACA) alleviated the oxidative stress response and BBB damage characterized by improving cell morphology, viability, apoptosis levels, TJ protein expression levels, and NaF flux. METH and HIV-Tat co-induced the activation and high protein expression of the TRPM2 channel, however, early intervention using 8-Bromoadenosine-5′-O-diphosphoribose (8-Br-ADPR), an inhibitor of TPRM2 channel, or TRPM2 gene knockdown attenuated the BBB damage. Oxidative stress inhibition reduced the activation and high protein expression of the TRPM2 channel in the *in vitro* model, which in turn reduced the oxidative stress response. Further, 8-Br-ADPR attenuated the effects of METH and

HIV-Tat on the BBB in tree shrews—namely, down-regulated TJ protein expression and increased BBB permeability to Evans blue (EB) and NaF. In summary, the TRPM2 channel can regulate METH- and HIV-Tat-induced oxidative stress and BBB injury, giving the channel potential for developing drug interventions to reduce BBB injury and neuropsychiatric symptoms in HIV-infected METH abusers.

Keywords: transient receptor potential melastatin 2 channel, methamphetamine, HIV-tat protein, blood-brain barrier, oxidative stress

INTRODUCTION

Methamphetamine (METH), a highly addictive synthetic drug characterized by high central excitability and relapse rates, is widely abused worldwide due to the simple synthesis process and low production cost (Huang et al., 2020). Long-term METH abuse damages the central nervous system (CNS), and the resultant neurotoxicity involves multiple mechanisms, including dopaminergic nerve terminal injury, neuronal excitatory toxicity, mitochondrial dysfunction, endoplasmic reticulum stress, neuroinflammation, and oxidative stress response (Mediouni et al., 2015; Northrop and Yamamoto, 2015; Gonçalves et al., 2017; Qie et al., 2017; Yang et al., 2018).

METH use is not uncommon among those infected with HIV, another major public health problem in the world today. Data from the Joint United Nations Programme on HIV/AIDS (UNAIDS) suggests that 37.9 m people were living with HIV at the end of 2018. When HIV-positive patients inject METH intravenously, they increase the risk of spreading HIV by sharing syringes. In the early stage of HIV infection, the virus can enter the CNS and induce HIV-associated neurocognitive disorders (HAND) (Atluri et al., 2015). HAND persistence is influenced by several factors, such as increased life expectancy with antiretroviral therapy, residual levels of the virus in patients' CNS, and the presence of HIV regulatory proteins such as HIV-Tat in the brain (Mediouni et al., 2015). HIV-Tat encoded by the HIV gene can not only activate HIV transcription and promote HIV replication (Atluri et al., 2015; Mediouni et al., 2015) but also cause neurotoxicity through neuronal excitatory toxicity, mitochondrial dysfunction, endoplasmic reticulum stress, glial cell activation, and oxidative stress response (Ma et al., 2014; Mediouni et al., 2015).

METH and HIV-Tat have a complex interaction. Mediouni et al. (Mediouni et al., 2015) believe that METH abuse can enhance the neurotoxicity of HIV-Tat, and their combined effects can lead to neurotransmitter metabolism disorder, oxidative stress response, and neuroinflammation. Other studies have shown that METH and HIV-Tat can co-induce autophagy and apoptosis of nerve cells (Qi et al., 2011; Li et al., 2018a; Zeng et al., 2018). To become toxic in the CNS, METH, and HIV must first break through the blood-brain barrier (BBB). The BBB is the diffusion barrier between the brain microvascular wall and the brain parenchyma, which is composed of brain microvascular endothelial cells (BMECs), tight junctions (TJs), pericytes, the basement membrane, and the astrocytes. TJs form the basic structure of the BBB, which is composed of three integral membrane proteins—Junctional adhesion molecule (JAM), Occludin, and Claudin, and some cytoplasmic accessory proteins—Zonula occludens (ZO)1, ZO_2, ZO_3, and others (Ballabh et al., 2004).

The BBB is a protective and selective permeability barrier that lets water, glucose, amino acids, and some fat-soluble molecules freely penetrate it while restricting neurotoxic substances (Abbott et al., 2006; Campos-Bedolla et al., 2014). However, when METH and HIV-Tat induce neurotoxicity, BBB injury often occurs. Several studies have shown that both METH and HIV-Tat can induce BMEC apoptosis (Ma et al., 2014; Jumnongprakhon et al., 2016; Jumnongprakhon et al., 2017; Qie et al., 2017), destroy the BMEC cytoskeleton (Avraham et al., 2004; Fernandes et al., 2014; Xue et al., 2019), reduce BMEC transepithelial electrical resistance (TEER) (Jumnongprakhon et al., 2016; Patel et al., 2017; Qie et al., 2017), and affect the expression and function of TJ proteins (Xu et al., 2012; Fernandes et al., 2014; Jiang et al., 2017b; Gonçalves et al., 2017; Qie et al., 2017; Xue et al., 2019), thus altering the BBB's permeability and destroying its structural integrity (Mcrae, 2016; Namyen et al., 2020). Moreover, when a combined exposure of both METH and HIV-Tat, the consequent BMEC damage and abnormal TJ protein expression are more serious (Patel et al., 2017; Li et al., 2018b). METH and HIV-Tat-induced synergistic damage to the BBB increase CNS exposure and the risk of HAND. Previous studies have demonstrated that METH and HIV-Tat can co-induce the oxidative stress response (Zeng et al., 2018), which has been shown to play an important role in BBB injury in rats (Li et al., 2018b). The exact mechanism for this process, however, remains unclear.

The transient receptor potential melastatin 2 (TRPM2) channel, a cation channel that belongs to the transient receptor potential superfamily, has gained much interest in recent years (Belrose and Jackson, 2018; Sita et al., 2018; Wang et al., 2018). It is widely distributed in tissues and cells such as the hippocampus, thalamus, striatum, cerebral cortex, endothelial cells, and glial cells (Turlova et al., 2018). Recent studies have shown that the channel is a cellular effector of oxidative stress and can be activated by many factors, including H_2O_2, reactive oxygen species (ROS), and tumor necrosis factor-alpha (TNF-α), therefore, it could mediate oxidative stress response, neuroinflammation, autophagy, and apoptosis (Alawieyah Syed Mortadza et al., 2018; Aminzadeh et al., 2018; Belrose and Jackson, 2018; Miyanohara et al., 2018; Sita et al., 2018; Wang et al., 2020). Besides, inhibition of the TRPM2 channel by 8-Br-cADPR (an inhibitor of the TRPM2 channel) may be a new treatment modality for ischemic acute kidney injury (Eraslan et al., 2019).

Based on the above background research, we hypothesize that the TRPM2 channel can regulate the damaging effects of METH and HIV-Tat on the BBB. Compared with rodents, the tree shrew, a novel model animal, has a more developed brain and is more similar to humans in anatomy, physiology, and genomics (Fan et al., 2013). Recently, the tree shrews have been used as experimental animals in some studies related to METH addiction and toxicity (Li et al., 2018a; Huang et al., 2020). Thus, the human brain microvascular endothelial cell line hCMEC/D3 and tree shrews are used as the research objects for *in vivo* and *in vitro* analyses of how METH and HIV-Tat co-induce oxidative stress injury to damage the BBB, and to identify the TRPM2 channel's function and mechanism in this process. The results present a novel theory of the BBB injury induced by METH and HIV-Tat and provide a new scientific basis for developing effective drug intervention targets for HIV-positive METH abusers.

MATERIALS AND METHODS

Materials

METH was purchased from the National Institutes for Food and Drug Control (Cat#: 171212-200603, Beijing, China). Recombinant HIV-1 Tat Clade-B was purchased from Prospec (Tat, Cat#: HIV-129, Rehovot, Israel). N-acetylcysteine amide (NACA, Cat#: A0737), 8-Bromo-cyclic adenosine diphosphate ribose (8-Br-cADPR, Cat#: B5416), Evans Blue (EB, Cat#: E2129), and sodium fluorescein (NaF, Cat#: F6377) were purchased from Sigma-Aldrich (Missouri, United States). DeadEnd™ Fluorometric TUNEL System was purchased from Progema (Cat#: G3250, Fitchburg, United States). The antibodies used were JAMA (Cat#: ab180821, 1:1,000, Abcam, United Kingdom), Occludin (Cat#: ab167161, 1:5,000, Abcam, United Kingdom), ZO1 (Cat#: ab216880, 1:1,000, Abcam, United Kingdom), TRPM2 (Cat#: ab11168, 1:1,000, Abcam, United Kingdom), β-Actin (Cat#: 21,338, 1:1,000, Signalway Antibody, United States), and secondary antibody (Cat#: L3012, 1:5,000, Signalway Antibody, United States).

Animal Experiments

Male tree shrews (120 to 160 g, 1-year-old) were supplied by the Center of Tree Shrew Germplasm Resources, the Institute of Medical Biology, the Chinese Academy of Medical Science, and Peking Union Medical College (Kunming, China). They were housed in a standard 12 h:12 h light/dark cycle at a room temperature of 23 ± 2°C, with access to food and water *ad libitum*, and give humanitarian care according to the 3R principle used in laboratory animals. All experiments were approved by the Institutional Ethics Committee of Kunming Medical University and were performed according to ethical standards described in the NIH guidelines. The tree shrews were randomly divided into six groups: 1) control (C) group; 2) 8-Br-cADPR (8-Br) group; 3) METH (M) group; 4) HIV-Tat (T) group; 5) METH + HIV-Tat (M + T) group; 6) 8-Br-cADPR + METH + HIV-Tat (8-Br + M + T) group. The animals in groups 1) and 2) were intraperitoneally injected with either saline (0.2 ml) or 8-Br-cADPR (40 μg/kg); 3) to 5) were injected with METH (8 mg/kg, intraperitoneal injection) and/or HIV-Tat (100 ng, tail intravenous injection); 6) were injected with 8-Br-cADPR (40 μg/kg, intraperitoneal injection) 0.5 h before exposure to METH and HIV-Tat. All the animals were treated for 10 consecutive days per the above requirements and euthanized 24 h after the final treatment. Their brains were then harvested and snap-frozen in liquid nitrogen for further analysis.

Evaluation of BBB Permeability in Brain Tissues

Six animals in each group were treated with EB (2%, 2 ml/kg, n = 3) or NaF (2%, 2 ml/kg, n = 3) by tail intravenous injection 1 h before the end of the experiment. Approximately 0.5 h later, the animals were euthanized with sodium pentobarbital (10%, 3 ml/kg) by intraperitoneal injection and perfused with 300 ml of heparinized saline (0.9% sodium chloride and 20 U/ml sodium heparin). The brains injected with EB were harvested and dipped in dimethyl sulfoxide (1 ml/100 mg brain tissue) for 24 h at 60°C. After centrifugation at 1000 g for 5 min, optical densities (ODs) of the supernatants were measured by spectrophotometer at 550 nm excitation wavelength and 620 nm emission wavelength to evaluate the EB content. Another three brains injected with NaF were then harvested and dipped in 5% trichloroacetic acid (1 ml/100 mg brain tissue). Following centrifugation at 12000 g for 5 min, the supernatants were taken and 5 mol/L NaOH (1:0.8) matched into the samples. ODs of the samples were then measured by spectrophotometer at 450 nm excitation wavelength and 525 nm emission wavelength to evaluate the NaF content.

Cell Cultures and Treatments

The human brain microvascular endothelial cell line hCMEC/D3 cells were purchased from the National Infrastructure of Cell Line Resource (Beijing, China). The cells were derived from human brain microvascular endothelium and shared characteristics with the BBB, including the expression of TJ proteins (Weksler et al., 2013). The cells were cultured in DMEM/high glucose (Hyclone, United States) supplemented with 10% FBS (Gibco, United States), 1% penicillin/streptomycin (Gibco, United States), and 1 ng/ml human basic fibroblast growth factor (Sigma-Aldrich, United States) in 5% CO_2 at 37°C. According to the experimental requirements, the cells were plated in 6-well plates, 24-well plates, or 96-well plates, respectively, and treated with different drugs for different durations when the cells reached appropriate confluence. A non-serum medium was used for drug treatments.

Lentiviral Transfection

shTRPM2 lentivirus (LV-shTRPM2) and shNC lentivirus (LV-shNC) were obtained from GenePharma Co., Ltd (Shanghai, China). The sequences were as follows: shTRPM2: 5′-GCA ATAAGGTTGACGCCATGG-3′; shNC (refers to an empty vector): 5′-TTCTCCGAACGTGTCACGT-3′. The titer of the virus was 5×10^8 TU/ml. According to the experimental

requirements, the cells were plated in 6-well plates, 24-well plates, or 96-well plates, and transfection with LV-shTRPM2 or LV-shNC (1:50, containing 5 μg/ml polybrene) was conducted when the cells reached 40% confluence. The medium was replaced 24 h after infection. The cells were further cultured for 24 h to 48 h, then used for subsequent experiments.

Real-Time qPCR

Total RNA was extracted from the cells infected by LV-shTRPM2 or LV-shNC using the TRIzol reagent (Invitrogen, United States). According to the manufacturer's instructions, the total RNA was synthesized into cDNA using the First Strand cDNA Synthesis Kit (Thermo Scientific, United States), and the real-time qPCR reaction was performed using the FastStart Universal SYBR Green Master (ROX) kit (Roche, Switzerland) in a real-time qPCR system (ABI 7300, United States). The total reaction volume was 20 μL. The relative expression of TRPM2 mRNA was calculated using the $2^{-\triangle\triangle CT}$ method. Each experiment was performed in triplicate wells and replicated.

The primers were designed and synthesized by Sangon Biotech Co., Ltd (Shanghai, China), and they were compatible with the Minimum Information for Publication of Quantitative Real-Time PCR Experiments (MIQE) guidelines. The primer sequences were as follows:

TRPM2: Sense: 5′-TTCGTGGATTCCTGAAAACATCA-3′; Antisense: 5′-CCAGCATCAGACAGTTTGGAAC-3′.

GAPDH: Sense: 5′-GAGCGAGATCCCTCCAAAAT-3′; Antisense: 5′-GCTGTTGTCATACTTCTCAT-3′.

Analysis of Cell Viability

The viability of hCMEC/D3 cells was quantified using the CCK8 kit (Beyotime, Shanghai, China). The cells were plated in 96-well plates and cultured in 5% CO_2 at 37°C. Following exposure to different drugs for different durations, the medium in each well was discarded and replaced with 90 μL of serum-free medium and 10 μL of CCK8 reagent. After being incubated at 37°C for 2 h, the ODs were determined at 450 nm using a universal microplate reader (BioTek, United States). Each experiment was conducted in triplicate wells and replicated.

Assessment of Apoptosis

The cells were plated in 24-well plates and cultured in 5% CO2 at 37°C. Following exposure to different drugs for different durations, the cells were fixed in a 4% methanol-free formaldehyde solution and permeabilized with 0.2% Triton® X-100 solution. Then, the cells were incubated with the TUNEL solution (Progma, United States) at 37°C for 1 h. After DAPI (Cat#: H-1200, Vectorlab, United States) were added to each well to stain nuclei, the fluorescence signals were observed by an inverted fluorescence microscope (Nikon TE2000U, Japan). The image capture area was randomly selected by a researcher who was blinded to the experimental conditions. Each experiment was conducted in triplicate wells and replicated, and three images were captured from each well. The apoptosis level was determined by the number of TUNEL-positive cells expressed as a percentage of the total cell number (analyzed by Image J software).

Measurement of ROS

Intracellular ROS levels were measured using commercial kits (Beyotime, Shanghai, China) according to the manufacturer's instructions. The cells were seeded briefly in 24-well plates and cultured in 5% CO_2 at 37°C. Following exposure to different drugs for different durations, 10 μM DCFH-DA via the non-serum medium was added to each well and incubated at 37°C for 20 min. The cells were subsequently washed three times with PBS. DCF fluorescence was measured at 488 nm excitation wavelength and 520 nm emission wavelength using an inverted fluorescence microscope (Nikon TE2000U, Japan). The image capture area was randomly selected by a researcher who was blinded to the experimental conditions. Each experiment was conducted in triplicate wells and replicated, and three images were captured from each well. The fluorescence intensity was analyzed by Image J software.

Measurement of Antioxidant Enzyme Activity and Malonaldehyde Level

Catalase (CAT), glutathione peroxidase (GSH-PX), and superoxide dismutase (SOD) activity and the malonaldehyde (MDA) level were measured using commercial kits (Nanjing Jiancheng Bioengineering Institute, Nanjing, China) according to the manufacturer instructions. The cells were seeded briefly in 6-well plates and cultured in 5% CO_2 at 37°C.

The decomposition of H_2O_2 by CAT can be stopped quickly by ammonium molybdate. The remaining H_2O_2 reacts with ammonium molybdate to form a light-yellow complex, and its absorbance measured at 405 nm can be used to calculate the CAT activity. GSH-PX can catalyze the reaction of H_2O_2 with GSH to generate H_2O and oxidized glutathione (GSSG). The consumption of GSH can reflect the activity of GSH-PX in this enzymatic reaction. GSH reacts with dithiodinitrobenzoic acid to produce a 5-thiodinitrobenzoic acid anion, which presents a relatively stable yellow color. Measuring its absorbance at 412 nm can be used to calculate the GSH content and indirectly calculate GSH-PX activity. The superoxide anion radical ($O_{2\cdot-}$) produced by the xanthine/xanthine oxidase reaction can oxidize hydroxylamine to form nitrite, which will appear purple-red under the action of the color reagent. SOD has a specific inhibitory effect on $O_{2\cdot-}$, so it can weaken the color reaction. Measuring its absorbance at 550 nm can be used to calculate the SOD activity. MDA can be condensed with thiobarbituric acid to form a red product, and its absorbance measured at 530 nm can be used to calculate the MDA level. Each experiment was conducted in triplicate wells and replicated.

Determination of Ca^{2+} Concentration

The concentration of Ca^{2+} in the hCMEC/D3 cells was determined via fluorescent probe Fura-2 AM (Invitrogen, USA). The cells were seeded briefly in 24-well plates and cultured in 5% CO_2 at 37°C. Following exposure to different drugs for different durations, the cells were loaded with 4 μM Fura-2 AM in Hank's balanced salt solution (HBSS) and incubated at 37°C for 50 min. The cells were then washed three times with HBSS, and further incubated at 37°C for

30 min. Ca^{2+} fluorescence was measured at 340/380 nm excitation wavelength and 510 nm emission wavelength using an inverted fluorescence microscope (Nikon TE2000U, Japan). The image capture area was randomly selected by a researcher who was blinded to the experimental conditions. Each experiment was conducted in triplicate wells and replicated, and three images were captured from each well. The fluorescence intensity was analyzed by Image J software.

Evaluation of the hCMEC/D3 Cells Permeability

The flux of NaF across the hCMEC/D3 cells was used to determine the permeability of brain endothelial monolayers. The cells were seeded in the upper inserts (Millipore, United States) of the Transwell system and cultured until the formation of a tight monolayer. Following exposure to different drugs for different durations, the medium in the Transwell system was replaced with HBSS, and 10 μg/ml NaF was added to the upper insert. After the cells were incubated at 37°C for 1 h, 100 μL medium was collected from the acceptor chamber. ODs of the samples were measured at 485 nm excitation wavelength and 535 nm emission wavelength by fluorescence multi-plate reader (BioTek, United States) to evaluate the concentrations of NaF from the top to bottom chamber. Each experiment was conducted in triplicate wells and replicated.

Western Blot Assay in Cells and Brain Tissues

The cells or brain tissues were washed twice with cold PBS, then homogenized in a protein extraction buffer (Beyotime, Shanghai, China) containing protease and phosphatase inhibitors and centrifuged at 14,000 g at 4°C for 15 min. The supernatant was collected, and the protein concentrations were measured using the Bradford Protein Assay kit (Beyotime, Shanghai, China). After the protein sample loading buffer was added, the samples were boiled at 99°C for 10 min. The samples were then separated by 8% SDS-PAGE and transferred to 0.45 μm polyvinylidene difluoride membranes (Millipore, Billerica, MA, United States). The membranes were blocked in 5% non-fat dry milk (diluted in the tris-buffered saline with 0.1% Tween 20 (TBST)) at room temperature for 1 h, then incubated in appropriate primary antibodies (diluted with 5% defatted milk) overnight at 4°C. Next, the membranes were washed three times for 10 min each with TBST and incubated with the secondary antibody (diluted with 5% defatted milk) at room temperature for 1 h. Finally, the membranes were detected using an enhanced chemiluminescent Plus Detection kit (Millipore, United States) and visualized using a Bio-Rad Imaging system (Bio-Rad, United States). This experiment was repeated in triplicate, and representative Western blot images were presented.

Data Analysis

Statistical analyses were performed using SPSS 21 (IBM SPSS, Chicago, United States) and GraphPad Prism 8 (GraphPad Software, United States). All data were represented as the mean ± SD. One-way ANOVA tests (analyzed post-hoc using the LSD test) and Student's t-tests were performed. $p < 0.05$ was considered statistically significant. The Bliss Independent model (Foucquier and Guedj, 2015) was used to calculate whether the changes in related indicators caused by METH and HIV-Tat had a synergistic effect. The calculation formula was as follows: $(Effect_{METH} + Effect_{Tat} - Effect_{METH} \times Effect_{Tat})/Effect_{METH+Tat}$. $Effect_{METH/Tat/METH+Tat}$ had to be normalized to ensure the value between 0 and one using the Max–Min formula: Zi = Xi−Min/Max−Min. According to the calculation formula, the effect value < 1 meant synergistic action, = 1 meant additive action, and >1 meant antagonistic action.

RESULTS

METH and HIV-Tat Induce Synergistic Injury to the BBB *in vitro*

The hCMEC/D3 cells were treated with METH (0.05 to 2.0 mM) or HIV-Tat (25 to 200 nM) for 24 h. As the drug concentrations increased, the expression levels of JAMA, Occludin, and ZO1 all showed a downward trend (**Figures 1A,B**). Compared with the control group, 0.5 mM METH and 100 nM HIV-Tat induced significant decreases in TJ protein expression levels (**Figures 1A,B**). This regimen was selected for subsequent cell experiments. Through an inverted microscope, the cells in the control group (C) were observed to have a full and transparent cell body, good morphology and refractive index, a smooth cell membrane, and a clear boundary. In the group METH (M), HIV-Tat (T), and METH + HIV-Tat (M + T), many cells shrank and became round. Some cells showed vacuole-like structures in their cytoplasm, and a few cells even floated off the wall and died (**Supplementary Figure S1A**). Compared with group C, the apoptosis levels in groups M, T, and M + T were significantly higher (**Figure 1C**), TJ protein expression levels significantly lower (**Figure 1D**), and the flux of NaF across the hCMEC/D3 cells were significantly higher (**Supplementary Figure S2B**). These indicators of the cells in group M + T changed more obvious compared to those in group M or T. The effect values were 0.879 (apoptosis), 0.879 (JAMA), 0.814 (Occludin), 0.657 (ZO1), and 0.821 (NaF), showing a synergistic effect (**Figures 1C,D** and **Supplementary Figure S2B**). These results demonstrate that METH and HIV-Tat jointly damage the BBB.

METH and HIV-Tat Co-induce Oxidative Stress to Damage the BBB *in vitro*

Previous studies have shown that METH- and HIV-Tat-induced injury to the BBB in SD rats is accompanied by a severe oxidative stress response (Li et al., 2018b). In this study, we found that METH and/or HIV-Tat decreased the CAT (**Figure 2B**), GSH-PX (**Figure 2C**), and SOD (**Figure 2D**) activities of the cells, while increased the ROS (**Figure 2A**) and MDA (**Figure 2E**) levels. The changes in these indicators of

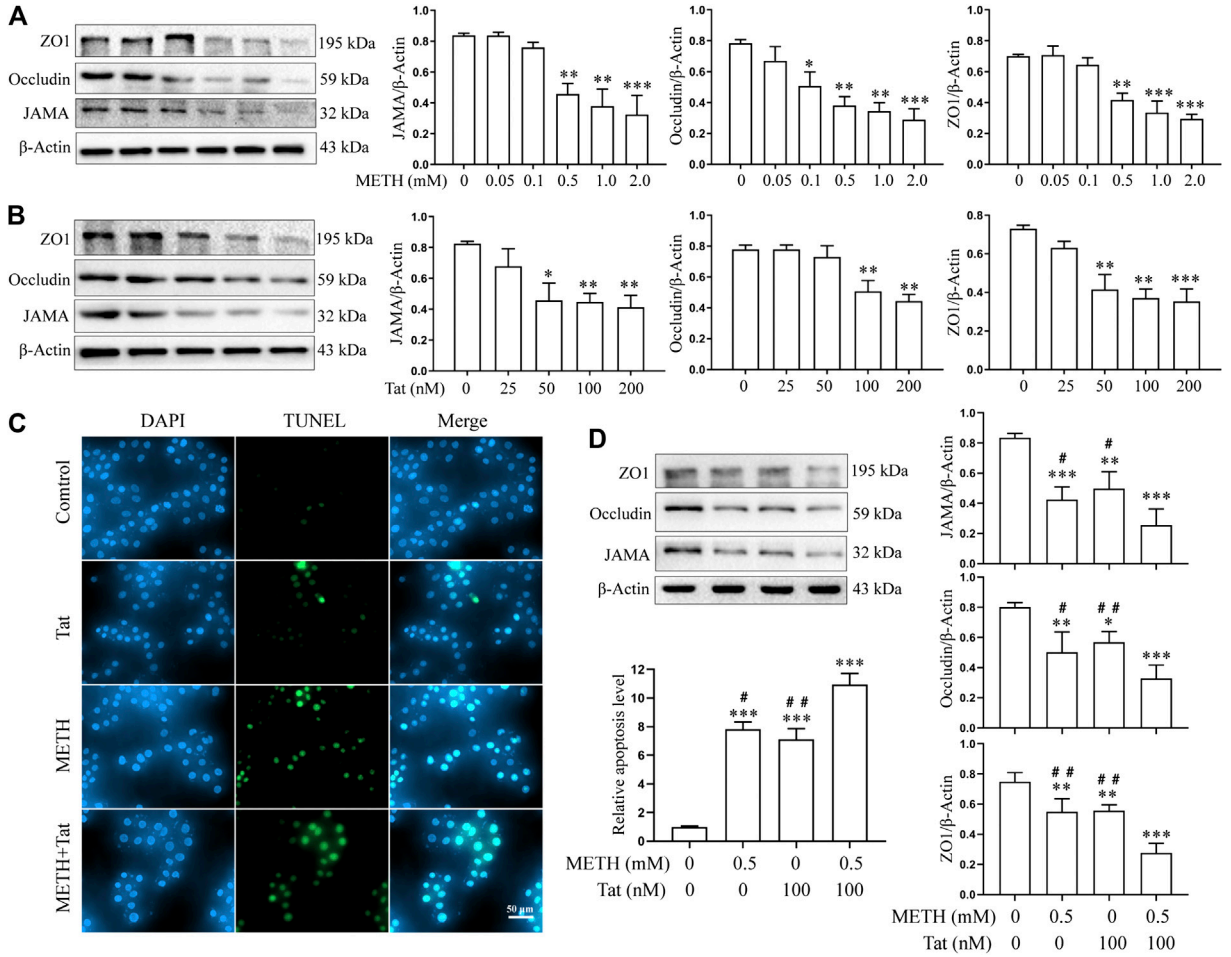

FIGURE 1 | METH and HIV-Tat synergistically damage the BBB model *in vitro*. **(A, B)** Western blot was performed to determine JAMA, Occludin, and ZO1 expression levels in the hCMEC/D3 cells treated with a gradient concentration of METH or HIV-Tat for 24 h. After the cells were treated with 0.5 mM of METH and/or 100 nM of HIV-Tat for 24 h, **(C)** apoptosis was assessed by TUNEL assay (Scale bar: 50 μm), apoptosis level was determined by the number of TUNEL-positive cells expressed as a percentage of the total cell number (analyzed by Image J software); **(D)** western blot was performed to determine JAMA, Occludin, and ZO1 expression levels. Compared with the control, $^{*}p < 0.05$, $^{**}p < 0.01$, $^{***}p < 0.001$; compared with the METH + HIV-Tat, $^{\#}p < 0.05$, $^{\#\#}p < 0.01$, n = 3.

the cells were more obvious in the group M + T compared with group M or T, where the effect values were 0.845 (CAT), 0.872 (GSH-PX), 0.876 (SOD), 0.903 (ROS), and 0.834 (MDA), indicating a synergic effect (**Figures 2A–E**). Then, we used the antioxidant NACA (1.0 mM, treat the cells for 1 h in advance) (**Supplementary Figure S1B**) to investigate the combined damaging effects of oxidative stress, HIV-Tat, and METH on the BBB. The cells were divided into four groups: control (C), NACA (N), METH + HIV-Tat (M + T), and NACA + METH + HIV-Tat (N + M + T). The NACA intervention improved the severe oxidative stress that had been synergistically induced by METH and HIV-Tat (**Figures 3A–E**). Furthermore, compared with the group M + T, the cell morphology (**Supplementary Figure S1C**), viability (**Figure 3F**), apoptosis levels (**Figure 3G**), TJ protein expression levels (**Figure 3H**), and NaF flux (**Supplementary Figure S2B**) all improved in the group N + M + T. These results demonstrate that METH and HIV-Tat co-induce oxidative stress to damage the BBB.

TRPM2 Channel Regulates METH- and HIV-Tat-Induced Synergistic Injury to the BBB *in vitro*

We then investigated whether the TRPM2 channel could regulate METH- and HIV-Tat-induced synergistic injury to the BBB *in vitro*. The hCMEC/D3 cells were transfected with LV-shTRPM2 or LV-shNC for 48 h, then western blot was performed to validate TRPM2 protein. We found that the band sized at 171 kDa was significantly decreased in group LV-shTRPM2 compared with the group LV-NC (**Supplementary Figure S3**). Thus, we confirmed that this antibody is indeed targeting the TRPM2 protein and the band sized at 171 kDa is the TRPM2 protein band. The TRPM2 protein

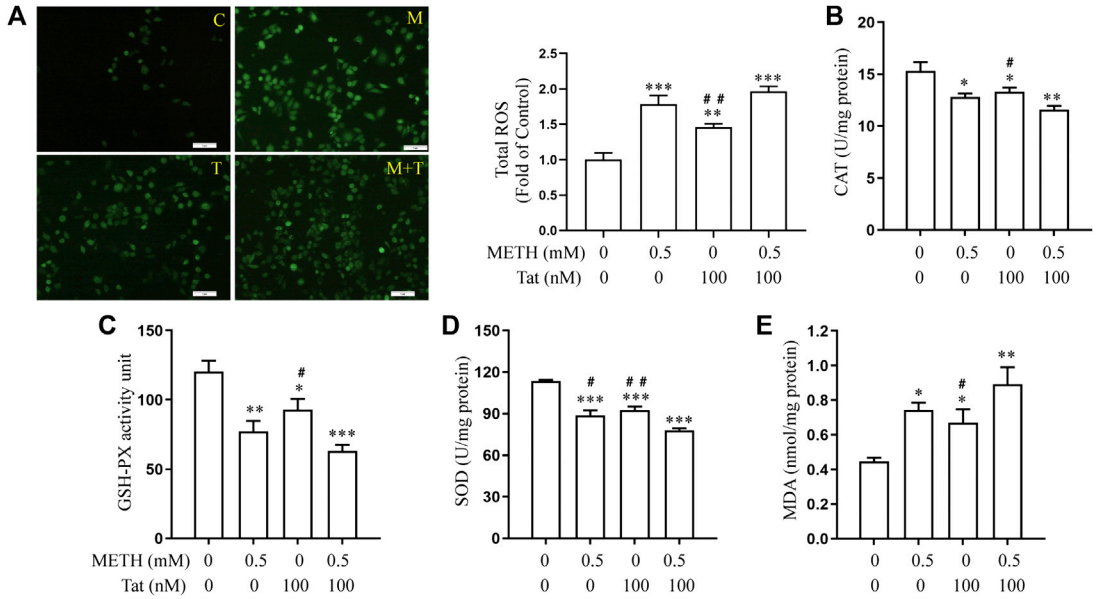

FIGURE 2 | METH and HIV-Tat synergistically induce oxidative stress responses. After the hCMEC/D3 cells were treated with 0.5 mM of METH and/or 100 nM of HIV-Tat for 24 h, **(A)** the ROS fluorescence was observed by an inverted fluorescence microscope (Scale bar: 1 μm), and the fluorescence intensity was analyzed by Image J software; **(B–E)** the activity of CAT, GSH-PX, and SOD and the level of MDA were measured using commercial kits. Compared with the control, $^{*}p < 0.05$, $^{**}p < 0.01$, $^{***}p < 0.001$; compared with the METH + HIV-Tat, $^{\#}p < 0.05$, $^{\#\#}p < 0.01$, n = 3. C=Control, M = 0.5 mM of METH, T = 100 nM of HIV-Tat, and M + T = 0.5 mM of METH+100 nM of HIV-Tat.

expression level increased by different degrees after the hCMEC/D3 cells were treated with METH (0.05 to 2.0 mM) or HIV-Tat (25 to 200 nM) for 24 h (**Figures 4A,B**). Compared to the cells treated with 0.5 mM METH or 100 nM HIV-Tat alone for 24 h, cells, where the two were combined, showed a more significant increase in TRPM2 protein expression, indicating a synergic effect (the effect value was 0.878) (**Figure 4C**). Furthermore, the intensity of Ca^{2+} fluorescence increased significantly in groups M, T, and M + T (METH and/or HIV-Tat exposure for 0.5 h) compared with group C. Compared with groups M or T, this phenomenon in group M + T was more obvious, with a synergistic effect (the effect value was 0.854) (**Figure 4D**). These results indicate that METH and/or HIV-Tat activate the TRPM2 channel.

8-BR-CADPR, an inhibitor of the TRPM2 channel (Eraslan et al., 2019; Alves-Lopes et al., 2020), was used to determine the role of the TRPM2 channel in METH- and HIV-Tat-induced co-injury to the BBB *in vitro*. The cells were divided into control (C), 8-BR-CADPR (8-BR), METH + HIV-Tat (M + T), and 8-BR-cadPR + METH + HIV-Tat (8-BR + M + T) groups. 30 μM 8-BR-CADPR was used to treat the cells for 0.5 h in advance according to the CCK8 results (**Supplementary Figure S1D**). We found that the 8-BR-CADPR intervention did not reduce the high TRPM2 protein expression caused by METH and HIV-Tat (**Figure 5A**). It was able, however, to reduce intracellular Ca^{2+} fluorescence intensity (METH and HIV-Tat exposure for 0.5 h) (**Figure 5B**), indicating that the TRPM2 channel had been inhibited. This inhibition improved the abnormal cell morphology (**Supplementary Figure S1E**), viability (**Figure 5C**), apoptosis levels (**Figure 5D**), TJ protein expression levels (**Figure 5E**), and NaF flux (**Supplementary Figure S2B**) caused by METH and HIV-Tat.

Lentivirus transfection technology was next used to investigate whether knockdown TRPM2 gene expression in hCMEC/D3 cells could reduce BBB injury induced by METH and HIV-Tat *in vitro*. Through an inverted fluorescence microscope, the lentivirus was observed to successfully transfect into the cells (**Supplementary Figure S1F**). qPCR results showed that the TRPM2 mRNA expression level of the LV-shTRPM2 transfected cells was extremely low compared to the negative control group (**Figure 6A**). After TRPM2 gene expression was knocked down, the METH- and HIV-Tat-induced high expression of TRPM2 protein (**Figure 6B**) and the increase in intracellular Ca^{2+} fluorescence intensity (METH and HIV-Tat exposure for 0.5 h) (**Figure 6C**) also decreased significantly, indicating that TRPM2 channels were inhibited. Like the inhibition of the TRPM2 channel via drug intervention, the TRPM2 gene knockdown was observed to improve abnormal cell morphology (**Supplementary Figure S1G**), viability (**Figure 6D**), apoptosis levels (**Figure 6E**), TJ protein expression levels (**Figure 6F**), and NaF flux (**Supplementary Figure S2C**) caused by METH and HIV-Tat. These results indicate that the TRPM2 channel regulates METH- and HIV-Tat-induced synergistic injury to the BBB *in vitro*.

TRPM2 Channel Regulates METH and HIV-Tat Co-Induced Oxidative Stress to Damage the BBB *in vitro*

The relationship between TRPM2 channels and oxidative stress was then examined in an *in vitro* model of METH- and HIV-Tat-induced synergistic injury to the BBB. After NACA intervention,

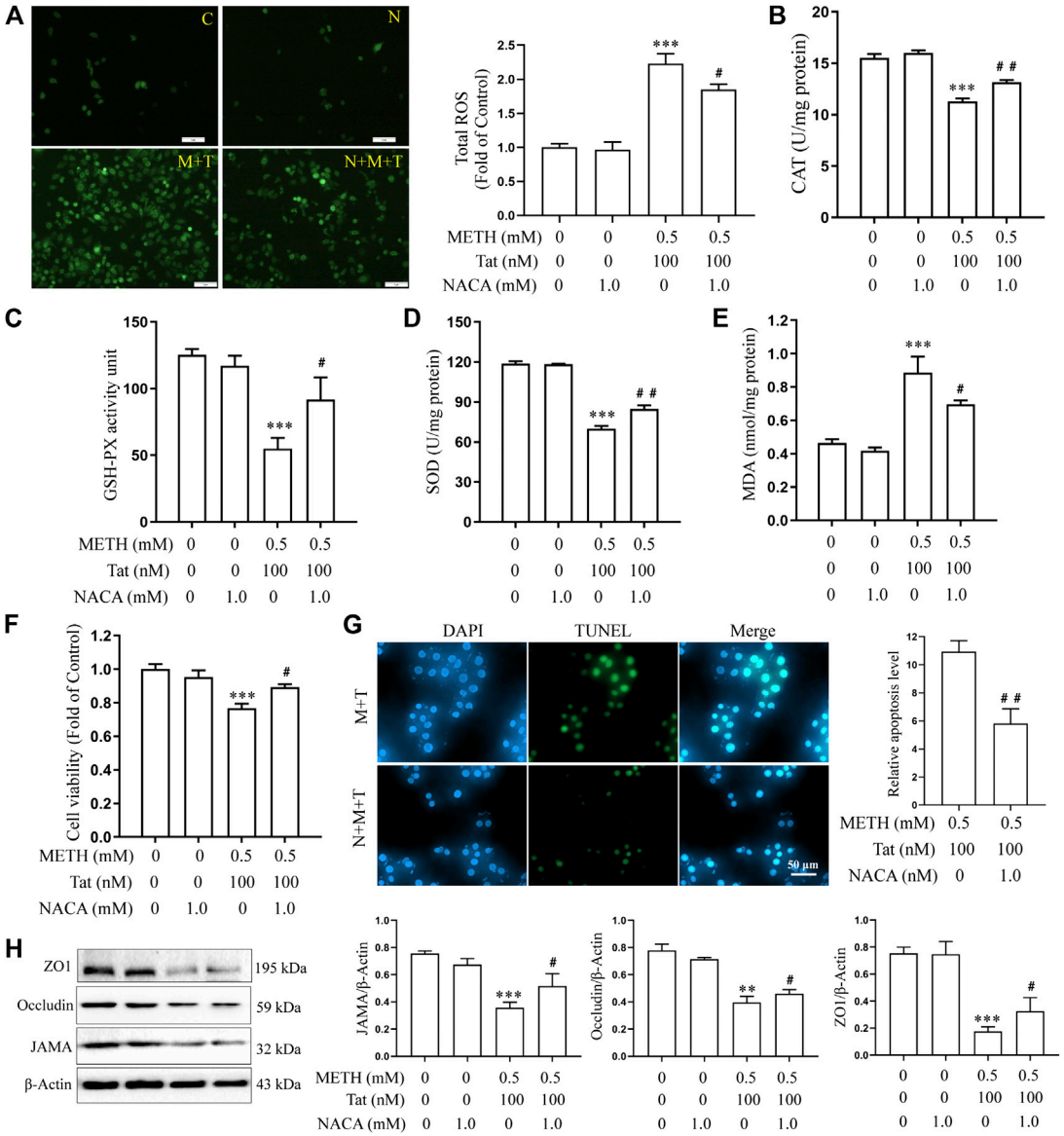

FIGURE 3 | METH and HIV-Tat synergistically induce oxidative stress that damages the BBB model *in vitro*. The hCMEC/D3 cells were treated with or without 1.0 mM of NACA for 1 h before 0.5 mM of METH and 100 nM of HIV-Tat for 24 h. **(A)** ROS fluorescence was observed by an inverted fluorescence microscope (Scale bar: 1 μm), and the fluorescence intensity was analyzed by Image J software; **(B–E)** the activity of CAT, GSH-PX, and SOD and the MDA level were measured using commercial kits; **(F)** the cell viability was measured using the CCK8 kit; **(G)** apoptosis was assessed via TUNEL assay (Scale bar: 50 μm), apoptosis level was determined by the number of TUNEL-positive cells expressed as a percentage of the total cell number (analyzed by Image J software); **(H)** western blot was performed to determine JAMA, Occludin, and ZO1 expression levels. Compared with the control, $^{**}p < 0.01$, $^{***}p < 0.001$; compared with the METH + HIV-Tat, $^{\#}p < 0.05$, $^{\#\#}p < 0.01$, n = 3. C=Control, N = 1.0 mM of NACA, M + T = 0.5 mM of METH+100 nM of HIV-Tat, and N + M + T = 1.0 mM of NACA+0.5 mM of METH+100 nM of HIV-Tat.

the high expression of TRPM2 protein (**Figure 7A**) and the increase in intracellular Ca^{2+} fluorescence intensity (METH and HIV-Tat exposure for 0.5 h) (**Figure 7B**) in hCMEC/D3 cells caused by METH and HIV-Tat decreased. On the contrary, oxidative stress also decreased when the TRPM2 channels were suppressed using drugs or knockdown techniques (**Figures 8A–J**). These results suggest that the TRPM2 channel is not only an effector of oxidative stress, but the channel can in turn affect oxidative stress. In sum, the TRPM2 channel regulates METH and HIV-Tat co-induced oxidative stress to damage the BBB *in vitro*.

TRPM2 Channel Regulates METH- and HIV-Tat-Induced Synergistic Injury to the BBB *in vivo*

The tree shrews were administered drugs according to the experimental procedure described above to determine whether

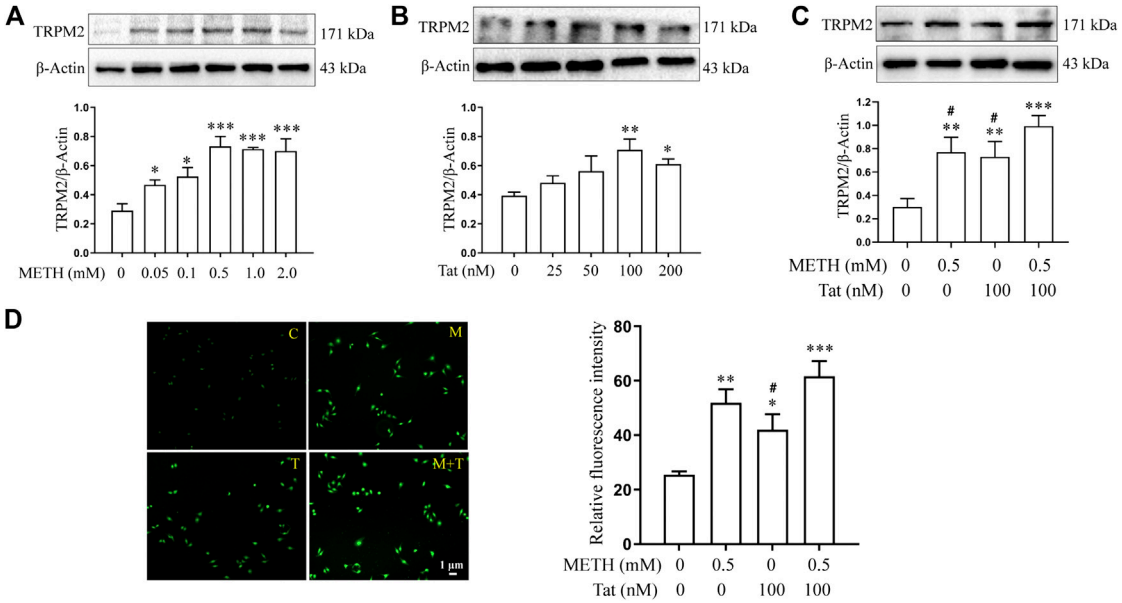

FIGURE 4 | METH and HIV-Tat synergistically activate the TRPM2 channel. **(A,B)** Western blot was performed to determine TRPM2 expression level in the hCMEC/D3 cells treated with a gradient concentration of METH or HIV-Tat for 24 h. After the cells were treated with 0.5 mM of METH and/or 100 nM of HIV-Tat for 24 h, **(C)** western blot was performed to determine the TRPM2 expression level; **(D)** the Ca^{2+} fluorescence was observed using an inverted fluorescence microscope (Scale bar: 1 μm), and the fluorescence intensity was analyzed using Image J software. Compared with the control, $^{*}p < 0.05$, $^{**}p < 0.01$, $^{***}p < 0.001$; compared with the METH + HIV-Tat, $^{\#}p < 0.05$, n = 3. C=Control, M = 0.5 mM of METH, T = 100 nM of HIV-Tat, and M + T = 0.5 mM of METH+100 nM of HIV-Tat. The Ca^{2+} fluorescence shown in **(D)** was detected after the cells were treated with 0.5 mM of METH and/or 100 nM of HIV-Tat for 0.5 h.

METH and Tat co-damage the BBB, as well as to explore the role of the TRPM2 channel in this process. Compared with group C, the JAMA, Occludin, and ZO1 expression levels in the prefrontal cortex of the tree shrews in groups M, T, and M + T decreased significantly (**Figure 9A**), while the EB and NaF content in the shrews' brain tissues increased significantly (**Figures 9C,D**). These changes were most prominent in the tree shrews from group M + T, where the effect values were 0.804 (JAMA), 0.817 (Occludin), 0.973 (ZO1), 0.707 (EB), and 0.533 (NaF), indicating a synergistic effect (**Figures 9A,C,D**). This suggests that METH and HIV-Tat can co-damage the tree shrew's BBB. We also found that Both METH and HIV-Tat induced high TRPM2 protein expression in the prefrontal cortex of the tree shrews (**Figure 9B**). This effect was most prominent in the group M + T, indicating a synergistic effect (the effect value was 0.712) (**Figure 9B**). TJ protein expression, meanwhile, increased significantly after the advance intervention of 8-BR-CADPR (**Figure 9A**). EB and NaF content also fell significantly after the intervention (**Figures 9C,D**), suggesting that BBB injury had improved. These results suggest that the TRPM2 channel can regulate METH- and HIV-Tat-induced synergistic injury to the BBB in tree shrews.

DISCUSSION

METH abuse and HIV infection are two major public health problems in the world today, and these issues are magnified by the high proportion of METH abusers within the HIV-positive population. METH abuse is closely related to increased HIV replication, enhanced HIV-Tat mediated neurotoxic effects, and neurocognitive impairment (Mediouni et al., 2015). A normally functioning BBB with a complete structure can maintain the internal and external environment stability of the CNS and protect it from external stimulation. METH and HIV-Tat, however, damage the BBB and greatly increase the incidence of HAND (Li et al., 2018b) (though the specific mechanism for this process has not been clarified in the existing literature). This study reveals that METH and HIV-Tat can co-induce oxidative stress to damage the BBB *in vitro*; specifically, the abnormal morphology of the hCMEC/D3 cells, decreased cell viability, increased apoptosis levels, reduced TJ protein expression levels, and increased the flux of NaF across the hCMEC/D3 cells. Drug interventions and gene knockdowns were shown to inhibit the TRPM2 channel, reducing injury to the BBB *in vitro*. *In vivo* experiments also proved that METH and HIV-Tat can increase BBB permeability and down-regulate the TJ protein expression levels in the tree shrews. Inhibiting the TRPM2 channel with drugs was shown to reduce BBB damage induced by METH and HIV-Tat in tree shrews.

As BMECs are an important part of the BBB, many studies have used primary BMEC (Avraham et al., 2004; Xu et al., 2012; Ma et al., 2014; Jiang et al., 2017b) or BMEC cell lines (Fernandes et al., 2014; Patel et al., 2017) to establish *in vitro* models of METH- or HIV-Tat-induced injury to the BBB. Qie et al. (Qie et al., 2017) found that bEnd.3 cells treated with 1.0 mM of METH for 24 h increased apoptosis and decreased viability, TEER, and TJ protein expression. Fernandes et al. (Fernandes et al., 2014) found that bEnd.3 cells lost and redistributed

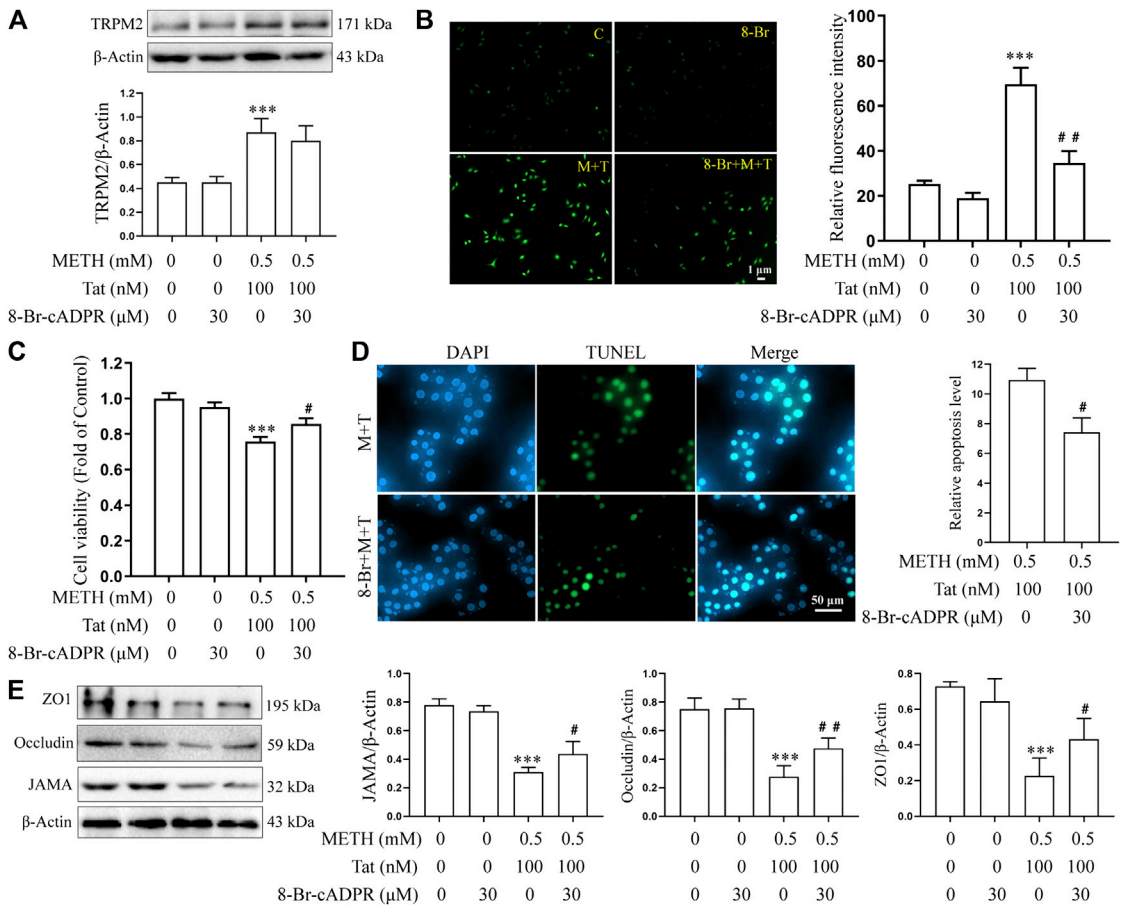

FIGURE 5 | 8-Br-cADPR attenuates damage to the BBB induced synergistically by METH and HIV-Tat *in vitro*. The hCMEC/D3 cells were treated with or without 30 μM of 8-Br-cADPR for 0.5 h before 0.5 mM of METH and 100 nM of HIV-Tat for 24 h. **(A)** Western blot was performed to determine the TRPM2 expression level; **(B)** the Ca^{2+} fluorescence was observed via an inverted fluorescence microscope (Scale bar: 1 μm); fluorescence intensity was analyzed using Image J software; **(C)** cell viability was measured using the CCK8 kit; **(D)** apoptosis was assessed via TUNEL assay (Scale bar: 50 μm), apoptosis level was determined by the number of TUNEL-positive cells expressed as a percentage of the total cell number (analyzed by Image J software); **(E)** western blot was performed to determine JAMA, Occludin, and ZO1 expression levels. Compared with the control, $^{***}p < 0.001$; compared with the METH + HIV-Tat, $^{\#}p < 0.05$, $^{\#\#}p < 0.01$, n = 3. C=Control, 8-Br = 30 μM of 8-Br-cADPR, M + T = 0.5 mM of METH+100 nM of HIV-Tat, and 8-Br + M + T = 30 μM of 8-Br-cADPR+0.5 mM of METH+100 nM of HIV-Tat. The Ca^{2+} fluorescence shown in **(B)** was detected after the cells were treated with or without 30 μM of 8-Br-cADPR for 0.5 h before 0.5 mM of METH and 100 nM of HIV-Tat for 0.5 h.

Claudin5 after exposure to 0.5 mM of METH for 24 h. Another study used the primary rats BMEC. Here, 0.1 mM of METH increased apoptosis and permeability while reducing TEER for 24 h (Jumnongprakhon et al., 2016). Besides, HIV-Tat increased apoptosis, decreased cell viability, and down-regulated Occludin expression (both mRNA and protein) of human BMECs (Xu et al., 2012; Ma et al., 2014).

Few studies, however, have reported the effects of both METH and HIV-Tat on BBB models *in vitro*. In the present research, hCMEC/D3 cells—which originate from the human microvascular endothelium, are similar to the BMECs in the BBB, and can express various TJ proteins (Weksler et al., 2013)—were studied. The cells were treated with gradient concentrations of METH (0.05 to 2.0 mM) or HIV-Tat (25 to 200 nM) for 24 h, and the expression levels of JAMA, Occludin, and ZO1 decreased in a dose-dependent manner. Compared with the control group, the cells treated with 0.5 mM of METH or 100 nM of HIV-Tat 24 h exhibited significantly reduced TJ protein expression levels. After combining the 0.5 mM of METH and 100 nM of HIV-Tat treat the cells for 24 h, the abnormal cell morphology, apoptosis levels, TJ protein expression levels, and NaF flux were more obvious than when METH or HIV-Tat were applied alone. This indicated that when combined, they caused more serious effects (effect value < 1), prompting the hypothesis that METH and HIV-Tat can co-induce BBB damage *in vitro*.

At present, not much research studies the link between synergistic BBB injury and METH and HIV-Tat through animal experiments. In one previous study, SD rats were given 10 mg/kg of METH and/or 50 ng/kg of HIV-Tat daily. After continuous treatment for seven days, BMEC edemas in the rats' cortical areas were observed via transmission electron microscopy, accompanied by several drinking vesicles. BBB permeability increased significantly, while the expression levels of Occludin, JAMA, claudin-5, and ZO1 decreased significantly.

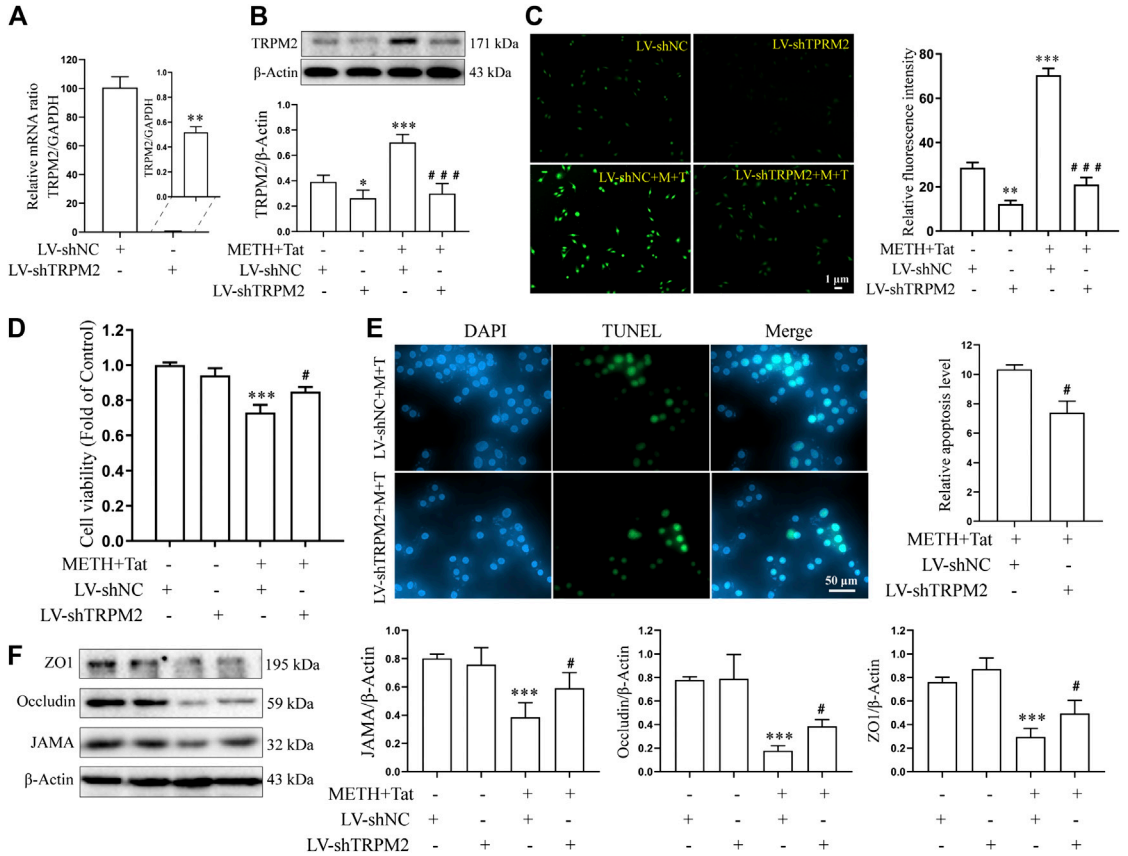

FIGURE 6 | TRPM2 gene knockdown attenuates damage to the BBB synergistically induced by METH and HIV-Tat *in vitro*. The hCMEC/D3 cells were transfected with LV-shTRPM2 or LV-shNC for 48 h before 0.5 mM of METH and 100 nM of HIV-Tat for 24 h. **(A)** Real-time qPCR was performed to determine the TRPM2 mRNA expression level; **(B)** western blot was performed to determine the TRPM2 expression level; **(C)** Ca^{2+} fluorescence was observed via an inverted fluorescence microscope (Scale bar: 1 μm), and fluorescence intensity was analyzed using Image J software; **(D)** cell viability was measured using the CCK8 kit; **(E)** apoptosis was assessed via TUNEL assay (Scale bar: 50 μm), apoptosis level was determined by the number of TUNEL-positive cells expressed as a percentage of the total cell number (analyzed by Image J software); **(F)** Western blot was performed to determine JAMA, Occludin, and ZO1 expression levels. Compared with the LV-shNC, $^{*}p < 0.05$, $^{**}p < 0.01$, $^{***}p < 0.001$; compared with the LV-shNC + METH + HIV-Tat, $^{\#}p < 0.05$, $^{\#\#\#}p < 0.001$, n = 3. LV-shNC = empty vector, LV-shTRPM2 = shTRPM2 lentivirus, LV-shNC + M+T = empty vector+0.5 mM of METH+100 nM of HIV-Tat, and LV-shTRPM2+M+T = shTRPM2 lentivirus+0.5 mM of METH+100 nM of HIV-Tat. The Ca^{2+} fluorescence shown in **(C)** was detected after the cells were transfected with LV-shTRPM2 or LV-shNC for 48 h before 0.5 mM of METH and 100 nM of HIV-Tat for 0.5 h.

These changes were most serious when METH and HIV-Tat were combined (Li et al., 2018b). In the present study, the tree shrew was used as an experimental animal to further verify whether METH and HIV-Tat can synergistically damage the BBB. Like previous reports, we found that METH and/or HIV-Tat administration for 10 consecutive days led to significant decreases in the expression levels of JAMA, Occludin, and ZO1 in the tree shrews' prefrontal cortex and increases in the concentrations of EB and NaF in the shrews' brain tissues. These changes are more serious when METH and HIV-Tat were used together (all effect values <1), indicating that METH and HIV-Tat can co-damage the BBB in the tree shrews.

The oxidative stress response is one of the mechanisms of METH and HIV-Tat that cause neurotoxicity (Mediouni et al., 2015; Yang et al., 2018). Both METH and HIV-Tat can induce excessive ROS production, impairing the defense abilities of antioxidant enzymes such as GSH-PX and SOD, then inducing autophagy and apoptosis of nerve cells by inhibiting the mTOR (Zeng et al., 2018). NADPH oxidase 2(NOX2) activation can cause intracellular ROS accumulation. This further inhibits the nuclear factor erythroid-2-related factor 2(Nrf2) from entering the cell nucleus, leading to the decrease of heme oxygenase-1(HO-1), NAD(P)H quinone oxidoreducpase-1 (NQO-1), γ-glutamylcysteine synthetase (γ-GCS), and SOD. This pathway is responsible for METH-induced oxidative stress injury in primary rats BMEC (Jumnongprakhon et al., 2016). The oxidative stress response induced by HIV-Tat is also related to damaged Nrf2 balances, manifests in the accumulation of ROS and nitric oxide in nerve cells, decreased GSH levels, and increased GSSG levels (Kim et al., 2015). Besides, Flora et al. (Flora et al., 2003) confirmed that METH and/or HIV-Tat can induce oxidative stress and activate redox-regulated transcription factors and inflammatory genes in the mouse brain.

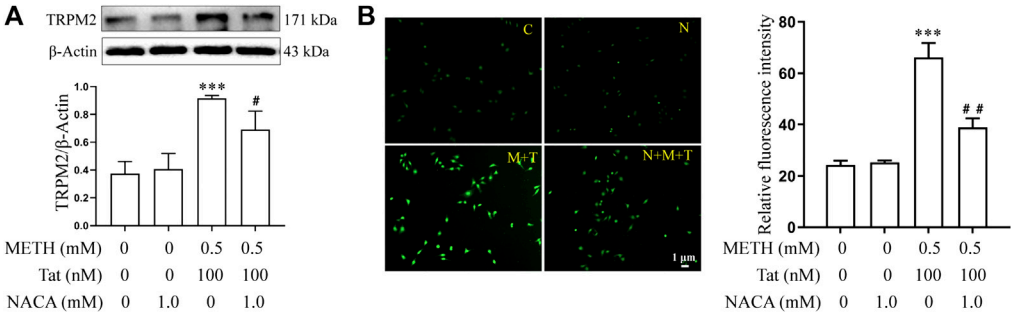

FIGURE 7 | NACA attenuates activation of TRPM2 channel synergistically induced by METH and HIV-Tat. The hCMEC/D3 cells were treated with or without 1.0 mM of NACA for 1 h before 0.5 mM of METH and 100 nM of HIV-Tat for 24 h. **(A)** Western blot was performed to determine the TRPM2 expression level; **(B)** Ca^{2+} fluorescence was observed using an inverted fluorescence microscope (Scale bar: 1 μm), and fluorescence intensity was analyzed using Image J software. Compared with the control, $^{***}p < 0.001$; compared with the METH + HIV-Tat, $^{\#}p < 0.05$, $^{\#\#}p < 0.01$, n = 3. C=Control, N = 1.0 mM of NACA, M + T = 0.5 mM of METH+100 nM of HIV-Tat, and N + M + T = 1.0 mM of NACA + 0.5 mM of METH+100 nM of HIV-Tat. The Ca^{2+} fluorescence shown in **(B)** was detected after the cells were treated with or without 1.0 mM of NACA for 1 h before 0.5 mM of METH and 100 nM of HIV-Tat for 0.5 h.

The role of oxidative stress in inducing BBB injury has been widely recognized (Pun et al., 2009; Northrop and Yamamoto, 2015; Namyen et al., 2020). Toborek et al. (Toborek et al., 2003) suggested that the increase of cellular oxidative stress may be a mechanism of BBB injury induced by HIV-Tat. A previous study confirmed that METH and HIV-Tat can co-damage the BBB in SD rats. NACA not only corrected the oxidative stress injury but also alleviated damage to the BBB induced by METH + HIV-Tat + GP120 (Banerjee et al., 2010). In the present research, similar results were obtained at a cellular level. We found that METH and HIV-Tat could both induce decreased CAT, GSH-PX, and SOD activity in hCMEC/D3 cells, as well as elevated ROS and MDA levels. These changes were most obvious (effect value <1) when METH and HIV-Tat acted together, suggesting that the combination synergistically induces the oxidative stress reaction. Here, NACA intervention not only reduced the severity of oxidative stress but also the damage to the BBB. These mediating effects were observed in the cells' improved morphology, decreased apoptosis levels, increased cell viability, TJ protein expression levels, and decreased the flux of NaF across the hCMEC/D3 cells.

As oxidative stress reaction cell receptors, TRPM2 channels can mediate the oxidative stress reaction—which in turn can mediate the occurrence and development of some nervous system diseases. Ostapchenko et al. (Ostapchenko et al., 2015) found that the landmark toxic protein present in Alzheimer's disease (AD), the amyloid β-protein (Aβ), can promote TRPM2 channel activation. In AD mice models, genetic ablation of TRPM2 was found to lighten the protein's neurotoxic effects and improve age-related memory defects. Intracellular ROS aggregation can activate NLRP3 inflammasomes by stimulating TRPM2 channels (Wang et al., 2020), or activate microglia cells and induce TNF- production (Alawieyah Syed Mortadza et al., 2018), a neuroinflammatory response induced by Aβ that appears to exacerbate AD (Aminzadeh et al., 2018). With Parkinson's disease (PD), there are also abnormal expressions and functions of the TRPM2 channel (Hermosura et al., 2008). Another mouse model of hypoxia and ischemic brain injury observed that the cerebral infarction area of TRM2 $^{+/-}$ and TRM2 $^{-/-}$ became reduced, the expression of inflammatory markers decreased, and sensorimotor functions improved (Huang et al., 2017). These studies all indicate that the TRPM2 channel is a potential drug intervention target for the treatment of a variety of neurodegenerative diseases (Wang et al., 2016; Yamamoto and Shimizu, 2016; Belrose and Jackson, 2018; Sita et al., 2018).

Research has shown that activating TRPM2 channels can also mediate H_2O_2-induced increased permeability of pulmonary artery endothelial cells and increased apoptosis (Hecquet et al., 2008; Hecquet and Malik, 2009; Hecquet et al., 2014). The TRPM2-activated Ca^{2+} signaling and VE-cadherin phosphorylation can regulate endotoxin-induced transmigration of polymorphonuclear neutrophils, resulting in the disassembly of adherens junctions and opening of the paracellular pathways in human lung microvascular endothelial cells (Mittal et al., 2017). Oxidative stress can also induce nitration of the TRPM2 channel Y1485 tyrosine, which plays an important role in peripheral cell damage in the BBB (Jiang et al., 2017a). The present study reveals that treatments using a gradient concentration of METH (0.05 to 2.0 mM) or HIV-Tat (25 to 200 nM) for 24 h increases the expression level of TRPM2 in hCMEC/D3 cells. The combination of 0.5 mM METH and 100 nM HIV-Tat increases the expression level of TRPM2 protein significantly (effect value <1). Also, both 0.5 mM of METH and/or 100 nM of HIV-Tat induce intracellular Ca^{2+} concentration to increase when treated for 0.5 h. When combined, METH and HIV-Tat had a synergic effect (effect value <1), suggesting that TRPM2 channels can be activated by METH, HIV-Tat, or both. Interventions using 8-BR-ADPR or TRPM2 gene expression knockdown to inhibit the TRPM2 channel improved the abnormal cell morphology caused by METH and HIV-Tat. The interventions also improved the observed decreased cell viability, increased apoptosis levels, decreased TJ protein expression levels, and increased NaF flux. *In vivo* experiments revealed that both METH and/or HIV-Tat can induce high expressions of TRPM2 proteins in the prefrontal

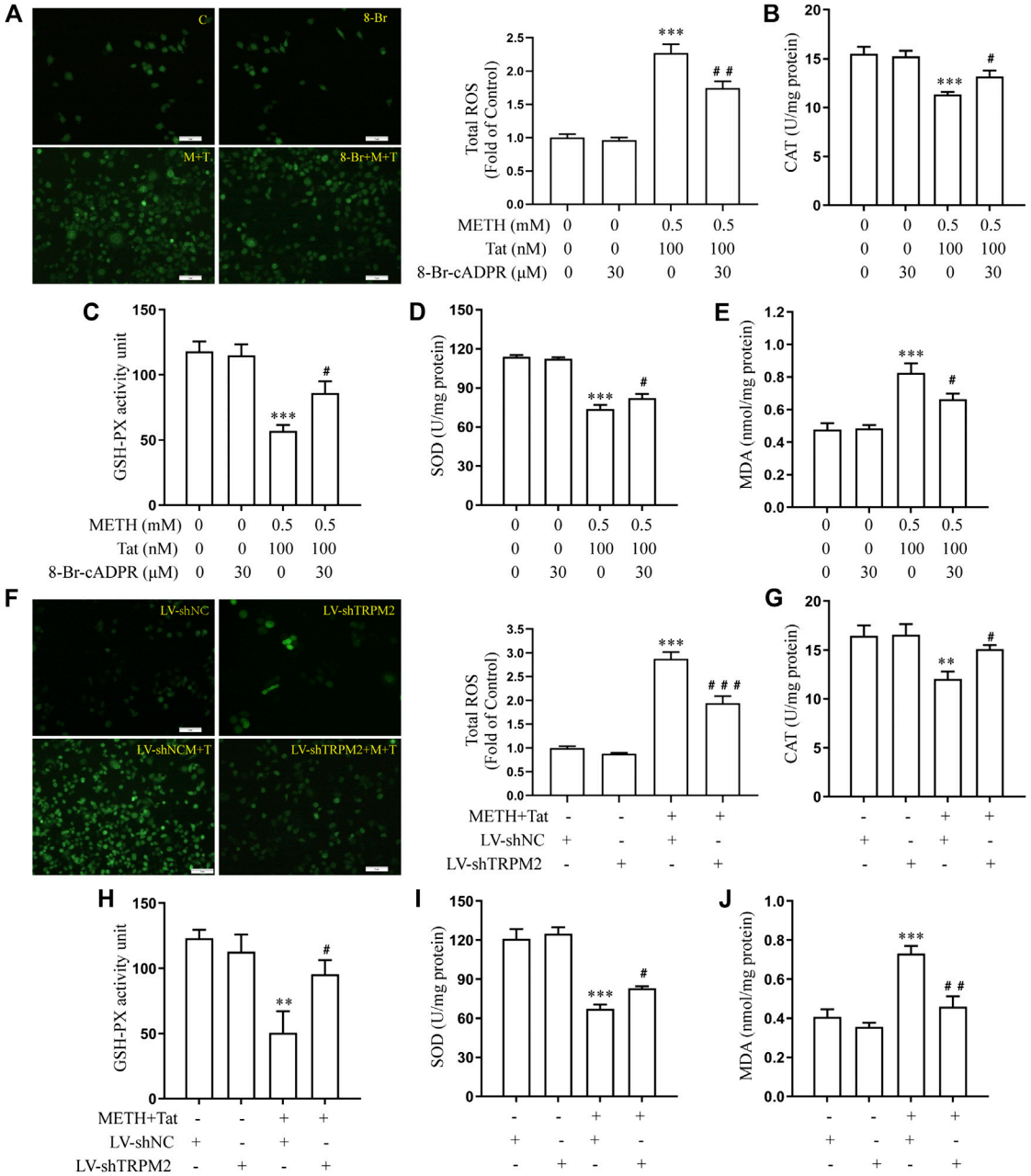

FIGURE 8 | 8-Br-cADPR and TRPM2 gene knockdown attenuate oxidative stress responses synergistically induced by METH and HIV-Tat. The hCMEC/D3 cells were transfected with LV-shTRPM2 or LV-shNC for 48 h or treated with or without 30 μM of 8-Br-cADPR for 0.5 h before 0.5 mM of METH and 100 nM of HIV-Tat for 24 h. **(A, F)** ROS fluorescence was observed via an inverted fluorescence microscope (Scale bar: 1 μm), and fluorescence intensity was analyzed using Image J software; **(B–E, G–J)** CAT, GSH-PX, and SOD activity and the level of MDA were measured using commercial kits. Compared with the control or LV-shNC, $^{**}p < 0.01$, $^{***}p < 0.001$; compared with the METH + HIV-Tat or LV-shNC + METH + HIV-Tat, $^{\#}p < 0.05$, $^{\#\#}p < 0.01$, n = 3. C=Control, 8-Br = 30 μM of 8-Br-cADPR, M + T = 0.5 mM of METH+100 nM of HIV-Tat, and 8-Br + M + T = 30 μM of 8-Br-cADPR+0.5 mM of METH+100 nM of HIV-Tat. LV-shNC = empty vector, LV-shTRPM2 = shTRPM2 lentivirus, LV-shNC + M+T = empty vector+0.5 mM of METH+100 nM of HIV-Tat, and LV-shTRPM2+M+T = shTRPM2 lentivirus+0.5 mM of METH+100 nM of HIV-Tat.

cortex of tree shrews, with a synergistic effect (effect value <1). Following drug administration to inhibit the TRPM2 channels, METH- and HIV-Tat-induced BBB injury improved, as shown by increased JAMA, Occludin, and ZO1 expression levels and decreased EB and NaF concentrations. This confirmed that the TRPM2 channel can regulate METH and HIV-Tat co-damage to the BBB both *in vivo* and *in vitro*.

The relationship between the oxidative stress response and TRPM2 channels when METH and HIV-Tat co-damage the BBB was also examined via an *in vitro* model. NACA intervention

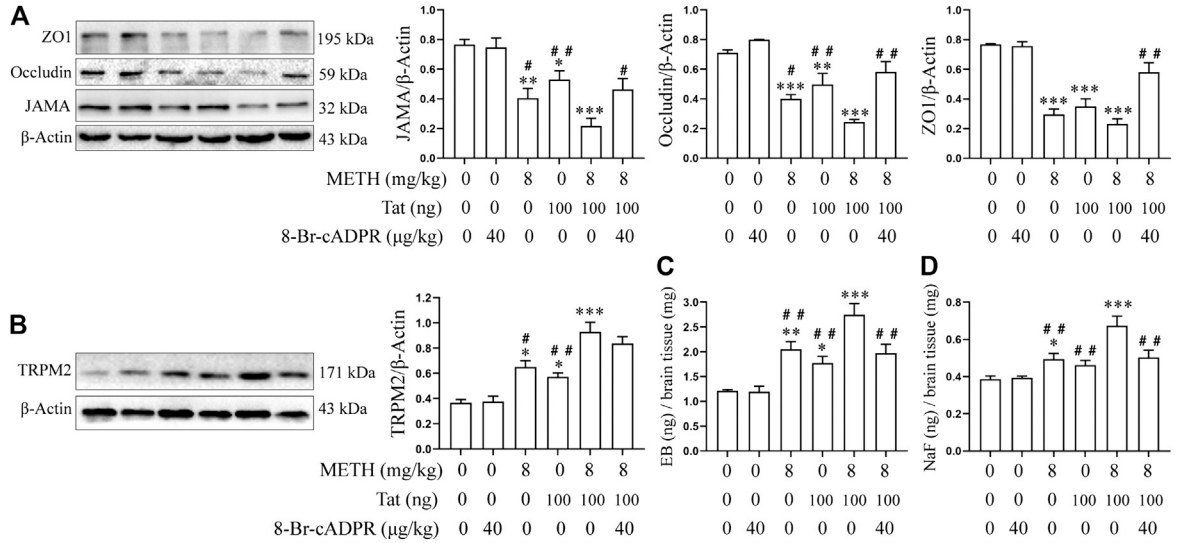

FIGURE 9 | 8-Br-cADPR attenuates synergistic METH- and HIV-Tat-induced BBB damage in tree shrews. All the animals were treated with METH and/or HIV-Tat with or without the intervention of 8-Br-cADPR for 10 consecutive days by the above administration regimen, then euthanized 24 h after the last treatment. Six tree shrews in each group were treated with EB or NaF by tail intravenous injection 1 h before the end of the last treatment. **(A,B)** Western blot was performed to determine JAMA, Occludin, ZO1, and TRPM2 expression levels in the prefrontal cortex of the tree shrews; **(C)** EB and **(D)** NaF quantitative analyses in a whole-brain context were used to detect the permeability of BBB. Compared with the control, $^{*}p < 0.05$, $^{**}p < 0.01$, $^{***}p < 0.001$; compared with the METH + HIV-Tat, $^{\#}p < 0.05$, $^{\#\#}p < 0.01$, n = 3.

reduced TRPM2 protein expression and TRPM2 channel activation caused by M + T. Intervention with 8-BR-ADPR or TRPM2 gene expression knockdown to inhibit the TRPM2 channel also attenuated oxidative stress injury caused by M + T. Previous studies had similar results in finding that H_2O_2 can activate protein kinase C (PKC) and NOX to produce excessive ROS, thus activating the TRPM2 channel. The TRPM2 channel can mediate lysosomal dysfunction and release lysosomal Zn^{2+}, but also induce mitochondrial Zn^{2+} accumulation, triggering mitochondrial dysfunction, and ROS production. Mitochondrial dysfunction can also enhance NOX-mediated ROS production and the oxidative stress response, which induces the delayed death of SH-SY5Y cells (Li and Jiang, 2019). A similar positive feedback mechanism was observed when Zn^{2+} induced microglia death by TRPM2 channel activation (Mortadza et al., 2017). Ozkaya et al. (Ozkaya and Naziroglu, 2020) found that oxidative stress-dependent TRPM2 activation plays an important role in cisplatin-induced optic neuron death in mice. Inhibition of the TRPM2 channel improved mitochondrial membrane depolarization caused by cisplatin, reduced ROS levels in the mitochondria and cytoplasm, and reduced optic nerve injury. These results are consistent with the results of the present study, suggesting that TRPM2 channels are not only effectors of oxidative stress response but also interact with each other.

Claudin-5 is a tight junction protein regulating the integrity and permeability of BBB. It warrants further investigation to characterize the role of claudin-5 on BBB injury by METH and HIV-Tat. Previous studies indicated that pro-inflammatory stimulation can down-regulate TJ protein expression levels in hCMEC/D3 cells (Lopez-Ramirez et al., 2012). Aβ peptides can increase hCMEC/D3 monolayer permeability (Tai et al., 2010). There are reports to study the effects of Tat and METH on BBB integrity and function using hCMEC/D3 cells (Patel et al., 2017). However, it is of biological significance to verify the effects of HIV-Tat and METH on BBB using primary human brain endothelial cells. Additionally, it warrants further investigation into the biological relevance and the characterization of the hCMEC/D3 for the BBB study. Also, the use of simple DMEM/high glucose medium with 10% FBS with human basic fibroblast growth factor promotes cell growth, but it lacks basic supplements needed for the culture of this cell type which might interfere with basic BBB properties. In the future, we plan to characterize the model with the suggested and published medium components (Weksler et al., 2005).

In sum, this study confirms that METH and HIV-Tat can co-induce oxidative stress to damage the BBB; the TRPM2 channel can regulate this BBB injury process. This research provides a new theory for explaining the mechanism of synergistic BBB injury by METH and HIV-Tat, and it presents the TRPM2 channel as a promising drug intervention target to reduce BBB injury and neuropsychiatric symptoms in HIV-infected METH abusers. Future research into synergistic BBB injury induced by METH and HIV-Tat proteins could further explore the specific interaction mechanism between the oxidative stress response and the TRPM2 channel, as well as the exact mechanism of the TRPM2 channel in mediating BBB injury.

DATA AVAILABILITY STATEMENT

The original contributions presented in the study are included in the article/**Supplementary Material**, further inquiries can be directed to the corresponding authors.

ETHICS STATEMENT

The animal study was reviewed and approved by the Institutional Ethics Committee of Kunming Medical University.

AUTHOR CONTRIBUTIONS

JH, RZ, SW, DZ, C-KL, GY, YL, LL, YX, SL, CW participated in literature search, experimental validation, data mining, bioinformatics analysis, and interpretation, writing the manuscript, creating figures and tables. XZ, JL supervised the study design, critically read and edited the manuscript. All authors read and approved the final manuscript.

FUNDING

This work was supported by the National Natural Science Foundation of China (82060382, 81660310 and 81960340), NHC Key Laboratory of Drug Addiction Medicine (2020DAMARA-008), Basic Research Program of Yunnan Province (202001AT070098), the Scientific Research Fund of Education Department of Yunnan Province (2019J1186 and 2018Y043).

SUPPLEMENTARY MATERIAL

The Supplementary Material for this article can be found online at: https://www.frontiersin.org/articles/10.3389/fphar.2021.619436/full#supplementary-material.

REFERENCES

Abbott, N. J., Ronnback, L., and Hansson, E. (2006). Astrocyte-endothelial interactions at the blood-brain barrier. *Nat. Rev. Neurosci.* 7, 41–53. doi:10.1038/nrn1824

Alawieyah Syed Mortadza, S., Sim, J. A., Neubrand, V. E., and Jiang, L. H. (2018). A critical role of TRPM2 channel in Abeta42 -induced microglial activation and generation of tumor necrosis factor-alpha. *Glia* 66, 562–575. doi:10.1002/glia.23265

Alves-Lopes, R., Neves, K. B., Anagnostopoulou, A., Rios, F. J., Lacchini, S., Montezano, A. C., et al. (2020). Crosstalk between vascular redox and calcium signaling in hypertension involves TRPM2 (transient receptor potential melastatin 2) cation channel. *Hypertension* 75, 139–149. doi:10.1161/HYPERTENSIONAHA.119.13861

Aminzadeh, M., Roghani, M., Sarfallah, A., and Riazi, G. H. (2018). TRPM2 dependence of ROS-induced NLRP3 activation in Alzheimer's disease. *Int. Immunopharmacol* 54, 78–85. doi:10.1016/j.intimp.2017.10.024

Atluri, V. S., Hidalgo, M., Samikkannu, T., Kurapati, K. R., Jayant, R. D., Sagar, V., et al. (2015). Effect of human immunodeficiency virus on blood-brain barrier integrity and function: an update. *Front. Cell Neurosci.* 9, 212. doi:10.3389/fncel.2015.00212

Avraham, H. K., Jiang, S., Lee, T. H., Prakash, O., and Avraham, S. (2004). HIV-1 Tat-mediated effects on focal adhesion assembly and permeability in brain microvascular endothelial cells. *J. Immunol.* 173, 6228–6233. doi:10.4049/jimmunol.173.10.6228

Ballabh, P., Braun, A., and Nedergaard, M. (2004). The blood-brain barrier: an overview: structure, regulation, and clinical implications. *Neurobiol. Dis.* 16, 1–13. doi:10.1016/j.nbd.2003.12.016

Banerjee, A., Zhang, X., Manda, K. R., Banks, W. A., and Ercal, N. (2010). HIV proteins (gp120 and Tat) and methamphetamine in oxidative stress-induced damage in the brain: potential role of the thiol antioxidant N-acetylcysteine amide. *Free Radic. Biol. Med.* 48, 1388–1398. doi:10.1016/j.freeradbiomed.2010.02.023

Belrose, J. C., and Jackson, M. F. (2018). TRPM2: a candidate therapeutic target for treating neurological diseases. *Acta Pharmacol. Sin.* 39, 722–732. doi:10.1038/aps.2018.31

Campos-Bedolla, P., Walter, F. R., Veszelka, S., and Deli, M. A. (2014). Role of the blood-brain barrier in the nutrition of the central nervous system. *Arch. Med. Res.* 45, 610–638. doi:10.1016/j.arcmed.2014.11.018

Eraslan, E., Tanyeli, A., Polat, E., and Polat, E. (2019). 8-Br-cADPR, a TRPM2 ion channel antagonist, inhibits renal ischemia-reperfusion injury. *J. Cell Physiol.* 234, 4572–4581. doi:10.1002/jcp.27236

Fan, Y., Huang, Z. Y., Cao, C. C., Chen, C. S., Chen, Y. X., Fan, D. D., et al. (2013). Genome of the Chinese tree shrew. *Nat. Commun.* 4, 1426. doi:10.1038/ncomms2416

Fernandes, S., Salta, S., Bravo, J., Silva, A. P., and Summavielle, T. (2014). Acetyl-L-carnitine prevents methamphetamine-induced structural damage on endothelial cells via ILK-related MMP-9 activity. *Mol. Neurobiol.* 53, 408–422. doi:10.1007/s12035-014-8973-5

Flora, G., Lee, Y. W., Nath, A., Hennig, B., Maragos, W., and Toborek, M. (2003). Methamphetamine potentiates HIV-1 Tat protein-mediated activation of redox-sensitive pathways in discrete regions of the brain. *Exp. Neurol.* 179, 60–70. doi:10.1006/exnr.2002.8048

Foucquier, J., and Guedj, M. (2015). Analysis of drug combinations: current methodological landscape. *Pharmacol. Res. Perspect.* 3, e00149. doi:10.1002/prp2.149

Gonçalves, J., Leitão, R. A., Higuera-Matas, A., Assis, M. A., Coria, S. M., Fontes-Ribeiro, C., et al. (2017). Extended-access methamphetamine self-administration elicits neuroinflammatory response along with blood-brain barrier breakdown. *Brain Behav. Immun.* 62, 306–317. doi:10.1016/j.bbi.2017.02.017

Hecquet, C. M., Ahmmed, G. U., Vogel, S. M., and Malik, A. B. (2008). Role of TRPM2 channel in mediating H2O2-induced Ca2+ entry and endothelial hyperpermeability. *Circ. Res.* 102, 347–355. doi:10.1161/CIRCRESAHA.107.160176

Hecquet, C. M., and Malik, A. B. (2009). Role of H(2)O(2)-activated TRPM2 calcium channel in oxidant-induced endothelial injury. *Thromb. Haemost.* 101, 619–625. doi:10.1160/TH08-10-0641

Hecquet, C. M., Zhang, M., Mittal, M., Vogel, S. M., Di, A., Gao, X., et al. (2014). Cooperative interaction of trp melastatin channel transient receptor potential (TRPM2) with its splice variant TRPM2 short variant is essential for endothelial cell apoptosis. *Circ. Res.* 114, 469–479. doi:10.1161/CIRCRESAHA.114.302414

Hermosura, M. C., Cui, A. M., Go, R. C., Davenport, B., Shetler, C. M., Heizer, J. W., et al. (2008). Altered functional properties of a TRPM2 variant in Guamanian ALS and PD. *Proc. Natl. Acad. Sci. U.S.A.* 105, 18029–18034. doi:10.1073/pnas.0808218105

Huang, J., Yang, G., Li, Z., Leung, C. K., Wang, W., Li, Y., et al. (2020). Involvement of dopamine D3 receptor and dopamine transporter in methamphetamine-induced behavioral sensitization in tree shrews. *Brain Behav.* 10, e01533. doi:10.1002/brb3.1533

Huang, S., Turlova, E., Li, F., Bao, M. H., Szeto, V., Wong, R., et al. (2017). Transient receptor potential melastatin 2 channels (TRPM2) mediate neonatal hypoxic-ischemic brain injury in mice. *Exp. Neurol.* 296, 32–40. doi:10.1016/j.expneurol.2017.06.023

Jiang, Q., Gao, Y., Wang, C., Tao, R., Wu, Y., Zhan, K., et al. (2017a). Nitration of TRPM2 as a molecular switch induces autophagy during brain pericyte injury. *Antioxid. Redox Signal.* 27, 1297–1316. doi:10.1089/ars.2016.6873

Jiang, W., Huang, W., Chen, Y., Zou, M., Peng, D., and Chen, D. (2017b). HIV-1 transactivator protein induces ZO-1 and neprilysin dysfunction in brain endothelial cells via the ras signaling pathway. *Oxid. Med. Cell Longev* 2017, 3160360. doi:10.1155/2017/3160360

Jumnongprakhon, P., Govitrapong, P., Tocharus, C., and Tocharus, J. (2016). Melatonin promotes blood-brain barrier integrity in methamphetamine-induced inflammation in primary rat brain microvascular endothelial cells. *Brain Res.* 1646, 182–192. doi:10.1016/j.brainres.2016.05.049

Jumnongprakhon, P., Sivasinprasasn, S., Govitrapong, P., Tocharus, C., and Tocharus, J. (2017). Activation of melatonin receptor (MT1/2) promotes P-gp transporter in methamphetamine-induced toxicity on primary rat brain microvascular endothelial cells. *Toxicol.* In Vitro 41, 42–48. doi:10.1016/j.tiv.2017.02.010

Kim, S. H., Smith, A. J., Tan, J., Shytle, R. D., and Giunta, B. (2015). MSM ameliorates HIV-1 Tat induced neuronal oxidative stress via rebalance of the glutathione cycle. *Am. J. Transl Res.* 7, 328–338.

Li, J., Wang, W., Tong, P., Leung, C. K., Yang, G., Li, Z., et al. (2018a). Autophagy induction by HIV-tat and methamphetamine in primary midbrain neuronal cells of tree shrews via the mTOR signaling and ATG5/ATG7 pathway. *Front. Neurosci.* 12, 921. doi:10.3389/fnins.2018.00921

Li, J., Zeng, B., Hu, X., Li, Z., Zhang, D., Yang, G., et al. (2018b). Protective effects of ginsenoside Rb1 against blood-brain barrier damage induced by human immunodeficiency virus-1 tat protein and methamphetamine in sprague-dawley rats. *Am. J. Chin. Med.* 46, 551–566. doi:10.1142/S0192415X18500283

Li, X., and Jiang, L. H. (2019). A critical role of the transient receptor potential melastatin 2 channel in a positive feedback mechanism for reactive oxygen species-induced delayed cell death. *J. Cell Physiol.* 234, 3647–3660. doi:10.1002/jcp.27134

Lopez-Ramirez, M. A., Fischer, R., Torres-Badillo, C. C., Davies, H. A., Logan, K., Pfizenmaier, K., et al. (2012). Role of caspases in cytokine-induced barrier breakdown in human brain endothelial cells. *J. Immunol.* 189, 3130–3139. doi:10.4049/jimmunol.1103460

Ma, R., Yang, L., Niu, F., and Buch, S. (2014). HIV tat-mediated induction of human brain microvascular endothelial cell apoptosis involves endoplasmic reticulum stress and mitochondrial dysfunction. *Mol. Neurobiol.* 53, 132–142. doi:10.1007/s12035-014-8991-3

Mcrae, M. (2016). HIV and viral protein effects on the blood brain barrier. *Tissue Barriers* 4, e1143543. doi:10.1080/21688370.2016.1143543

Mediouni, S., Garibaldi Marcondes, M. C., Miller, C., Mclaughlin, J. P., and Valente, S. T. (2015). The cross-talk of HIV-1 Tat and methamphetamine in HIV-associated neurocognitive disorders. *Front. Microbiol.* 6, 1164. doi:10.3389/fmicb.2015.01164

Mittal, M., Nepal, S., Tsukasaki, Y., Hecquet, C. M., Soni, D., Rehman, J., et al. (2017). Neutrophil activation of endothelial cell-expressed TRPM2 mediates transendothelial neutrophil migration and vascular injury. *Circ. Res.* 121, 1081–1091. doi:10.1161/CIRCRESAHA.117.311747

Miyanohara, J., Kakae, M., Nagayasu, K., Nakagawa, T., Mori, Y., Arai, K., et al. (2018). TRPM2 channel aggravates CNS inflammation and cognitive impairment via activation of microglia in chronic cerebral hypoperfusion. *J. Neurosci.* 38, 3520–3533. doi:10.1523/JNEUROSCI.2451-17.2018

Mortadza, S. S., Sim, J. A., Stacey, M., and Jiang, L. H. (2017). Signalling mechanisms mediating Zn2+-induced TRPM2 channel activation and cell death in microglial cells. *Sci. Rep.* 7, 45032. doi:10.1038/srep45032

Namyen, J., Permpoonputtana, K., Nopparat, C., Tocharus, J., Tocharus, C., and Govitrapong, P. (2020). Protective effects of melatonin on methamphetamine-induced blood-brain barrier dysfunction in rat model. *Neurotox. Res.* 37, 640–660. doi:10.1007/s12640-019-00156-1

Northrop, N. A., and Yamamoto, B. K. (2015). Methamphetamine effects on blood-brain barrier structure and function. *Front. Neurosci.* 9, 69. doi:10.3389/fnins.2015.00069

Ostapchenko, V. G., Chen, M., Guzman, M. S., Xie, Y. F., Lavine, N., Fan, J., et al. (2015). The transient receptor potential melastatin 2 (TRPM2) channel contributes to β-amyloid oligomer-related neurotoxicity and memory impairment. *J. Neurosci.* 35, 15157–15169. doi:10.1523/JNEUROSCI.4081-14.2015

Ozkaya, D., and Naziroglu, M. (2020). Curcumin diminishes cisplatin-induced apoptosis and mitochondrial oxidative stress through inhibition of TRPM2 channel signaling pathway in mouse optic nerve. *J. Recept Signal. Transduct Res.* 40, 97–108. doi:10.1080/10799893.2020.1720240

Patel, S., Leibrand, C. R., Palasuberniam, P., Couraud, P. O., Weksler, B., Jahr, F. M., et al. (2017). Effects of HIV-1 tat and methamphetamine on blood-brain barrier integrity and function in vitro. *Antimicrob. Agents Chemother.* 61, e01307–e01317. doi:10.1128/AAC.01307-17

Pun, P. B., Lu, J., and Moochhala, S. (2009). Involvement of ROS in BBB dysfunction. *Free Radic. Res.* 43, 348–364. doi:10.1080/10715760902751902

Qi, L., Gang, L., Hang, K. W., Ling, C. H., Xiaofeng, Z., Zhen, L., et al. (2011). Programmed neuronal cell death induced by HIV-1 tat and methamphetamine. *Microsc. Res. Tech.* 74, 1139–1144. doi:10.1002/jemt.21006

Qie, X., Wen, D., Guo, H., Xu, G., Liu, S., Shen, Q., et al. (2017). Endoplasmic reticulum stress mediates methamphetamine-induced blood-brain barrier damage. *Front. Pharmacol.* 8, 639. doi:10.3389/fphar.2017.00639

Sita, G., Hrelia, P., Graziosi, A., Ravegnini, G., and Morroni, F. (2018). TRPM2 in the brain: role in health and disease. *Cells* 7, 82. doi:10.3390/cells7070082

Tai, L. M., Holloway, K. A., Male, D. K., Loughlin, A. J., and Romero, I. A. (2010). Amyloid-beta-induced occludin down-regulation and increased permeability in human brain endothelial cells is mediated by MAPK activation. *J. Cell Mol. Med.* 14, 1101–1112. doi:10.1111/j.1582-4934.2009.00717.x

Toborek, M., Lee, Y. W., Pu, H., Malecki, A., Flora, G., Garrido, R., et al. (2003). HIV-Tat protein induces oxidative and inflammatory pathways in brain endothelium. *J. Neurochem.* 84, 169–179. doi:10.1046/j.1471-4159.2003.01543.x

Turlova, E., Feng, Z. P., and Sun, H. S. (2018). The role of TRPM2 channels in neurons, glial cells and the blood-brain barrier in cerebral ischemia and hypoxia. *Acta Pharmacol. Sin.* 39, 713–721. doi:10.1038/aps.2017.194

Wang, J., Jackson, M. F., and Xie, Y. F. (2016). Glia and TRPM2 channels in plasticity of central nervous system and Alzheimer's diseases. *Neural Plast.* 2016, 1680905. doi:10.1155/2016/1680905

Wang, L., Negro, R., and Wu, H. (2020). TRPM2, linking oxidative stress and Ca^{2+} permeation to NLRP3 inflammasome activation. *Curr. Opin. Immunol.* 62, 131–135. doi:10.1016/j.coi.2020.01.005

Wang, L., Fu, T. M., Zhou, Y., Xia, S., Greka, A., and Wu, H. (2018). Structures and gating mechanism of human TRPM2. *Science* 362, eaav4809. doi:10.1126/science.aav4809

Weksler, B., Romero, I. A., and Couraud, P. O. (2013). The hCMEC/D3 cell line as a model of the human blood brain barrier. *Fluids Barriers CNS* 10, 16. doi:10.1186/2045-8118-10-16

Weksler, B. B., Subileau, E. A., Perrière, N., Charneau, P., Holloway, K., Leveque, M., et al. (2005). Blood-brain barrier-specific properties of a human adult brain endothelial cell line. *FASEB J.* 19, 1872–1874. doi:10.1096/fj.04-3458fje

Xu, R., Feng, X., Xie, X., Zhang, J., Wu, D., and Xu, L. (2012). HIV-1 Tat protein increases the permeability of brain endothelial cells by both inhibiting occludin expression and cleaving occludin via matrix metalloproteinase-9. *Brain Res.* 1436, 13–19. doi:10.1016/j.brainres.2011.11.052

Xue, Y., He, J. T., Zhang, K. K., Chen, L. J., Wang, Q., and Xie, X. L. (2019). Methamphetamine reduces expressions of tight junction proteins, rearranges F-actin cytoskeleton and increases the blood brain barrier permeability via the RhoA/ROCK-dependent pathway. *Biochem. Biophys. Res. Commun.* 509, 395–401. doi:10.1016/j.bbrc.2018.12.144

Yamamoto, S., and Shimizu, S. (2016). Targeting TRPM2 in ROS-coupled diseases. *Pharmaceuticals* 9. doi:10.3390/ph9030057

Yang, X., Wang, Y., Li, Q., Zhong, Y., Chen, L., Du, Y., et al. (2018). The main molecular mechanisms underlying methamphetamine- induced neurotoxicity and implications for pharmacological treatment. *Front. Mol. Neurosci.* 11, 186. doi:10.3389/fnmol.2018.00186

Zeng, X. F., Li, Q., Li, J., Wong, N., Li, Z., Huang, J., et al. (2018). HIV-1 Tat and methamphetamine co-induced oxidative cellular injury is mitigated by N-acetylcysteine amide (NACA) through rectifying mTOR signaling. *Toxicol. Lett.* 299, 159–171. doi:10.1016/j.toxlet.2018.09.009

Conflict of Interest: The authors declare that the research was conducted in the absence of any commercial or financial relationships that could be construed as a potential conflict of interest.

frontiers in Pharmacology

ORIGINAL RESEARCH
published: 09 April 2021
doi: 10.3389/fphar.2021.652865

Disrupting Reconsolidation by Systemic Inhibition of mTOR Kinase via Rapamycin Reduces Cocaine-Seeking Behavior

*Fushen Zhang[1†], Shihao Huang[1†], Haiyan Bu[1†], Yu Zhou[2], Lixiang Chen[1], Ziliu Kang[1], Liangpei Chen[2], He Yan[3], Chang Yang[1], Jie Yan[3], Xiaohong Jian[1] and Yixiao Luo[1]**

[1]Key Laboratory of Molecular Epidemiology of Hunan Province, School of Medicine, Hunan Normal University, Changsha, China, [2]Yiyang Medical College, Yiyang, China, [3]Department of Forensic Science, School of Basic Medical Science, Central South University, Changsha, China

Drug addiction is considered maladaptive learning, and drug-related memories aroused by the presence of drug related stimuli (drug context or drug-associated cues) promote recurring craving and reinstatement of drug seeking. The mammalian target of rapamycin signaling pathway is involved in reconsolidation of drug memories in conditioned place preference and alcohol self-administration (SA) paradigms. Here, we explored the effect of mTOR inhibition on reconsolidation of addiction memory using cocaine self-administration paradigm. Rats received intravenous cocaine self-administration training for 10 consecutive days, during which a light/tone conditioned stimulus was paired with each cocaine infusion. After acquisition of the stable cocaine self-administration behaviors, rats were subjected to nosepoke extinction (11 days) to extinguish their behaviors, and then received a 15 min retrieval trial with or without the cocaine-paired tone/light cue delivery or without. Immediately or 6 h after the retrieval trial, rapamycin (10 mg/kg) was administered intraperitoneally. Finally, cue-induced reinstatement, cocaine-priming-induced reinstatement and spontaneous recovery of cocaine-seeking behaviors were assessed in rapamycin previously treated animals, respectively. We found that rapamycin treatment immediately after a retrieval trial decreased subsequent reinstatement of cocaine seeking induced by cues or cocaine itself, and these effects lasted at least for 28 days. In contrast, delayed intraperitoneal injection of rapamycin 6 h after retrieval or rapamycin injection without retrieval had no effects on cocaine-seeking behaviors. These findings indicated that mTOR inhibition within the reconsolidation time-window impairs the reconsolidation of cocaine associated memory, reduces cocaine-seeking behavior and prevents relapse, and these effects are retrieval-dependent and temporal-specific.

Keywords: mTOR, rapamycin, reconsolidation, drug memory, self-administration

OPEN ACCESS

Edited by:
M Foster Olive,
Arizona State University, United States

Reviewed by:
Devin Mueller,
Kent State University, United States
James Mark Otis,
Medical University of South Carolina, United States

****Correspondence:***
Yixiao Luo
luoyx@hunnu.edu.cn

[†]These authors have contributed equally to this work

Specialty section:
This article was submitted to Neuropharmacology, a section of the journal Frontiers in Pharmacology

Received: *13 January 2021*
Accepted: *16 March 2021*
Published: *09 April 2021*

Citation:
Zhang F, Huang S, Bu H, Zhou Y, Chen L, Kang Z, Chen L, Yan H, Yang C, Yan J, Jian X and Luo Y (2021) Disrupting Reconsolidation by Systemic Inhibition of mTOR Kinase via Rapamycin Reduces Cocaine-Seeking Behavior. Front. Pharmacol. 12:652865. doi: 10.3389/fphar.2021.652865

INTRODUCTION

Drug addiction is defined as a chronic psychiatric disease with a high rate of relapse even after a long period of withdrawal. Addicted individuals experience intense drug craving that can persist long after withdrawal, leading to high relapse rates. Additionally, they exert compulsive seeking and drug-taking behaviors that are difficult to control despite the serious adverse consequences of drug abuse. The critical problem of drug addiction is to prevent and reduce relapse after withdrawal (Grant et al.,

1996; Childress et al., 1999; Kilts et al., 2001). To date, there are no available pharmacological or non-pharmacological therapies to treat drug addiction and prevent relapse completely (Nestler, 2001; Hyman et al., 2006; Volkow and Boyle, 2018; Ahmed et al., 2020). Much evidence shows that the persistence of drug memory and the difficulty in eliminating are the root causes of compulsive drug use behavior, drug-seeking behavior, and relapse after withdrawal (Childress et al., 1986; Kelley, 2004; Torregrossa et al., 2011). Hence, elucidating the neurobiological mechanisms of drug memory and disrupting it through various interventions seem to be an effective way to treat drug addiction and prevent relapse after withdrawal.

The formation of conditioned associations between repeated drug abuse and associative context is essential for the generation and maintenance of addiction-related behaviors. Exploring the neural mechanisms underlying the associated learning process in the formation of drug memories will help us understand addictive behaviors from the perspective of maladaptive learning and memory and develop new treatments to prevent relapse (O'Brien et al., 1998). Chronic use of addictive drugs leads to adaptive changes in plasticity in the central nervous system, which may be related to the pathological memories formed between repeated exposure to drugs and drug-associated cues (Everitt et al., 1999; Jentsch and Taylor, 1999). There are similar processes between drug memory and normal learning memory, such as consolidation and reconsolidation (Dudai, 1996; McGaugh, 2000; Nader et al., 2000; Sara, 2000; Nader and Hardt, 2009).

Consolidation and reconsolidation are specific phases in which the memory becomes unstable after acquisition or reactivation and can be disrupted, requiring *de novo* protein synthesis to be restabilized (McGaugh, 2000; Sara, 2000; Nader and Hardt, 2009). Interfering with consolidation or reconsolidation can disrupt drug memory and consequently attenuate the drug seeking or reinstatement in gold-standard animal models of addiction (Hellemans et al., 2006; Robbins et al., 2008). Drug memory can be activated during the reconsolidation process by controlled re-exposure to drug-context or cues, which provides operability to interfering with drug memory. Current research on drug memory is mainly focused on the reconsolidation (Lee et al., 2005; Milton et al., 2008a; Milton et al., 2008b; Taylor et al., 2009; Sanchez et al., 2010; Wells et al., 2013). Interfering with reconsolidation is a promising strategy for the treatment of drug addiction and relapse prevention.

The mammalian target of rapamycin (mTOR) signaling pathway is well known to exert complex physiological functions *in vivo*, especially, plays a critical role in gene transcription regulation and protein translation initiation via modulating downstream target proteins (Sabatini et al., 1994; Schmelzle and Hall, 2000; Laplante and Sabatini, 2012). Reconsolidation is a protein synthesis-dependent process (Nader et al., 2000; Dudai, 2006). Therefore, the activity of mTOR probably regulates reconsolidation of drug memories. Previous studies have shown that inhibition of the activity of mTOR signaling pathway can disrupt spatial memory consolidation, as well as the consolidation and reconsolidation of contextual fear memory (Dash et al., 2006; Parsons et al., 2006). The mTOR signaling pathway has also been reported to be involved in reconsolidation of drug memories in conditioned place preference (CPP) and alcohol self-administration (SA) animal models (Barak et al., 2013; Lin et al., 2014). However, whether or not disruption of reconsolidation by mTOR inhibition could inhibit drug-seeking behaviors and prevent relapse still remains largely unknown.

It is generally accepted that rapamycin is the specific inhibitor of mammalian target of rapamycin (Brown et al., 1994; Sabatini et al., 1994; Abraham and Wiederrecht, 1996). In the present study, we investigated the role of mTOR via rapamycin in the reconsolidation of cocaine-associated memory using a cocaine self-administration model. We also assessed the effects of mTOR inhibition on cue-induced- and cocaine priming-induced reinstatement of drug seeking and on spontaneous recovery of cocaine-seeking.

MATERIALS AND METHODS

Subjects

Male Sprague Dawley rats (weighing 260–280 g on arrival) were obtained from the Tianqin Laboratory Animal Technology Co. Ltd., China. Rats were housed in groups of five under controlled temperature (23 ± 2°C) and humidity (50 ± 5%), and maintained on a 12 h light/dark cycle (lights off at 8:00, lights on at 20:00) with access to food and water ad libitum. All of the rats were handled 3 min per day for 5 days before the surgeries. All animal procedures were performed in accordance with the Guide of Hunan province for the Care and Use of Laboratory Animals, and the experiments were approved by the Local Committee on Animal Care and Use and Protection of the Hunan Normal University. All the experiments were performed during the dark phase.

Intravenous Surgery

Rats (weighing 300–320 g at the time of surgery) were anesthetized with sodium pentobarbital (60 mg/kg, i. p.). Catheters were inserted into the right jugular vein with the tip terminating at the opening of the right atrium as described previously (Lu et al., 2005). The cannulae were anchored to the skull with stainless steel screws and dental cement. A stainless steel stylet blocker was inserted into each cannula to maintain patency and prevent infection (Xue et al., 2012). Rats were then housed individually for 5–7 days to recover before the training sessions began.

Behavioral Procedures

Intravenous Cocaine Self-Administration Training

The operant chambers used (AniLab Software and Instruments, Ningbo, China) were equipped with two nosepoke operandi (AniLab Software and Instruments, Ningbo, China) located 5 cm above the chamber floor. Nosepokes in the left side (active) operandum led to cocaine infusions that were accompanied by a 5 s tone-light cue. Nosepokes in the right side (inactive) operandum were also recorded but had no programmed consequences. Rats were trained to self-administer cocaine hydrochloride (0.75 mg/kg/infusion) during three 1 h daily sessions separated by 5 min over 10 days. The

sessions began at the onset of the dark cycle (8:00–20:00). A fixed-ratio one reinforcement schedule was used, with a 40 s timeout period after each infusion. Each session began with the illumination of a houselight that remained on for the entire session. The number of drug infusions was limited to 20 per hour to prevent death by overdose (Xue et al., 2012; Luo et al., 2015). We excluded a total of nine rats from the experiments: four rats due to catheter patency failure and five rats due to failure to acquire cocaine self-administration.

Nosepoke Extinction

During extinction, the conditions were the same as during cocaine self-administration training, except that cocaine was no longer available and without the tone-light cue (Shi et al., 2015).

Retrieval Trial

A 15 min retrieval to reactivate cocaine-associated memories began 24 h after the last nosepoke extinction session. The retrieval conditions were the same as during cocaine self-administration training except that active nosepokes with no reward cocaine.

Cue Extinction

During extinction, the conditions were the same as during cocaine self-administration training, with the exception that no cocaine injections were given with the delivery of cue (tone/light).

Cue-Induced Reinstatement Test

Rats were returned to the same self-administration context and recorded the number of nosepokes to both operandi (active and inactive) for 1 h. The conditions were the same as during cocaine self-administration training except that cocaine injections were not given upon active nosepoking.

Priming-Induced Reinstatement Test

For priming-induced reinstatement test, rats were injected with cocaine (5 mg/kg, i. p.) 5 min before the start of the session. Rats then were placed in the same self-administration context and recorded the number of nosepokes to both operandi (active and inactive) was recorded for 1 h. The conditions were the same as during cocaine self-administration training except that active nosepokes were not reinforced with cocaine.

Spontaneous Recovery Test

For a spontaneous recovery test, active and inactive operandi nosepokes were recorded for 1 h after 28 days withdrawal. The testing conditions were similar to those during the cue-induced reinstatement test.

Experimental Design

Experiment 1: Effect of Immediate Rapamycin Administration After Retrieval of Cocaine cue Memory on Subsequent cue-Induced + Priming-Induced Reinstatement

Rats received three 1-h daily sessions of intravenous cocaine self-administration training for 10 days, and 24 h after training, all rats then underwent 11 consecutive days of daily nosepoke extinction training. 24 h after the last nosepoke extinction session, the rats were divided into two groups: 1) Intraperitoneal injection of rapamycin (10 mg/kg, i. p.) immediately after a 15 min retrieval trial (Retrieval + Rapa); 2) Intraperitoneal injection of vehicle (0.3 ml/kg, i. p.) immediately after a 15 min retrieval trial (Retrieval + Vel). The doses of rapamycin were chosen based on previous studies (Lin et al., 2014; Zubedat and Akirav, 2017). On Day 23, a cue-induced reinstatement test was performed to verify whether the administration of rapamycin immediately after retrieval of cocaine cue memory destroys the expression of cocaine cue memory in rats. 24 h after the cue-induced reinstatement test, rats received daily cue extinction session for two consecutive days. 24 h later, on Day 26, rats were tested for cocaine priming-induced reinstatement (**Figure 1A**).

Experiment 2: Effect of Immediate Rapamycin Administration After Retrieval of Cocaine cue Memory on Subsequent Cue-Induced Reinstatement and Spontaneous Recovery

Rats received three 1 h daily sessions of intravenous cocaine self-administration training for 10 days, and 24 h after training, all rats then underwent 11 consecutive days of daily nosepoke extinction training. 24 h after the last nosepoke extinction session, the rats were divided into two groups: 1) Intraperitoneal injection of rapamycin (10 mg/kg, i. p.) immediately after a 15 min retrieval trial (Retrieval + Rapa); 2) Intraperitoneal injection of vehicle (0.3 ml/kg, i. p.) immediately after a 15 min retrieval trial (Retrieval + Vel). 24 h after the last extinction session, rats underwent the cue-induced reinstatement test. To confirm the long-term inhibition effect of rapamycin on cocaine-seeking behavior in rats, 28 days after the cue-induced reinstatement test, all rats were tested for spontaneous recovery on Day 58 (**Figure 2A**).

Experiment 3: Effect of Rapamycin Treatment on Subsequent Cue-Induced + Priming-Induced Reinstatement in Non-retrieved Controls

The experimental procedure for Experiment 3 was the same as in Experiment 1, except that injection of rapamycin was made 24 h after the last nosepoke extinction session without the retrieval trial session (**Figure 3A**).

Experiment 4: Effect of Delayed Rapamycin Treatment After Retrieval of Cocaine Cue Memory on Subsequent Cue-Induced + Priming-Induced Reinstatement

The experimental procedure for Experiment 4 was the same as in Experiment 1, except that rapamycin was administered intraperitoneally 6 h after the retrieval trial session (**Figure 4A**).

Statistical Analysis

The data were analyzed using repeated measures ANOVAs with between-subjects factor of treatment condition and within-subjects factor of test condition followed by Tukey's *post-hoc* test in each experiment (see results). The values are presented as

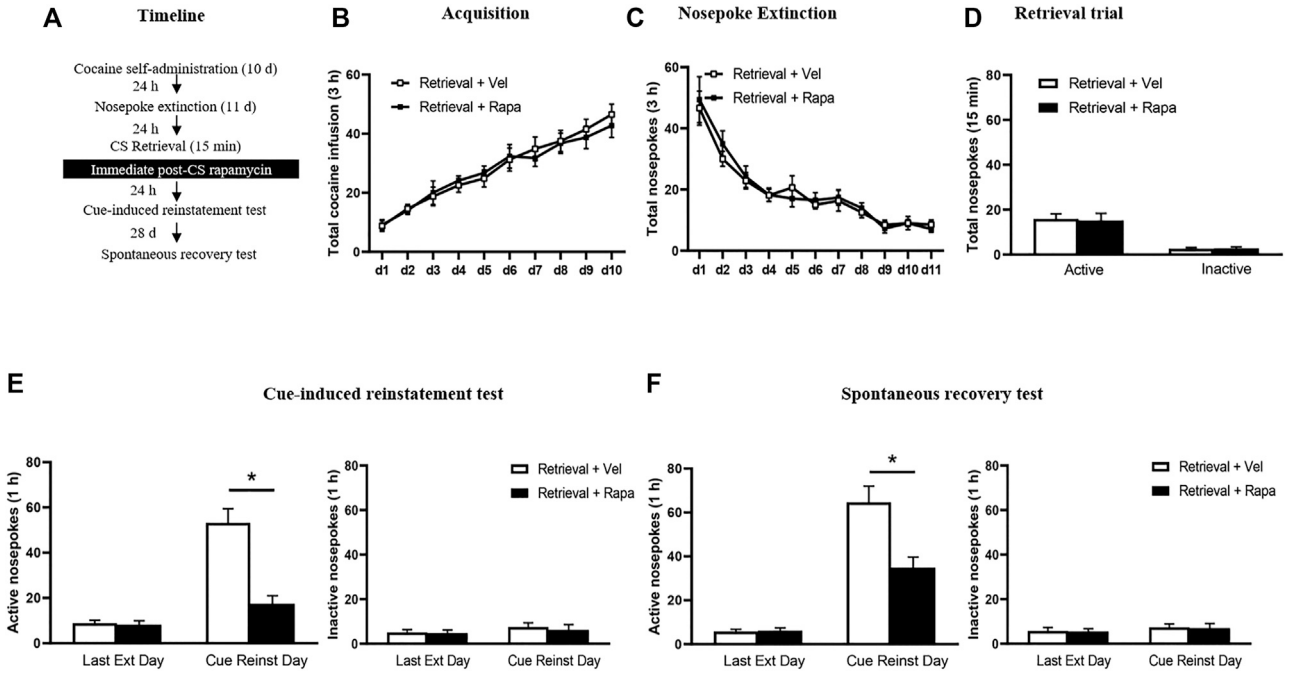

FIGURE 1 | Rapamycin administration immediately after retrieval of cocaine cue memory reduces subsequent cue-induced reinstatement of cocaine seeking behavior. **(A)** Experimental procedure. **(B)** Total number of cocaine infusions across acquisition of cocaine self-administration sessions. **(C)** Total number of active nosepoke responses across nosepoke response extinction. **(D)** Nosepoke responses during retrieval trial. **(E)** Active **(left)** and inactive **(right)** nosepoke responses during the last session of the nosepoke extinction sessions and the cue-induced reinstatement test. **(F)** Active **(left)** and inactive **(right)** nosepoke responses during the last session of the cue extinction sessions and the priming-induced reinstatement test. *Different from the Retrieval + Veh group, $p < 0.05$.

the mean ± S.E.M. Values of $p < 0.05$ were considered statistically significant.

RESULTS

Experiment 1: Rapamycin Administration Immediately After Retrieval of Cocaine Cue Memory Reduces Subsequent Reinstatement of Cocaine-Seeking Behavior

In Experiment 1, we test the effect of immediate rapamycin administration after retrieval of cocaine cue memory on cue-induced and priming-induced reinstatement of cocaine seeking behaviors (**Figure 1**). Results were analyzed by repeated measures-ANOVA, with the treatment condition (Retrieval + Rapa, Retrieval + Veh) as a between-subjects factor and test condition as a within-subjects factor. There was no difference between two groups in the total numbers of cocaine infusions during acquisition (with the treatment condition as a between-subjects factor and the different training days as a within-subject factor) [main effect of the training day: $F_{(9,126)} = 36.620$, $p < 0.001$; main effect of the treatment condition: $F_{(1,14)} = 0.035$, $p = 0.854$; interaction of training day × treatment condition: $F_{(9,126)} = 0.299$, $p = 0.974$] (**Figure 1B**). Furthermore, statistical analysis of the number of active nosepokes in extinction session revealed no group difference in the Retrieval + Rapa group and the Retrieval + Veh group [main effect of the extinction day: $F_{(10,140)} = 32.410$, $p < 0.001$; main effect of the treatment condition: $F_{(1,14)} = 0.508$, $p = 0.488$; interaction of extinction day × treatment condition: $F_{(10,140)} = 0.331$, $p = 0.971$] (**Figure 1C**). For the retrieval trial, there were no group differences in the numbers of nosepokes [main effect of the different nosepokes: $F_{(1,14)} = 42.61$, $p < 0.001$; main effect of the treatment condition: $F_{(1,14)} = 0.01549$, $p = 0.9027$; interaction of different nosepokes × treatment condition: $F_{(1,14)} = 0.03614$, $p = 0.8519$] (**Figure 1D**). However, there was a significant difference in active nosepokes between two groups in the cue reinstatement tests [main effect of the test condition: $F_{(1,14)} = 45.940$, $p < 0.001$; main effect of the treatment condition: $F_{(1,14)} = 28.342$, $p < 0.001$; interaction of test condition × treatment condition: $F_{(1,14)} = 19.710$, $p = 0.001$]; *Post hoc* shown that drug-seeking in the Retrieval + Rapa group was significantly reduced compared to the Retrieval + Veh group in the cue-induced reinstatement test ($p < 0.05$) (**Figure 1E** left column). There was no significant difference in inactive nosepokes [main effect of the test condition: $F_{(1,14)} = 1.575$, $p = 0.230$; main effect of the treatment condition: $F_{(1,14)} = 0.172$, $p = 0.684$; interaction of test condition × treatment condition: $F_{(1,14)} = 0.080$, $p = 0.781$] (**Figure 1E** right column). For priming-induced reinstatement tests, repeated measures-ANOVA revealed a significant effect of active nosepokes [main effect of the test condition: $F_{(1,14)} = 88.352$, $p < 0.001$; main effect of the treatment condition: $F_{(1,14)} = 11.98$,

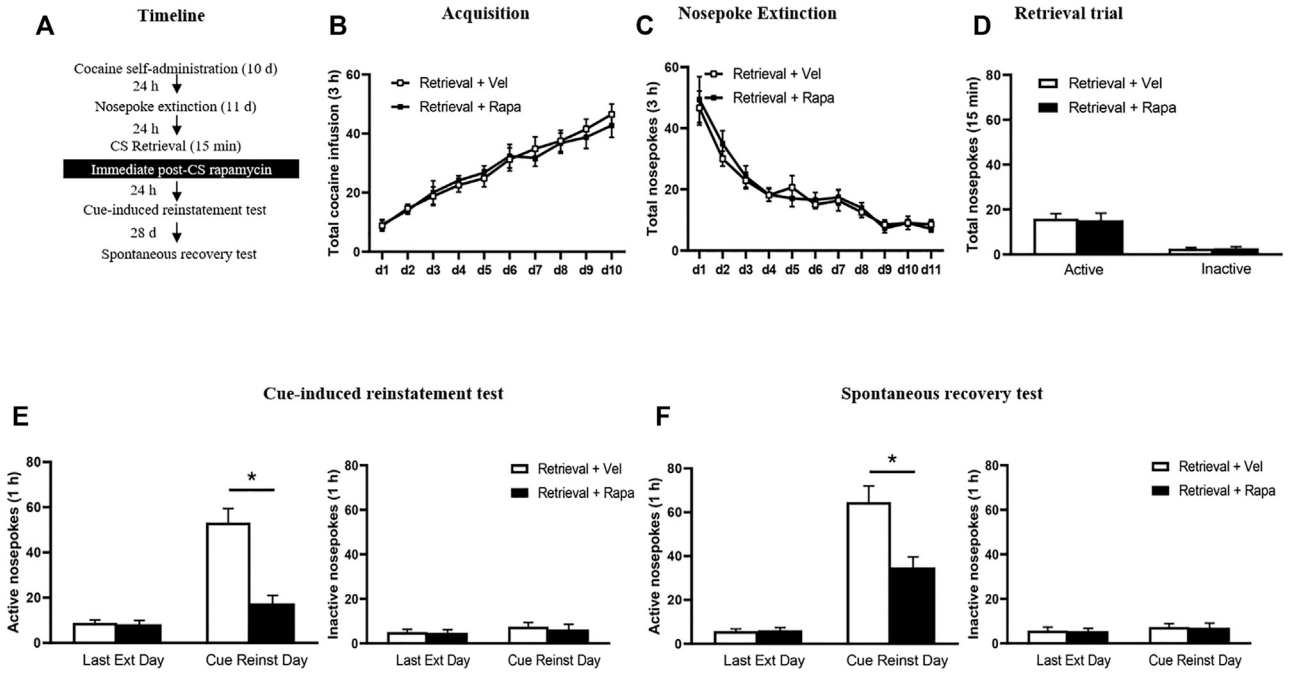

FIGURE 2 | Rapamycin administration immediately after retrieval of cocaine cue memory decreases subsequent spontaneous recovery of cocaine seeking behavior. **(A)** Experimental procedure. **(B)** Total number of cocaine infusions across acquisition of cocaine self-administration sessions. **(C)** Total number of active nosepoke responses across nosepoke response extinction. **(D)** Nosepoke responses during retrieval trial. **(E)** Active **(left)** and inactive **(right)** nosepoke responses during the last session of the nosepoke extinction sessions and the cue-induced reinstatement test. **(F)** Active **(left)** and inactive **(right)** nosepoke responses during the last session of the cue extinction sessions and the spontaneous recovery test. *Different from the Retrieval + Veh group, $p < 0.05$.

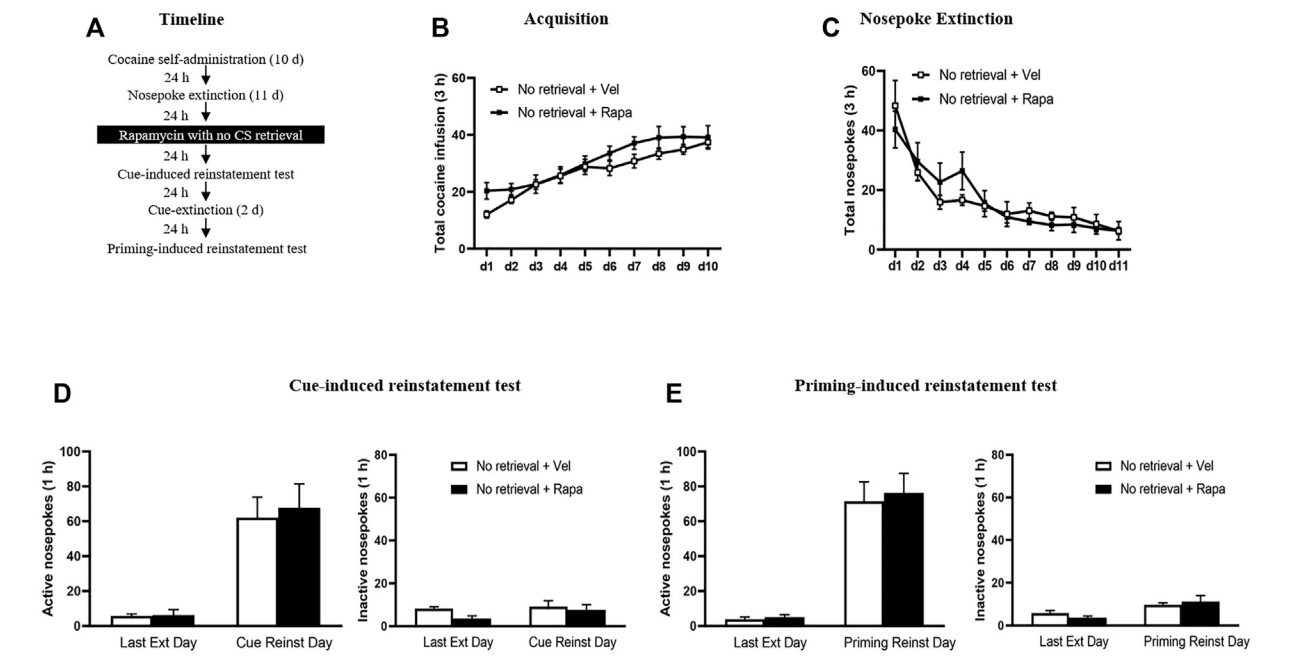

FIGURE 3 | Rapamycin treatment without retrieval has no effects on subsequent reinstatement of cocaine seeking behavior. **(A)** Experimental procedure. **(B)** Total number of cocaine infusions across acquisition of cocaine self-administration sessions. **(C)** Total number of active nosepoke responses across nosepoke response extinction. **(D)** Active **(left)** and inactive **(right)** nosepoke responses during the last session of the nosepoke extinction sessions and the cue-induced reinstatement test. **(E)** Active **(left)** and inactive **(right)** nosepoke responses during the last session of the cue extinction sessions and the priming-induced reinstatement test.

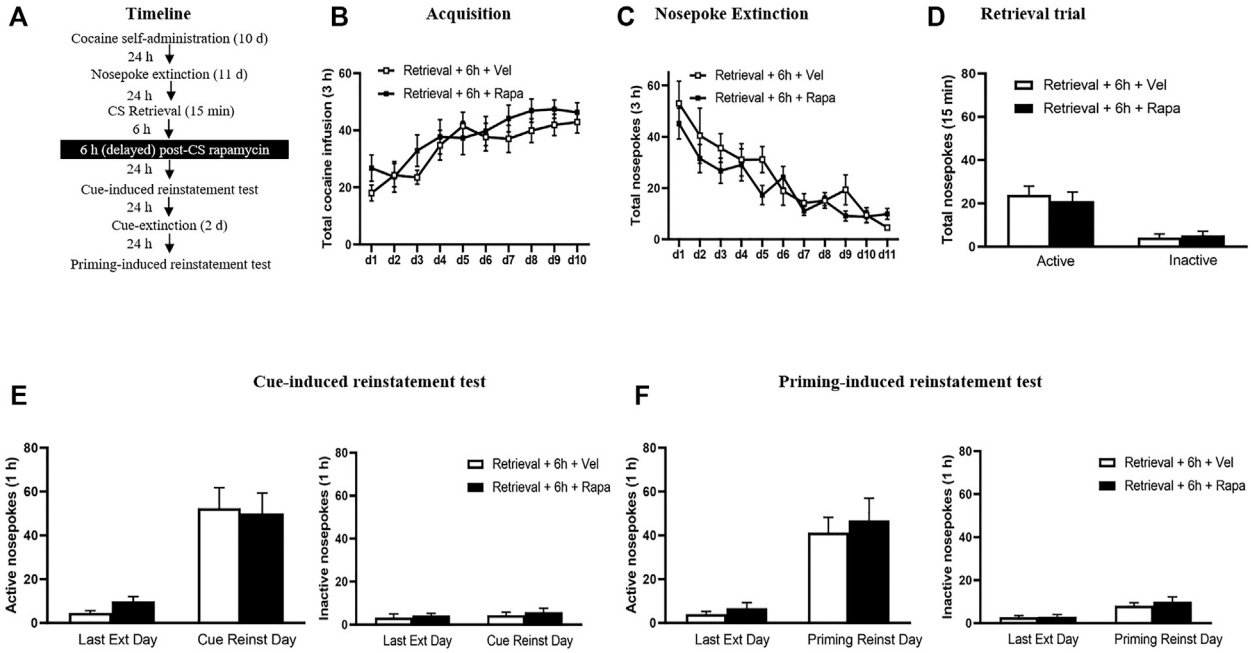

FIGURE 4 | Rapamycin treatment 6 h after retrieval of cocaine cue memory has no effects on subsequent reinstatement of cocaine seeking behavior. **(A)** Experimental procedure. **(B)** Total number of cocaine infusions across acquisition of cocaine self-administration sessions. **(C)** Total number of active nosepoke responses across nosepoke response extinction. **(D)** Nosepoke responses during retrieval trial. **(E)** Active **(left)** and inactive **(right)** nosepoke responses during the last session of the nosepoke extinction sessions and the cue-induced reinstatement test. **(F)** Active **(left)** and inactive **(right)** nosepoke responses during the last session of the cue extinction sessions and the priming-induced reinstatement test.

p = 0.004; interaction of test condition × treatment condition: $F_{(1,14)}$ = 10.560, p = 0.006;]; *Post hoc* shown that drug-seeking in the Retrieval + Rapa group was significantly reduced compared to the Retrieval + Veh group in the priming-induced reinstatement test (p < 0.05) (**Figure 1F** left column), but no significant difference in inactive nosepokes [main effect of the test condition: $F_{(1,14)}$ = 0.654, p = 0.432; main effect of the treatment condition: $F_{(1,14)}$ = 0.066, p = 0.801; interaction of test condition × treatment condition: $F_{(1,14)}$ = 0.001, p = 0.975] (**Figure 1F** right column). In summary, these results scxuggest that inhibition of mTOR kinase by rapamycin disrupts cocaine addiction memory and suppresses cue-induced and priming-induced reinstatement of cocaine-seeking behavior.

Experiment 2: Rapamycin Administration Immediately After Retrieval of Cocaine Cue Memory Decreases Spontaneous Recovery of Cocaine-Seeking Behavior

In Experiment 2, we investigated the effect of rapamycin administration immediately after retrieval of cocaine cue memory on subsequent reinstatement and spontaneous recovery tests of cocaine seeking behaviors (**Figure 2**). The results were analyzed by repeated-measures ANOVA, with the treatment condition (Retrieval + Rapa, Retrieval Veh) as a between-subjects factor and the test condition as a within-subjects factor. There was no significant difference between the two groups in total numbers of cocaine infusions during acquisition (with the treatment condition as a between-subjects factor and the different training days as a within-subject factor) [main effect of the training day: $F_{(9,171)}$ = 41.518, p < 0.001; main effect of the treatment condition: $F_{(1,19)}$ = 0.077, p = 0.785; interaction of training day × treatment condition: $F_{(9,171)}$ = 0.757, p = 0.656] (**Figure 2B**). In addition, statistical analysis of the numbers of active nosepokes during the extinction session revealed no significant group differences between the Retrieval + Rapa group and the Retrieval + Veh group [main effect of the extinction day: $F_{(10,190)}$ = 30.187, p < 0.001; main effect of the treatment condition: $F_{(1,19)}$ = 0.193, p = 0.665; interaction of extinction day × treatment condition: $F_{(10,190)}$ = 0.265, p = 0.988] (**Figure 2C**). For the retrieval trial, there were no group differences in the numbers of nosepokes [main effect of the different nosepokes: $F_{(1,19)}$ = 29.68, p < 0.001; main effect of the treatment condition: $F_{(1,19)}$ = 0.2486, p = 0.6238; interaction of different nosepokes × treatment condition: $F_{(119)}$ = 0.0484, p = 0.8282] (**Figure 2D**). However, there was a significant difference in active nosepokes between these groups in the cue-induced reinstatement test [main effect of the test condition: $F_{(1,\ 18)}$ = 55.265, p < 0.001; main effect of the treatment condition: $F_{(1,18)}$ = 19.091, p < 0.001; interaction of test condition × treatment condition: $F_{(1,18)}$ = 14.283, p = 0.001]; *Post hoc* shown that drug-seeking in the Retrieval + Rapa group was significantly reduced as compared to the Retrieval + Veh group during the cue-induced reinstatement test (p < 0.05) (**Figure 2E** left column), but no significant difference in inactive nosepokes [main effect of the test condition: $F_{(1,19)}$ < 0.001, p = 0.989; main effect of the

treatment condition: $F_{(1,19)} = 0.295$, $p = 0.593$; interaction of test condition × treatment condition: $F_{(1,19)} = 0.085$, $p = 0.773$] (**Figure 2E** right column). Furthermore, repeated-measures ANOVA revealed a significant effect of active nosepokes in the spontaneous recovery test [main effect of the test condition: $F_{(1,19)} = 60.320$, $p < 0.001$; main effect of the treatment condition: $F_{(1,19)} = 11.220$, $p = 0.003$; interaction of test condition × treatment condition: $F_{(1,19)} = 15.444$, $p = 0.001$]; *Post hoc* shown that drug-seeking in the Retrieval + Rapa group was significantly reduced as compared to the Retrieval + Veh group in the spontaneous recovery test ($p < 0.05$) (**Figure 2F** left column), but no significant difference in inactive nosepokes [main effect of the test condition: $F_{(1,19)} = 0.987$, $p < 0.001$; main effect of the treatment condition: $F_{(1,19)} = 0.150$, $p = 0.703$; interaction of test condition × treatment condition: $F_{(1,19)} = 0.012$, $p = 0.915$] (**Figure 2F** right column). These results indicate that inhibition of mTOR kinase by rapamycin treatment disrupts cocaine addiction memory and suppresses spontaneous recovery of cocaine-seeking behavior.

Experiment 3: Rapamycin Treatment Without Retrieval has No Effects on Subsequent Reinstatement of Cocaine-Seeking Behavior

In Experiment 3, we examined whether rapamycin disrupting reconsolidation of cocaine memory was retrieval dependent. After the cocaine self-administer acquisition and extinction, rats administered rapamycin or vehicle but without a retrieval trial (**Figure 3**). There was no significant difference between the groups in the total numbers of cocaine infusions during acquisition (with the treatment condition as a between-subjects factor and the different training days as a within-subject factor) [main effect of the training day: $F_{(9,144)} = 29.498$, $p < 0.001$; main effect of the treatment condition: $F_{(1,16)} = 2.014$, $p = 0.175$; interaction of training day × treatment condition: $F_{(9,144)} = 0.943$, $p = 0.490$] (**Figure 3B**). Furthermore, statistical analysis on the number of active nosepokes during the extinction session revealed that there were no group difference in the Retrieval + Rapa group and the Retrieval + Veh group [main effect of the extinction day: $F_{(10,160)} = 18.906$, $p < 0.001$; main effect of the treatment condition: $F_{(1,16)} = 0.044$, $p = 0.837$; interaction of extinction day × treatment condition: $F_{(10,160)} = 0.735$, $p = 0.691$] (**Figure 3C**). In addition, there was no significant difference in active nosepokes between these groups during the reinstatement tests [main effect of the test condition: $F_{(1,16)} = 39.240$, $p < 0.001$; main effect of the treatment condition: $F_{(1,16)} = 0.122$, $p = 0.732$; interaction of test condition × treatment condition: $F_{(1,16)} = 0.074$, $p = 0.789$] (**Figure 3D** left column), no significant difference in inactive nosepokes [main effect of the test condition: $F_{(1,16)} = 1.493$, $p = 0.239$; main effect of the treatment condition: $F_{(1,16)} = 2.419$, $p = 0.139$; interaction of test condition × treatment condition: $F_{(1,16)} = 0.620$, $p = 0.443$] (**Figure 3D** right column). For priming-induced reinstatement tests, repeated-measures ANOVA revealed no significant effect of active nosepokes [main effect of the test condition: $F_{(1,16)} = 75.577$, $p < 0.001$; main effect of the treatment condition: $F_{(1,16)} = 0.152$, $p = 0.701$; interaction of test condition × treatment condition: $F_{(1,16)} = 0.053$, $p = 0.821$] (**Figure 3F** left column), no significant difference in inactive nosepokes [main effect of the test condition: $F_{(1,16)} = 10.826$, $p = 0.005$; main effect of the treatment condition: $F_{(1,16)} = 0.031$, $p = 0.862$; interaction of test condition × treatment condition: $F_{(1,16)} = 1.111$, $p = 0.307$] (**Figure 3F** right column). There is no significant difference between the groups in all tests (all $p > 0.05$). Therefore, the results of Experiment 3 indicate that the effect of rapamycin in Experiment 1 depends on the retrieval trial and that rapamycin administration without a retrieval trial has no effects on subsequent cue-induced and priming-induced reinstatement of cocaine-seeking behavior.

Experiment 4: Delayed Rapamycin Treatment Following Retrieval of Cocaine Cue Memory has No Effects on Subsequent Reinstatement of Cocaine-Seeking Behavior

In Experiment 4, we examined whether the rapamycin treatment outside the sensitive time window could disrupted the reconsolidation of cocaine memory. We assessed the effect of rapamycin administration 6 h after retrieval of cocaine cue memory on cue-induced and priming-induced reinstatement of cocaine seeking behaviors (**Figure 4**). During the acquisition sessions, there was no significant difference between two groups in the total numbers of cocaine infusions (with the treatment condition as a between-subjects factor and the different training days as a within-subject factor) [main effect of the training day: $F_{(9,117)} = 15.687$, $p < 0.001$; main effect of the treatment condition: $F_{(1,13)} = 0.701$, $p = 0.418$; interaction of training day × treatment condition: $F_{(9,117)} = 1.021$, $p = 0.427$] (**Figure 4B**). Furthermore, statistical analysis of the numbers of active nosepokes during the extinction sessions revealed no group difference in the Retrieval + Rapa group and the Retrieval + Veh group [main effect of the extinction day: $F_{(10,130)} = 17.667$, $p < 0.001$; main effect of the treatment condition: $F_{(1,13)} = 1.088$, $p = 0.316$; interaction of extinction day × treatment condition: $F_{(10,130)} = 1.080$, $p = 0.383$] (**Figure 4C**). For the retrieval trial, there were no group differences in the numbers of nosepokes [main effect of the different nosepokes: $F_{(1,13)} = 57.10$, $p < 0.001$; main effect of the treatment condition: $F_{(1,13)} = 0.06455$, $p = 0.8034$; interaction of different nosepokes × treatment condition: $F_{(1,13)} = 0.7395$, $p = 0.4054$] (**Figure 4D**). For the reinstatement tests, there was no differences in both active [main effect of the test condition: $F_{(1,13)} = 49.409$, $p < 0.001$; main effect of the treatment condition: $F_{(1,13)} = 0.040$, $p = 0.845$; interaction of test condition × treatment condition: $F_{(1,13)} = 0.382$, $p = 0.547$] (**Figure 4E** left column), and inactive [main effect of the test condition: $F_{(1,13)} = 0.693$, $p = 0.420$; main effect of the treatment condition: $F_{(1,13)} = 0.620$, $p = 0.445$; interaction of test condition × treatment condition: $F_{(1,13)} = 0.028$, $p = 0.870$] (**Figure 4E** right column) nosepokes between the two groups. For priming-induced reinstatement tests, repeated-measures ANOVA revealed no significant effect of active nosepokes [main effect

of the test condition: $F_{(1,13)} = 43.008$, $p < 0.001$; main effect of the treatment condition: $F_{(1,13)} = 0.349$, $p = 0.565$; interaction of test condition × treatment condition: $F_{(1,13)} = 0.058$, $p = 0.814$] (**Figure 4F** left column), and no significant difference in inactive nosepokes [main effect of the test condition: $F_{(1,13)} = 11.956$, $p = 0.004$; main effect of the treatment condition: $F_{(1,13)} = 0.690$, $p = 0.421$; interaction of test condition × treatment condition: $F_{(1,13)} = 0.204$, $p = 0.659$] (**Figure 4F** right column). There is no significant difference between the groups in all tests (all $p > 0.05$). These findings indicate that the effect of mTOR kinase inhibition via rapamycin on blocking reinstatement of cocaine seeking is time-limited, that is, this effect must occur within 6 h after retrieval.

DISCUSSION

The study first identified the critical role of mTOR in reconsolidation in the classic cocaine cue memory model. The main findings of this study are following: 1) Systemic administration of rapamycin immediately after retrieval of cocaine cue memory effectively reduced the cocaine-seeking behavior induced by drug-associated cues and the reinstatement of cocaine seeking induced by cocaine in rats; 2) The inhibitory effect of systemic rapamycin administration immediately after retrieval of cocaine cue memory on cocaine-seeking behavior persisted for least 28 days; 3) rapamycin when administered intraperitoneally with a 6 h delay or without a retrieval trial had no effects on cue-induced and cocaine-priming-induced reinstatement of cocaine-seeking behavior, indicating that the inhibitory effects of rapamycin on cocaine-seeking behavior is retrieval-dependent and temporal-specific.

In the current study, we utilized a classic intravenous cocaine self-administration paradigm to investigate the effect of rapamycin on drug memory reconsolidation. After establishing a stable pattern of cocaine self-administration, nosepoke behavior was extinguished. According to previous studies, nosepoke behavior in two operandi did not accompanied by light/tone stimulus during nosepoke extinction sessions, while during the retrieval trial session, the rats were exposed to the training chamber for 15 min and active nosepoke behavior was accompanied by tone/light stimulus (Lee et al., 2005; Sanchez et al., 2010; Wells et al., 2013; Shi et al., 2015). We have demonstrated that intraperitoneal injection of rapamycin immediately after memory retrieval inhibits mTOR activity. On the following test day, we found that inhibiting mTOR activity reduces the reinstatement of cocaine-seeking behavior induced by cued, subsequent cocaine-priming, and spontaneous recovery. However, inhibition of mTOR activity did not affect subsequent cue-induced behavior and cocaine-priming-induced cocaine-seeking when administered with a 6 h delay or without retrieval. These results indicate that the administration of rapamycin immediately after retrieval of cocaine cue memory disrupts the reconsolidation process of cocaine cue memory, rather than it inhibits the expression of cocaine cue memory. Growing evidence demonstrates that reconsolidation is a *de novo* protein-dependent process, which is completed within 6 h after retrieval. The effectiveness of interventions that destroy reconsolidation depends on the time window and the manipulation of memory retrieval (Nader et al., 2000; Alberini, 2005; Dudai, 2006; Luo et al., 2015). Our results indicate that inhibition of mTOR activity by rapamycin on the destruction of cocaine cue memory is retrieval-dependent and temporal-specific. These findings are consistent with the memory reconsolidation theory. These behavioral experiments demonstrate that the activity of mTOR mediates the reconsolidation of cocaine cue memory, and such process can be disrupted by rapamycin leading to a reduction of cocaine-seeking and prevention of relapse. However, the limitation of the current study is that we use systemic injections of rapamycin to block reconsolidation, which can't identify the mTOR activity of specific brain areas is involved in the reconsolidation of cocaine cue memory using the self-administration rats model. Previous studies have been shown that basolateral amydala (BLA) and nucleus accumbens core (NAcc) is critically involved in the reconsolidation of drug memories (Lee et al., 2005; Sanchez et al., 2010; Otis et al., 2015; Shi et al., 2015; Rich et al., 2016; Hafenbreidel et al., 2017; Bender B. N. and Torregrossa M. M., 2020). Considering mTOR is extensively expressed in the above mentioned brain regions (Caron et al., 2015) and rapamycin could cross the brain-blood barrier (Cloughesy et al., 2008), systemic injection of rapamycin could inhibit the activity of mTOR in the BLA and NAc. Therefore, the activity of mTOR in amygdala and/or NAc could be required for the reconsolidation of cocaine cue memories (Luo et al., 2013; Bender B. N. and Torregrossa M. M., 2020). Our future study will use microinjection method to identify the mTOR activity of specific brain areas is required for reconsolidation of cocaine cue memory in the rat self-administration model.

The mTOR signaling pathway regulates the downstream eukaryotic translation initiation factor, the eIF4E-binding protein 1 (4E-BP1) and ribosomal protein S6 kinases (S6Ks), it thus plays a critical role in the protein translation process (Peterson et al., 1999; Choi et al., 2002). mTOR alters the binding state of eIF4E and 4E-BP1 phosphorylation level to regulate the initiation of eukaryotic protein translation (Proud, 2007). mTOR activation increases the phosphorylation level of downstream S6Ks and promotes peptide chain elongation during protein translation (Wang et al., 2001; Holz et al., 2005). Hence, the mTOR signaling pathway regulates protein synthesis in eukaryotic cells via regulating the activity of downstream target proteins 4E-BP1 and S6Ks. Reconsolidation is a protein synthesis-dependent process, thus the mTOR signaling pathway may regulate reconsolidation of cocaine addiction memory through these mechanisms.

In addition, the mTOR signaling pathway can also affect the protein's translation, synthesis, apoptosis, and the occurrence and proliferation of tumor cells by regulating ribosome synthesis and downstream gene transcription (Sabatini et al., 1994). Furthermore, the activity of mTOR can also regulate downstream protein kinases, such as the activity of Akt and protein kinase C (PKC), and regulate the biosynthesis and metabolism of cytoskeleton-related proteins (Sarbassov et al., 2004; Sarbassov et al., 2005). Meanwhile, the protein kinases

including PKA, PKC, Akt, and biosynthesis and metabolism of cytoskeleton protein have been found to be involved in reconsolidation (Milton and Everitt, 2010; Neasta et al., 2010; Sanchez et al., 2010; Neasta et al., 2014; Ben Hamida et al., 2019; Morisot et al., 2019; Bender B. N. and Torregrossa M. M., 2020). Thus, we speculate that the mTOR signaling pathway may regulate the reconsolidation of cocaine addiction memory by affecting the protein kinase system and cytoskeleton proteins. Consistently, some previous studies have demonstrated that changes in synaptic plasticity mediated by mTORC1 and its downstream target proteins regulate alcohol intake and drug-seeking behavior in rats (Neasta et al., 2010; Neasta et al., 2014; Ben Hamida et al., 2019; Morisot et al., 2019).

Previous studies have also shown that immediate intraperitoneal rapamycin injection after reactivating memory by exposure to drug-associated environment can disrupt reconsolidation of cocaine, morphine, and alcohol-induced addiction memory in the CPP conditioned place preference paradigm (Lin et al., 2014). In the alcohol self-administration paradigm, it was also found that the activity of mTORC1 in CeA was increased after memory reactivation, and inhibition of mTOR1 activity in CeA with rapamycin was reported to destroy reconsolidation of alcohol addiction memory causing a reduction in reinstatement of alcohol-seeking behavior in rats (Barak et al., 2013). Both CPP and SA paradigms are classic animal models used to investigate addiction memory, but there are essential differences between them. The CPP model is based on classical conditioning learning and memory model, while the self-administration is based on operant conditioning. During the CPP conditioning, the experimental animals passively receive addictive drugs, and the dose is relatively lower as compared to the SA model. In intravenous self-administration model, experimental animals need to actively complete certain operational behaviors to obtain addictive drugs (de Wit and Stewart, 1981; Cami and Farre, 2003). Therefore, the SA paradigm mimics the characteristics of human drug addiction more closely that the CPP paradigm. In addition, a previous study found that microinjections of rapamycin into the nucleus accumbens (NAc) 30 min before the cocaine cue-induced reinstatement test inhibits the expression of drug-seeking behavior induced by the drug-associated cue in SA model. In this study, rapamycin was administered before the cue-induced drug-seeking behavior test, which verified the role of mTOR activity in the expression of cocaine addiction memory in rats. It has also been shown that exposure to the cocaine-associated environment increases the mTOR activity and the phosphorylation level of the p70s6k-rps6 downstream pathway in the rat NAc core, but not the NAc shell (Wang et al., 2010). Our results indicate that reactivation of cocaine addiction memory activates the mTOR signaling pathway, and we can deduce that the mTOR signaling pathway is involved in memory reconsolidation. Consistent with these previous studies, the present research further identifies the critical role of the mTOR signaling pathway in reconsolidation of addiction memory using the operational cocaine cue memory model.

In summary, our findings demonstrated that the mTOR activity plays a critical role in the reconsolidation of cocaine cue memory using the operational cocaine SA paradigm. Administration of rapamycin immediately after memory reactivation disrupts reconsolidation of the cocaine cue memory, leading to a reduction in reinstatement of cocaine seeking behavior in rats. The present study identifies the mTOR signaling pathway as a promising target for treating cocaine addiction and preventing relapse.

DATA AVAILABILITY STATEMENT

The raw data supporting the conclusions of this article will be made available by the authors, without undue reservation.

ETHICS STATEMENT

The animal study was reviewed and approved by the Local Committee on Animal Care and Use and Protection of the Hunan Normal University.

AUTHOR CONTRIBUTIONS

YL and XJ designed and supervised this study. FZ, SH, HB, LC, LC, HY, YZ, and ZK carried out main experiments. FZ, SH, and HB prepared the manuscript. JY and CY analyze the data. YL and XJ contributed to manuscript revision with contributions from all of the other authors.

FUNDING

This work was supported in part by the Natural Science Foundation of China (no. 81771434, and 81501150), Outstanding Innovative Youth Training Program of Changsha (kq1905032). Hunan province college students research learning and innovative experiment project (S201910542034).

REFERENCES

Abraham, R. T., and Wiederrecht, G. J. (1996). Immunopharmacology of rapamycin. *Annu. Rev. Immunol.* 14, 483–510. doi:10.1146/annurev.immunol.14.1.483

Ahmed, S. H., Badiani, A., Miczek, K. A., and Müller, C. P. (2020). Non-pharmacological factors that determine drug use and addiction. *Neurosci. Biobehavioral Rev.* 110, 3–27. doi:10.1016/j.neubiorev.2018.08.015

Alberini, C. M. (2005). Mechanisms of memory stabilization: are consolidation and reconsolidation similar or distinct processes?. *Trends Neurosciences* 28, 51–56. doi:10.1016/j.tins.2004.11.001

Barak, S., Liu, F., Hamida, S. B., Yowell, Q. V., Neasta, J., Kharazia, V., et al. (2013). Disruption of alcohol-related memories by mTORC1 inhibition prevents relapse. *Nat. Neurosci.* 16, 1111–1117. doi:10.1038/nn.3439

Ben Hamida, S., Laguesse, S., Morisot, N., Park, J.-H., Phuamluong, K., Berger, A. L., et al. (2019). Mammalian target of rapamycin complex 1 and its downstream effector collapsin response mediator protein-2 drive reinstatement of alcohol reward seeking. *Addict. Biol.* 24, 908–920. doi:10.1111/adb.12653

Bender, B. N., and Torregrossa, M. M. (2020a). Molecular and circuit mechanisms regulating cocaine memory. *Cell Mol Life Sci.* 77(19):3745-3768. doi:10.1007/s00018-020-03498-8

Bender, B. N., and Torregrossa, M. M. (2020b). Molecular and circuit mechanisms regulating cocaine memory. *Cell. Mol. Life Sci.* 77, 3745–3768. doi:10.1007/s00018-020-03498-8

Brown, E. J., Albers, M. W., Bum Shin, T., Ichikawa, K., Keith, C. T., Lane, W. S., et al. (1994). A mammalian protein targeted by G1-arresting rapamycin-receptor complex. *Nature* 369, 756–758. doi:10.1038/369756a0

Camí, J., and Farré, M. (2003). Drug addiction. *N. Engl. J. Med.* 349, 975–986. doi:10.1056/nejmra023160

Caron, A., Baraboi, E.-D., Laplante, M., and Richard, D. (2015). DEP domain-containing mTOR-interacting protein in the rat brain: distribution of expression and potential implication. *J. Comp. Neurol.* 523, 93–107. doi:10.1002/cne.23668

Childress, A. R., Mclellan, A. T., and O'Brien, C. P. (1986). Role of conditioning factors in the development of drug dependence. *Psychiatr. Clin. North America* 9, 413–425. doi:10.1016/s0193-953x(18)30603-8

Childress, A. R., Mozley, P. D., Mcelgin, W., Fitzgerald, J., Reivich, M., and O'Brien, C. P. (1999). Limbic activation during cue-induced cocaine craving. *Ajp* 156, 11–18. doi:10.1176/ajp.156.1.11

Choi, J. H., Bertram, P. G., Drenan, R., Carvalho, J., Zhou, H. H., and Zheng, X. F. S. (2002). The FKBP12-rapamycin-associated protein (FRAP) is a CLIP-170 kinase. *EMBO Rep.* 3, 988–994. doi:10.1093/embo-reports/kvf197

Cloughesy, T. F., Yoshimoto, K., Nghiemphu, P., Brown, K., Dang, J., Zhu, S., et al. (2008). Antitumor activity of rapamycin in a Phase I trial for patients with recurrent PTEN-deficient glioblastoma. *Plos Med.* 5, e8. doi:10.1371/journal.pmed.0050008

Dash, P. K., Orsi, S. A., and Moore, A. N. (2006). Spatial memory formation and memory-enhancing effect of glucose involves activation of the tuberous sclerosis complex-Mammalian target of rapamycin pathway. *J. Neurosci.* 26, 8048–8056. doi:10.1523/jneurosci.0671-06.2006

De Wit, H., and Stewart, J. (1981). Reinstatement of cocaine-reinforced responding in the rat. *Psychopharmacology* 75, 134–143. doi:10.1007/bf00432175

Dudai, Y. (1996). Consolidation: fragility on the road to the engram. *Neuron* 17, 367–370. doi:10.1016/s0896-6273(00)80168-3

Dudai, Y. (2006). Reconsolidation: the advantage of being refocused. *Curr. Opin. Neurobiol.* 16, 174–178. doi:10.1016/j.conb.2006.03.010

Everitt, B. J., Parkinson, J. A., Olmstead, M. C., Arroyo, M., Robledo, P., and Robbins, T. W. (1999). Associative processes in addiction and reward the role of amygdala-ventral striatal subsystems. *Ann. NY Acad Sci* 877, 412–438. doi:10.1111/j.1749-6632.1999.tb09280.x

Grant, S., London, E. D., Newlin, D. B., Villemagne, V. L., Liu, X., Contoreggi, C., et al. (1996). Activation of memory circuits during cue-elicited cocaine craving. *Proc. Natl. Acad. Sci.* 93, 12040–12045. doi:10.1073/pnas.93.21.12040

Hafenbreidel, M., Rafa Todd, C., and Mueller, D. (2017). Infralimbic GluN2A-containing NMDA receptors modulate reconsolidation of cocaine self-administration memory. *Neuropsychopharmacol* 42, 1113–1125. doi:10.1038/npp.2016.288

Hellemans, K. G. C., Everitt, B. J., and Lee, J. L. C. (2006). Disrupting reconsolidation of conditioned withdrawal memories in the basolateral amygdala reduces suppression of heroin seeking in rats. *J. Neurosci.* 26, 12694–12699. doi:10.1523/jneurosci.3101-06.2006

Holz, M. K., Ballif, B. A., Gygi, S. P., and Blenis, J. (2005). mTOR and S6K1 mediate assembly of the translation preinitiation complex through dynamic protein interchange and ordered phosphorylation events. *Cell* 123, 569–580. doi:10.1016/j.cell.2005.10.024

Hyman, S. E., Malenka, R. C., and Nestler, E. J. (2006). Neural mechanisms of addiction: the role of reward-related learning and memory. *Annu. Rev. Neurosci.* 29, 565–598. doi:10.1146/annurev.neuro.29.051605.113009

Jentsch, J. D., and Taylor, J. R. (1999). Impulsivity resulting from frontostriatal dysfunction in drug abuse: implications for the control of behavior by reward-related stimuli. *Psychopharmacology* 146, 373–390. doi:10.1007/pl00005483

Kelley, A. E. (2004). Memory and addiction. *Neuron* 44, 161–179. doi:10.1016/j.neuron.2004.09.016

Kilts, C. D., Schweitzer, J. B., Quinn, C. K., Gross, R. E., Faber, T. L., Muhammad, F., et al. (2001). Neural activity related to drug craving in cocaine addiction. *Arch. Gen. Psychiatry* 58, 334–341. doi:10.1001/archpsyc.58.4.334

Laplante, M., and Sabatini, D. M. (2012). mTOR signaling in growth control and disease. *Cell* 149, 274–293. doi:10.1016/j.cell.2012.03.017

Lee, J. L. C., Di Ciano, P., Thomas, K. L., and Everitt, B. J. (2005). Disrupting reconsolidation of drug memories reduces cocaine-seeking behavior. *Neuron* 47, 795–801. doi:10.1016/j.neuron.2005.08.007

Lin, J., Liu, L., Wen, Q., Zheng, C., Gao, Y., Peng, S., et al. (2014). Rapamycin prevents drug seeking via disrupting reconsolidation of reward memory in rats. *Int. J. Neuropsychopharm.* 17, 127–136. doi:10.1017/s1461145713001156

Lu, L., Hope, B. T., Dempsey, J., Liu, S. Y., Bossert, J. M., and Shaham, Y. (2005). Central amygdala ERK signaling pathway is critical to incubation of cocaine craving. *Nat. Neurosci.* 8, 212–219. doi:10.1038/nn1383

Luo, Y.-X., Xue, Y.-X., Shen, H.-W., and Lu, L. (2013). Role of amygdala in drug memory. *Neurobiol. Learn. Mem.* 105, 159–173. doi:10.1016/j.nlm.2013.06.017

Luo, Y. X., Xue, Y. X., Liu, J. F., Shi, H. S., Jian, M., Han, Y., et al. (2015). A novel UCS memory retrieval-extinction procedure to inhibit relapse to drug seeking. *Nat. Commun.* 6, 7675. doi:10.1038/ncomms8675

Mcgaugh, J. L. (2000). Memory--a century of consolidation. *Science* 287, 248–251. doi:10.1126/science.287.5451.248

Milton, A. L., and Everitt, B. J. (2010). The psychological and neurochemical mechanisms of drug memory reconsolidation: implications for the treatment of addiction. *Eur. J. Neurosci.* 31, 2308–2319. doi:10.1111/j.1460-9568.2010.07249.x

Milton, A. L., Lee, J. L. C., Butler, V. J., Gardner, R., and Everitt, B. J. (2008a). Intra-amygdala and systemic antagonism of NMDA receptors prevents the reconsolidation of drug-associated memory and impairs subsequently both novel and previously acquired drug-seeking behaviors. *J. Neurosci.* 28, 8230–8237. doi:10.1523/jneurosci.1723-08.2008

Milton, A. L., Lee, J. L. C., and Everitt, B. J. (2008b). Reconsolidation of appetitive memories for both natural and drug reinforcement is dependent on -adrenergic receptors. *Learn. Mem.* 15, 88–92. doi:10.1101/lm.825008

Morisot, N., Phamluong, K., Ehinger, Y., Berger, A. L., Moffat, J. J., and Ron, D. (2019). mTORC1 in the orbitofrontal cortex promotes habitual alcohol seeking. *Elife* 8. doi:10.7554/elife.51333

Nader, K., and Hardt, O. (2009). A single standard for memory: the case for reconsolidation. *Nat. Rev. Neurosci.* 10, 224–234. doi:10.1038/nrn2590

Nader, K., Schafe, G. E., and Le Doux, J. E. (2000). Fear memories require protein synthesis in the amygdala for reconsolidation after retrieval. *Nature* 406, 722–726. doi:10.1038/35021052

Neasta, J., Barak, S., Hamida, S. B., and Ron, D. (2014). mTOR complex 1: a key player in neuroadaptations induced by drugs of abuse. *J. Neurochem.* 130, 172–184. doi:10.1111/jnc.12725

Neasta, J., Ben Hamida, S., Yowell, Q., Carnicella, S., and Ron, D. (2010). Role for mammalian target of rapamycin complex 1 signaling in neuroadaptations underlying alcohol-related disorders. *Proc. Natl. Acad. Sci.* 107, 20093–20098. doi:10.1073/pnas.1005554107

Nestler, E. J. (2001). Molecular neurobiology of addiction. *Am. J. Addict.* 10, 201–217. doi:10.1080/105504901750532094

O'brien, C. P., Childress, A. R., Ehrman, R., and Robbins, S. J. (1998). Conditioning factors in drug abuse: can they explain compulsion?. *J. Psychopharmacol.* 12, 15–22. doi:10.1177/026988119801200103

Otis, J. M., Werner, C. T., and Mueller, D. (2015). Noradrenergic regulation of fear and drug-associated memory reconsolidation. *Neuropsychopharmacol* 40, 793–803. doi:10.1038/npp.2014.243

Parsons, R. G., Gafford, G. M., and Helmstetter, F. J. (2006). Translational control via the mammalian target of rapamycin pathway is critical for the formation and stability of long-term fear memory in amygdala neurons. *J. Neurosci.* 26, 12977–12983. doi:10.1523/jneurosci.4209-06.2006

Peterson, R. T., Desai, B. N., Hardwick, J. S., and Schreiber, S. L. (1999). Protein phosphatase 2A interacts with the 70-kDa S6 kinase and is activated by

inhibition of FKBP12-rapamycinassociated protein. *Proc. Natl. Acad. Sci.* 96, 4438–4442. doi:10.1073/pnas.96.8.4438

Proud, C. G. (2007). Signalling to translation: how signal transduction pathways control the protein synthetic machinery. *Biochem. J.* 403, 217–234. doi:10.1042/bj20070024

Rich, M. T., Abbott, T. B., Chung, L., Gulcicek, E. E., Stone, K. L., Colangelo, C. M., et al. (2016). Phosphoproteomic analysis reveals a novel mechanism of CaMKII regulation inversely induced by cocaine memory extinction versus reconsolidation. *J. Neurosci.* 36, 7613–7627. doi:10.1523/jneurosci.1108-16.2016

Robbins, T. W., Ersche, K. D., and Everitt, B. J. (2008). Drug addiction and the memory systems of the brain. *Ann. N. Y Acad. Sci.* 1141, 1–21. doi:10.1196/annals.1441.020

Sabatini, D. M., Erdjument-Bromage, H., Lui, M., Tempst, P., and Snyder, S. H. (1994). RAFT1: a mammalian protein that binds to FKBP12 in a rapamycin-dependent fashion and is homologous to yeast TORs. *Cell* 78, 35–43. doi:10.1016/0092-8674(94)90570-3

Sanchez, H., Quinn, J. J., Torregrossa, M. M., and Taylor, J. R. (2010). Reconsolidation of a cocaine-associated stimulus requires amygdalar protein kinase A. *J. Neurosci.* 30, 4401–4407. doi:10.1523/jneurosci.3149-09.2010

Sara, S. J. (2000). Retrieval and reconsolidation: toward a neurobiology of remembering. *Learn. Mem.* 7, 73–84. doi:10.1101/lm.7.2.73

Sarbassov, D. D., Ali, S. M., Kim, D. H., Guertin, D. A., Latek, R. R., Erdjument-Bromage, H., et al. (2004). Rictor, a novel binding partner of mTOR, defines a rapamycin-insensitive and raptor-independent pathway that regulates the cytoskeleton. *Curr. Biol.* 14, 1296–1302. doi:10.1016/j.cub.2004.06.054

Sarbassov, D. D., Guertin, D. A., Ali, S. M., and Sabatini, D. M. (2005). Phosphorylation and regulation of Akt/PKB by the rictor-mTOR complex. *Science* 307, 1098–1101. doi:10.1126/science.1106148

Schmelzle, T., and Hall, M. N. (2000). TOR, a central controller of cell growth. *Cell* 103, 253–262. doi:10.1016/s0092-8674(00)00117-3

Shi, H. S., Luo, Y. X., Yin, X., Wu, H. H., Xue, G., Geng, X. H., et al. (2015). Reconsolidation of a cocaine associated memory requires DNA methyltransferase activity in the basolateral amygdala. *Sci. Rep.* 5, 13327. doi:10.1038/srep13327

Taylor, J. R., Olausson, P., Quinn, J. J., and Torregrossa, M. M. (2009). Targeting extinction and reconsolidation mechanisms to combat the impact of drug cues on addiction. *Neuropharmacology* 56 (Suppl. 1), 186–195. doi:10.1016/j.neuropharm.2008.07.027

Torregrossa, M. M., Corlett, P. R., and Taylor, J. R. (2011). Aberrant learning and memory in addiction. *Neurobiol. Learn. Mem.* 96, 609–623. doi:10.1016/j.nlm.2011.02.014

Volkow, N. D., and Boyle, M. (2018). Neuroscience of addiction: relevance to prevention and treatment. *Ajp* 175, 729–740. doi:10.1176/appi.ajp.2018.17101174

Wang, X., Li, W., Williams, M., Terada, N., Alessi, D. R., and Proud, C. G. (2001). Regulation of elongation factor 2 kinase by p90RSK1 and p70 S6 kinase. *EMBO J.* 20, 4370–4379. doi:10.1093/emboj/20.16.4370

Wang, X., Luo, Y.-x., He, Y.-y., Li, F.-q., Shi, H.-s., Xue, L.-f., et al. (2010). Nucleus accumbens core mammalian target of rapamycin signaling pathway is critical for cue-induced reinstatement of cocaine seeking in rats. *J. Neurosci.* 30, 12632–12641. doi:10.1523/jneurosci.1264-10.2010

Wells, A. M., Arguello, A. A., Xie, X., Blanton, M. A., Lasseter, H. C., Reittinger, A. M., et al. (2013). Extracellular signal-regulated kinase in the basolateral amygdala, but not the nucleus accumbens core, is critical for context-response-cocaine memory reconsolidation in rats. *Neuropsychopharmacol* 38, 753–762. doi:10.1038/npp.2012.238

Xue, Y.-X., Luo, Y.-X., Wu, P., Shi, H.-S., Xue, L.-F., Chen, C., et al. (2012). A memory retrieval-extinction procedure to prevent drug craving and relapse. *Science* 336, 241–245. doi:10.1126/science.1215070

Zubedat, S., and Akirav, I. (2017). The involvement of cannabinoids and mTOR in the reconsolidation of an emotional memory in the hippocampal-amygdala-insular circuit. *Eur. Neuropsychopharmacol.* 27, 336–349. doi:10.1016/j.euroneuro.2017.01.011

Conflict of Interest: The authors declare that the research was conducted in the absence of any commercial or financial relationships that could be construed as a potential conflict of interest.

frontiers in Pharmacology

ORIGINAL RESEARCH
published: 12 April 2021
doi: 10.3389/fphar.2021.624127

Cocaine Reduces the Neuronal Population While Upregulating Dopamine D2-Receptor-Expressing Neurons in Brain Reward Regions: Sex-Effects

Kevin Clare[1], Chelsea Pan[1], Gloria Kim[1], Kicheon Park[1], Juan Zhao[2], Nora D. Volkow[3], Zhicheng Lin[2]* and Congwu Du[1]**

[1]Department of Biomedical Engineering, Stony Brook University, Stony Brook, NY, United States, [2]Laboratory of Psychiatric Neurogenomics, Basic Neuroscience Division, McLean Hospital, Belmont, MA, United States, [3]National Institute on Drug Abuse, Bethesda, MD, United States

OPEN ACCESS

Edited by:
Qi Wang,
Southern Medical University, China

Reviewed by:
Briac Halbout,
University of California Irvine, United States
Teng Chen,
Xi'an Jiaotong University, China

***Correspondence:**
Nora D. Volkow
nvolkow@nida.nih.gov
Zhicheng Lin
Zhicheng_Lin@hms.harvard.edu
Congwu Du
congwu.du@stonybrook.edu

Specialty section:
This article was submitted to Neuropharmacology, a section of the journal Frontiers in Pharmacology

Received: 30 October 2020
Accepted: 08 February 2021
Published: 12 April 2021

Citation:
Clare K, Pan C, Kim G, Park K, Zhao J, Volkow ND, Lin Z and Du C (2021) Cocaine Reduces the Neuronal Population While Upregulating Dopamine D2-Receptor-Expressing Neurons in Brain Reward Regions: Sex-Effects. Front. Pharmacol. 12:624127. doi: 10.3389/fphar.2021.624127

Addiction to cocaine is associated with dysfunction of the dopamine mesocortical system including impaired dopamine-2 receptor (D2r) signaling. However, the effects of chronic cocaine on neuronal adaptations in this system have not been systematically examined and data available is mostly from males. Here, we investigated changes in the total neuronal density and relative concentration of D2r-expressing neurons in the medial prefrontal cortex (mPFC), dorsal striatum (Dstr), nucleus accumbens (NAc), and ventral tegmental area (VTA) in both male and female mice passively exposed to cocaine for two weeks. In parallel experiments, we measured mRNA levels for *Drd2* and for opioid peptides (m*Penk* and m*Pdyn*). Through a combination of large field of view fluorescent imaging with BAC transgenic D2r-eGFP mice and immunostaining, we observed that cocaine exposed mice had a higher density of D2r-positive cells that was most prominent in mPFC and VTA and larger for females than for males. This occurred amidst an overall significant decrease in neuronal density (measured with NeuN) in both sexes. However, increases in *Drd2* mRNA levels with cocaine were only observed in mPFC and Dstr in females, which might reflect the limited sensitivity of the method. Our findings, which contrast with previous findings of cocaine-induced downregulation of D2r binding availability, could reflect a phenotypic shift in neurons that did not previously express *Drd2* and merits further investigation. Additionally, the neuronal loss particularly in mPFC with chronic cocaine might contribute to the cognitive impairments observed with cocaine use disorder.

Keywords: cocaine, dopamine-2 receptor, dynorphin, enkephalin, neuroadaptation, sex differences

INTRODUCTION

Addiction is a chronic disease which manifests by compulsive drug seeking and use that is difficult to control despite harmful consequences (Koob and Volkow, 2016). The involvement of dopamine in drug reinforcement is well recognized, but its role in addiction is less clear (Uhl et al., 2002). Imaging studies in drug addicted individuals have shown that dopamine function is markedly disrupted as reflected by decreases in dopamine (DA) release and in DA D2 receptor (D2r) availability in striatum

(Volkow and Fowler, 2000). The reduced striatal D2r availability is associated with reduced activity in the medial and ventral prefrontal cortex–regions involved in salience attribution and motivation, which could underlie the compulsiveness of drug taking in addiction (Jasinska et al., 2015; Porrino et al., 2016). In parallel, studies in laboratory animals have also documented the involvement of the dopamine mesocortical system in addiction, including the substantia nigra (SN) and ventral tegmental area (VTA) midbrain regions with their striatal targets to dorsal striatum (Dstr) and nucleus accumbens (NAc) and cortical targets to the medial prefrontal cortex (mPFC) (Koob and Volkow, 2010). Preclinical studies have also reported reduced D2r levels in Dstr and NAc along with evidence of neuronal loss in mPFC and striatal regions with chronic cocaine exposure (Stefański et al., 2007; George et al., 2008). However, the systematic analyses of changes in D2r and neuronal loss in the various regions of the DA mesocortical system with chronic cocaine exposure as a function of sex to our knowledge has not been investigated. This is relevant since women when compared to men transition faster from occasional to compulsive cocaine intake and those with cocaine use disorder experience more cravings, withdrawal symptoms, and worse outcomes (Griffin et al., 1989; Robbins et al., 1999; Van Etten and Anthony, 2001; Becker and Koob, 2016). Similarly, studies in laboratories animals have reported significant sex differences in the locomotor and rewarding effects of cocaine (Kokane and Perrotti, 2020).

Here we aimed to assess the changes in total neuronal density and in the density of D2r expressing neurons in mesocortical dopamine regions (Dstr, NAc, VTA, and PFC) after repeated cocaine exposure. For this purpose, we combined a transgenic mouse model of D2r-enhanced GFP (D2r-eGFP) with immunostaining and fluorescence microscopy, which allowed us to separately visualize and quantify D2r-expressing and non-D2r neurons (Gong et al., 2003). In a separate group of wild-type (WT) mice we assessed the effects of cocaine on mRNA levels of D2r (m*Drd2*) and proenkephalin (m*Penk*) genes, which are genes that are co-expressed in D2r expressing neurons in striatum. As control, we measured the prodynorphin (m*Pdyn*) gene, which in striatum is expressed in dopamine 1 (D1) receptor expressing neurons (Whitfield et al., 2015). We hypothesized that chronic cocaine would result in neuronal loss and loss of D2r expressing neurons in striatum and PFC in parallel with a reduction in the mRNA levels of *Drd2* and *Penk*. We anticipate that the effects would be greater in females than in male mice.

MATERIALS AND METHODS

Animals and Drug Treatments

All experiments were approved by the Institutional Animal Care and Use Committee at Stony Brook University. The transgenic mouse strain, Tg(Drd2-eGFP)S118Gsat (in which eGFP was expressed under the *Drd2* promoter; D2r-eGFP (Gong et al., 2003)) as well as C57BL/6 WT animals were used. We studied 74 mice (age 4 months, males and females) comprised of two genotypes derived from C57BL/6 background, of whom 48 were used for immunohistochemistry and fluorescent microscopy imaging (**Figures 1A,C**; **Table 1**), and 26 for mRNA quantification (**Figure 1B**; **Table 1**). The mRNA and D2r immunostaining quantification studies were done in WT C57BL/6. All animals were kept on a reverse 12 h on/off light cycle with *ad libitum* access to food and water.

The protocol of the drug pretreatment is illustrated in **Figure 1**. For all experiments, animals received the same treatment schedule: Cocaine mice received daily intraperitoneal (i.p.) injections of 30 mg/kg cocaine for 14 consecutive days followed by 24 h withdrawal prior to euthanizing. This dose of cocaine was chosen because previous studies had demonstrated its ability to recreate addiction behaviors and our imaging studies have shown that this protocol induced pathophysiological changes relevant to clinical adverse consequences from cocaine use including cerebral ischemia and transient ischemic attacks (Zombeck et al., 2009; Rappeneau et al., 2015; You et al., 2017). The control group was injected i.p. with 10cc/kg of saline daily following the same protocol as the cocaine treatment group.

Immunohistochemistry

Mice were given a lethal dose of anesthesia and then perfused transcardially with cold 1x phosphate buffered saline (PBS) followed by 4% paraformaldehyde (PFA). The brain tissue was collected and immersed in 4% PFA overnight at 4°C for further fixation. After 24 h in PFA, the tissue was transferred to a 30% sucrose solution in 1x PBS to cryoprotect it. The brain was then frozen at −80°C until sectioning. Similar to prior investigations into D2r expression, sections with a thickness of 50 µm were collected in mPFC, Dstr, NAc and VTA (**Figures 2–6** provide location of sampling) (Lawhorn et al., 2013; Cheng et al., 2017; Gagnon et al., 2017; Wei et al., 2018; Dobbs et al., 2019). These sections were free floated and transferred to slides prior to staining. Slides were either stained on the same day (for Group 1B, Group 3, Group 4B, and Group 6 in **Table 1**) or frozen at −80°C for imaging without staining (Group 1A and Group 4A).

The Tg(Drd2-eGFP)S118Gsat mice were divided into two groups, one received saline (n = 19; **Table 1**: Group 1A,B) and the other cocaine (n = 23; **Table 1**: Group 4A,B). Each group comprised two subgroups, one (Group 1A and 4A in **Table 1**) was used to measure D2r fluorescence intensity in the striatum and the other (Group 1B and Group 4B in **Table 1**) was used for GFP and NeuN staining. For immunohistochemistry, we first washed the slides 3 times with 1x PBS followed by blocking with a solution containing 4% donkey serum, 0.03% Triton-X and 30 mg/ml of Bovine Serum Albumin (BSA) in 1x PBS. After blocking at room temperature for 1 h, slides were washed 5 times and the primary antibody solution containing 4% donkey serum, 0.03% Triton-X, chicken anti-GFP antibody (1: 200, Thermofischer), and mouse anti-Neun antibody (1:200, Millpore) added. The slides were incubated in the solution at 4°C overnight on a shaker at 100 rpm. Prior to adding the secondary antibody solution, the slides were washed 6 times with 1x PBS followed by addition of the secondary antibody. This solution included 4% donkey serum, 0.03% Triton-X, Alexa-fluro 488 donkey anti-chicken (1:200, Jackson Immunoresearch), and Alex-fluro 594 donkey anti-mouse (1:200, Jackson Immunoresearch). After incubating in the secondary antibody at 4°C overnight on a shaker, the slides were washed 6 times with 1x PBS and a mounting media containing DAPi added. Slides were then cover slipped and imaged on a fluorescent microscope.

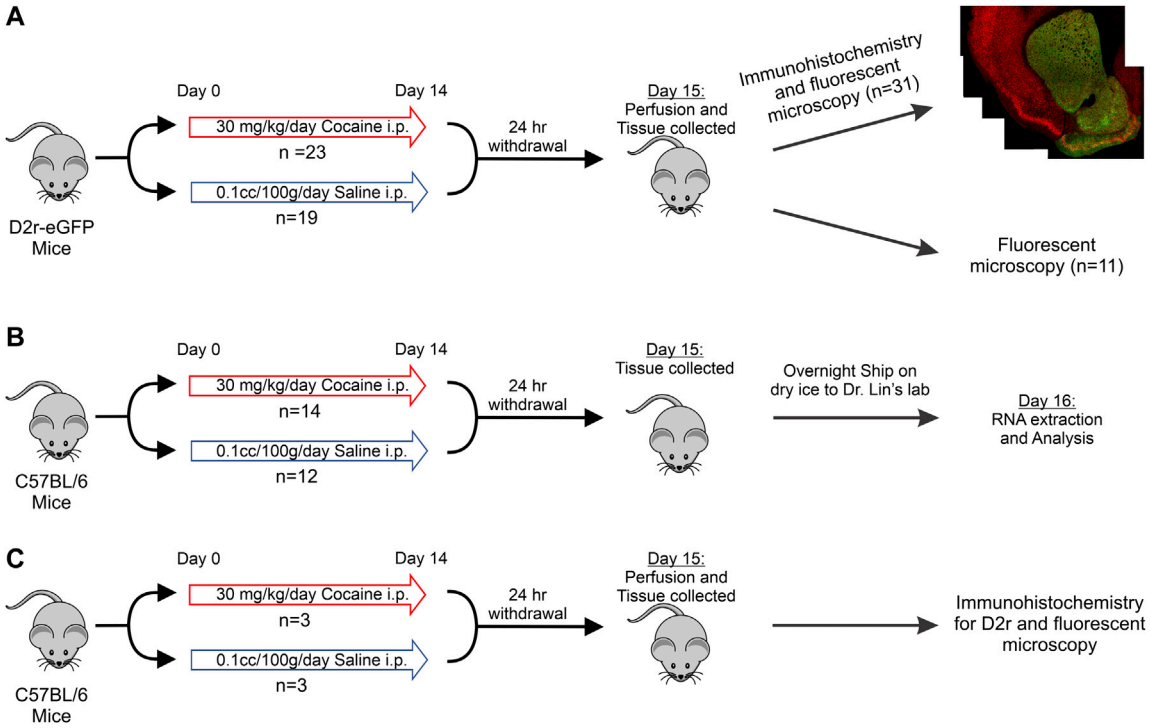

FIGURE 1 | Schematic of the experimental protocol and timeline. **(A)**: D2r-eGFP tissue collection with immunohistochemistry for eGFP and NeuN or no immunohistochemistry for eGFP intensity quantification; **(B)**: C57BL/6 tissue collection and mRNA analysis; **(C)**: Drug treatment, immunohistochemistry, and imaging of Drd2 in C57BL/6 mice.

We chose NeuN over other neuronal CNS markers, such as synaptophysin, to quantify the neuronal population for it localizes only in the nuclei of neurons and not in glia and its nuclear location allows easy segmentation and quantification of neuronal density (Gusel'nikova and Korzhevskiy, 2015).

To detect D2r expression in C57BL/6 mice (**Table 1**: Group 3 and 6), the same protocol as outlined above for immunohistochemistry was utilized with the primary antibody rabbit anti-Drd2 (1:200, Millipore Sigma, AB5084P) and the secondary antibody Alex-fluro 594 donkey anti-rabbit (1:200, Jackson Immunoresearch).

Fluorescent Microscopy and Image Analysis

Images were captured on a Nikon fluorescent microscope under white light at 4x to evaluate the A/P location of the section followed by imaging at 10X for each brain region. Accurate representation was achieved by nine random single focal images for each condition via different animals. Specifically, for each animal we created a mosaic of the brain region for three different brain sections. Each mosaic was composed of multiple images (~40, as illustrated in **Figure 1A**) and montaged together to compose a large field of view image while retaining resolution for cell counting. In total, we obtained from each animal 12 sets of images, 3 for mPFC, 3 for Dstr, 3 for NAc and 3 for VTA with an average image dimension of 1.5 mm × 1.2 mm x 0.05 mm (length x width x depth).

Density of cells in each image was quantified using a custom ImageJ (NIH) macro to count the number of cells in the brain region. For each brain section, we quantified 3 ROI. Therefore, for a brain region (i.e., mPFC) with 14 control mice, a total of 126 ROIs were analyzed (3 ROI/section * 3 sections/animal * 14 animals = 126). Meanwhile, a total of 117 ROI were analyzed for the mixed mPFC cocaine group (n = 17; 3 ROI/section * 3 sections/animal * 17 animals = 153). The cell number from the macro was normalized to the volume of the brain region quantified to compute cell density. Once the cell density for each brain region was obtained, we averaged them to calculate the cell density for each specific region. Data are presented as the percent change in cell density relative to the saline controls for a specific group (i.e. percent change in D2r cell density in male cocaine exposed mice is relative to D2r cell density in saline exposed male mice).

Images for quantifying D2r-eGFP signaling without immunohistochemistry were capture on a Nikon fluorescent microscope at 10X. In total, 25 images from 6 control animals and 18 images from 5 cocaine animals were obtained from the dorsal striatum. The signal to noise ratio (SNR) was calculated by measuring the average intensity of GFP positive cells relative to background fluorescence intensity.

RNA Extraction

Two groups of C57BL/6 background mice were used for molecular analysis, half received saline (10cc/kg, i.p. daily

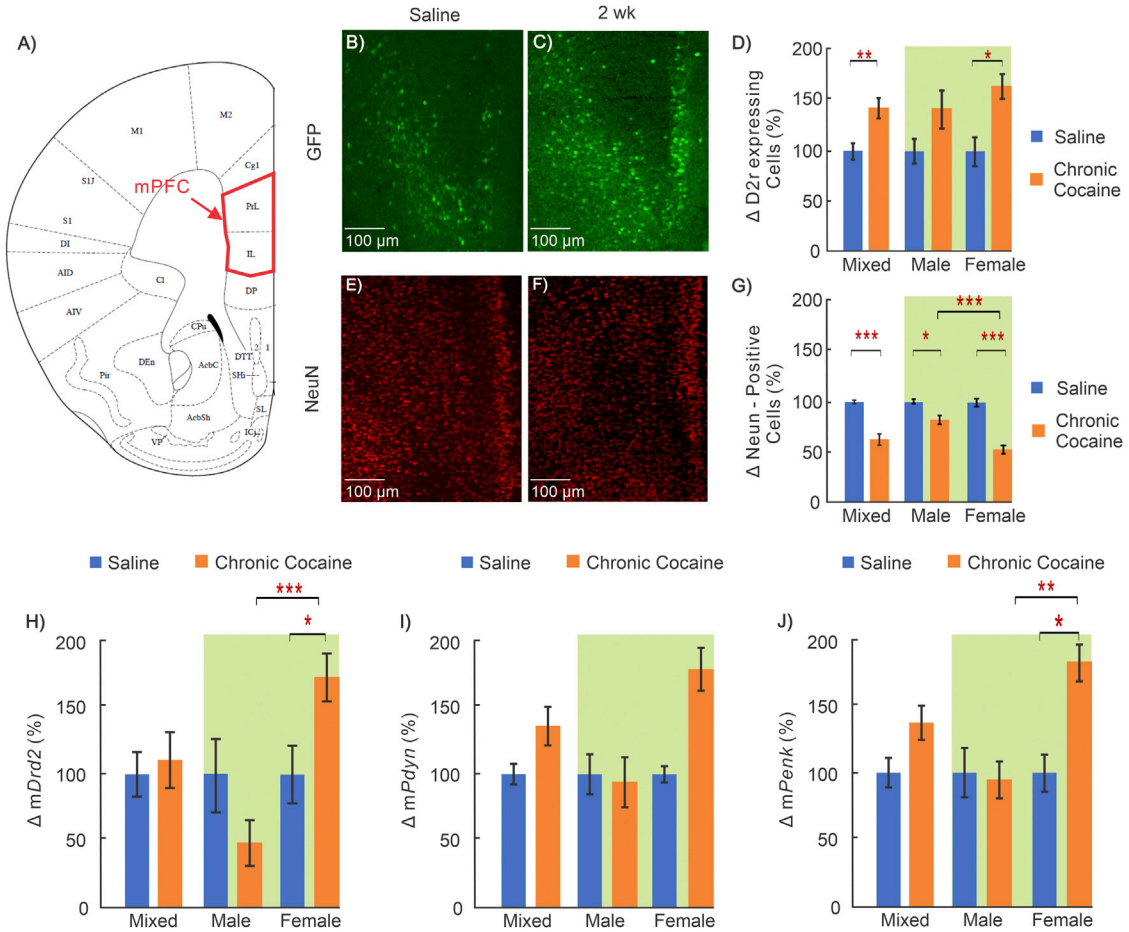

FIGURE 2 | Cocaine effects in medial prefrontal cortex (mPFC). **(A)**: Mouse brain atlas showing the location of the microscopic images in mPFC (George and Franklin, 2001); **(B–C)**: "Zoom-in" GFP in mPFC of a saline and cocaine treated animal; **(D)**: Comparison of D2r-GFP expressing neurons in mPFC in saline (n = 14; 5 ♀, 9 ♂) and cocaine (n = 13; 6 ♀, 7 ♂) treated animals. **(E–F)**: Corresponding NeuN images in mPFC of a saline treated and cocaine treated mouse; **(G)**: Comparison of neurons in mPFC between saline (n = 10; 5 ♀, 5 ♂) and cocaine treated animals (n = 10; 6 ♀, 4 ♂); **(H–J)**: Comparison of mRNA levels between saline (n = 12; 6 ♀, 6 ♂) and cocaine (n = 14; 7 ♀, 7 ♂) treated WT mice for *Drd2* **(H)**, *Pdyn* **(I)**, and *Penk* **(J)**. Mixed: males and females; female: females only; male: males only; *: $p < 0.05$; **: $p < 0.005$; ***: $p < 0.001$. Blue bars correspond to saline and orange ones to cocaine treated mice. Green background indicates data included in two-way ANOVA. Values show averages and SE.

for 14 days; Group 2 in **Table 1**), and the other cocaine (30 mg/kg/day, i.p. daily for 14 days; Group 5 in **Table 1**). Twenty-four hours after completion of the 14 days treatment period, animals were deeply anesthetized with isoflurane and decapitated. The brain tissue was then collected from mPFC, Dstr, NAc and VTA through manual dissection using a mouse brain atlas to ensure accurate and consistent dissection. The brain tissue samples were frozen at −80°C for 5 h and shipped overnight on dry ice to Dr. Lin's laboratory for RNA analysis. Total RNA was isolated by using TRIzol reagents (Ambion, MA, United States) following the manufacturer's protocol. 30 µl RNase-free water was used for reconstitution. RNA concentration was determined with NanoDrop Lit (Thermoscientific, MA, United States). Usually 3 µg RNA could be extracted from 3 mg of mouse brain tissue. Samples were stored at −80°C till cDNA synthesis.

cDNA Synthesis

100 ng RNA was reverse transcribed into cDNA using a Verso cDNA synthesis kit (Thermoscientific, MA, United States) with oligo dT primers following the manufacturer's protocol. cDNA was diluted by 10 folds with DNase-free water for mRNA quantification or stored at −20°C.

Quantitative Reverse Transcription Polymerase Chain Reaction (qRT-PCR) and Quantification of Relative mRNA Levels

All qRT-PCR primers used in this study were designed as intron-spanning. Two pairs of primers were designed for each gene so that the one with better performance, that is, single peak in melting curve and/or lower Ct value, was selected for estimation of its amplification coefficient (AC). Those selected primers are listed in **Table 2**.

TABLE 1 | Experimental Design: Animals, Pretreatment, Experimental approaches.

Animal	Pretreatment	Experimental metric	Groups (n)	Quantification	Brain regions analyzed
I: Controls (n = 34)	0.9% saline (0.2 cc/100 g/day, i.p.)	Fluorescence in Tg(Drd2-eGFP) S118Gsat	**1A)** No IHC (n = 5 ♂)	D2r fluorescence intensity	Dstr
			1B) GFP and Neun IHC (n = 14; 9♂ 5♀)	D2r cell and Neun counting	Dstr, VTA, NAc and mPFC
		mRNA in WT mice	**2)** rt-PCR (n = 12; 6♂ 6♀)	mRNA density	Dstr, VTA, NAc and mPFC
		D2r fluorescence in WT mice	**3)** D2r IHC (n = 3♂)	D2r cell counting	Dstr
II: Cocaine-animals (n = 40)	Cocaine (30 mg/kg/day, i.p.)	Fluorescence in Tg(Drd2-eGFP) S118Gsat	**4A)** No IHC (n = 6 ♂)	D2r fluorescence intensity	Dstr
			4B) GFP and Neun IHC (n = 17; 7♂ 10♀)	D2r cell and Neun counting	Dstr, NAc VTA, mPFC
		mRNA in WT mice	**5)** rt-PCR (n = 14; 7♂ 7♀)	mRNA density	Dstr, NAc VTA, mPFC
		D2r fluorescence in WT mice	**6)** D2r IHC (n = 3♂)	D2r cell counting	Dstr

Samples were amplified in triple and incubated in the Bio-Rad CFX Connect real-time system (Bio-rad, CA, United States). The qRT-PCR condition was 95°C for 30 s, then for 40 cycles of 95°C for 10 s, 55°C for 20 s and 72°C for 30 s using Ssoadvanced universal SYBR Green supermix (Bio-rad, 172–5271, CA, United States) in a final volume of 12.5 μL, containing 2 μL of diluted cDNA and a final concentration of 0.5 μmol/L for forward and reverse primers. To estimate an AC, 1:2 serial dilutions of a starting cDNA sample prepared 8 cDNA concentrations, and the Ct vs log cDNA concentration plot, or standard curve, was constructed to calculate the Ct slope. AC was calculated from the Ct slope of the standard curve using the formula: $AC = 10^{-1/slope}$. This AC was used in data analysis for relative mRNA levels. Standard curve was generated by using the same reaction system and qRT-PCR condition as for samples. Data were normalized with respect to the reference gene *Gapdh*. Results are presented as percent change relative to saline control.

Statistics

The mean value, standard deviation, and standard error of the experimental results obtained from the immunochemistry, fluorescence imaging and qRT-PCR were calculated using Microsoft Excel. Statistics were carried out using SPSS (IBM). A three factor ANOVA was used to identify interactions between sex, treatment, and brain region and a p-value less than 0.05 was considered significant. Student T-tests were initially used to compare the differences in the "Mixed" groups (combined males and females) between controls and cocaine-exposed mice as the two groups only differ by one factor (treatment). If the t-test yielded a significant outcome for the whole group, we then investigated how each sex contributed to the outcome of the mixed group through two-way ANOVAs. Male and female data in each brain region were compared using a two factor (sex and treatment) ANOVA. When significant interactions or main effects were found, pairwise comparisons were used with a Bonferroni corrected p-value of less than 0.0167 indicating significance.

TABLE 2 | qRT-PCR primers validated, selected and used in this study.

Primer	Sequence	Tm (GC + AT)	AC
mPdyn1f	CAGGACCTGGTGCCGCCCTCAGAG	82°C	1.960
mPdyn1r	CGCTTCTGGTTGTCC CACTTCAGC	76°C	
mDrd2f	GCATGGCTGTATCCAGAGAG	62°C	1.978
mDrd2r	CCCACCACCTCCAGATAGAC	64°C	
mPenk1f	CGACATCAATTTCCTGGCGT	60°C	1.954
mPenk1r	AGATCCTTGCAGGTCTCCCA	62°C	
mGapdhf	AGGCCGGATGTGTTCG	52°C	2.017
mGapdhr	TTACCAGAGTTAAAAGCAGCC	60°C	

RESULTS

To assess whether chronic cocaine exposure induces alterations at the tissue and neuronal levels, we combined a D2r-eGFP transgenic mouse model with immunostaining fluorescence techniques. Immunohistochemistry was used to enhance GFP visualization of D2r-positive cells in order to count them and the neuronal nuclei indicator NeuN was used to quantify the total neuronal population. The single-cell resolution of microscope imaging enabled us to define the density of D2r-GFP+ (positive) neurons (D2r-expressing neurons) and the total density for all neurons. Comparisons between control and cocaine treated animals allowed us to assess changes from chronic cocaine exposure in the 4 brain regions.

Interaction Between Treatment, Brain Region and Sex

Three-way ANOVAs of sex, treatment, and brain regional effects were conducted to identify potential interplay between these variables and are summarized in **Table 3**. A significant three-way interaction among the variables was revealed for neuronal (NeuN) density ($F_{(3,65)} = 5.757$, $p = 0.001$) and *Pdyn* mRNA levels ($F_{(3,88)} = 3.791$, $p = 0.013$) but not for D2r-GFP fluorescence, m*Drd2* or m*Penk*. Significant treatment x region interaction was observed for NeuN ($p = 0.009$) and for *Pdyn* ($p = 0.01$) and *Penk* ($p = 0.017$) mRNA levels, but not for D2r-GFP or m*Drd2*.

TABLE 3 | Outcome of 3-way ANOVA.

	NeuN	D2r-eGFP	m*Drd2*	m*PDyn*	m*Penk*
Treatment	$p = 1.50 \times 10^{-16}$	$p = 5.10 \times 10^{-10}$	$p = 0.732$	$p = 1.4 \times 10^{-5}$	$p = 0.06$
Sex	$p = 0.077$	$p = 0.002$	$p = 3.64 \times 10^{-4}$	$p = 0.253$	$p = 0.025$
Brain region	$p = 0.009$	$p = 0.656$	$p = 0.121$	$p = 0.01$	$p = 0.017$
Sex x brain region	$p = 0.001$	$p = 0.784$	$p = 0.103$	$p = 0.013$	$p = 0.079$
Brain region x treatment	$p = 0.009$	$p = 0.883$	$p = 0.12$	$p = 0.01$	$p = 0.017$
Sex x treatment	$p = 0.077$	$p = 0.007$	$p = 3.64 \times 10^{-4}$	$p = 0.253$	$p = 0.026$
Treatment x sex x brain region	$p = 0.001$	$p = 0.604$	$p = 0.103$	$p = 0.013$	$p = 0.079$

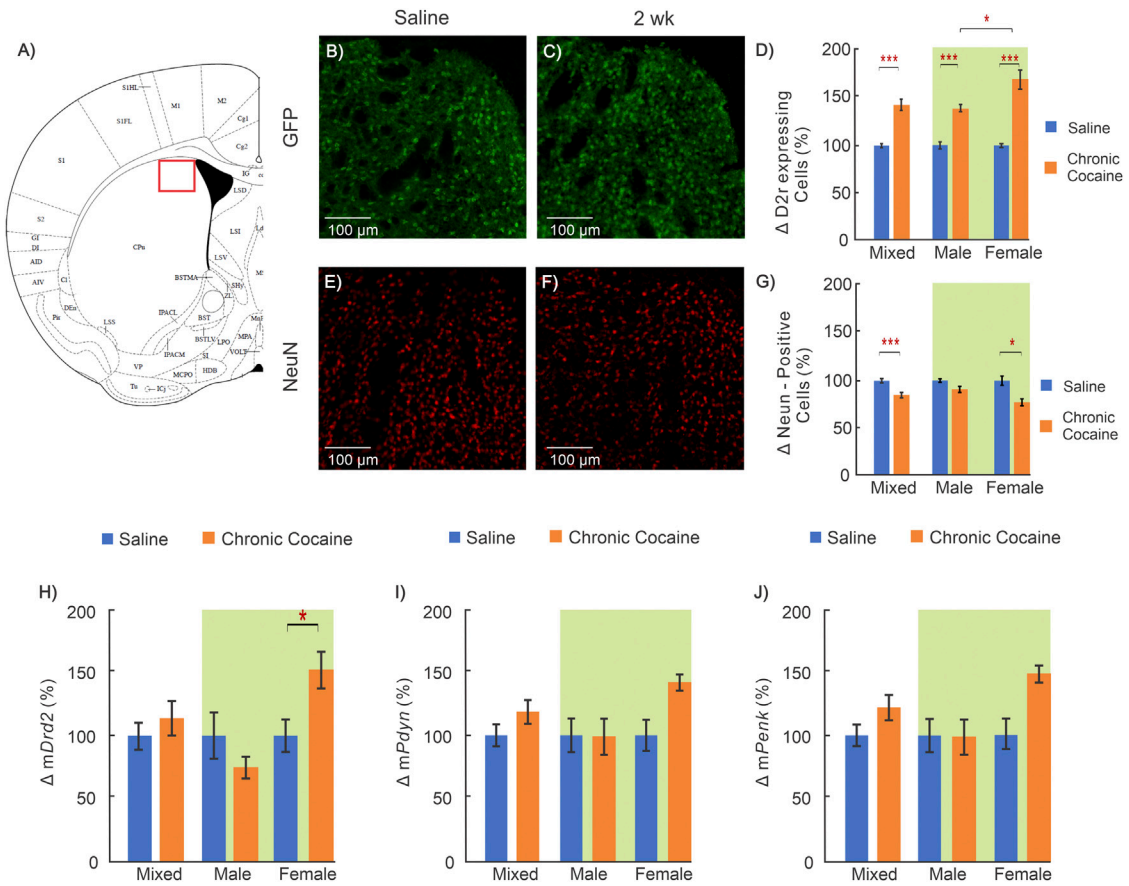

FIGURE 3 | Cocaine effects in dorsal striatum (Dstr). **(A)**: Mouse brain atlas shows location where images were obtained for Dstr (George and Franklin, 2001) ; **(B-C)**: "Zoom-in" GFP images of a control and a cocaine exposed animal; **(D)**: Comparison of D2r-GFP expressing neurons in Dstr between saline (n = 12; 5 ♀, 7 ♂) and chronic cocaine (n = 11; 5 ♀, 6 ♂) exposed animals (2 weeks); **(E-F)**: Corresponding NeuN images of a saline treated and a cocaine exposed mouse; **(G)**: Comparison of neurons between controls (n = 11; 5 ♀, 6 ♂) and cocaine (n = 10; 6 ♀, 4 ♂) exposed animals; **(H-J)**: Comparison of mRNA levels between control (n = 12; 6 ♀, 6 ♂) and cocaine (n = 14; 7 ♀, 7 ♂) animals for *Drd2* **(H)**, for *Pdyn* **(I)** and *Penk* **(J)**. Mixed: males and females; female: females only; male: males only; *: $p < 0.05$; **: $p < 0.005$; ***: $p < 0.001$. Blue bars correspond to saline and orange to cocaine treated mice. Data for two-way ANOVA highlighted in green. Values show averages and SE.

Significant treatment x sex interaction was found for both D2r-GFP ($p = 0.007$) and *Drd2* mRNA ($p = 0.00036$), along with *Penk* mRNA ($p = 0.026$), but not for NeuN or *Pdyn* mRNA. Sex-region interactions were observed for NeuN and *Pdyn* mRNA only. In the three-way ANOVA with the independent variables sex, treatment, and brain region, significant treatment effects were observed on NeuN ($p = 1.5 \times 10^{-16}$), D2r-GFP ($p = 5.1 \times 10^{-10}$) and m*Pdyn* ($p = 1.4 \times 10^{-5}$); significant sex effects were recognized on both D2r-GFP ($p = 0.002$) and *Drd2* mRNA levels ($p = 0.00036$), also for m*Penk* ($p = 0.025$) but not for NeuN or m*Pdyn*. Among all the genes examined, *Drd2* showed the most significant interactions between treatment and sex. To evaluate a treatment-sex interaction in a particular brain region, two-way ANOVA was performed in the following analyses.

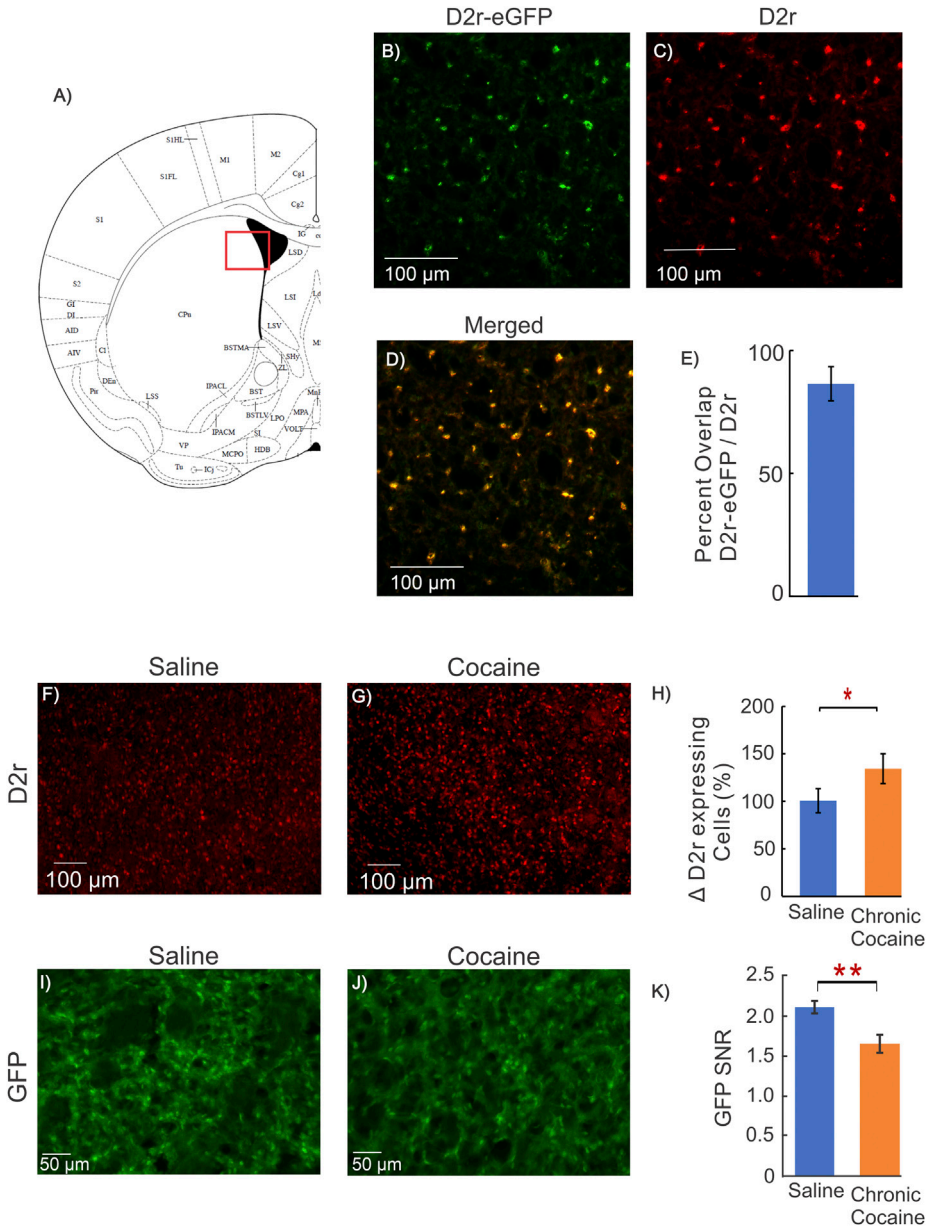

FIGURE 4 | Dstr D2r Response in Cocaine WT mice and fluorescent intensity measure. **(A)**: Mouse brain atlas showing location of imaging in (George and Franklin, 2001); **(B–D)**: Representative images from a mouse brain of the co-localization of GFP from D2r-eGFP reporter line (green), D2r antibody (red), and merged (yellow) obtained from the dorsal striatum; **(E)**: Quantification of overlap of GFP and D2r antibody, indicating that GFP of the D2r-eGFP transgenic mouse reports cellular D2r expression; **(F, G)**: Representative images of D2r positive cell density in the dorsal striatum of a WT animal obtained using an antibody directed against D2r for a control (saline) and cocaine mouse; **(H)**: Quantification of the density of D2r-positive cells for 3 saline and 3 cocaine treated C57BL/6 male mice, indicating the D2r-neuronal expression increase after chronic cocaine exposure ($p = 0.02$); **(I–J)**: Representative images of *ex-vivo* GFP expression without immunohistochemistry from a control and a cocaine treated animal; **(K)**: Comparison of GFP Signal-to-Noise Ratio (SNR = GFP expression per D2r neuron/background noise) between control and cocaine treated mice. The GFP of D2r neurons in cocaine treated mice (1.66 ± 0.08, n = 6, m = 25) was significantly lower than in controls (2.11 ± 0.05, n = 5, m = 18, $p = 0.002$, Student t-test). Blue bars correspond to saline and orange bars to chronic cocaine. Values are means and SE.

Chronic Cocaine's Effect on the Medial Prefrontal Cortex (mPFC)

Representative images from a control mouse used to quantify D2r-eGFP expressing neurons (green cells) and the total neuronal population (red cells) are shown in **Figures 2B,E**, respectively, and those in a cocaine treated animal are shown in **Figures 2C,F**, respectively. The differences in the density of D2r-expressing neurons and of total neuron numbers between control and cocaine treated animals are summarized in **Figures 2D,G**. Specifically, when males and females are grouped together

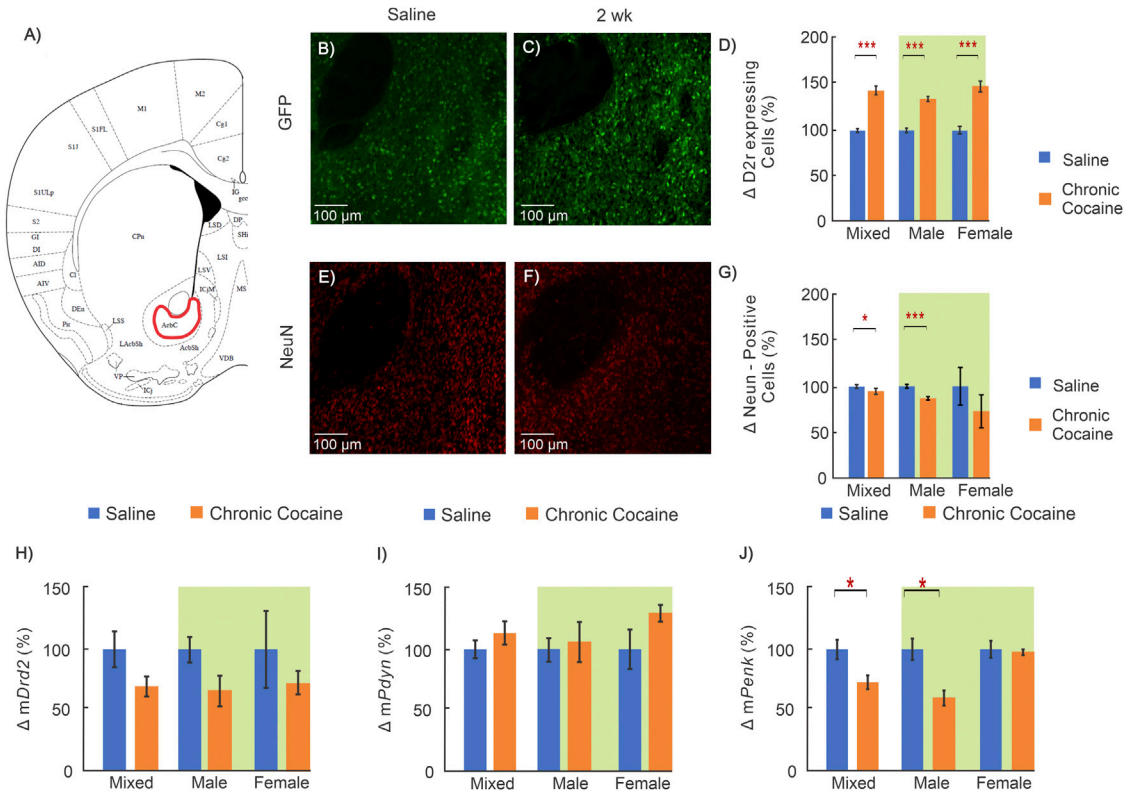

FIGURE 5 | Effects of cocaine in nucleus accumbens (NAc). **(A)**: Brain atlas of the location in NAc where images were obtained (George and Franklin, 2001); **(B, E)**: "Zoom-in" GFP and NeuN sections in NAc for a representative control; and **(C, F)**: for a representative cocaine mouse; **(D)** Results comparing D2r-GFP expressing neurons in NAc for saline (blue, n = 12; 5 ♀, 7 ♂) and cocaine exposed mice (orange, n = 11; 6 ♀, 5 ♂); and **(G)**: results for differences in total neurons (saline = 11; 5 ♀, 6 ♂, cocaine = 10; 6 ♀, 4 ♂); **(H–J)**: Results in WT mice comparing mRNA levels for **(H)**: *Drd2*, **(I)**: *Pdyn* and **(J)**: *Penk* between saline (blue, n = 12; 6 ♀,6 ♂) and cocaine treated (orange, n = 14; 7 ♀,7 ♂) animals. Mixed: including both male of female; female: female animal only; male: male only; Two-way ANOVA data indicated with green background; *: $p < 0.05$; **: $p < 0.005$; ***: $p < 0.001$.

(i.e., defined as 'mixed' shown in **Figure 2D**), the density of D2r-expressing neurons was 45 ± 10% higher in cocaine treated than in controls (n_{saline} = 14, $n_{cocaine}$ = 13, p = 0.003). A two-way ANOVA of sex and treatment revealed a significant main effect of treatment on D2r-expressing neuron density too ($F_{(1,23)}$ = 9.82, p = 0.005). Pairwise comparison tests showed that increases in D2r-eGFP cell density were significant only in females (i.e. Females: 60 ± 12%, n_{saline} = 5, $n_{cocaine}$ = 6, p = 0.016), but not males (Males: 38 ± 17%, n_{saline} = 9, $n_{cocaine}$ = 7, p = 0.08). In contrast, the number of NeuN positive cells (reflecting total neuron count) in mPFC was 35 ± 6% lower (mixed group) in cocaine exposed animals compared to controls (n_{saline} = 10, $n_{cocaine}$ = 10, $p < 0.001$). A two-way ANOVA for NeuN density found a significant interaction between sex and treatment ($F_{(1,17)}$ = 17.28, $p < 0.001$). Pairwise comparison of neuronal density showed that the density was lower in both male (Males: 16 ± 5% decrease, n_{saline} = 5, $n_{cocaine}$ = 4, p = 0.01) and females (47 ± 5% decrease, n_{saline} = 5, $n_{cocaine}$ = 6, $p < 0.001$). The decrease in neuronal density with cocaine was larger in females than in males ($p < 0.001$).

Receptor transcription levels were evaluated using qRT-PCR to measure mRNA of *Drd2*, *Pdyn*, and *Penk* in mPFC. Two way ANOVA for m*Drd2* demonstrated a significant interaction between sex and treatment ($F_{(1,22)}$ = 8.74, p = 0.007). Pairwise comparison revealed that the mRNA for *Drd2* in female mice exposed to cocaine was greater than control (76 ± 18%; n_{saline} = 6, $n_{cocaine}$ = 7, p = 0.016) and was significantly larger than m*Drd2* in cocaine treated males (p = 3.1 × 10^{-4}). Similar to m*Drd2*, two-way ANOVA of m*Penk* revealed a significant interaction between sex and treatment ($F_{(1,22)}$ = 4.37, p = 0.048) with pairwise comparison demonstrating that after cocaine, female m*Penk* levels were significantly higher than female saline control (81 ± 19%; n_{saline} = 6, $n_{cocaine}$ = 7, p = 0.01), and male cocaine treated mice ($n_{cocaine,\ male}$ = 7, $n_{cocaine,\ female}$ = 7, p = 0.007). (**Figures 2H-J**).

Chronic Cocaine's Effect on the Dorsal Striatum (Dstr)

The Dstr is implicated in the neuroadaptations associated with the transition from controlled to habitual cocaine intake (Everitt et al., 2008; Koob and Volkow, 2010). **Figure 3** summarizes the cocaine-associated changes in Dstr. A

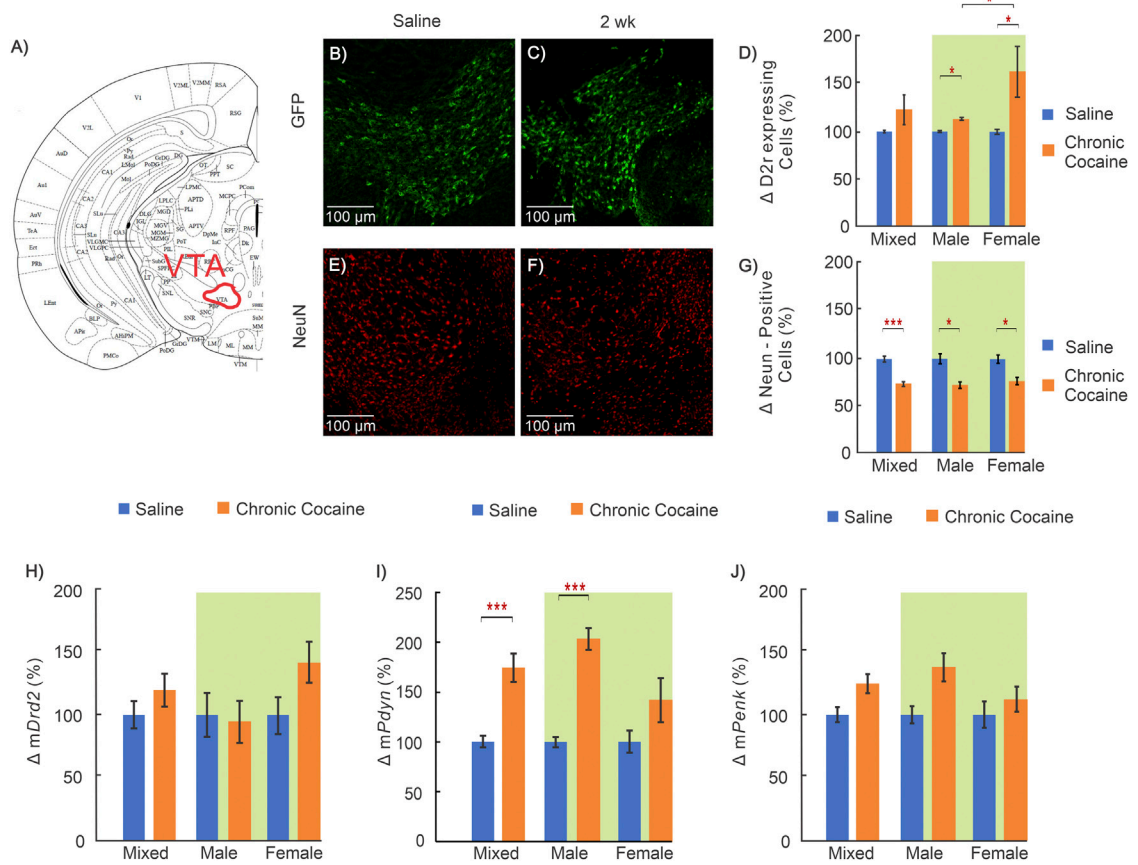

FIGURE 6 | Effects of cocaine in the ventral tegmental area (VTA) **(A)**: Mouse brain atlas showing location of VTA where images were obtained (George and Franklin, 2001); **(B—C)**: "Zoom-in" GFP representative images in a control and **(E–F)** for a cocaine exposed animal for D2r-GFP and NeuN respectively; **(D)**: Comparison of D2r-GFP expressing neurons between saline (blue, n = 11; 5 ♀, 6 ♂) and cocaine animals (orange, n = 11; 6 ♀, 5 ♂); **(G)**: Comparison of total neuronal population between saline (n = 9; 4 ♀, 5 ♂) and cocaine (n = 10; 5 ♀, 5 ♂) exposed animals; **(H–J)**: Comparison of mRNA levels between control (n = 12; 6 ♀, 6 ♂) and cocaine (n = 14; 7 ♀, 7 ♂) animals for *Drd2* **(H)**, *Pdyn* **(I)**, and *Penk* **(J)**. Mixed: males and females; female: females only; male: males only; Data compared with two-way ANOVA indicated by green background; *: $p < 0.05$; **: $p < 0.005$; ***: $p < 0.001$.

significant interaction between sex and treatment remained for the density of D2r-expressing neurons in the Dstr when a two-way ANOVA was performed ($F_{(1,19)} = 8.07$, $p = 0.01$). Pairwise analysis found that both cocaine exposed males (32 ± 4% increase; $n_{saline} = 7$, $n_{cocaine} = 6$, $p < 0.001$) and females (63 ± 11% increase; $n_{saline} = 5$, $n_{cocaine} = 5$, $p < 0.001$) showed significantly higher density of D2r-expressing neurons in Dstr than controls, with female mice having the greatest increases ($n_{cocaine,\ male} = 6$, $n_{cocaine,\ female} = 5$,$p = 0.013$) (**Figure 3D**). The density of neurons labeled by NeuN was analyzed using a two-way ANOVA which revealed a significant main effect of treatment ($F_{(1,17)} = 18.93$, $p < 0.001$). Pairwise comparisons found that female mice exposed to cocaine had significantly lower neuronal density than female saline controls(24 ± 6% decrease; $n_{saline} = 5$, $n_{cocaine} = 6$, $p = 0.006$) (**Figure 3G**).

Two-way ANOVA was run for *Drd2, Penk,* and *Pdyn* mRNA levels in the Dstr. The ANOVA showed a significant interaction between sex and treatment for m*Drd2* ($F_{(1,22)} = 8.25$, $p = 0.009$) but not for m*Penk* or m*Pdyn*. Pairwise analysis determined that in cocaine treated female mice, the level of m*Drd2* was significantly higher compared to female controls (53 ± 14% increase; $n_{saline} = 6$, $n_{cocaine} = 7$, $p = 0.016$) whereas males showed a non-significant decrease (26%; $n_{saline} = 6$, $n_{cocaine} = 7$, $p = 0.2$) (**Figure 3H**).

Using immunohistochemistry, we observed an increase in the number of D2r-positive neurons in mPFC and Dstr in mice exposed to cocaine. To confirm this, we utilized an antibody that binds to the D2r protein, which we measured in the dorsal striatum of WT animals to quantify differences between saline and cocaine treated mice. **Figure 4F,G** show representative images of D2r positive cell density in the dorsal striatum of WT mice exposed to saline and cocaine pretreatment. Comparison of the density of D2r-positive cells between saline (n = 3) and cocaine treated (n = 3) C57BL/6 mice showed ~ 36% increase in the cocaine exposed group compared to controls ($p = 0.02$, **Figure 4H**); which is in close agreement to the results observed in the D2r-eGFP mice (**Figures 3B–D**).

To assess the effects of cocaine on *Drd2* expression levels at the neuronal level. we used D2r-GFP fluorescence intensity as a marker of *Drd2* expression in Dstr neurons. Prior studies in BAC transgenic mice showed an association between

fluorescence intensity (no immunohistochemistry) and gene expression (Zhou et al., 2011; Crook and Housman, 2012; Lawhorn et al., 2013). To confirm that the GFP observed in the D2r-eGFP reporter line corresponded to D2r expression we assessed the co-localization of the D2r-eGFP signal with that of the D2r antibody in the dorsal striatum. **Figure 4B-D** show the representative images from a mouse's brain of the co-localization of GFP from D2r-eGFP reporter line (green), D2r antibody (red), and merged (yellow). The overlap between eGFP and D2r staining was 86 ± 7% (n = 3), indicating that D2r-eGFP represents cells expressing D2r. The comparison of D2r intensity between controls (**Table 1**: Group 1A) and cocaine-exposed mice (**Table 1**: Group 4A) is summarized in **Figure 4I-K**. Cocaine exposed mice showed a decrease in normalized GFP fluorescence, i.e., ratio of GFP fluorescence over the background (ΔGFP-SNR = 0.44 ± 0.10 decrease; n_{saline} = 5, $n_{cocaine}$ = 6, p = 0.002) relative to controls (**Figure 4K**).

Taken together these results suggests that cocaine increased the number of D2r-expressing neurons amid an associated reduction of the total neuronal population. Findings also suggest that the level of expression of the *Drd2* gene in D2r-expressing neurons, as evidence by decreased fluorescence intensity, was lower in cocaine exposed mice than in controls.

Chronic Cocaine's Effect on the Nucleus Accumbens (NAc)

A two-way ANOVA for sex and treatment was conducted on D2r-expressing neurons in the NAc. The ANOVA revealed a significant interaction between sex and treatment ($F_{(1,19)}$ = 6.621, p = 0.019) for this brain region. Pairwise comparison showed the number of D2r-expressing neurons increased in both sexes though females had a 96% greater increase than males (Males: 24 ± 3%, n_{saline} = 7, $n_{cocaine}$ = 5, p < 0.001; Females: 47 ± 6%, n_{saline} = 5, $n_{cocaine}$ = 6, p < 0.001; Male cocaine v female cocaine p = 0.014) (**Figure 5D**). Two way ANOVA for NeuN-positive cells showed a main effect of treatment ($F_{(1,17)}$ = 15.87, p < 0.001) with pairwise analysis revealing that D2r-expressing neurons in male cocaine-exposed mice were decreased by 20 ± 2% (n_{saline} = 6, $n_{cocaine}$ = 4, p < 0.001) (**Figure 5G**).

Drd2 mRNA levels did not show a treatment effect neither in male nor female mice (**Figure 5H**). For *Penk* mRNA levels there was a significant effect of treatment ($F_{(1,22)}$ = 4.86, p = 0.038). In cocaine treated males m*Penk* levels were decreased by 42 ± 8% (n_{saline} = 6, $n_{cocaine}$ = 7, p = 0.007) whereas females showed no changes (3 ± 3% NS) (**Figure 5J**). The *Pdyn* mRNA levels did not show a treatment effect neither in male nor female mice (**Figure 5I**).

Chronic Cocaine's Effect on the Ventral Tegmental Area (VTA)

In the VTA, which is the location of dopamine neurons that project to NAc, the number of D2r-positive cells was increased in cocaine treated mice compared to controls. Two-way ANOVA revealed a significant main effect of treatment ($F_{(1,17)}$ = 5.51, p = 0.031) with pairwise comparisons demonstrating both male and female mice had a significant increase in the density of D2r- neurons following cocaine exposure (Males: 9 ± 3%, n_{saline} = 6, $n_{cocaine}$ = 5, p = 0.016; Females: 64 ± 3%, n_{saline} = 5, $n_{cocaine}$ = 6, p = 0.008) (**Figure 6D**). Similarly, two-way ANOVA for NeuN revealed a significant main effect of treatment. Conversely to GFP, pairwise comparison found NeuN positive cells were decreased by 27 ± 4% (n_{saline} = 5, $n_{cocaine}$ = 5, p = 0.005) in males and 25 ± 4% (n_{saline} = 5, $n_{cocaine}$ = 5, p = 0.006) in female cocaine-expose mice compared to sex matched saline-exposed mice (**Figure 6G**). The mRNA for *Drd2* and *Penk* did not differ between groups (**Figures 6H,J**). Analysis of *Pdyn* mRNA results using two-way ANOVA demonstrated significant effect of treatment ($F_{(1,22)}$ = 24.38, p < 0.001). Pairwise comparisons found m*Pdyn* was significantly increased in cocaine-exposed male mice by 117 ± 13% (n_{saline} = 6, $n_{cocaine}$ = 7, p < 0.001) (**Figure 6I**).

DISCUSSION

Here we assessed the effects of chronic cocaine (2 weeks passive exposure) on D2r-expressing neurons and the total neuronal population in the dopamine mesocortical system. Based on findings reporting decreased D2r availability in striatum we expected to observe a reduction in D2r-expressing neurons. However, contrary to our hypothesis, we found a significant increase in the number of D2r-expressing neurons in mPFC, Dstr, NAc, and VTA in cocaine exposed mice that was stronger in females than males. These increases occurred amidst decreases in the total number of neurons in mPFC and Dstr and these changes were also larger in cocaine exposed females than males. Cocaine exposed females also showed increases in *Drd2* mRNA levels in mPFC and Dstr, consistent with the findings of increases in D2r-expressing neurons, whereas in males there were no significant changes in *Drd2* mRNA. Similarly, whereas m*Penk* were increased in cocaine exposed females in mPFC; in cocaine-exposed males m*Pdyn* was increased in VTA and m*Penk* was decreased in NAc compared to male saline controls.

To our knowledge, this is the first report of an upregulation in the number of neurons that express *Drd2* in the dopamine mesocortical system in animals chronically exposed to cocaine. The increases in D2r-expressing neurons was larger in mPFC and VTA of females exposed to cocaine than in males. Though in females there were parallel increases in *Drd2* mRNA in mPFC and Dstr, this was not the case for NAc or VTA nor was it observed in males. The reason for the discrepancies between the increases in the number of D2r-expressing neurons and the lack of changes in mRNA *Drd2* levels in the VTA and NAc of both sexes and in the Dstr of males is unclear. This divergence in the results of the two methodologies indicates that the increase in the number of D2r-expressing neurons was not reflected in the *Drd2* expression measures averaged at the tissue level. In other words, the changes in expression of *Drd2* as reflected by the number of cells that expressed eGFP regulated by the *Drd2* promoter provided different results from the measures obtained when averaging mRNA levels across all cells in the tissue. Such a discrepancy could reflect the fact that with eGFP transcription of the *Drd2* gene, even if it happened at a very low level, it will lead to fluorescence of the neuron making it detectable whereas in the

tissue the varying levels of mRNA would be averaged across all cells diluting the signal.

We interpret the increase in D2r-expressing neurons amidst a decrease in the total number of neurons to reflect a phenotypic shift in some of the surviving neurons that result in activation of a previously silent *Drd2* gene. Indeed, reports have shown that striatal neurons can undergo phenotypic shifts when dopamine (DA) neurons are damaged or activated. For example, Tande et al. reported a 2-fold increase in the number of striatal neurons expressing the dopamine transporter in macaques exposed to MPTP (1-methyl-4-phenyl-1,2,3,6-tetrahydropyridine) that reflected a phenotypic shift of pre-existing small spiny GABAergic interneurons (Tandé et al., 2006). In addition, Dela Cruz et al. reported an increase in the number of tyrosine hydroxylase immunoreactive neurons in the VTA after deep brain stimulation (Dela Cruz et al., 2015). These studies provide supporting evidence that changes in dopamine signaling can trigger phenotypic neuronal transdifferentiation within the mesocortical dopamine system. To our knowledge, our study is the first to document an increase in the number of D2r expressing neurons following chronic cocaine exposure. However, increases in the number of neurons expressing a particular molecule are not unique to cocaine or the dopamine mesocortical system. Specifically, a recent histochemistry study reported that chronic morphine increased the number of hypothalamic neurons that expressed hypocretin that was not due to neurogenesis and this finding was corroborated in postmortem brains of heroin users (Thannickal et al., 2018). Evidence for shifts in neuronal phenotypes is considered by some to be another form of neuroplasticity (Dulcis et al., 2017). Future studies are needed to determine if the increases in the number of D2r expressing neurons with chronic cocaine reflects transdifferentiation and if so, to identify the neuronal types within the mesocortical system that activate a previously silent *Drd2* gene and the mechanisms that drive it.

Cocaine mediates its effects by inhibiting the dopamine transporter thus increasing extracellular DA. Increases in DA levels underlie cocaine's rewarding effects but have also been implicated in excitotoxicity through enhanced glutamatergic stimulation (Kerkerian et al., 1987; Olney et al., 1991; Dauer and Przedborski, 2003) including NMDA receptor mediated cell swelling (Dodt et al., 1993; Colwell and Levine, 1996). Studies have shown that D2r activation reduces NMDA excitotoxic cell swelling and triggers internalization of AMPA glutamate receptors (Cepeda et al., 1998; Zou et al., 2005) supporting a role of D2r in mitigating excitotoxicity. Therefore, our observation of an increase in the density of D2r-postive cells may be a compensatory mechanism to reduce excitotoxic effects of cocaine-induced DA increases and presumably also to decrease DA release through overexpression of D2r auto-receptors. The neuronal loss reported in our investigation may reflect a failure of this compensatory mechanism.

The sex differences in response to cocaine could reflect the previously reported dimorphism in synapse and neuronal function in brain reward regions. Specifically, Wissman et al. using voltage clamp recording of neurons in the NAc revealed that female rats have higher basal miniature excitatory postsynaptic potential (mEPSC) than males in the NAc core but not shell, and chronic cocaine increased mEPSC to a greater extent in females than males (Wissman et al., 2011). Sex hormones may underlie some of these differences since they influence basal neuronal activity and synaptic DA kinetics. Estrus females have increased basal VTA activity as compared to non-estrus and male mice and release two times more DA into the synapse with tonic stimulation and display impaired synaptic D2-autoreceptor function (Calipari et al., 2017).

In contrast we observed a decrease in D2r-eGFP fluorescence intensity across the Dstr of cocaine exposed mice, which we interpret to reflect a reduction in the overall expression of D2r in the tissue (Zhou et al., 2011; Crook and Housman, 2012). The increase in the number of D2r-expressing neurons with a simultaneous reduced fluorescence intensity in the tissue (measured only in Dstr) suggests that while more neurons expressed *Drd2* those neurons might have had lower *Drd2* expression levels. Alternatively, this apparent discrepancy could also reflect a redistribution of fluorescence in D2r expressing neurons in cocaine exposed mice if a phenotypic shift in expression of D2r occurred in small interneurons instead of the typical D2r expression in striatal MSN. Indeed in the MPTP model of Parkinson's disease, an increase in tyrosine hydroxylase and DAT expressing neurons in the striatum occurred by the phenotypic transformation of small interneurons (Tandé et al., 2006). Regardless, such a marked disruption of D2r expression could unbalance DA signaling in the reward pathway contributing to compulsive cocaine seeking as observed with optogenetic inhibition of D2r-expressing neurons (Baik, 2013; Song et al., 2014).

The dopamine receptors D1r and D2r exert opposite effects on neuronal excitability with D1r increasing and D2r decreasing it (Alvarez, 2016). D1r and D2r expressing neurons in the striatum also have distinct expression patterns for endogenous opioids; enkephalin is mainly co-expressed in D2r whereas dynorphin is mainly co-expressed in D1r-expressing neurons (Surmeier et al., 1998; Gerfen and Surmeier, 2011; Gangarossa et al., 2013). Thus, we also quantified mRNA for proenkephalin (m*Penk*) and prodynorphin (m*Pdyn*). We measured the mRNA levels of m*Pdyn* as a control since it is expressed in D1r- expressing cells to contrast it with the changes in mRNA levels in D2r and m*Penk*, which are expressed in D2r-expressing cells. Females exposed to chronic cocaine only showed elevated levels of m*Penk* in the PFC whereas males showed decreases in m*Penk* in NAc and increases in m*Pdyn* in VTA. Dynorphin, the protein product of m*Pdyn*, reduces firing of DA neurons in the VTA (Muschamp et al., 2014; Baimel et al., 2017). The upregulation of dynorphin in the VTA suggest that chronic cocaine exposure might lead to a reduction in DA neuronal firing and in DA release.

After chronic cocaine we observed a decrease in the density of cells which stained positive for NeuN, which suggests neuronal loss after chronic cocaine exposure. A reduction in neuronal nuclei following cocaine exposure has been previously reported in *ex-vivo* and *in-vitro* studies and has been attributed to cocaine's neurotoxic effects (George et al., 2008; Lepsch et al., 2015). The *in-vitro* study of Lepsch et al. reported a reduction of NeuN in

cultured primary striatal neurons exposed to cocaine due to activation of apoptotic pathways (Lepsch et al., 2015) triggered by nitrosylation of glyceraldehyde-3-phosphate dehydrogenase by nitric oxide leading to activation of p53 and its downstream components PUMA and Bax (Xu et al., 2013; Guha et al., 2016). Thus, the global decrease in neurons observed in the cocaine exposed mice in our study could reflect cocaine's apoptotic effects. In addition, both clinical and animal studies have documented cocaine induced vasoconstriction leading to cerebral ischemia in cocaine addicted individuals and in laboratory animals exposed to cocaine (Treadwell and Robinson, 2007; You et al., 2017). NeuN levels have been shown to decrease in response to ischemia and thus neuronal loss with cocaine could also reflects its vasoconstrictive effects (Gusel'nikova and Korzhevskiy, 2015).

The decrease in the neuronal population following chronic cocaine exposure was largest in mPFC and it was stronger in females than males. These findings are consistent with prior reports of neuronal loss in PFC associated with cocaine exposure in rodents and in postmortem brain studies documenting loss of DA neurons in cocaine users and neuronal loss in multiple brain regions in polysubstance users (Büttner and Weis, 2006; George et al., 2008; Little et al., 2009). They could also explain the reduction of cerebral blood flow, metabolic activity, and cortical thickness in the frontal cortex of cocaine users (Volkow et al., 1988; Hirsiger et al., 2019). Notably the study documenting loss of DA neurons in cocaine users led to the speculation of an increased risk for Parkinson's disease in cocaine users that as of now has not been corroborated.

Our results show that the detrimental effects from cocaine exposure on the female are greater than the male brain, which are in agreement with previous reports from preclinical and clinical studies. In rodents, sex-dependent behavioral differences in response to cocaine have been observed. After passive exposure to cocaine for 9 days, cocaine treated females had greater increases in activity and rearing behaviors than cocaine treated males (van Haaren and Meyer, 1991). In self-administration experiments, female rats self-administer cocaine more times than males and also escalate drug taking faster. (Algallal et al., 2020). In humans, progression from substance use to substance dependence appears to be faster in females than males, also they appear to consume higher doses and have more difficulty in achieving and maintaining abstinence (O'Brien & Anthony, 2005; Gallop et al., 2007). Similarly, brain imaging studies of stimulant-dependent females showed that compared to males, they had larger decreases in gray matter volumes in frontal, limbic, temporal and parietal regions (Tanabe et al., 2013; Regner et al., 2015), consistent with the loss of neurons we observed in the female mice, which was most prominent in PFC. Among all the genes examined *Drd2* displayed the most significant sex effects and the most significant sex-treatment interactions, supporting a view that D2r might contribute to sex differences in cocaine behaviors.

The transgenic mouse model that we used to visualize D2r-expressing neurons was shown by a prior study to display a two-fold upregulation of *Drd2* mRNA (Kramer et al., 2011). However since we compared D2r-eGFP changes between naïve and chronic cocaine animals, any potential baseline differences in the transgenic model should not affect the comparison analyses. To confirm that the GFP in the D2r-eGFP reporter line corresponded to D2r expression, we assessed the co-localization of the D2r-eGFP signal and the D2r antibody. The high overlap (i.e., 86 ± 7%, $n = 3$) between eGFP and D2r staining indicates that D2r-eGFP is representative of cells expressing D2r.

Limitations of this study are as follows: 1) in our study we used passive cocaine administration and findings might differ with self-administering animals, which is more relevant to the clinical situation. The passive cocaine model however allowed us to remove the confounds due to dose differences; 2) we did not record behavior which would have allowed us to correlate behavioral changes with the changes in D2r expressing neurons. These would have been desirable since prior studies mostly done in males have shown that D2r availability modulates cocaine's effects. Mice and rats with suppressed or absent D2 receptors show increased locomotion during cocaine self-administration compared to wildtypes but do not differ in the time to acquisition of cocaine self-administration (Chausmer et al., 2002; de Jong et al., 2015). When the role of D2r in cocaine relapse and seeking was studied, systemic administration of D2 agonist enhanced cocaine seeking whereas administration of the D2r antagonist raclopride into the VTA inhibited relapse to cocaine seeking (Wise et al., 1990; Xue et al., 2011); 3) we did not measure the protein levels of D2r, enkephalin and dynorphin, which would have allowed us to assess the association between the changes in mRNA and the levels of protein expression. 4) Technically, use of isoflurane in brain harvesting might systemically interfere with gene activity (Staib-Lasarzik et al., 2014; Ko et al., 2019). Additionally, while we interpret our findings of increases in D2r-expressing neurons to reflect expression of *Drd2* in neurons where the gene was previously silent, further work is needed to corroborate this. Future investigations will need to assess the consequences of these changes in brain function and behaviors relevant to cocaine addiction.

In summary, we performed a systematic assessment of the total neuronal population and of the subset of neurons expressing D2r in response to chronic cocaine using immunohistochemistry and a transgenic D2r-eGFP mouse line. This approach revealed an increase in the number of neurons expressing *Drd2* and a decrease in total neuron numbers in mPFC, Dstr, NAc, and VTA that was more severe for females than males. We interpret our findings to suggest evidence that cocaine triggers neuronal transdifferentiation in regions of the dopamine mesocortical system, but further work is needed to corroborate this.

DATA AVAILABILITY STATEMENT

The data that support the findings of this study are available from the corresponding authors upon reasonable request.

ETHICS STATEMENT

The animal study was reviewed and approved by the Stony Brook University Institutional Animal Care and Use Committee.

AUTHOR CONTRIBUTIONS

NV, CD, and ZL designed research; KC and CP carried out the experiments and imaging process and analysis, GK, KP performed the partial immunohistochemistry experiments. JZ and ZL conducted the genetic studies. KC, CD, ZL and NV contributed significantly to data interpretation, discussing the results, and writing the manuscript.

FUNDING

This work was supported in part by National Institutes of Health (NIH) grants 2R01 DA029718 (CD), RF1DA048808 (YP and CD), R21DA042597 (CD), R01DA021409 (ZL), and NIH's Intramural Program of NIAAA (NV). The authors have no conflicts to disclose.

ACKNOWLEDGMENTS

The authors would like to acknowledge Angela Chen who assisted in collected and processing tissue samples, Weiguo Zhong for helping with data analysis, and Dr. Craig Allen for assistance in drug treatment. The authors would also like to thank the NIDA drug supply program for providing the cocaine used in this study.

REFERENCES

Algallal, H., Allain, F., Ndiaye, N. A., and Samaha, A. N. (2020). Sex differences in cocaine self-administration behaviour under long access versus intermittent access conditions. *Addict. Biol.* 25, e12809. doi:10.1111/adb.12809

Alvarez, V. A. (2016). Clues on the coding of reward cues by the nucleus accumbens. *Proc. Natl. Acad. Sci. U.S.A.* 113, 2560–2562. doi:10.1073/pnas.1601162113

Baik, J.-H. (2013). Dopamine Signaling in reward-related behaviors. *Front. Neural Circuits* 7, 152. doi:10.3389/fncir.2013.00152

Baimel, C., Lau, B. K., Qiao, M., and Borgland, S. L. (2017). Projection-target-defined effects of orexin and dynorphin on VTA dopamine neurons. *Cell Rep.* 18, 1346–1355. doi:10.1016/j.celrep.2017.01.030

Becker, J. B., and Koob, G. F. (2016). Sex differences in animal models: focus on addiction. *Pharmacol. Rev.* 68, 242–263. doi:10.1124/pr.115.011163

Büttner, A., and Weis, S. (2006). Neuropathological alterations in drug abusers: the involvement of neurons, glial, and vascular systems. *Fsmp* 2, 115–126. doi:10.1385/fsmp:2:2:115

Calipari, E. S., Juarez, B., Morel, C., Walker, D. M., Cahill, M. E., Ribeiro, E., et al. (2017). Dopaminergic dynamics underlying sex-specific cocaine reward. *Nat. Commun.* 8, 13877. doi:10.1038/ncomms13877

Cepeda, C., Colwell, C. S., Itri, J. N., Gruen, E., and Levine, M. S. (1998). Dopaminergic modulation of early signs of excitotoxicity in visualized rat neostriatal neurons. *Eur. J. Neurosci.* 10, 3491–3497. doi:10.1046/j.1460-9568.1998.00357.x

Chausmer, A. L., Elmer, G. I., Rubinstein, M., Low, M. J., Grandy, D. K., and Katz, J. L. (2002). Cocaine-induced locomotor activity and cocaine discrimination in dopamine D2 receptor mutant mice. *Psychopharmacology* 163, 54–61. doi:10.1007/s00213-002-1142-y

Cheng, Y., Huang, C. C. Y., Ma, T., Wei, X., Wang, X., Lu, J., et al. (2017). Distinct synaptic strengthening of the striatal direct and indirect pathways drives alcohol consumption. *Biol. Psychiatry* 81, 918–929. doi:10.1016/j.biopsych.2016.05.016

Colwell, C. S., and Levine, M. S. (1996). Glutamate receptor-induced toxicity in neostriatal cells. *Brain Res.* 724, 205–212. doi:10.1016/0006-8993(96)00323-x

Crook, Z. R., and Housman, D. E. (2012). Dysregulation of dopamine receptor D2 as a sensitive measure for Huntington disease pathology in model mice. *Proc. Natl. Acad. Sci. U.S.A.* 109, 7487–7492. doi:10.1073/pnas.1204542109

Dauer, W., and Przedborski, S. (2003). Parkinson's disease: mechanisms and models. *Neuron* 39, 889–909. doi:10.1016/s0896-6273(03)00568-3

de Jong, J. W., Roelofs, T. J., Mol, F. M., Hillen, A. E., Meijboom, K. E., Luijendijk, M. C., et al. (2015). Reducing ventral tegmental dopamine D2 receptor expression selectively boosts incentive motivation. *Neuropsychopharmacology* 40, 2085–2095. doi:10.1038/npp.2015.60

Dela Cruz, J. A., Hescham, S., Adriaanse, B., Campos, F. L., Steinbusch, H. W., Rutten, B. P., et al. (2015). Increased number of TH-immunoreactive cells in the ventral tegmental area after deep brain stimulation of the anterior nucleus of the thalamus. *Brain Struct. Funct.* 220, 3061–3066. doi:10.1007/s00429-014-0832-7

Dobbs, L. K., Kaplan, A. R., Bock, R., Phamluong, K., Shin, J. H., Bocarsly, M. E., et al. (2019). D1 receptor hypersensitivity in mice with low striatal D2 receptors facilitates select cocaine behaviors. *Neuropsychopharmacology* 44, 805–816. doi:10.1038/s41386-018-0286-3

Dodt, H. U., Hager, G., and Zieglgänsberger, W. (1993). Direct observation of neurotoxicity in brain slices with infrared videomicroscopy. *J. Neurosci. Methods* 50, 165–171. doi:10.1016/0165-0270(93)90005-c

Dulcis, D., Lippi, G., Stark, C. J., Do, L. H., Berg, D. K., and Spitzer, N. C. (2017). Neurotransmitter switching regulated by miRNAs controls changes in social preference. *Neuron* 95, 1319–1333.e5. doi:10.1016/j.neuron.2017.08.023

Everitt, B. J., Belin, D., Economidou, D., Pelloux, Y., Dalley, J. W., and Robbins, T. W. (2008). Review. Neural mechanisms underlying the vulnerability to develop compulsive drug-seeking habits and addiction. *Philos. Trans. R. Soc. London B Biol. Sci.* 363, 3125–3135. doi:10.1098/rstb.2008.0089

Gagnon, D., Petryszyn, S., Sanchez, M. G., Bories, C., Beaulieu, J. M., De Koninck, Y., et al. (2017). Striatal neurons expressing D1 and D2 receptors are morphologically distinct and differently affected by dopamine denervation in mice. *Sci. Rep.* 7, 41432. doi:10.1038/srep41432

Gallop, R. J., Crits-Christoph, P., Ten Have, T. R., Barber, J. P., Frank, A., Griffin, M. L., et al. (2007). Differential transitions between cocaine use and abstinence for men and women. *J. Consult. Clin. Psychol.* 75, 95–103. doi:10.1037/0022-006X.75.1.95

Gangarossa, G., Espallergues, J., Mailly, P., De Bundel, D., de Kerchove d'Exaerde, A., Hervé, D., et al. (2013). Spatial distribution of D1R- and D2R-expressing medium-sized spiny neurons differs along the rostro-caudal axis of the mouse dorsal striatum. *Front. Neural Circuits* 7, 124. doi:10.3389/fncir.2013.00124

George, O., Mandyam, C. D., Wee, S., and Koob, G. F. (2008). Extended access to cocaine self-administration produces long-lasting prefrontal cortex-dependent working memory impairments. *Neuropsychopharmacology* 33, 2474–2482. doi:10.1038/sj.npp.1301626

George, P., and Franklin, K. (2001). *The mouse brain in stereotaxic coordinates*. 2nd Edn. Cambridge, MA: Academic Press, 360.

Gerfen, C. R., and Surmeier, D. J. (2011). Modulation of striatal projection systems by dopamine. *Annu. Rev. Neurosci.* 34, 441–466. doi:10.1146/annurev-neuro-061010-113641

Gong, S., Zheng, C., Doughty, M. L., Losos, K., Didkovsky, N., Schambra, U. B., et al. (2003). A gene expression atlas of the central nervous system based on bacterial artificial chromosomes. *Nature* 425, 917–925. doi:10.1038/nature02033

Griffin, M. L., Weiss, R. D., Mirin, S. M., and Lange, U. (1989). A comparison of male and female cocaine abusers. *Arch. Gen. Psychiatry* 46, 122–126. doi:10.1001/archpsyc.1989.01810020024005

Guha, P., Harraz, M. M., and Snyder, S. H. (2016). Cocaine elicits autophagic cytotoxicity via a nitric oxide-GAPDH signaling cascade. *Proc. Natl. Acad. Sci. U.S.A.* 113, 1417–1422. doi:10.1073/pnas.1524860113

Gusel'nikova, V. V., and Korzhevskiy, D. E. (2015). NeuN as a neuronal nuclear antigen and neuron differentiation marker. *Acta Naturae* 7, 42–47. 10.32607/20758251-2015-7-2-42-47.

Hirsiger, S., Hänggi, J., Germann, J., Vonmoos, M., Preller, K. H., Engeli, E. J. E., et al. (2019). Longitudinal changes in cocaine intake and cognition are linked to cortical thickness adaptations in cocaine users. *Neuroimage Clin.* 21, 101652. doi:10.1016/j.nicl.2019.101652

Jasinska, A. J., Chen, B. T., Bonci, A., and Stein, E. A. (2015). Dorsal medial prefrontal cortex (MPFC) circuitry in rodent models of cocaine use: implications for drug addiction therapies. *Addict. Biol.* 20, 215–226. doi:10.1111/adb.12132

Kerkerian, L., Dusticier, N., and Nieoullon, A. (1987). Modulatory effect of dopamine on high-affinity glutamate uptake in the rat striatum. *J. Neurochem.* 48, 1301–1306. doi:10.1111/j.1471-4159.1987.tb05661.x

Ko, M. J., van Rijn, R. M., and van Rijn, R. M. (2019). Response: commentary: commonly used anesthesia/euthanasia methods for brain collection differentially impact MAPK activity in male and female C57bl/6 mice. *Front. Cell Neurosci.* 13, 379. doi:10.3389/fncel.2019.00379

Kokane, S. S., and Perrotti, L. I. (2020). Sex differences and the role of estradiol in mesolimbic reward circuits and vulnerability to cocaine and opiate addiction. *Front. Behav. Neurosci.* 14, 74. doi:10.3389/fnbeh.2020.00074

Koob, G. F., and Volkow, N. D. (2016). Neurobiology of addiction: a neurocircuitry analysis. *Lancet Psychiatry* 3, 760–773. doi:10.1016/S2215-0366(16)00104-8

Koob, G. F., and Volkow, N. D. (2010). Neurocircuitry of addiction. *Neuropsychopharmacology* 35, 217–238. doi:10.1038/npp.2009.110

Kramer, P. F., Christensen, C. H., Hazelwood, L. A., Dobi, A., Bock, R., Sibley, D. R., et al. (2011). Dopamine D2 receptor overexpression alters behavior and physiology in drd2-EGFP mice. *J. Neurosci.* 31, 126–132. doi:10.1523/JNEUROSCI.4287-10.2011

Lawhorn, C., Edusei, E., Zhou, Y., Ho, A., and Kreek, M. J. (2013). Acute binge pattern cocaine administration induces region-specific effects in D1-r- and D2-r-expressing cells in eGFP transgenic mice. *Neuroscience* 253, 123–131. doi:10.1016/j.neuroscience.2013.08.032

Lepsch, L. B., Planeta, C. S., and Scavone, C. (2015). Cocaine causes apoptotic death in rat mesencephalon and striatum primary cultures. *Biomed. Res. Int.* 2015, 750752. doi:10.1155/2015/750752

Little, K. Y., Ramssen, E., Welchko, R., Volberg, V., Roland, C. J., and Cassin, B. (2009). Decreased brain dopamine cell numbers in human cocaine users. *Psychiatry Res.* 168, 173–180. doi:10.1016/j.psychres.2008.10.034

Muschamp, J. W., Hollander, J. A., Thompson, J. L., Voren, G., Hassinger, L. C., Onvani, S., et al. (2014). Hypocretin (orexin) facilitates reward by attenuating the antireward effects of its cotransmitter dynorphin in ventral tegmental area. *Proc. Natl. Acad. Sci. U.S.A.* 111, E1648–E1655. doi:10.1073/pnas.1315542111

Olney, J. W., Labruyere, J., Wang, G., Wozniak, D. F., Price, M. T., and Sesma, M. A. (1991). NMDA antagonist neurotoxicity: mechanism and prevention. *Science* 254, 1515–1518. doi:10.1126/science.1835799

O'Brien, M. S., and Anthony, J. C. (2005). Risk of becoming cocaine dependent: epidemiological estimates for the United States, 2000–2001. *Neuropsychopharmacology* 30, 1006–1018. doi:10.1038/sj.npp.1300681

Porrino, L. J., Beveridge, T. J., Smith, H. R., and Nader, M. A. (2016). Functional consequences of cocaine expectation: findings in a non-human primate model of cocaine self-administration. *Addict. Biol.* 21, 519–529. doi:10.1111/adb.12231

Rappeneau, V., Morel, A. L., El Yacoubi, M., Vaugeois, J. M., Denoroy, L., and Bérod, A. (2015). Enhanced cocaine-associated contextual learning in female H/rouen mice selectively bred for depressive-like behaviors: molecular and neuronal correlates. *Int. J. Neuropsychopharmacol.* 18. doi:10.1093/ijnp/pyv022

Regner, M. F., Dalwani, M., Yamamoto, D., Perry, R. I., Sakai, J. T., Honce, J. M., et al. (2015). Sex differences in gray matter changes and brain-behavior relationships in patients with stimulant dependence. *Radiology* 277, 801–812. doi:10.1148/radiol.2015142541

Robbins, S. J., Ehrman, R. N., Childress, A. R., and O'Brien, C. P. (1999). Comparing levels of cocaine cue reactivity in male and female outpatients. *Drug Alcohol Depend.* 53, 223–230. doi:10.1016/s0376-8716(98)00135-5

Song, S. S., Kang, B. J., Wen, L., Lee, H. J., Sim, H. R., Kim, T. H., et al. (2014). Optogenetics reveals a role for accumbal medium spiny neurons expressing dopamine D2 receptors in cocaine-induced behavioral sensitization. *Front. Behav. Neurosci.* 8, 336. doi:10.3389/fnbeh.2014.00336

Staib-Lasarzik, I., Kriege, O., Timaru-Kast, R., Pieter, D., Werner, C., Engelhard, K., et al. (2014). Anesthesia for euthanasia influences mRNA expression in healthy mice and after traumatic brain injury. *J. Neurotrauma* 31, 1664–1671. doi:10.1089/neu.2013.3243

Stefański, R., Ziółkowska, B., Kuśmider, M., Mierzejewski, P., Wyszogrodzka, E., Kołomańska, P., et al. (2007). Active versus passive cocaine administration: differences in the neuroadaptive changes in the brain dopaminergic system. *Brain Res.* 1157, 1–10. doi:10.1016/j.brainres.2007.04.074

Surmeier, D. J., Yan, Z., and Song, W. J. (1998). Coordinated expression of dopamine receptors in neostriatal medium spiny neurons. *Adv. Pharmacol.* 42, 1020–1023. doi:10.1523/JNEUROSCI.16-20-06579.1996

Tanabe, J., York, P., Krmpotich, T., Miller, D., Dalwani, M., Sakai, J. T., et al. (2013). Insula and orbitofrontal cortical morphology in substance dependence is modulated by sex. *AJNR Am. J. Neuroradiol.* 34, 1150–1156. doi:10.3174/ajnr.A3347

Tandé, D., Höglinger, G., Debeir, T., Freundlieb, N., Hirsch, E. C., and François, C. (2006). New striatal dopamine neurons in MPTP-treated macaques result from a phenotypic shift and not neurogenesis. *Brain* 129, 1194–1200. doi:10.1093/brain/awl041

Thannickal, T. C., John, J., Shan, L., Swaab, D. F., Wu, M. F., Ramanathan, L., et al. (2018). Opiates increase the number of hypocretin-producing cells in human and mouse brain and reverse cataplexy in a mouse model of narcolepsy. *Sci. Transl. Med.* 10, eaao4953. doi:10.1126/scitranslmed.aao4953

Treadwell, S. D., and Robinson, T. G. (2007). Cocaine use and stroke. *Postgrad. Med. J.* 83, 389–394. doi:10.1136/pgmj.2006.055970

Uhl, G. R., Hall, F. S., and Sora, I. (2002). Cocaine, reward, movement and monoamine transporters. *Mol. Psychiatry* 7, 21–26. doi:10.1038/sj/mp/4000964

Van Etten, M. L., and Anthony, J. C. (2001). Male-female differences in transitions from first drug opportunity to first use: searching for subgroup variation by age, race, region, and urban status. *J. Womens Health Gend. Based Med.* 10, 797–804. doi:10.1089/15246090152636550

van Haaren, F., and Meyer, M. E. (1991). Sex differences in locomotor activity after acute and chronic cocaine administration. *Pharmacol. Biochem. Behav.* 39, 923–927. doi:10.1016/0091-3057(91)90054-6

Volkow, N. D., and Fowler, J. S. (2000). Addiction, a disease of compulsion and drive: involvement of the orbitofrontal cortex. *Cereb. Cortex* 10, 318–325. doi:10.1093/cercor/10.3.318

Volkow, N. D., Mullani, N., Gould, K. L., Adler, S., and Krajewski, K. (1988). Cerebral blood flow in chronic cocaine users: a study with positron emission tomography. *Br. J. Psychiatry* 152, 641–648. doi:10.1192/bjp.152.5.641

Wei, X., Ma, T., Cheng, Y., Huang, C. C. Y., Wang, X., Lu, J., et al. (2018). Dopamine D1 or D2 receptor-expressing neurons in the central nervous system. *Addict. Biol.* 23, 569–584. doi:10.1111/adb.12512

Whitfield, T. W., Schlosburg, J. E., Wee, S., Gould, A., George, O., Grant, Y., et al. (2015). κ Opioid receptors in the nucleus accumbens shell mediate escalation of methamphetamine intake. *J. Neurosci.* 35, 4296–4305. doi:10.1523/JNEUROSCI.1978-13.2015

Wise, R. A., Murray, A., and Bozarth, M. A. (1990). Bromocriptine self-administration and bromocriptine-reinstatement of cocaine-trained and heroin-trained lever pressing in rats. *Psychopharmacology* 100, 355–360. doi:10.1007/BF02244606

Wissman, A. M., McCollum, A. F., Huang, G. Z., Nikrodhanond, A. A., and Woolley, C. S. (2011). Sex differences and effects of cocaine on excitatory synapses in the nucleus accumbens. *Neuropharmacology* 61, 217–227. doi:10.1016/j.neuropharm.2011.04.002

Xu, R., Serritella, A. V., Sen, T., Farook, J. M., Sedlak, T. W., Baraban, J., et al. (2013). Behavioral effects of cocaine mediated by nitric oxide-GAPDH transcriptional signaling. *Neuron* 78, 623–630. doi:10.1016/j.neuron.2013.03.021

Xue, Y., Steketee, J. D., Rebec, G. V., and Sun, W. (2011). Activation of D_2-like receptors in rat ventral tegmental area inhibits cocaine-reinstated drug-seeking behavior. *Eur. J. Neurosci.* 33, 1291–1298. doi:10.1111/j.1460-9568.2010.07591.x

You, J., Volkow, N. D., Park, K., Zhang, Q., Clare, K., Du, C., et al. (2017). Cerebrovascular adaptations to cocaine-induced transient ischemic attacks in the rodent brain. *JCI Insight* 2, e90809. doi:10.1172/jci.insight.90809

Zhou, Y., Litvin, Y., Piras, A. P., Pfaff, D. W., and Kreek, M. J. (2011). Persistent increase in hypothalamic arginine vasopressin gene expression during

protracted withdrawal from chronic escalating-dose cocaine in rodents. *Neuropsychopharmacology* 36, 2062–2075. doi:10.1038/npp.2011.97

Zombeck, J. A., Gupta, T., and Rhodes, J. S. (2009). Evaluation of a pharmacokinetic hypothesis for reduced locomotor stimulation from methamphetamine and cocaine in adolescent versus adult male C57BL/6J mice. *Psychopharmacology* 201, 589–599. doi:10.1007/s00213-008-1327-0

Zou, S., Li, L., Pei, L., Vukusic, B., Van Tol, H. H., Lee, F. J., et al. (2005). Protein-protein coupling/uncoupling enables dopamine D2 receptor regulation of AMPA receptor-mediated excitotoxicity. *J. Neurosci.* 25, 4385–4395. doi:10.1523/JNEUROSCI.5099-04.2005

Conflict of Interest: The authors declare that the research was conducted in the absence of any commercial or financial relationships that could be construed as a potential conflict of interest.

frontiers in Pharmacology

ORIGINAL RESEARCH
published: 16 April 2021
doi: 10.3389/fphar.2021.632757

The Effects of Repeated Morphine Treatment on the Endogenous Cannabinoid System in the Ventral Tegmental Area

*Hong Zhang[1], Austin A. Lipinski[2], Erika Liktor-Busa[1], Angela F. Smith[1], Aubin Moutal[1], Rajesh Khanna[1], Paul R. Langlais[2], Tally M. Largent-Milnes[1] and Todd W. Vanderah[1]**

[1]Department of Pharmacology, College of Medicine, University of Arizona, Tucson, AZ, United States, [2]Department of Medicine, Division of Endocrinology, College of Medicine, University of Arizona, Tucson, AZ, United States

OPEN ACCESS

Edited by:
Jianfeng Liu,
Texas A and M University,
United States

Reviewed by:
Ying Han,
Peking University, China
Katia Befort,
Laboratoire de Neurosciences Cognitives et Adaptatives (LNCA),
France

***Correspondence:**
Todd W. Vanderah
vanderah@email.arizona.edu

Specialty section:
This article was submitted to Neuropharmacology, a section of the journal Frontiers in Pharmacology

Received: 24 November 2020
Accepted: 26 February 2021
Published: 16 April 2021

Citation:
Zhang H, Lipinski AA, Liktor-Busa E, Smith AF, Moutal A, Khanna R, Langlais PR, Largent-Milnes TM and Vanderah TW (2021) The Effects of Repeated Morphine Treatment on the Endogenous Cannabinoid System in the Ventral Tegmental Area. Front. Pharmacol. 12:632757. doi: 10.3389/fphar.2021.632757

The therapeutic utility of opioids is diminished by their ability to induce rewarding behaviors that may lead to opioid use disorder. Recently, the endogenous cannabinoid system has emerged as a hot topic in the study of opioid reward but relatively little is known about how repeated opioid exposure may affect the endogenous cannabinoid system in the mesolimbic reward circuitry. In the present study, we investigated how sustained morphine may modulate the endogenous cannabinoid system in the ventral tegmental area (VTA) of Sprague Dawley rats, a critical region in the mesolimbic reward circuitry. Studies here using proteomic analysis and quantitative real-time PCR (qRT-PCR) found that the VTA expresses 32 different proteins or genes related to the endogenous cannabinoid system; three of these proteins or genes (PLCγ2, ABHD6, and CB2R) were significantly affected after repeated morphine exposure (CB2R was only detected by qRT-PCR but not proteomics). We also identified that repeated morphine treatment does not alter either anandamide (AEA) or 2-arachidonoylglycerol (2-AG) levels in the VTA compared to saline treatment; however, there may be diminished levels of anandamide (AEA) production in the VTA 4 h after a single morphine injection in both chronic saline and morphine pretreated cohorts. Treating the animals with an inhibitor of 2-AG degradation significantly decreased repeated opioid rewarding behavior. Taken together, our studies reveal a potential influence of sustained opioids on the endocannabinoid system in the VTA, suggesting that the endogenous cannabinoid system may participate in the opioid-induced reward.

Keywords: opioids, endocannabinnoid, cannabinoid receptor, endogenous cannabinoid system, ventral tegmental area, reward

Abbreviation: 2-AG, 2-arachidonoylglycerol; ABHD6, α/β-hydrolase domain containing 6; AEA, anandamide; CB1R, cannabinoid receptor 1; CB2R, Cannabinoid receptor 2; CPP, conditioned place preference; DAGLα, diacylglycerol lipase; ECS, endogenous cannabinoid system; GO, Gene Ontology; MAGL, monoglyceride lipase; NAc, nucleus accumbens; PLCγ2, phospholipase Cgamma-2; VTA, ventral tegmental area.

INTRODUCTION

The opioid epidemic is a severe health problem in the United States. It is estimated that over 10 million Americans misused prescription opioids and approximate two million of them have use disorders (SAMHSA, 2019). This high prevalence of opioid misusers/abusers is coupled to a striking increase in emergency room visits and overdose deaths due to non-medical use of opioids (Kolodny et al., 2015). Recently, this situation is even getting worse due to the social isolation and overwhelming despair associated with the COVID-19 pandemic (Volkow, 2020). Despite these significant detriments associated with opioids, 50 million Americans who are suffering from pain still need opioids–as they remain the current most effective analgesics (Dahlhamer et al., 2018). This dilemma has now become a challenging question for the medical community and requires further research to suppress the addictive potential of opioids especially for long-term use.

Opioid-induced reward is an initial but critical step toward opioid abuse and addiction (Fields and Margolis, 2015). Therefore, exploring the underlying mechanisms of opioid reward is essential to develop novel therapies for the treatment of the opioid epidemic. The mesolimbic circuitry is the major component of the brain reward system (Volkow and Morales, 2015). This circuitry is comprised of dopaminergic neurons projecting from the ventral tegmental area (VTA) of the midbrain to the nucleus accumbens (NAc) in the ventral forebrain (Volkow and Morales, 2015). The activation of these dopaminergic neurons is thought to directly encode for a reward prediction signal by producing a rapid, phasic dopamine release in the NAc (Volkow and Morales, 2015), which, at least in part, mediates opioid-induced reward.

The endogenous cannabinoid system (ECS), formed by cannabinoid receptors, lipid-derived endogenous ligands, and enzymes that synthesize and degrade the endogenous ligands, has recently been implicated in the process of rewarding behavior formation mediated by the mesolimbic circuitry. As it was shown previously, the blockade of cannabinoid receptor 1 (CB1R) in the VTA or NAc significantly suppressed morphine-induced conditioned place preference (CPP) or heroin self-administration (Caillé and Parsons, 2006; Rashidy-Pour et al., 2013); while administration of a selective Cannabinoid receptor 2 (CB2R) agonist JWH015 effectively attenuated acute morphine-induced dopamine release in the NAc, as well as attenuated morphine-induced rewarding behavior when co-administered with morphine (Grenald et al., 2017). Additionally, systemic administration of an endocannabinoid 2-arachidonyl glycerol (2-AG) or the inhibitor of its degrading enzyme MAGL, JZL184, significantly enhanced dopamine release in NAc (Oleson et al., 2012; De Luca et al., 2014). Interestingly, another study utilizing a dual FAAH (the primary enzymes that hydrolyzes the endocannabinoid anandamide (AEA) in the brain)-MAGL inhibitor, SA-57, reduced heroin-reinforced nose poke behavior and the progressive ratio break point for heroin (Wilkerson et al., 2017). Although distinct phenomena might be observed from different studies, current evidence strongly suggests the ECS can modulate and possibly participate in the development of opioid reward.

Current data propose that the ECS modulates opioid reward primarily via a disinhibitory feedback loop mediated by the 2-AG/CB1R axis in the mesolimbic circuitry (Zlebnik and Cheer, 2016). During periods of burst firing, VTA dopamine neurons release 2-AG onto the presynaptic GABAergic terminals in VTA (Lecca et al., 2012). The CB1R activation by 2-AG disinhibits the GABA-mediated inhibition of dopamine neurons, thus enhancing dopamine neuron activity (Melis et al., 2004; Riegel and Lupica, 2004; Fitzgerald et al., 2012). Recently, studies showed that CB2Rs are functionally expressed on the VTA dopamine neurons and can significantly suppress the activity of these neurons in the presence of cocaine, suggesting a potential ECS-mediated modulatory mechanism of opioid reward (Zhang et al., 2014; Zhang et al., 2017).

Considering the major impact of the endocannabinoid system on the rewarding effects of opioids, one important question is how the ECS in the mesolimbic reward circuitry responds to sustained exposure of opioids. To date, only a few studies have explored this research question (Rubino et al., 1997; Cichewicz et al., 2001; Gonzalez et al., 2002; González et al., 2003; Viganò et al., 2003; Viganò et al., 2004; Caillé et al., 2007; Jin et al., 2014). However, none of these studies have investigated the possible changes in the VTA. Additionally, most of these studies merely focused on analyzing the expression of CB1Rs, which lack a comprehensive understanding of the alterations in the whole ECS. Therefore, our present study sought to 1) obtain a thorough picture of the ECS-related proteins expressed in the VTA and their possible alterations induced by repeated opioid treatment through unbiased quantitative proteomics and 2) investigate the VTA levels of the two major endocannabinoids (AEA and 2-AG) by *in vivo* microdialysis after repeated morphine treatment.

MATERIALS AND METHODS

Animals

Two hundred and twenty-three male Sprague Dawley rats (7–8 weeks old), purchased from Envigo (Indianapolis, IN), were maintained in a climate-controlled room on a 12 h light-dark cycle and allowed food and water *ad libitum*. Rats were housed three per cage for all experiments except for those that received guide cannula implantation, which were housed individually. All procedures were approved by the University of Arizona Animal Care and Use Committee (Approval #06–110) and adhere to the guidelines issued by the National Institutes of Health and the International Association for the Study of Pain.

Drug Treatment

MJN110, a selective MAGL inhibitor (MAGL IC_{50} = 9.1 nM, over 1,000-fold selectivity vs. FAAH (Niphakis et al., 2013)), was purchased from Cayman Chemical (#17583, Ann Arbor, MI). JWH015, a selective CB2R agonist (CB2R Ki = 13.8 nM, 28-fold selectivity vs. CB1R (Showalter et al., 1996)), was purchased from Tocris (#1341, Minneapolis, MN). MJN110 and JWH015 were dissolved in a vehicle solution consisting of 10% dimethyl sulfoxide, 10% Tween-80, and 80% saline for injection (1 ml/kg, i. p.) with dosages of 5 and 3 mg/kg, respectively,

based on the previous studies (Niphakis et al., 2013; Grenald et al., 2017; Thompson et al., 2020). Morphine sulfate was obtained from the NIDA Drug Supply program and was dissolved in saline for injection (1 ml/kg). Sustained morphine administration as previously described was performed by intraperitoneal injections of morphine sulfate to rats at a dose of 5 mg/kg twice daily (9:00 am and 5:00 pm) for five consecutive days (Viganò et al., 2003; Tumati et al., 2012; Campbell et al., 2013), which was intended to mimic the repeated use and systemic administration of opioids in humans (Ballantyne and Mao, 2003; Abrams et al., 2011; Surratt et al., 2011; Volkow and McLellan, 2016). For conditioned place preference testing, rats received a total of five injections of morphine at a dose of 10 mg/kg intraperitoneally over five consecutive days.

Ventral Tegmental Area Tissue Collection

One hour after the last morphine or saline injection, rats were anesthetized with ketamine (80 mg/kg)/xylazine (10 mg/kg) mix and transcardially perfused with phosphate buffered saline (pH 7.4). Brains were carefully removed, and the VTA tissues (bilateral) were rapidly dissected on ice by using disposable biopsy punches (1 mm diameter) according to the Paxinos and Watson Atlas (Paxinos and Watson, 2007). Immediately after tissue harvest, the VTA samples were snap frozen in liquid nitrogen and then stored at −80°C until they were used for proteomics, western blotting, and quantitative real-time polymerase chain reaction.

Proteomics Analysis

In-gel Digestion

Each VTA sample (3–4 mg VTA tissue from one rat) was lyzed in 60 µL chilled RIPA buffer (#89900, Thermo Scientific, Rockford, IL) with protease inhibitor cocktail (1: 50 dilution, #B14002, Bimake, Houston, TX). Immediately after adding the lysis buffer, samples were homogenized via ultrasonication (3 short bursts) and centrifuged at 15,000 g for 10 min at 4°C. The supernatant was transferred into a clean 1.5 ml tube, and the protein concentration in the tissue lysates were determined using Pierce BCA protein assay kit (#23225, Thermo Scientific, Rockford, IL). The protein concentration of each sample was ~2–3 µg/µL 100 µg boiled tissue lysate was separated by SDS-PAGE and stained with Bio-Safe Coomassie G-250 Stain (#1610786; Biorad, Hercules, CA). Each lane of the SDS-PAGE gel was cut into seven slices. The gel slices were subjected to trypsin digestion and the resulting peptides were purified by C^{18}-based desalting exactly as previously described (Kruse et al., 2017; Parker et al., 2019).

Mass Spectrometry and Database Search

HPLC-ESI-MS/MS was performed in positive ion mode on a Thermo Scientific Orbitrap Fusion Lumos tribrid mass spectrometer fitted with an EASY-Spray Source (Thermo Scientific, San Jose, CA). NanoLC was performed as previously described (Kruse et al., 2017; Parker et al., 2019). Tandem mass spectra were extracted from Xcalibur "RAW" files and charge states were assigned using the ProteoWizard 2.1. x msConvert script using the default parameters. The fragment mass spectra were searched against the rattus SwissProt_2018 database (8,068 entries) using Mascot (Matrix Science, London, United Kingdom; version 2.4) using the default probability cut-off score. The search variables that were used were: 10 ppm mass tolerance for precursor ion masses and 0.5 Da for product ion masses; digestion with trypsin; a maximum of two missed tryptic cleavages; variable modifications of oxidation of methionine and phosphorylation of serine, threonine, and tyrosine. Cross-correlation of Mascot search results with X! Tandem was accomplished with Scaffold (version Scaffold_4.8.7; Proteome Software, Portland, OR, United States). Probability assessment of peptide assignments and protein identifications were made using Scaffold. Only peptides with ≥95% probability were considered.

Label-free Peptide/protein Quantification and Identification

Progenesis QI for proteomics software (version 2.4, Nonlinear Dynamics Ltd., Newcastle upon Tyne, United Kingdom) was used to perform ion-intensity based label-free quantification. In brief, in an automated format, raw files were imported and converted into two-dimensional maps (y-axis = time, x-axis = m/z) followed by selection of a reference run for alignment purposes. An aggregate data set containing all peak information from all samples was created from the aligned runs, which was then further narrowed down by selecting only +2, +3, and +4 charged ions for further analysis. The samples were then grouped and a peak list of fragment ion spectra from only the top eight most intense precursors of a feature was exported in Mascot generic file (.mgf) format and searched against the rattus SwissProt_2018 database (8,068 entries) using Mascot (Matrix Science, London, United Kingdom; version 2.4). The search variables that were used were: 10 ppm mass tolerance for precursor ion masses and 0.5 Da for product ion masses; digestion with trypsin; a maximum of two missed tryptic cleavages; variable modifications of oxidation of methionine and phosphorylation of serine, threonine, and tyrosine; 13C = 1. The resulting Mascot. xml file was then imported into Progenesis, allowing for peptide/protein assignment, while peptides with a Mascot Ion Score of <25 were not considered for further analysis. Protein quantification was performed using only non-conflicting peptides and precursor ion-abundance values were normalized in a run to those in a reference run (not necessarily the same as the alignment reference run). Principal component analysis and unbiased hierarchal clustering analysis (heat map) was performed in Perseus (Tyanova et al., 2016; Tyanova and Cox, 2018) while Volcano plots were generated in Rstudio. Gene ontology (GO) and Kyoto Encyclopedia of Genes and Genomes (KEGG) pathway enrichment analysis was performed with DAVID (Huang et al., 2009).

Western Blotting

Tissue lysates were prepared as for the proteomics analysis (methods above). Protein samples from each tissue lysate were resolved on 10% SDS-polyacrylamide gels (Criterion TGX, Bio-rad, Hercules, CA) and subsequently transferred to

polyvinylidene difluoride (PVDF) membranes (Bio-rad, Hercules, CA). PVDF Membrane was blocked with 5% BSA in Tris-buffered saline containing 0.5% (v/v) Tween-20 (TBST) for 1 h at room temperature, and then incubated with different primary antibodies, including anti-rat CB1R antibody (rabbit polyclonal, 1:1,000 dilution), anti-rat DAGLα antibody (rabbit polyclonal, 1:4,000 dilution), anti-rat MAGL antibody (rabbit polyclonal, 1:2,000 dilution), and anti-α-tubulin (cp06, Calbiochem; mouse monoclonal, 1:50,000 dilution). All antibodies were diluted in Tris-buffered saline containing 0.5% (v/v) Tween-20 (TBST) and 3% (w/v) bovine serum albumin (BSA). Anti-rat CB1, DAGLα, and MAGL antibodies are kind gifts from Dr Ken Mackie. HRP-linked anti-rabbit IgG (7,074, Cell Signaling, Danvers, MA) and HRP-linked anti-mouse IgG (7,076, Cell Signaling, Danvers, MA) were used as the secondary antibodies for corresponding primary antibodies. The membranes were developed by using Clarity Western ECL substrate (#1705061, Bio-rad, Hercules, CA), and the blots were detected by GeneMate Blue Lite Autorad films (BioExpress, Kaysville, UT) and later quantitated with ImageJ 1.50i (Wayne Rasband, NIH, United States). All data were normalized to the α-tubulin signal for each sample. To probe a second protein on the same membranes, the membranes were washed in TBST and then stripped in the OneMinute Plus stripping buffer (GM6015, GM Biosciences, Frederick, MD). After a second run of wash in TBST, the membranes were blocked and then stained with another primary antibody.

Quantitative Real-Time Polymerase Chain Reaction

Quantitative real-time polymerase chain reaction (qRT-PCR) was performed as described previously (Ibrahim et al., 2017). RNA was extracted from VTA tissues using TRIzol reagent (#15596026, Invitrogen, Carlsbad, CA) according to the manufacturer's protocol. Briefly, samples were homogenized in 500 μL TRIzol reagent, and then 100 μL chloroform was added to each homogenate. After centrifugation, the upper aqueous phase containing RNA was transferred to a new tube and total RNA was subsequently precipitated after adding 250 μL isopropanol to the aqueous phase. Following by another centrifugation, the RNA precipitates were washed with 75% ethanol and resuspended in 20 μL DEPC-treated water (ThermoFisher, Grand Island, NY). cDNA was generated immediately after RNA extraction using the Maxima Reverse transcriptase kit (#K1641, ThermoFisher, Grand Island, NY) according to its manufacturer's protocol. qRT-PCR analysis was performed using 5x HOT FIREPol EvaGreen qPCR Mix Plus (08–25–00001, Solis Biodyne, Estonia) on a CFX connect real-time PCR detection system (Bio-rad, Hercules, CA) according to the manufactures protocol. The relative mRNA expression for CB1R and CB2R genes was normalized to β-actin mRNA level and calculated with the ΔΔCt method (Livak and Schmittgen, 2001). The sequences of all specific primers were listed below: Rat CB1R (forward 5'- ACCTAC CTGATGTTCTGGATTGGG -3', reverse 5'- CGTGTGGAT GATGATGCTCTTCTG -3′), Rat CB2R (forward 5'- CTCGTA CCTGTTCATCGGCA -3', reverse 5'- GTATCGGTCAACAGC GGTCA -3') and Rat β-actin (forward TAAGGCCAACCGTGA AAAGATGA -3', reverse 5'- TAAGGCCAACCGTGAAAAGAT GA -3'). The primers for ABHD6 and PLCγ2 were acquired from Qiagen RT2 qPCR Primer Assays (ABHD6: PPR46100A-200 (NM_001007680); PLCγ2: PPR44457A-200 (NM_017168)).

In vivo Endocannabinoid Analysis

Cannulation Implantation

Rats were anesthetized with ketamine (80 mg/kg)/xylazine (10 mg/kg) mix and secured in a stereotaxic apparatus (Stoelting, Wood Dale, IL). A unilateral microdialysis guide cannula (20 mm, MAB 2/6/9.20. G, SciPro, Sanborn, NY) was implanted into the ventral tegmental area (VTA) according to the Paxinos and Watson Atlas (Paxinos and Watson, 2007): AP −5.9 mm, ML +0.5 mm, and DV −8.2 mm from bregma. The guide cannula was fixed in place with skull screws and dental cement. All rats were injected with the antibiotic gentamicin (8 mg/kg, s. c.) to prevent infection. Morphine treatment started on the same day of surgery. Due to the small nuclei target, the successful rate of the cannula placement is ~50%, with a total of n = 44 rats excluded for off target placement.

In vivo Microdialysis of Endocannabinoids in Awake Animals

In vivo Microdialysis experiments were conducted on the last day of repeated morphine treatment. The performance of microdialysis was modified from previous studies (Buczynski and Parsons, 2010; Wiskerke et al., 2012; Grenald et al., 2017). Two hours prior to sample collection, rats were lightly anesthetized for ~2 min with 2% isoflurane for smooth insertion of a microdialysis probe (1 mm PES membrane and 15kD cut-off; MAB 6.20.1; 1 mm protruded beyond guide cannula) through and secured in the guide cannula. Immediately after probe insertion, the isoflurane anesthesia was discontinued and artificial cerebral spinal fluid (aCSF) containing 10% (w/v) hydroxypropyl-β-cyclodextrin (#16169, Cayman Chemical, Ann Arbor, MI) was perfused through the microdialysis probe and equilibrated within the brain tissue at a flow rate of 1 μL/min. Following this 2 h baseline period, all rats were injected with morphine (5 mg/kg, i. p.) and dialysate samples were collected every 30 min (30 μL total volume at each time point) for a total of 4 h. Collected samples were frozen in dry ice after each 30 min interval and subsequently stored at −80°C until further analysis. Upon completion, rats were sacrificed, and their brains were harvested and fixed in 10% formalin solution to verify cannula placement. Coronal slices containing the VTA were sectioned at a thickness of 40 μm on a cryostat. Guide cannula placements were verified visually and only those rats with correct cannula placement were used for final analysis.

Quantification of Endocannabinoid Contents in Microdialysates

Analysis of 2-AG and AEA contents in microdialysates was performed by the University of Arizona *Cancer* Center Analytical Chemistry Core on an Ultivo triple quadrupole mass spectrometer combined with a 1,290 Infinity II UPLC

system (Agilent, Palo Alto, CA). Samples for analysis were prepared by mixing 10 µL internal standard solution (a mixture of 5.213 nM d_4-AEA and 5.688 nM d_4-2-AG in acetonitrile) to 20 µL microdialysate and then centrifuged at 15,800 xg for 5 min at 4°C. The supernatant was transferred to autosampler vials and 5 µL was injected for analysis. Chromatographic separation was achieved using an isocratic system of 21% 1 mM ammonium fluoride and 79% methanol on an Acquity UPLC BEH C-18 1.7u 2.1 × 100 mm column (Waters, Milford, MA) maintained at 60°C with a flow rate of 400 µL/min. After each injection the column was washed with 90% methanol for 1 min and then re-equilibrated for 5 min prior to the next injection. The mass spectrometer was operated in electrospray positive mode with a gas temperature of 150°C at a flow of 5 L/min, nebulizer at 15 psi, capillary voltage of 4,500 V, sheath gas at 400°C with a flow of 12 L/min and nozzle voltage of 300 V. The transitions monitored were: *m/z*348.3→*m/z*287.3 (d_0-AEA), *m/z*352.3→*m/z*287.4 (d_4-AEA), *m/z*379.3→*m/z*287.2 and 269.2 (d_0-2-AG), and *m/z*348.3→*m/z*287.2 and 296.1 (d_4-2-AG). As 2-AG is reported to be relatively unstable and can rapidly convert to 1-AG (Caillé et al., 2007), the 2-AG and 1-AG peak areas were combined for all analyses in the present study. The quantification of AEA and 2-AG was achieved by using calibration curves, which were prepared by serial dilution of AEA and 2-AG stock solutions in 80% acetonitrile. The stock solutions of AEA, 2-AG, d_4-AEA and d_4-2-AG were purchased from Cayman Chemical (Ann Arbor, MI).

Conditioned Place Preference

The procedure of conditioned place preference (CPP) was modified from our previous studies (Grenald et al., 2017; Sandweiss et al., 2018). Rats were preconditioned to a three-chambered CPP apparatus (San Diego Instruments, San Diego, CA) for 15 min to acquire their baseline preference for the two side chambers. Only rats that showed no basal preference (<80% of the total time) or aversion (>20% of the total time) to any end chambers were used and randomly assigned for further conditioning experiments over the next 5 days. In our experiments, approximate 10–20% rats were excluded every time due to basal preference. In the morning session of the first conditioning day, rats were pretreated with MJN110 (5 mg/kg, i. p.), JWH015 (3 mg/kg, i. p.) or vehicle, and then were returned to their home cages. To ensure that JWH015 is on board and interacting at CB2R, animals were injected with morphine (10 mg/kg, i. p.) or saline 30 min after the pretreatment. This treatment time point has been applied frequently by previous studies using JWH015 or similar compounds (Ma et al., 2012; Verty et al., 2015; Zhang et al., 2018). Immediately after morphine/saline treatment, animals were confined to one end chamber (drug-paired chamber) for 15 min. In the afternoon session, all rats were pretreated with vehicle followed by an injection of saline and paired with opposite end chamber (non-drug paired chamber) as a control. All chambers were thoroughly cleaned after each trial to prevent effects of scent on behavior in the following trials. The same procedures were repeated on the conditioning days 2–5 while the morning and afternoon sessions in days 2–4 were inverted to counter-balance a putative effect of the circadian rhythm. In the morning of the test day (day 6), rats could explore all chambers of the CPP box freely for 15 min and the total time they spent in each chamber was recorded to determine their chamber preference. The chamber preference is presented as CPP score, which is calculated as below:

CPP difference score = Time spent in drug-paired chamber on the test day
– Time spent in drug-paired chamber on baseline day

Statistical Analysis

Power analyses were performed on cumulated data using G*Power 3.1 software (Faul et al., 2009) to estimate the optimal numbers of animals required for each experiment, and we found the adequate statistical separation for each group to detect 0.80 between groups at $p < 0.05$. ANOVA was used to analyze the expression difference between repeated morphine and saline-treated samples in the proteomic analysis. Two-way ANOVA with Tukey's and Sidak's multiple comparisons tests were used to analyze the time effect and group difference of the endocannabinoid production, respectively. Unpaired *t* test was used to compare the expression difference in proteomic analysis, western blotting, qRT-PCR and MAGL activity assay. One-way ANOVA with Dunnett's multiple comparisons test was used to analyze the CPP tests. All data are presented as mean ± standard error of the mean (SEM) and a value of $p < 0.05$ was accepted as statistically significant. GraphPad Prism 8.0 (Graph Pad Inc., San Diego, CA) was used to perform statistical analyses and generate plots.

RESULTS

The Effects of Sustained Morphine on the Ventral Tegmental Area Proteome

To obtain a global picture of protein expression alterations in the VTA endogenous cannabinoid system after sustained opioid exposure, we carried out HPLC-ESI-MS/MS-based proteomic analysis of VTA tissues harvested from sustained morphine or saline-treated rats (**Figure 1A**). This analysis identified 3,680 total proteins across a total of 56 fractions from eight biological samples (**Supplementary Table S1**). 162 identified proteins were significantly ($p < 0.05$) affected by sustained morphine exposure, 37 of which had over 2-fold expression difference (**Figure 1B**; **Supplementary Table S1**). Of the 162 significantly regulated proteins, the expression levels of 117 were decreased after sustained morphine exposure and the levels of 45 were increased. Unbiased principal component analysis (PCA) of the 162 significantly affected proteins from the 2-way ANOVA analysis suggested a good consistency among the samples within each treatment group (**Figure 1C**), data that were supported by unbiased hierarchical clustering analysis (**Figure 1D**). The Gene Ontology (GO) enrichment and KEGG analyses of the significantly affected proteins were performed for GO-Molecular Function, Cellular Component and Biological Process as well as KEGG pathways, and the

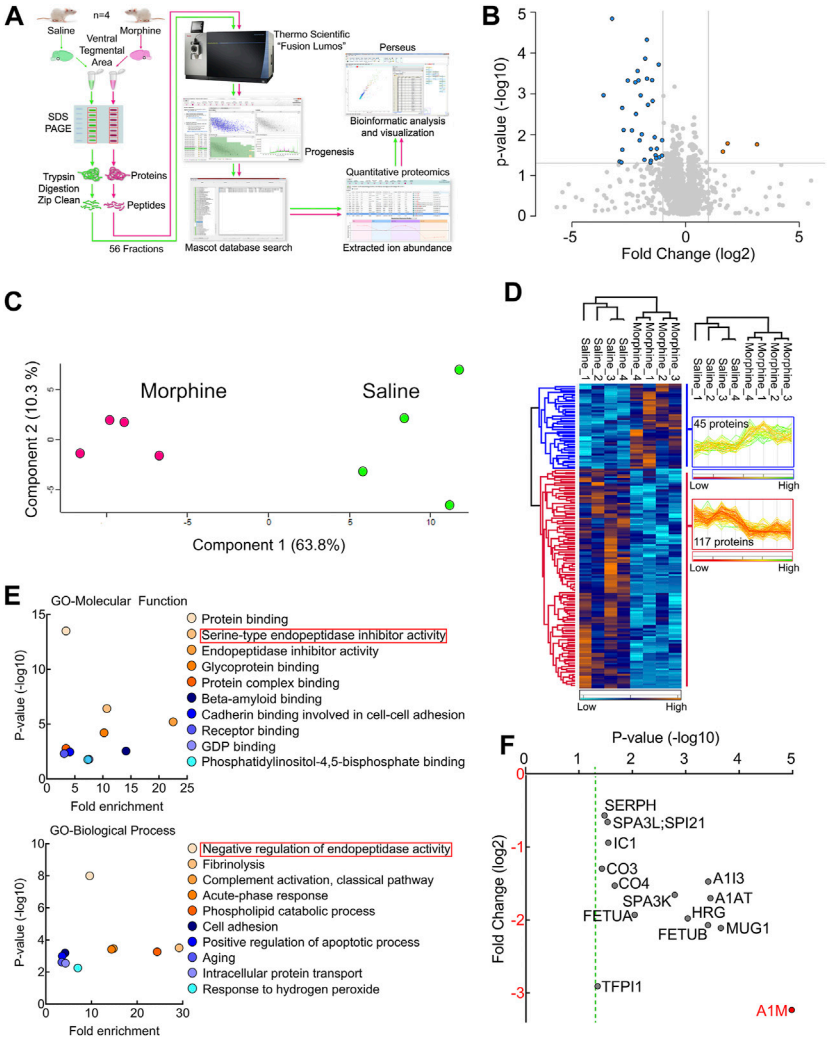

FIGURE 1 | Proteomic analysis of the endogenous cannabinoid system-related proteins in rat VTA. **(A)** Experimental design for VTA tissue collection. **(B)** Schematic diagram of the label-free quantitative proteomics experimental approach. VTA tissues acquired from repeated morphine- or saline-treated rats were processed and used for performing proteomic analysis as described in Methods and Materials. **(C)** A volcano plot of the proteins identified in the VTA tissues treated with sustained morphine or saline. Above the horizontal gray line represents the cut-off for a *p* value of <0.05 while the two vertical lines represent the cut-off values of 2-fold change in either the positive or negative direction. **(D)** Unbiased principal component analysis (PCA) of the 162 significantly affected proteins from the 2-way ANOVA analysis of the quantitative proteomics data revealed that the protein expression differences of the individual biological samples within each group were consistent. **(E)** Unbiased hierarchical clustering of the 162 significantly affected proteins in the sustained morphine vs. saline treatment groups confirmed that the expression patterns across the different individual biological samples cluster together. **(F)** Scatter plots of the Gene Ontology (GO) enrichment findings for the significantly affected proteins after repeated morphine treatment. **(G)** Scatter plot of the endopeptidase inhibitors that are significantly affected by repeated morphine treatment. The Fold Change axis is labeled red to represent that treatment with morphine results in a decrease in the endopeptidase inhibitor proteins identified. The vertical dashed green line represents the *p* cut-off value of <0.05. α-1-macroglobulin is labeled in red to highlight the most significantly affected protein after morphine treatment. *n* = 4 per group.

results are presented in **Figure 1E**; **Supplementary Table S2**. Interestingly, our analyses of GO-Molecular Function and GO-Biological Process suggest that the endopeptidase inhibitors are the most affected proteins in the VTA following repeated morphine treatment (All 14 proteins were reduced significantly and 11 of them had over 2-fold reduction in expression; **Figures 1E, F**; **Supplementary Table S3**). α-1-macroglobulin was the most significantly affected protein out of all 3,680 proteins, which has the largest fold change loss after morphine treatment of all the significantly affected proteins related to endopeptidase activity (labeled red in **Figure 1F**).

Sustained Morphine Induces Proteomic Changes in the Ventral Tegmental Area Endogenous Cannabinoid System

In the proteomic analysis, 31 endogenous cannabinoid system-related proteins were detected in the VTA (**Table 1**). Two of these proteins, phospholipase Cγ-2 (PLCγ2) and α/β-hydrolase

TABLE 1 | Expression alterations of the endogenous cannabinoid system-related proteins in the VTA after chronic morphine exposure.

Protein name	Gene name	MW (kDa)[a]	Fold change[b]	Anova P value[c]
Receptors for cannabinoids				
Cannabinoid receptor 1	CNR1	52.8	0.85	0.380
Transient receptor potential cation channel subfamily V member 1	TRPV1	94.9	0.54	0.924
Enzymes related to endocannabinoid synthesis				
1-Phosphatidylinositol 4,5-bisphosphate phosphodiesterase beta-1	PLCB1	138.3	1.04	0.595
1-Phosphatidylinositol 4,5-bisphosphate phosphodiesterase beta-3	PLCB3	139.4	0.88	0.164
1-Phosphatidylinositol 4,5-bisphosphate phosphodiesterase beta-4	PLCB4	134.4	1.04	0.721
1-Phosphatidylinositol 4,5-bisphosphate phosphodiesterase delta-1	PLCD1	85.9	1.01	0.971
1-Phosphatidylinositol 4,5-bisphosphate phosphodiesterase delta-4	PLCD4	88.9	0.64	0.059
1-Phosphatidylinositol 4,5-bisphosphate phosphodiesterase gamma-1	PLCG1	148.5	0.90	0.134
1-Phosphatidylinositol 4,5-bisphosphate phosphodiesterase gamma-2	PLCG2	147.6	0.63	0.035*
Glycerophosphodiester phosphodiesterase 1	GDE1	37.6	0.72	0.089
N-acyl-phosphatidylethanolamine-hydrolyzing phospholipase D	NAPEPLD	45.7	1.07	0.913
Phosphatidylinositol 3,4,5-trisphosphate 5-phosphatase 1	SHIP1	133.5	0.87	0.923
Sn1-specific diacylglycerol lipase alpha	DAGLA	115.2	0.53	0.107
Enzymes related to endocannabinoid degradation				
Arachidonate 12-lipoxygenase, 12 R type	ALOX12 B	80.7	0.92	0.354
Cytochrome P450 2C70	CYP2C70	56.1	1.07	0.365
Cytochrome P450 2D4	CYP2D4	56.6	1.04	0.833
Cytochrome P450 4F5	CYP4F5	60.6	0.72	0.105
Fatty-acid amide hydrolase 1	FAAH1	63.3	1.14	0.305
Monoacylglycerol lipase, abhydrolase domain containing 6	ABHD6	38.3	0.69	0.031*
Monoacylglycerol lipase, abhydrolase domain containing 12	ABHD12	45.3	1.03	0.648
Monoglyceride lipase	MGLL	33.5	1.00	0.956
N-acylethanolamine-hydrolyzing acid amidase	NAAA	40.3	0.81	0.410
Endocannabinoid transport proteins				
Fatty acid-binding protein 5	FABP5	15.1	0.85	0.495
Fatty acid-binding protein 7	FABP7	14.9	0.97	0.810
Heat shock 70 kDa protein 1 A	HSPA1A	70.1	1.59	0.143
Heat shock 70 kDa protein 1-like	HSPA1L	70.5	0.80	0.975
Heat shock-related 70 kDa protein 2	HSPA2	69.6	1.20	0.491
Heat shock 70 kDa protein 4	HSPA4	94.0	1.04	0.668
Heat shock 70 kDa protein 13	HSPA13	51.8	0.95	0.734
Heat shock 70 kDa protein 14	HSPA14	54.4	1.29	0.283
Regulatory protein				
CB1 cannabinoid receptor-interacting protein 1	CNRIP1	18.6	1.08	0.619

[a]*MW, molecular weight.*

[b]*Expression difference is presented as the fold change of the protein abundance in the tissues after chronic morphine treatment: fold change = protein expression level (after sustained morphine treatment)/protein expression level (after saline treatment).*

[c]*$p < 0.05$.

domain containing 6 (ABHD6), were significantly downregulated after sustained morphine exposure. To verify the results of our proteomic analysis, we examined the expression of PLCγ2 and ABHD6 as well as several proteins that are demonstrated as the major contributors to the endocannabinoid signaling in the central nervous system, including diacylglycerol lipase α (DAGLα), monoglyceride lipase (MAGL) and CB1R, using either western blotting or qPCR. Consistent with our proteomic data, DAGLα, MAGL and CB1R were not significantly altered in the VTA after repeated morphine treatment (DAGLα: t (10) = 1.27, $p = 0.23$; MAGL: t (10) = 1.73, $p = 0.11$; CB1R: t (10) = 0.47, $p = 0.65$) (**Figures 2A–F**), yet findings for the PLCγ2 using qPCR demonstrated PLCγ2 was significantly downregulated after morphine treatment (t (10) = 8.65, $p < 0.0001$) (**Figure 3A**). These results indicate the accuracy and reproducibility of the proteomic analysis (t (10) = 1.70, $p = 0.12$). Interestingly, ABHD6 detected by qPCR was not shown to be altered by sustained morphine (**Figure 3B**), suggesting its downregulation detected by proteomics may not be controlled at the transcription level.

CB2R, a critical member of the endogenous cannabinoid system, was recently demonstrated as playing a key role in drug addiction (Xi et al., 2011; Navarrete et al., 2013; Ortega-Álvaro et al., 2015; Grenald et al., 2017). However, due to its low expression level in the central nervous system, this receptor was not detected with current mass spectrometry-based or antibody-based techniques (Cécyre et al., 2014; Marchalant et al., 2014; Li and Kim, 2015). To examine the expression of CB2R in the VTA, we employed quantitative real-time PCR. Our results showed that sustained morphine significantly decreased the mRNA expression level of CB2Rs by 17% (t (10) = 2.82, $p < 0.05$) (**Figure 3C**). In contrast, no significant difference of CB1R expression between repeated morphine-treated and saline-treated groups was found (t (10) = 0.77, $p = 0.46$) (**Figure 3D**), which is consistent with our previous protein observation (**Figure 2F**).

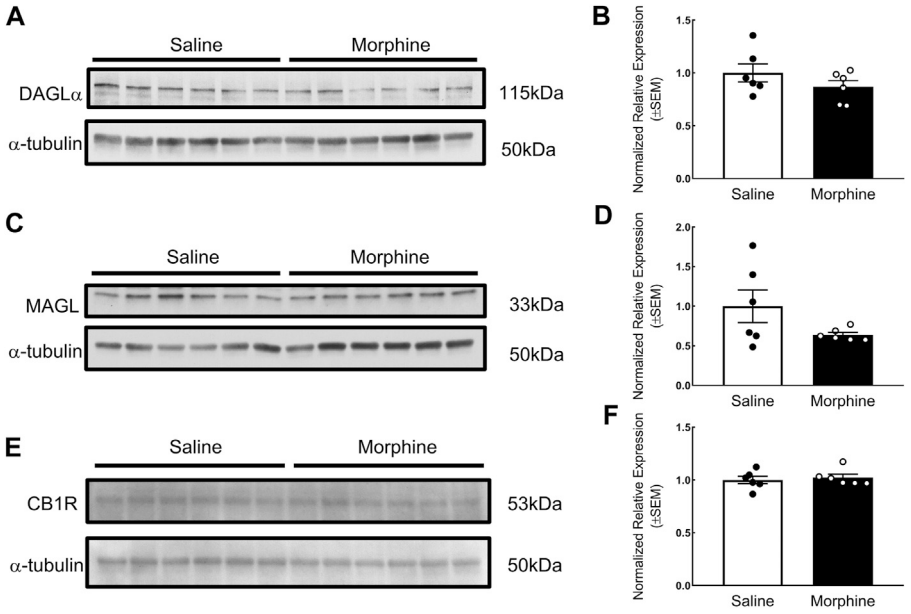

FIGURE 2 | Verification of the effects of sustained morphine on DAGLα, MAGL and CB1R expression in the VTA. Rats were sacrificed after repeated morphine or saline treatment, and the VTA tissues were then collected and prepared for western blot analysis. **(A, C and E)** Samples were analyzed for the expression of DAGLα, MAGL, and CB1R. **(B, D and F)** Relative expression levels of DAGLα, MAGL, and CB1R were determined by densitometric analysis and normalized to *a*-tubulin (as internal control) in each lane. No significant difference in the expression of DAGLα, MAGL, and CB1R was observed between two treatment groups. Values represent the mean ± SEM, $n = 6$ per group.

The Effects of Sustained Morphine on the Production of Endocannabinoids in the Ventral Tegmental Area

Next, to determine the influence of sustained morphine on the production of the endocannabinoids 2-AG and AEA, we employed *in vivo* microdialysis in the VTA of awake rats after sustained morphine administration (**Figures 4A,B**). Our results found that, one day after repeated morphine treatment, the production of 2-AG in the VTA was not significantly changed compared to saline-treated group (Interaction: F (11, 187) = 0.72, $p = 0.71$; Time: F (2.714, 46.14) = 1.60, $p = 0.21$; Column factor: F (1, 17) = 0.32, $p = 0.58$; Subject: F (17, 187) = 31.89, $p < 0.0001$) (**Figure 4C**; t = −120–0 min). However, considering the possibility that sustained morphine-induced 2-AG alteration have returned to the baseline level, we performed an additional injection of morphine (5 mg/kg, i. p.) to both sustained morphine-treated and saline treated rats and determined whether the 2-AG production may be altered compared to the baseline levels. Again, no significant difference of 2-AG production was identified compared to baseline levels or between two treatment groups (**Figure 4C**).

In addition to 2-AG, we also investigated the effects of sustained morphine on AEA production. Similarly, no significant difference in AEA production was observed between repeated morphine-treated and saline treated rats before (baseline session; $t = -120–0$ min) or after the morphine challenge in both groups (morphine challenge session; $t = 0–240$ min) (Interaction: F (11, 198) = 0.41, $p = 0.95$; Time: F (2.045, 36.80) = 6.84, $p < 0.01$; Column factor: F (1, 18) = 0.02, $p = 0.88$; Subject: F (18, 198) = 59.01, $p < 0.0001$) (**Figure 4D**). Interestingly, we did identify a significant difference in AEA production between the baseline ($t = -90$ to 0 min) and the last time point of the morphine challenge session ($t = 240$ min) when data from both groups (chronic-saline and -morphine) were combined ($t = -90$ to 0 min vs. $t = 240$ min: $p < 0.05$) (**Figure 4D**), something not seen with 2-AG levels. The placement of all microdialysis guide cannulas was verified after experiments (**Figures 4E,F**).

The Modulatory Effects of 2-AG and CB2R on Sustained Morphine-Induced Reward

Lastly, we briefly investigated the possible roles of the proteins and genes regulated by sustained morphine in the modulation of opioid reward hoping to identify potential target(s) for the treatment of opioid reward and addiction. According to the proteomic data, we found that the expression of PLCγ2 and ABHD6 was downregulated by repeated morphine treatment. These two proteins are possibly implicated in the production of 2-AG (Blankman et al., 2007; Kadamur and Ross, 2013). Although the *in vivo* microdialysis showed that sustained morphine does not modulate 2-AG level in VTA, it is still possible that 2-AG can exert regulatory effects on sustained morphine-induced reward. To examine this idea, we facilitated the production of endogenous 2-AG on sustained morphine-induced reward pharmacologically using conditioned place preference assay (**Figure 5A**). Our results showed that rats receiving sustained morphine exhibited a

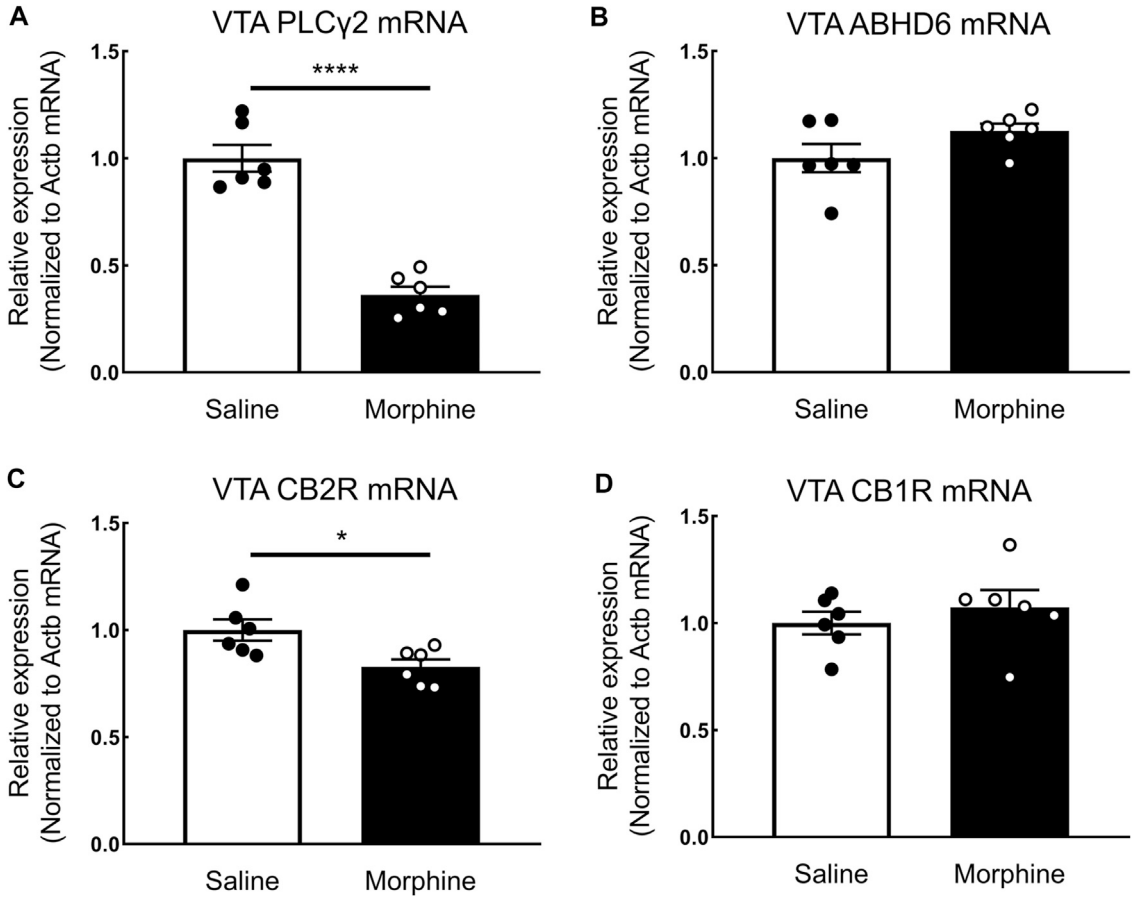

FIGURE 3 | The effects of sustained morphine on the mRNA expression of PLCγ2, ABHD6, CB1Rs, and CB2Rs in the VTA. Rats were sacrificed after sustained morphine or saline treatment, and the VTA tissues were then collected and prepared for qRT-PCR analysis. Relative mRNA expression levels of **(A)** PLCγ2, **(B)** ABHD6, **(C)** CB2R, and **(D)** CB1R were determined by ΔΔCT method and normalized to β-actin mRNA level. PLCγ2 and CB2R mRNA expression was significantly decreased in repeated morphine treatment, but no significant difference in ABHD6 and CB1 expression was observed between two treatment groups. *$p < 0.05$, ****$p < 0.0001$, morphine vs. saline. Values represent the mean ± SEM, $n = 6$ per group.

significant preference to the drug-paired chamber compared to the saline-treated rats reflecting by both CPP difference score and percentage of rats presenting CPP ($F(5, 79) = 9.62$, $p < 0.0001$; Vehicle + Morphine vs. Vehicle + Saline: $p < 0.0001$; CPP (>50°s): 88.89 vs. 18.18%) (**Figures 5B,C**). Increasing endogenous 2-AG tone by pretreatment with the selective MAGL inhibitor, MJN110 (5 mg/kg, i. p.), significantly reduced the time that animals spent in morphine-paired chambers and the proportion of animals showing CPP (Vehicle + Morphine vs. MJN110 + Morphine: $p < 0.01$; CPP (>50°s): 88.89 vs. 35.71%) (**Figures 5B,C**). Interestingly, we found that the rats received MJN110 alone showed a trend of aversion to drug-paired chamber although no statistically significant difference was observed in the CPP difference score compared to Vehicle-Saline group (Vehicle + Saline vs. MJN110 + Saline: $p = 0.64$; CPA (<50°s): 45.45 vs. 61.54%) (**Figures 5B,C**).

CB2R is another member of the endocannabinoid system we found to be regulated by repeated morphine treatment. Previously, the activation of CB1R has been repeatedly demonstrated to promote opioid-induced reward (Chaperon et al., 1998; Navarro et al., 2001; Caillé and Parsons, 2003, 2006; De Vries et al., 2003; Solinas et al., 2003; Singh et al., 2004; Rashidy-Pour et al., 2013; He et al., 2019). In the present study, we sought to investigate if CB2R can modulate sustained morphine-induced rewarding behaviors. We pre-treated the rats with a selective CB2R agonist, JWH015 (3 mg/kg, i. p.), prior to morphine or saline treatment. The results showed that the activation of CB2Rs markedly inhibited morphine-induced preference (Vehicle + Morphine vs. JWH015 + Morphine: $p < 0.05$; CPP (>50°s): 88.89 vs. 56.25%) (**Figures 5B,C**), while JWH015 treatment alone did not present preference to any chamber (**Figures 5B,C**).

DISCUSSION

The ECS has emerged as a hot topic in the study of opioid reward, given the large body of evidence linking this system to the formation and development of opioid reward, withdrawal and addiction (Chaperon et al., 1998; Ledent et al., 1999; Navarro

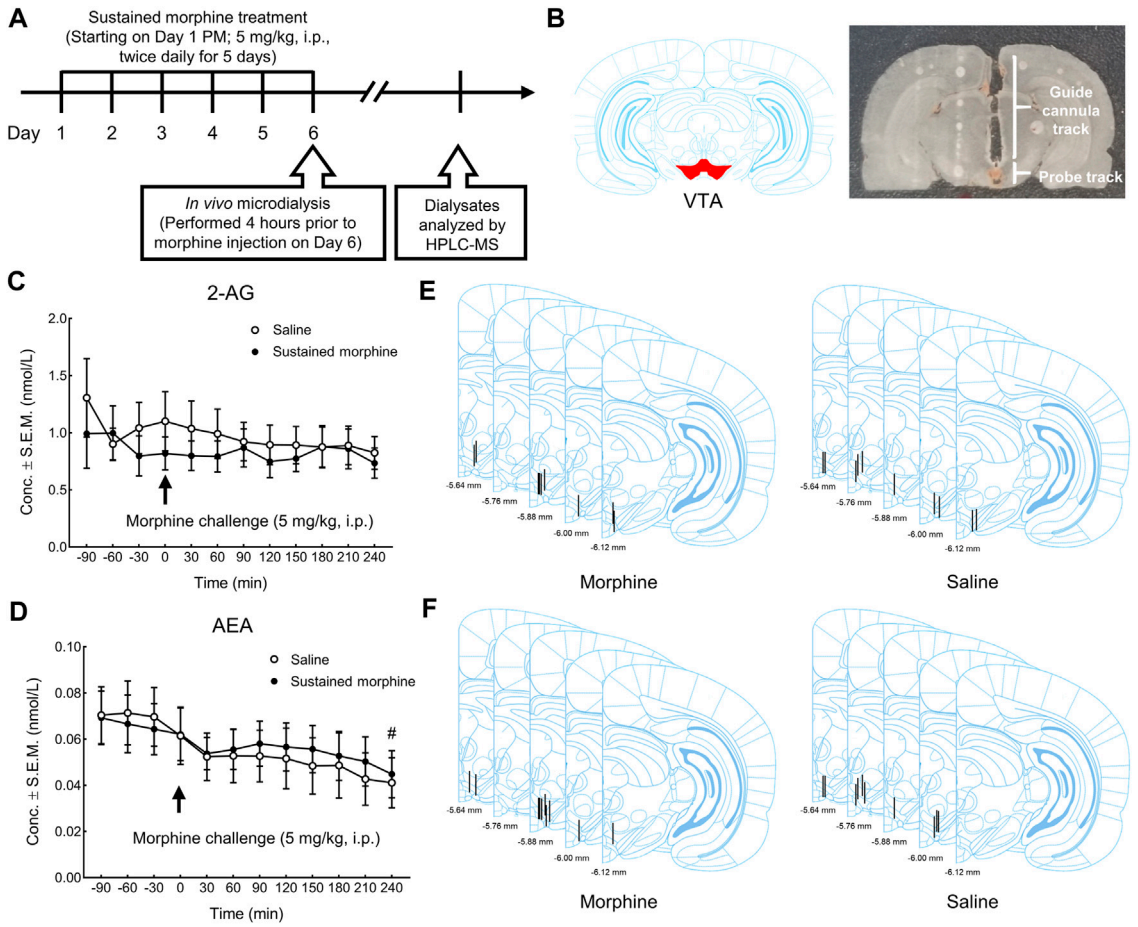

FIGURE 4 | The effects of sustained morphine on the production of 2-AG and AEA in the VTA. *In vivo* microdialysis was performed on rats one day after repeated morphine treatment to determine the alterations of endocannabinoids in VTA. Microdialysis samples were collected every 30 min for a total of 6 h. After the first 2 h baseline (t = −120–0 min), all rats received an additional injection of morphine and the changes in the production of endocannabinoids was observed for the next 4 h (t = 0–240 min). **(A)** Experimental design for *in vivo* microdialysis of endocannabinoids. **(B)** Representative brain section of microdialysis guide cannula/probe implantation. **(C, D)** no significant difference in the production of either 2-AG or AEA was observed between treatment groups at baseline session or in the morphine challenge session. However, a significant time effect in AEA production was observed between the baseline period and the last time point of the morphine challenge session (t = 240 min). **(E, F)** Anatomical representatives of microdialysis guide cannula placements in VTA for the studies of 2-AG and AEA. $^{\#}p < 0.05$, t = 240 min vs. baseline (t = −90 to 0 min). Values represent the mean ± SEM, n = 9–10 per group.

et al., 2001; Caillé and Parsons, 2003, 2006; De Vries et al., 2003; Solinas et al., 2003; Singh et al., 2004; Solinas et al., 2005; Luchicchi et al., 2010; Rashidy-Pour et al., 2013; Grenald et al., 2017; He et al., 2019). Recent studies showing promising synergistic effects of cannabinoids and opioids in chronic pain treatment further stimulate the interest of using cannabinoids to treat opioid abuse potential (Cichewicz, 2004; Tham et al., 2005; Bushlin et al., 2010; Abrams et al., 2011; Kazantzis et al., 2016; Grenald et al., 2017). However, very few studies have investigated the possible changes of ECS in the VTA - a key brain region mediating reward, in the presence of opioids, and no study has provided a comprehensive proteomic analysis of VTA following repeated opioid administration.

In the present studies using unbiased global proteomic analysis, we identified the expression of 31 proteins that belong to five different categories of the endogenous cannabinoid system in the VTA. Two proteins, PLCγ2, and ABHD6, were significantly downregulated by repeated morphine treatment. PLCγ2 is an enzyme belonging to the phospholipase C family that selectively hydrolyzes phosphatidylinositol 4, 5-biphosphate and generates diacylglycerol (DAG) (Kadamur and Ross, 2013). As DAG is the precursor of 2-AG, this downregulation of PLCγ2 may directly reduce the levels of 2-AG in the VTA. It is also possible that this decreased PLCγ2 expression may be a mechanism by which opioids modulate growth factor receptor-mediated synaptic regulation. Indeed, PLCγ2 is primarily activated by tyrosine protein kinases, such as growth factor receptors (Kadamur and Ross, 2013). ABHD6 is a newly identified member of the endocannabinoid system and contributes to approximate 4% of 2-AG hydrolysis measured in the whole mouse brain (Blankman et al., 2007), yet the ABHD6 activity is even higher than MAGL in select brain regions including select areas of the cortex, hippocampus, striatum

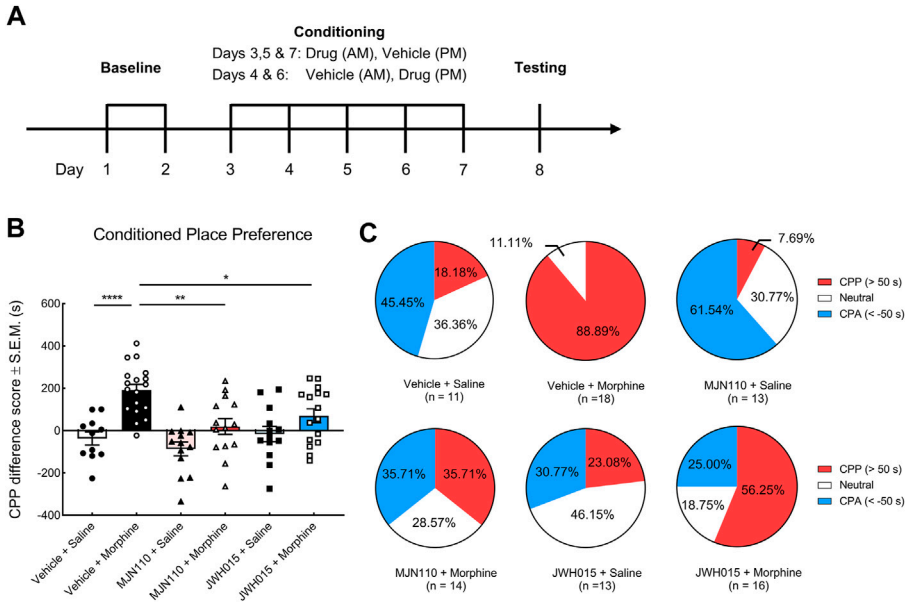

FIGURE 5 | The effects of systemic MJN110 and JWH015 on the sustained morphine-induced conditioned place preference. Conditioned place preference was employed to investigate the modulatory effects of a selective MAGL inhibitor, MJN110, and a selective CB2R agonist, JWH015, on sustained morphine-induced reward. **(A)** Experimental design of conditioned place preference assay. After baseline testing to establish approximate equal times in the two end chambers, rats were paired with a treatment and one of the end chambers for 5°days. Their chamber preference (access to all chambers) was tested on day 8 with no treatment administered. **(B)** Rats that received sustained morphine presented a strong preference toward the drug-paired chamber but not saline-treated rats. MJN110 significantly suppressed morphine-induced preference. MJN110 may produce aversive effect on rats but no statistic difference was observed compared to the results from vehicle-saline-treated rats. JWH015 attenuated morphine-induced preference but did not alter the preference in saline-treated rats. **(C)** Pie plots showing the percentages of rats exhibiting conditioned place preference, aversion or no preference. CPP (red): Animals presenting remarked conditioned place preference (CPP difference score >50°s); CPA (blue): Animals presenting remarked conditioned place aversion (CPP difference score < −50°s); Neutral (white), Animals presenting no remarked preference or aversion (CPP difference score between −50 and 50°s). or $^{*}p < 0.05$, $^{**}p < 0.01$, $^{****}p < 0.0001$. Values represent the mean ± SEM, n = 11–18 per group.

and cerebellum (Baggelaar et al., 2017). Previous evidence suggests that ABHD6 controls the long-term synaptic depression in the central nervous system mediated via the 2-AG/CB1R axis or an endocannabinoid-independent AMPA receptor pathway (Marrs et al., 2010; Wei et al., 2016; Cao et al., 2019). The downregulation of ABHD6 expression following sustained morphine exposure may be a mechanism underlying opioid-mediated long-term synaptic depression and participate in opioid reward. Interestingly, our qPCR result showed that the expression of ABHD6 was not altered at the mRNA level, suggesting its downregulation detected by the proteomics is not at the transcription level. CB2R is a critical member of the endogenous cannabinoid system but is barely detected by current mass spectrometry-based techniques due to its low expression level (Marchalant et al., 2014). Our qRT-PCR experiments found that CB2R was significantly decreased by repeated morphine treatment. This downregulation of CB2R may be involved in a regulatory process of sustained morphine in the facilitation of the rewarding behavior (Xi et al., 2011; Navarrete et al., 2013; Ortega-Álvaro et al., 2015; Grenald et al., 2017). Overall, these studies suggest that sustained opioids exert regulatory effects on the VTA endogenous cannabinoid system.

Interestingly, our proteomic analysis indicates the endopeptidase inhibitors, particularly serine-type endopeptidase inhibitors, including α-1-macroglobulin, was the most significantly affected protein due to repeated morphine with over a 9-fold decrease. Considering the essential roles of these endopeptidase inhibitors in the regulation of synaptic plasticity and inflammation (Falkenberg et al., 1995; Almonte and Sweatt, 2011; Wang and Sama, 2012; Wake et al., 2016; Krause et al., 2019; Zhang et al., 2020), the modulation of these proteins by repeated morphine treatment may implicate novel regulatory mechanisms of opioids in the mediation of reward and addiction. It is worth mentioning that 18 out of the 45 upregulated proteins in our proteomic analysis were found to possess cleavage sites recognized by serine-type endopeptidases (Predicted by a peptidase database MEROPS (Rawlings et al., 2018); (**Supplementary Table S4**), suggesting the upregulation of these proteins may be attributed to the reduction of those endopeptidase inhibitors. As some of these upregulated proteins participate in the regulation of protein translation (**Supplementary Table S4**) this may indicate a novel pathway that opioids control different biological processes.

We also examined the modulatory effects of sustained morphine on the VTA levels of endocannabinoids, 2-AG and AEA. Our results exhibited that sustained morphine did not alter the production of either 2-AG or AEA in the VTA. These results are consistent with the unaltered protein expression of the major regulators of endocannabinoid production or degradation, such as DAGLα, MAGL, NAPE-PLD, and FAAH, and this lack of

alteration is not affected by the time of the last morphine injection. In contrast, previous studies showed that sustained opioid changes the production of these endocannabinoids in several brain regions associated with reward process (i.e., striatum) although the extent and direction may vary (González et al., 2003; Viganò et al., 2003; Viganò et al., 2004; Caillé et al., 2007). Currently, we do not know the actual reasons why endocannabinoids are regulated differently among distinct brain regions, yet previous studies show that the changes of endocannabinoid production are not universal in all tested brain regions (González et al., 2003; Viganò et al., 2003; Viganò et al., 2004). Furthermore, the pattern of the drug administration may also play a role here as a substantial difference of the neurochemical, proteomic and genomic effects were observed when drugs were applied noncontingently or by free-choice self-administration (Jacobs et al., 2003). When sustained morphine was applied via daily injection (non-contingent), the AEA level in the NAc shell was not altered while self-administration (contingent) of heroin significantly increased AEA production (Viganò et al., 2004; Caillé et al., 2007). Lastly, different dosages and duration of opioid treatment may also influence the results. Interestingly, our study found that a single dose of morphine just prior to VTA-microdialysis collection significantly reduced AEA production in both sustained morphine- and saline-treated rats, suggesting that opioids may induce an acute regulation of AEA production in the VTA. The actual significance for this phenomenon is unclear and no other study has reported this result. Considering the relative higher affinity of AEA to CB1Rs than to CB2Rs as well as the facilitatory effect of CB1Rs on opioid-induced CPP, this reduction of AEA after morphine treatment may reflect a negative feedback mechanism in opioid reward. However, it is also possible that this reduction of AEA could be a result of handling stress on animals and/or a depletion of AEA after a 240 min period of collection. This did not occur for 2-AG levels suggesting less evidence for stress handling of animals, yet the regulation of the endogenous cannabinoids may be under different stress controls and cannot be ruled out. Further experiments analyzing the AEA alteration in acute saline-treated rats will address this question.

Although 2-AG does not seem to be modulated by sustained morphine, we found that modulating 2-AG production can regulate sustained morphine-induced reward. Our study identified that enhancing systemic 2-AG tone by a selective MAGL inhibitor, MJN110, significantly attenuated morphine-induced preference, suggesting an inhibitory effect of 2-AG on the rewarding behavior of morphine. Interestingly, we also found that activation of CB2Rs with a selective CB2R agonist, JWH015, significantly decreased sustained morphine-induced reward, suggestive of an opposite role of CB2Rs in opioid reward compared to CB1Rs. This result also suggests that the inhibitory effect of 2-AG on opioid reward is possibly mediated via CB2R rather than CB1R that promotes the opioid-induced rewarding behaviors. The functional difference of CB1R and CB2R in opioid reward may be caused by their distinct localization in the VTA. Previous studies found that CB1Rs are abundantly expressed on synaptic terminals targeting dopaminergic neurons in the VTA, indicating that CB1Rs serve as an autoreceptor and disinhibit GABAergic suppression of dopaminergic neuron activity (Fitzgerald et al., 2012; Van Bockstaele, 2012; Rashidy-Pour et al., 2013). In contrast, CB2Rs are primarily located on postsynaptic dopaminergic neurons, suggesting an inhibitory role of this receptor in reward process. Although no study has directly demonstrated this idea in opioid reward, this seems to be true in cocaine-induced reward (Zhang et al., 2014; Zhang et al., 2017). Further studies that directly modulating the CB2Rs expressed on the VTA dopaminergic neurons will provide the answer.

The endogenous cannabinoid and opioid systems are two critical neuromodulatory systems, which share similar pharmacological features, including the downstream signaling of μ-opioid receptors (MORs) and CB1Rs and behavioral outcomes (analgesia, sedation and reward) (Wenzel and Cheer, 2018). Recent evidence shows that these two systems are functionally interacted in the modulation of reward and addiction. Δ9-Tetrahydrocannabinol (THC)-induced CPP is eliminated in MOR-knockout mice (Ghozland et al., 2002) and THC self-administration is attenuated by opioid receptor antagonist naloxone (Braida et al., 2001; Justinova et al., 2004). Reciprocally, genetic depletion of CB1Rs or the application of CB1R antagonist rimonabant blocks opioid-induced CPP and self-administration (Ledent et al., 1999; Martin et al., 2000; Cossu et al., 2001; Navarro et al., 2001; Navarro et al., 2004; Caillé and Parsons, 2006). Currently, the underlying mechanisms of the functional interactions between the two systems remains to be elucidated, but the interactions between MOR and CB1R may be an explanation (Wenzel and Cheer, 2018). Indeed, these two receptors are both expressed on the GABAergic terminals in the VTA (Mátyás et al., 2008; Kudo et al., 2014), and the blockade of either receptor significantly decreases drug-induced dopamine release in the NAc (Chen et al., 1990; Tanda et al., 1997; Mascia et al., 1999). Importantly, Schoffelmeer et al. reported that MOR and CB1R may form heterodimers in the NAc and can cause synergistic suppression of GABA release, providing the possibility that the MOR and CB1R in the VTA may follow a similar pattern although additional *in vivo* studies are necessary to demonstrate if this is the case in the VTA (Schoffelmeer et al., 2006). Our present study provided evidence suggesting additional components of the endocannabinoid system may also involve in the functional interactions between the endogenous cannabinoid and opioid systems. However, more specific data using genetically modified animals are required to confirm this thought.

Overall, our current study provides a better picture of the ECS-related proteins expressed in the VTA and identified the expression of several proteins/genes (i.e., PLCγ2, ABHD6, and CB2R) were reduced after systemic sustained morphine exposure. We also evaluated the VTA levels of 2-AG and AEA; finding that AEA was reduced after acute exposure to morphine. These studies, for the first time, offer a comprehensive picture of the alterations of the VTA endocannabinoid system following sustained morphine exposure in male rats, providing several uncharacterized targets that may play a role in the regulation of opioid reward and addiction. Similar studies are ongoing in females to determine whether there are sex differences in the ECS after repeated morphine. It is also necessary to mention that systemic administration of morphine was performed in this study to

mimic the route of administration and repeated use of opioids in humans (Ballantyne and Mao, 2003; Surratt et al., 2011; Volkow and McLellan, 2016) with the understanding that alterations in the ECS in the VTA may be direct or indirect. Lastly, our study identified the possibility that broad manipulation of the endocannabinoid system may mitigate opioid abuse potential directly addressing the ongoing opioid epidemic.

DATA AVAILABILITY STATEMENT

The mass spectrometry proteomics data have been deposited to the ProteomeXchange Consortium via the PRIDE partner repository with the dataset identifier PXD023096 and 10.6019/PXD023096.

ETHICS STATEMENT

The animal study was reviewed and approved by University of Arizona Animal Care and Use Committee.

AUTHOR CONTRIBUTIONS

HZ, TL-M, and TV contributed to the study concept and design; HZ, AL, EL-B, AS, and PL contributed to the acquisition of data; HZ, PL, EL-B and TL performed data analysis; HZ, AM, RK, PL, TL-M, and TV wrote the manuscript. All authors read and approved the final manuscript.

FUNDING

This work was supported by the National Institutes of Health (NIH-NCI grant R01CA142115 and NIH-NIDA grant 1P01DA041307–01 (TV and TL-M); P30CA023074 (UA Cancer Center Analytical Chemistry Core)). Research was also supported by the Comprehensive Pain and Addiction Center, Health Sciences, University of Arizona.

ACKNOWLEDGMENTS

We appreciate Kenneth Mackie at Indiana University Bloomington for providing anti-DAGLα, MAGL, and CB1R antibodies for our experiments, John Streicher at the University of Arizona, who provided help with the RNA experiments, and Kevin Doubleday for his expertize in RStudio.

SUPPLEMENTARY MATERIAL

The Supplementary Material for this article can be found online at: https://www.frontiersin.org/articles/10.3389/fphar.2021.632757/full#supplementary-material.

REFERENCES

Abrams, D. I., Couey, P., Shade, S. B., Kelly, M. E., and and Benowitz, N. L. (2011). Cannabinoid-opioid interaction in chronic pain. *Clin. Pharmacol. Ther.* 90(6), 844–851. doi:10.1038/clpt.2011.188

Almonte, A. G., and and Sweatt, J. D. (2011). Serine proteases, serine protease inhibitors, and protease-activated receptors: roles in synaptic function and behavior. *Brain Res.* 1407, 107–122. doi:10.1016/j.brainres.2011.06.042

Baggelaar, M. P., van Esbroeck, A. C. M., van Rooden, E. J., Florea, B. I., Overkleeft, H. S., Marsicano, G., et al. (2017). Chemical proteomics maps brain region specific activity of endocannabinoid hydrolases. *ACS Chem. Biol.* 12 (3), 852–861. doi:10.1021/acschembio.6b01052

Ballantyne, J. C., and and Mao, J. (2003). Opioid therapy for chronic pain. *N. Engl. J. Med.* 349 (20), 1943–1953. doi:10.1056/nejmra025411

Blankman, J. L., Simon, G. M., and and Cravatt, B. F. (2007). A comprehensive profile of brain enzymes that hydrolyze the endocannabinoid 2-arachidonoylglycerol. *Chem. Biol.* 14 (12), 1347–1356. doi:10.1016/j.chembiol.2007.11.006

Braida, D., Pozzi, M., Parolaro, D., and and Sala, M. (2001). Intracerebral self-administration of the cannabinoid receptor agonist CP 55,940 in the rat: interaction with the opioid system. *Eur. J. Pharmacol.* 413 (2-3), 227–234. doi:10.1016/s0014-2999(01)00766-x

Buczynski, M. W., and and Parsons, L. H. (2010). Quantification of brain endocannabinoid levels: methods, interpretations and pitfalls. *Br. J. Pharmacol.* 160 (3), 423–42. doi:10.1111/j.1476-5381.2010.00787.x

Bushlin, I., Rozenfeld, R., and and Devi, L. A., (2010). Cannabinoid-opioid interactions during neuropathic pain and analgesia. *Curr. Opin. Pharmacol.* 10 (1), 80–86. doi:10.1016/j.coph.2009.09.009

Cécyre, B., Thomas, S., Ptito, M., Casanova, C., and and Bouchard, J. F. (2014). Evaluation of the specificity of antibodies raised against cannabinoid receptor type 2 in the mouse retina. *Naunyn-schmiedeberg's Arch. Pharmacol.* 387 (2), 175–184. doi:10.1007/s00210-013-0930-8

Caillé, S., Alvarez-Jaimes, L., Polis, I., Stouffer, D. G., and and Parsons, L. H. (2007). Specific alterations of extracellular endocannabinoid levels in the nucleus accumbens by ethanol, heroin, and cocaine self-administration. *J. Neurosci.* 27 (14), 3695–3702. doi:10.1523/jneurosci.4403-06.2007

Caillé, S., and and Parsons, L. H. (2006). Cannabinoid modulation of opiate reinforcement through the ventral striatopallidal pathway. *Neuropsychopharmacol* 31 (4), 804–813. doi:10.1038/sj.npp.1300848

Caillé, S., and and Parsons, L. H. (2003). SR141716A reduces the reinforcing properties of heroin but not heroin-induced increases in nucleus accumbens dopamine in rats. *Eur. J. Neurosci.* 18 (11), 3145–3149. doi:10.1111/j.1460-9568.2003.02961.x

Campbell, L. A., Avdoshina, V., Rozzi, S., and and Mocchetti, I. (2013). CCL5 and cytokine expression in the rat brain: differential modulation by chronic morphine and morphine withdrawal. *Brain Behav. Immun.* 34, 130–140. doi:10.1016/j.bbi.2013.08.006

Cao, J. K., Kaplan, J., and and Stella, N. (2019). ABHD6: its place in endocannabinoid signaling and beyond. *Trends Pharmacol. Sci.* 40 (4), 267–277. doi:10.1016/j.tips.2019.02.002

Chaperon, F., Soubrié, P., Puech, A. J., and and Thiébot, M. H. (1998). Involvement of central cannabinoid (CB 1) receptors in the establishment of place conditioning in rats. *Psychopharmacology* 135 (4), 324–332. doi:10.1007/s002130050518

Chen, J., Paredes, W., Li, J., Smith, D., Lowinson, J., and and Gardner, E. L. (1990). Δ9-Tetrahydrocannabinol produces naloxone-blockable enhancement of presynaptic basal dopamine efflux in nucleus accumbens of conscious, freely-moving rats as measured by intracerebral microdialysis. *Psychopharmacology* 102 (2), 156–162. doi:10.1007/bf02245916

Cichewicz, D. L., Haller, V. L., and and Welch, S. P. (2001). Changes in opioid and cannabinoid receptor protein following short-term combination treatment with

delta(9)-tetrahydrocannabinol and morphine. *J. Pharmacol. Exp. Ther.* 297 (1), 121–127.

Cichewicz, D. L. (2004). Synergistic interactions between cannabinoid and opioid analgesics. *Life Sci.* 74 (11), 1317–1324. doi:10.1016/j.lfs.2003.09.038

Cossu, G., Ledent, C., Fattore, L., Imperato, A., Böhme, G. A., Parmentier, M., et al. (2001). Cannabinoid CB1 receptor knockout mice fail to self-administer morphine but not other drugs of abuse. *Behav. Brain Res.* 118 (1), 61–65. doi:10.1016/s0166-4328(00)00311-9

Dahlhamer, J., Lucas, J., Zelaya, C., Nahin, R., Mackey, S., DeBar, L., et al. (2018). Prevalence of chronic pain and high-impact chronic pain among adults - United States, 2016. *MMWR Morb. Mortal. Wkly. Rep.* 67 (36), 1001–1006. doi:10.15585/mmwr.mm6736a2

De Luca, M. A., Valentini, V., Bimpisidis, Z., Cacciapaglia, F., Caboni, P., and and Di Chiara, G. (2014). Endocannabinoid 2-arachidonoylglycerol self-administration by sprague-dawley rats and stimulation of *in vivo* dopamine transmission in the nucleus accumbens shell. *Front. Psychiatry* 5, 140. doi:10.3389/fpsyt.2014.00140

De Vries, T. J., Homberg, J. R., Binnekade, R., Raasø, H., and and Schoffelmeer, A. N. M. (2003). Cannabinoid modulation of the reinforcing and motivational properties of heroin and heroin-associated cues in rats. *Psychopharmacology* 168 (1-2), 164–169. doi:10.1007/s00213-003-1422-1

Falkenberg, C., Allhorn, M., Th✆gersen, I. B., Valnickova, Z., Pizzo, S. V., Salvesen, G., et al. (1995). α1-Microglobulin destroys the proteinase inhibitory activity of α1-inhibitor-3 by complex formation. *J. Biol. Chem.* 270 (9), 4478–4483. doi:10.1074/jbc.270.9.4478

Faul, F., Erdfelder, E., Buchner, A., and and Lang, A. G. (2009). Statistical power analyses using G*Power 3.1: tests for correlation and regression analyses. *Behav. Res. Methods* 41 (4), 1149–1160. doi:10.3758/brm.41.4.1149

Fields, H. L., and and Margolis, E. B. (2015). Understanding opioid reward. *Trends Neurosci.* 38 (4), 217–225. doi:10.1016/j.tins.2015.01.002

Fitzgerald, M. L., Shobin, E., and and Pickel, V. M. (2012). Cannabinoid modulation of the dopaminergic circuitry: implications for limbic and striatal output. *Prog. Neuro-Psychopharmacol. Biol. Psychiatry* 38 (1), 21–29. doi:10.1016/j.pnpbp.2011.12.004

Ghozland, S., Matthes, H. W. D., Simonin, F., Filliol, D., Kieffer, B. L., and and Maldonado, R. (2002). Motivational effects of cannabinoids are mediated by μ-opioid and κ-opioid receptors. *J. Neurosci.* 22 (3), 1146–1154. doi:10.1523/jneurosci.22-03-01146.2002

González, S., Schmid, P., Fernández-ruiz, J., Krebsbach, R., Schmid, H., and and Ramos, J. (2003). Region-dependent changes in endocannabinoid transmission in the brain of morphine-dependent rats. *Addict. Biol.* 8 (2), 159–166. doi:10.1080/1355621031000117383

González, S., Fernández-Ruiz, J., Sparpaglione, V., Parolaro, D., and and Ramos, J. A. (2002). Chronic exposure to morphine, cocaine or ethanol in rats produced different effects in brain cannabinoid CB1 receptor binding and mRNA levels. *Drug Alcohol Depend.* 66 (1), 77–84. doi:10.1016/s0376-8716(01)00186-7

Grenald, S. A., Young, M. A., Wang, Y., Ossipov, M. H., Ibrahim, M. M., Largent-Milnes, T. M., et al. (2017). Synergistic attenuation of chronic pain using mu opioid and cannabinoid receptor 2 agonists. *Neuropharmacology* 116, 59–70. doi:10.1016/j.neuropharm.2016.12.008

He, X. H., Jordan, C. J., Vemuri, K., Bi, G. H., Zhan, J., Gardner, E. L., et al. (2019). Cannabinoid CB1 receptor neutral antagonist AM4113 inhibits heroin self-administration without depressive side effects in rats. *Acta Pharmacol. Sin.* 40 (3), 365–373. doi:10.1038/s41401-018-0059-x

Huang, D. W., Sherman, B. T., and and Lempicki, R. A. (2009). Systematic and integrative analysis of large gene lists using DAVID bioinformatics resources. *Nat. Protoc.* 4 (1), 44–57. doi:10.1038/nprot.2008.211

Ibrahim, M. M., Patwardhan, A., Gilbraith, K. B., Moutal, A., Yang, X., Chew, L. A., et al. (2017). Long-lasting antinociceptive effects of green light in acute and chronic pain in rats. *Pain* 158, 347–360. doi:10.1097/j.pain.0000000000000767

Jacobs, E. H., Smit, A. B., de Vries, T. J., and and Schoffelmeer, A. N. M. (2003). Neuroadaptive effects of active versus passive drug administration in addiction research. *Trends Pharmacol. Sci.* 24 (11), 566–573. doi:10.1016/j.tips.2003.09.006

Jin, L., Pan, L., Guo, Y., Zheng, Y., Nie, Z., and and Zhu, R. (2014). Expression and localization of cannabinoid receptor 1 in rats' brain treated with acute and repeated morphine. *Acta Neurobiol. Exp. (Wars)* 74 (3), 288–297.

Justinova, Z., Tanda, G., Munzar, P., and and Goldberg, S. R. (2004). The opioid antagonist naltrexone reduces the reinforcing effects of Delta 9 tetrahydrocannabinol (THC) in squirrel monkeys. *Psychopharmacology (Berl)* 173 (1-2), 186–194. doi:10.1007/s00213-003-1693-6

Kadamur, G., and and Ross, E. M. (2013). Mammalian phospholipase C. *Annu. Rev. Physiol.* 75, 127–154. doi:10.1146/annurev-physiol-030212-183750

Kazantzis, N. P., Casey, S. L., Seow, P. W., Mitchell, V. A., and and Vaughan, C. W. (2016). Opioid and cannabinoid synergy in a mouse neuropathic pain model. *Br. J. Pharmacol.* 173 (16), 2521–2531. doi:10.1111/bph.13534

Kolodny, A., Courtwright, D. T., Hwang, C. S., Kreiner, P., Eadie, J. L., Clark, T. W., et al. (2015). The prescription opioid and heroin crisis: a public health approach to an epidemic of addiction. *Annu. Rev. Public Health* 36 (1), 559–574. doi:10.1146/annurev-publhealth-031914-122957

Krause, K., Azouz, F., Nakano, E., Nerurkar, V. R., and and Kumar, M. (2019). Deletion of pregnancy zone protein and murinoglobulin-1 restricts the pathogenesis of west nile virus infection in mice. *Front. Microbiol.* 10, 259. doi:10.3389/fmicb.2019.00259

Kruse, R., Krantz, J., Barker, N., Coletta, R. L., Rafikov, R., Luo, M., et al. (2017). Characterization of the CLASP2 protein interaction network identifies SOGA1 as a microtubule-associated protein. *Mol. Cell Proteomics* 16 (10), 1718–1735. doi:10.1074/mcp.ra117.000011

Kudo, T., Konno, K., Uchigashima, M., Yanagawa, Y., Sora, I., Minami, M., et al. (2014). GABAergic neurons in the ventral tegmental area receive dual GABA/enkephalin-mediated inhibitory inputs from the bed nucleus of the stria terminalis. *Eur. J. Neurosci.* 39 (11), 1796–1809. doi:10.1111/ejn.12503

Lecca, S., Melis, M., Luchicchi, A., Muntoni, A. L., and and Pistis, M. (2012). Inhibitory inputs from rostromedial tegmental neurons regulate spontaneous activity of midbrain dopamine cells and their responses to drugs of abuse. *Neuropsychopharmacol* 37 (5), 1164–1176. doi:10.1038/npp.2011.302

Ledent, C., Valverde, O., Cossu, G., Petitet, F., Aubert, J. F., Beslot, F., et al. (1999). Unresponsiveness to cannabinoids and reduced addictive effects of opiates in CB1 receptor knockout mice. *Science* 283 (5400), 401–404. doi:10.1126/science.283.5400.401

Li, Y., and and Kim, J. (2015). Neuronal expression of CB2 cannabinoid receptor mRNAs in the mouse hippocampus. *Neuroscience* 311, 253–267. doi:10.1016/j.neuroscience.2015.10.041

Livak, K. J., and and Schmittgen, T. D. (2001). Analysis of relative gene expression data using real-time quantitative PCR and the 2−ΔΔCT method. *Methods* 25 (4), 402–408. doi:10.1006/meth.2001.1262

Luchicchi, A., Lecca, S., Carta, S., Pillolla, G., Muntoni, A. L., Yasar, S., et al. (2010). Effects of fatty acid amide hydrolase inhibition on neuronal responses to nicotine, cocaine and morphine in the nucleus accumbens shell and ventral tegmental area: involvement of PPAR-α nuclear receptors. *Addict. Biol.* 15 (3), 277–88. doi:10.1111/j.1369-1600.2010.00222.x

Mátyás, F., Urbán, G. M., Watanabe, M., Mackie, K., Zimmer, A., Freund, T. F., et al. (2008). Identification of the sites of 2-arachidonoylglycerol synthesis and action imply retrograde endocannabinoid signaling at both GABAergic and glutamatergic synapses in the ventral tegmental area. *Neuropharmacology* 54 (1), 95–107. doi:10.1016/j.neuropharm.2007.05.028

Ma, Z., Gu, X., Zhang, W., and and Ren, B. (2012). The effect of cannabinoid receptor 2 agonist JWH015 on the hyperalgesia induced by remifentanil: 14AP2-3. *Eur. J. Anaesthesiol. | EJA* 29, 195. doi:10.1097/00003643-201206001-00647

Marchalant, Y., Brownjohn, P. W., Bonnet, A., Kleffmann, T., and and Ashton, J. C. (2014). Validating antibodies to the cannabinoid CB2 receptor. *J. Histochem. Cytochem.* 62 (6), 395–404. doi:10.1369/0022155414530995

Marrs, W. R., Blankman, J. L., Horne, E. A., Thomazeau, A., Lin, Y. H., Coy, J., et al. (2010). The serine hydrolase ABHD6 controls the accumulation and efficacy of 2-AG at cannabinoid receptors. *Nat. Neurosci.* 13 (8), 951–957. doi:10.1038/nn.2601

Martin, M., Ledent, C., Parmentier, M., Maldonado, R., and and Valverde, O. (2000). Cocaine, but not morphine, induces conditioned place preference and sensitization to locomotor responses in CB1 knockout mice. *Eur. J. Neurosci.* 12 (11), 4038–4046. doi:10.1046/j.1460-9568.2000.00287.x

Mascia, M. S., Obinu, M. C., Ledent, C., Parmentier, M., Böhme, G. A., Imperato, A., et al. (1999). Lack of morphine-induced dopamine release in the nucleus accumbens of cannabinoid CB1 receptor knockout mice. *Eur. J. Pharmacol.* 383 (3), R1–R2. doi:10.1016/s0014-2999(99)00656-1

Melis, M., Pistis, M., Perra, S., Muntoni, A. L., Pillolla, G., and and Gessa, G. L. (2004). Endocannabinoids mediate presynaptic inhibition of glutamatergic

transmission in rat ventral tegmental area dopamine neurons through activation of CB1 receptors. *J. Neurosci.* 24 (1), 53–62. doi:10.1523/jneurosci.4503-03.2004

Navarrete, F., Rodríguez-Arias, M., Martín-García, E., Navarro, D., García-Gutiérrez, M. S., Aguilar, M. A., et al. (2013). Role of CB2 cannabinoid receptors in the rewarding, reinforcing, and physical effects of nicotine. *Neuropsychopharmacol* 38 (12), 2515–2524. doi:10.1038/npp.2013.157

Navarro, M., Carrera, M. R. A., Del Arco, I., Trigo, J. M., Koob, G. F., and and Rodríguez de Fonseca, F. (2004). Cannabinoid receptor antagonist reduces heroin self-administration only in dependent rats. *Eur. J. Pharmacol.* 501 (1-3), 235–237. doi:10.1016/j.ejphar.2004.08.022

Navarro, M., Carrera, M. R. A., Fratta, W., Valverde, O., Cossu, G., Fattore, L., et al. (2001). Functional interaction between opioid and cannabinoid receptors in drug self-administration. *J. Neurosci.* 21 (14), 5344–5350. doi:10.1523/jneurosci.21-14-05344.2001

Niphakis, M. J., Cognetta, A. B., 3rd, Chang, J. W., Buczynski, M. W., Parsons, L. H., Byrne, F., et al. (2013). Evaluation of NHS carbamates as a potent and selective class of endocannabinoid hydrolase inhibitors. *ACS Chem. Neurosci.* 4 (9), 1322–1332. doi:10.1021/cn400116z

Oleson, E. B., Beckert, M. V., Morra, J. T., Lansink, C. S., Cachope, R., Abdullah, R. A., et al. (2012). Endocannabinoids shape accumbal encoding of cue-motivated behavior via CB1 receptor activation in the ventral tegmentum. *Neuron* 73 (2), 360–373. doi:10.1016/j.neuron.2011.11.018

Ortega-Álvaro, A., Ternianov, A., Aracil-Fernández, A., Navarrete, F., García-Gutiérrez, M. S., and and Manzanares, J. (2015). Role of cannabinoid CB_2 receptor in the reinforcing actions of ethanol. *Addict. Biol.* 20 (1), 43–55. doi:10.1111/adb.12076

Parker, S. S., Krantz, J., Kwak, E. A., Barker, N. K., Deer, C. G., Lee, N. Y., et al. (2019). Insulin induces microtubule stabilization and regulates the microtubule plus-end tracking protein network in adipocytes. *Mol. Cell Proteomics* 18 (7), 1363–1381. doi:10.1074/mcp.ra119.001450

Paxinos, G., and and Watson, C. (2007). *The rat brain in stereotaxic coordinates*. Amsterdam: Elsevier.

Rashidy-Pour, A., Pahlevani, P., Vaziri, A., Shaigani, P., Zarepour, L., Vafaei, A. A., et al. (2013). Involvement of CB1 receptors in the ventral tegmental area in the potentiation of morphine rewarding properties in acquisition but not expression in the conditioned place preference model. *Behav. Brain Res.* 247, 259–267. doi:10.1016/j.bbr.2013.03.015

Rawlings, N. D., Barrett, A. J., Thomas, P. D., Huang, X., Bateman, A., and and Finn, R. D. (2018). The MEROPS database of proteolytic enzymes, their substrates and inhibitors in 2017 and a comparison with peptidases in the PANTHER database. *Nucleic Acids Res.* 46 (D1), D624-d632. doi:10.1093/nar/gkx1134

Riegel, A. C., and and Lupica, C. R. (2004). Independent presynaptic and postsynaptic mechanisms regulate endocannabinoid signaling at multiple synapses in the ventral tegmental area. *J. Neurosci.* 24 (49), 11070–11078. doi:10.1523/jneurosci.3695-04.2004

Rubino, T., Tizzoni, L., Viganò, D., Massi, P., and and Parolaro, D. (1997). Modulation of rat brain cannabinoid receptors after chronic morphine treatment. *Neuroreport* 8 (15), 3219–3223. doi:10.1097/00001756-199710200-00007

SAMHSA (2019). *K*ey substance use and mental health indicators in the United States: Results from the 2018 national Survey on drug Use and health *(HHS publication No. PEP19-5068, NSDUH series H-54)*. Rockville, MD: Center for Behavioral Health Statistics and Quality, Substance Abuse and Mental Health Services Administration.

Schoffelmeer, A., Hogenboom, F., Wardeh, G., and and Devries, T. (2006). Interactions between CB1 cannabinoid and μ opioid receptors mediating inhibition of neurotransmitter release in rat nucleus accumbens core. *Neuropharmacology* 51 (4), 773–781. doi:10.1016/j.neuropharm.2006.05.019

Showalter, V. M., Compton, D. R., Martin, B. R., and and Abood, M. E. (1996). Evaluation of binding in a transfected cell line expressing a peripheral cannabinoid receptor (CB2): identification of cannabinoid receptor subtype selective ligands. *J. Pharmacol. Exp. Ther.* 278 (3), 989–999.

Singh, M. E., Verty, A. N. A., McGregor, I. S., and and Mallet, P. E. (2004). A cannabinoid receptor antagonist attenuates conditioned place preference but not behavioural sensitization to morphine. *Brain Res.* 1026 (2), 244–253. doi:10.1016/j.brainres.2004.08.027

Solinas, M., Panlilio, L. V., Antoniou, K., Pappas, L. A., and and Goldberg, S. R. (2003). The cannabinoid CB1 antagonist N-piperidinyl-5-(4-chlorophenyl)-1-(2,4-dichlorophenyl) -4-methylpyrazole-3-carboxamide (SR-141716A) differentially alters the reinforcing effects of heroin under continuous reinforcement, fixed ratio, and progressive ratio schedules of drug self-administration in rats. *J. Pharmacol. Exp. Ther.* 306 (1), 93–102. doi:10.1124/jpet.102.047928

Solinas, M., Panlilio, L. V., Tanda, G., Makriyannis, A., Matthews, S. A., and and Goldberg, S. R. (2005). Cannabinoid agonists but not inhibitors of endogenous cannabinoid transport or metabolism enhance the reinforcing efficacy of heroin in rats. *Neuropsychopharmacol* 30 (11), 2046–2057. doi:10.1038/sj.npp.1300754

Surratt, H., Kurtz, S. P., and and Cicero, T. J. (2011). Alternate routes of administration and risk for HIV among prescription opioid abusers. *J. Addict. Dis.* 30 (4), 334–341. doi:10.1080/10550887.2011.609805

Tanda, G., Pontieri, F. E., and and Di Chiara, G. (1997). Cannabinoid and heroin activation of mesolimbic dopamine transmission by a common μ1 opioid receptor mechanism. *Science* 276 (5321), 2048–2050. doi:10.1126/science.276.5321.2048

Tham, S. M., Angus, J. A., Tudor, E. M., and and Wright, C. E. (2005). Synergistic and additive interactions of the cannabinoid agonist CP55,940 with μ opioid receptor and α 2 -adrenoceptor agonists in acute pain models in mice. *Br. J. Pharmacol.* 144 (6), 875–884. doi:10.1038/sj.bjp.0706045

Thompson, A. L., Grenald, S. A., Ciccone, H. A., BassiriRad, N., Niphakis, M. J., Cravatt, B. F., et al. (2020). The endocannabinoid system Alleviates pain in a murine model of cancer-induced bone pain. *J. Pharmacol. Exp. Ther.* 373 (2), 230–238. doi:10.1124/jpet.119.262337

Tumati, S., Largent-Milnes, T. M., Keresztes, A., Ren, J., Roeske, W. R., Vanderah, T. W., et al. (2012). Repeated morphine treatment-mediated hyperalgesia, allodynia and spinal glial activation are blocked by co-administration of a selective cannabinoid receptor type-2 agonist. *J. Neuroimmunol.* 244 (1-2), 23–31. doi:10.1016/j.jneuroim.2011.12.021

Tyanova, S., and and Cox, J. (2018). Perseus: a bioinformatics platform for integrative analysis of proteomics data in cancer research. *Methods Mol. Biol.* 1711, 133–148. doi:10.1007/978-1-4939-7493-1_7

Tyanova, S., Temu, T., Sinitcyn, P., Carlson, A., Hein, M. Y., Geiger, T., et al. (2016). The Perseus computational platform for comprehensive analysis of (prote) omics data. *Nat. Methods* 13 (9), 731–740. doi:10.1038/nmeth.3901

Van Bockstaele, E. J. (2012). Cannabinoid receptor signaling and modulation of monoamines: implications for psychiatric and neurological disorders. *Prog. Neuro-Psychopharmacol. Biol. Psychiatry* 38 (1), 1–3. doi:10.1016/j.pnpbp.2012.01.002

Verty, A. N., Stefanidis, A., McAinch, A. J., Hryciw, D. H., and and Oldfield, B. (2015). Anti-obesity effect of the CB2 receptor agonist JWH-015 in diet-induced obese mice. *PLoS One* 10 (11), e0140592. doi:10.1371/journal.pone.0140592

Viganò, D., Grazia Cascio, M., Rubino, T., Fezza, F., Vaccani, A., Di Marzo, V., et al. (2003). Chronic morphine modulates the contents of the endocannabinoid, 2-arachidonoyl glycerol, in rat brain. *Neuropsychopharmacol* 28 (6), 1160–1167. doi:10.1038/sj.npp.1300117

Viganò, D., Valenti, M., Grazia Cascio, M., Di Marzo, V., Parolaro, D., and and Rubino, T. (2004). Changes in endocannabinoid levels in a rat model of behavioural sensitization to morphine. *Eur. J. Neurosci.* 20 (7), 1849–1857. doi:10.1111/j.1460-9568.2004.03645.x

Volkow, N. D. (2020). Collision of the COVID-19 and addiction epidemics. *Ann. Intern. Med.* 173 (1), pp. 61–62. doi:10.7326/m20-1212

Volkow, N. D., and and McLellan, A. T. (2016). Opioid abuse in chronic pain - misconceptions and mitigation strategies. *N. Engl. J. Med.* 374 (13), 1253–1263. doi:10.1056/nejmra1507771

Volkow, N. D., and and Morales, M. (2015). The brain on drugs: from reward to addiction. *Cell* 162 (4), 712–725. doi:10.1016/j.cell.2015.07.046

Wake, H., Mori, S., Liu, K., Morioka, Y., Teshigawara, K., Sakaguchi, M., et al. (2016). Histidine-rich glycoprotein prevents septic lethality through regulation of immunothrombosis and inflammation. *EBioMedicine* 9, 180–194. doi:10.1016/j.ebiom.2016.06.003

Wang, H., and and E. Sama, A. (2012). Anti-inflammatory role of fetuin-A in injury and infection. *Curr. Mol. Med.* 12 (5), 625–633. doi:10.2174/156652412800620039

Wei, M., Zhang, J., Jia, M., Yang, C., Pan, Y., Li, S., et al. (2016). α/β-Hydrolase domain-containing 6 (ABHD6) negatively regulates the surface delivery and synaptic function of AMPA receptors. *Proc. Natl. Acad. Sci. USA* 113 (19), E2695–E2704. doi:10.1073/pnas.1524589113

Wenzel, J. M., and and Cheer, J. F. (2018). Endocannabinoid regulation of reward and reinforcement through interaction with dopamine and endogenous opioid signaling. *Neuropsychopharmacol.* 43 (1), 103–115. doi:10.1038/npp.2017.126

Wilkerson, J. L., Ghosh, S., Mustafa, M., Abdullah, R. A., Niphakis, M. J., Cabrera, R., et al. (2017). The endocannabinoid hydrolysis inhibitor SA-57: intrinsic antinociceptive effects, augmented morphine-induced antinociception, and attenuated heroin seeking behavior in mice. *Neuropharmacology* 114, 156–167. doi:10.1016/j.neuropharm.2016.11.015

Wiskerke, J., Irimia, C., Cravatt, B. F., De Vries, T. J., Schoffelmeer, A. N. M., Pattij, T., et al. (2012). Characterization of the effects of reuptake and hydrolysis inhibition on interstitial endocannabinoid levels in the brain: an *in vivo* microdialysis study. *ACS Chem. Neurosci.* 3 (5), 407–417. doi:10.1021/cn300036b

Xi, Z. X., Peng, X. Q., Li, X., Song, R., Zhang, H. Y., Liu, Q. R., et al. (2011). Brain cannabinoid CB2 receptors modulate cocaine's actions in mice. *Nat. Neurosci.* 14 (9), 1160–1166. doi:10.1038/nn.2874

Zhang, H. Y., Gao, M., Liu, Q. R., Bi, G. H., Li, X., Yang, H. J., et al. (2014). Cannabinoid CB2receptors modulate midbrain dopamine neuronal activity and dopamine-related behavior in mice. *Proc. Natl. Acad. Sci. USA* 111 (46), E5007–E5015. doi:10.1073/pnas.1413210111

Zhang, H. Y., Gao, M., Shen, H., Bi, G.-H., Yang, H. J., Liu, Q. R., et al. (2017). Expression of functional cannabinoid CB2receptor in VTA dopamine neurons in rats. *Addict. Biol.* 22 (3), 752–765. doi:10.1111/adb.12367

Zhang, M., Dong, L., Zou, H., Li, J., Li, Q., Wang, G., et al. (2018). Effects of cannabinoid type 2 receptor agonist AM1241 on morphine-induced antinociception, acute and chronic tolerance, and dependence in mice. *J. Pain* 19 (10), 1113–1129. doi:10.1016/j.jpain.2018.04.009

Zhang, H., Largent-Milnes, T. M., and and Vanderah, T. W. (2020). Glial neuroimmune signaling in opioid reward. *Brain Res. Bull.* 155, 102–111. doi:10.1016/j.brainresbull.2019.11.012

Zlebnik, N. E., and and Cheer, J. F. (2016). Drug-induced alterations of endocannabinoid-mediated plasticity in brain reward regions. *J. Neurosci.* 36 (40), 10230–10238. doi:10.1523/jneurosci.1712-16.2016

Conflict of Interest: RK is the co-founder of Regulonix LLC, a company developing non-opioids drugs for chronic pain. In addition, RK has patents US10287334 and US10441586 issued to Regulonix LLC.

The remaining authors declare that the research was conducted in the absence of any commercial or financial relationships that could be construed as a potential conflict of interest.

frontiers in Pharmacology

REVIEW
published: 10 May 2021
doi: 10.3389/fphar.2021.679905

The Role of Chinese Herbal Therapy in Methamphetamine Abuse and its Induced Psychiatric Symptoms

*Lin Chen[1], Qin Ru[2], Qi Xiong[2], Mei Zhou[2], Kai Yue[2] and Yuxiang Wu[1]**

[1]Department of Health and Physical Education, Jianghan University, Wuhan, China, [2]Wuhan Institutes of Biomedical Sciences, Jianghan University, Wuhan, China

Repeated intake of methamphetamine (METH) leads to drug addiction, the inability to control intake, and strong drug cravings. It is also likely to cause psychiatric impairments, such as cognitive impairment, depression, and anxiety. Because the specific neurobiological mechanisms involved are complex and have not been fully and systematically elucidated, there is no established pharmacotherapy for METH abuse. Studies have found that a variety of Chinese herbal medicines have significant therapeutic effects on neuropsychiatric symptoms and have the advantage of multitarget comprehensive treatment. We conducted a systematic review, from neurobiological mechanisms to candidate Chinese herbal medicines, hoping to provide new perspectives and ideas for the prevention and treatment of METH abuse.

Keywords: addiction, psychiatric impairment, neurobiological mechanisms, chinese herbal medicines, METH abuse

OPEN ACCESS

Edited by:
Qi Wang,
Southern Medical University, China

Reviewed by:
Feng Chen,
Augusta University, United States
Yadong Guo,
Central South University, China

****Correspondence:***
Yuxiang Wu
yxwu@jhun.edu.cn

Specialty section:
This article was submitted to Neuropharmacology, a section of the journal Frontiers in Pharmacology

Received: *12 March 2021*
Accepted: *16 April 2021*
Published: *10 May 2021*

Citation:
Chen L, Ru Q, Xiong Q, Zhou M, Yue K and Wu Y (2021) The Role of Chinese Herbal Therapy in Methamphetamine Abuse and its Induced Psychiatric Symptoms. Front. Pharmacol. 12:679905. doi: 10.3389/fphar.2021.679905

INTRODUCTION

Psychostimulants, including methamphetamine (METH) and other amphetamines (AMPHs), are inferior to marijuana and have become the most diffusely used class of drugs globally (United Nations, 2020). The abuse of METH and other AMPHs has become a serious public health problem and a growing global concern. Regardless of the person, family, country, or society, the abuse of METH has led to an obvious increase in various burdens, including the consumption of public health resources (Siefried et al., 2020).

METH can cross the blood-brain barrier and act on the central nervous system. It mainly alters neurotransmission by interfering with dopamine (DA), DA transporters (DAT), and increasing the DA concentration in the brain (Brensilver et al., 2013). Repeated use of METH leads to chronic recurrent drug dependence that is characterized by compulsive, uncontrolled drug use and intense cravings (Brensilver et al., 2013; Mizoguchi and Yamada, 2019). METH is more likely to cause psychiatric impairments than traditional opioids (Glasner-Edwards and Mooney, 2014; Eslami-Shahrbabaki et al., 2015). Related epidemiological and clinical studies have suggested that people abusing METH have a significantly increased risk of schizophrenia (Callaghan et al., 2012) and are more prone to cognitive impairment (Wagner et al., 2013; Potvin et al., 2018; Mizoguchi and Yamada, 2019), depression (Marshall and Werb, 2010), anxiety (McKetin et al., 2016), and suicide attempts (Glasner-Edwards et al., 2008).

The Neurobiological Mechanisms Involved in Methamphetamine Abuse

METH indirectly activates DA, 5-hydroxytryptamine (5-HT), glutamate (Glu), and adrenaline receptors by increasing monoamine transmitters in the synaptic cleft, producing a series of

TABLE 1 | The effect of METH on neurotransmitters, their addictive effects, and/or psychiatric impairment.

		Addictive effects and/or major psychiatric impairment	Neurotransmitters	Receptor or target	Effect
METH impairment	Addictive effects	METH dependence	DA	D1, D2, D3, DAT	DA release and reuptake imbalances; DA receptor activation
			5-HT	SERT	Release of 5-HT; increases synthesis and release of DA
			Glu	D1	Increased glu and DA release via D1 receptor-mediated glutamate disinhibition
			GABA	GABAA	Inhibits the GABAB receptor signaling pathway
	Neuronal injury	Memory and cognitive deficits	DA	D1, D2, D3, DAT, HCN1	DA release and reuptake imbalances and apoptosis pathways activation
			Glu	mGluR5 and GluNR2B	Deduced glutamate homeostasis, decreased expression of mGluR5 and GluNR2B
		Anxiety and depression	Monoamine neurotransmitters	Monoamine neurotransmitters receptor	Monoamine neurotransmitters depletion
				Apoptotic signaling pathways	Apoptosis
				Mitochondria and endoplasmic reticulum	Stress cascading activation
			Neuronal (damage)	Microglia and astrocytes	Inflammation and overactivation
				BDNF and NGF	Neurotrophic action
				Toxic dopamine quinone, oxygen free radicals, hydrogen peroxide, and increased ROS in neuron cells	Oxidative stress

METH = methamphetamine; R = receptor; 5-HT = 5-hydroxytryptamine; D or DA = dopamine; DAT = Dopamine transporter; SERT = 5-HT transporter; GABA = gamma-aminobutyric acid; Glu = glutamate; NR2B = N-methyl-D-aspartate receptor subtype-2B; HCN1 = hyperpolarization-activated and cyclic nucleotide-gated cation 1; BDNF = brain derived neurotrophic factor; NGF = nerve growth factor.

physiological effects (Cruickshank and Dyer, 2009). In the central nervous system, METH can indirectly stimulate adrenaline receptors, causing increased alertness, vitality, and attention. METH also induces the release of DA, which can induce pleasure. Working memory and reasoning ability can be enhanced by activating D1 receptors and α_2 adrenergic receptors in the prefrontal cortex (PFC); excited 5-HT receptors have antianxiety effects, making people feel relaxed and confident (Berridge, 2006; Weinshenker and Schroeder, 2007). These positive drug-induced experiences are the main reasons why METH is widely abused. However, long-term heavy use of METH can produce significant toxic effects on the nervous system, which not only leads to abnormal brain function but also damages the brain structure. At the beginning of this manuscript, we reviewed the neurobiological mechanisms of METH addiction, including cognitive dysfunction, anxiety, depression, oxidative stress, and inflammation. The specific neurobiological mechanisms of METH addiction are summarized in **Table 1**.

Methamphetamine and Addiction

Chronic METH abuse elicits compulsive craving and dependency (Miner et al., 2019). The neurobiological mechanism of METH addiction has been studied for several years. The 'incentive-sensitization theory' of addiction is the most widely recognized classical theory about METH-induced behavioral hypersensitization and rewarding (Siefried et al., 2020). METH stimulates the brain's reward system, leading to drug-related overstimulation, compulsive motivation, and excessive drug intake (Cruickshank and Dyer, 2009). The neural circuits involved in METH addiction are extensive and complex, involving many brain nuclei and brain regions, neurotransmitters, and protein mediators (Kauer and Malenka, 2007). Among them, the DA system is the most studied, and other systems are also involved to varying degrees.

The balanced state of release and reuptake of DA is an important prerequisite for DA to participate in various physiological activities. METH inhibits DA reuptake by the DAT and enhances synaptic DA release. Therefore, METH can activate DA receptors in the brain reward system to induce reward-motivated behavior (Volz et al., 2007). Different DA receptors play different roles in METH addiction. The D1 receptor is closely involved in METH-induced drug administration, location preference, and drug-seeking behaviour, while the D2 receptor is involved in METH-mediated neurotoxicity (Carati and Schenk, 2011). Studies have also found that the D3 receptor (D3R) is closely involved in METH addiction and has also been proven to play an important role in METH-induced hypersensitization in rats (Jiang et al., 2018). An increase in striatal D3R dopaminergic neurotransmission is associated with compulsive drug-seeking behavior in METH addicts. D3R antagonists may serve as a therapeutic tool for craving and relapse in METH addicts (Boileau et al., 2016).

In addition to DA, 5-HT is another important neurotransmitter in the processes leading to METH-induced nerve injury and addiction. METH can cause a dramatic

increase and release of serotonin in the body, which is due to its indirect effect on the 5-HT transporter (SERT) (Sora et al., 2009). Moreover, the 5-HT system and the DA system interact in the mechanism of METH addiction. On the one hand, METH promotes the endogenous release of 5-HT through an independent mechanism of the 5-HT reuptake transporter (Scearce-Levie et al., 1999). On the other hand, a large amount of endogenous 5-HT can increase the synthesis and release of DA, and the regulation of the release of DA in the central 'reward system' may be the mechanism of the 5-HT system in METH drug addiction (Thomas et al., 2010). However, the interaction between the 5-HT and DA systems needs to be further investigated.

In addition, glutamate, as the 'assistant' of DA, has attracted much attention because of its involvement in the sensitization and plasticity of neurons in the central nervous system, and glutamate neurotoxicity is an important cause of pathological changes in the nervous system. During METH abuse, due to D1 receptor-mediated glutamate disinhibition in the cortical striatum, extracellular DA increases, leading to a sharp increase in glutamate in the striatum (Trudeau et al., 2014). METH can also increase the activity of glutamate neurons in the ventral tegmental area (VTA), thus inducing an increase in DA release in the nucleus accumbens (NAc) and PFC (Mark et al., 2007).

METH-induced addiction also involves gamma-aminobutyric acid (GABA) neurons and their receptor signaling pathways. METH can affect the activity of the GABAA receptor and decrease the potential induced by the GABAA receptor, which may be caused by the competitive binding of METH to the GABAA receptor (Hondebrink et al., 2013). METH can also inhibit the GABAB receptor signaling pathway of GABA neurons in the VTA region (Padgett et al., 2012). GABA receptor agonists can counteract METH-induced GABA neuron damage and conditioned positional preference (CPP) behavior in rats (Voigt et al., 2011).

Methamphetamine and Cognitive Deficits

Cognition involves various intellectual capabilities, such as memory, attention, processing speed, and multitasking ability (Potvin et al., 2018). Cognitive abilities are necessary to function in society, and METH abuse can lead to cognitive problems that interfere with daily life (Dean et al., 2013). Previous researchers have been interested in understanding the cognitive deficits caused by METH because of its neurotoxic properties. Long-term METH abuse can cause permanent brain damage, which translates into persistent cognitive deficits. It is commonly believed that METH is an addictive drug with neurotoxic properties that damages the nervous system and induces cognitive impairment (Scott et al., 2007; Panenka et al., 2013).

To date, several cognitive deficits have been identified in METH addicts, including reaction time, working or attention memory, learning and memory, motor skills, information processing speed, and executive function deficits. Studies have shown that continuous METH use can cause medium effect-size cognitive impairment (Scott et al., 2007). A recent report also revealed that moderate impairments occur in most cognitive categories, including attention, verbal fluency, learning and memory, executive function, and visual and working memory. However, the societal consequences of METH cognitive impairment also need to be understood (Potvin et al., 2018).

METH has been found to cause abnormal changes in several neurotransmitters, such as DA overflow, leading to memory deficits (Nordahl et al., 2003). METH abuse has persistent adverse effects on the dopaminergic system, including DA release, reuptake, transport, and metabolism (Moszczynska and Callan, 2017; Anneken et al., 2018). Recent studies have shown that METH abuse can cause excessive release of DA in the PFC, activate neuronal apoptosis pathways, and eventually lead to impaired memory function (Long et al., 2017). Chronic use of antipsychotics causes downregulation of D1 receptors in the PFC, which severely damages working memory (Castner et al., 2000). Therefore, D1 receptor regulation in the PFC plays an important role in working memory and is an important target for the treatment of cognitive dysfunction (Thompson et al., 2014; Wang et al., 2019).

Prefrontal glutamatergic dysregulation may also impact recognition memory (Barker et al., 2007). Repeated METH exposure alters neuronal firing states and reduces glutamate homeostasis (Parsegian and See, 2014). METH decreases the expression of mGluR5 and GluNR2B in the cortex after two weeks of abstinence (Reichel et al., 2011). Because blocking both mGluR5-and GluNR2B-containing N-methyl-D-aspartate (NMDA) receptors impairs memory, these receptors are important in memory and cognitive function (Barker and Warburton, 2008).

Methamphetamine and Depression

The severity of METH exposure is associated with increased rates of anxiety and depression (Glasner-Edwards et al., 2009). METH abusers with depression are more likely to alleviate depressive symptoms by taking drugs again and continue to use METH at a much higher rate than other populations. METH addicts also have significantly higher rates of depressive symptoms after withdrawal (Nakama et al., 2008). Studies have proven that the negative mood of addicts is closely associated with drug craving (Quello et al., 2005). METH abuse can lead to or worsen depressive and other psychiatric symptoms, which can increase the likelihood of further METH abuse (Glasner-Edwards et al., 2009; May et al., 2020).

Abuse of METH induces the release of neurotransmitters that cause feelings of euphoria, thereby affecting the brain's reward pathways (Glasner-Edwards and Mooney, 2014). METH induces rapid accumulation of monoamine neurotransmitters in brain synapses, which interact with DA, norepinephrine, and SERT in neurons to produce pharmacological effects (Cruickshank and Dyer, 2009). The DA level in the brain can affect emotional conditions such as depression and anxiety, leading to pathological changes such as reward effects and drug craving (Cadet and Brannock, 1998; Siefried et al., 2020). In METH addicts, long-term abuse of METH severely impairs the structure and function of the brain's monoamine transmitter system and eventually leads to the depletion of monoamine neurotransmitters in the brain (Cadet et al., 2003). METH abuse can also lead to the release of

monoamine transmitters such as DA, norepinephrine, 5-HT, and other neurotransmitters (Rothman and Baumann, 2003; Panenka et al., 2013). Concretely, chronic abuse of METH can deplete DA reserves in the brain and reduce DA receptor availability (London, 2016). In summary, long-term METH abuse depletes reserves of DA in the brain and reduces the availability of DA receptors (Alex and Pehek, 2007; Ferrucci et al., 2013). METH can also have a negative impact on motor and executive function, which are usually associated with anxiety and depression (Rusyniak, 2013). Recent studies have demonstrated that METH can induce neuropathological changes through apoptotic signaling pathways in the rodent brain. Data suggest that mitochondria- and endoplasmic reticulum-mediated cascade activation is involved in METH-induced apoptosis and that neuronal apoptosis aggravates the occurrence of depression (Cadet et al., 2003).

Microglia are mainly involved in the regulation of inflammation in the central nervous system and protect the brain against injury and damage (Graeber and Streit, 2010). However, microglial overactivation can induce the release of various cytokines, reactive oxygen species, and nitrogen species, ultimately leading to neuronal damage. A study found that the inflammation induced by METH exposure may play an important role in neuronal damage (Beardsley and Hauser, 2014). Clinically, neuropsychiatric impairments, including cognitive deficits, depression, and anxiety that have been found in METH addicts, are associated with the inflammatory response (Sadek et al., 2007; Zorick et al., 2010). Elevated levels of the proinflammatory cytokines interleukin-1β (IL-1β), interleukin-2 (IL-2), interleukin-6 (IL-6), and tumor necrosis factor-α (TNF-α) in plasma were obviously associated with severe neurocognitive impairment in METH addicts (Loftis et al., 2011). It has been suggested that METH-induced neuroinflammation in the striatum may be the common basis of depression and cognitive deficits in METH addicts (Krasnova et al., 2016).

Research has shown that brain-derived neurotrophic factor (BDNF) plays an increasingly important role in anxiety and depression. BDNF is involved in the pathophysiological process of depression and plays an antidepressant role (Heyman et al., 2012; Archer et al., 2014). Physical exercise has been found to reverse the physical and neurological damage caused by METH exposure by increasing BDNF release, which is the basis for antidepressant effects (Huang et al., 2019). Studies have shown that other neurotrophic factors, such as nerve growth factor (NGF) and BDNF, also play a key role in the neurophysiological mechanisms that relieve depression (Overstreet et al., 2010; Hochstrasser et al., 2013).

Methamphetamine and Neuronal Injury

Core mechanisms of nervous system damage caused by METH include over release of monoamine transmitters, oxidative stress, mitochondrial dysfunction, and inflammation (Krasnova and Cadet, 2009; Shin et al., 2012). These mechanisms may be the common pathological basis for METH-induced neuropsychiatric disorders such as addiction, impairments in learning, memory and cognition, anxiety, and depression, and it is necessary to highlight these mechanisms here.

High concentrations of DA in the cytoplasm produce toxic dopamine quinone, oxygen free radicals, hydrogen peroxide, and increased reactive oxygen species (ROS) in neuronal cells, resulting in oxidative stress, mitochondrial dysfunction, and damage to the presynaptic membrane (Cadet and Brannock, 1998; Lin et al., 2012). Studies have shown that tyrosine hydroxylase inhibitors inhibit DA synthesis and thus protect against neurotoxic effects caused by DA autoxidation (Krasnova and Cadet, 2009). Excessive release of DA in the synaptic cleft can cause the loss of the synaptic termini of dopaminergic neurons. DAT inhibitors have been shown to inhibit METH-induced DA release and thus have a protective effect on synaptic terminals (Shaerzadeh et al., 2018). Increased DA release in the synaptic cleft also induces apoptosis of postsynaptic neurons by activating D1 and D2 receptors, and this effect is inhibited by D1 and/or D2 receptor antagonists (Xu et al., 2005). Antioxidants help to alleviate nerve damage caused by METH and are neuroprotective (Imam et al., 2001). Protein kinase Cδ (PKCδ) is also involved in METH-induced oxidative stress and dopaminergic neurotoxicity. Inhibition of PKCδ activity can prevent METH-induced neurotoxicity (Wen et al., 2016).

Mitochondrial dysfunction is another mechanism of METH neurotoxicity. METH causes adenosine triphosphate (ATP) depletion and mitochondrial complex II inhibition. Mitochondrial complex substrates (decylubiquinone or nicotinamide) have been shown to attenuate METH-induced striatal dopaminergic neuron damage (Stephans et al., 1998; Brown et al., 2005).

The inflammatory response of the central nervous system induced by METH is a complex, interactive, and regulated process. This may be related to the symptoms of mental disorders caused by METH (Huckans et al., 2015). Microglia, astrocytes, and a series of inflammation-related factors form a network of cascade pathways. When the inflammatory response is overactivated, microglia and astrocytes can regulate each other through inflammatory cell mediators and jointly regulate changes in other factors in the inflammatory pathway. The increase in inflammatory factors can stimulate or induce microglia and astrocytes (Potula et al., 2010; Liu et al., 2012; Chen et al., 2015; Lloyd et al., 2017). Signal changes in nuclear factor-κB (NF-κB) acts as a 'local pivotal factor' in the control of midstream inflammation, controlling the activation of many inflammatory pathways (Mitchell and Carmody, 2018). Upstream factors, such as toll-like receptor-4 (TLR4), signal transducer and activator of transcription 3 (STAT3), extracellular signal-regulated kinase (ERK), serine-threonine kinase (AKT), and phosphatidylinositol 3-kinase (PI3K), signal changes in NF-κB signalling (Park et al., 2017), NF-κB activation, and transcription of various inflammatory cytokines, such as IL-1β, IL-6, and TNF-α, thereby mediating the cellular inflammatory response (Hou et al., 2017). D2-deficient brain regions show a significant inflammatory response. D2 agonists inhibit NF-κB phosphorylation and downstream inflammatory cytokine and chemokine production (Han et al., 2017). Due to the complex environment of the central nervous system, there are still many upstream and downstream factors of inflammation-related pathways, and their relationships have not been fully elucidated and need to be further studied.

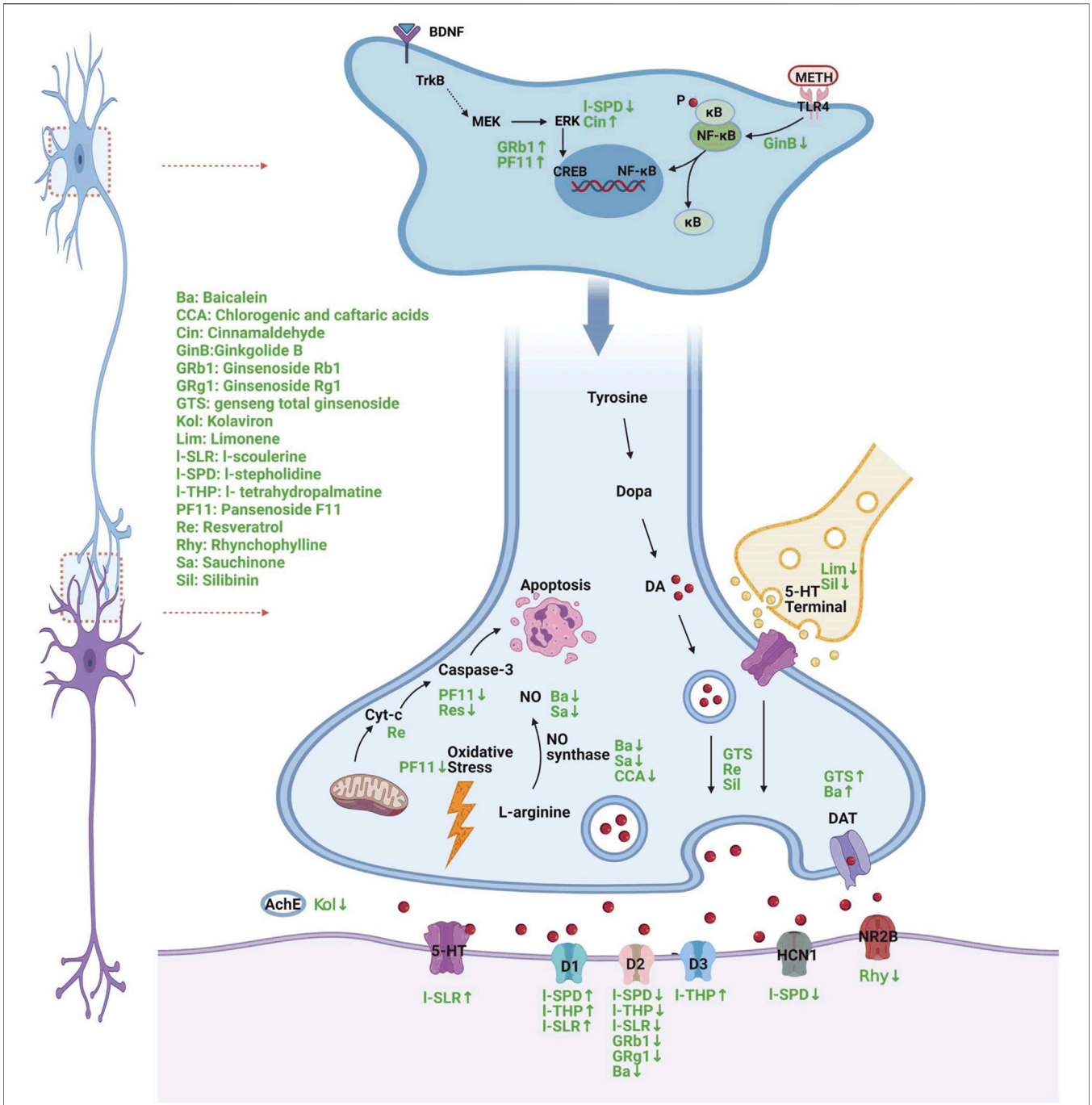

FIGURE 1 | A diagram of the mechanism of different Chinese herbs in the treatment of METH-induced neuropsychiatric injury (Created with BioRender.com). ®↓ symbol indicates decrease and ↑ symbol indicates increase following METH treatment.

Candidate Chinese Herbal Medicine of Methamphetamine Abuse

METH abuse, addiction, and the resulting mental symptoms have become an increasingly important problem to be solved. Unfortunately, because the specific neurobiological mechanisms involved are complex and have not been fully and systematically elucidated, to date, there is no established pharmacotherapy for METH abuse (Siefried et al., 2020).

In recent years, research on the therapeutic effect of Chinese herbal medicine on METH has received increasing attention and has made remarkable progress. Studies have found that a variety of Chinese herbal medicines have significant therapeutic effects

on psychiatric symptoms, such as addiction, depression, and cognitive impairment, induced by METH abuse and have the advantage of multitarget comprehensive treatment. We conducted a systematic review to provide new perspectives and ideas for the prevention and treatment of METH abuse. The detailed neural mechanism is illustrated in **Figure 1**.

Tetrahydroprotoberberines

Tetrahydroprotoberberines (THPBs) are a series of alkaloids isolated from the traditional Chinese analgesic drug Yanhuasol that act on the dopaminergic system of the CNS and have a far-reaching effect (Jin and Sun, 1995). *l*-Tetrahydropalmatine (*l*-THP) and *l*-stepholidine (*l*-SPD) are members of the THPB family. They have unique pharmacological characteristics as D1 receptor agonists and D2 receptor antagonists (Jin et al., 2002) and have been proven to have value in the clinical treatment of drug dependence (Chu et al., 2008).

l-THP acts in the brain and induces the release of endogenous opioids such as endorphins, enkephalins, and kephalins. This may be the underlying mechanism for treating drug dependence (Jin and Sun, 1995). The reward effect in the process of METH addiction is mainly caused by the increase of DA, and the blocking effect of *l*-THP on the DA receptor in the reward system can weaken the reward effect of METH, reduce the euphoria it produces, and finally reduce the mental dependence on METH (Jin and Sun, 1995). Our other study also found that *l*-THP inhibits METH self-administration and reinstatement in rats (Gong et al., 2016). *l*-THP can suppress METH-induced rewarding in CPP mice (Su et al., 2013), and the *l*-THP inhibitory effect may be associated with the inhibition of ERK phosphorylation in the NAc and PFC (Su et al., 2020). *l*-THP inhibits METH-induced behavioral sensitization by upregulating 5-HT neuronal activity and increasing the expression of the D3 receptor (Yun, 2014a). *l*-THP treatment also has a potential protective role on METH-induced spatial memory impairment in mice (Cao et al., 2018).

l-SPD, a partial agonist of the D1 receptor and antagonist of the D2 receptor (Natesan et al., 2008), has a therapeutic effect on memory damage induced by METH. *l*-SPD can also attenuate METH-induced locomotor sensitization behavior in a dose-dependent manner (Ma et al., 2014). A recent study proved that *l*-SPD alleviates memory deficits in Alzheimer's disease rats by affecting dopaminergic pathways and synaptic plasticity (Hao et al., 2015). Our previous study also demonstrated that *l*-SPD pre-treatment rescues METH-induced memory deficits by suppressing upregulated HCN1 channels and the dopaminergic pathway (Zhou et al., 2019).

l-scoulerine (*l*-SLR, an *l*-SPD analogue) is not only a D1 receptor agonist and D2 receptor antagonist but also a 5-HT1A receptor partial agonist. Pre-treatment with *l*-SLR reduces the chronic behavioral sensitization and METH-induced expression of CPP in mice. *l*-SLR also inhibits the anxiety-like behaviors induced by METH in zebrafish (Mi et al., 2016).

The effects of these traditional Chinese medicine (TCM) THPBs are summarized in **Table 2**.

Ginsenoside

Ginseng is a perennial, succulent root and a family of plants known as araliaceae. Ginseng is mainly divided into American ginseng panaxquinquefolium and Korean ginseng panax ginseng. Over many years, in traditional medicine, ginseng has played a positive role in invigorating qi, calming nerves, and enhancing immunity. It has also been used as an anxiolytic, antidepressant, and memory enhancer (Lacaille-Dubois and Wagner, 1996). Ginseng prevents morphine-, cocaine-, and METH-induced tolerance and dependence in rodents (Tokuyama and Takahashi, 2001; Kim et al., 2005). Ginseng also reduces the hyperstimulation induced by METH and cocaine even after discontinuation for 30 days (Tokuyama et al., 1996).

It has been suggested that ginseng total saponin (GTS) attenuates hyperlocomotion and CPP induced by METH in rodents (Kim et al., 1996; Tokuyama and Takahashi, 2001; Kim et al., 2005). GTS modulates the activity of the dopaminergic system by reducing DA reuptake and then affecting brain DA concentrations (Lacaille-Dubois and Wagner, 1996).

Pansenoside F11 (PF11) is a special ginsenoside that is found in American ginseng but not in Korean ginseng. PF11 can reduce DA levels by regulating dopaminergic and GABA neurons in the NAc and thus exerts an inhibitory effect on METH addiction-induced behavior (Fu et al., 2016). PF11 has a neuroprotective effect and can antagonize the neurotoxic effects caused by METH addiction (Wu et al., 2003).

Ginsenoside Re can effectively prevent METH-induced mitochondrial dysfunction, oxidative damage, microglial activation, activation of proapoptotic factors, and degeneration of dopaminergic neurons by inhibiting the PKCδ gene (Shin et al., 2014; Nam et al., 2015). Both single and repeated administration of ginsenosides Rb1 and Rg1 (major components of GTS) inhibit the behavioral sensitization and CPP induced by METH (Kim et al., 1998).

One of the clinical indications of ginseng is antidepressant effects (Kennedy and Scholey, 2003). In forced swimming tasks, PF11 shortens METH-induced long periods of immobility and increases the incubation period of the Morris water maze task, suggesting that PF11 alleviates memory decline and depression-like behavior (Wu et al., 2003). A study found that ginseng saponin Rb1 has an antidepressant effect associated with the BDNF- tyrosine kinase B (TrkB) signaling pathways and that the combination of BDNF and TrkB regulates PI3K through at least three intracellular signal transduction pathways. These different signal transduction pathways ultimately regulate cell proliferation, differentiation, and apoptosis through the cyclic adenosine monophosphate response element binding protein (CREB)-dependent activation of transcription factors and are critical to play an antidepressant role (Lee et al., 2016; Kang et al., 2019). Therefore, ginseng (saponin) is also a potential candidate drug for METH-induced depression.

The effects of the TCM ginseng are summarized in **Table 3**.

Others

Scutellariae baicalensis Georgi (*Huang Qin*) belongs to the labiaceae family. It has many clinical therapeutic effects.

TABLE 2 | Summarized effects of TCM Corydalis and Stephania therapy on METH abuse and other psychiatric symptoms.

Herb	Compound	Types of functional impairment	Symptoms and experiment	Animal	Effective dose	Receptor or signaling pathway molecule	Author [Ref.]
Corydalis and Stephania	*l*-THP	METH dependence	METH self-administration and METH-induced reinstatement	Rat	*l*-THP 5 mg/kg	DA receptor	Gong et al. (2016)
			CPP	Mice	*l*-THP (10 and 20 mg/kg)		Su et al. (2013)
					l-THP 10 mg/kg	ERK phosphorylation	Su et al. (2020)
		Behavioral sensitization	Locomotor activity	Rat and mice	*l*-THP (10 and 15 mg/kg)	5-HT and D3 receptor	Yun (2014a)
		Memory and cognitive function impairment	Spatial memory impairment	Mice	*l*-THP (10 and 20 mg/kg)	DA receptor	Cao et al. (2018)
	l-SPD	Behavioral sensitization	Locomotor sensitization behavior	Rat	*l*-SPD (5 and 10 mg/kg, i.p.)	DA receptor	Ma et al. (2014)
		Memory and cognitive function impairment	Memory deficits	Mice	*l*-SPD (10 mg/kg, i.p.)	Dopaminergic pathway and HCN1 channels	Zhou et al. (2019)
	l-SLR	Behavioral sensitization METH dependence	Behavioral sensitization CPP	Mice	*l*-SLR (5 mg/kg)	D2 receptor antagonist, D1 receptor agonist	Mi et al. (2016)
		Anxiety-like behaviors	Anxiety-like behaviors	Zebrafish		5-HT1A receptor partial agonist	

METH = methamphetamine; 5-HT = 5-hydroxytryptamine; D or DA = dopamine; ERK = extracellular-regulated kinase; HCN1 = hyperpolarization-activated and cyclic nucleotide-gated cation 1; l-THP = l-tetrahydropalmatine; l-SPD = l-stepholidine; l-SLR = l-scoulerine; CPP = conditioned place preference.

TABLE 3 | Summarized effects of TCM ginseng therapy on METH abuse and other psychiatric symptoms.

Herb	Compound	Types of functional impairment	Symptoms and experiment	Animal	Effective dose	Receptor or signaling pathway molecule	Author [Ref.]
Ginseng	GTS	Behavioral sensitization	Hyperlocomotion	Mice	200 mg/kg	Modulated reuptake of dopamine and complex pharmacological actions between dopamine receptors and a serotonergic/adenosine A2A/delta-opioid receptor	Tokuyama et al. (1996)
		METH dependence	CPP				
	Ginsenoside Rb1 and Rg1	Behavioral sensitization	Hyperlocomotion	Mice	100 and 200 mg/kg, respectively	Postsynaptic DA receptors	Kim et al. (1998)
		METH dependence	CPP		100 mg/kg, respectively		
	Ginsenoside Rb1	Anxiety-like behaviors and stress	Immobilization stress	Rat	40 mg/kg	BDNF - TrkB signaling pathways	Kang et al. (2019)
			Anxiety-like responses and post-traumatic stress		30 mg/kg	CREB	Lee et al. (2016)
	Pansenoside F11	METH dependence	CPP	Mice	4 or 8 mg/kg/day p.o	Reduce DA level by regulating dopaminergic and GABA neurons	Fu et al. (2016)
		Neurotoxic	Neurotoxic		4 and 8 mg/kg, p.o., two times at 4 h intervals, 60 min prior to METH administration	Neuroprotective	Wu et al. (2003)
		Depression	Prolonged immobility time in the forced swimming task				
		Memory and cognitive function impairment	Increased latency in morris water maze task				
	Ginsenoside Re	Neurotoxic	Oxidative damage, mitochondrial dysfunction	Mice	10 and 20 mg/kg, p.o., twice a day, 8 or 19 days	PKCδ gene	Shin et al. (2014)
			Microglial activation and dopaminergic degeneration	Human neuroblastoma dopaminergic SH-SY5Y cell lines	100 μM		Nam et al. (2015)

METH = methamphetamine; 5-HT = 5-hydroxytryptamine; D or DA = dopamine; GABA = gamma-aminobutyric acid; BDNF = brain derived neurotrophic factor; TrkB = tyrosine kinase B; CREB = cAMP-response element binding protein; PKC = protein kinase C; GTS = ginseng total saponin; CPP = conditioned place preference

TABLE 4 | Summarized effects of other TCM therapy on METH abuse and other psychiatric symptoms.

Herb	Compound	Types of functional impairment	Symptoms and experiment	Animal	Effective dose	Receptor or signaling pathway molecule	Author [Ref.]
Scutellariae baicalensis Georgi	Baicalein	Memory and cognitive function impairment	Memory deficits, amnesia	Mice	1 mg/kg	D2 receptors	Wong et al. (2014)
Uncaria alkaloids	Rhynchophylline	Neurotoxic	Oxidative damage	Mice	1 mg/kg	Dopamine transporter	Liu et al. (2006)
		Neurotoxic	Dopaminergic neurotoxicity				
		METH dependence	Dopaminergic neurotoxicity		1 mg/kg	Elevated NO level	Liu et al. (2006)
			CPP		40 and 80 mg/kg	Reduce NR2B expression	Li et al. (2014)
Clerodendrum inerme	Hispidulin	Behavioral sensitization	Hyperlocomotion	Mice	10,30, and 100 mg/kg, ip; 10 nmol, intracerebellar microinjection (i.c.b.)	Activate GABAA receptors	Liao et al. (2016)
G. kola seeds	Kolaviron	Behavioral sensitization	Stereotypic behaviors	Rat	200, 400, and 800 mg/kg, po., 4 weeks	Inhibition of acetylcholinesterase	Ijomone and Obi (2013)
Saururus chinensis	Sauchinone	Memory and cognitive function impairment	Negative effects of METH on learning and memory	Mice	10 mg/kg, po	Degeneration of dopaminergic nerve terminals, NO synthase	Jang et al. (2012)
		Neurotoxic	Neurotoxicity				
		Neurotoxic	Attenuated the METH-induced degeneration of dopaminergic nerve terminals, reduced the glial cell activation, inhibited the synthesis of NO				
Coffee beans	Chlorogenic and caftaric acids	METH dependence	CPP	Rat	10 mg/kg, ip	NO synthase inhibitor	Kim et al. (2013)
		Oxidative stress	Oxidative stress		60 mg/kg chlorogenic acid and 40 mg/kg caftaric acid	Antioxidant stress	Koriem and Soliman (2014)
Grape	Resveratrol	Behavioral sensitization	Dopamine overflow	Rat	Repeated resveratrol treatment (1–20 mg/kg)	Reduce DA release	Miller et al. (2013)
Lemon	Limonene	Behavioral sensitization	Neuron apoptotic	Neuronal N27 cell lines	10 μM	Caspase-3 dependent pathway	Kanthasamy et al. (2011)
			Hyperlocomotion	Rat and mice	200, 400, and 600 mg/kg, i.p	5-HT neuronal function and DA release	Yun (2014b)
Ginkgo biloba	Ginkgolide B	Nerve inflammation	Microglial activation	BV2 cells lines	120–240 μM	TLR4-NF-κb signaling pathway	Wan et al. (2017)
Silybum Marianum	Silibinin	Memory and cognitive function impairment	Cognitive deficits	Mice	200 mg/kg, po.,qd, 7 days	DA and 5-HT system	Lu et al. (2010)
Cassia siamea Lamk	Barakol	Neurotoxic	Decreases of DA and 5-HT	Mice	100 mg/kg, ip	Dopaminergic receptors	Sukma et al. (2002)
		Behavioral sensitization	Hyperlocomotion				
Cortex cinnamomi	Cinnamaldehyde	Neurotoxic	Neurotoxicity	Rat	40 mg/kg, ip	ERK pathway	Saeed et al. (2018)
		Memory and cognitive function impairment	Learning and cognition deficits				

METH = methamphetamine; NO = nitric oxide; 5-HT = 5-hydroxytryptamine; D or DA = dopamine; GABA = gamma-aminobutyric acid; NR2B = N-methyl-D-aspartate receptor subtype-2B; ERK = extracellular-regulated kinase; TLR4-NF-κB = toll-like receptor 4-nuclear factor-κB; CPP = conditioned place preference

Baicalein is an active ingredient isolated from *Huang Qin* roots that has anti-inflammatory and free radical scavenging effects. Studies have shown that baicalein has a powerful neuroprotective effect (Sowndhararajan et al., 2017). A recent study confirmed that baicalein ameliorates METH-induced memory loss and amnesia through D2 receptors in mice. Baicalein also reduces METH-induced hippocampal lipid peroxidation and peroxynitrite production in mice (Wong et al., 2014). Baicalein attenuates the loss of DAT (Wu et al., 2006) and affects the DA concentration in METH-intoxicated mice in a dose-dependent manner (Liu et al., 2006). In the striatum, baicalein protects neurons from METH-induced reductions in NO content (Liu et al., 2006).

Uncaria alkaloids are commonly used in TCM (Shi et al., 2003). In the central nervous system, rhynchophylline has anti-convulsive, sedative, memory repair, and anti-epileptic effects (Li et al., 2015). Rhynchophylline is a noncompetitive NMDA receptor antagonist and a calcium channel blocker. It can reduce the CPP behavior of animals by reducing the expression of NR2B protein and thus reduces psycho-dependence after METH abuse (Li et al., 2014).

Hispidulin, the active constituent of the *C. inerme* ethanolic group, also decreases hyperlocomotion induced by METH (Chen et al., 2012; Huang et al., 2015). Hispidulin inhibits METH-induced behavioral sensitization, possibly by activation of the GABAA receptor α6 subunit (Liao et al., 2016).

Kolaviron, the biflavone complex in kola seeds, alleviates the stereotypical behavior induced by a single dose of METH in mice and alleviates the negative effects of METH on learning and memory. Brain histological studies also show that kolaviron preconditioning protects the hippocampus from METH-induced neurotoxicity. Kolaviron may restore METH-induced cognitive impairment by inhibiting acetylcholinesterase (Ijomone and Obi, 2013).

Possible protective effects of sauchinone against METH abuse have also been discussed. Sauchinone attenuates METH-induced dopaminergic nerve terminal degeneration. In addition, sauchinone reduces glial cell activation and inhibits the synthesis of NO through the suppression of NO synthase (Jang et al., 2012). Kim and coworkers found that sauchinone shows a dose-dependent protective effect, inhibiting the expression and acquisition of CPP induced by METH (Kim et al., 2013).

Chlorogenic acid and caftaric acid can eliminate hepatotoxicity and reverse the increase in oxidative stress induced by METH (Koriem and Soliman, 2014). Resveratrol also reduces METH-induced DA overload in the brains of rats (Miller et al., 2013). Resveratrol has a protective effect on METH-induced caspase-3-dependent apoptosis (Kanthasamy et al., 2011). Limonene reduces METH-induced hyperlocomotion in a dose-dependent manner (Yun, 2014b).

Ginkgolide B inhibits microglial cell activation induced by METH, possibly through the TLR4-NF-κB signaling pathway (Wan et al., 2017). Silibinin can reduce cognitive impairment and decrease DA and 5-HT associated with METH abuse (Lu et al., 2010). Barakol, the main component of *cassia seeds*, reduces hyperactivity induced by METH in a dose-dependent manner by inhibiting dopaminergic receptors (Sukma et al., 2002). Cinnamaldehyde can reduce METH-induced nerve damage and enhances learning and cognitive abilities through activation of the ERK pathway in the PFC (Saeed et al., 2018).

The effects of other TCM are summarized in **Table 4**.

DISCUSSION

METH dependence and its related neurological and psychiatric problems involve multiple transmitter systems in multiple brain regions. METH dependence is caused by very complex mechanisms involving DA, Glu, 5-HT, acetylcholine, and GABA. With a history of more than 200 years, TCM drug rehabilitation has accumulated rich experience and formed a set of unique theories and methods. The treatment philosophy of TCM drug abstinence is to support healthy qi and eliminate toxic drugs, and this philosophy highlights the characteristics of treatment based on syndrome differentiation. More importantly, TCM compounds also have multitarget effects that are similar to cocktail therapy, aiming to address METH substance dependence and the neuropsychiatric problems derived from this complex multitarget intractable encephalopathy. TCM can be regarded as a useful attempt and exploration. Unfortunately, only a few TCM or chemical constituents have sufficient literature to identify promising candidates for METH abuse. Further basic and clinical studies are needed.

AUTHOR CONTRIBUTIONS

The authors declare that there LC and YW contributed to conception and design of the study. LC organized the database. QR performed the statistical analysis. LC and YW wrote the first draft of the manuscript. All authors contributed to manuscript revision, read, and approved the submitted version.

FUNDING

This study was supported by the Wuhan Municipal Science and Technology Bureau (Grant No. 2019020701011499) and the National Natural Science Foundation of China (Grant No. 81971775 to LC and 82071970 to YW).

REFERENCES

Alex, K. D., and Pehek, E. A. (2007). Pharmacologic Mechanisms of Serotonergic Regulation of Dopamine Neurotransmission. *Pharmacol. Ther.* 113, 296–320. doi:10.1016/j.pharmthera.2006.08.004

Anneken, J. H., Angoa-Perez, M., Sati, G. C., Crich, D., and Kuhn, D. M. (2018). Assessing the Role of Dopamine in the Differential Neurotoxicity Patterns of Methamphetamine, Mephedrone, Methcathinone and 4-methylmethamphetamine. *Neuropharmacology* 134, 46–56. doi:10.1016/j.neuropharm.2017.08.033

Archer, T., Josefsson, T., and Lindwall, M. (2014). Effects of Physical Exercise on Depressive Symptoms and Biomarkers in Depression. *CNS Neurol. Disord. Drug Targets* 13, 1640–1653. doi:10.2174/1871527313666141130203245

Barker, G. R. I., Bird, F., Alexander, V., and Warburton, E. C. (2007). Recognition Memory for Objects, Place, and Temporal Order: a Disconnection Analysis of the Role of the Medial Prefrontal Cortex and Perirhinal Cortex. *J. Neurosci.* 27, 2948–2957. doi:10.1523/jneurosci.5289-06.2007

Barker, G. R. I., and Warburton, E. C. (2008). NMDA Receptor Plasticity in the Perirhinal and Prefrontal Cortices Is Crucial for the Acquisition of Long-Term Object-In-Place Associative Memory. *J. Neurosci.* 28, 2837–2844. doi:10.1523/jneurosci.4447-07.2008

Beardsley, P. M., and Hauser, K. F. (2014). Glial Modulators as Potential Treatments of Psychostimulant Abuse. *Adv. Pharmacol.* 69, 1–69. doi:10.1016/b978-0-12-420118-7.00001-9

Berridge, C. W. (2006). Neural Substrates of Psychostimulant-Induced Arousal. *Neuropsychopharmacol* 31, 2332–2340. doi:10.1038/sj.npp.1301159

Boileau, I., Payer, D., Rusjan, P. M., Houle, S., Tong, J., McCluskey, T., et al. (2016). Heightened Dopaminergic Response to Amphetamine at the D3 Dopamine Receptor in Methamphetamine Users. *Neuropsychopharmacol* 41, 2994–3002. doi:10.1038/npp.2016.108

Brensilver, M., Heinzerling, K. G., and Shoptaw, S. (2013). Pharmacotherapy of Amphetamine-type Stimulant Dependence: an Update. *Drug Alcohol. Rev.* 32, 449–460. doi:10.1111/j.1465-3362.2012.00423.x

Brown, J. M., Quinton, M. S., and Yamamoto, B. K. (2005). Methamphetamine-induced Inhibition of Mitochondrial Complex II: Roles of Glutamate and Peroxynitrite. *J. Neurochem.* 95, 429–436. doi:10.1111/j.1471-4159.2005.03379.x

Cadet, J. L., and Brannock, C. (1998). Invited Review Free Radicals and the Pathobiology of Brain Dopamine Systems. *Neurochem. Int.* 32, 117–131. doi:10.1016/s0197-0186(97)00031-4

Cadet, J. L., Jayanthi, S., and Deng, X. (2003). Speed Kills: Cellular and Molecular Bases of Methamphetamine-induced Nerve Terminal Degeneration and Neuronal Apoptosis. *FASEB J.* 17, 1775–1788. doi:10.1096/fj.03-0073rev

Callaghan, R. C., Cunningham, J. K., Allebeck, P., Arenovich, T., Sajeev, G., Remington, G., et al. (2012). Methamphetamine Use and Schizophrenia: a Population-Based Cohort Study in California. *Am. J. Psychiatry* 169, 389–396. doi:10.1176/appi.ajp.2011.10070937

Cao, G., Zhang, Y., Zhu, L., Zhu, J., Zhao, N., Dong, N., et al. (2018). The Inhibitory Effect of Levo-Tetrahydropalmatine on the Methamphetamine-Induced Spatial Memory Impairment in Mice. *Neurosci. Lett.* 672, 34–39. doi:10.1016/j.neulet.2018.02.018

Carati, C., and Schenk, S. (2011). Role of Dopamine D1- and D2-like Receptor Mechanisms in Drug-Seeking Following Methamphetamine Self-Administration in Rats. *Pharmacol. Biochem. Behav.* 98, 449–454. doi:10.1016/j.pbb.2011.02.010

Castner, S. A., Williams, G. V., and Goldman-Rakic, P. S. (2000). Reversal of Antipsychotic-Induced Working Memory Deficits by Short-Term Dopamine D1 Receptor Stimulation. *Science* 287, 2020–2022. doi:10.1126/science.287.5460.2020

Chen, H. L., Lee, H. J., Huang, W. J., Chou, J. F., Fan, P. C., Du, J. C., et al. (2012). Clerodendrum Inerme Leaf Extract Alleviates Animal Behaviors, Hyperlocomotion, and Prepulse Inhibition Disruptions, Mimicking Tourette Syndrome and Schizophrenia. *Evid. Based Complement. Alternat Med.* 2012, 284301. doi:10.1155/2012/284301

Chen, S.-H., Oyarzabal, E. A., Sung, Y.-F., Chu, C.-H., Wang, Q., Chen, S.-L., et al. (2015). Microglial Regulation of Immunological and Neuroprotective Functions of Astroglia. *Glia* 63, 118–131. doi:10.1002/glia.22738

Chu, H., Jin, G., Friedman, E., and Zhen, X. (2008). Recent Development in Studies of Tetrahydroprotoberberines: Mechanism in Antinociception and Drug Addiction. *Cell Mol. Neurobiol.* 28, 491–499. doi:10.1007/s10571-007-9179-4

Cruickshank, C. C., and Dyer, K. R. (2009). A Review of the Clinical Pharmacology of Methamphetamine. *Addiction* 104, 1085–1099. doi:10.1111/j.1360-0443.2009.02564.x

Dean, A. C., Groman, S. M., Morales, A. M., and London, E. D. (2013). An Evaluation of the Evidence that Methamphetamine Abuse Causes Cognitive Decline in Humans. *Neuropsychopharmacol* 38, 259–274. doi:10.1038/npp.2012.179

Eslami-Shahrbabaki, M., Fekrat, A., and Mazhari, S. (2015). A Study of the Prevalence of Psychiatric Disorders in Patients with Methamphetamine-Induced Psychosis. *Addict. Health* 7, 37–46.

Ferrucci, M., S. Giorgi, F., Bartalucci, A., L. Busceti, C., and Fornai, F. (2013). The Effects of Locus Coeruleus and Norepinephrine in Methamphetamine Toxicity. *Curr. Neuropharmacol.* 11, 80–94. doi:10.2174/157015913804999522

Fu, K., Lin, H., Miyamoto, Y., Wu, C., Yang, J., Uno, K., et al. (2016). Pseudoginsenoside-F11 Inhibits Methamphetamine-Induced Behaviors by Regulating Dopaminergic and GABAergic Neurons in the Nucleus Accumbens. *Psychopharmacology* 233, 831–840. doi:10.1007/s00213-015-4159-8

Glasner-Edwards, S., Marinelli-Casey, P., Hillhouse, M., Ang, A., Mooney, L. J., Rawson, R., et al. (2009). Depression Among Methamphetamine Users. *J. Nerv Ment. Dis.* 197, 225–231. doi:10.1097/nmd.0b013e31819db6fe

Glasner-Edwards, S., Mooney, L. J., Marinelli-Casey, P., Hillhouse, M., Ang, A., Rawson, R., et al. (2008). Risk Factors for Suicide Attempts in Methamphetamine-dependent Patients. *Am. J. Addict.* 17, 24–27. doi:10.1080/10550490701756070

Glasner-Edwards, S., and Mooney, L. J. (2014). Methamphetamine Psychosis: Epidemiology and Management. *CNS Drugs* 28, 1115–1126. doi:10.1007/s40263-014-0209-8

Gong, X., Yue, K., Ma, B., Xing, J., Gan, Y., Wang, D., et al. (2016). Levo-tetrahydropalmatine, a Natural, Mixed Dopamine Receptor Antagonist, Inhibits Methamphetamine Self-Administration and Methamphetamine-Induced Reinstatement. *Pharmacol. Biochem. Behav.* 144, 67–72. doi:10.1016/j.pbb.2016.01.010

Graeber, M. B., and Streit, W. J. (2010). Microglia: Biology and Pathology. *Acta Neuropathol.* 119, 89–105. doi:10.1007/s00401-009-0622-0

Han, X., Li, B., Ye, X., Mulatibieke, T., Wu, J., Dai, J., et al. (2017). Dopamine D2receptor Signalling Controls Inflammation in Acute Pancreatitisviaa PP2A-dependent Akt/NF-κB Signalling Pathway. *Br. J. Pharmacol.* 174, 4751–4770. doi:10.1111/bph.14057

Hao, J.-R., Sun, N., Lei, L., Li, X.-Y., Yao, B., Sun, K., et al. (2015). L-Stepholidine Rescues Memory Deficit and Synaptic Plasticity in Models of Alzheimer's Disease via Activating Dopamine D1 Receptor/PKA Signaling Pathway. *Cell Death Dis.* 6, e1965. doi:10.1038/cddis.2015.315

Heyman, E., Gamelin, F.-X., Goekint, M., Piscitelli, F., Roelands, B., Leclair, E., et al. (2012). Intense Exercise Increases Circulating Endocannabinoid and BDNF Levels in Humans-Possible Implications for Reward and Depression. *Psychoneuroendocrinology* 37, 844–851. doi:10.1016/j.psyneuen.2011.09.017

Hochstrasser, T., Ehrlich, D., Sperner-Unterweger, B., and Humpel, C. (2013). Antidepressants and Anti-inflammatory Drugs Differentially Reduce the Release of NGF and BDNF from Rat Platelets. *Pharmacopsychiatry* 46, 29–34. doi:10.1055/s-0032-1314843

Hondebrink, L., Tan, S., Hermans, E., van Kleef, R. G. D. M., Meulenbelt, J., and Westerink, R. H. S. (2013). Additive Inhibition of Human α1β2γ2 GABAA Receptors by Mixtures of Commonly Used Drugs of Abuse. *Neurotoxicology* 35, 23–29. doi:10.1016/j.neuro.2012.12.003

Hou, J., Jiang, S., Zhao, J., Zhu, D., Zhao, X., Cai, J. C., et al. (2017). N-Myc-Interacting Protein Negatively Regulates TNF-Alpha-Induced NF-kappaB Transcriptional Activity by Sequestering NF-kappaB/p65 in the Cytoplasm. *Sci. Rep.* 7, 14579. doi:10.1038/s41598-017-15074-5

Huang, J., Zheng, Y., Gao, D., Hu, M., and Yuan, T. (2019). Effects of Exercise on Depression, Anxiety, Cognitive Control, Craving, Physical Fitness and Quality of Life in Methamphetamine-Dependent Patients. *Front. Psychiatry* 10, 999. doi:10.3389/fpsyt.2019.00999

Huang, W.-J., Lee, H.-J., Chen, H.-L., Fan, P.-C., Ku, Y.-L., and Chiou, L.-C. (2015). Hispidulin, a Constituent of Clerodendrum Inerme that Remitted Motor Tics,

Alleviated Methamphetamine-Induced Hyperlocomotion without Motor Impairment in Mice. *J. Ethnopharmacology* 166, 18–22. doi:10.1016/j.jep.2015.03.001

Huckans, M., Fuller, B. E., Chalker, A. L. N., Adams, M., and Loftis, J. M. (2015). Plasma Inflammatory Factors Are Associated with Anxiety, Depression, and Cognitive Problems in Adults with and without Methamphetamine Dependence: An Exploratory Protein Array Study. *Front. Psychiatry* 6, 1–13. doi:10.3389/fpsyt.2015.00178

Ijomone, O. M., and Obi, A. U. (2013). Kolaviron, Isolated from Garcinia Kola, Inhibits Acetylcholinesterase Activities in the hippocampus and Striatum of Wistar Rats. *Ann. Neurosci.* 20, 42–46. doi:10.5214/ans.0972.7531.200203

Imam, S. Z., el-Yazal, J., Newport, G. D., Itzhak, Y., Cadet, J. L., Slikker, W., Jr., et al. (2001). Methamphetamine-induced Dopaminergic Neurotoxicity: Role of Peroxynitrite and Neuroprotective Role of Antioxidants and Peroxynitrite Decomposition Catalysts. *Ann. N. Y Acad. Sci.* 939, 366–380. doi:10.1111/j.1749-6632.2001.tb03646.x

Jang, E. Y., Park, K. A., Lee, J. R., Yang, C. H., and Hwang, M. (2012). Protective Effect of Sauchinone on Methamphetamine-Induced Neurotoxicity in Mice. *J. Pharmacol. Sci.* 118, 531–536. doi:10.1254/jphs.11207sc

Jiang, L., Zhu, R., Bu, Q., Li, Y., Shao, X., Gu, H., et al. (2018). Brain Renin-Angiotensin System Blockade Attenuates Methamphetamine-Induced Hyperlocomotion and Neurotoxicity. *Neurotherapeutics* 15, 500–510. doi:10.1007/s13311-018-0613-8

Jin, G.-Z., and Sun, B.-C. (1995). Neuropharmacological Effects of (−)-Stepholidine and its Analogues on Brain Dopaminergic System. *Adv. Exp. Med. Biol.* 363, 27–28. doi:10.1007/978-1-4615-1857-0_5

Jin, G.-Z., Zhu, Z.-T., and Fu, Y. (2002). (−)-Stepholidine: a Potential Novel Antipsychotic Drug with Dual D1 Receptor Agonist and D2 Receptor Antagonist Actions. *Trends Pharmacol. Sci.* 23, 4–7. doi:10.1016/s0165-6147(00)01929-5

Kang, X., Hong, W., Xie, K., Tang, H., Tang, J., Luo, S., et al. (2019). Ginsenoside Rb1 Pretreatment Reverses Hippocampal Changes in BDNF/TrkB mRNA and Protein in Rats Subjected to Acute Immobilization Stress. *Drug Des. Devel. Ther.* 13, 2127–2134. doi:10.2147/dddt.s201135

Kanthasamy, K., Gordon, R., Jin, H., Anantharam, V., Ali, S., G. Kanthasamy, A., et al. (2011). Neuroprotective Effect of Resveratrol against Methamphetamine-Induced Dopaminergic Apoptotic Cell Death in a Cell Culture Model of Neurotoxicity. *Curr. Neuropharmacol.* 9, 49–53. doi:10.2174/157015911795017353

Kauer, J. A., and Malenka, R. C. (2007). Synaptic Plasticity and Addiction. *Nat. Rev. Neurosci.* 8, 844–858. doi:10.1038/nrn2234

Kennedy, D. O., and Scholey, A. B. (2003). Ginseng: Potential for the Enhancement of Cognitive Performance and Mood. *Pharmacol. Biochem. Behav.* 75, 687–700. doi:10.1016/s0091-3057(03)00126-6

Kim, D. H., Yang, C. H., and Hwang, M. (2013). Sauchinone Blocks Methamphetamine-Induced Hyperlocomotion and Place Preference in Mice. *Phytomedicine* 20, 1071–1075. doi:10.1016/j.phymed.2013.04.006

Kim, H.-C., Shin, E.-J., Jang, C.-G., Lee, M.-K., Eun, J.-S., Hong, J.-T., et al. (2005). Pharmacological Action of Panax Ginseng on the Behavioral Toxicities Induced by Psychotropic Agents. *Arch. Pharm. Res.* 28, 995–1001. doi:10.1007/bf02977391

Kim, H.-S., Hong, Y.-T., Oh, K.-W., Seong, Y.-H., Rheu, H.-M., Cho, D.-H., et al. (1998). Inhibition by Ginsenosides Rb1 and Rg1 of Methamphetamine-Induced Hyperactivity, Conditioned Place Preference and Postsynaptic Dopamine Receptor Supersensitivity in Mice. *Gen. Pharmacol. Vasc. Syst.* 30, 783–789. doi:10.1016/s0306-3623(97)00330-3

Kim, H.-S., Jang, C.-G., Park, W.-K., Oh, K.-W., Rheu, H.-M., Cho, D.-H., et al. (1996). Blockade by Ginseng Total Saponin of Methamphetamine-Induced Hyperactivity and Conditioned Place Preference in Mice. *Gen. Pharmacol. Vasc. Syst.* 27, 199–204. doi:10.1016/0306-3623(95)02023-3

Koriem, K. M., and Soliman, R. E. (2014). Chlorogenic and Caftaric Acids in Liver Toxicity and Oxidative Stress Induced by Methamphetamine. *J. Toxicol.* 2014, 583494. doi:10.1155/2014/583494

Krasnova, I. N., and Cadet, J. L. (2009). Methamphetamine Toxicity and Messengers of Death. *Brain Res. Rev.* 60, 379–407. doi:10.1016/j.brainresrev.2009.03.002

Krasnova, I. N., Justinova, Z., and Cadet, J. L. (2016). Methamphetamine Addiction: Involvement of CREB and Neuroinflammatory Signaling Pathways. *Psychopharmacology* 233, 1945–1962. doi:10.1007/s00213-016-4235-8

Lacaille-Dubois, M. A., and Wagner, H. (1996). A Review of the Biological and Pharmacological Activities of Saponins. *Phytomedicine* 2, 363–386. doi:10.1016/s0944-7113(96)80081-x

Lee, B., Sur, B., Cho, S.-G., Yeom, M., Shim, I., Lee, H., et al. (2016). Ginsenoside Rb1 Rescues Anxiety-like Responses in a Rat Model of Post-traumatic Stress Disorder. *J. Nat. Med.* 70, 133–144. doi:10.1007/s11418-015-0943-3

Li, J., Liu, W., Peng, Q., Jiang, M., Luo, C., Guo, Y., et al. (2014). Effect of Rhynchophylline on Conditioned Place Preference on Expression of NR2B in Methamphetamine-dependent Mice. *Biochem. Biophysical Res. Commun.* 452, 695–700. doi:10.1016/j.bbrc.2014.08.127

Li, Y., Yang, W., Zhu, Q., Yang, J., and Wang, Z. (2015). Protective Effects on Vascular Endothelial Cell in N'-nitro-L-arginine (L-NNA)-induced Hypertensive Rats from the Combination of Effective Components of Uncaria Rhynchophylla and Semen Raphani. *Biosci. Trends* 9, 237–244. doi:10.5582/bst.2015.01087

Liao, Y.-H., Lee, H.-J., Huang, W.-J., Fan, P.-C., and Chiou, L.-C. (2016). Hispidulin Alleviated Methamphetamine-Induced Hyperlocomotion by Acting at α6 Subunit-Containing GABAA Receptors in the Cerebellum. *Psychopharmacology* 233, 3187–3199. doi:10.1007/s00213-016-4365-z

Lin, M., Chandramani-Shivalingappa, P., Jin, H., Ghosh, A., Anantharam, V., Ali, S., et al. (2012). Methamphetamine-induced Neurotoxicity Linked to Ubiquitin-Proteasome System Dysfunction and Autophagy-Related Changes that Can Be Modulated by Protein Kinase C Delta in Dopaminergic Neuronal Cells. *Neuroscience* 210, 308–332. doi:10.1016/j.neuroscience.2012.03.004

Liu, X., Silverstein, P. S., Singh, V., Shah, A., Qureshi, N., and Kumar, A. (2012). Methamphetamine Increases LPS-Mediated Expression of IL-8, TNF-Alpha and IL-1 Beta in Human Macrophages through Common Signaling Pathways. *PLoS One* 7. doi:10.1371/journal.pone.0033822

Liu, Y. Y., Yeh, P. H., Wang, G. J., Huang, S. W., Chi, C. W., Ho, L. K., et al. (2006). Baicalein Reverses the Methamphetamine-Induced Striatal Dopaminergic Neurotoxicity in Mice. *J. Food Drug Anal.* 14, 317–322.

Lloyd, S. A., Corkill, B., Bruster, M. C., Roberts, R. L., and Shanks, R. A. (2017). Chronic Methamphetamine Exposure Significantly Decreases Microglia Activation in the Arcuate Nucleus. *J. Chem. Neuroanat.* 82, 5–11. doi:10.1016/j.jchemneu.2017.03.001

Loftis, J. M., Choi, D., Hoffman, W., and Huckans, M. S. (2011). Methamphetamine Causes Persistent Immune Dysregulation: A Cross-Species, Translational Report. *Neurotox Res.* 20, 59–68. doi:10.1007/s12640-010-9223-x

London, E. D. (2016). Impulsivity, Stimulant Abuse, and Dopamine Receptor Signaling. *Adv. Pharmacol.* 76, 67–84. doi:10.1016/bs.apha.2016.01.002

Long, J.-D., Liu, Y., Jiao, D.-L., Wang, Y.-J., Zan, G.-Y., Ju, Y.-Y., et al. (2017). The Neuroprotective Effect of Memantine on Methamphetamine-Induced Cognitive Deficits. *Behav. Brain Res.* 323, 133–140. doi:10.1016/j.bbr.2017.01.042

Lu, P., Mamiya, T., Lu, L., Mouri, A., Niwa, M., Kim, H.-C., et al. (2010). Silibinin Attenuates Cognitive Deficits and Decreases of Dopamine and Serotonin Induced by Repeated Methamphetamine Treatment. *Behav. Brain Res.* 207, 387–393. doi:10.1016/j.bbr.2009.10.024

Ma, B. M., Yue, K., Xing, J. Q., Gong, X. K., Ru, Q., Chen, L., et al. (2014). l-Stepholidine Blocks Methamphetamine-Induced Locomotor Sensitization in Mice. *Amr* 998-999, 156–159. doi:10.4028/www.scientific.net/amr.998-999.156

Mark, K. A., Quinton, M. S., Russek, S. J., and Yamamoto, B. K. (2007). Dynamic Changes in Vesicular Glutamate Transporter 1 Function and Expression Related to Methamphetamine-Induced Glutamate Release. *J. Neurosci.* 27, 6823–6831. doi:10.1523/jneurosci.0013-07.2007

Marshall, B. D. L., and Werb, D. (2010). Health Outcomes Associated with Methamphetamine Use Among Young People: a Systematic Review. *Addiction* 105, 991–1002. doi:10.1111/j.1360-0443.2010.02932.x

May, A. C., Aupperle, R. L., and Stewart, J. L. (2020). Dark Times: The Role of Negative Reinforcement in Methamphetamine Addiction. *Front. Psychiatry* 11, 114. doi:10.3389/fpsyt.2020.00114

McKetin, R., Gardner, J., Baker, A. L., Dawe, S., Ali, R., Voce, A., et al. (2016). Correlates of Transient versus Persistent Psychotic Symptoms Among Dependent Methamphetamine Users. *Psychiatry Res.* 238, 166–171. doi:10.1016/j.psychres.2016.02.038

Mi, G., Gao, Y., Yan, H., Jin, X., Ye, E., Liu, S., et al. (2016). l-Scoulerine Attenuates Behavioural Changes Induced by Methamphetamine in Zebrafish and Mice. *Behav. Brain Res.* 298, 97–104. doi:10.1016/j.bbr.2015.09.039

Miller, D. K., Oelrichs, C. E., Sage, A. S., Sun, G. Y., and Simonyi, A. (2013). Repeated Resveratrol Treatment Attenuates Methamphetamine-Induced Hyperactivity and [3H]dopamine Overflow in Rodents. *Neurosci. Lett.* 554, 53–58. doi:10.1016/j.neulet.2013.08.051

Miner, N. B., Phillips, T. J., and Janowsky, A. (2019). The Role of Biogenic Amine Transporters in Trace Amine-Associated Receptor 1 Regulation of Methamphetamine-Induced Neurotoxicity. *J. Pharmacol. Exp. Ther.* 371, 36–44. doi:10.1124/jpet.119.258970

Mitchell, J. P., and Carmody, R. J. (2018). NF-κB and the Transcriptional Control of Inflammation. *Int. Rev. Cell Mol. Biol.* 335, 41–84. doi:10.1016/bs.ircmb.2017.07.007

Mizoguchi, H., and Yamada, K. (2019). Methamphetamine Use Causes Cognitive Impairment and Altered Decision-Making. *Neurochem. Int.* 124, 106–113. doi:10.1016/j.neuint.2018.12.019

Moszczynska, A., and Callan, S. P. (2017). Molecular, Behavioral, and Physiological Consequences of Methamphetamine Neurotoxicity: Implications for Treatment. *J. Pharmacol. Exp. Ther.* 362, 474–488. doi:10.1124/jpet.116.238501

Nakama, H., Chang, L., Cloak, C., Jiang, C., Alicata, D., and Haning, W. (2008). Association between Psychiatric Symptoms and Craving in Methamphetamine Users. *Am. J. Addict.* 17, 441–446. doi:10.1080/10550490802268462

Nam, Y., Wie, M. B., Shin, E.-J., Nguyen, T.-T. L., Nah, S.-Y., Ko, S. K., et al. (2015). Ginsenoside Re Protects Methamphetamine-Induced Mitochondrial Burdens and Proapoptosis via Genetic Inhibition of Protein Kinase C δ in Human Neuroblastoma Dopaminergic SH-SY5Y Cell Lines. *J. Appl. Toxicol.* 35, 927–944. doi:10.1002/jat.3093

Natesan, S., Reckless, G. E., Barlow, K. B. L., Odontiadis, J., Nobrega, J. N., Baker, G. B., et al. (2008). The Antipsychotic Potential of L-Stepholidine-A Naturally Occurring Dopamine Receptor D1 Agonist and D2 Antagonist. *Psychopharmacology* 199, 275–289. doi:10.1007/s00213-008-1172-1

Nordahl, T. E., Salo, R., and Leamon, M. (2003). Neuropsychological Effects of Chronic Methamphetamine Use on Neurotransmitters and Cognition: A Review. *J. Neuropsychiatry Clin. Neurosci.* 15, 317–325. doi:10.1176/jnp.15.3.317

Overstreet, D. H., Fredericks, K., Knapp, D., Breese, G., and McMichael, J. (2010). Nerve Growth Factor (NGF) Has Novel Antidepressant-like Properties in Rats. *Pharmacol. Biochem. Behav.* 94, 553–560. doi:10.1016/j.pbb.2009.11.010

Padgett, C. L., Lalive, A. L., Tan, K. R., Terunuma, M., Munoz, M. B., Pangalos, M. N., et al. (2012). Methamphetamine-Evoked Depression of GABAB Receptor Signaling in GABA Neurons of the VTA. *Neuron* 73, 978–989. doi:10.1016/j.neuron.2011.12.031

Panenka, W. J., Procyshyn, R. M., Lecomte, T., MacEwan, G. W., Flynn, S. W., Honer, W. G., et al. (2013). Methamphetamine Use: A Comprehensive Review of Molecular, Preclinical and Clinical Findings. *Drug Alcohol Dependence* 129, 167–179. doi:10.1016/j.drugalcdep.2012.11.016

Park, J. H., Seo, Y. H., Jang, J. H., Jeong, C. H., Lee, S., and Park, B. (2017). Asiatic Acid Attenuates Methamphetamine-Induced Neuroinflammation and Neurotoxicity through Blocking of NF-Kappa B/STAT3/ERK and Mitochondria-Mediated Apoptosis Pathway. *J. Neuroinflamm* 14. doi:10.1186/s12974-017-1009-0

Parsegian, A., and See, R. E. (2014). Dysregulation of Dopamine and Glutamate Release in the Prefrontal Cortex and Nucleus Accumbens Following Methamphetamine Self-Administration and during Reinstatement in Rats. *Neuropsychopharmacol* 39, 811–822. doi:10.1038/npp.2013.231

Potula, R., Hawkins, B. J., Cenna, J. M., Fan, S. S., Dykstra, H., Ramirez, S. H., et al. (2010). Methamphetamine Causes Mitrochondrial Oxidative Damage in Human T Lymphocytes Leading to Functional Impairment. *J. Immunol.* 185, 2867–2876. doi:10.4049/jimmunol.0903691

Potvin, S., Pelletier, J., Grot, S., Hebert, C., Barr, A. M., and Lecomte, T. (2018). Cognitive Deficits in Individuals with Methamphetamine Use Disorder: A Meta-Analysis. *Addict. Behav.* 80, 154–160. doi:10.1016/j.addbeh.2018.01.021

Quello, S. B., Brady, K. T., and Sonne, S. C. (2005). Mood Disorders and Substance Use Disorder: A Complex Comorbidity. *Sci. Pract. Perspect.* 3, 13–21. doi:10.1151/spp053113

Reichel, C. M., Schwendt, M., McGinty, J. F., Olive, M. F., and See, R. E. (2011). Loss of Object Recognition Memory Produced by Extended Access to Methamphetamine Self-Administration Is Reversed by Positive Allosteric Modulation of Metabotropic Glutamate Receptor 5. *Neuropsychopharmacol* 36, 782–792. doi:10.1038/npp.2010.212

Rothman, R. B., and Baumann, M. H. (2003). Monoamine Transporters and Psychostimulant Drugs. *Eur. J. Pharmacol.* 479, 23–40. doi:10.1016/j.ejphar.2003.08.054

Rusyniak, D. E. (2013). Neurologic Manifestations of Chronic Methamphetamine Abuse. *Psychiatr. Clin. North. Am.* 36, 261–275. doi:10.1016/j.psc.2013.02.005

Sadek, J. R., Vigil, O., Grant, I., Heaton, R. K., and Group, H. (2007). The Impact of Neuropsychological Functioning and Depressed Mood on Functional Complaints in HIV-1 Infection and Methamphetamine Dependence. *J. Clin. Exp. Neuropsychol.* 29, 266–276. doi:10.1080/13803390600659384

Saeed, M., Ghadiri, A., Hadizadeh, F., Attaranzadeh, A., Alavi, M. S., and Etemad, L. (2018). Cinnamaldehyde Improves Methamphetamine-Induced Spatial Learning and Memory Deficits and Restores ERK Signaling in the Rat Prefrontal Cortex. *Iran J. Basic Med. Sci.* 21, 1316–1321. doi:10.22038/IJBMS.2018.35368.8427

Scearce-Levie, K., Viswanathan, S. S., and Hen, R. (1999). Locomotor Response to MDMA Is Attenuated in Knockout Mice Lacking the 5-HT1B Receptor. *Psychopharmacology (Berl)* 141, 154–161. doi:10.1007/s002130050819

Scott, J. C., Woods, S. P., Matt, G. E., Meyer, R. A., Heaton, R. K., Atkinson, J. H., et al. (2007). Neurocognitive Effects of Methamphetamine: a Critical Review and Meta-Analysis. *Neuropsychol. Rev.* 17, 275–297. doi:10.1007/s11065-007-9031-0

Shaerzadeh, F., Streit, W. J., Heysieattalab, S., and Khoshbouei, H. (2018). Methamphetamine Neurotoxicity, Microglia, and Neuroinflammation. *J. Neuroinflammation* 15, 341. doi:10.1186/s12974-018-1385-0

Shi, J. S., Yu, J. X., Chen, X. P., and Xu, R. X. (2003). Pharmacological Actions of Uncaria Alkaloids, Rhynchophylline and Isorhynchophylline. *Acta Pharmacologica Sinica* 24, 97–101.

Shin, E. J., Duong, C. X., Nguyen, X. T., Li, Z., Bing, G., Bach, J. H., et al. (2012). Role of Oxidative Stress in Methamphetamine-Induced Dopaminergic Toxicity Mediated by Protein Kinase Cdelta. *Behav. Brain Res.* 232, 98–113. doi:10.1016/j.bbr.2012.04.001

Shin, E. J., Shin, S. W., Nguyen, T. T. L., Park, D. H., Wie, M. B., Jang, C. G., et al. (2014). Ginsenoside Re Rescues Methamphetamine-Induced Oxidative Damage, Mitochondrial Dysfunction, Microglial Activation, and Dopaminergic Degeneration by Inhibiting the Protein Kinase C Delta Gene. *Mol. Neurobiol.* 49, 1400–1421. doi:10.1007/s12035-013-8617-1

Siefried, K. J., Acheson, L. S., Lintzeris, N., and Ezard, N. (2020). Pharmacological Treatment of Methamphetamine/Amphetamine Dependence: A Systematic Review. *CNS Drugs* 34, 337–365. doi:10.1007/s40263-020-00711-x

Sora, I., Li, B., Fumushima, S., Fukui, A., Arime, Y., Kasahara, Y., et al. (2009). Monoamine Transporter as a Target Molecule for Psychostimulants. *Int. Rev. Neurobiol.* 85, 29–33. doi:10.1016/s0074-7742(09)85003-4

Sowndhararajan, K., Deepa, P., Kim, M., Park, S. J., and Kim, S. (2017). Baicalein as a Potent Neuroprotective Agent: A Review. *Biomed. Pharmacother.* 95, 1021–1032. doi:10.1016/j.biopha.2017.08.135

Stephans, S. E., Whittingham, T. S., Douglas, A. J., Lust, W. D., and Yamamoto, B. K. (1998). Substrates of Energy Metabolism Attenuate Methamphetamine-Induced Neurotoxicity in Striatum. *J. Neurochem.* 71, 613–621. doi:10.1046/j.1471-4159.1998.71020613.x

Su, H., Sun, T., Wang, X., Du, Y., Zhao, N., Zhu, J., et al. (2020). Levo-tetrahydropalmatine Attenuates Methamphetamine Reward Behavior and the Accompanying Activation of ERK Phosphorylation in Mice. *Neurosci. Lett.* 714, 134416. doi:10.1016/j.neulet.2019.134416

Su, H. L., Zhu, J., Chen, Y. J., Zhao, N., Han, W., Dang, Y. H., et al. (2013). Roles of Levo-Tetrahydropalmatine in Modulating Methamphetamine Reward Behavior. *Physiol. Behav.* 118, 195–200. doi:10.1016/j.physbeh.2013.05.034

Sukma, M., Chaichantipyuth, C., Murakami, Y., Tohda, M., Matsumoto, K., and Watanabe, H. (2002). CNS Inhibitory Effects of Barakol, a Constituent of Cassia Siamia Lamk. *J. Ethnopharmacol* 83, 87–94. doi:10.1016/s0378-8741(02)00206-4

Thomas, D. M., Angoa Perez, M., Francescutti-Verbeem, D. M., Shah, M. M., and Kuhn, D. M. (2010). The Role of Endogenous Serotonin in Methamphetamine-Induced Neurotoxicity to Dopamine Nerve Endings of the Striatum. *J. Neurochem.* 115, 595–605. doi:10.1111/j.1471-4159.2010.06950.x

Thompson, J. L., Rosell, D. R., Slifstein, M., Girgis, R. R., Xu, X. Y., Ehrlich, Y., et al. (2014). Prefrontal Dopamine D1 Receptors and Working Memory in Schizotypal Personality Disorder: A PET Study with [C-11]NNC112. *Psychopharmacology* 231, 4231–4240. doi:10.1007/s00213-014-3566-6

Tokuyama, S., and Takahashi, M. (2001). [Pharmacological and Physiological Effects of Ginseng on Actions Induced by Opioids and Psychostimulants]. *Nihon Yakurigaku Zasshi* 117, 195–201. doi:10.1254/fpj.117.195

Tokuyama, S., Takahashi, M., and Kaneto, H. (1996). The Effect of Ginseng Extract on Locomotor Sensitization and Conditioned Place Preference Induced by Methamphetamine and Cocaine in Mice. *Pharmacol. Biochem. Behav.* 54, 671–676. doi:10.1016/0091-3057(96)00021-4

Trudeau, L. E., Hnasko, T. S., Wallen-Mackenzie, A., Morales, M., Rayport, S., and Sulzer, D. (2014). The Multilingual Nature of Dopamine Neurons. *Prog. Brain Res.* 211, 141–164. doi:10.1016/b978-0-444-63425-2.00006-4

United Nations (2020). *World Drug Report 2020*. Vienna, Austria: United Nations publication.

Voigt, R. M., Herrold, A. A., Riddle, J. L., and Napier, T. C. (2011). Administration of GABA(B) Receptor Positive Allosteric Modulators Inhibit the Expression of Previously Established Methamphetamine-Induced Conditioned Place Preference. *Behav. Brain Res.* 216, 419–423. doi:10.1016/j.bbr.2010.08.034

Volz, T. J., Hanson, G. R., and Fleckenstein, A. E. (2007). The Role of the Plasmalemmal Dopamine and Vesicular Monoamine Transporters in Methamphetamine-Induced Dopaminergic Deficits. *J. Neurochem.* 101, 883–888. doi:10.1111/j.1471-4159.2006.04419.x

Wagner, D., Becker, B., Koester, P., Gouzoulis-Mayfrank, E., and Daumann, J. (2013). A Prospective Study of Learning, Memory, and Executive Function in New MDMA Users. *Addiction* 108, 136–145. doi:10.1111/j.1360-0443.2012.03977.x

Wan, F., Zang, S., Yu, G., Xiao, H., Wang, J., and Tang, J. (2017). Ginkgolide B Suppresses Methamphetamine-Induced Microglial Activation through TLR4-NF-kappaB Signaling Pathway in BV2 Cells. *Neurochem. Res.* 42, 2881–2891. doi:10.1007/s11064-017-2309-6

Wang, M., Datta, D., Enwright, J., Galvin, V., Yang, S. T., Paspalas, C., et al. (2019). A Novel Dopamine D1 Receptor Agonist Excites Delay-dependent Working Memory-Related Neuronal Firing in Primate Dorsolateral Prefrontal Cortex. *Neuropharmacology* 150, 46–58. doi:10.1016/j.neuropharm.2019.03.001

Weinshenker, D., and Schroeder, J. P. (2007). There and Back Again: A Tale of Norepinephrine and Drug Addiction. *Neuropsychopharmacol* 32, 1433–1451. doi:10.1038/sj.npp.1301263

Wen, D., An, M. L., Gou, H. Y., Liu, X., Liu, L., Ma, C. L., et al. (2016). Cholecystokinin-8 Inhibits Methamphetamine-Induced Neurotoxicity via an Anti-oxidative Stress Pathway. *Neurotoxicology* 57, 31–38. doi:10.1016/j.neuro.2016.08.008

Wong, Y. K., Chou, M. K., Shen, Y. C., Wang, Y. H., Yen, J. C., Chen, C. F., et al. (2014). Preventive Effect of Baicalein on Methamphetamine-Induced Amnesia in the Passive Avoidance Test in Mice. *Pharmacology* 93, 278–285. doi:10.1159/000365008

Wu, C. F., Liu, Y. L., Song, M., Liu, W., Wang, J. H., Li, X., et al. (2003). Protective Effects of Pseudoginsenoside-F11 on Methamphetamine-Induced Neurotoxicity in Mice. *Pharmacol. Biochem. Behav.* 76, 103–109. doi:10.1016/s0091-3057(03)00215-6

Wu, P. H., Shen, Y. C., Wang, Y. H., Chi, C. W., and Yen, J. C. (2006). Baicalein Attenuates Methamphetamine-Induced Loss of Dopamine Transporter in Mouse Striatum. *Toxicology* 226, 238–245. doi:10.1016/j.tox.2006.06.015

Xu, W., Zhu, J. P., and Angulo, J. A. (2005). Induction of Striatal Pre- and Postsynaptic Damage by Methamphetamine Requires the Dopamine Receptors. *Synapse* 58, 110–121. doi:10.1002/syn.20185

Yun, J. (2014a). L-tetrahydropalmatine Inhibits Methamphetamine-Induced Locomotor Activity via Regulation of 5-HT Neuronal Activity and Dopamine D3 Receptor Expression. *Phytomedicine* 21, 1287–1291. doi:10.1016/j.phymed.2014.07.003

Yun, J. (2014b). Limonene Inhibits Methamphetamine-Induced Locomotor Activity via Regulation of 5-HT Neuronal Function and Dopamine Release. *Phytomedicine* 21, 883–887. doi:10.1016/j.phymed.2013.12.004

Zhou, M., Gong, X. K., Ru, Q., Xiong, Q., Chen, L., Si, Y. R., et al. (2019). The Neuroprotective Effect of L-Stepholidine on Methamphetamine-Induced Memory Deficits in Mice. *Neurotoxicity Res.* 36, 376–386. doi:10.1007/s12640-019-00069-z

Zorick, T., Nestor, L., Miotto, K., Sugar, C., Hellemann, G., Scanlon, G., et al. (2010). Withdrawal Symptoms in Abstinent Methamphetamine-dependent Subjects. *Addiction* 105, 1809–1818. doi:10.1111/j.1360-0443.2010.03066.x

Conflict of Interest: The authors declare that the research was conducted in the absence of any commercial or financial relationships that could be construed as a potential conflict of interest.

frontiers in Pharmacology

ORIGINAL RESEARCH
published: 30 June 2021
doi: 10.3389/fphar.2021.705813

High-Frequency Deep Brain Stimulation of the Substantia Nigra Pars Reticulata Facilitates Extinction and Prevents Reinstatement of Methamphetamine-Induced Conditioned Place Preference

Libo Zhang[1,2†], Shiqiu Meng[2†], Wenjun Chen[2†], Yun Chen[2], Enze Huang[2], Guipeng Zhang[2], Yisen Liang[2], Zengbo Ding[2], Yanxue Xue[2], Yun Chen[1], Jie Shi[1,2]* and Yu Shi[1]**

[1]Shenzhen Public Service Platform for Clinical Application of Medical Imaging, Shenzhen Key Laboratory for Drug Addiction and Medication Safety, Department of Ultrasound, Peking University Shenzhen Hospital, Shenzhen, China, [2]National Institute on Drug Dependence and Beijing Key Laboratory of Drug Dependence, Peking University, Beijing, China

Persistent and stable drug memories lead to a high rate of relapse among addicts. A number of studies have found that intervention in addiction-related memories can effectively prevent relapse. Deep brain stimulation (DBS) exhibits distinct therapeutic effects and advantages in the treatment of neurological and psychiatric disorders. In addition, recent studies have also found that the substantia nigra pars reticulata (SNr) could serve as a promising target in the treatment of addiction. Therefore, the present study aimed to investigate the effect of DBS of the SNr on the reinstatement of drug-seeking behaviors. Electrodes were bilaterally implanted into the SNr of rats before training of methamphetamine-induced conditioned place preference (CPP). High-frequency (HF) or low-frequency (LF) DBS was then applied to the SNr during the drug-free extinction sessions. We found that HF DBS, during the extinction sessions, facilitated extinction of methamphetamine-induced CPP and prevented drug-primed reinstatement, while LF DBS impaired the extinction. Both HF and LF DBS did not affect locomotor activity or induce anxiety-like behaviors of rats. Finally, HF DBS had no effect on the formation of methamphetamine-induced CPP. In conclusion, our results suggest that HF DBS of the SNr could promote extinction and prevent reinstatement of methamphetamine-induced CPP, and the SNr may serve as a potential therapeutic target in the treatment of drug addiction.

Keywords: deep brain stimulation, substantia nigra pars reticulata, methamphetamine, extinction, relapse

OPEN ACCESS

Edited by:
Di Wen,
Hebei Medical University, China

Reviewed by:
Xiangdong Tang,
Sichuan University, China
Ti-Fei Yuan,
Shanghai Jiao Tong University, China
Hongxian Shen,
Central South University, China

***Correspondence:**
Yu Shi
shiyu@pkuszh.com
Jie Shi
shijie@bjmu.edu.cn
Yun Chen
chenyun@pkuszh.com;

†These authors have contributed equally to this work

Specialty section:
This article was submitted to Neuropharmacology, a section of the journal Frontiers in Pharmacology

Received: *06 May 2021*
Accepted: *10 June 2021*
Published: *30 June 2021*

Citation:
Zhang L, Meng S, Chen W, Chen Y, Huang E, Zhang G, Liang Y, Ding Z, Xue Y, Chen Y, Shi J and Shi Y (2021) High-Frequency Deep Brain Stimulation of the Substantia Nigra Pars Reticulata Facilitates Extinction and Prevents Reinstatement of Methamphetamine-Induced Conditioned Place Preference. Front. Pharmacol. 12:705813. doi: 10.3389/fphar.2021.705813

INTRODUCTION

Persistent and stable drug memories are considered a major contributor to the intense craving and relapse in drug addiction, which are difficult to eliminate (Hyman and Malenka, 2001; Kauer and Malenka, 2007). Even after extinction, when being re-exposed to drug-associated cues, the original drug memories would be reactivated and cause drug-seeking behaviors, leading to a high relapse rate

among addicts (Conklin and Tiffany, 2002; Milton and Everitt, 2012b; Chen et al., 2019b). It has been found that extinction combined with other interventions, such as the retrieval–extinction procedure, can facilitate elimination of drug memories and prevent relapse (He et al., 2011; Xue et al., 2012; Xue et al., 2014; Luo et al., 2015; Liu et al., 2019), which provides a new avenue for the treatment of addiction (Milton and Everitt, 2012a).

Deep brain stimulation (DBS) is an FDA-approved therapy for essential tremor (Schuurman et al., 2000; Opri et al., 2020), Parkinson's disease (Rosin et al., 2011; Okun, 2012; Katz et al., 2015), idiopathic dystonia (Kleiner-Fisman et al., 2007; Elkaim et al., 2019), and severe obsessive-compulsive disorder (Figee et al., 2013; Wu et al., 2021) and exhibits potential therapeutic effects in the treatment of some other neurological and psychiatric disorders, such as depression (Kennedy et al., 2011; Holtzheimer et al., 2017; Crowell et al., 2019), anorexia nervosa (Lipsman et al., 2013; Lipsman et al., 2017), and addiction (Luigjes et al., 2012; Creed et al., 2015). In addition, unlike pharmacotherapy, DBS has the advantages of adjusting stimulus parameters and starting and stopping stimulation at any time based on the condition of patients, and it also produces minimal side effects when used in clinical application (Kringelbach et al., 2007).

Preclinical and clinical studies have indicated that DBS may be effective in the treatment of cocaine (Creed et al., 2015), morphine (Martinez-Rivera et al., 2016), and heroin (Chen et al., 2019a) addiction. For example, studies have proven that high-frequency (HF) DBS of the nucleus accumbens suppresses seeking behavior and reinstatement of cocaine and methamphetamine (Vassoler et al., 2008; Muller et al., 2013; Vassoler et al., 2013; Batra et al., 2017). However, research has also found that HF DBS of the nucleus accumbens could decrease natural reward-seeking behaviors (Guercio et al., 2015). Meanwhile, it has also been found that DBS can exert distinct effects *via* different stimulus parameters (Schor and Nelson, 2019). Thus, proper targets and parameters of DBS in the treatment of addiction are yet to be identified (Wang et al., 2018).

Substantia nigra pars reticulata (SNr) is a part of the basal ganglia which is involved in various brain functions such as sleep and motivation (Liu et al., 2020; Lai et al., 2021) and diseases including PD (Du et al., 2018; Willard et al., 2019; Sitzia et al., 2020) and seizures (Wicker et al., 2019; Chen et al., 2020). The most dominant neuronal cells in the SNr are GABAergic neurons, and previous studies have found that the SNr serves as a superb DBS target for the treatment of PD-related symptoms (Chastan et al., 2009; Valldeoriola et al., 2019). Evidence also suggests that PD and addiction share certain common mechanisms which involve the striatum (Villalba and Smith, 2013), the major input areas of the SNr (Van Den Berge et al., 2017), making it possible to apply DBS of the SNr to the treatment of addiction. A recent study has also found that GABA neurons in the SNr play important roles in opioid reward and relapse, and activation of SNr GABA neurons decreased heroin-primed reinstatement (Galaj et al., 2020). Thus, the SNr has great potential to be an effective target of addiction treatment.

Here, we investigated the impacts of HF and low-frequency (LF) DBS of the SNr on extinction of methamphetamine-induced conditioned place preference (CPP) and methamphetamine-primed reinstatement in rats. We also examined the effects on locomotor ability, anxiety-like behaviors, and formation of methamphetamine-induced place preference.

MATERIALS AND METHODS

Animals

Male Sprague-Dawley rats (260–280 g), purchased from Beijing Vital River Laboratory Animal Technology Co., Ltd., were housed five per cage prior to the implantation of electrodes. All rats were given access to freely available food and water with a reverse 12/12 h light/dark cycle. All procedures were performed in accordance with the National Institutes of Health's Guide for the Care and Use of Laboratory Animals and were approved by the Biomedical Ethics Committee for Animal Use and Protection of Peking University.

Implanting the Stimulating Electrodes

After a period of adaptation, the rats were anesthetized with isoflurane and placed in a stereotaxic apparatus. Stainless steel bipolar electrodes were bilaterally implanted into the SNr at the following coordinates: anterior/posterior, −5.3 mm; medial/lateral, 2.3 mm; and dorsal/ventral, −8.2 mm. Electrodes were secured to the skull with anchoring screws and dental acrylic cement. The rats were housed individually after the surgery and allowed 3–5 days of recovery before behavioral experiments.

Conditioned Place Preference

The CPP procedure in a three-chamber apparatus was performed using an unbiased, counterbalanced protocol as described previously (Liang et al., 2017).

Baseline preference was assessed by placing the rats in the center chamber of the CPP apparatus and allowing them to explore all three chambers freely for 15 min. Rats that showed a strong unconditioned preference for either of the side chambers (i.e., >540 s) were excluded from the experiments. Then the rats were trained for eight consecutive days with alternating injections of methamphetamine (1 mg/kg, i. p.) or saline (1 ml/kg, i. p.) and were confined to the conditioning chambers for 45 min after each injection before being returned to their home cages. The test for the expression of methamphetamine-induced CPP was identical to the initial baseline preference assessment and was performed on the following day after training. After the establishment of CPP, all rats were divided into sham and HF (or LF) DBS groups in an unbiased random manner.

DBS was continuously delivered for 60 min before the extinction sessions. This duration of stimulation was selected based on previous studies showing that 60 min of DBS is sufficient to produce behavioral changes in rats (Martinez-Rivera et al., 2016; Fakhrieh-Asl et al., 2020). A total of six or nine extinction sessions were performed for HF DBS or LF DBS, respectively, until the rats showed no obvious place preference for either chamber. Similar to the expression test, the rats were allowed to move freely between compartments during each extinction session. On the last day, all of the rats received an injection of

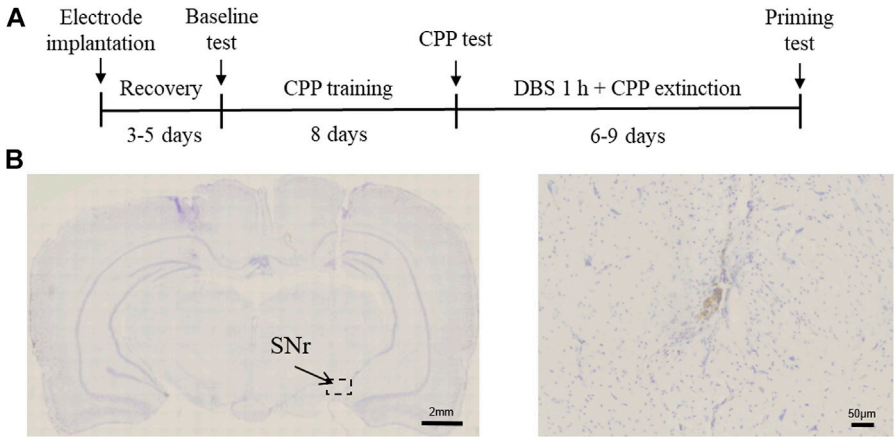

FIGURE 1 | Experimental design and electrode implantation site. **(A)** Experimental timeline. **(B)** Nissl's staining of the SNr DBS site.

methamphetamine (1 mg/kg) without DBS and were tested immediately for CPP. The time spent (in seconds) in the methamphetamine-paired chamber minus the time spent in the saline-paired chamber was calculated as the index of the CPP score.

In the experiment of investigating the effect of HF DBS on CPP formation, rats were divided into sham or HF DBS groups based on the baseline preference before training. During the methamphetamine-pairing trials in training, the rats received 60-min sham or HF DBS in their home cages and were then given an injection of methamphetamine (1 mg/kg) and placed into the drug-paired chamber for 45 min. During the saline-pairing trials, the rats received an injection of saline and were placed into the saline-paired chamber for 45 min. The procedure for the test of expression of methamphetamine-induced CPP was identical to that described above.

Deep Brain Stimulation

Monophasic square pulses were delivered to the SNr using a current-based stimulator through a cable connected to the implanted electrodes. The stimulation parameters were HF (130 Hz) or LF (20 Hz) pulse frequencies, 150 μA pulse amplitude, and 100 μs pulse width (Martinez-Rivera et al., 2016). In sham DBS experiments, the rats were connected to the external cable but did not receive electrical stimulation.

Elevated Plus Maze

The elevated plus maze was used to determine anxiety-like behavior as previously described (Xue et al., 2015; Fang et al., 2018). The elevated plus maze consisted of four arms set in a plus-shaped configuration. The apparatus was elevated 70 cm above the floor. The two open arms were 50 cm long and 10 cm wide. The two closed arms were 50 cm long and 10 cm wide with 40-cm-high walls. All rats received a 60-min DBS (sham, HF, or LF) in their home cages, and then each rat was placed in the central zone of the elevated plus maze with its head facing an open arm. The rat was allowed to freely explore the elevated plus maze for 5 min under dim illumination. The number of entries into and time (in seconds) spent on the open arms were recorded.

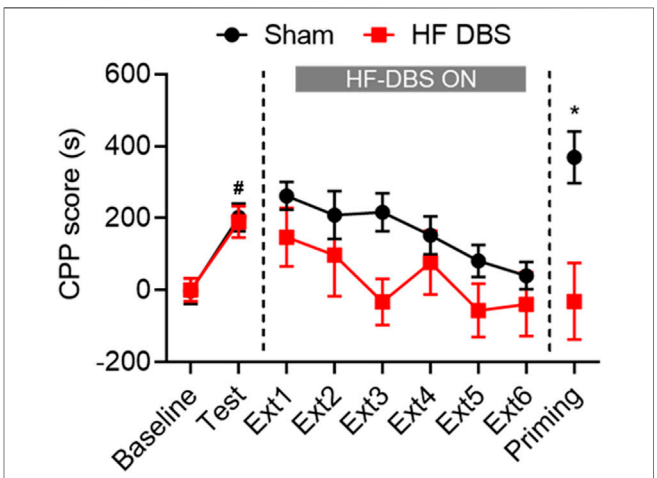

FIGURE 2 | HF DBS of the SNr facilitated extinction and prevented the reinstatement of methamphetamine-induced CPP. Methamphetamine (1 mg/kg) induced a significant preference for the drug-paired side in both groups, and sham DBS or HF DBS (130 Hz, 150 μA, 100 μs) was then applied to the SNr during each of the drug-free extinction sessions (15 min). HF DBS caused a significant decrease in CPP scores compared with the sham DBS. After full extinction, a priming injection of methamphetamine (1 mg/kg) was given to the sham DBS and HF DBS groups, and only the sham DBS group, but not the HF DBS group, showed reinstatement of drug-seeking behavior. Data are shown as mean ± SEM. $^{\#}p < 0.05$ compared with baseline (sham and HF DBS), $^{*}p < 0.05$ compared with HF DBS. Sham DBS: $n = 8$; HF DBS: $n = 8$.

Open Field Test

The open field test apparatus consisted of a square arena that was 75 cm long, 75 cm wide, and 40 cm high, which was divided into 25 equal squares on the floor of the arena. All rats received a 60-min DBS (sham, HF, or LF) in their home cages, and then each individual rat was placed in the center of the arena and allowed to freely explore for 5 min. The number of crossings (i.e., entering the adjacent square with all four paws) was considered as the index of locomotor activity.

Histology

The animals were anesthetized and transcardially perfused with 0.01 M phosphate buffer solution, followed by 4% paraformaldehyde in 0.2 M phosphate buffer. The brain was extracted, post-fixed overnight at 4°C, and cryoprotected in 30% sucrose in 0.2 M phosphate buffer. The cannula placements were confirmed in 25-μm-thick sections using Nissl staining by light microscopy. Rats with misplaced cannulae were excluded from the statistical analysis.

Statistical Analysis

The paired *t* test was used to compare the baseline and the test of the CPP scores from the methamphetamine conditioning phase. Two-way repeated measures ANOVA was applied to analyze the differences in CPP scores of extinction sessions between the sham and HF/LF DBS groups. The unpaired *t* test was used to compare the differences in CPP scores of methamphetamine conditioning or drug-primed reinstatement between the sham DBS and DBS groups. One-way ANOVA was performed to measure the locomotor activity and anxiety-like behaviors of rats between the sham, LF, and HF DBS groups. Data are shown as mean ± SEM, and the statistical analyses and plotting of the graphs were performed using GraphPad Prism 8 (GraphPad Software, California, United States).

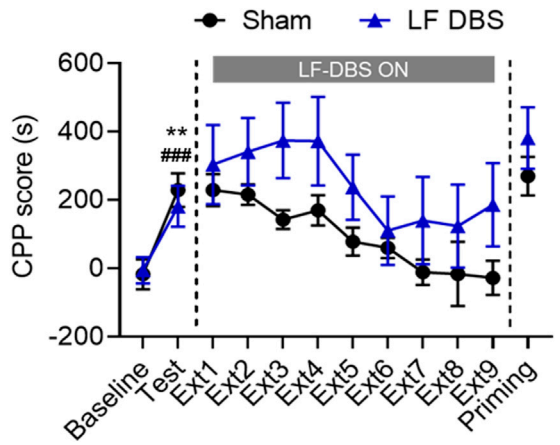

FIGURE 3 | LF DBS of the SNr impaired the methamphetamine-induced CPP extinction and had no effect on methamphetamine-primed reinstatement. After methamphetamine conditioning (1 mg/kg), sham DBS or LF DBS (20 Hz, 150 μA, 100 μs) was delivered into the SNr during each of the drug-free extinction sessions (15 min). LF DBS significantly impaired the extinction sessions compared with the sham DBS. A priming injection of methamphetamine (1 mg/kg) was given to the sham DBS and LF DBS groups, and both groups of rats exhibited significant drug-seeking behaviors. Data are shown as mean ± SEM. $^{**}p < 0.01$ (sham DBS) and $^{\#\#\#}p < 0.0001$ compared with baseline (LF DBS). Sham DBS: $n = 7$; LF DBS: $n = 6$.

RESULTS

High-Frequency Deep Brain Stimulation of the Substantia Nigra Pars Reticulata Facilitated Extinction and Prevented the Reinstatement of Methamphetamine-Induced Conditioned Place Preference

To examine the effect of SNr DBS on extinction and drug-primed reinstatement of methamphetamine-induced CPP, rats were first trained for 8 days with regard to conditioned place preference. After the rats acquired a preference for methamphetamine, DBS was delivered to the SNr for 60 min before each extinction test, and at the end of extinction, an injection of methamphetamine was given to evaluate the reinstatement of drug-seeking behavior (**Figures 1A,B**). Rats with misplacement of electrodes were excluded from the study.

As shown in **Figure 2**, two groups of rats exhibited significant preference for the drug-paired side after methamphetamine conditioning (paired *t* test: Sham DBS: $t_7 = 3.308$, $p < 0.05$; HF DBS: $t_7 = 2.868$, $p < 0.05$). Sham or HF DBS was then delivered to the SNr during the drug-free extinction phase, and a two-way repeated measures ANOVA showed overall significant differences in the CPP scores across DBS ($F_{(1,\ 14)} = 5.122$, $p < 0.05$) and extinction sessions ($F_{(3.112,\ 43.57)} = 3.089$, $p < 0.05$) but not DBS × extinction session interactions ($F_{(5,\ 70)} = 0.4994$, $p = 0.7756$), which suggests that HF DBS of the SNr facilitated the extinction of methamphetamine-seeking behavior.

Following the last extinction test, all rats received a priming injection of methamphetamine and were tested for reinstatement of drug-seeking behavior. Rats in the HF DBS group showed no significant preference for the methamphetamine-paired side, while those in the sham DBS group exhibited a dramatic increase in CPP scores compared with the HF DBS group (unpaired *t* test, $t_{14} = 2.178$, $p < 0.05$). Therefore, HF DBS of the SNr blocked the methamphetamine-primed reinstatement of the extinguished drug-seeking behavior.

Low-Frequency Deep Brain Stimulation of the Substantia Nigra Pars Reticulata Impaired the Extinction of Methamphetamine-Induced Conditioned Place Preference and Had No Effect on Methamphetamine-Primed Reinstatement

Since studies have proven that LF DBS generally has different effects compared with HF DBS on the excitability of the stimulated brain region (Kringelbach et al., 2007; Wang et al., 2018), we examined the effects of LF DBS on the extinction of methamphetamine-induced CPP. As shown in **Figure 3**, after conditioning, the rats showed an overall preference for the drug-paired side (paired *t* test: Sham DBS: $t_6 = 4.003$, $p < 0.01$; LF DBS: $t_5 = 11.17$, $p < 0.0001$). The two groups of rats both underwent extinction until the methamphetamine-seeking behavior of the sham DBS rats was fully extinguished. A two-way repeated measures ANOVA revealed that rats that received LF DBS of the SNr before the extinction sessions exhibited overall significantly higher CPP scores during extinction across DBS ($F_{(1,\ 11)} = 6.473$, $p < 0.05$) and extinction sessions ($F_{(3.737,\ 41.11)} = 5.041$, $p < 0.01$) but not DBS × extinction session interactions ($F_{(8,\ 88)} = 0.5160$, $p = 0.8415$) compared with the sham DBS group. Then all rats received an injection of methamphetamine for the drug-priming test, and the unpaired *t* test revealed no significant difference in the CPP scores between the sham DBS

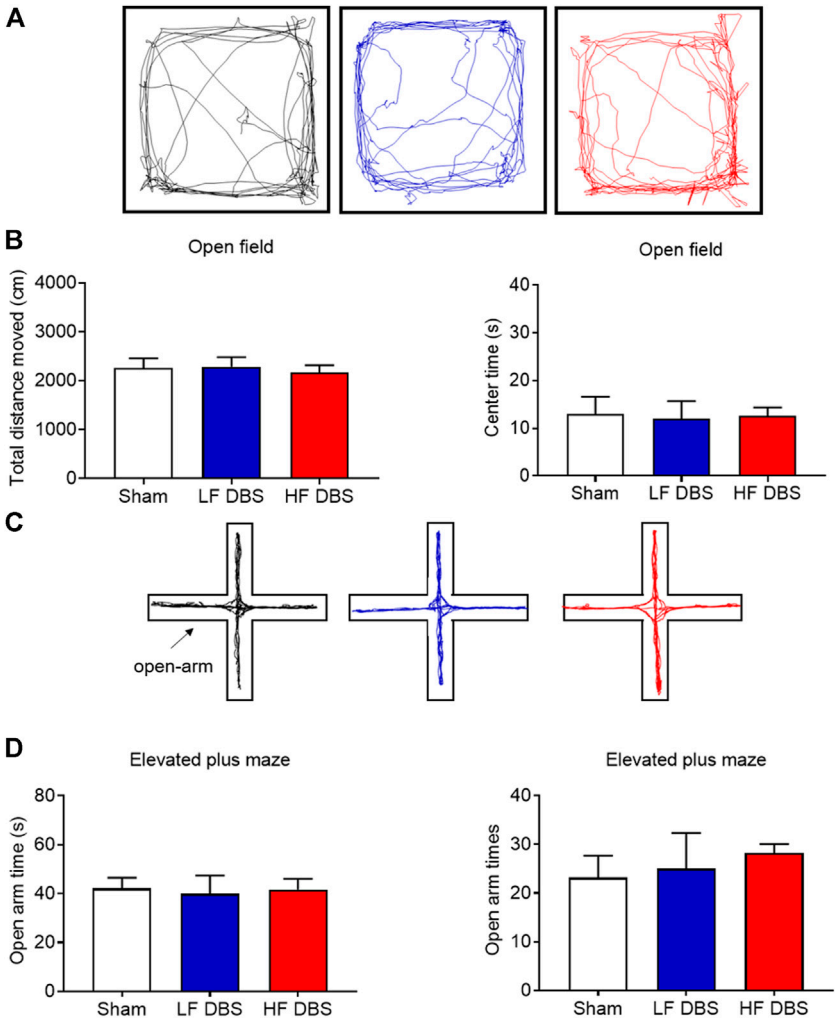

FIGURE 4 | DBS of the SNr did not affect locomotor activity and anxiety-like behavior. **(A)** Representative activity traces of sham, LF, and HF DBS groups in the open field test. **(B)** Total distance traveled and time in the central zone in the open field test. **(C)** Representative activity traces of sham, LF, and HF DBS rats in the elevated plus maze test. **(D)** Time and entries in the open arms of the elevated plus maze test. Data are shown as mean ± SEM. n = 6 for all groups.

and LF DBS groups (t_{11} = 1.374, p = 0.1969). Thus, LF DBS of the SNr impaired the extinction of methamphetamine-induced CPP and produced no effect on reinstatement.

Deep Brain Stimulation of the Substantia Nigra Pars Reticulata Did Not Affect Locomotor Activity and Anxiety-Like Behavior

To rule out the possibility that SNr DBS may have adverse effects on locomotor activity and induce anxiety-like behavior, we used the open field test and the elevated plus maze test to measure these behaviors. HF DBS or LF DBS was delivered into the SNr for 60 min before the tests. One-way ANOVA showed that there was no significant difference in the distance traveled ($F_{(2, 15)}$ = 0.1107, p = 0.8959) and the time in the central zone ($F_{(2, 15)}$ = 0.02149, p = 0.9788) between the HF DBS, LF DBS, and sham DBS groups in the open field test (**Figures 4A,B**). Also, no significant difference was found in the open-arm time ($F_{(2, 15)}$ = 0.04105, p = 0.9599) and entries ($F_{(2, 15)}$ = 0.2453, p = 0.7856) between the HF DBS, LF DBS, and sham DBS groups in the elevated plus maze test (**Figures 4C,D**). Therefore, SNr DBS had no effect on locomotor activity and did not induce anxiety-like behavior in rats.

High-Frequency Deep Brain Stimulation of the Substantia Nigra Pars Reticulata Had No Effect on the Formation of Methamphetamine-Induced Place Preference

Finally, we investigated the effect of HF DBS of the SNr on the rewarding effects of methamphetamine. As shown in **Figure 5**, rats received HF DBS of the SNr before the CPP training, and the

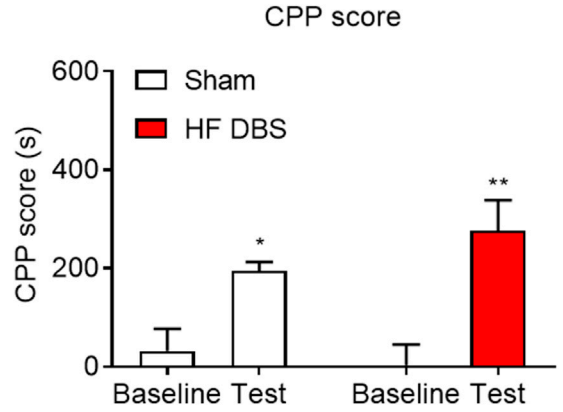

FIGURE 5 | HF DBS of the SNr had no effect on the formation of methamphetamine-induced place preference. Both sham DBS and HF DBS groups exhibited a significant preference for the drug-paired side after the methamphetamine conditioning (1 mg/kg), while no difference was found in the CPP scores between the two groups. Data are shown as mean ± SEM. *$p < 0.05$ (sham DBS) and **$p < 0.01$ (HF DBS) compared with baseline. Sham DBS: $n = 8$; HF DBS: $n = 8$.

paired t test showed that both sham ($t_7 = 3.494$, $p < 0.05$) and HF ($t_7 = 4.859$, $p < 0.01$) DBS groups formed a significant preference for the drug-paired side, and there was no significant difference in the CPP scores between the two groups (unpaired t test, $t_{14} = 1.272$, $p = 0.2241$), indicating that HF DBS of the SNr in the conditioning phase had no effect on the rewarding effects of methamphetamine.

DISCUSSION

Our data demonstrated that HF and LF DBS of the SNr produced distinct effects on the extinction of methamphetamine-induced CPP. HF DBS of the SNr facilitated the extinction of methamphetamine-induced CPP and blocked drug-primed reinstatement, while LF DBS suppressed extinction. It is worth noting that HF DBS of the SNr did not affect the reinforcing properties of methamphetamine. These findings suggest that the SNr could be a potential DBS target for the treatment of addiction, although proper stimulation parameters and phases need to be chosen.

The SNr is the ventral part of the substantia nigra. Recent evidence has implied that abnormalities of the substantia nigra are involved in the pathophysiology of addiction (Sharpe et al., 2014; Cassidy et al., 2020), and acute methamphetamine administration could induce neuronal death in the substantia nigra (Sabrini et al., 2020). The substantia nigra also plays a crucial role in the relapse to drug seeking (Hyman et al., 2006; Madsen et al., 2012; Pelloux et al., 2018). However, there is still a lack of sufficient evidence on the exact role of the SNr in addiction, and whether intervention in the SNr can be applied in addiction treatment needs further verification.

On the other hand, the SNr is the convergence region of the striatal output pathways, which comprises striatonigral neurons in the direct pathway and striatopallidal neurons in the indirect pathway (Deniau et al., 2007; Phillips et al., 2020). Evidence suggests that the D1-expressing medium spiny neurons of the direct pathway in the striatum project to the SNr GABA neurons and exhibit D1-mediated presynaptic facilitation (Chuhma et al., 2011). Numerous studies have confirmed that the direct pathway is crucial to drug-seeking behaviors (Cui et al., 2014; Volkow and Morales, 2015; Yager et al., 2019; Salery et al., 2020), and inhibition of the activity of striatal neurons in the direct pathway could suppress cue-induced cocaine-seeking behaviors without affecting the formation of cocaine addiction (Yager et al., 2019). Thus, modulating the activity of the SNr may regulate addiction by affecting striatum activity. Studies also found that HF DBS of the SNr produced negative changes in the cerebral blood volume (CBV) in the striatum, and it also evoked positive CBV changes in multiple basal ganglia nuclei as well as the zona incerta and the ventral tegmental area (Van Den Berge et al., 2017), while existing evidence proved that these brain regions play a crucial role in addiction (Hikida et al., 2010; Mahler et al., 2014; Shen et al., 2014). Therefore, electrical stimulation of the SNr may affect addiction by modulating the neural activity of related brain regions.

In the present study, we attempted to investigate the beneficial effects of DBS of the SNr in the treatment of methamphetamine addiction by using the free access CPP extinction paradigm in rats. The stimulation parameters used in previous studies are mainly LF (10–40 Hz) and HF (100–400 Hz) stimulation, while the medium-frequency (40–60 Hz) stimulation has almost no effect on modulating the functional connectivity of the SNr (Creed et al., 2015; Martinez-Rivera et al., 2016; Van Den Berge et al., 2017; Fakhrieh-Asl et al., 2020). Our results indicated that HF DBS of the SNr promoted extinction and subsequently blocked the drug-primed reinstatement. However, we also found that LF DBS of the SNr suppressed the extinction. Besides, HF DBS of the SNr had no effect on the development of methamphetamine-induced CPP. These results suggest that the stages of addiction and the stimulation parameters should be considered when using SNr DBS in the treatment of addiction. On the other hand, DBS has the ability to modulate the synaptic plasticity, which may also contribute to strengthening the extinction memory and suppressing the subsequent reinstatement of drug-seeking behaviors (Kauer and Malenka, 2007; Creed et al., 2015; Lee et al., 2016; Ni et al., 2018). The mechanism of DBS that promotes extinction may be that HF DBS causes long-term potentiation of the SNr and leads to a decrease in the activity of the dorsal striatum, which plays a critical role in the extinction of the addiction memory, in line with the previous findings (Martinez-Rivera et al., 2016; Yager et al., 2019).

Despite the efficacy of DBS in the treatment of a variety of diseases, the underlying mechanisms of these effects remain unclear. Indeed, it is a limitation of the present study that we did not investigate the mechanisms of the effects of DBS of the SNr on extinction and reinstatement of methamphetamine-induced CPP. Studies have found that DBS could enhance the transmission from the stimulation target and activate surrounding fiber pathways simultaneously, leading to a complex pattern of excitatory and inhibitory effects (Miocinovic et al., 2013). Furthermore, consistent

with our findings, different frequencies of DBS could produce distinct effects. Acute LF DBS of the nucleus accumbens combined with the dopamine D1 receptor antagonist SCH23390 effectively abolishes the behavioral sensitization of cocaine (Creed et al., 2015). LF DBS of the dorsal ventral striatum strengthens the morphine extinction memory, whereas HF DBS of the dorsal ventral striatum impairs extinction training and the subsequent extinction memory (Martinez-Rivera et al., 2016). Additionally, HF DBS of the OFC prevents the development of morphine place preference and blocks the drug-primed reinstatement of morphine-seeking behavior (Fakhrieh-Asl et al., 2020).

In conclusion, we have found that HF DBS of the SNr facilitated the extinction of methamphetamine-induced CPP and blocked methamphetamine-primed reinstatement, while LF DBS of the SNr impaired extinction. Meanwhile, HF DBS of the SNr neither affected locomotor activity nor caused anxiety-like behaviors. Moreover, it had no effect on the formation of methamphetamine-induced CPP. Our findings may provide potential targets and options for the future clinical application of DBS in the treatment of addiction.

DATA AVAILABILITY STATEMENT

The raw data supporting the conclusion of this article will be made available by the authors, without undue reservation.

ETHICS STATEMENT

The animal study was reviewed and approved by the Biomedical Ethics Committee for Animal Use and Protection of Peking University.

AUTHOR CONTRIBUTIONS

LZ, YC (Shenzhen), JS, and YS designed the study. LZ, SM, WC, EH, GZ, YL, and ZD performed the experiments. LZ, SM, WC, YC (Beijing), and YX analyzed the data and prepared the manuscript together. All the authors have read and approved the final version of the manuscript.

FUNDING

This work was supported by the Shenzhen Science and Technology Innovation Committee (Grant no. JCYJ20170412171856582), the Shenzhen Development and Reform Commission (Grant no. XMHT20190104001), the National Natural Science Foundation of China (Grant nos. U1802283, 81821092, and 81901352), and the Beijing Municipal Science and Technology Commission (Grant no. Z181100001518005).

REFERENCES

Batra, V., Tran, T. L. N., Caputo, J., Guerin, G. F., Goeders, N. E., and Wilden, J. (2017). Intermittent Bilateral Deep Brain Stimulation of the Nucleus Accumbens Shell Reduces Intravenous Methamphetamine Intake and Seeking in Wistar Rats. *Jns* 126 (4), 1339–1350. doi:10.3171/2016.4.JNS152524

Cassidy, C. M., Carpenter, K. M., Konova, A. B., Cheung, V., Grassetti, A., Zecca, L., et al. (2020). Evidence for Dopamine Abnormalities in the Substantia Nigra in Cocaine Addiction Revealed by Neuromelanin-Sensitive MRI. *Am. J. Psychiatry* 177 (11), 1038–1047. doi:10.1176/appi.ajp.2020.20010090

Chastan, N., Westby, G. W. M., Yelnik, J., Bardinet, E., Do, M. C., Agid, Y., et al. (2009). Effects of Nigral Stimulation on Locomotion and Postural Stability in Patients with Parkinson's Disease. *Brain* 132 (Pt 1), 172–184. doi:10.1093/brain/awn294

Chen, B., Xu, C., Wang, Y., Lin, W., Wang, Y., Chen, L., et al. (2020). A Disinhibitory Nigra-Parafascicular Pathway Amplifies Seizure in Temporal Lobe Epilepsy. *Nat. Commun.* 11 (1), 923. doi:10.1038/s41467-020-14648-8

Chen, L., Li, N., Ge, S., Lozano, A. M., Lee, D. J., Yang, C., et al. (2019a). Long-term Results after Deep Brain Stimulation of Nucleus Accumbens and the Anterior Limb of the Internal Capsule for Preventing Heroin Relapse: An Open-Label Pilot Study. *Brain Stimulation* 12 (1), 175–183. doi:10.1016/j.brs.2018.09.006

Chen, Y.-Y., Zhang, L.-B., Li, Y., Meng, S.-Q., Gong, Y.-M., Lu, L., et al. (2019b). Post-retrieval Extinction Prevents Reconsolidation of Methamphetamine Memory Traces and Subsequent Reinstatement of Methamphetamine Seeking. *Front. Mol. Neurosci.* 12, 157. doi:10.3389/fnmol.2019.00157

Chuhma, N., Tanaka, K. F., Hen, R., and Rayport, S. (2011). Functional Connectome of the Striatal Medium Spiny Neuron. *J. Neurosci.* 31 (4), 1183–1192. doi:10.1523/JNEUROSCI.3833-10.2011

Conklin, C. A., and Tiffany, S. T. (2002). Applying Extinction Research and Theory to Cue-Exposure Addiction Treatments. *Addiction* 97 (2), 155–167. doi:10.1046/j.1360-0443.2002.00014.x

Creed, M., Pascoli, V. J., and Lüscher, C. (2015). Refining Deep Brain Stimulation to Emulate Optogenetic Treatment of Synaptic Pathology. *Science* 347 (6222), 659–664. doi:10.1126/science.1260776

Crowell, A. L., Riva-Posse, P., Holtzheimer, P. E., Garlow, S. J., Kelley, M. E., Gross, R. E., et al. (2019). Long-Term Outcomes of Subcallosal Cingulate Deep Brain Stimulation for Treatment-Resistant Depression. *Am. J. Psychiatry* 176 (11), 949–956. doi:10.1176/appi.ajp.2019.18121427

Cui, Y., Ostlund, S. B., James, A. S., Park, C. S., Ge, W., Roberts, K. W., et al. (2014). Targeted Expression of μ-opioid Receptors in a Subset of Striatal Direct-Pathway Neurons Restores Opiate Reward. *Nat. Neurosci.* 17 (2), 254–261. doi:10.1038/nn.3622

Deniau, J. M., Mailly, P., Maurice, N., and Charpier, S. (2007). The Pars Reticulata of the Substantia Nigra: a Window to Basal Ganglia Output. *Prog. Brain Res.* 160, 151–172. doi:10.1016/S0079-6123(06)60009-5

Du, G., Lewis, M. M., Sica, C., He, L., Connor, J. R., Kong, L., et al. (2018). Distinct Progression Pattern of Susceptibility MRI in the Substantia Nigra of Parkinson's Patients. *Mov Disord.* 33 (9), 1423–1431. doi:10.1002/mds.27318

Elkaim, L. M., Alotaibi, N. M., Sigal, A., Alotaibi, H. M., Lipsman, N., Kalia, S. K., et al. (2019). Deep Brain Stimulation for Pediatric Dystonia: a Meta-analysis with Individual Participant Data. *Dev. Med. Child. Neurol.* 61 (1), 49–56. doi:10.1111/dmcn.14063

Fakhrieh-Asl, G., Sadr, S. S., Karimian, S. M., and Riahi, E. (2020). Deep Brain Stimulation of the Orbitofrontal Cortex Prevents the Development and Reinstatement of Morphine Place Preference. *Addict. Biol.* 25 (4), e12780. doi:10.1111/adb.12780

Fang, Q., Li, Z., Huang, G.-D., Zhang, H.-H., Chen, Y.-Y., Zhang, L.-B., et al. (2018). Traumatic Stress Produces Distinct Activations of GABAergic and Glutamatergic Neurons in Amygdala. *Front. Neurosci.* 12, 387. doi:10.3389/fnins.2018.00387

Figee, M., Luigjes, J., Smolders, R., Valencia-Alfonso, C.-E., van Wingen, G., de Kwaasteniet, B., et al. (2013). Deep Brain Stimulation Restores Frontostriatal Network Activity in Obsessive-Compulsive Disorder. *Nat. Neurosci.* 16 (4), 386–387. doi:10.1038/nn.3344

Galaj, E., Han, X., Shen, H., Jordan, C. J., He, Y., Humburg, B., et al. (2020). Dissecting the Role of GABA Neurons in the VTA versus SNr in Opioid Reward. *J. Neurosci.* 40 (46), 8853–8869. doi:10.1523/JNEUROSCI.0988-20.2020

Guercio, L. A., Schmidt, H. D., and Pierce, R. C. (2015). Deep Brain Stimulation of the Nucleus Accumbens Shell Attenuates Cue-Induced Reinstatement of Both

Cocaine and Sucrose Seeking in Rats. *Behav. Brain Res.* 281, 125–130. doi:10.1016/j.bbr.2014.12.025

He, Y.-Y., Xue, Y.-X., Wang, J.-s., Fang, Q., Liu, J.-F., Xue, L.-F., et al. (2011). PKMζ Maintains Drug Reward and Aversion Memory in the Basolateral Amygdala and Extinction Memory in the Infralimbic Cortex. *Neuropsychopharmacology* 36 (10), 1972–1981. doi:10.1038/npp.2011.63

Hikida, T., Kimura, K., Wada, N., Funabiki, K., and Nakanishi, S. (2010). Distinct Roles of Synaptic Transmission in Direct and Indirect Striatal Pathways to Reward and Aversive Behavior. *Neuron* 66 (6), 896–907. doi:10.1016/j.neuron.2010.05.011

Holtzheimer, P. E., Husain, M. M., Lisanby, S. H., Taylor, S. F., Whitworth, L. A., McClintock, S., et al. (2017). Subcallosal Cingulate Deep Brain Stimulation for Treatment-Resistant Depression: a Multisite, Randomised, Sham-Controlled Trial. *The Lancet Psychiatry* 4 (11), 839–849. doi:10.1016/S2215-0366(17)30371-1

Hyman, S. E., and Malenka, R. C. (2001). Addiction and the Brain: the Neurobiology of Compulsion and its Persistence. *Nat. Rev. Neurosci.* 2 (10), 695–703. doi:10.1038/35094560

Hyman, S. E., Malenka, R. C., and Nestler, E. J. (2006). Neural Mechanisms of Addiction: the Role of Reward-Related Learning and Memory. *Annu. Rev. Neurosci.* 29, 565–598. doi:10.1146/annurev.neuro.29.051605.113009

Katz, M., Luciano, M. S., Carlson, K., Luo, P., Marks, W. J., Jr., Larson, P. S., et al. (2015). Differential Effects of Deep Brain Stimulation Target on Motor Subtypes in Parkinson's Disease. *Ann. Neurol.* 77 (4), 710–719. doi:10.1002/ana.24374

Kauer, J. A., and Malenka, R. C. (2007). Synaptic Plasticity and Addiction. *Nat. Rev. Neurosci.* 8 (11), 844–858. doi:10.1038/nrn2234

Kennedy, S. H., Giacobbe, P., Rizvi, S. J., Placenza, F. M., Nishikawa, Y., Mayberg, H. S., et al. (2011). Deep Brain Stimulation for Treatment-Resistant Depression: Follow-Up after 3 to 6 Years. *Am. J. Psychiatry* 168 (5), 502–510. doi:10.1176/appi.ajp.2010.10081187

Kleiner-Fisman, G., Lin Liang, G. S., Moberg, P. J., Ruocco, A. C., Hurtig, H. I., Baltuch, G. H., et al. (2007). Subthalamic Nucleus Deep Brain Stimulation for Severe Idiopathic Dystonia: Impact on Severity, Neuropsychological Status, and Quality of Life. *J. Neurosurg.* 107 (1), 29–36. doi:10.3171/JNS-07/07/0029

Kringelbach, M. L., Jenkinson, N., Owen, S. L. F., and Aziz, T. Z. (2007). Translational Principles of Deep Brain Stimulation. *Nat. Rev. Neurosci.* 8 (8), 623–635. doi:10.1038/nrn2196

Lai, Y.-Y., Kodama, T., Hsieh, K.-C., Nguyen, D., and Siegel, J. M. (2021). Substantia Nigra Pars Reticulata-Mediated Sleep and Motor Activity Regulation. *Sleep* 44 (1). doi:10.1093/sleep/zsaa151

Lee, J., Finkelstein, J., Choi, J. Y., and Witten, I. B. (2016). Linking Cholinergic Interneurons, Synaptic Plasticity, and Behavior during the Extinction of a Cocaine-Context Association. *Neuron* 90 (5), 1071–1085. doi:10.1016/j.neuron.2016.05.001

Liang, J., Li, J.-L., Han, Y., Luo, Y.-X., Xue, Y.-X., Zhang, Y., et al. (2017). Calpain-GRIP Signaling in Nucleus Accumbens Core Mediates the Reconsolidation of Drug Reward Memory. *J. Neurosci.* 37 (37), 8938–8951. doi:10.1523/JNEUROSCI.0703-17.2017

Lipsman, N., Lam, E., Volpini, M., Sutandar, K., Twose, R., Giacobbe, P., et al. (2017). Deep Brain Stimulation of the Subcallosal Cingulate for Treatment-Refractory Anorexia Nervosa: 1 Year Follow-Up of an Open-Label Trial. *The Lancet Psychiatry* 4 (4), 285–294. doi:10.1016/S2215-0366(17)30076-7

Lipsman, N., Woodside, D. B., Giacobbe, P., Hamani, C., Carter, J. C., Norwood, S. J., et al. (2013). Subcallosal Cingulate Deep Brain Stimulation for Treatment-Refractory Anorexia Nervosa: a Phase 1 Pilot Trial. *The Lancet* 381 (9875), 1361–1370. doi:10.1016/S0140-6736(12)62188-6

Liu, D., Li, W., Ma, C., Zheng, W., Yao, Y., Tso, C. F., et al. (2020). A Common Hub for Sleep and Motor Control in the Substantia Nigra. *Science* 367 (6476), 440–445. doi:10.1126/science.aaz0956

Liu, J. F., Tian, J., and Li, J. X. (2019). Modulating Reconsolidation and Extinction to Regulate Drug Reward Memory. *Eur. J. Neurosci.* 50 (3), 2503–2512. doi:10.1111/ejn.14072

Luigjes, J., van den Brink, W., Feenstra, M., van den Munckhof, P., Schuurman, P. R., Schippers, R., et al. (2012). Deep Brain Stimulation in Addiction: a Review of Potential Brain Targets. *Mol. Psychiatry* 17 (6), 572–583. doi:10.1038/mp.2011.114

Luo, Y. X., Xue, Y. X., Liu, J. F., Shi, H. S., Jian, M., Han, Y., et al. (2015). A Novel UCS Memory Retrieval-Extinction Procedure to Inhibit Relapse to Drug Seeking. *Nat. Commun.* 6, 7675. doi:10.1038/ncomms8675

Madsen, H. B., Brown, R. M., Short, J. L., and Lawrence, A. J. (2012). Investigation of the Neuroanatomical Substrates of Reward Seeking Following Protracted Abstinence in Mice. *J. Physiol.* 590 (10), 2427–2442. doi:10.1113/jphysiol.2011.225219

Mahler, S. V., Vazey, E. M., Beckley, J. T., Keistler, C. R., McGlinchey, E. M., Kaufling, J., et al. (2014). Designer Receptors Show Role for Ventral Pallidum Input to Ventral Tegmental Area in Cocaine Seeking. *Nat. Neurosci.* 17 (4), 577–585. doi:10.1038/nn.3664

Martínez-Rivera, F. J., Rodriguez-Romaguera, J., Lloret-Torres, M. E., Do Monte, F. H., Quirk, G. J., and Barreto-Estrada, J. L. (2016). Bidirectional Modulation of Extinction of Drug Seeking by Deep Brain Stimulation of the Ventral Striatum. *Biol. Psychiatry* 80 (9), 682–690. doi:10.1016/j.biopsych.2016.05.015

Milton, A. L., and Everitt, B. J. (2012b). The Persistence of Maladaptive Memory: Addiction, Drug Memories and Anti-relapse Treatments. *Neurosci. Biobehavioral Rev.* 36 (4), 1119–1139. doi:10.1016/j.neubiorev.2012.01.002

Milton, A. L., and Everitt, B. J. (2012a). Wiping Drug Memories. *Science* 336 (6078), 167–168. doi:10.1126/science.1221691

Miocinovic, S., Somayajula, S., Chitnis, S., and Vitek, J. L. (2013). History, Applications, and Mechanisms of Deep Brain Stimulation. *JAMA Neurol.* 70 (2), 163–171. doi:10.1001/2013.jamaneurol.45

Müller, U. J., Voges, J., Steiner, J., Galazky, I., Heinze, H.-J., Möller, M., et al. (2013). Deep Brain Stimulation of the Nucleus Accumbens for the Treatment of Addiction. *Ann. N.Y. Acad. Sci.* 1282, 119–128. doi:10.1111/j.1749-6632.2012.06834.x

Ni, Z., Kim, S. J., Phielipp, N., Ghosh, S., Udupa, K., Gunraj, C. A., et al. (2018). Pallidal Deep Brain Stimulation Modulates Cortical Excitability and Plasticity. *Ann. Neurol.* 83 (2), 352–362. doi:10.1002/ana.25156

Okun, M. S. (2012). Deep-brain Stimulation for Parkinson's Disease. *N. Engl. J. Med.* 367 (16), 1529–1538. doi:10.1056/NEJMct1208070

Opri, E., Cernera, S., Molina, R., Eisinger, R. S., Cagle, J. N., Almeida, L., et al. (2020). Chronic Embedded Cortico-Thalamic Closed-Loop Deep Brain Stimulation for the Treatment of Essential Tremor. *Sci. Transl. Med.* 12 (572), eaay7680. doi:10.1126/scitranslmed.aay7680

Pelloux, Y., Hoots, J. K., Cifani, C., Adhikary, S., Martin, J., Minier-Toribio, A., et al. (2018). Context-induced Relapse to Cocaine Seeking after Punishment-Imposed Abstinence Is Associated with Activation of Cortical and Subcortical Brain Regions. *Addict. Biol.* 23 (2), 699–712. doi:10.1111/adb.12527

Phillips, R. S., Rosner, I., Gittis, A. H., and Rubin, J. E. (2020). The Effects of Chloride Dynamics on Substantia Nigra Pars Reticulata Responses to Pallidal and Striatal Inputs. *Elife* 9. doi:10.7554/eLife.55592

Rosin, B., Slovik, M., Mitelman, R., Rivlin-Etzion, M., Haber, S. N., Israel, Z., et al. (2011). Closed-loop Deep Brain Stimulation Is superior in Ameliorating Parkinsonism. *Neuron* 72 (2), 370–384. doi:10.1016/j.neuron.2011.08.023

Sabrini, S., Russell, B., Wang, G., Lin, J., Kirk, I., and Curley, L. (2020). Methamphetamine Induces Neuronal Death: Evidence from Rodent Studies. *Neurotoxicology* 77, 20–28. doi:10.1016/j.neuro.2019.12.006

Salery, M., Trifilieff, P., Caboche, J., and Vanhoutte, P. (2020). From Signaling Molecules to Circuits and Behaviors: Cell-type-specific Adaptations to Psychostimulant Exposure in the Striatum. *Biol. Psychiatry* 87 (11), 944–953. doi:10.1016/j.biopsych.2019.11.001

Schor, J. S., and Nelson, A. B. (2019). Multiple Stimulation Parameters Influence Efficacy of Deep Brain Stimulation in Parkinsonian Mice. *J. Clin. Invest.* 129 (9), 3833–3838. doi:10.1172/JCI122390

Schuurman, P. R., Bosch, D. A., Bossuyt, P. M. M., Bonsel, G. J., van Someren, E. J. W., de Bie, R. M. A., et al. (2000). A Comparison of Continuous Thalamic Stimulation and Thalamotomy for Suppression of Severe Tremor. *N. Engl. J. Med.* 342 (7), 461–468. doi:10.1056/NEJM200002173420703

Sharpe, A. L., Varela, E., Bettinger, L., and Beckstead, M. J. (2014). Methamphetamine Self-Administration in Mice Decreases GIRK Channel-Mediated Currents in Midbrain Dopamine Neurons. *Int. J. Neuropsychopharmacol.* 18 (5), pyu073. doi:10.1093/ijnp/pyu073

Shen, H.-W., Gipson, C. D., Huits, M., and Kalivas, P. W. (2014). Prelimbic Cortex and Ventral Tegmental Area Modulate Synaptic Plasticity Differentially in Nucleus Accumbens during Cocaine-Reinstated Drug Seeking. *Neuropsychopharmacology* 39 (5), 1169–1177. doi:10.1038/npp.2013.318

Sitzia, G., Mantas, I., Zhang, X., Svenningsson, P., and Chergui, K. (2020). NMDA Receptors Are Altered in the Substantia Nigra Pars Reticulata and Their Blockade Ameliorates Motor Deficits in Experimental Parkinsonism. *Neuropharmacology* 174, 108136. doi:10.1016/j.neuropharm.2020.108136

Valldeoriola, F., Muñoz, E., Rumià, J., Roldán, P., Cámara, A., Compta, Y., et al. (2019). Simultaneous Low-Frequency Deep Brain Stimulation of the Substantia Nigra Pars Reticulata and High-Frequency Stimulation of the Subthalamic Nucleus to Treat Levodopa Unresponsive Freezing of Gait in Parkinson's Disease: A Pilot Study. *Parkinsonism Relat. Disord.* 60, 153–157. doi:10.1016/j.parkreldis.2018.09.008

Van Den Berge, N., Albaugh, D. L., Salzwedel, A., Vanhove, C., Van Holen, R., Gao, W., et al. (2017). Functional Circuit Mapping of Striatal Output Nuclei Using Simultaneous Deep Brain Stimulation and fMRI. *Neuroimage* 146, 1050–1061. doi:10.1016/j.neuroimage.2016.10.049

Vassoler, F. M., Schmidt, H. D., Gerard, M. E., Famous, K. R., Ciraulo, D. A., Kornetsky, C., et al. (2008). Deep Brain Stimulation of the Nucleus Accumbens Shell Attenuates Cocaine Priming-Induced Reinstatement of Drug Seeking in Rats. *J. Neurosci.* 28 (35), 8735–8739. doi:10.1523/JNEUROSCI.5277-07.2008

Vassoler, F. M., White, S. L., Hopkins, T. J., Guercio, L. A., Espallergues, J., Berton, O., et al. (2013). Deep Brain Stimulation of the Nucleus Accumbens Shell Attenuates Cocaine Reinstatement through Local and Antidromic Activation. *J. Neurosci.* 33 (36), 14446–14454. doi:10.1523/JNEUROSCI.4804-12.2013

Villalba, R. M., and Smith, Y. (2013). Differential Striatal Spine Pathology in Parkinson's Disease and Cocaine Addiction: a Key Role of Dopamine? *Neuroscience* 251, 2–20. doi:10.1016/j.neuroscience.2013.07.011

Volkow, N. D., and Morales, M. (2015). The Brain on Drugs: From Reward to Addiction. *Cell* 162 (4), 712–725. doi:10.1016/j.cell.2015.07.046

Wang, T. R., Moosa, S., Dallapiazza, R. F., Elias, W. J., and Lynch, W. J. (2018). Deep Brain Stimulation for the Treatment of Drug Addiction. *Neurosurg. Focus* 45 (2), E11. doi:10.3171/2018.5.FOCUS18163

Wicker, E., Beck, V. C., Kulick-Soper, C., Kulick-Soper, C. V., Hyder, S. K., Campos-Rodriguez, C., et al. (2019). Descending Projections from Thesubstantia Nigra Pars Reticulatadifferentially Control Seizures. *Proc. Natl. Acad. Sci. USA* 116, 27084–27094. doi:10.1073/pnas.1908176117

Willard, A. M., Isett, B. R., Whalen, T. C., Mastro, K. J., Ki, C. S., Mao, X., et al. (2019). State Transitions in the Substantia Nigra Reticulata Predict the Onset of Motor Deficits in Models of Progressive Dopamine Depletion in Mice. *Elife* 8. doi:10.7554/eLife.42746

Wu, H., Hariz, M., Visser-Vandewalle, V., Zrinzo, L., Coenen, V. A., Sheth, S. A., et al. (2021). Deep Brain Stimulation for Refractory Obsessive-Compulsive Disorder (OCD): Emerging or Established Therapy? *Mol. Psychiatry* 26 (1), 60–65. doi:10.1038/s41380-020-00933-x

Xue, Y.-X., Luo, Y.-X., Wu, P., Shi, H.-S., Xue, L.-F., Chen, C., et al. (2012). A Memory Retrieval-Extinction Procedure to Prevent Drug Craving and Relapse. *Science* 336 (6078), 241–245. doi:10.1126/science.1215070

Xue, Y.-X., Xue, L.-F., Liu, J.-F., He, J., Deng, J.-H., Sun, S.-C., et al. (2014). Depletion of Perineuronal Nets in the Amygdala to Enhance the Erasure of Drug Memories. *J. Neurosci.* 34 (19), 6647–6658. doi:10.1523/JNEUROSCI.5390-13.2014

Xue, Y.-X., Zhu, Z.-Z., Han, H.-B., Liu, J.-F., Meng, S.-Q., Chen, C., et al. (2015). Overexpression of Protein Kinase Mζ in the Prelimbic Cortex Enhances the Formation of Long-Term Fear Memory. *Neuropsychopharmacology* 40 (9), 2146–2156. doi:10.1038/npp.2015.56

Yager, L. M., Garcia, A. F., Donckels, E. A., and Ferguson, S. M. (2019). Chemogenetic Inhibition of Direct Pathway Striatal Neurons Normalizes Pathological, Cue-Induced Reinstatement of Drug-Seeking in Rats. *Addict. Biol.* 24 (2), 251–264. doi:10.1111/adb.12594

Conflict of Interest: The authors declare that the research was conducted in the absence of any commercial or financial relationships that could be construed as a potential conflict of interest.

frontiers in Pharmacology

ORIGINAL RESEARCH
published: 06 July 2021
doi: 10.3389/fphar.2021.705254

Cocaine-Induced Changes in Tonic Dopamine Concentrations Measured Using Multiple-Cyclic Square Wave Voltammetry *in vivo*

*Jason Yuen[1,2], Abhinav Goyal[1,3], Aaron E. Rusheen[1,3], Abbas Z. Kouzani[4], Michael Berk[2], Jee Hyun Kim[2], Susannah J. Tye[5], Charles D. Blaha[1], Kevin E. Bennet[1,6], Dong-Pyo Jang[7], Kendall H. Lee[1,8], Hojin Shin[1] and Yoonbae Oh[1,8]**

[1]Department of Neurologic Surgery, Mayo Clinic, Rochester, MN, United States, [2]Deakin University, IMPACT—the Institute for Mental and Physical Health and Clinical Translation, School of Medicine, Barwon Health, Geelong, VIC, Australia, [3]Medical Scientist Training Program, Mayo Clinic, Rochester, MN, United States, [4]School of Engineering, Deakin University, Geelong, VIC, Australia, [5]Queensland Brain Institute, The University of Queensland, St Lucia, QLD, Australia, [6]Division of Engineering, Mayo Clinic, Rochester, MN, United States, [7]Department of Biomedical Engineering, Hanyang University, Seoul, Korea, [8]Department of Biomedical Engineering, Mayo Clinic, Rochester, MN, United States

OPEN ACCESS

Edited by:
Jianfeng Liu,
Texas A&M University, United States

Reviewed by:
Alexander G. Zestos,
American University, United States
Sara Raulerson Jones,
Wake Forest School of Medicine, United States
Adrian Michael,
University of Pittsburgh, United States

***Correspondence:**
Yoonbae Oh
oh.yoonbae@mayo.edu

Specialty section:
This article was submitted to Neuropharmacology, a section of the journal Frontiers in Pharmacology

Received: *05 May 2021*
Accepted: *24 June 2021*
Published: *06 July 2021*

Citation:
Yuen J, Goyal A, Rusheen AE, Kouzani AZ, Berk M, Kim JH, Tye SJ, Blaha CD, Bennet KE, Jang D-P, Lee KH, Shin H and Oh Y (2021) Cocaine-Induced Changes in Tonic Dopamine Concentrations Measured Using Multiple-Cyclic Square Wave Voltammetry in vivo. *Front. Pharmacol. 12:705254. doi: 10.3389/fphar.2021.705254*

For over 40 years, *in vivo* microdialysis techniques have been at the forefront in measuring the effects of illicit substances on brain tonic extracellular levels of dopamine that underlie many aspects of drug addiction. However, the size of microdialysis probes and sampling rate may limit this technique's ability to provide an accurate assessment of drug effects in microneural environments. A novel electrochemical method known as multiple-cyclic square wave voltammetry (M-CSWV), was recently developed to measure second-to-second changes in tonic dopamine levels at microelectrodes, providing spatiotemporal resolution superior to microdialysis. Here, we utilized M-CSWV and fast-scan cyclic voltammetry (FSCV) to measure changes in tonic or phasic dopamine release in the nucleus accumbens core (NAcc) after acute cocaine administration. Carbon-fiber microelectrodes (CFM) and stimulating electrodes were implanted into the NAcc and medial forebrain bundle (MFB) of urethane anesthetized (1.5 g/kg i.p.) Sprague-Dawley rats, respectively. Using FSCV, depths of each electrode were optimized by determining maximal MFB electrical stimulation-evoked phasic dopamine release. Changes in phasic responses were measured after a single dose of intravenous saline or cocaine hydrochloride (3 mg/kg; n = 4). In a separate group, changes in tonic dopamine levels were measured using M-CSWV after intravenous saline and after cocaine hydrochloride (3 mg/kg; n = 5). Both the phasic and tonic dopamine responses in the NAcc were augmented by the injection of cocaine compared to saline control. The phasic and tonic levels changed by approximately x2.4 and x1.9, respectively. These increases were largely consistent with previous studies using FSCV and microdialysis. However, the minimal disruption/disturbance of neuronal tissue by the CFM may explain why the baseline tonic dopamine values (134 ± 32 nM) measured by M-CSWV were found to be 10-fold higher when compared to conventional microdialysis. In this study, we demonstrated phasic dopamine dynamics in the NAcc with acute cocaine administration. M-CSWV was able to record rapid changes in tonic levels of dopamine, which cannot be achieved with other

current voltammetric techniques. Taken together, M-CSWV has the potential to provide an unprecedented level of physiologic insight into dopamine signaling, both *in vitro* and *in vivo*, which will significantly enhance our understanding of neurochemical mechanisms underlying psychiatric conditions.

Keywords: cocaine, tonic dopamine, addiction, voltammetry, nucleus accumbens, neuroscience, psychiatry, mental disorders

INTRODUCTION

Substance dependence is a global public health problem. A 2019 survey revealed 20.4 million people aged 12 or older in the United States suffered from substance use disorder (Substance Abuse and Mental Health Services Administration, 2020). Around 40–60% of patients experience relapse within one year of treatment discharge (McLellan et al., 2000), which is hypothesized to be a result of long-term neuroplastic changes after chronic drug use (Kalivas and O'Brien, 2008). Therefore, it is important to understand the neurobiology of addiction in order to improve our treatment strategies.

Dopamine is widely implicated in addiction. Its functions include determining the incentive value of naturally occurring positive rewarding stimuli (e.g., food, water, and conspecific mates) (Blaha and Phillips, 1996). Previous studies have also demonstrated that dopamine release in the nucleus accumbens, dorsal striatum, and the prefrontal cortex is a cardinal feature in models of addiction, with dopamine receptor blockade in these areas disrupting drug-seeking behaviors (Berke and Hyman, 2000; Ito et al., 2002; Vanderschuren et al., 2005; Murray et al., 2012; Zbukvic et al., 2016; Hodebourg et al., 2019). However, measuring dopamine with high temporal and spatial resolution *in vivo* is a major challenge.

There are generally two distinct patterns of spike firing exhibited by neuronal dopamine-containing cells in the mammalian midbrain: tonic activity and phasic burst activity (Grace, 1991; Grace, 2016). Phasic activity causes a transient and robust release of dopamine in the synapse that serves as a learning signal for neural plasticity (Schultz, 2007). Tonic activity refers to continuous spontaneous extra-synaptic dopamine release driven by pacemaker-like firing of dopamine neurons, providing a relatively homeostatic extracellular level of dopamine (i.e., tonic concentration) in the striatum thought to modulate behavioral flexibility (Goto et al., 2007).

Tonic concentrations of dopamine in the brain have been typically quantified in the sub-nM range using microdialysis (Watson et al., 2006; Gu et al., 2015). Microdialysis has been utilized for sampling neurochemical substances, such as dopamine with high selectivity and sensitivity. However, it has several drawbacks when compared to electrochemical techniques (Robinson et al., 2003; Heien et al., 2004; Chefer et al., 2009; Rodeberg et al., 2017; Kim et al., 2021). These include limited temporal resolution ($\geq$ 1 min) in comparison to voltammetry (milliseconds to seconds), and the relatively large dimensions of dialysis probes (typically > 200 μm), resulting in variable physicochemical characteristics, tissue damage, and relatively low spatiotemporal resolution (Morelli et al., 1992; Di Chiara et al., 1993; Blaha et al., 1996; Chefer et al., 2009; Oh et al., 2018; Rusheen et al., 2020). For these reasons, and the fact that it requires continuous sampling from the brain and laboratory analysis, its application in the human nervous system is limited.

In contrast, electrochemical methods, such as fast-scan cyclic voltammetry (FSCV), have features that are well-suited to quantitatively measure changes in extracellular dopamine concentrations (Millar, 1997; Robinson et al., 2003; Huffman and Venton, 2009; Lama et al., 2012). FSCV provides excellent temporal resolution (milliseconds time response) and detection sensitivity (<5 nM). In this technique, a carbon-fiber microelectrode (CFM, diameter typically <10 μm) is held at a resting potential and then ramped to an electric potential sufficient to oxidize and reduce the electroactive species before the potential is returned to the resting potential (Robinson et al., 2003). This results in a measured current, which yields a cyclic voltammogram. The electrical scan takes less than 10 ms and is repeated every 100 ms (corresponding to a rate of 10 Hz). The voltammogram gives a chemical signature, which can be used to identify the chemical species of interest and quantify phasic changes in extracellular concentration. However, because of a large capacitive current which must be subtracted out to resolve the faradaic current, the application of conventional FSCV provides only measurements of phasic changes in neurochemical concentrations (Howell et al., 1986). FSCV cannot measure dysregulation in tonic concentrations of neurotransmitters (minutes to hours) that are likely to be important characteristics of many neurologic and psychiatric conditions (Dreher and Burnod, 2002; Berke, 2018).

For the measurement of tonic dopamine levels in the brain in real time, several electrochemical techniques were developed such as fast-scan controlled-adsorption voltammetry (FSCAV) (Atcherley et al., 2013), square wave voltammetry (Taylor et al., 2019), and convolution-based current removal technique (Johnson et al., 2017). Among these techniques, FSCAV from Heien and colleagues has been applied to study tonic dopamine levels in various experiment setups (Atcherley et al., 2015; Burrell et al., 2015; Abdalla et al., 2017). FSCAV utilizes adsorption properties of dopamine to the carbon microelectrode using multiple conventional FSCV waveforms. We have previously developed a technique that uses cyclic square wave voltammetric waveforms, called Multiple-Cyclic Square Wave Voltammetry (M-CSWV). The time resolution is 10 s, which is slower than FSCV but is well-matched to the timescale of changes in tonic concentrations of dopamine relevant to the pathologies of interest (Schultz, 2007). Since M-CSWV utilizes square waveforms, M-CSWV is able to harvest higher dimensional data for analysis that leads to higher sensitivity and selectivity than other tonic level measurement techniques (Kim et al., 2019; Kim et al., 2021).

In this study, we aim to elucidate the acute effects of cocaine administration on phasic dopamine release by using FSCV and tonic dopamine levels by using M-CSWV in the nucleus accumbens core (NAcc). Cocaine is one of the most common illicit drugs with an increasing prevalence of use and dependence (John and Wu, 2017).

MATERIALS AND METHODS

Animal Subjects

Nine male Sprague-Dawley rats (Envigo, United States) were used for this study. Rats were kept in social housing in an Association for Assessment and Accreditation of Laboratory Animal Care International (AAALAC) accredited vivarium following a standard 12-h light/dark cycle at constant temperature (21°C) and humidity (45%) with ad libitum food and water. The present studies were approved by the Institutional Animal Care and Use Committee (IACUC), Mayo Clinic, Rochester, MN. The NIH Guide for the Care and Use of Laboratory Animals guidelines (Department of Health and Human Services, NIH publication No. 86-23, revised 1985) were followed for all aspects of animal care.

Electrode Fabrication

CFMs were fabricated using an established standardized CFM design at Mayo Clinic. (Chang et al., 2013; Oh et al., 2016). Briefly, each microelectrode involved isolating and inserting a single carbon fiber (AS4, diameter = 7 μm; Hexel, Dublin, CA) into a silica tube (20 μM ID, 90 μM OD, 10 μM coat with polyimide; Polymicro Technologies, Phoenix, AZ). The connection between the carbon fiber and the silica tubing was covered with epoxy resin. The silica tubing was then attached to a nitinol (Nitinol #1, an alloy of nickel and titanium; Fort Wayne Metals, IN) extension wire with a silver-based conductive paste (Chang et al., 2013). The carbon fiber attached nitinol wire was insulated with polyimide tubing (0.0089″ID, 0.0134″OD, 0.00225″ WT; Vention Medical, Salem, NH) up to the carbon fiber sensing part. The exposed carbon fiber was then trimmed under a dissecting microscope to a length of 50 μm. Teflon-coated silver (Ag) wire (A-M systems, Inc., Sequim, WA) was prepared as an Ag/AgCl counter-reference electrode by chlorinating the exposed tip in saline with a 9 V dry cell battery. CFMs were pretested in a flow cell prior to coating deposition with a PEDOT:Nafion deposition solution (Vreeland et al., 2015), which minimized the effect of *in vivo* biofouling.

Implantation of Recording and Stimulating Electrodes

Each rat was anesthetized with urethane (1.5 g/kg i.p.; Sigma-Aldrich, St Louis, MO) and administered buprenorphine (0.05–0.1 mg/kg s.c, Par Pharmaceutical, Chestnut Ridge, NY, United States) for analgesia. Following anesthesia, they were placed in a stereotaxic frame (David Kopf Instruments, Tujunga, CA). Respiratory rate (RespiRAT, Intuitive Measurement Systems), hind-paw and tail pinch were used to monitor the physiological state and depth of anesthesia. Using a standard rat atlas (Paxinos and Watson, 2007), three trephine holes were drilled, the first for placement of a CFM into the NAcc (AP 1.2 mm, ML 2.0 mm, DV 6–7 mm from dura), the second for a stimulating electrode into the medial forebrain bundle (MFB) (twisted bipolar stimulating electrode—Plastics One, MS 303/2, Roanoke, VA, with the tips separated by 1 mm; AP −4.6 mm, ML 1.3 mm, DV 8–9 mm from dura), and a third for an Ag/AgCl into the contralateral cortex (Clark et al., 2010) (**Figure 1A**).

Drug Administration and Recordings

The stimulating electrode in the MFB and CFM in the NAcc were first adjusted to obtain a robust stimulation-evoked dopamine signal via FSCV (−0.4–1.3 V sweep; 10 Hz). MFB was chosen as it is known to induce dopamine release in the NAcc (Ng et al., 1991; Shu et al., 2013). For the phasic dopamine group, evoked responses (60 Hz, 0.2 mA, 2 ms pulse width, 2 s duration) were recorded at pre-, 5, 10, and 20, 30 40, 50, 60 min post-injection. This was performed using WINCS Harmoni system (Lee et al., 2017), a wireless neurochemical sensing system. Cocaine hydrochloride (Sigma-Aldrich, St. Louis, MO) at a single bolus of 3 mg/kg i.v., was used. Cocaine hydrochloride was given for 5-min duration in all cases.

For the tonic dopamine group, the system was switched to the M-CSWV sensing technique with electrodes at the same position after identification of an optimal CFM position in the NAcc using FSCV. Cocaine at the same dose and route as above was administered after baseline and post-saline recording. Further recordings were performed for another 90 min to monitor the potentially lasting effects of cocaine on tonic dopamine levels. Dynamic background subtraction and capacitive background current modeling was used to eliminate large capacitive background currents, allowing tonic dopamine concentrations to be measured every 10 s (Oh et al., 2018). Because of the uniqueness of the waveform, the voltammetric outcome of M-CSWV provides a wealth of electrochemical information beyond that provided by conventional FSCV (**Figures 1B–D**).

Calibration of Electrodes

After experimentation, changes in dopamine release for phasic studies were determined by calibration of CFMs using a flow cell injection apparatus; whereas for tonic dopamine levels, calibration with dopamine solutions were used (Oh et al., 2018). The media used consisted of TRIS buffer (15 mM tris, 3.25 mM KCl, 140 mM NaCl, 1.2 mM CaCl2, 1.25 mM NaH2PO4, 1.2 mM MgCl2, and 2.0 mM Na2SO4, with the pH adjusted to 7.4) (Oh et al., 2018).

Modelling Dopamine Dynamics

Measurement of phasic dopamine release using FSCV offers many important applications, including modeling dopamine release and reuptake kinetics, and modeling the effects of pharmacologic agents on these processes. To quantitatively characterize the effects of cocaine administration on synaptic dopamine release, we used the restricted diffusion model of Walters et al. (Walters et al., 2015). This model proposes that the synapse-electrode system consists of two anatomically separated compartments and allows for restricted diffusion from the synaptic compartment to the electrode

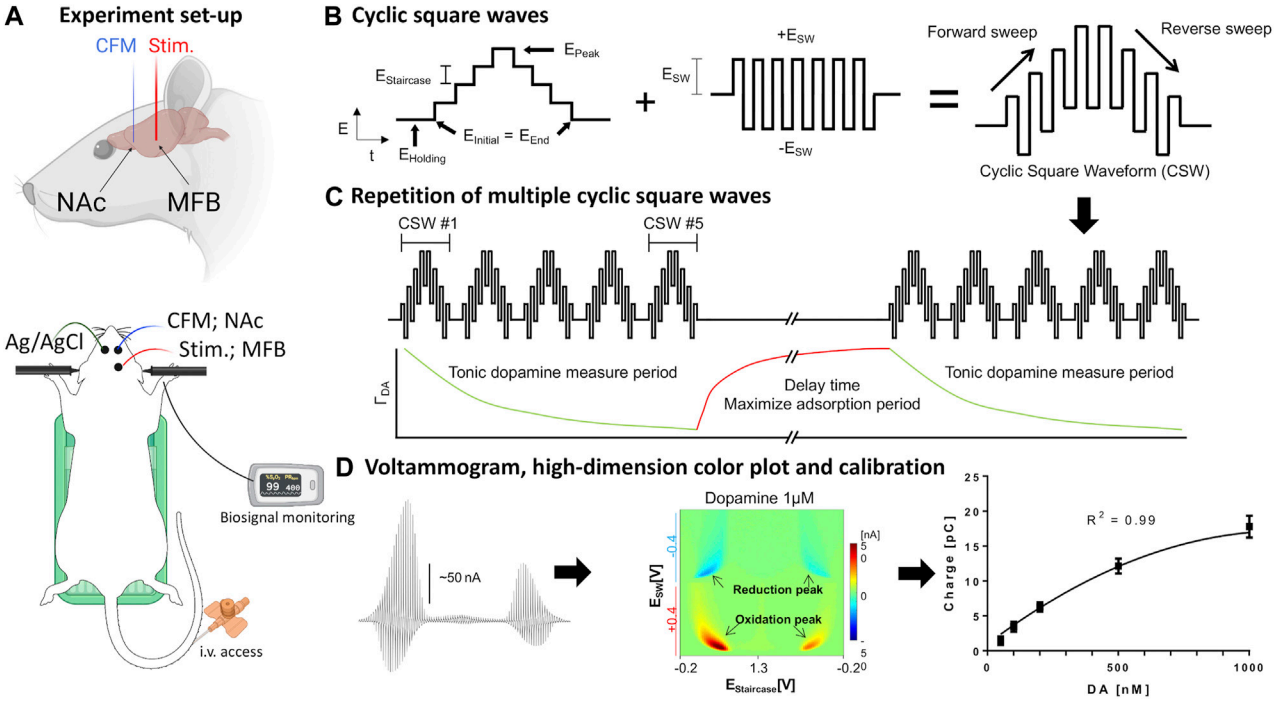

FIGURE 1 | Set-up of *in vivo* voltammetry experiment. **(A)** Rat surgery set-up. Recording and stimulating electrodes were inserted unilaterally into the core of the nucleus accumbens and medial forebrain bundle, respectively. The counter-reference Ag/AgCl electrode was inserted contralaterally into cortical tissue. The rat is placed in a stereotactic frame with tail vein access, heating pad, and pulse oximetry monitoring. **(B,C)** Schematic design of waveform-CSWV applied to the CFM and its response. **(D)** Left-to-right: Raw voltammogram after removal of background currents, high-dimensional pseudo-color plot, M-CSWV signal calibration with tonic dopamine experiment (n = 4 electrodes). Figures adopted from (Oh et al., 2018) with permission. *Ag/AgCl*, silver chloride reference electrode; *CFM*, carbon-fiber electrode; *CSW*, cyclic square wave; *MFB*, medial forebrain bundle; *NAc*, nucleus accumbens; *stim.*, bipolar stimulating electrode. Parts of the Figure were created with Biorender.com.

TABLE 1 | Parameters calculated for the FSCV response pre-cocaine and 10 min post-cocaine, based on the model by Walters et al. (Walters et al., 2015). N = 4 rats. S.E.M. values provided. One-tailed paired *t*-test was performed. A range is provided in the reference values to account for the slow and fast dopamine domains (dorsal striatal measurements based on medial forebrain bundle stimulation).

Parameters	Best-fit estimates (cocaine)		*p*-value
	Pre-drug	Post-drug	
Dopamine release per stimulus pulse, R_P (mols X 10^{-21})	6.98 ± 3.26	16.0 ± 3.34	0.093
Modifier for dopamine release, k_R (s^{-1})	–0.65 ± 4.72	–0.18 ± 0.20	Comparison cannot be made as some values were zero
Constant for dopamine uptake, k_U (s^{-1})	1.08 ± 0.53	0.36 ± 0.09	0.028
Constant for dopamine transport, k_T (s^{-1})	1.40 ± 0.22	1.40 ± 0.42	0.428

compartment. This allows for more accurate fitting of *in vivo* data compared to previous models such as the diffusion gap model. We applied the restricted diffusion model to our data to extract best-fit estimates for the parameters R_p, k_R, k_U, and k_T (see **Table 1** for more information). Best fit was evaluated with root mean square error (RMSE). The model was fit to five sets of stimulation-induced phasic dopamine releases with saline onboard, and five sets with cocaine on board, 5 min after administration.

Statistical Analysis

Statistical analysis was performed using ratio two-tailed paired *t*-tests (PRISM 8, GraphPad). Significance was set at $p < 0.05$. In the phasic experiments, three planned paired *t*-tests were performed (response at 5 min after cocaine vs baseline, saline, 60 min post-cocaine). In the tonic experiments, the peak level after cocaine injection was compared to baseline and saline levels.

RESULTS

Phasic Response and Dopamine Dynamics

Cocaine administration consistently led to enhancement of stimulation-evoked dopamine responses (**Figure 2**). The evoked phasic response at 5 min after cocaine injection was significantly higher than saline control (ratio two-tailed paired *t*-test, $p = 0.0124$, $n = 4$ rats), baseline (ratio two-tailed paired *t*-test, $p = 0.0326$, $n = 4$

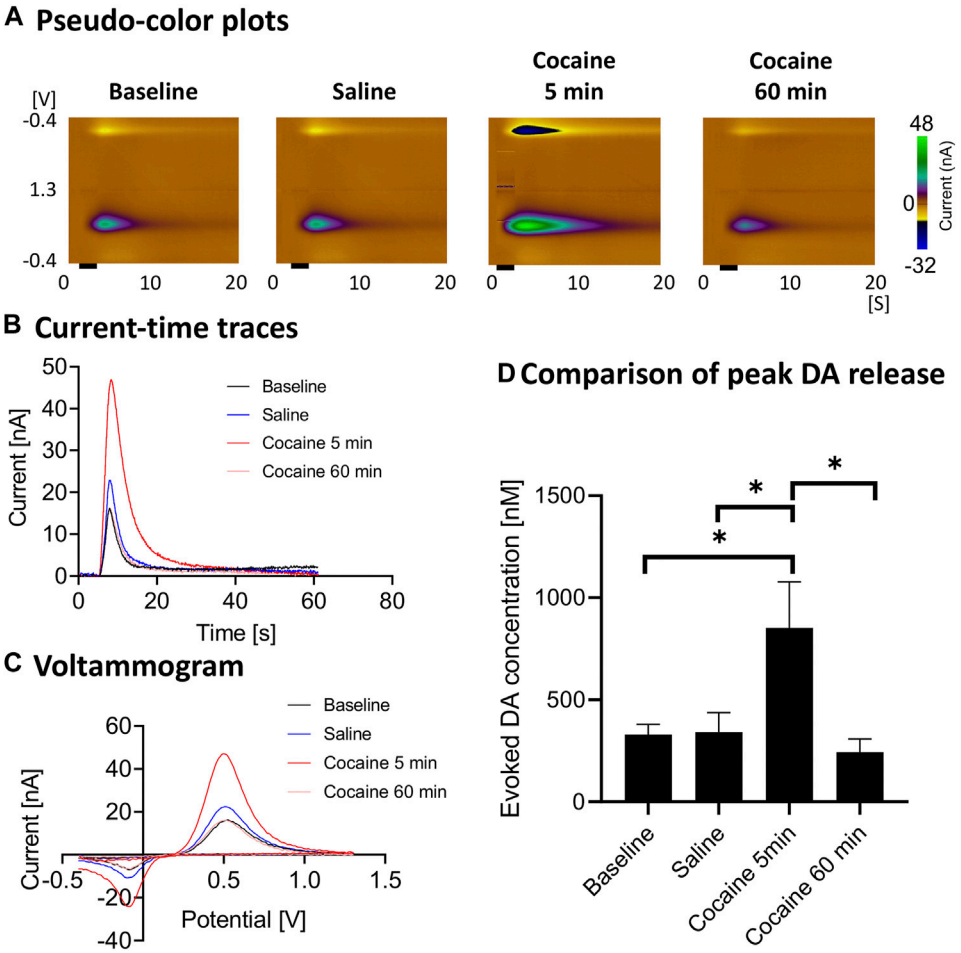

FIGURE 2 | Peak and gradual decay of cocaine-induced changes in stimulation-evoked dopamine release. *In vivo* FSCV measurements in the nucleus accumbens core showing augmented dopamine responses to cocaine injection (3 mg/kg, i.v.). Responses were measured following medial forebrain bundle stimulation (2 s, biphasic, 300 μA, 2 ms pulse width). **(A)** Representative pseudo-color plots pre- and post-cocaine injection, **(B)** Oxidative current-time traces, **(C)** Voltammograms (at the peak) and **(D)** Maximum change in dopamine concentration with medial forebrain bundle stimulation at different time points (n = 4 rats). Black bar represents electrical stimulation (2 s). *denotes $p < 0.05$. n = 4 rats. *DA*, dopamine.

rats) and 60 min after cocaine administration (ratio two-tailed paired t-test, $p = 0.0225$, $n = 4$ rats). With repeated stimulation performed for 60 min after injection, the peak level dropped to the pre-injection baseline level (**Figures 2B,D**).

Using the restricted diffusion model discussed in the Methods section, the reuptake parameters for our experiments were calculated both before and after cocaine administration (**Table 1**). This model includes dopamine release per stimulus pulse and kinetic terms for dopamine reuptake, transport, and release. Cocaine, a dopamine reuptake inhibitor, would be expected to decrease the kinetic parameter for reuptake. Indeed, this is what was found ($p = 0.028$) (**Table 1**). Cocaine administration did not significantly influence the values of the other kinetic parameters.

Tonic Response

As measured by M-CSWV, a representative example of the temporal changes in tonic dopamine levels in response to cocaine administration is shown in **Figure 3**. There were variations in the temporal pattern and time to peak changes in concentration (**Figure 3A**). Baseline recordings were taken for 30 min (**Figure 3B**), and saline was injected as a control (**Figure 3C**). Cocaine was injected 90 min later and showed a significant increase in tonic dopamine levels (**Figures 3D–F**). The tonic dopamine levels were measured for 60–70 min post cocaine injection. Overall, cocaine injections significantly increased dopamine levels in NAcc from 134 ± 32 nM to 281 ± 60 nM (ratio two-tailed paired t-test, $p = 0.002$, $n = 5$ rats) (**Figure 3F**).

DISCUSSION

This is the first study to characterize changes in tonic dopamine levels in the NAcc in the presence of cocaine in near real-time with an electrochemical technique *in vivo*. By utilizing the M-CSWV technique with its unrivaled temporal resolution and high spatial resolution provided by CFMs, we have

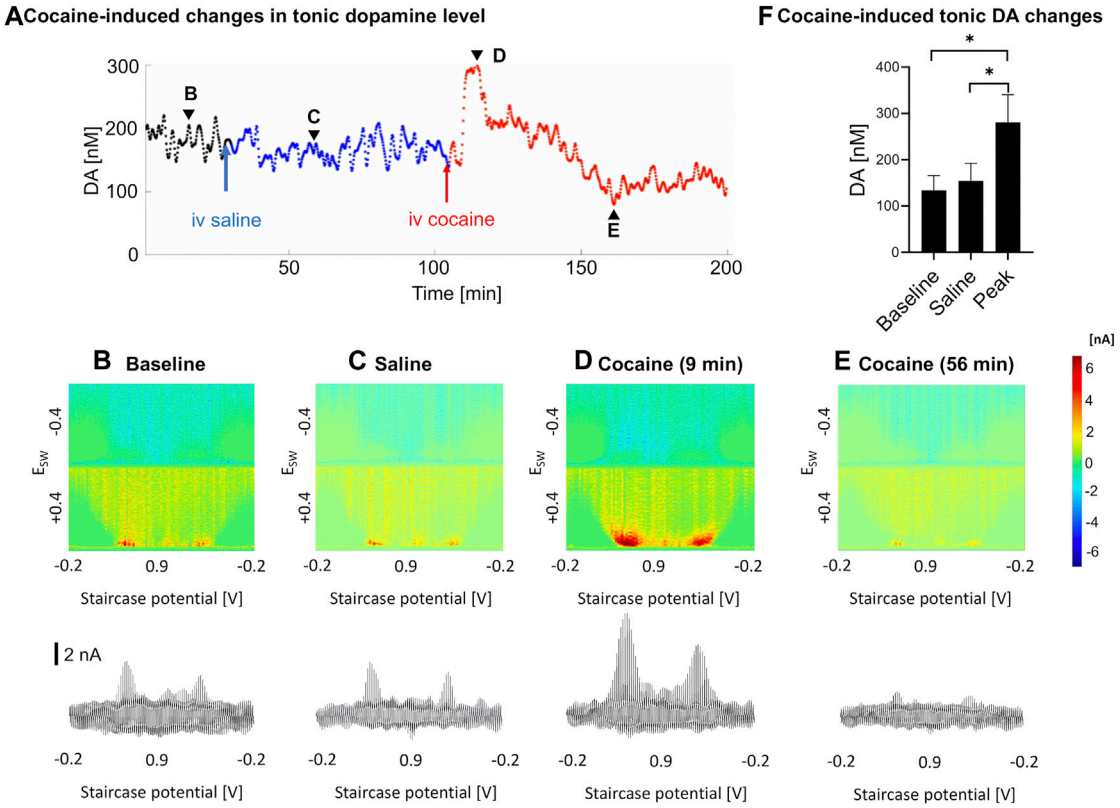

FIGURE 3 | An example of tonic dopamine measurements obtained from the nucleus accumbens core in a single rat with saline then cocaine i.v. injections. **(A)**. Changes in tonic dopamine concentration over time, where the black line denotes the stabilization period, blue line denotes control (saline) and red line denotes post-cocaine measurements. **(B–E)**. High-dimension color plots and voltammograms pre- and post-injections, corresponding to the time points (arrowheads) in **(A)**, respectively, **(F)** Comparison of tonic dopamine concentrations pre- and post-(peak) injection. Ratio two-tailed paired *t*-test, $p = 0.002$, $n = 5$ rats. See supplementary information for a video of the experiment. *DA*, dopamine.

demonstrated a more precise picture of how tonic dopamine dynamics change in response to acute cocaine administration.

Effects of Cocaine on Phasic Dopamine Release

The main findings of our study (see **Figures 2A–D**) are consistent with the literature which has shown that cocaine (and opioids) leads to increases in dopamine responses in the core of the nucleus accumbens as measured using FSCV (Aragona et al., 2008; Vander Weele et al., 2014). Aside from the robust increase in stimulation-evoked dopamine release after cocaine administration, dopamine release appeared to drop to below pre-cocaine levels (see **Figure 2D**). However, this did not reach statistical significance with this sample size. This may be due to blockade of dopamine reuptake by cocaine leading to decreased releasable vesicular pool over the course of the cocaine effect, as well as the effect of continuous stimulation. However, the latter is less likely to be the main contributor, given the synapses were provided at least 10 min to recover between stimulations. Further experiments would help to confirm this phenomenon. Also, the reuptake constant, k_U was lowered after cocaine administration, which is expected since cocaine is a competitive antagonist of the dopamine transporter and k_U is directly proportional to reuptake rate (see **Table 1**). Cocaine administration would not be expected to influence kinetic parameters for transport between the synapse and the electrode. Consistent with these expectations, these other parameters were not significantly influenced by cocaine administration.

From previous studies, it was found that the NAcc appears to consist of a patchwork of domains that show distinct dopamine kinetics, each demonstrating slow and/or fast evoked responses when the MFB is stimulated (Shu et al., 2013). The dopamine phasic response within the core is also heterogenous in response to cocaine self-administration (Owesson-White et al., 2009). This may explain why there are differences in our values, compared to values published by Walters et al. (2015), as well as the fact that we used different pharmacological agents. The differences may be accounted for by different stimulation parameters, especially the duration of stimulation. However, they do have similar orders of magnitude, which is expected, as both cocaine and nomifensine act by limiting the reuptake of dopamine. As far as we are aware, no studies have used this model to evaluate the evoked response

of cocaine, therefore, our results could provide a benchmark for future studies.

Effects of Cocaine on Tonic Dopamine Levels

In previous microdialysis studies where cocaine was given acutely (Bradberry et al., 1993; Pontieri et al., 1995), intravenous cocaine led to rapid rise in nucleus accumbens tonic dopamine levels, which peaked at 10–20 min (where dopamine was measured at 10–20 min intervals). Peak levels of dopamine varied between 150 to 400% of baseline. In addition, in pharmacokinetic studies, cocaine was eliminated in a biexponential manner after i.v. administration with mean elimination half-lives of 4.4 and 24.8 min, with a rapidly decaying serum concentration (Ma et al., 1999; Sun and Lau, 2001). In our study, a trough was observed in a subset of samples after the peak but not in all (see **Figure 3A**). This may be due to dopamine depletion after the sharp increase. This may be analogous to the small drop in the mean phasic response at ~60 min compared to pre-cocaine baseline. Further experiments are needed to confirm this phenomenon.

Previous studies have shown that dopamine release varies widely among test subjects and within dopaminergic structures (Verheij et al., 2008; Owesson-White et al., 2009; Shu et al., 2013), necessitating a trial-and-error approach where the depths of CFM and stimulating electrodes are continually adjusted until the so-called "hotspot" is found. This hotspot is thought to occur when the CFM is close to a site of large synaptic release of dopamine. Variations in the location and behavior of these hotspots may explain the variable effects we see after cocaine administration in our study.

Overall, the present results suggest that M-CSWV can measure drug-induced changes in tonic dopamine levels with high temporal and spatial resolution when compared to microdialysis. Most of these studies used microdialysis with a temporal resolution of 10–20 min (Bradberry et al., 1993; Pontieri et al., 1995; Cadoni et al., 2000). Despite recent developments to reduce the resolution from 20 min down to 1 min (Gu et al., 2015; Ngo et al., 2017), M-CSWV still provides a much higher time resolution with the added benefit of spatial resolution and minimal tissue disruption when used with CFMs.

It is important to note however, that there are two major differences in our M-CSWV results in comparison to microdialysis. First, the tonic dopamine concentrations are very different in magnitude. Our baseline dopamine levels, determined by post-*in vivo* calibration, were at around 100–200 nM; whereas microdialysis studies commonly report values between 10 to 20 nM (Bradberry et al., 1993; Cadoni et al., 2000). Although the order of magnitude differs by a factor of ten, our values are broadly consistent with previous accumbal and striatal dopamine concentrations measured by various electrochemical techniques (Blaha, 1996; Atcherley et al., 2015; Johnson et al., 2017; Oh et al., 2018; Taylor et al., 2019; Barath et al., 2020). The possibility that other interferents such as norepinephrine, which has similar electrochemical properties as dopamine, may be a contributing factor in the differences is unlikely since other studies have demonstrated that the amount of norepinephrine and serotonin in the NAcc is comparatively low (Andrews and Lucki, 2001; McKittrick and Abercrombie, 2007; Zhang et al., 2020). Therefore, the disparities likely represent the fundamental differences between microdialysis and electrochemical techniques. Previous studies have suggested that the traumatized layer of tissue of the order of 200 μm caused by the relatively large diameter of the microdialysis probe may lead to a reduction in dopamine extraction, although relative changes could still be measured (Peters and Michael, 1998; Bungay et al., 2003; Borland et al., 2005). This is minimized by the relatively small diameter of the carbon fibers used in voltammetry. Being able to identify tonic values may help to quantify differences between subjects, as well as the diagnosis of different pathologies, especially given some neuropathological diseases are known to be driven by degeneration and depletion of neurotransmitters such as dopamine (Denys et al., 2004; Beitz, 2014; Oliva and Wanat, 2016; Maia and Conceicao, 2018). With these advantages, there is a strong argument that dopamine levels measured by M-CSWV can serve as important biomarkers for monitoring treatments with rapid bioavailability such as deep brain stimulation.

The other major difference is the relative change in magnitude. Rather than a 400% increase as in the described literature, in our study the dopamine signal mostly doubled. This may again be attributed to the underestimation of baseline in microdialysis, as well as the possibility that cocaine-induced increases in synaptic dopamine may be affected by factors related to the physical presence of the microdialysis probe, such as the formation of a layer of traumatized tissue (Di Chiara et al., 1993; Blaha et al., 1996). The rate and dose of drug administration may also have an impact (Minogianis et al., 2019). As mentioned in the Methods section, the rate was controlled at 5-min duration to avoid overdosing. The use of different anesthetic agents in other studies, such as chloral hydrate, may also lead to discrepancies in results (Bradberry et al., 1993).

Our study focused on the NAcc, so the results should not be generalized to the nucleus accumbens shell, since they are distinct subdivisions of the accumbens or other regions. For example, in one *in vitro* FSCV study, dopamine uptake in the shell was approximately one-third of that measured in the core, and the former was less sensitive to both cocaine and nomifensine (dopamine reuptake inhibitor) (Jones et al., 1996). Also, intravenous cocaine increased extracellular dopamine in the shell more markedly than in the core of the rat nucleus accumbens. Another study utilized immunochemistry to demonstrate that dopaminergic axons in the shell contained lower densities of dopamine transporter than those in the core (Nirenberg et al., 1997). This suggests a more tightly regulated phasic dopamine transmission in this subregion and highlights the value of both phasic and tonic measurements across both regions for future work. In addition, Dreyer *et al.* utilized a computer model to interpret *in vivo* FSCV data from the NAcc and shell after rodents were administered cocaine (Dreyer et al., 2016). After studying the dynamics involved in presynaptic terminal autoreceptor feedback, they concluded that extracellular dopamine concentrations in the core resulted

from constant dopamine firing, whereas the shell concentrations reflected dynamic firing patterns. This supported our decision to record from the NAcc using this new tonic dopamine measurement method.

While our technique focuses on a single analyte, dopamine, and therefore may not be as comprehensive as microdialysis studies, precise measurement of dopamine alone is still highly important. Dopamine has a major role in the reward circuit and is one of the key neurotransmitters in the pathophysiology of addiction (Berke and Hyman, 2000). Newer techniques have also been devised to voltammetrically measure serotonin with high sensitivity and selectivity, which can be incorporated in future study designs (Shin et al., 2020). DLight, which is a new technique that uses genetically encoded indicators based on fluorescent proteins with microscopy also allows measurements of neurochemicals with high temporal resolution (Patriarchi et al., 2018). However, the need for a viral vector currently limits its potential use in human subjects.

Another notable characteristic of this study is that the animal experiments were performed under anesthesia in an acute setting using a single dose of cocaine. While we appreciate that addiction is often secondary to chronic drug use in humans, acute experiments offer insight into the first step of the pathophysiological process. Additionally, this study paves the way for future chronic experiments by proving the feasibility of this technique to study the effects of other drugs of abuse. In the future, it is our intention to apply the M-CSWV intraoperatively, particularly in the context of neurological (e.g., Parkinson's disease) and psychiatric (e.g., addiction) disorders.

Although cocaine is known to enhance dopamine transmission in the nucleus accumbens, this is the first study that utilized M-CSWV to measure accumbal tonic dopamine levels, and to characterize the effect of cocaine on these levels in near real-time. Overall, this technique provides unprecedented insight into the temporal changes in dopamine dynamics, and it will likely be of much value in future addiction studies.

Supplementary video. An example of tonic dopamine measurements obtained from the NAcc in a single rat with saline then cocaine i.v. injections. Upper panel shows the color plot and the lower panel shows the changes in tonic dopamine concentration over time, where the black line denotes the stabilization period, blue line denotes control (saline) and red line denotes post-cocaine measurements.

DATA AVAILABILITY STATEMENT

The data presented in the study are included in the article, further inquiries can be directed to the corresponding author.

ETHICS STATEMENT

The animal study was reviewed and approved by the Institutional Animal Care and Use Committee (IACUC), Mayo Clinic, Rochester, MN.

AUTHOR CONTRIBUTIONS

KL, D-PJ, and YO conceptualized the study. JY, AR, and HS conducted experiments and collected the data. JY, YO, and HS designed the analyses. JY and HS conducted the analyses. AG and HS assisted in software and conducting the analysis on phasic responses. JY drafted the first manuscript. AK, MB, JK, ST, CB, KB, KL, D-PJ, and YO critically reviewed and revised the manuscript. KL, HS, and YO supervised all aspects of this work. JY drafted the figures. All authors accepted the final version of the article.

FUNDING

This research was supported by the NIH R01NS112176 award and Minnesota Partnership for Biotechnology and Medical Genomics Grant MNP #19.13. Training grant funding for AR was supported by NIH F31NS115202-01A1, NIH R25GM055252-23, NIH TL1TR002380-03, and NIH T32GM065841-17. MB is supported by a NHMRC Senior Principal Research Fellowship (1156072).

SUPPLEMENTARY MATERIAL

The Supplementary Material for this article can be found online at: https://www.frontiersin.org/articles/10.3389/fphar.2021.705254/full#supplementary-material

REFERENCES

Abdalla, A., Atcherley, C. W., Pathirathna, P., Samaranayake, S., Qiang, B., Peña, E., et al. (2017). *In Vivo* Ambient Serotonin Measurements at Carbon-Fiber Microelectrodes. *Anal. Chem.* 89 (18), 9703–9711. doi:10.1021/acs.analchem.7b01257

Andrews, C., and Lucki, I. (2001). Effects of Cocaine on Extracellular Dopamine and Serotonin Levels in the Nucleus Accumbens. *Psychopharmacology* 155 (3), 221–229. doi:10.1007/s002130100704

Aragona, B. J., Cleaveland, N. A., Stuber, G. D., Day, J. J., Carelli, R. M., and Wightman, R. M. (2008). Preferential Enhancement of Dopamine Transmission within the Nucleus Accumbens Shell by Cocaine Is Attributable to a Direct Increase in Phasic Dopamine Release Events. *J. Neurosci.* 28 (35), 8821–8831. doi:10.1523/JNEUROSCI.2225-08.2008

Atcherley, C. W., Laude, N. D., Parent, K. L., and Heien, M. L. (2013). Fast-scan Controlled-Adsorption Voltammetry for the Quantification of Absolute Concentrations and Adsorption Dynamics. *Langmuir* 29 (48), 14885–14892. doi:10.1021/la402686s

Atcherley, C. W., Wood, K. M., Parent, K. L., Hashemi, P., and Heien, M. L. (2015). The Coaction of Tonic and Phasic Dopamine Dynamics. *Chem. Commun.* 51 (12), 2235–2238. doi:10.1039/c4cc06165a

Barath, A. S., Rusheen, A. E., Rojas Cabrera, J. M., Price, J. B., Owen, R. L., Shin, H., et al. (2020). Hypoxia-Associated Changes in Striatal Tonic Dopamine Release: Real-Time *In Vivo* Measurements with a Novel Voltammetry Technique. *Front. Neurosci.* 14, 869. doi:10.3389/fnins.2020.00869

Beitz, J. M. (2014). Parkinson S Disease a Review. *Front. Biosci.* S6, 65–74. doi:10.2741/s415

Berke, J. D., and Hyman, S. E. (2000). Addiction, Dopamine, and the Molecular Mechanisms of Memory. *Neuron* 25 (3), 515–532. doi:10.1016/s0896-6273(00)81056-9

Berke, J. D. (2018). What Does Dopamine Mean?. *Nat. Neurosci.* 21 (6), 787–793. doi:10.1038/s41593-018-0152-y

Blaha, C. D., and Phillips, A. G. (1996). A Critical Assessment of Electrochemical Procedures Applied to the Measurement of Dopamine and its Metabolites during Drug-Induced and Species-Typical Behaviours. *Behav. Pharmacol.* 7 (7), 675–708. doi:10.1097/00008877-199611000-00014

Blaha, C. D., Coury, A., and Phillips, A. G. (1996). Does Monoamine Oxidase Inhibition by Pargyline Increase Extracellular Dopamine Concentrations in the Striatum?. *Neuroscience* 75 (2), 543–550. doi:10.1016/0306-4522(96)00289-8

Blaha, C. D. (1996). Evaluation of Stearate-Graphite Paste Electrodes for Chronic Measurement of Extracellular Dopamine Concentrations in the Mammalian Brain. *Pharmacol. Biochem. Behav.* 55 (3), 351–364. doi:10.1016/s0091-3057(96)00104-9

Borland, L. M., Shi, G., Yang, H., and Michael, A. C. (2005). Voltammetric Study of Extracellular Dopamine Near Microdialysis Probes Acutely Implanted in the Striatum of the Anesthetized Rat. *J. Neurosci. Methods* 146 (2), 149–158. doi:10.1016/j.jneumeth.2005.02.002

Bradberry, C. W., Nobiletti, J. B., Elsworth, J. D., Murphy, B., Jatlow, P., and Roth, R. H. (1993). Cocaine and Cocaethylene: Microdialysis Comparison of Brain Drug Levels and Effects on Dopamine and Serotonin. *J. Neurochem.* 60 (4), 1429–1435. doi:10.1111/j.1471-4159.1993.tb03305.x

Bungay, P. M., Newton-Vinson, P., Isele, W., Garris, P. A., and Justice, J. B. (2003). Microdialysis of Dopamine Interpreted with Quantitative Model Incorporating Probe Implantation Trauma. *J. Neurochem.* 86 (4), 932–946. doi:10.1046/j.1471-4159.2003.01904.x

Burrell, M. H., Atcherley, C. W., Heien, M. L., and Lipski, J. (2015). A Novel Electrochemical Approach for Prolonged Measurement of Absolute Levels of Extracellular Dopamine in Brain Slices. *ACS Chem. Neurosci.* 6 (11), 1802–1812. doi:10.1021/acschemneuro.5b00120

Cadoni, C., Solinas, M., and Di Chiara, G. (2000). Psychostimulant Sensitization: Differential Changes in Accumbal Shell and Core Dopamine. *Eur. J. Pharmacol.* 388 (1), 69–76. doi:10.1016/s0014-2999(99)00824-9

Chang, S.-Y., Kimble, C. J., Kim, I., Paek, S. B., Kressin, K. R., Boesche, J. B., et al. (2013). Development of the Mayo Investigational Neuromodulation Control System: toward a Closed-Loop Electrochemical Feedback System for Deep Brain Stimulation. *Jns* 119 (6), 1556–1565. doi:10.3171/2013.8.JNS122142

Chefer, V. I., Thompson, A. C., Zapata, A., and Shippenberg, T. S. (2009). Overview of Brain Microdialysis. *Curr. Protoc. Neurosci.* 47, 2009 Chapter 7, Unit7.1. doi:10.1002/0471142301.ns0701s47

Clark, J. J., Sandberg, S. G., Wanat, M. J., Gan, J. O., Horne, E. A., Hart, A. S., et al. (2010). Chronic Microsensors for Longitudinal, Subsecond Dopamine Detection in Behaving Animals. *Nat. Methods* 7 (2), 126–129. doi:10.1038/nmeth.1412

Denys, D., Zohar, J., and Westenberg, H. G. (2004). The Role of Dopamine in Obsessive-Compulsive Disorder: Preclinical and Clinical Evidence. *J. Clin. Psychiatry* 65 (Suppl. 14), 11–17. doi:10.4088/jcp.v65n0803

Di Chiara, G., Carboni, E., Morelli, M., Cozzolino, A., Tanda, G. L., Pinna, A., et al. (1993). Stimulation of Dopamine Transmission in the Dorsal Caudate Nucleus by Pargyline as Demonstrated by Dopamine and Acetylcholine Microdialysis and Fos Immunohistochemistry. *Neuroscience* 55 (2), 451–456. doi:10.1016/0306-4522(93)90514-g

Dreher, J. C., and Burnod, Y. (2002). An Integrative Theory of the Phasic and Tonic Modes of Dopamine Modulation in the Prefrontal Cortex. *Neural Netw.* 15 (4-6), 583–602. doi:10.1016/s0893-6080(02)00051-5

Dreyer, J. K., Vander Weele, C. M., Lovic, V., and Aragona, B. J. (2016). Functionally Distinct Dopamine Signals in Nucleus Accumbens Core and Shell in the Freely Moving Rat. *J. Neurosci.* 36 (1), 98–112. doi:10.1523/jneurosci.2326-15.2016

Goto, Y., Otani, S., and Grace, A. (2007). The Yin and Yang of Dopamine Release: a New Perspective. *Neuropharmacology* 53 (5), 583–587. doi:10.1016/j.neuropharm.2007.07.007

Grace, A. A. (1991). Phasic versus Tonic Dopamine Release and the Modulation of Dopamine System Responsivity: a Hypothesis for the Etiology of Schizophrenia. *Neuroscience* 41 (1), 1–24. doi:10.1016/0306-4522(91)90196-u

Grace, A. A. (2016). Dysregulation of the Dopamine System in the Pathophysiology of Schizophrenia and Depression. *Nat. Rev. Neurosci.* 17 (8), 524–532. doi:10.1038/nrn.2016.57

Gu, H., Varner, E. L., Groskreutz, S. R., Michael, A. C., and Weber, S. G. (2015). *In Vivo* Monitoring of Dopamine by Microdialysis with 1 Min Temporal Resolution Using Online Capillary Liquid Chromatography with Electrochemical Detection. *Anal. Chem.* 87 (12), 6088–6094. doi:10.1021/acs.analchem.5b00633

Heien, M. L., Johnson, M. A., and Wightman, R. M. (2004). Resolving Neurotransmitters Detected by Fast-Scan Cyclic Voltammetry. *Anal. Chem.* 76 (19), 5697–5704. doi:10.1021/ac0491509

Hodebourg, R., Murray, J. E., Fouyssac, M., Puaud, M., Everitt, B. J., and Belin, D. (2019). Heroin Seeking Becomes Dependent on Dorsal Striatal Dopaminergic Mechanisms and Can Be Decreased by N-acetylcysteine. *Eur. J. Neurosci.* 50 (3), 2036–2044. doi:10.1111/ejn.13894

Howell, J. O., Kuhr, W. G., Ensman, R. E., and Mark Wightman, R. (1986). Background Subtraction for Rapid Scan Voltammetry. *J. Electroanal. Chem. Interfacial Electrochem.* 209(1), 77–90. doi:10.1016/0022-0728(86)80187-5

Huffman, M. L., and Venton, B. J. (2009). Carbon-fiber Microelectrodes for *In Vivo* Applications. *Analyst* 134 (1), 18–24. doi:10.1039/b807563h

Ito, R., Dalley, J. W., Robbins, T. W., and Everitt, B. J. (2002). Dopamine Release in the Dorsal Striatum during Cocaine-Seeking Behavior under the Control of a Drug-Associated Cue. *J. Neurosci.* 22 (14), 6247–6253. doi:10.1523/jneurosci.22-14-06247.2002

John, W. S., and Wu, L.-T. (2017). Trends and Correlates of Cocaine Use and Cocaine Use Disorder in the United States from 2011 to 2015. *Drug and Alcohol Depend.* 180, 376–384. doi:10.1016/j.drugalcdep.2017.08.031

Johnson, J. A., Hobbs, C. N., and Wightman, R. M. (2017). Removal of Differential Capacitive Interferences in Fast-Scan Cyclic Voltammetry. *Anal. Chem.* 89 (11), 6166–6174. doi:10.1021/acs.analchem.7b01005

Jones, S. R., O'Dell, S. J., Marshall, J. F., and Wightman, R. M. (1996). Functional and Anatomical Evidence for Different Dopamine Dynamics in the Core and Shell of the Nucleus Accumbens in Slices of Rat Brain. *Synapse* 23 (3), 224–231. doi:10.1002/(sici)1098-2396(199607)23:3<224::aid-syn12>3.0.co;2-z

Kalivas, P. W., and O'Brien, C. (2008). Drug Addiction as a Pathology of Staged Neuroplasticity. *Neuropsychopharmacol* 33 (1), 166–180. doi:10.1038/sj.npp.1301564

Kim, J., Oh, Y., Park, C., Kang, Y. M., Shin, H., Kim, I. Y., et al. (2019). Comparison Study of Partial Least Squares Regression Analysis and Principal Component Analysis in Fast-Scan Cyclic Voltammetry. *Int. J. Electrochem. Sci.* 14 (7), 5924–5937. doi:10.20964/2019.07.03

Kim, J., Barath, A. S., Rusheen, A. E., Rojas Cabrera, J. M., Price, J. B., Shin, H., et al. (2021). Automatic and Reliable Quantification of Tonic Dopamine Concentrations *In Vivo* Using a Novel Probabilistic Inference Method. *ACS Omega* 6 (10), 6607–6613. doi:10.1021/acsomega.0c05217

Lama, R. D., Charlson, K., Anantharam, A., and Hashemi, P. (2012). Ultrafast Detection and Quantification of Brain Signaling Molecules with Carbon Fiber Microelectrodes. *Anal. Chem.* 84 (19), 8096–8101. doi:10.1021/ac301670h

Lee, K. H., Lujan, J. L., Trevathan, J. K., Ross, E. K., Bartoletta, J. J., Park, H. O., et al. (2017). WINCS Harmoni: Closed-Loop Dynamic Neurochemical Control of Therapeutic Interventions. *Sci. Rep.* 7, 46675. doi:10.1038/srep46675

Ma, F., Falk, J. L., and Lau, C. E. (1999). Cocaine Pharmacodynamics after Intravenous and Oral Administration in Rats: Relation to Pharmacokinetics. *Psychopharmacology* 144 (4), 323–332. doi:10.1007/s002130051014

Maia, T. V., and Conceição, V. A. (2018). Dopaminergic Disturbances in Tourette Syndrome: An Integrative Account. *Biol. Psychiatry* 84 (5), 332–344. doi:10.1016/j.biopsych.2018.02.1172

McKittrick, C. R., and Abercrombie, E. D. (2007). Catecholamine Mapping within Nucleus Accumbens: Differences in Basal and Amphetamine-Stimulated Efflux of Norepinephrine and Dopamine in Shell and Core. *J. Neurochem.* 100 (5), 1247–1256. doi:10.1111/j.1471-4159.2006.04300.x

McLellan, A. T., Lewis, D. C., O'Brien, C. P., and Kleber, H. D. (2000). Drug Dependence, a Chronic Medical Illness. *JAMA* 284 (13), 1689–1695. doi:10.1001/jama.284.13.1689

Millar, J. (1997). *In Vivo* detection of Neurotransmitters with Fast Cyclic Voltammetry. *Methods Mol. Biol.* 72, 251–266. doi:10.1385/0-89603-394-5:251

Minogianis, E. A., Shams, W. M., Mabrouk, O. S., Wong, J. M. T., Brake, W. G., Kennedy, R. T., et al. (2019). Varying the Rate of Intravenous Cocaine Infusion Influences the Temporal Dynamics of Both Drug and Dopamine Concentrations in the Striatum. *Eur. J. Neurosci.* 50 (3), 2054–2064. doi:10.1111/ejn.13941

Morelli, M., Carboni, E., Cozzolino, A., Tanda, G. L., Pinna, A., and Chiara, G. (1992). Combined Microdialysis and Fos Immunohistochemistry for the Estimation of Dopamine Neurotransmission in the Rat Caudate-Putamen. *J. Neurochem.* 59 (3), 1158–1160. doi:10.1111/j.1471-4159.1992.tb08359.x

Murray, J. E., Belin, D., and Everitt, B. J. (2012). Double Dissociation of the Dorsomedial and Dorsolateral Striatal Control over the Acquisition and Performance of Cocaine Seeking. *Neuropsychopharmacol* 37 (11), 2456–2466. doi:10.1038/npp.2012.104

Ng, J. P., Hubert, G. W., and Justice, J. B., Jr. (1991). Increased Stimulated Release and Uptake of Dopamine in Nucleus Accumbens after Repeated Cocaine Administration as Measured by *In Vivo* Voltammetry. *J. Neurochem.* 56 (5), 1485–1492. doi:10.1111/j.1471-4159.1991.tb02042.x

Ngo, K. T., Varner, E. L., Michael, A. C., and Weber, S. G. (2017). Monitoring Dopamine Responses to Potassium Ion and Nomifensine by *In Vivo* Microdialysis with Online Liquid Chromatography at One-Minute Resolution. *ACS Chem. Neurosci.* 8 (2), 329–338. doi:10.1021/acschemneuro.6b00383

Nirenberg, M. J., Chan, J., Pohorille, A., Vaughan, R. A., Uhl, G. R., Kuhar, M. J., et al. (1997). The Dopamine Transporter: Comparative Ultrastructure of Dopaminergic Axons in Limbic and Motor Compartments of the Nucleus Accumbens. *J. Neurosci.* 17 (18), 6899–6907. doi:10.1523/jneurosci.17-18-06899.1997

Oh, Y., Park, C., Kim, D. H., Shin, H., Kang, Y. M., DeWaele, M., et al. (2016). Monitoring *In Vivo* Changes in Tonic Extracellular Dopamine Level by Charge-Balancing Multiple Waveform Fast-Scan Cyclic Voltammetry. *Anal. Chem.* 88 (22), 10962–10970. doi:10.1021/acs.analchem.6b02605

Oh, Y., Heien, M. L., Park, C., Kang, Y. M., Kim, J., Boschen, S. L., et al. (2018). Tracking Tonic Dopamine Levels *In Vivo* Using Multiple Cyclic Square Wave Voltammetry. *Biosens. Bioelectron.* 121, 174–182. doi:10.1016/j.bios.2018.08.034

Oliva, I., and Wanat, M. J. (2016). Ventral Tegmental Area Afferents and Drug-dependent Behaviors. *Front. Psychiatry* 7, 30. doi:10.3389/fpsyt.2016.00030

Owesson-White, C. A., Ariansen, J., Stuber, G. D., Cleaveland, N. A., Cheer, J. F., Mark Wightman, R., et al. (2009). Neural Encoding of Cocaine-Seeking Behavior Is Coincident with Phasic Dopamine Release in the Accumbens Core and Shell. *Eur. J. Neurosci.* 30 (6), 1117–1127. doi:10.1111/j.1460-9568.2009.06916.x

Patriarchi, T., Cho, J. R., Merten, K., Howe, M. W., Marley, A., Xiong, W.-H., et al. (2018). Ultrafast Neuronal Imaging of Dopamine Dynamics with Designed Genetically Encoded Sensors. *Science* 360 (6396), eaat4422. doi:10.1126/science.aat4422

Paxinos, G., and Watson, C. (2007). *The Rat Brain in Stereotaxic Coordinates*. Amsterdam; Boston: Academic Press/Elsevier.

Peters, J. L., and Michael, A. C. (1998). Modeling Voltammetry and Microdialysis of Striatal Extracellular Dopamine: the Impact of Dopamine Uptake on Extraction and Recovery Ratios. *J. Neurochem.* 70 (2), 594–603. doi:10.1046/j.1471-4159.1998.70020594.x

Pontieri, F. E., Tanda, G., and Di Chiara, G. (1995). Intravenous Cocaine, Morphine, and Amphetamine Preferentially Increase Extracellular Dopamine in the "shell" as Compared with the "core" of the Rat Nucleus Accumbens. *Proc. Natl. Acad. Sci.* 92 (26), 12304–12308. doi:10.1073/pnas.92.26.12304

Robinson, D. L., Venton, B. J., Heien, M. L. A. V., and Wightman, R. M. (2003). Detecting Subsecond Dopamine Release with Fast-Scan Cyclic Voltammetry *In Vivo*. *Clin. Chem.* 49 (10), 1763–1773. doi:10.1373/49.10.1763

Rodeberg, N. T., Sandberg, S. G., Johnson, J. A., Phillips, P. E. M., and Wightman, R. M. (2017). Hitchhiker's Guide to Voltammetry: Acute and Chronic Electrodes for *In Vivo* Fast-Scan Cyclic Voltammetry. *ACS Chem. Neurosci.* 8 (2), 221–234. doi:10.1021/acschemneuro.6b00393

Rusheen, A. E., Gee, T. A., Jang, D. P., Blaha, C. D., Bennet, K. E., Lee, K. H., et al. (2020). Evaluation of Electrochemical Methods for Tonic Dopamine Detection *In Vivo*. *Trac Trends Anal. Chem.* 132, 116049. doi:10.1016/j.trac.2020.116049

Schultz, W. (2007). Behavioral Dopamine Signals. *Trends Neurosciences* 30 (5), 203–210. doi:10.1016/j.tins.2007.03.007

Shin, H., Oh, Y., Park, C., Kang, Y., Cho, H. U., Blaha, C. D., et al. (2020). Sensitive and Selective Measurement of Serotoninin VivoUsing Fast Cyclic Square-Wave Voltammetry. *Anal. Chem.* 92 (1), 774–781. doi:10.1021/acs.analchem.9b03164

Shu, Z., Taylor, I. M., and Michael, A. C. (2013). The Dopamine Patchwork of the Rat Nucleus Accumbens Core. *Eur. J. Neurosci.* 38 (8), 3221–3229. doi:10.1111/ejn.12319

Substance Abuse and Mental Health Services Administration (2020). *Key Substance Use and Mental Health Indicators in the United States: Results from the 2019 National Survey on Drug Use and Health (HHS Publication No. PEP20-07-01-001, NSDUH Series H-55)*. Rockville, MD: Center for Behavioral Health Statistics and Quality, Substance Abuse and Mental Health Services Administration. Available at: https://www.samhsa.gov/data/ (Accessed March 20, 2021).

Sun, L., and Lau, C. E. (2001). Simultaneous Pharmacokinetic Modeling of Cocaine and its Metabolites, Norcocaine and Benzoylecgonine, after Intravenous and Oral Administration in Rats. *Drug Metab. Dispos* 29 (9), 1183–1189.

Taylor, I. M., Patel, N. A., Freedman, N. C., Castagnola, E., and Cui, X. T. (2019). Direct *In Vivo* Electrochemical Detection of Resting Dopamine Using Poly(3,4-ethylenedioxythiophene)/Carbon Nanotube Functionalized Microelectrodes. *Anal. Chem.* 91 (20), 12917–12927. doi:10.1021/acs.analchem.9b02904

Vander Weele, C. M., Porter-Stransky, K. A., Mabrouk, O. S., Lovic, V., Singer, B. F., Kennedy, R. T., et al. (2014). Rapid Dopamine Transmission within the Nucleus Accumbens: Dramatic Difference between Morphine and Oxycodone Delivery. *Eur. J. Neurosci.* 40 (7), 3041–3054. doi:10.1111/ejn.12709

Vanderschuren, L. J. M. J., Di Ciano, P., and Everitt, B. J. (2005). Involvement of the Dorsal Striatum in Cue-Controlled Cocaine Seeking. *J. Neurosci.* 25 (38), 8665–8670. doi:10.1523/JNEUROSCI.0925-05.2005

Verheij, M. M. M., de Mulder, E. L. W., De Leonibus, E., van Loo, K. M. J., and Cools, A. R. (2008). Rats that Differentially Respond to Cocaine Differ in Their Dopaminergic Storage Capacity of the Nucleus Accumbens. *J. Neurochem.* 105 (6), 2122–2133. doi:10.1111/j.1471-4159.2008.05323.x

Vreeland, R. F., Atcherley, C. W., Russell, W. S., Xie, J. Y., Lu, D., Laude, N. D., et al. (2015). Biocompatible PEDOT:Nafion Composite Electrode Coatings for Selective Detection of Neurotransmitters *In Vivo*. *Anal. Chem.* 87 (5), 2600–2607. doi:10.1021/ac502165f

Walters, S. H., Robbins, E. M., and Michael, A. C. (2015). Modeling the Kinetic Diversity of Dopamine in the Dorsal Striatum. *ACS Chem. Neurosci.* 6 (8), 1468–1475. doi:10.1021/acschemneuro.5b00128

Watson, C. J., Venton, B. J., and Kennedy, R. T. (2006). *In Vivo* measurements of Neurotransmitters by Microdialysis Sampling. *Anal. Chem.* 78 (5), 1391–1399. doi:10.1021/ac0693722

Zbukvic, I. C., Ganella, D. E., Perry, C. J., Madsen, H. B., Bye, C. R., Lawrence, A. J., et al. (2016). Role of Dopamine 2 Receptor in Impaired Drug-Cue Extinction in Adolescent Rats. *Cereb. Cortex* 26 (6), 2895–2904. doi:10.1093/cercor/bhw051

Zhang, Z., Oh, Y., Adams, S. D., Bennet, K. E., and Kouzani, A. Z. (2021). An FSCV Deep Neural Network: Development, Pruning, and Acceleration on an FPGA. *IEEE J. Biomed. Health Inform.* 25, 2248–2259. doi:10.1109/JBHI.2020.3037366

Conflict of Interest: The authors declare that the research was conducted in the absence of any commercial or financial relationships that could be construed as a potential conflict of interest.

frontiers in Pharmacology

ORIGINAL RESEARCH
published: 19 July 2021
doi: 10.3389/fphar.2021.716394

The Role of HSP90α in Methamphetamine/ Hyperthermia-Induced Necroptosis in Rat Striatal Neurons

Lv-shuang Liao[1,2], Shuang Lu[1], Wei-tao Yan[1], Shu-chao Wang[3], Li-min Guo[1], Yan-di Yang[1], Kai Huang[4], Xi-min Hu[1,5], Qi Zhang[1], Jie Yan[6,7] and Kun Xiong[1,8]**

[1]Department of Anatomy and Neurobiology, School of Basic Medical Sciences, Central South University, Changsha, China, [2]School of Physical Education, Hunan Institute of Science and Technology, Yueyang, China, [3]Center for Medical Research, The Second Xiangya Hospital of Central South University, Changsha, China, [4]Department of Human Anatomy and Histoembryolog, School of Basic Medical Sciences, Shaoyang University, Shaoyang, China, [5]Department of Dermatology, Xiangya Hospital, Central South University, Changsha, China, [6]Department of Forensic Science, School of Basic Medical Science, Central South University, Changsha, China, [7]School of Basic Medical Science, Xinjiang Medical University, Urumqi, China, [8]Hunan Key Laboratory of Ophthalmology, Changsha, China

OPEN ACCESS

Edited by:
Di Wen,
Hebei Medical University, China

Reviewed by:
Chun-Xia Yi,
Amsterdam University Medical Center, Netherlands
Pingming Qiu,
Southern Medical University, China
Guo Guo Qing,
Jinan University, China

***Correspondence:**
Kun Xiong
xiongkun2001@163.com
Jie Yan
wills212156@csu.edu.cn

Specialty section:
This article was submitted to Neuropharmacology, a section of the journal Frontiers in Pharmacology

Received: *28 May 2021*
Accepted: *07 July 2021*
Published: *19 July 2021*

Citation:
Liao L, Lu S, Yan W, Wang S, Guo L, Yang Y, Huang K, Hu X, Zhang Q, Yan J and Xiong K (2021) The Role of HSP90α in Methamphetamine/ Hyperthermia-Induced Necroptosis in Rat Striatal Neurons. Front. Pharmacol. 12:716394. doi: 10.3389/fphar.2021.716394

Methamphetamine (METH) is one of the most widely abused synthetic drugs in the world. The users generally present hyperthermia (HT) and psychiatric symptoms. However, the mechanisms involved in METH/HT-induced neurotoxicity remain elusive. Here, we investigated the role of heat shock protein 90 alpha (HSP90α) in METH/HT (39.5°C)-induced necroptosis in rat striatal neurons and an *in vivo* rat model. METH treatment increased core body temperature and up-regulated LDH activity and the molecular expression of canonical necroptotic factors in the striatum of rats. METH and HT can induce necroptosis in primary cultures of striatal neurons. The expression of HSP90α increased following METH/HT injuries. The specific inhibitor of HSP90α, geldanamycin (GA), and *HSP90α* shRNA attenuated the METH/HT-induced upregulation of receptor-interacting protein 3 (RIP3), phosphorylated RIP3, mixed lineage kinase domain-like protein (MLKL), and phosphorylated MLKL. The inhibition of HSP90α protected the primary cultures of striatal neurons from METH/HT-induced necroptosis. In conclusion, HSP90α plays an important role in METH/HT-induced neuronal necroptosis and the HSP90α-RIP3 pathway is a promising therapeutic target for METH/HT-induced neurotoxicity in the striatum.

Keywords: methamphetamine, hyperthermia, heat shock protein 90 alpha, necroptosis, receptor-interacting protein 3

INTRODUCTION

Methamphetamine (METH) is one of the most widely abused synthetic drugs in the world. METH abuse can cause irreversible damage to many systems, such as the nervous system, the cardiovascular system, the digestive system, and the skin (Cadet et al., 2007; Paratz et al., 2016). In particular, the nervous system is one of the most important targets of METH (Degenhardt et al., 2010; Ren et al., 2016). Additionally to its strong addiction properties, METH has a strong toxic effect on the entire nervous system. Striatal neurons are extensively linked to multiple brain regions related to addiction,

learning, and memory. They also play essential roles in stimulating and maintaining movement, emotional control, reward effect, and drug dependence (Alexander et al., 1986; Calabresi et al., 1997). Unfortunately, striatal neurons are very sensitive to METH-induced neurotoxicity (Granado et al., 2010; Yamamoto et al., 2010; Valian et al., 2017; Granado et al., 2018; Lu et al., 2021). Studies have shown the degeneration of dopaminergic terminals and the death of cell bodies in the striatum following METH treatment (Zhu et al., 2009; Ares-Santos et al., 2014). Apoptosis is the most focused type of neuronal cell death. However, the inhibition of the apoptotic pathway only partially inhibited METH-induced cell death (Kanthasamy et al., 2011), suggesting that other forms of cell death may also be involved in METH-induced neurotoxicity.

Necroptosis is a regulated variant of necrosis that displays a necrotic morphological feature (Font-Belmonte et al., 2020). Necroptosis can be regulated, initiated, transmitted, and executed by specific factors and blocked by several inhibitors, such as Necrostatin-1 (Nec-1) (He et al., 2009; Weinlich et al., 2017; Wang et al., 2018c; Lin et al., 2020; Hu et al., 2021; Jiang et al., 2021; Yan et al., 2021). The main factors that participate in necroptosis include receptor-interacting serine/threonine-protein 1 (RIP1), receptor-interacting serine/threonine-protein 3 (RIP3), and mixed lineage kinase domain-like protein (MLKL) (Huang et al., 2013; Ding et al., 2015; Liu et al., 2016; Shang et al., 2017; Wang et al., 2018a; Yuan et al., 2019). In this pathway, RIP3 phosphorylation is a key step in the occurrence of necroptosis. Therefore, RIP3 has been the core and characteristic molecule in the study of necroptosis (Meng et al., 2015). Although Ares-Santos' experiments demonstrated that the neurons in the striatum showed obvious necrotic phenotypes after METH treatment (Ares-Santos et al., 2014), it is still unknown whether METH can induce necroptosis in the striatal neurons that are sensitive to METH neurotoxicity.

Hyperthermia (HT) is a critical mechanism in METH-induced neurotoxicity (Tata and Yamamoto, 2007; Krasnova and Cadet, 2009). A single medium or high dose of METH will cause HT (39–40°C), which is usually maintained for several hours (Behrouzvaziri et al., 2015; Wu et al., 2016). HT aggravates the oxidative stress and excitotoxicity caused by METH (Chauhan et al., 2014) and increases the damage to the nervous system (e.g., neuron death) (He et al., 2004). An elevated core body temperature can rapidly upregulate a variety of stress proteins, such as heat shock proteins (HSPs) (Yan et al., 2006). HSP90 belongs to one of the subfamilies of the HSPs family. It consists of two subtypes, the stress-inducible HSP90α and the constitutively expressed HSP90β (Voss et al., 2000; Sreedhar et al., 2004; Grad et al., 2010). It has been suggested that the up-regulated HSP90α acts as a molecular chaperone that stabilizes RIP1 and RIP3 and mediates necroptosis (Li et al., 2015; Li et al., 2016; Wang et al., 2018b). Our previous studies showed the significant upregulation of HSP90 mRNA in rat cortical neurons exposed to METH treatment (Xiong et al., 2017). Meanwhile, our preliminary results showed an upregulation of RIP3 and phosphorylated RIP3 (p-RIP3) in cortical brain sections of patients who died from a METH overdose (Guo et al., 2020). Based on the METH-induced HT and the possible modulatory role of HSP90α on necroptosis, we asked whether HSP90α had a significant impact on METH/HT-induced necroptosis in striatal neurons. Our investigation shed new light on the regulatory mechanism of METH/HT-induced injury.

MATERIALS AND METHODS

Primary Striatal Neuron Cultures and *in vitro* Model Preparation

All experimental procedures were approved by the Medical Ethics Committee of the Third Xiangya Hospital of Central South University in accordance with the Guidelines for the Care and Use of Laboratory Animals (U.S. National Institutes of Health). Primary cultures of rat striatum tissues were separated from fetal Sprague-Dawley (SD) rats (embryonic day 17). In brief, rat striatum tissues were extracted with the aid of a dissecting microscope under sterile conditions. The striatum tissues were digested at 37°C for 10 min in Dulbecco's modified Eagle's medium (DMEM, GE Health care, Logan Utah, United States) containing 0.02% papain and then the tissues were gently triturated for 20 times and filtered through a 70 μm nylon cell sieve, followed with 5 min centrifugation. After resuspension in plating medium consisted of DMEM supplemented with 10% heat-inactivated fetal bovine serum (FBS), 5% heat-inactivated horse serum, 1 mM L-glutamine, cells were counted and plated onto flasks or plates precoated with poly-D-lysine (10 μg/ml, Sigma-Aldrich, St. Louis, United States) at a density of 6×10^5 cells/ml. Cells were maintained at 37°C for 4 h in a 5% CO_2 incubator after plating, followed by replacing the plating medium with neurobasal medium (Thermo Scientific, MA, United States) supplemented with 2% B27 (Thermo Scientific). Half of the culture media were replaced every 2 days. On the 7th day, the cultures were exposed to indicated concentration of METH applied by Changsha City Public Security Bureau, China, cultured in a 5% CO_2 incubator at 39.5°C for 3 or 6 h. The cell cultures in the normal control group were still cultured in a 5% CO_2 incubator at 37°C in parallel.

In vivo METH Administration

Male SD rats, each weighing 200–210 g at the beginning of the experiment, were obtained from the Animal Center of Central South University. Animals were housed in a temperature (23 ± 2°C) and humidity (50 ± 5%) controlled animal facility. All experimental rats were housed together in 50 × 35 × 20 cm cages (n = 3/cage) and were maintained on a 12 h light/dark cycle with free access to food and water. METH (10 mg/kg) or saline were administered to rats every 2 h in four successive intraperitoneal (i.p.) injections. Rats were sacrificed by decapitation at 1, 12, or 24 h after the last injection of METH or saline. The rectal temperature of rats was monitored by an electronic thermometer throughout METH treatment, at 30 min after each injection, and rectal temperature 30 min before METH treatment was considered as the baseline.

Drug Preparation and Administration

For *in vitro* experiments, we pretreated primary cultured neurons with 20 μM Nec-1 (Sigma-Aldrich) diluted with DMSO for 2 h

before conducting METH and 39.5°C treatment to determine the rate of necroptosis (Vieira et al., 2014). 50, 100, 300, and 900 nM HSP90 inhibitor Geldanamycin (GA) (Cell Signaling Technology, MA, United States) diluted with DMSO were picked and added into the primary striatal neuronal medium for 24 h before conducting METH and 39.5°C treatment. For *in vivo* experiments, GA was diluted with 1% DMSO (diluted with saline) to a final concentration of 1.6 mM. After anesthetized by i.p. injection of 1% pentobarbital sodium (6 ml/kg), rats were placed into a stereotaxic frame. A 23-gauge stainless steel guide cannula attached to a 10 μl Hamilton® syringe was stereotactically inserted (coordinates: striatum: AP + 0.9 mm, lateral −2.2 mm, −4.4 mm beneath the pial surface). 5 μl GA or dilute DMSO was injected 1 h before METH administration at a rate of 0.5 μl/min (Wen et al., 2008; Yin et al., 2017). Following the intracerebral injection, rats were removed from the stereotaxic device and maintained at a rectal temperature of 37°C throughout surgery and recovery.

Lentivirus Infection in Primary Cultured Striatal Neurons

The lentivirus kit containing three shRNA sequences of HSP90α gene and one negative control sequence was purchased from Jikai gene (Shanghai, China). The sequences are as following: Hsp90aa1-RNAi Sequence 1: GACAGCAAACATGGAGAG AAT, Hsp90aa1-RNAi Sequence 2: GCTTTCAGAGCTGTT GAGATA, Hsp90aa1-RNAi Sequence 3: AAGTACATTGAT CAAGAAGAA. Firstly, we conducted the pretest study to explore the suitable concentration of the lentivirus for infecting primary cultured striatal neurons. Four concentrations (MOI:1, MOI:3, MOI:5, and MOI:10) of the negative control lentivirus were applied to infect primary cultured neurons on the 4th day after planting in plates. Then change the medium after infecting for 24 h, and continue to infect for 72 h. The GFP positive cells were captured by a fluorescence microscope. The formal experiment was carried out for infecting primary cultured neurons at MOI:3 after infecting for 72 h. The rate of knocking down of HSP90α was detected by western blot.

Propidium Iodide Staining

Propidium iodide (PI) staining was used to identify necrotic cells (Shang et al., 2014; Guo et al., 2020). At the indicated time points, cell cultures on the coverslips were washed three times with PBS and then incubated with 10 μg/ml PI dye in a 5% CO_2 incubator at 37°C for 10 min. Then, cell cultures were perfused with 4% paraformaldehyde (PF) for 20 min at room temperature (RT) followed by washing three times in PBS buffer and covered the slides with an anti-fading mounting solution containing DAPI (Vector Laboratories, CA, United States). Images acquired with a fluorescence microscope using the same exposure time were captured for five random fields of each group. The percentages of PI-positive cells, which were analyzed in every intact captured image using ImageJ software (National Institutes of Health, MD, United States), are calculated from the number of PI-positive cells divided by the number of DAPI-positive cells.

Lactate Dehydrogenase Release Assay

The release of lactate dehydrogenase (LDH) into the extracellular space/supernatant is considered to be an important feature of broken cell membrane integrity (Kumar et al., 2018; Parhamifar et al., 2019). The LDH assay is a non-radioactive colorimetric assay. For *in vitro* analysis, we used the LDH cytotoxicity assay kit (Beyotime, Shanghai, China) to determine the LDH released from necrotic cells in each group. In brief, cell culture plates were centrifuged at 1,500 rpm for 5 min, followed by harvesting the cell-free culture supernatants from each well of the plate and then incubated with the working reagent mixture at RT for 30 min. Subsequently, the optical density of each well in the assay was measured with a microplate reader at the wavelength of 490 and 650 nm. The optical density is directly proportional to the LDH activity and the percentage of necrotic cells. The percentages of necrotic cell death are equal to the optical density of the treated group minus control group/LDH releasing reagent treated group minus control group, which was calculated from three independent experiments. The LDH cytotoxicity assay kit (Nanjing Jiancheng Bioengineering Institute, Nanjing, China) was used for the *in vivo* analysis according to the manufacturer's instructions. In brief, rats were anesthetized with 10% chloral hydrate and then sacrificed by decapitation. Rat striatum tissues were quickly removed and immediately homogenized in 0.86% ice-cold NaCl by sonication, then tissue homogenates were centrifuged at 2,500 rpm for 10 min. The supernatant solutions were collected before incubation with the working reagent mixture for 30 min at 37°C. The optical density of each group was detected with a microplate reader at the wavelength of 450 nm. The percentage of necrotic cell death was measured by the color intensity of treated group minus negative control group/standard group minus blank control group, according to the manufacturer's instructions.

Immunofluorescence Staining

For *in vitro* experiments, at the indicated time points, cell cultures on the coverslips were washed three times with PBS and fixed with 4% PF for 20 min. For *in vivo* experiments, the rats received intracardiac perfusion with saline and 4% PF. The brains were then dehydrated in a series of 15 and 30% sucrose solutions before dissection. Coronal slices (20 μm thickness) encompassing the striatum were collected and then used for staining. After three times washed in PBS again, cell cultures on the coverslips and slices were blocked at RT in blocking buffer, i.e., PBS containing 0.3% Triton X-100 and 5% normal bovine serum for 1–2 h. Incubate cell coverslips and slices with primary antibodies against the following targets at 4°C overnight: HSP90α (1:100, Abcam, Cambridge, United Kingdom), RIP3 (1:100, Sigma-Aldrich), TH (1:200, Abclonal, Wuhan, China; 1:200, Santa Cruz, TX, United States), Map-2 (1:100, Proteintech Group, IL, United States). The next day, coverslips and slices were moved to RT for 30 min, washed three times with PBS, and then incubated with Alexa-conjugated secondary antibodies (1: 200, Jackson ImmunoResearch, PA, United States) for 2 h at RT with gentle fluctuation. The coverslips were washed three times with PBS, followed by covering with an anti-fading mounting solution containing DAPI (Vector Laboratories). All the staining

procedures were in parallel and images were captured using the same settings at five random fields of view on each coverslip with a fluorescence microscope.

Western Blot Detection

At the indicated time points, the cultured neurons and the rat striatum tissues were harvested, washed twice with ice-cold PBS, and then dissociated with RIPA buffer contained 1% phosphorylated inhibitors and 1% protease inhibitors (CWBIO, Beijing, China). The extracts were centrifuged at 12,000 rpm for 20 min at 4°C, and the supernatant was transferred to a new tube. We measured the protein concentration of these samples by BCA assay. After unifying the concentration, we added 5× loading buffer, boiled them for 5 min, centrifuged them at 1,000 rpm for 5 min. The total loading protein for each lane is 20 μg. The samples were loaded in 8–12% SDS-PAGE gel and then transferred the protein from the gel to a PVDF membrane (Millipore, MA, United States) in ice-cold transfer buffer. After washing with TBST for once, the membranes were blocked with 5% skim milk at RT for 1–2 h to wipe off the non-specific protein band. The membranes were incubated with primary antibody (RIP3, 1:1,000; HSP90α, 1:1,000; MLKL, 1:500; GAPDH, 1:5,000 (Beyotime) at 4°C overnight. The next day, after washing the membrane with TBST three times, the membranes were incubated with the homologous HRP-conjugated secondary antibody (1:2,500, Jackson ImmunoResearch) at RT for 1.5 h. And then high sensitivity chemiluminescence reagent (CWBIO) was used to visualize the immunoreactive bands. Integrated density values of specific proteins, which quantified by ImageJ software, were normalized to the GAPDH values.

Phos-Tag™ SDS-PAGE

The concentration of acrylamide SDS-PAGE gel for RIP3 and MLKL was 8%, the concentration of phos-tag™ (Wako Pure Chemical Industries, Japan) was 50 μM. The protocol was similar to western blot (WB) but the operation before transferring onto the PVDF membrane. Before transferring onto the membrane, the gel needed to be washed with transferring buffer containing 1 mM EDTA for 15 min, then with transferring buffer without EDTA for 15 min to get rid of Mn^{2+}.

Co-Immunoprecipitation

Primary cultured neurons were harvested and lysed in cold immunoprecipitation (IP) extraction buffer containing 1% phosphatase and 1% protease inhibitor and the protein solution medium was separated by centrifugation at 12,000 rpm at 4°C for 20 min. Four micrograms of HSP90α antibody and IgG (Abclonal) were pre-incubated with protein A/G agarose beads (Santa Cruz) for 8 h at RT and washed with GLB^+ buffer for five times. Then 500 μg protein from extracted protein was incubated with protein A/G agarose beads coupled with primary antibody at 4°C for 24 h with gentle fluctuating. On the following day, the mixture was pre-washed five times with cold GLB^+ buffer, and proteins were eluted with prepared 1× loading buffer by boiling for 5 min and centrifuge for 5 min at 10,000 rpm to collect the supernatant and subjected to SDS-PAGE.

Statistical Analysis

To ensure consistency of the results, all experiments were replicated at least three times. Figure panels were assembled using Photoshop CC (Adobe Systems Incorporated, CA, United States). The measurement data are analysed by GraphPad Prism 5 (GraphPad Software Inc., CA, United States) and presented as the mean ± standard deviation. Statistical significance was set at $p < 0.05$.

RESULTS

METH Treatment Increased the Core Body Temperature and Up-Regulated LDH Activity and the Molecular Expression of Canonical Necroptotic Factors in the Striatum of Rats

HT is an important contributor to METH-induced neurotoxicity (Yamamoto et al., 2010). It usually reaches a peak 30 min after METH treatment. To determine whether our METH and HT insult rat model was successful, we measured core body temperatures before the first METH or saline injection and 30 min after each METH or saline injection. As shown in **Figure 1A**, there was no significant difference in the basal body temperature of rats treated with a saline solution. Compared to the saline controls, METH treatment (4 × 10 mg/kg, every 2 h, i.p.) significantly increased core body temperatures. The temperatures also increased with the number of injections and reached about 39.5°C 30 min after the fourth METH injection, similar to the previous study (Chauhan et al., 2014). These results indicate that the rats treated with METH displayed higher temperatures than the rats treated with saline. We also conducted LDH cytotoxicity assays *in vivo* (**Figure 1B**). Compared with the saline group, we observed a higher LDH release in the METH treatment group.

The increased expression of RIP3 and MLKL mRNA or protein *in vivo* has been reported in various diseases or physiological conditions (Guo et al., 2020). The activated forms of RIP3 and MLKL are optimal biomarkers to detect necrosis and to assess the diagnosis or prognostic of diseases related to necrotic injuries (He et al., 2016; Hu et al., 2021). Therefore, we first speculated whether METH administration could cause the corresponding molecular changes in the striatum of rat brains (**Figures 1C–G**). The phos-tag SDS-PAGE results (the upper bands) showed that the expression of p-RIP3, total RIP3 (t-RIP3), and phosphorylated MLKL (p-MLKL) in the rat striatum were higher in the binge METH treatment group than in the control groups. Together, these results indicate that METH administration and METH-induced HT may induce necroptosis in the striatum of rats.

METH and HT Induced Necroptosis in Primary Cultures of Striatal Neurons

The purity of the striatal neuronal cells was assessed on the 7th day by immunoreactivity to microtubule association protein-2

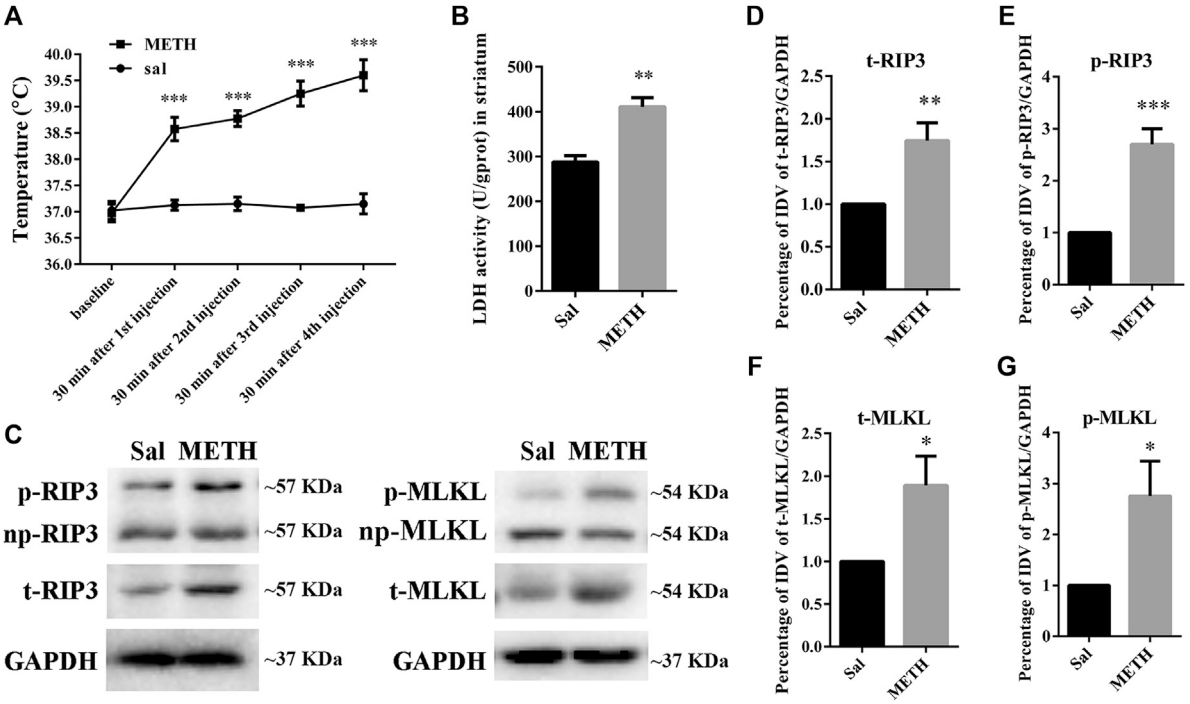

FIGURE 1 | Changes in core body temperature, LDH activity, and canonical necroptotic factors expression in the striatum of rats following METH administration. Rats were sacrificed by decapitation at 24 h after the last injection of METH (4 × 10 mg/kg, every 2 h, i.p.) or saline. **(A)** METH treatment increased core body temperature. Data were analyzed by RM two-way analysis of variance (ANOVA) which was carried out with GraphPad Prism 5 software ($n = 3$). ***$p < 0.001$ vs. baseline. **(B)** Necrosis in the striatum of rats was determined by LDH cytotoxicity assay. Data were analyzed by unpaired 2-tailed Student's t test ($n = 3$). **$p < 0.01$ vs. Sal group. **(C)** p-RIP3, RIP3, p-MLKL, and MLKL protein levels in the rat striatum were detected by phos-tag SDS-PAGE and WB after METH administration. **(D–G)** Statistical analysis of WB of p-RIP3, RIP3, p-MLKL, and MLKL expression. np, non-phosphorylated protein; t, total protein; Sal, saline group. Data were analyzed by unpaired 2-tailed Student's t test ($n = 3$). *$p < 0.05$, **$p < 0.01$, ***$p < 0.001$ vs. Sal group.

(Map-2). In all, 90.5 ± 2.06% of the cells were Map-2 positive (**Supplementary Figure 1**). To observe whether striatal neurons are injured by METH and HT, we incubated our cultured neurons with 2 and 4 mM METH at 39.5°C for 3 or 6 h and observed the change in neuronal morphology under a light microscope. The results showed that 2 mM of METH + 39.5°C for 3 h damaged the neurites. The degree of damage to the neurites increased with a higher concentration of METH and HT duration time. After exposure to 4 mM of METH + 39.5°C for 6 h, the neurons were severely damaged and presented obvious necrosis-like features as the neuronal body began to swell and the massive neurites broke and fractured (**Figure 2A**). These results showed that METH and HT induced neuronal necrosis-like cell death.

To determine whether necroptosis occurred in primary cultures of striatum neurons exposed to METH and HT, we employed the necroptosis inhibitor Nec-1 and two necrosis detecting methods. We did not observe any apparent PI-positive cells (necrotic cells) after PI staining in the control group. We detected necrotic cells after treating the neurons with METH for 3 and 6 h and HT exacerbated the injury. The number of necrotic cells increased with METH concentration and HT treatment time (**Figure 2B**). The quantitative analysis of the number of necrotic cells showed that their number increased dramatically in the METH and HT treatment groups. However, the number of necrotic cells in the Nec-1 + 4 mM of METH + 39.5°C treatment group was lower than in the 4 mM of METH + 39.5°C group after 6 h (**Figure 2C**). The LDH release results also showed that the treatment with Nec-1 significantly decreased the number of necrotic cells induced by METH and HT for 6 h. The multiple comparisons test among groups showed that necrotic cell death in HT + METH 4 mM treatment for 6 h group was more than single HT and single METH treatment for 6 h group (**Figure 2D**). Thus, we performed the analysis 6 h after treatment to further study the mechanism of METH/HT-induced neuronal injury. Collectively, these results suggest that METH and HT induce necroptosis in primary cultures of striatum neurons.

We detected the changes in the expression of several canonical necroptotic molecules following METH and HT treatment (**Figure 3A**). Our results showed that the level of p-RIP3, t-RIP3, and p-MLKL was higher in both 39.5°C treatment groups than in the control groups. The band thickness of p-RIP3, t-RIP3, p-MLKL, and t-MLKL was remarkably increased in the 4 mM METH + 39.5°C group. The quantitative analysis of the WB showed that METH slightly increased p-RIP3, t-RIP3, p-MLKL, and t-MLKL levels. However, the co-treatment with METH and HT significantly increased the expression of both canonical necroptotic molecules. The level of p-RIP3, t-RIP3, *p*-MLKL, and t-MLKL increased rapidly in the cells

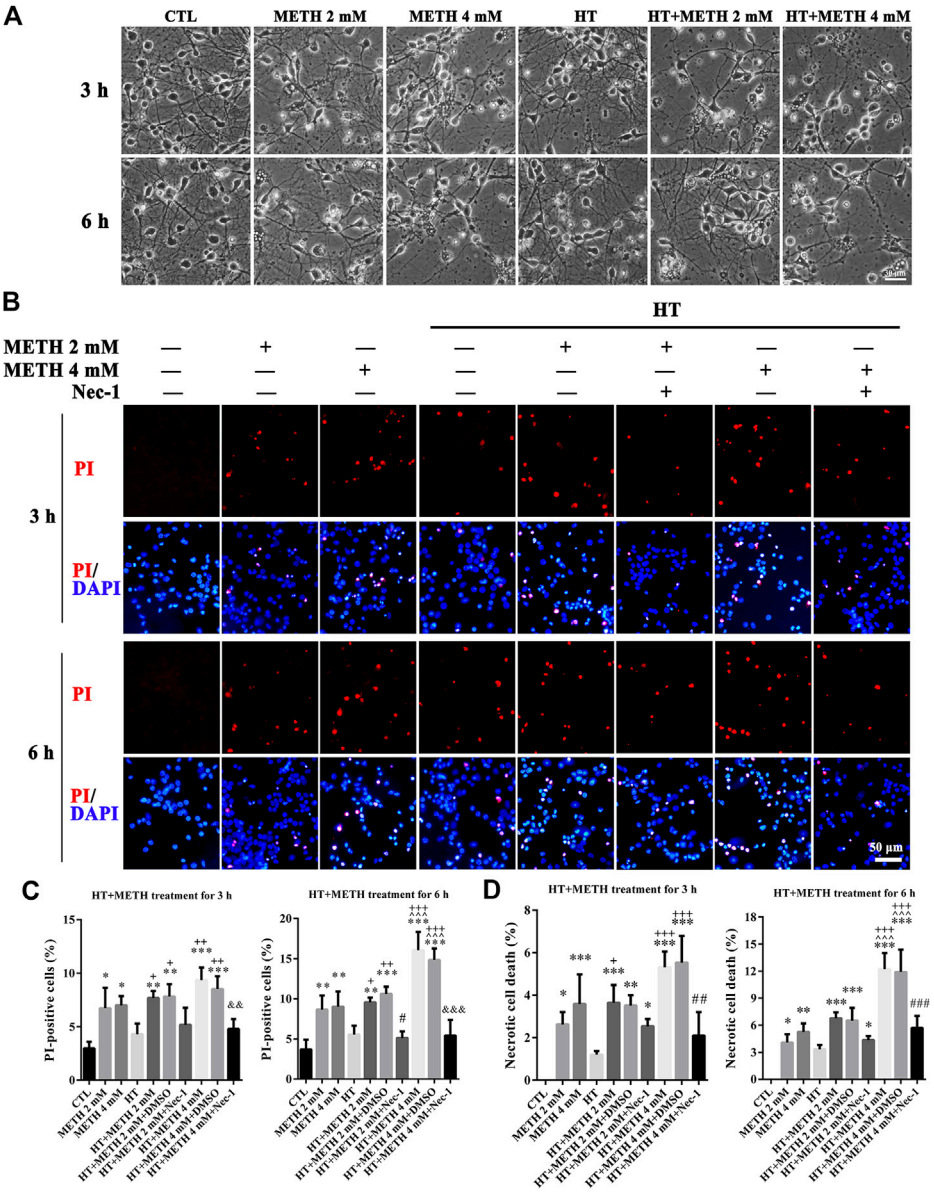

FIGURE 2 | METH/HT-induced cell morphological changes and Nec-1 pre-treatment attenuated the METH/HT-induced necrosis in striatal neurons. **(A)** Cell morphological changes of striatal neurons treated with METH for 3 and 6 h under a light microscope. *Scale bar* = 30 μm **(B)** PI (red)/DAPI (blue) double staining of striatal neurons pre-treated with Nec-1 after 3 and 6 h of METH/HT. *Scale bar* = 50 μm. **(C)** Statistical analysis of the PI/DAPI double staining of necrotic cells. Data were analyzed by one-way ANOVA, followed by a Tukey multiple comparisons posttest ($n = 3$). $^{*}p < 0.05$, $^{**}p < 0.01$, $^{***}p < 0.001$ vs. CTL group; $^{\wedge\wedge}p < 0.05$ vs. METH 4 mM; $^{+}p < 0.05$, $^{++}p < 0.01$, $^{+++}p < 0.001$ vs. HT; $^{\#}p < 0.05$ vs. HT + METH 2 mM group; $^{\&\&}p < 0.01$, $^{\&\&\&}p < 0.001$ vs. HT + METH 4 mM group. **(D)** The percentage of necrotic neuron death after METH/HT treatment and pre-treatment with Nec-1 was determined with LDH release assays. Data were analyzed by one-way ANOVA, followed by a Tukey multiple comparisons posttest ($n = 3$). $^{*}p < 0.05$, $^{**}p < 0.01$, $^{***}p < 0.001$ *vs.* CTL group; $^{\wedge\wedge}p < 0.05$ vs. METH 4 mM; $^{+}p < 0.05$, $^{+++}p < 0.001$ vs. HT; $^{\#\#}p < 0.01$, $^{\#\#\#}p < 0.001$ vs. HT + METH 4 mM group.

treated with 4 mM METH at 39.5°C for 6 h (**Figures 3B–E**). Thus, we performed further experiments at the concentration of 4 mM of METH.

HSP90α Was Involved in METH/HT-Induced Necrosis in Primary Cultures of Striatal Neurons

HSP90α acts as a molecular chaperone to stabilize RIP3 and mediate necroptosis (Li et al., 2016). Our IP results showed that the interaction between HSP90α and RIP3 was increased in the 4 mM METH + 39.5°C treatment for 6 h group compared to that in the control group (**Figure 4A**). Our WB results showed that a single METH treatment did not upregulate the expression of HSP90α. HSP90α expression was, however, significantly increased following METH and HT co-treatment (**Figure 4B**). The quantitative analysis of the WB showed that HSP90α expression significantly increased in cells treated with 4 mM METH at 39.5°C for 6 h (**Figure 4C**). These results suggest

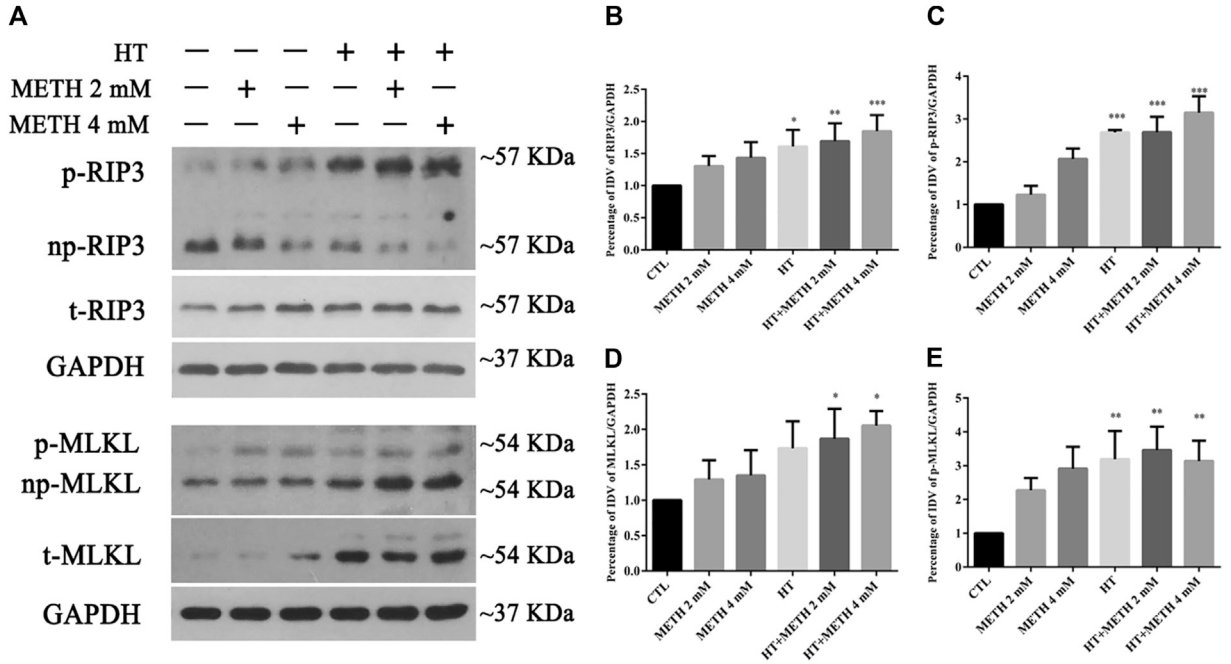

FIGURE 3 | Detection of RIP3, p-RIP3, MLKL, and p-MLKL expression by WB after METH/HT injury in striatal neurons. **(A)** p-RIP3, RIP3, p-MLKL, and MLKL protein levels in primary cultures of striatal neurons detected by phos-tag SDS-PAGE and WB after 6 h of METH treatment at 39.5°C. **(B–E)** Statistical analysis of WB of p-RIP3, RIP3, p-MLKL, and MLKL expression. Data were analyzed by one-way ANOVA, followed by a Tukey multiple comparisons posttest ($n = 3$). $^{*}p < 0.05$, $^{**}p < 0.01$, $^{***}p < 0.001$ vs. CTL group.

that the increase in HSP90α levels may be related to METH/HT-induced necroptosis in primary cultures of striatal neurons.

We found above that the expression of HSP90α increased following METH and HT treatment and detected a potential interactive relationship between RIP3 and HSP90α. Therefore, we predicted that HSP90α might be involved in METH/HT-induced necrosis in primary cultures of striatal neurons. The cells were treated with GA, an HSP90α inhibitor, for 24 h before adding METH and HT to determine whether HSP90α could mediate striatum neuronal necroptosis. Firstly, we found the best working concentration of GA with literature reviews and experimental verifications (Chen et al., 2012). The LDH release results showed that a pre-treatment with 50 nM, 100 nM, and 300 nM GA protected the striatum neurons from necrosis following METH and HT insults (**Figure 4D**). The PI staining also indicated that treatment with 50 and 100 nM GA effectively reduced the number of PI-positive cells after METH and HT insults (**Figure 4E**). The statistical analysis for the PI staining showed that the number of necrotic cells was remarkably reduced in all the GA pre-treatment groups as compared to that of the METH/HT groups (**Figure 4F**). These results suggest that GA could, at least partially, rescue METH/HT-induced necrosis in primary cultures of striatal neurons.

As HSP90α might decrease METH/HT-induced necroptosis in striatal neurons, we next investigated how HSP90α might regulate the process of protection. First, we measured the level of RIP3 (acting as a client and downstream molecule of HSP90α), p-RIP3, and its downstream molecules MLKL and p-MLKL following treatment with GA in the METH/HT groups. The phos-tag SDS-PAGE results showed that METH and HT increased the level of t-RIP3, p-RIP3, t-MLKL, and p-MLKL. This effect was reversed in cells pre-treated with GA (**Figure 5A**). The statistical analysis showed that GA treatment decreased the expression level of t-RIP3, p-RIP3, t-MLKL, and p-MLKL (**Figures 5B–F**). GA pre-treatments did not affect the expression of HSP90α following METH and HT. This may be because GA mainly binds to the N-terminal ATP-binding domain of HSP90 and inhibits its ATP-dependent chaperone activity (Guo et al., 2005; Hermane et al., 2019). These results suggest that GA can protect striatal neurons from METH/HT-induced necroptosis by decreasing the levels of t-RIP3/MLKL and p-RIP3/MLKL. Collectively, the above results indicate that HSP90α might be involved in METH/HT-induced necrosis in primary cultures of striatal neurons.

HSP90α shRNA Partially Protected Primary Cultures of Striatal Neurons From METH/HT-Induced Necroptosis

Four lentivirus concentrations (MOI:1, MOI:3, MOI:5, MOI:10) were used to explore the suitable lentivirus infective concentration for further experiments. The results showed that the GFP expression at MOI:3 and MOI:5 was optimal with a GFP-positive cell rate above 80% (**Supplementary Figure 2**). Thus, MOI: 3 was selected for further experiments. The results from the

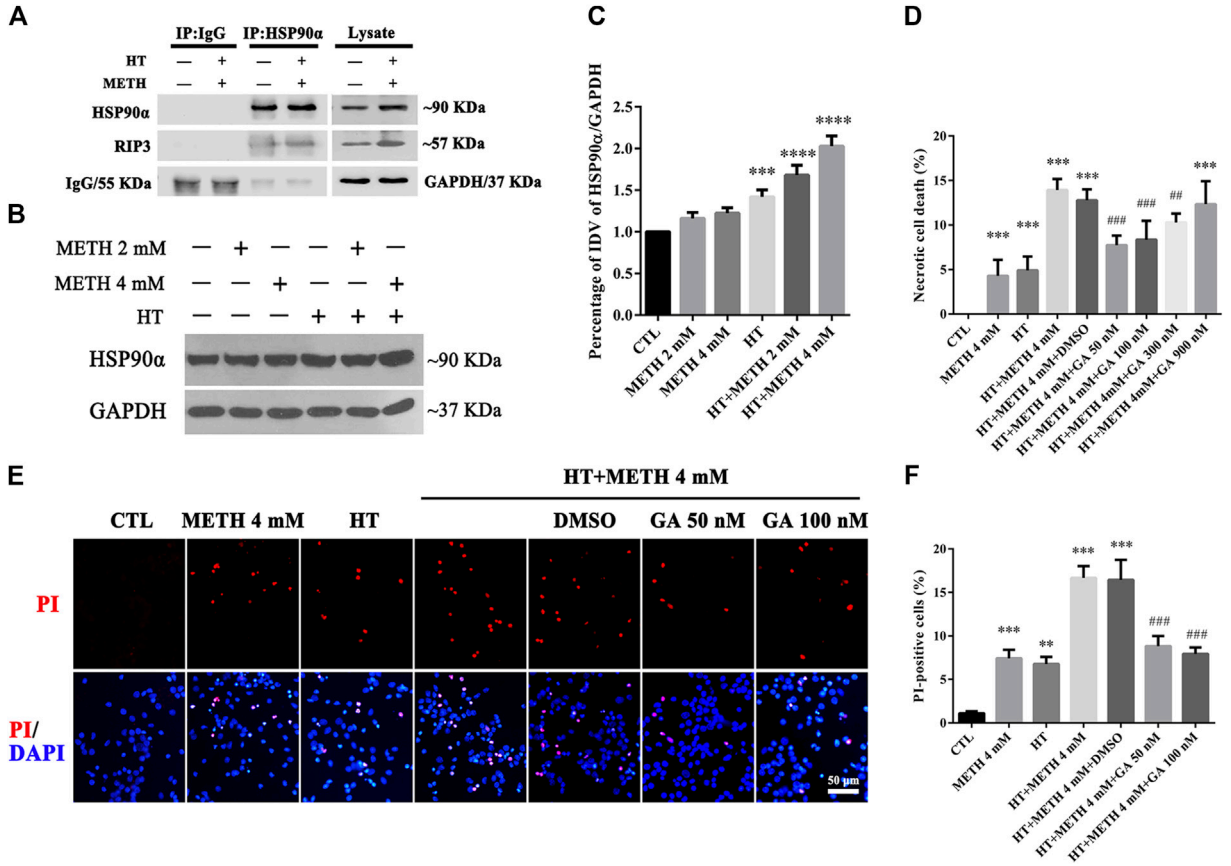

FIGURE 4 | HSP90α interacts with RIP3 and GA pretreatment protected primary striatal neurons from METH/HT-induced necrosis. **(A)** Detection of HSP90α and RIP3 interaction in primary cultures of neurons by IP **(B)** WB of HSP90α expression after METH treatment for 6 h at 39.5°C. **(C)** Statistical analysis of WB of HSP90α expression. Data were analyzed by one-way ANOVA, followed by a Tukey multiple comparisons posttest (n = 3). ***p < 0.001; ****p < 0.0001 vs. CTL group **(D)** Percentage of necrotic neuron death after METH/HT treatment and pre-treatment with GA as determined by LDH release assays. Data were analyzed by one-way ANOVA, followed by a Tukey multiple comparisons posttest (n = 3). ***p < 0.001 vs. CTL group; ##p < 0.01, ###p < 0.001 vs. HT + METH 4 mM group **(E)** PI (red)/DAPI (blue) double staining of striatal neurons after METH/HT and pre-treatment with GA. *Scale bar* = 50 μm. **(F)** Statistical analysis of PI/DAPI double staining of necrotic cells. Data were analyzed by one-way ANOVA, followed by a Tukey multiple comparisons posttest (n = 3). **p < 0.01, ***p < 0.001 vs. CTL group; ###p < 0.001 vs. HT + METH 4 mM group.

WB revealed that shRNA #2-3 lentiviruses pretreatment reduced the expression of HSP90α. The shRNA #3 sequence had the highest silencing efficiency (**Figures 6A,B**). The LDH release results confirmed that necrosis was significantly decreased in the shRNA #2-3 lentiviruses + METH and HT group as compared to the METH and HT group without lentiviral treatment (**Figure 6C**). We observed few PI-positive cells (necrotic cells) in the control group and an increased number of necrotic cells following METH and HT treatment for 6 h. The number of necrotic cells was reduced in the shRNA #1-3 lentiviruses + METH and HT group compared to that in the METH and HT group without lentiviral treatment (**Figure 6D**). The quantitative analysis of the necrotic cell numbers showed that it was lower in the shRNA #1-3 lentiviruses + METH and HT group than in the METH and HT group. Of the three sequences, the shRNA #3 lentivirus-transfected group had the lowest number of necrotic cells (**Figure 6E**). Therefore, the shRNA #3 lentivirus sequence was chosen in the following infective experiment. Collectively, these results suggest that *HSP90α* shRNA decreased METH/HT-induced necrosis in striatal neurons.

To further investigate the regulatory role of HSP90α in METH/HT-induced necrosis, we inhibited the function and expression of HSP90α using a specific shRNA. The phos-tag SDS-PAGE results showed that the upregulation of HSP90α, t-RIP3, p-RIP3, t-MLKL, and *p*-MLKL induced by METH/HT decreased in the shRNA #3 lentivirus-transfected group compared with that in the METH/HT-treated group (**Figure 6F**). Our statistical analysis showed that the expression level of HSP90α, t-RIP3, p-RIP3, t-MLKL, and p-MLKL increased in the HT + METH groups, the HT + METH + Reagent group, and the HT + METH + NC group but decreased in the HT + METH + #3 *HSP90α* shRNA group (**Figures 6G–K**). The immunofluorescence (IF) staining showed that both the expression of HSP90α (green) and RIP3 (red)

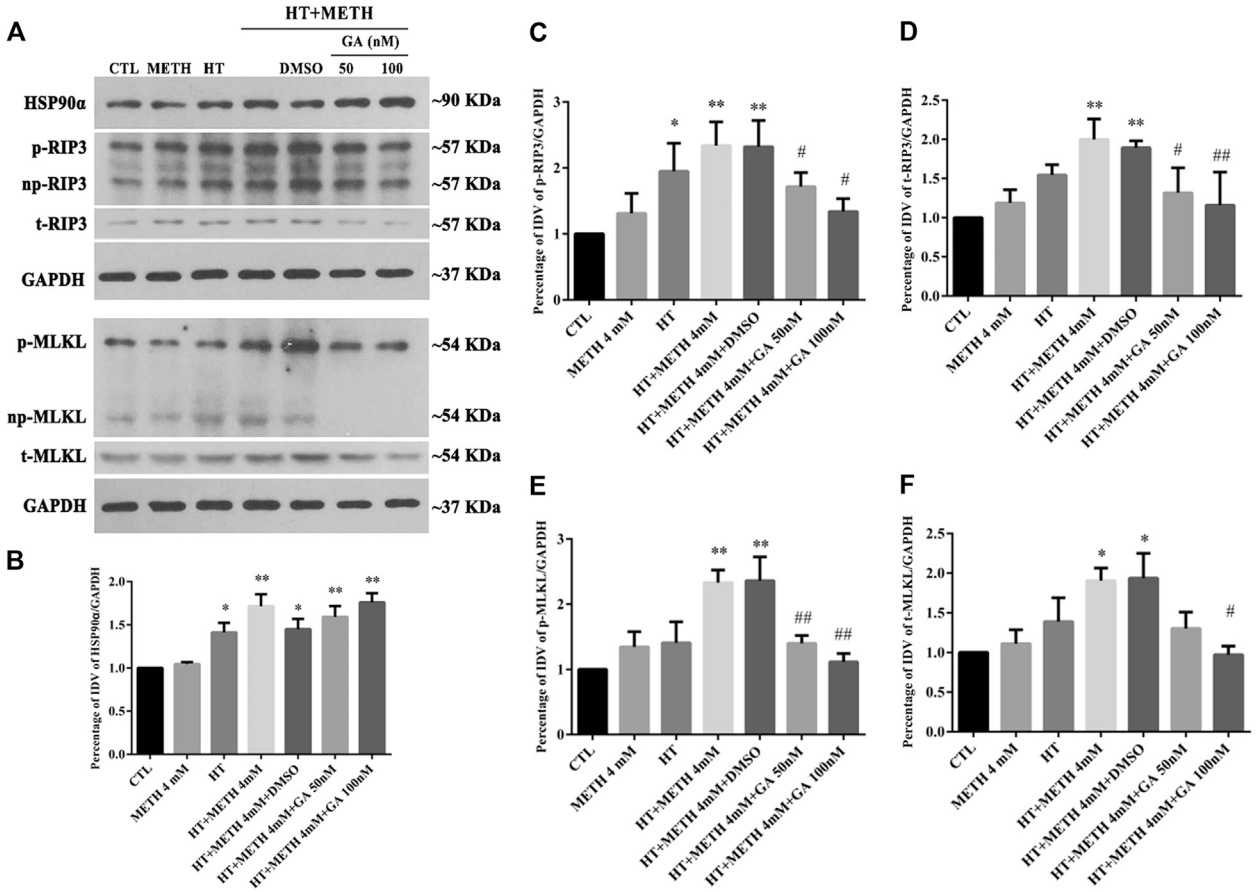

FIGURE 5 | Detection of HSP90α, RIP3, p-RIP3, MLKL, and *p*-MLKL in striatal neurons following METH/HT injury and pre-treatment with GA. **(A)** WB of HSP90α, RIP3, p-RIP3, MLKL, and p-MLKL after treatment with METH/HT for 6 h and pre-treatment with 50 and 100 nM GA. **(B–F)** Statistical analysis of WB of HSP90α, RIP3, p-RIP3, MLKL, and p-MLKL expression. Data were analyzed by one-way ANOVA, followed by a Tukey multiple comparisons posttest ($n = 3$). $^{*}p < 0.05$, $^{**}p < 0.01$ vs. CTL group; $\#p < 0.05$, $\#\#p < 0.01$ vs. HT + METH 4 mM group.

increased following METH and HT treatment. However, the knockdown of HSP90α by shRNA not only attenuated the IF intensity of HSP90α but also of RIP3 (**Figure 7**). Taken together, these results suggest that HSP90α inhibition can partially protect striatal neurons from METH/HT-induced necroptosis by decreasing the expression of RIP3 and MLKL.

Inhibition of HSP90α Protected Striatal Neurons from METH/HT-Induced Necroptosis *in vivo*

To investigate whether the expression of HSP90α and RIP3 changed following METH and HT insults *in vivo*, we administered METH or a saline solution to rats and detected the expression of HSP90α and RIP3 1, 12, or 24 h after the last injection. The IF intensity of HSP90α (red) was increased 1 h after METH administration and was sustained even 24 h after the METH insult (**Figure 8A**). We did not detect obvious RIP3-positive (green) cells by immunostaining in the saline group but their number slightly increased after 1 h and significantly increased after 24 h in the METH group (**Figure 8B**). Generally, neuronal death is observed with one-day intervals in rats. After one day, cell death may no longer be evident as the dying cells may have undergone phagocytosis before lysis (Deng et al., 1999; Sabrini et al., 2019). Thus, we performed our experiments 24 h after the METH insult. The phos-tag SDS-PAGE results showed that p-RIP3, RIP3, p-MLKL, and MLKL in rat striatum cells were dramatically up-regulated 24 h after METH and METH + vehicle administration compared to that in the saline groups. On the other hand, HSP90α inhibition significantly blocked the expression of the METH/HT-induced canonical necroptotic molecules (**Figures 9A–F**). LDH cytotoxicity assays *in vivo* were also conducted. Compared with the saline group, we observed an increased LDH release in the METH and METH + vehicle groups. However, the increased LDH release was decreased in the GA pre-treatment groups (**Figure 9G**). These results demonstrate that HSP90α inhibition can partially protect striatal neurons from METH/HT-induced necroptosis.

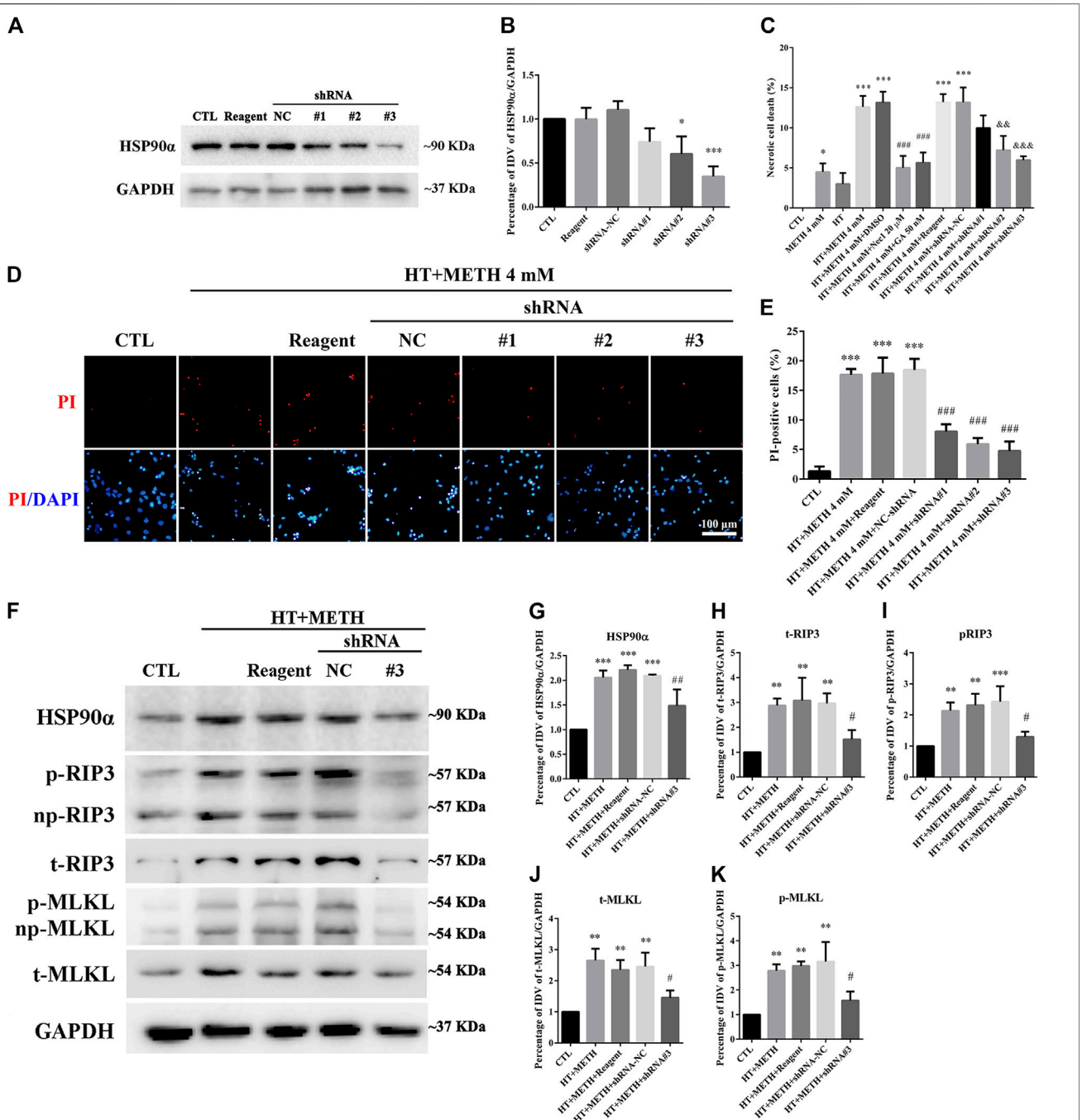

FIGURE 6 | *HSP90α* shRNA protected primary striatal neurons from METH/HT-induced necrosis. **(A)** The protein level of HSP90α after infection with lentivirus in primary cultures of striatal neurons detected by WB. Reagent, infection reagent without shRNA group; NC, infection reagent with negative control of shRNA group; #1-3, infection reagent with the indicated sequence of *HSP90α* shRNA group **(B)** Statistical analysis of HSP90α WB. Data were analyzed by one-way ANOVA, followed by a Tukey multiple comparisons posttest ($n = 3$). $^{*}p < 0.05$, $^{***}p < 0.001$ vs. CTL group. **(C)** The percentage of necrotic neuron death after METH/HT treatment and pre-treatment with Nec-1, GA, and *HSP90α* shRNA was determined with LDH release assays. Data were analyzed by one-way ANOVA, followed by a Tukey multiple comparisons posttest ($n = 3$). $^{*}p < 0.05$, $^{***}p < 0.001$ vs. CTL group; $^{###}p < 0.001$, $^{\&\&}p < 0.01$, $^{\&\&\&}p < 0.001$ vs. HT + METH 4 mM group, respectively. **(D)** PI (red)/DAPI (blue) double staining of striatal neurons after METH/HT treatment and pre-treatment with *HSP90α* shRNA. *Scale bar* = 50 μm. **(E)** Statistical analysis of the PI/DAPI double staining of necrotic cells. Data were analyzed by one-way ANOVA, followed by a Tukey multiple comparisons posttest ($n = 3$). $^{***}p < 0.001$ vs. CTL group; $^{###}p < 0.001$ vs. HT + METH 4 mM group. **(F)** WB of HSP90α, RIP3, p-RIP3, MLKL, and p-MLKL after METH/HT treatment for 6 h and pre-treatment with HSP90α shRNA. **(G–K)** Statistical analysis of WB of HSP90α, RIP3, p-RIP3, MLKL, and p-MLKL expression. Data were analyzed by one-way ANOVA, followed by a Tukey multiple comparisons posttest ($n = 3$). $^{**}p < 0.01$, $^{***}p < 0.001$ vs. CTL group; $^{\#}p < 0.05$, $^{\#\#}p < 0.01$ vs. HT + METH 4 mM group.

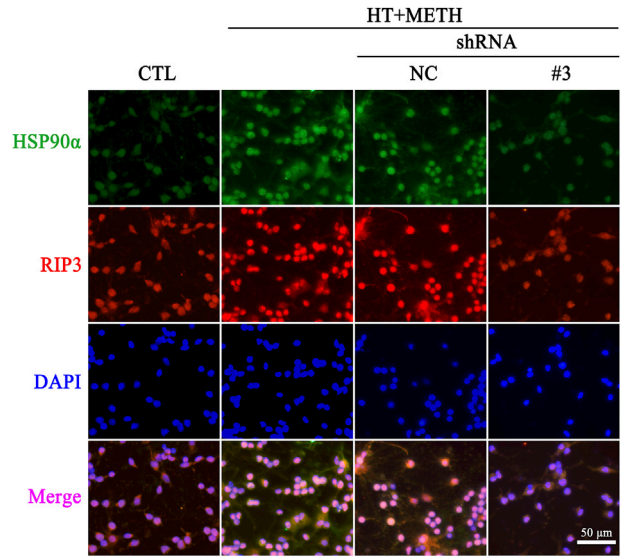

FIGURE 7 | IF of HSP90α (green) and RIP3 (red) in striatal neurons following METH/HT injury and pre-treatment with *HSP90α* shRNA. *Scale bar* = 50 μm.

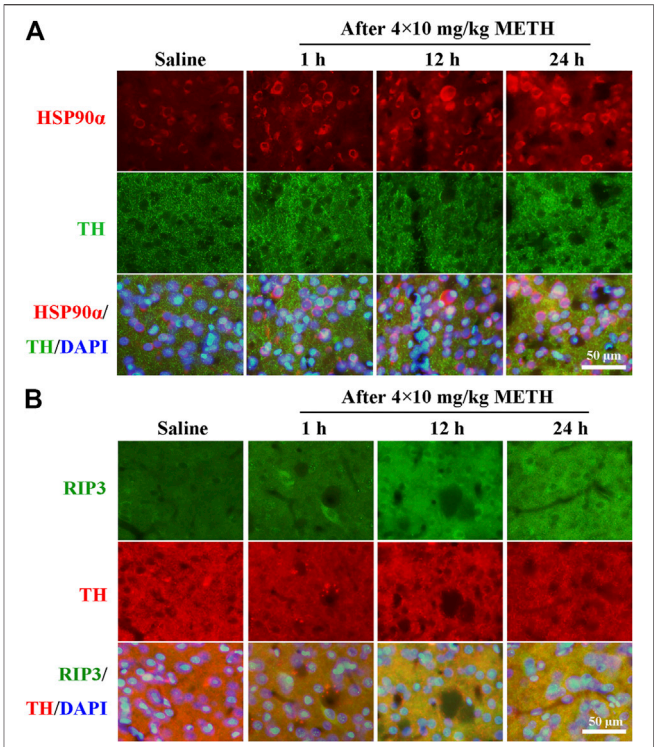

FIGURE 8 | Detection of HSP90α and RIP3-positive cells in the rats' striatum following METH administration by IF. **(A)** IF staining of HSP90α (red) and tyrosine hydroxylase (TH) (green) 1, 12, and 24 h after the last injection of a binge dose of METH (4 × 10 mg/kg, every 2 h, i.p.) or saline. **(B)** IF staining of RIP3 (green) and TH (red) 1, 12, and 24 h after the last injection of a binge dose of METH. *Scale bar* = 50 μm in all panels.

DISCUSSION

In this study, we first demonstrated that METH and HT insults might lead to the upregulation of HSP90α, RIP3, and MLKL. Furthermore, the upregulation of HSP90α induced by METH and HT plays a regulatory role in the phosphorylation of RIP3 and subsequent necroptosis. Finally, by using an animal *in vivo* model, we demonstrated the role of HSP90α in METH/HT-induced necroptosis in the rat striatum. These results provided potential therapeutic targets and clinical diagnostic biomarkers for future use.

METH-induced HT allegedly results from the activation of dopaminergic (Mechan et al., 2002) and serotonergic (Herin et al., 2005) receptors in the thermoregulatory circuits of the hypothalamus, the direct or indirect activation of the sympathetic nervous system, the loss of vasoconstriction-mediated heat dissipation (Sprague et al., 2018), cerebrovascular damage, an increased level of oxidative stress and calcium entry, which contribute to METH-induced neurotoxicity in a dose-dependent manner (Miller and O'Callaghan, 2003; Yamamoto et al., 2010). Humans presented pathological HT during acute intoxication by METH (Kojima et al., 1984; Buffum and Shulgin, 2001; Marco et al., 2021). Additionally, HT can also markedly promote METH-induced neurotoxicity in rodents and non-human primates in similar ranges (Crean et al., 2006; Crean et al., 2007; Gutierrez et al., 2018). Thus, animal *in vivo* and *in vitro* models have been highly useful in identifying the neurochemical and physiological mechanisms of METH-induced HT. Several dose regimens of METH administration have been evaluated in rodent studies, i.e., single high dose (40 mg/kg) or binge doses (4 × 10 mg/kg, 2–3 h intervals), and escalating doses (1–10 mg/kg, twice a day, at 5 h intervals, for 10 days) of METH and chronic voluntary oral METH intake (Yang et al., 2018). The core body temperature of rats reached 38–39.5°C for 5 h after a single high dose of METH, while a binge dose (4 × 10 mg/kg, every 2 h, i.p.) caused an HT of 39–40°C for at least 6 h (Herring et al., 2008; Chauhan et al., 2014). In the present study, a binge dose of METH significantly increased the core body temperature to 38.5–39.5°C compared with the saline controls. The measured core body temperature was slightly lower than that observed in Chauhan et al.'s study, which may be caused by the differences in the experimental environment (Raineri et al., 2015), the weight of the rats (Bowyer et al., 1993), and the experimental equipment. Thus, we performed our HT experiments *in vitro* at 39.5°C.

HSP is a group of highly conserved proteins that respond to several stressors, including heat stress. They also play a role in cellular repair and the induction of thermotolerance (Yan et al., 2006). As an important chaperone molecule, HSP90 supports the folding of many important proteins, including signalling proteins and transcription factors. In response to stress, *HSP* gene expression is activated by *cis*-acting promoter elements which consist of variations of an inverted repeat sequence (nGAAn) called heat shock elements (HSE) and a homotrimeric DNA-binding transcription factor--heat shock factor 1 (HSF1) in eukaryotic cells (Ahn and Thiele, 2003). The denatured protein produced by heat shock or other types of stress, creates binding sites for HSP90 and changes the balance such

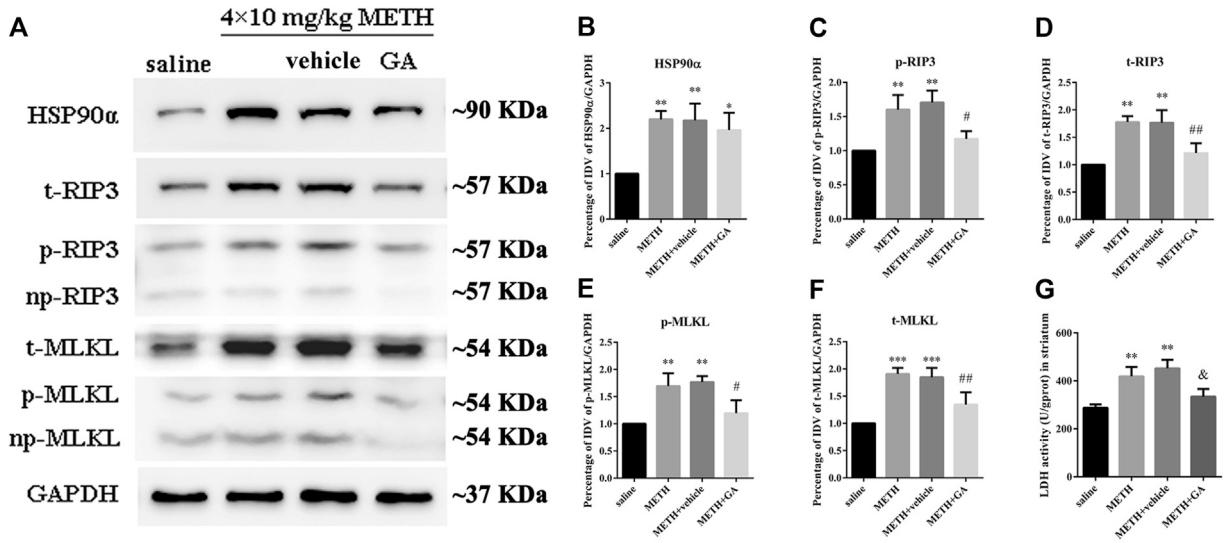

FIGURE 9 | HSP90α inhibition by brain stereotactic injections of GA attenuated the METH/HT-induced upregulation of RIP3, p-RIP3, MLKL, and p-MLKL and the LDH activity in the rats' striatum following a binge dose of METH. **(A)** WB of HSP90α, RIP3, p-RIP3, MLKL, and p-MLKL following a binge dose of METH administration and pre-treatment with GA by brain stereotactic injections. **(B–F)** Statistical analysis of WB of HSP90α, RIP3, p-RIP3, MLKL, and p-MLKL expression. Data were analyzed by one-way ANOVA, followed by a Tukey multiple comparisons posttest ($n = 3$). $^{*}p < 0.05$, $^{**}p < 0.01$, $^{***}p < 0.001$ vs. saline group; $\#p < 0.05$, $\#\#p < 0.01$ vs. METH group. **(G)** Necrosis in the striatum of rats was determined by LDH cytotoxicity assay. Data were analyzed by one-way ANOVA, followed by a Tukey multiple comparisons posttest ($n = 3$). $^{**}p < 0.01$ vs. saline group; $\&p < 0.05$ vs. METH group.

as to release HSF1, then activated HSF1 binds to HSEs, HSEs are required to induce the expression of many genes central to the proteostasis network, including general chaperones of the heat shock protein classes HSP70 and HSP90 (Xiao and Lis, 1988; Lepock, 2005). In turn, cytosolic HSP70 and HSP90 have both been implicated in the negative regulation of HSF1 activity (Akerfelt et al., 2010). HSP90α is an isoform of HSP90, which plays an essential role in the response to external stimuli (Grad et al., 2010). For HSP90α gene expression, Zhang et al. reported that the 5' flanking sequences play a critical role in both constitutive expression and stress-induced expression of the human HSP90α gene (Zhang et al., 1999). HSP90α expression and extracellular secretion increase rapidly to protect the cells from damage in response to elevated temperature, infection, or oxidative stress (ROS) (Chatterjee et al., 2007). However, some studies indicated that the up-regulation of HSP90α could stabilize death-related proteins that mediate cell death (Li et al., 2015; Li et al., 2016). In our study, the co-treatment with METH and HT increased HSP90α expression more than HT or METH alone. The inhibition of HSP90α partially protected the primary cultures of striatal neurons from METH/HT injuries. These results suggest the regulatory role of the high expression of HSP90α in promoting METH/HT-induced injuries in striatal neurons.

In this study and many others, the concentration of METH used to promote cell death is in the millimolar range, which is several orders of magnitude higher than that in the blood of abusers. For example, the mean blood concentration of METH in human abusers (e.g., arrested by police in Kern County, CA) was estimated at 2.0 μM ($n = 105$) with a maximum of 11.1 μM (Melega et al., 2007). Melega et al. also reported that the concentration of METH in the blood and brain necessary to induce neurotoxicity *in vivo* after intravenous administration (1–5 mg/kg) varies between 1 and 10 μM. However, METH is distributed preferentially in the brain rather than in the plasma. Thus, the concentration of METH in the brain should be higher than in the blood (Melega et al., 1995). The concentrations of METH in the frontal cortex, striatum, and cerebellum of rats were more than 10-fold higher than in the plasma (Melega et al., 1995). In humans, the common dose of a well-adopted abuser is 1 g or more METH per day (Simon et al., 2002; Melega et al., 2007). In these cases, the blood concentration of METH may increase to the millimolar range (Badisa et al., 2019). Meanwhile, systemic responses, such as immune responses and HT, might play crucial roles in METH-induced toxicity *in vivo* (Papageorgiou et al., 2019; Marco et al., 2021). Therefore, the concentration of METH used to promote direct neurotoxicity *in vitro* should be higher than the one required *in vivo*. A millimolar range concentration is often used to study the mechanism of METH neurotoxicity in culture studies (Huang et al., 2009; Chen et al., 2020). In our study, we administered 4 mM METH, which is similar to several studies investigating METH-induced neurotoxicity (Huang et al., 2015; Huang et al., 2017). Moreover, we observed a particularly obvious increase in necrotic cell death 6 h after treatment with 4 mM METH, suggesting a high level of neuronal cytotoxicity. Therefore, we used this concentration to mimic the impact of high doses of METH in individuals who are acutely exposed to the substance. The sub-toxic effects of lower doses of METH (0.1, 0.5, and 1 mM) on neurons will be investigated in our future research. In our *in vivo* experiments,

we administered binge doses of METH because they can cause more severe damage to the neurons compared to a single METH administration (Ares-Santos et al., 2014). This mode of administration is also closer to an overdose in humans (Davidson et al., 2001).

METH primarily affects multiple functional areas in the human brain (Lu et al., 2019). The striatum is associated with movement disorders and is involved in the control of attention, executive function, motivated behaviours, and neuropsychiatric conditions, such as compulsive disorders, psychoses, and addictive behaviours (Zhu et al., 2006; Granado et al., 2013; Potvin et al., 2018). METH exposure can cause neuronal apoptosis and autophagy. A loss of approximately 25% of striatal neurons has been reported 24 h after METH exposure (Zhu et al., 2005). Many studies indicated that the death of striatal neurons occurred by apoptosis and autophagy after METH exposure (Zhu et al., 2006). For example, C/EBPβ was involved in METH-induced DDIT4-mediated neuronal autophagy and Trib3-mediated neuronal apoptosis (Huang et al., 2019). Xu et al. suggested that nuclear protein 1 (Nupr1/com1/p8) was involved in neuronal apoptosis and autophagy caused by high doses of METH through the endoplasmic reticulum (ER) stress signalling pathway (Xu et al., 2017). However, the inhibition of these molecules cannot protect all the neurons, indicating that apoptosis and autophagy may mediate the degeneration of only some of them. Since necrosis was discovered, it was mainly believed that it was a form of cell death that cannot be accurately intervened. When the necroptosis process was discovered, the research on necrosis received more attention. Multiple molecules are involved in necroptosis. The TNFα-regulated pathway, which is mediated by RIP1, RIP3, and MLKL is the most extensive and important (Sun et al., 2012; Liao et al., 2017; Ruan et al., 2019; Wang et al., 2020; Wu et al., 2020). This pathway is briefly described as follows: the death ligands bind to the corresponding receptors to pass the death signal into the cells. RIP1 can then bind RIP3 in the cytoplasm to form complex-II, which in turn promotes the phosphorylation of RIP3. This may cause an excessive accumulation of ROS (Chtourou et al., 2015) and the aggregation and translocation of phosphorylated MLKL to the cell membrane to form pores. The formation of these pores can deregulate the balance in the concentration of metal ions inside and outside the cell membrane and eventually promote cell necrosis (Cho et al., 2009; Sun et al., 2012). Our previous study showed that treatment with 4 mM METH for 12 h induced necroptosis in the cortical neurons of rats *in vitro* (Xiong et al., 2016), and cortical neurons showed signs of necroptosis after treatment with 1 mM METH at 39°C (Guo et al., 2020). Additionally, Zhao et al. reported that necroptosis occurred in the striatum of human and mice brain samples exposed to METH and the RIP3/MLKL/Drp1 pathway played an essential role in the mechanism of METH-induced neuronal programmed necrosis (Zhao et al., 2021). However, it is still unclear whether METH-induced HT can induce necroptosis in striatal neurons. In this study, METH combined with HT triggered necroptosis in striatal neurons after 6 h. The inhibition of HSP90α decreased the METH/HT-induced upregulation of p-RIP3, RIP3, p-MLKL, and MLKL, suggesting that HSP90α may mediate necroptosis by regulating the phosphorylation of RIP3. Interestingly, pyroptosis, an inflammasome-associated regulatory necrosis, is closely associated with the pathogenesis of neurodegenerative diseases (Wang et al., 2019; Huang et al., 2021) and METH induces ER stress that mediates GSDME-dependent pyroptosis in hippocampal neuronal cells (Liu et al., 2020). That is to say, METH abuse may cause a variety of regulatory cell necrosis. We postulate that different regulatory necrosis can be triggered under METH/HT injuries and the neural cells can experience extensive crosstalk between different types of cell death. Further research is needed to clarify this hypothesis.

In conclusion, our results indicated that HSP90α had a significant impact on METH/HT-induced necroptosis in striatal neurons. These results provide a deeper understanding of the regulatory mechanism of METH/HT-induced injury.

DATA AVAILABILITY STATEMENT

The original contributions presented in the study are included in the article/**Supplementary Material**, further inquiries can be directed to the corresponding authors.

ETHICS STATEMENT

The animal study was reviewed and approved by the Medical Ethics Committee of the Third Xiangya Hospital of Central South University.

AUTHOR CONTRIBUTIONS

KX and JY designed the study. L-S L conducted the experiments, analyzed the data, and prepared the article and images. SL, W-T Y, S-C W, L-M G, Y-D Y, X-M H, and QZ conducted the experiments, prepared the article and images, collected and analyzed the data and literature. KH prepared the article and images. KX, JY, and L-S L revised the article. All authors approved the final version of the article. All authors agreed to be accountable for all aspects of the study to ensure that questions related to the accuracy or integrity of any part of the work are appropriately investigated and resolved.

FUNDING

The work was supported by the grants from the National Natural Science Foundation of China (Nos. 81772134, 81772024, 82060339, 81971891, and 81571939), the Tianshan Xuesong Project of Xinjiang (No. 2019XS04), Hunan Provincial Innovation Foundation for Postgraduate (Nos. CX20190139 and CX20200116), the Fundamental Research Funds for the Central Universities of Central South University (Nos.

2019zzts083 and 2020zzts218), and the Subject of Hunan Provincial Department of Education (No.17C1422).

ACKNOWLEDGMENTS

The authors thank all the authors for their contribution to this work. L-S L would like to thank KX and JY for their guidance. The authors would like to thank Professor Jufang Huang for providing the experimental platform. The authors would like to thank the language-editing service provided by Wordvice.

SUPPLEMENTARY MATERIAL

The Supplementary Material for this article can be found online at: https://www.frontiersin.org/articles/10.3389/fphar.2021.716394/full#supplementary-material

REFERENCES

Ahn, S. G., and Thiele, D. J. (2003). Redox Regulation of Mammalian Heat Shock Factor 1 Is Essential for Hsp Gene Activation and protection from Stress. *Genes Dev.* 17 (4), 516–528. doi:10.1101/gad.1044503

Akerfelt, M., Morimoto, R. I., and Sistonen, L. (2010). Heat Shock Factors: Integrators of Cell Stress, Development and Lifespan. *Nat. Rev. Mol. Cel Biol* 11 (8), 545–555. doi:10.1038/nrm2938

Alexander, G. E., DeLong, M. R., and Strick, P. L. (1986). Parallel Organization of Functionally Segregated Circuits Linking Basal Ganglia and Cortex. *Annu. Rev. Neurosci.* 9, 357–381. doi:10.1146/annurev.ne.09.030186.002041

Ares-Santos, S., Granado, N., Espadas, I., Martinez-Murillo, R., and Moratalla, R. (2014). Methamphetamine Causes Degeneration of Dopamine Cell Bodies and Terminals of the Nigrostriatal Pathway Evidenced by Silver Staining. *Neuropsychopharmacology* 39 (5), 1066–1080. doi:10.1038/npp.2013.307

Badisa, R. B., Wiley, C., Randell, K., Darling-Reed, S. F., Latinwo, L. M., Agharahimi, M., et al. (2019). Identification of Cytotoxic Markers in Methamphetamine Treated Rat C6 Astroglia-like Cells. *Sci. Rep.* 9 (1), 9412. doi:10.1038/s41598-019-45845-1

Behrouzvaziri, A., Fu, D., Tan, P., Yoo, Y., Zaretskaia, M. V., Rusyniak, D. E., et al. (2015). Orexinergic Neurotransmission in Temperature Responses to Methamphetamine and Stress: Mathematical Modeling as a Data Assimilation Approach. *PLoS One* 10 (5), e0126719. doi:10.1371/journal.pone.0126719

Bowyer, J. F., Gough, B., Slikker, W., Jr., Lipe, G. W., Newport, G. D., and Holson, R. R. (1993). Effects of a Cold Environment or Age on Methamphetamine-Induced Dopamine Release in the Caudate Putamen of Female Rats. *Pharmacol. Biochem. Behav.* 44 (1), 87–98. doi:10.1016/0091-3057(93)90284-z

Buffum, J. C., and Shulgin, A. T. (2001). Overdose of 2.3 Grams of Intravenous Methamphetamine: Case, Analysis and Patient Perspective. *J. Psychoactive Drugs* 33 (4), 409–412. doi:10.1080/02791072.2001.10399926

Cadet, J. L., Krasnova, I. N., Jayanthi, S., and Lyles, J. (2007). Neurotoxicity of Substituted Amphetamines: Molecular and Cellular Mechanisms. *Neurotox Res.* 11 (3-4), 183–202. doi:10.1007/bf03033567

Calabresi, P., De Murtas, M., and Bernardi, G. (1997). The Neostriatum beyond the Motor Function: Experimental and Clinical Evidence. *Neuroscience* 78 (1), 39–60. doi:10.1016/s0306-4522(96)00556-8

Chatterjee, A., Dimitropoulou, C., Drakopanayiotakis, F., Antonova, G., Snead, C., Cannon, J., et al. (2007). Heat Shock Protein 90 Inhibitors Prolong Survival, Attenuate Inflammation, and Reduce Lung Injury in Murine Sepsis. *Am. J. Respir. Crit. Care Med.* 176 (7), 667–675. doi:10.1164/rccm.200702-291OC

Chauhan, H., Killinger, B. A., Miller, C. V., and Moszczynska, A. (2014). Single and Binge Methamphetamine Administrations Have Different Effects on the Levels of Dopamine D2 Autoreceptor and Dopamine Transporter in Rat Striatum. *Int. J. Mol. Sci.* 15 (4), 5884–5906. doi:10.3390/ijms15045884

Chen, W. W., Yu, H., Fan, H. B., Zhang, C. C., Zhang, M., Zhang, C., et al. (2012). RIP1 Mediates the protection of Geldanamycin on Neuronal Injury Induced by Oxygen-Glucose Deprivation Combined with zVAD in Primary Cortical Neurons. *J. Neurochem.* 120 (1), 70–77. doi:10.1111/j.1471-4159.2011.07526.x

Chen, X., Qiu, F., Zhao, X., Lu, J., Tan, X., Xu, J., et al. (2020). Astrocyte-Derived Lipocalin-2 Is Involved in Mitochondrion-Related Neuronal Apoptosis Induced by Methamphetamine. *ACS Chem. Neurosci.* 11 (8), 1102–1116. doi:10.1021/acschemneuro.9b00559

Cho, Y. S., Challa, S., Moquin, D., Genga, R., Ray, T. D., Guildford, M., et al. (2009). Phosphorylation-driven Assembly of the RIP1-RIP3 Complex Regulates Programmed Necrosis and Virus-Induced Inflammation. *Cell* 137 (6), 1112–1123. doi:10.1016/j.cell.2009.05.037

Chtourou, Y., Slima, A. B., Makni, M., Gdoura, R., and Fetoui, H. (2015). Naringenin Protects Cardiac Hypercholesterolemia-Induced Oxidative Stress and Subsequent Necroptosis in Rats. *Pharmacol. Rep.* 67 (6), 1090–1097. doi:10.1016/j.pharep.2015.04.002

Crean, R. D., Davis, S. A., and Taffe, M. A. (2007). Oral Administration of (+/-)3,4-methylenedioxymethamphetamine and (+)methamphetamine Alters Temperature and Activity in Rhesus Macaques. *Pharmacol. Biochem. Behav.* 87 (1), 11–19. doi:10.1016/j.pbb.2007.03.015

Crean, R. D., Davis, S. A., Von Huben, S. N., Lay, C. C., Katner, S. N., and Taffe, M. A. (2006). Effects of (+/-)3,4-methylenedioxymethamphetamine, (+/-)3,4-methylenedioxyamphetamine and Methamphetamine on Temperature and Activity in Rhesus Macaques. *Neuroscience* 142 (2), 515–525. doi:10.1016/j.neuroscience.2006.06.033

Davidson, C., Gow, A. J., Lee, T. H., and Ellinwood, E. H. (2001). Methamphetamine Neurotoxicity: Necrotic and Apoptotic Mechanisms and Relevance to Human Abuse and Treatment. *Brain Res. Brain Res. Rev.* 36 (1), 1–22. doi:10.1016/s0165-0173(01)00054-6

Degenhardt, L., Mathers, B., Guarinieri, M., Panda, S., Phillips, B., Strathdee, S. A., et al. (2010). Meth/amphetamine use and Associated HIV: Implications for Global Policy and Public Health. *Int. J. Drug Pol.* 21 (5), 347–358. doi:10.1016/j.drugpo.2009.11.007

Deng, X., Ladenheim, B., Tsao, L. I., and Cadet, J. L. (1999). Null Mutation of C-Fos Causes Exacerbation of Methamphetamine-Induced Neurotoxicity. *J. Neurosci.* 19 (22), 10107–10115.

Ding, W., Shang, L., Huang, J. F., Li, N., Chen, D., Xue, L. X., et al. (2015). Receptor Interacting Protein 3-induced RGC-5 Cell Necroptosis Following Oxygen Glucose Deprivation. *BMC Neurosci.* 16, 49. doi:10.1186/s12868-015-0187-x

Font-Belmonte, E., González-Rodríguez, P., and Fernández-López, A. (2020). Necroptosis in Global Cerebral Ischemia: a Role for Endoplasmic Reticulum Stress. *Neural Regen. Res.* 15 (3), 455–456. doi:10.4103/1673-5374.266054

Grad, I., Cederroth, C. R., Walicki, J., Grey, C., Barluenga, S., Winssinger, N., et al. (2010). The Molecular Chaperone Hsp90alpha Is Required for Meiotic Progression of Spermatocytes beyond Pachytene in the Mouse. *PLoS One* 5 (12), e15770. doi:10.1371/journal.pone.0015770

Granado, N., Ares-Santos, S., and Moratalla, R. (2013). Methamphetamine and Parkinson's Disease. *Parkinsons Dis.* 2013, 308052. doi:10.1155/2013/308052

Granado, N., Ares-Santos, S., O'Shea, E., Vicario-Abejon, C., Colado, M. I., and Moratalla, R. (2010). Selective Vulnerability in Striosomes and in the Nigrostriatal Dopaminergic Pathway after Methamphetamine Administration : Early Loss of TH in Striosomes after Methamphetamine. *Neurotox Res.* 18 (1), 48–58. doi:10.1007/s12640-009-9106-1

Granado, N., Ares-Santos, S., Tizabi, Y., and Moratalla, R. (2018). Striatal Reinnervation Process after Acute Methamphetamine-Induced Dopaminergic Degeneration in Mice. *Neurotox Res.* 34 (3), 627–639. doi:10.1007/s12640-018-9925-z

Guo, L. M., Wang, Z., Li, S. P., Wang, M., Yan, W. T., Liu, F. X., et al. (2020). RIP3/MLKL-mediated Neuronal Necroptosis Induced by Methamphetamine at 39 Degrees C. *Neural Regen. Res.* 15 (5), 865–874. doi:10.4103/1673-5374.268902

Guo, W., Reigan, P., Siegel, D., Zirrolli, J., Gustafson, D., and Ross, D. (2005). Formation of 17-Allylamino-Demethoxygeldanamycin (17-AAG) Hydroquinone by NAD(P)H:quinone Oxidoreductase 1: Role of 17-AAG Hydroquinone in Heat Shock Protein 90 Inhibition. *Cancer Res.* 65 (21), 10006–10015. doi:10.1158/0008-5472.CAN-05-2029

Gutierrez, A., Williams, M. T., and Vorhees, C. V. (2018). A Single High Dose of Methamphetamine Reduces Monoamines and Impairs Egocentric and Allocentric Learning and Memory in Adult Male Rats. *Neurotox Res.* 33 (3), 671–680. doi:10.1007/s12640-018-9871-9

He, J., Xu, H., Yang, Y., Zhang, X., and Li, X. M. (2004). Neuroprotective Effects of Olanzapine on Methamphetamine-Induced Neurotoxicity Are Associated with an Inhibition of Hyperthermia and Prevention of Bcl-2 Decrease in Rats. *Brain Res.* 1018 (2), 186–192. doi:10.1016/j.brainres.2004.05.060

He, S., Huang, S., and Shen, Z. (2016). Biomarkers for the Detection of Necroptosis. *Cell Mol Life Sci* 73 (11-12), 2177–2181. doi:10.1007/s00018-016-2192-3

He, S., Wang, L., Miao, L., Wang, T., Du, F., Zhao, L., et al. (2009). Receptor Interacting Protein Kinase-3 Determines Cellular Necrotic Response to TNF-Alpha. *Cell* 137 (6), 1100–1111. doi:10.1016/j.cell.2009.05.021

Herin, D. V., Liu, S., Ullrich, T., Rice, K. C., and Cunningham, K. A. (2005). Role of the Serotonin 5-HT2A Receptor in the Hyperlocomotive and Hyperthermic Effects of (+)-3,4-methylenedioxymethamphetamine. *Psychopharmacology (Berl)* 178 (4), 505–513. doi:10.1007/s00213-004-2030-4

Hermane, J., Eichner, S., Mancuso, L., Schroder, B., Sasse, F., Zeilinger, C., et al. (2019). New Geldanamycin Derivatives with Anti Hsp Properties by Mutasynthesis. *Org. Biomol. Chem.* 17 (21), 5269–5278. doi:10.1039/c9ob00892f

Herring, N. R., Schaefer, T. L., Gudelsky, G. A., Vorhees, C. V., and Williams, M. T. (2008). Effect of +-methamphetamine on Path Integration Learning, Novel Object Recognition, and Neurotoxicity in Rats. *Psychopharmacology (Berl)* 199 (4), 637–650. doi:10.1007/s00213-008-1183-y

Hu, X. M., Li, Z. X., Lin, R. H., Shan, J. Q., Yu, Q. W., Wang, R. X., et al. (2021). Guidelines for Regulated Cell Death Assays: A Systematic Summary, A Categorical Comparison, A Prospective. *Front Cel Dev Biol* 9, 634690. doi:10.3389/fcell.2021.634690

Huang, E., Huang, H., Guan, T., Liu, C., Qu, D., Xu, Y., et al. (2019). Involvement of C/EBPbeta-related Signaling Pathway in Methamphetamine-Induced Neuronal Autophagy and Apoptosis. *Toxicol. Lett.* 312, 11–21. doi:10.1016/j.toxlet.2019.05.003

Huang, J. F., Shang, L., Zhang, M. Q., Wang, H., Chen, D., Tong, J. B., et al. (2013). Differential Neuronal Expression of Receptor Interacting Protein 3 in Rat Retina: Involvement in Ischemic Stress Response. *BMC Neurosci.* 14, 16. doi:10.1186/1471-2202-14-16

Huang, W., Xie, W. B., Qiao, D., Qiu, P., Huang, E., Li, B., et al. (2015). Caspase-11 Plays an Essential Role in Methamphetamine-Induced Dopaminergic Neuron Apoptosis. *Toxicol. Sci.* 145 (1), 68–79. doi:10.1093/toxsci/kfv014

Huang, Y. N., Wu, C. H., Lin, T. C., and Wang, J. Y. (2009). Methamphetamine Induces Heme Oxygenase-1 Expression in Cortical Neurons and Glia to Prevent its Toxicity. *Toxicol. Appl. Pharmacol.* 240 (3), 315–326. doi:10.1016/j.taap.2009.06.021

Huang, Y. N., Yang, L. Y., Wang, J. Y., Lai, C. C., Chiu, C. T., and Wang, J. Y. (2017). L-ascorbate Protects against Methamphetamine-Induced Neurotoxicity of Cortical Cells via Inhibiting Oxidative Stress, Autophagy, and Apoptosis. *Mol. Neurobiol.* 54 (1), 125–136. doi:10.1007/s12035-015-9561-z

Huang, Y., Wang, S., Huang, F., Zhang, Q., Qin, B., Liao, L., et al. (2021). c-FLIP Regulates Pyroptosis in Retinal Neurons Following Oxygen-Glucose Deprivation/recovery via a GSDMD-Mediated Pathway. *Ann. Anat.* 235, 151672. doi:10.1016/j.aanat.2020.151672

Jiang, N., Zhang, X., Gu, X., Li, X., and Shang, L. (2021). Progress in Understanding the Role of lncRNA in Programmed Cell Death. *Cell Death Discov* 7 (1), 30. doi:10.1038/s41420-021-00407-1

Kanthasamy, K., Gordon, R., Jin, H., Anantharam, V., Ali, S., Kanthasamy, A. G., et al. (2011). Neuroprotective Effect of Resveratrol against Methamphetamine-Induced Dopaminergic Apoptotic Cell Death in a Cell Culture Model of Neurotoxicity. *Curr. Neuropharmacol* 9 (1), 49–53. doi:10.2174/157015911795017353

Kojima, T., Une, I., Yashiki, M., Noda, J., Sakai, K., and Yamamoto, K. (1984). A Fatal Methamphetamine Poisoning Associated with Hyperpyrexia. *Forensic Sci. Int.* 24 (1), 87–93. doi:10.1016/0379-0738(84)90156-7

Krasnova, I. N., and Cadet, J. L. (2009). Methamphetamine Toxicity and Messengers of Death. *Brain Res. Rev.* 60 (2), 379–407. doi:10.1016/j.brainresrev.2009.03.002

Kumar, P., Nagarajan, A., and Uchil, P. D. (2018). Analysis of Cell Viability by the Lactate Dehydrogenase Assay. *Cold Spring Harb Protoc.* 2018 (6). doi:10.1101/pdb.prot095497

Lepock, J. R. (2005). How Do Cells Respond to Their thermal Environment?. *Int. J. Hyperthermia* 21 (8), 681–687. doi:10.1080/02656730500307298

Li, D., Li, C., Li, L., Chen, S., Wang, L., Li, Q., et al. (2016). Natural Product Kongensin A Is a Non-canonical HSP90 Inhibitor that Blocks RIP3-dependent Necroptosis. *Cell Chem Biol* 23 (2), 257–266. doi:10.1016/j.chembiol.2015.08.018

Li, D., Xu, T., Cao, Y., Wang, H., Li, L., Chen, S., et al. (2015). A Cytosolic Heat Shock Protein 90 and Cochaperone CDC37 Complex Is Required for RIP3 Activation during Necroptosis. *Proc. Natl. Acad. Sci. U S A.* 112 (16), 5017–5022. doi:10.1073/pnas.1505244112

Liao, L., Shang, L., Li, N., Wang, S., Wang, M., Huang, Y., et al. (2017). Mixed Lineage Kinase Domain-like Protein Induces RGC-5 Necroptosis Following Elevated Hydrostatic Pressure. *Acta Biochim. Biophys. Sin (Shanghai)* 49 (10), 879–889. doi:10.1093/abbs/gmx088

Lin, D. Q., Cai, X. Y., Wang, C. H., Yang, B., and Liang, R. S. (2020). Optimal Concentration of Necrostatin-1 for Protecting against Hippocampal Neuronal Damage in Mice with Status Epilepticus. *Neural Regen. Res.* 15 (5), 936–943. doi:10.4103/1673-5374.268903

Liu, X., Shi, F., Li, Y., Yu, X., Peng, S., Li, W., et al. (2016). Post-translational Modifications as Key Regulators of TNF-Induced Necroptosis. *Cell Death Dis* 7 (7), e2293. doi:10.1038/cddis.2016.197

Liu, Y., Wen, D., Gao, J., Xie, B., Yu, H., Shen, Q., et al. (2020). Methamphetamine Induces GSDME-dependent Cell Death in Hippocampal Neuronal Cells through the Endoplasmic Reticulum Stress Pathway. *Brain Res. Bull.* 162, 73–83. doi:10.1016/j.brainresbull.2020.06.005

Lu, S., Liao, L., Zhang, B., Yan, W., Chen, L., Yan, H., et al. (2019). Antioxidant Cascades Confer Neuroprotection in Ethanol, Morphine, and Methamphetamine Preconditioning. *Neurochem. Int.* 131, 104540. doi:10.1016/j.neuint.2019.104540

Lu, S., Yang, Y., Liao, L., Yan, W., Xiong, K., and Yan, J. (2021). iTRAQ-Based Proteomic Analysis of the Rat Striatum in Response to Methamphetamine Preconditioning. *Acta Biochim. Biophys. Sin (Shanghai)* 53 (5), 636–639. doi:10.1093/abbs/gmab024

Marco, C. A., Gupta, K., Lubov, J., Jamison, A., and Murray, B. P. (2021). Hyperthermia Associated with Methamphetamine and Cocaine Use. *Am. J. Emerg. Med.* 42, 20–22. doi:10.1016/j.ajem.2020.12.083

Mechan, A. O., Esteban, B., O'Shea, E., Elliott, J. M., Colado, M. I., and Green, A. R. (2002). The Pharmacology of the Acute Hyperthermic Response that Follows Administration of 3,4-methylenedioxymethamphetamine (MDMA, 'ecstasy') to Rats. *Br. J. Pharmacol.* 135 (1), 170–180. doi:10.1038/sj.bjp.0704442

Melega, W. P., Cho, A. K., Harvey, D., and Laćan, G. (2007). Methamphetamine Blood Concentrations in Human Abusers: Application to Pharmacokinetic Modeling. *Synapse* 61 (4), 216–220. doi:10.1002/syn.20365

Melega, W. P., Williams, A. E., Schmitz, D. A., DiStefano, E. W., and Cho, A. K. (1995). Pharmacokinetic and Pharmacodynamic Analysis of the Actions of D-Amphetamine and D-Methamphetamine on the Dopamine Terminal. *J. Pharmacol. Exp. Ther.* 274 (1), 90–96.

Meng, L., Jin, W., and Wang, X. (2015). RIP3-mediated Necrotic Cell Death Accelerates Systematic Inflammation and Mortality. *Proc. Natl. Acad. Sci. U S A.* 112 (35), 11007–11012. doi:10.1073/pnas.1514730112

Miller, D. B., and O'Callaghan, J. P. (2003). Elevated Environmental Temperature and Methamphetamine Neurotoxicity. *Environ. Res.* 92 (1), 48–53. doi:10.1016/s0013-9351(02)00051-8

Papageorgiou, M., Raza, A., Fraser, S., Nurgali, K., and Apostolopoulos, V. (2019). Methamphetamine and its Immune-Modulating Effects. *Maturitas* 121, 13–21. doi:10.1016/j.maturitas.2018.12.003

Paratz, E. D., Cunningham, N. J., and MacIsaac, A. I. (2016). The Cardiac Complications of Methamphetamines. *Heart Lung Circ.* 25 (4), 325–332. doi:10.1016/j.hlc.2015.10.019

Parhamifar, L., Andersen, H., and Moghimi, S. M. (2019). Lactate Dehydrogenase Assay for Assessment of Polycation Cytotoxicity. *Methods Mol. Biol.* 1943, 291–299. doi:10.1007/978-1-4939-9092-4_18

Potvin, S., Pelletier, J., Grot, S., Hebert, C., Barr, A. M., and Lecomte, T. (2018). Cognitive Deficits in Individuals with Methamphetamine Use Disorder: A Meta-Analysis. *Addict. Behav.* 80, 154–160. doi:10.1016/j.addbeh.2018.01.021

Raineri, M., González, B., Rivero-Echeto, C., Muñiz, J. A., Gutiérrez, M. L., Ghanem, C. I., et al. (2015). Differential Effects of Environment-Induced Changes in Body Temperature on Modafinil's Actions against Methamphetamine-Induced Striatal Toxicity in Mice. *Neurotox Res.* 27 (1), 71–83. doi:10.1007/s12640-014-9493-9

Ren, W., Tao, J., Wei, Y., Su, H., Zhang, J., Xie, Y., et al. (2016). Time-Dependent Serum Brain-Derived Neurotrophic Factor Decline during Methamphetamine Withdrawal. *Medicine (Baltimore)* 95 (5), e2604. doi:10.1097/MD.0000000000002604

Ruan, Z. H., Xu, Z. X., Zhou, X. Y., Zhang, X., and Shang, L. (2019). Implications of Necroptosis for Cardiovascular Diseases. *Curr. Med. Sci.* 39 (4), 513–522. doi:10.1007/s11596-019-2067-6

Sabrini, S., Russell, B., Wang, G., Lin, J., Kirk, I., and Curley, L. (2019). Methamphetamine Induces Neuronal Death: Evidence from Rodent Studies. *Neurotoxicology* 77, 20–28. doi:10.1016/j.neuro.2019.12.006

Shang, L., Ding, W., Li, N., Liao, L., Chen, D., Huang, J., et al. (2017). The Effects and Regulatory Mechanism of RIP3 on RGC-5 Necroptosis Following Elevated Hydrostatic Pressure. *Acta Biochim. Biophys. Sin (Shanghai)* 49 (2), 128–137. doi:10.1093/abbs/gmw130

Shang, L., Huang, J. F., Ding, W., Chen, S., Xue, L. X., Ma, R. F., et al. (2014). Calpain: a Molecule to Induce AIF-Mediated Necroptosis in RGC-5 Following Elevated Hydrostatic Pressure. *BMC Neurosci.* 15, 63. doi:10.1186/1471-2202-15-63

Simon, S. L., Richardson, K., Dacey, J., Glynn, S., Domier, C. P., Rawson, R. A., et al. (2002). A Comparison of Patterns of Methamphetamine and Cocaine Use. *J. Addict. Dis.* 21 (1), 35–44. doi:10.1300/j069v21n01_04

Sprague, J. E., Riley, C. L., and Mills, E. M. (2018). Body Temperature Regulation and Drugs of Abuse. *Handb Clin. Neurol.* 157, 623–633. doi:10.1016/b978-0-444-64074-1.00036-7

Sreedhar, A. S., Kalmár, E., Csermely, P., and Shen, Y. F. (2004). Hsp90 Isoforms: Functions, Expression and Clinical Importance. *FEBS Lett.* 562 (1-3), 11–15. doi:10.1016/s0014-5793(04)00229-7

Sun, L., Wang, H., Wang, Z., He, S., Chen, S., Liao, D., et al. (2012). Mixed Lineage Kinase Domain-like Protein Mediates Necrosis Signaling Downstream of RIP3 Kinase. *Cell* 148 (1-2), 213–227. doi:10.1016/j.cell.2011.11.031

Tata, D. A., and Yamamoto, B. K. (2007). Interactions between Methamphetamine and Environmental Stress: Role of Oxidative Stress, Glutamate and Mitochondrial Dysfunction. *Addiction* 102 (Suppl. 1), 49–60. doi:10.1111/j.1360-0443.2007.01770.x

Valian, N., Ahmadiani, A., and Dargahi, L. (2017). Escalating Methamphetamine Regimen Induces Compensatory Mechanisms, Mitochondrial Biogenesis, and GDNF Expression, in Substantia Nigra. *J. Cel Biochem* 118 (6), 1369–1378. doi:10.1002/jcb.25795

Vieira, M., Fernandes, J., Carreto, L., Anuncibay-Soto, B., Santos, M., Han, J., et al. (2014). Ischemic Insults Induce Necroptotic Cell Death in Hippocampal Neurons through the Up-Regulation of Endogenous RIP3. *Neurobiol. Dis.* 68, 26–36. doi:10.1016/j.nbd.2014.04.002

Voss, A. K., Thomas, T., and Gruss, P. (2000). Mice Lacking HSP90beta Fail to Develop a Placental Labyrinth. *Development* 127 (1), 1–11.

Wang, M., Wan, H., Wang, S., Liao, L., Huang, Y., Guo, L., et al. (2020). RSK3 Mediates Necroptosis by Regulating Phosphorylation of RIP3 in Rat Retinal Ganglion Cells. *J. Anat.* 237 (1), 29–47. doi:10.1111/joa.13185

Wang, S., Yuan, Y. H., Chen, N. H., and Wang, H. B. (2019). The Mechanisms of NLRP3 Inflammasome/pyroptosis Activation and Their Role in Parkinson's Disease. *Int. Immunopharmacol* 67, 458–464. doi:10.1016/j.intimp.2018.12.019

Wang, Z., Guo, L. M., Wang, S. C., Chen, D., Yan, J., Liu, F. X., et al. (2018a). Progress in Studies of Necroptosis and its Relationship to Disease Processes. *Pathol. Res. Pract.* 214 (11), 1749–1757. doi:10.1016/j.prp.2018.09.002

Wang, Z., Guo, L. M., Wang, Y., Zhou, H. K., Wang, S. C., Chen, D., et al. (2018b). Inhibition of HSP90alpha Protects Cultured Neurons from Oxygen-Glucose Deprivation Induced Necroptosis by Decreasing RIP3 Expression. *J. Cel Physiol* 233 (6), 4864–4884. doi:10.1002/jcp.26294

Wang, Z., Guo, L. M., Zhou, H. K., Qu, H. K., Wang, S. C., Liu, F. X., et al. (2018c). Using Drugs to Target Necroptosis: Dual Roles in Disease Therapy. *Histol. Histopathol* 33 (8), 773–789. doi:10.14670/hh-11-968

Weinlich, R., Oberst, A., Beere, H. M., and Green, D. R. (2017). Necroptosis in Development, Inflammation and Disease. *Nat. Rev. Mol. Cel Biol* 18 (2), 127–136. doi:10.1038/nrm.2016.149

Wen, X. R., Li, C., Zong, Y. Y., Yu, C. Z., Xu, J., Han, D., et al. (2008). Dual Inhibitory Roles of Geldanamycin on the C-Jun NH2-terminal Kinase 3 Signal Pathway through Suppressing the Expression of Mixed-Lineage Kinase 3 and Attenuating the Activation of Apoptosis Signal-Regulating Kinase 1 via Facilitating the Activation of Akt in Ischemic Brain Injury. *Neuroscience* 156 (3), 483–497. doi:10.1016/j.neuroscience.2008.08.006

Wu, H., Kong, L., Cheng, Y., Zhang, Z., Wang, Y., Luo, M., et al. (2016). Corrigendum to "Metallothionein Plays a Prominent Role in the Prevention of Diabetic Nephropathy by Sulforaphane via Up-Regulation of Nrf2" [Free Radic. Biol. Med. 89 (2015) 431-42]. *Free Radic. Biol. Med.* 97 (621). doi:10.1016/j.freeradbiomed.2016.06.022

Wu, X., Hu, X., Zhang, Q., Liu, F., and Xiong, K. (2020). Regulatory Role of Chinese Herbal Medicine in Regulated Neuronal Death. *CNS Neurol. Disord. Drug Targets*. doi:10.2174/1871527319666200730165011

Xiao, H., and Lis, J. T. (1988). Germline Transformation Used to Define Key Features of Heat-Shock Response Elements. *Science* 239 (4844), 1139–1142. doi:10.1126/science.3125608

Xiong, K., Liao, H., Long, L., Ding, Y., Huang, J., and Yan, J. (2016). Necroptosis Contributes to Methamphetamine-Induced Cytotoxicity in Rat Cortical Neurons. *Toxicol. Vitro* 35, 163–168. doi:10.1016/j.tiv.2016.06.002

Xiong, K., Long, L., Zhang, X., Qu, H., Deng, H., Ding, Y., et al. (2017). Overview of Long Non-coding RNA and mRNA Expression in Response to Methamphetamine Treatment *In Vitro*. *Toxicol. Vitro* 44, 1–10. doi:10.1016/j.tiv.2017.06.009

Xu, X., Huang, E., Tai, Y., Zhao, X., Chen, X., Chen, C., et al. (2017). Nupr1 Modulates Methamphetamine-Induced Dopaminergic Neuronal Apoptosis and Autophagy through CHOP-Trib3-Mediated Endoplasmic Reticulum Stress Signaling Pathway. *Front. Mol. Neurosci.* 10, 203. doi:10.3389/fnmol.2017.00203

Yamamoto, B. K., Moszczynska, A., and Gudelsky, G. A. (2010). Amphetamine Toxicities: Classical and Emerging Mechanisms. *Ann. N. Y Acad. Sci.* 1187, 101–121. doi:10.1111/j.1749-6632.2009.05141.x

Yan, W. T., Lu, S., Yang, Y. D., Ning, W. Y., Cai, Y., Hu, X. M., et al. (2021). Research Trends, Hot Spots and Prospects for Necroptosis in the Field of Neuroscience. *Neural Regen. Res.* 16 (8), 1628–1637. doi:10.4103/1673-5374.303032

Yan, Y. E., Zhao, Y. Q., Wang, H., and Fan, M. (2006). Pathophysiological Factors Underlying Heatstroke. *Med. Hypotheses* 67 (3), 609–617. doi:10.1016/j.mehy.2005.12.048

Yang, X., Wang, Y., Li, Q., Zhong, Y., Chen, L., Du, Y., et al. (2018). The Main Molecular Mechanisms Underlying Methamphetamine- Induced Neurotoxicity and Implications for Pharmacological Treatment. *Front. Mol. Neurosci.* 11, 186. doi:10.3389/fnmol.2018.00186

Yin, X. H., Han, Y. L., Zhuang, Y., Yan, J. Z., and Li, C. (2017). Geldanamycin Inhibits Fas Signaling Pathway and Protects Neurons against Ischemia. *Neurosci. Res.* 124, 33–39. doi:10.1016/j.neures.2017.05.003

Yuan, J., Amin, P., and Ofengeim, D. (2019). Necroptosis and RIPK1-Mediated Neuroinflammation in CNS Diseases. *Nat. Rev. Neurosci.* 20 (1), 19–33. doi:10.1038/s41583-018-0093-1

Zhang, S. L., Yu, J., Cheng, X. K., Ding, L., Heng, F. Y., Wu, N. H., et al. (1999). Regulation of Human Hsp90alpha Gene Expression. *FEBS Lett.* 444 (1), 130–135. doi:10.1016/s0014-5793(99)00044-7

Zhao, X., Lu, J., Chen, X., Gao, Z., Zhang, C., Chen, C., et al. (2021). Methamphetamine Exposure Induces Neuronal Programmed Necrosis by Activating the Receptor-Interacting Protein Kinase 3 -related Signalling Pathway. *Faseb j* 35 (5), e21561. doi:10.1096/fj.202100188R

Zhu, J. P., Xu, W., and Angulo, J. A. (2005). Disparity in the Temporal Appearance of Methamphetamine-Induced Apoptosis and Depletion of Dopamine Terminal Markers in the Striatum of Mice. *Brain Res.* 1049 (2), 171–181. doi:10.1016/j.brainres.2005.04.089

Zhu, J. P., Xu, W., and Angulo, J. A. (2006). Methamphetamine-induced Cell Death: Selective Vulnerability in Neuronal Subpopulations of the Striatum in Mice. *Neuroscience* 140 (2), 607–622. doi:10.1016/j.neuroscience.2006.02.055

Zhu, J., Xu, W., Wang, J., Ali, S. F., and Angulo, J. A. (2009). The Neurokinin-1 Receptor Modulates the Methamphetamine-Induced Striatal Apoptosis and Nitric Oxide Formation in Mice. *J. Neurochem.* 111 (3), 656–668. doi:10.1111/j.1471-4159.2009.06330.x

Conflict of Interest: The authors declare that the research was conducted in the absence of any commercial or financial relationships that could be construed as a potential conflict of interest.

frontiers in Pharmacology

ORIGINAL RESEARCH
published: 26 July 2021
doi: 10.3389/fphar.2021.716703

Antibiotics Attenuate Methamphetamine-Induced Hepatotoxicity by Regulating Oxidative Stress and TLR4/MyD88/Traf6 Axis

Li-Jian Chen[1†], Jie-Tao He[1,2†], Ming Pan[3†], Jia-Li Liu[1], Kai-Kai Zhang[1], Jia-Hao Li[1], Li-Bin Wang[4], Ling-Ling Xu[4], Yu-Kui Chen[4], Qin-Yao Zhang[4], Dong-Ri Li[5], Jing-Tao Xu[6]* and Xiao-Li Xie[4]**

[1]Department of Forensic Pathology, School of Forensic Medicine, Southern Medical University, Guangzhou, China, [2]Department of Basic Medicine and Biomedical Engineering, School of Medicine, Foshan University, Foshan, China, [3]Department of Anesthesiology, Dalian Municipal Central Hospital, Dalian, China, [4]Department of Toxicology, School of Public Health (Guangdong Provincial Key Laboratory of Tropical Disease Research), Southern Medical University, Guangzhou, China, [5]Department of Forensic Evidence Science, School of Forensic Medicine, Southern Medical University, Guangzhou, China, [6]Department of Forensic Clinical Medicine, School of Forensic Medicine, Southern Medical University, Guangzhou, China

Methamphetamine (METH) is a major psychostimulant drug of abuse worldwide, and its neurotoxicity has been studied extensively. In addition to neurotoxicity, METH can also induce hepatotoxicity. The underlying mechanism of intestinal microorganisms in METH-induced hepatotoxicity remains unclear. In this study, mice have received antibiotics intragastrically or PBS once each day for 1 week, followed by METH or saline. The antibiotics attenuated METH-induced hepatotoxicity as evidenced by histopathological observation and biochemical analysis; furthermore, they alleviated METH-induced oxidative stress. The effect of antibiotics on METH-induced hepatotoxicity was investigated using RNA-sequencing (RNA-seq). The RNA-seq results demonstrated that antibiotics could regulate 580 differentially expressed genes (DEGs), of which 319 were upregulated after METH treatment and then downregulated with antibiotic pretreatment and 237 were first downregulated after METH administration and then upregulated after antibiotic pretreatment, in addition to 11 upregulated and 13 downregulated ones simultaneously in METH and antibiotic-pretreated groups. RNA-seq analyses revealed that TLR4 is one of the hub genes. Western blot analysis indicated that antibiotics inhibited the increase of TLR4, MyD88 and Traf6 induced by METH. This research suggests that antibiotics may play an important role in preventing METH-induced liver injury by regulating oxidative stress and TLR4/MyD88/Traf6 axis, though further investigation is required.

Keywords: methamphetamine, antibiotics, hepatotoxicity, RNA-seq, RT-qPCR

OPEN ACCESS

Edited by:
Zeng Xiao Feng,
Kunming Medical University, China

Reviewed by:
Wu Xu,
China Medical University, China
Luyang Tao,
Soochow University, China

****Correspondence:***
Dong-Ri Li
lidongri@smu.edu.cn
Jing-Tao Xu
xjt3080@smu.edu.cn
Xiao-Li Xie
xiexiaoli1999@126.com

†These authors have contributed equally to this work

Specialty section:
This article was submitted to Experimental Pharmacology and Drug Discovery, a section of the journal Frontiers in Pharmacology

Received: *29 May 2021*
Accepted: *28 June 2021*
Published: *26 July 2021*

Citation:
Chen L-J, He J-T, Pan M, Liu J-L, Zhang K-K, Li J-H, Wang L-B, Xu L-L, Chen Y-K, Zhang Q-Y, Li D-R, Xu J-T and Xie X-L (2021) Antibiotics Attenuate Methamphetamine-Induced Hepatotoxicity by Regulating Oxidative Stress and TLR4/MyD88/Traf6 Axis. Front. Pharmacol. 12:716703. doi: 10.3389/fphar.2021.716703

HIGHLIGHTS

- Methamphetamine (METH) induces hepatotoxicity in mice.
- Antibiotics alleviate METH-induced hepatotoxicity by regulating oxidative stress and TLR4/MyD88/Traf6 pathway.
- Clearance of microbiota by antibiotics suggested that gut flora may involve in protecting antibiotic preconditioning on METH-mediated hepatotoxicity.

INTRODUCTION

Abuse of METH has become a major worldwide health problem (Xu et al., 2019; Xu and Liu, 2019). As known, METH is harmful to multiple organs (e.g., the brain, heart, liver, lung, kidney, and spleen), and the current research mainly focuses on its neurotoxicity (Liu et al., 2017; Moratalla et al., 2017; Zhang et al., 2017; Yang et al., 2018), and METH-induced hepatic injury has recently been studied (Dias Da Silva et al., 2013; Halpin et al., 2013). Previous studies found that globulin increased, albumin decreased, and albumin/globulin decreased in METH-abuser serum, indicating that METH would induce hepatic disease and inflammation (Zhao et al., 2020). Eskandari et al. reported that METH cytotoxicity was related to oxidative stress and subsequent mitochondrial membrane conformation changes and cytochrome c release into the cytosol (Eskandari et al., 2014). However, preconditioning of chlorogenic and caftaric acids could prevent liver toxicity and oxidative stress induced by METH injections (Koriem and Soliman, 2014). Similarly, our team demonstrated that METH induced hepatotoxicity by inducing cell cycle arrest and activating apoptosis (Wang et al., 2017) and luteolin exerted protective effects against METH hepatotoxicity by suppressing apoptosis, autophagy, and inflammation in rats (Qu et al., 2020; Zhang et al., 2021).

Accumulating evidence suggested that intestinal flora overgrowth might improve translocation of enteric bacteria and their metabolites to the liver through the portal venous system and lead to inflammation, oxidative stress, and other liver diseases (Berg and Garlington, 1979; Albillos, 2003; Meng et al., 2018). Intestinal microbiological disorders are crucial for developing liver diseases, such as non-alcoholic fatty liver disease (NAFLD), alcoholic liver disease (ALD), cirrhosis, non-alcoholic steatohepatitis (NASH), and viral hepatitis (Milosevic et al., 2019; Albhaisi et al., 2020). Our previous studies have demonstrated that METH induces a decrease in the abundance of intestinal probiotics in the gut and increases the conditionally pathogenic bacteria with pro-inflammatory effects (Chen et al., 2021). Using antibiotics in mice liver disease models clearly demonstrates that targeting intestinal flora can alleviate hepatic inflammation by reducing lipopolysaccharide transport to the liver (Tripathi et al., 2018; Mu and Zhu, 2019). Oral non-absorbable antibiotics can reduce inflammation caused by bacterial translocation (Bajaj et al., 2018; Mendoza et al., 2020). Inflammation was reported to play a significant function in the pathophysiology of neuropsychiatric diseases, and minocycline has potent neuroprotective and anti-inflammatory effects that reduce behavior and dopaminergic neurotoxicity in mice after METH treatment (Hashimoto, 2008; Hashimoto et al., 2013). However, the exact mechanisms of antibiotics on METH-induced hepatotoxicity have not been elucidated.

Herein, mice were pretreated with non-absorbable antibiotics, followed by METH injection. Histopathology and biochemical analyses were conducted to determine hepatic damage, and RNA-seq was performed for a potential mechanism of the protective effects of antibiotic pretreatment in METH. Overall, our findings may provide novel evidence for prevention and therapy of METH-induced hepatotoxicity.

MATERIALS AND METHODS

Chemicals

METH was purchased from the National Institute for the Control of Pharmaceutical and Biological Products (Beijing, China), with a purity > 99.0%. Vancomycin, neomycin sulfate, metronidazole, and ampicillin were obtained from Sangon Biotech (Shanghai, China).

Animals and Treatments

The six- to eight-week-old BABL/c mice purchased from the Laboratory Animal Center of Southern Medical University were accommodated in specific-pathogen-free conditions for a week with accessible water and food. The animal procedure was carried out according to the National Institutes of Health Guide for the Care and Use of Laboratory Animals of Southern Medical University (Ethical Committee Approval Code: L2018123).

Mice were randomly divided into four groups with eight per group: control, antibiotic, METH, and antibiotic pretreatment. Briefly, based on the METH model of escalating dose/multiple binge, the doses were as follows (Chen et al., 2021): days 1–2, 1.5 mg/kg; days 3–4, 4.5 mg/kg; days 5–6, 7.5 mg/kg; and days 7–8, 10 mg/kg, four injections a day every 2 h. Mice received antibiotics (vancomycin, 100 mg/kg; neomycin sulfate, 200 mg/kg; metronidazole, 200 mg kg; and ampicillin, 200 mg/kg) and were gavaged once a day for 1 week (Gregory et al., 2015; Hu et al., 2017), and the following week, they were simultaneously injected with METH as mentioned above. All mice were deeply anesthetized with pentobarbital (45 mg/kg i.p.) within 24 h of the final dose. Blood samples were collected and centrifuged (4°C, 1,2000 r/min, 10 min) and then stored at −80°C until biochemical analysis. The liver tissues were removed and weighed, a portion was fixed with formalin buffered with 10% PBS, and others were stored at −80°C for further analysis.

Histological Analysis: Determination of Aspartate Transaminase and Alanine Aminotransferase Levels in Serum

The liver tissue was dehydrated, embedded in paraffin, sectioned (3 μm thickness), and stained with hematoxylin and eosin (H&E) (Xie et al., 2019). The pathological morphology of liver tissue was

observed under an optical microscope (Olympus, Tokyo, Japan). The activities of serum alanine aminotransferase (ALT) and aspartate aminotransferase (AST) were measured with the ELISA kit (MEIMIAN, Jiangsu, China) following the manufacturer's instructions.

Biochemical Analysis in Liver

Liver tissue (not less than 100 mg) was homogenized with 200 μl PBS (pH = 7.2–7.4, concentration 0.01 mol/L) and centrifuged (12,000 g/min) at 4°C for 10 min. The supernatant was taken to measure protein concentration using the BCA kit (Thermo Scientific, MA, United States). SOD and ROS concentrations in liver tissue were detected using the ELISA kit (MEIMIAN, Jiangsu, China) following the reagent protocol.

RNA-seq Analyses

RNA Extraction, Library Preparation, and Illumina HiSeq X Ten/NovaSeq 6000 Sequencing

Total RNA of liver was extracted with TRIzol® reagent (Invitrogen), and gDNA was removed using DNase I (TaKara). The RNA-seq transcriptome library was prepared using 1 μg total RNA according to TruSeq™ RNA Sample Preparation Kit from Illumina (San Diego, CA, United States). The RNA-seq process is as follows: isolate mRNA, fragment mRNA, synthesize cDNA, connect adaptor, select fragment, PCR cycles, and Illumina HiSeq X Ten/NovaSeq 6000 sequence.

Read Mapping

Quality control of raw data was conducted with SeqPrep (https://github.com/jstjohn/SeqPrep) and Sickle (https://github.com/najoshi/sickle). The clean reads were separately compared with the reference genome using HISAT2 software (http://ccb.jhu.edu/software/hisat2/index.shtml) (Kim et al., 2015). StringTie (https://ccb.jhu.edu/software/stringtie/index.shtml? t=example) was used to assemble the mapped reads of each sample in a reference-based approach (Pertea et al., 2015).

Differential Expression Analysis and Functional Enrichment

To identify the difference of DEGs among different samples, the transcripts per million reads (TPM) method calculated the expression level of each transcript.

DEGs with fold change ≥2 or ≤0.5 were considered to be significantly differentially expressed genes. GO functional enrichment and KEGG pathway analysis were carried out through Goatools (https://github.com/tanghaibao/Goatools) and KOBAS (http://kobas.cbi.pku.edu.cn/home.do) (Xie et al., 2011). PPI analysis was conducted with Cytoscape 3.7.1 software.

Real-Time Quantitative Polymerase Chain Reaction Analysis

To verify RNA-seq results, four genes (Acaca, Chrna4, Nr1d2, and Csrnp1) were randomly selected for real-time quantitative PCR (RT-qPCR) analysis. Total RNA was extracted with TRIzol® reagent (Invitrogen, MA, United States), and RNA quality was detected with a NanoDrop 2000 Spectrophotometer (Thermo Scientific, MA, United States) (Zhou et al., 2020). Total RNA was converted to cDNA using Hifair™ II First-Strand cDNA Synthesis SuperMix (YEASEN, Shanghai, China). Real-time quantitative PCR (RT-qPCR) was performed on a LightCycler® 96 System (Roche Life Science, Penzberg, Germany) using Hieff™ qPCR SYBR Green Master Mix (No Rox Plus, YEASEN, Shanghai, China) to quantify mRNA expression. Primers were designed with Primer3 web software (http://primer3.ut.ee/) (**Table 1**). The gene expression was normalized to β-actin. Relative quantification was calculated using the CT ($2^{-\Delta\Delta Ct}$) method.

Western Blot Analysis

The total liver tissue protein was extracted with lysis buffer (RIPA lysis buffer: PMSF: phosphatase inhibitors = 100: 1: 1). The Pierce™ BCA Protein Assay Kit (Thermo Scientific, MA, United States) was used to measure the protein concentration. 20 μg of proteins was resolved by 12% SDS-PAGE and transferred to PVDF membranes. The membranes were blocked with 5% skim milk at room temperature for 2 h, incubated with primary antibodies overnight at 4°C, and then incubated with appropriate secondary antibodies for 2 h at room temperature. Protein bands were revealed using chemiluminescence reagents (Thermo Scientific, MA, United States). The grayscale was calculated by ImageJ (version 1.8.0) software with normalization to that of β-actin. The antibodies and their dilutions were as follows: TLR4 (1:1,000; Santa Cruz, CA, United States), MyD88 (1:1,000; CST), Traf6 (1:1,000; Santa Cruz, CA, United States), and GAPDH (1:1,000; Proteintech).

Statistical Analysis

All results were reported as mean ± SEM. Statistical analysis was performed using GraphPad Prism 8.0 software. Statistical significance was calculated using one-way ANOVA followed by the Bonferroni post hoc test for multiple comparisons. p-Values < 0.05 were considered statistically significant (*/#p < 0.05, **/##p < 0.01, and ***/###p < 0.001).

RESULTS

Antibiotics Attenuated Methamphetamine-Induced Hepatotoxicity

Antibiotic and METH treatment significantly decreased the body and liver weights of mice (**Figures 1A,B**). Antibiotic pretreatment tends to alleviate METH-induced body and liver weight loss, with a non-significant difference (**Figures 1A,B**). Histopathological analysis revealed that karyopyknosis and extensive cytoplasmic damage (vacuolar degeneration) in METH-treated mice were ameliorated by antibiotic pretreatment (**Figure 1C**). However, there is no noticeable damage in hepatocytes' morphology in control and antibiotic groups (**Figure 1C**). Similarly, serum ALT and AST activities were remarkably increased after METH administration but decreased with antibiotic pretreatment (**Figures 1D,E**).

TABLE 1 | Primers for RT-qPCR analysis.

Gene	F	R
Csrnp1	5′-TTCATTCACACCCTCACCCG-3′	5′-CCAGGGAGGCTACCTTCTCT-3′
Nr1d2	5′-CCACCTGCAGAATGACACC-3′	5′-AGATGCATCCTCCCTCCAGT-3′
Chrna4	5′-CTGCCCCAACTTTCTGCAAC-3′	5′-TGGCCACGTATTTCCAGTCC-3′
Acaca	5′-TTGCCATGGGGATCCCTCTA-3′	5′-GCTGTTCCTCAGGCTCACAT-3′
β-Actin	5′-CTGGTCGTACCACAGGCATT-3′	5′-TGCTAGGAGCCAGAGCAGTA-3′

Antibiotic Pretreatment Mitigated Methamphetamine-Induced ROS and SOD Levels

To further investigate the protective effect of antibiotics on METH-induced liver injury, ROS and SOD concentrations in liver were measured. As illustrated in **Figure 2**, antibiotic cocktail pretreatment dramatically relieved METH-induced ROS and SOD elevation activities.

RNA-seq

Principal Correlation Analysis and Differentially Expressed Genes

PCA intuitively showed a clear correlation between the gene expression of samples in the group and apparent separation and distinction among the three groups (**Figure 3A**). A total of 580 DEGs were identified ($|\log_2$ (fold change)$| \geq 1$), of which 319 were upregulated after METH treatment and then downregulated with antibiotic pretreatment and 237 were first downregulated after METH administration and then upregulated after antibiotic pretreatment, in addition to 11 upregulated and 13 downregulated ones simultaneously in METH and antibiotic-pretreated groups (**Figures 3B–D**).

GO and KEGG Pathway Enrichment Analyses

To further predict the relationship between biological function and DEGs, GO analysis was carried out in three categories: molecular function, biological process, and cell composition (**Figure 4A**). KEGG analysis revealed that 580 DEGs were enriched in 15 pathways (**Figure 4B**), contributing to the study of gene and expression information of the whole network. **Figure 4B** displays enrichment of KEGG pathways, including AMPK and PPAR signaling pathways, fatty acid biosynthesis, and cholesterol and retinol metabolisms.

PPI Analysis

The PPI analysis allows us to better understand molecular mechanisms of core signaling pathways and core genes (Fei et al., 2020). The more connections or the closer to circle center of genes might be related to underlying mechanisms of METH hepatotoxicity and antibiotic protection (**Figure 5A**). The hub genes corresponding to the top-ranked proteins were selected by Cytoscape software, and these genes mostly interacted with other DEGs such as Pnpla2, Pnpla5, Pnpla3, Fasn, Acly, and TLR4 (**Figure 5B**, **Figure 6**).

Validation of the RNA-seq Results via Real-Time Quantitative Polymerase Chain Reaction

To verify RNA-seq results' accuracy, four genes (Chrna4, Acaca, Nr1d2, and Csrnp1) were randomly selected for RT-qPCR analysis. Acaca and Chrna4 were upregulated DEGs in the METH group compared with the control group and downregulated after antibiotic pretreatment, while Nr1d2 and Csrnp1 were reversed. The RT-qPCR results followed those of RNA-seq (**Figure 7**). However, RNA-seq was not conducted in the antibiotic group, and RT-qPCR data certified no difference compared to the control group.

Pretreatment of Antibiotics Alleviates Methamphetamine-Induced Inflammation via TLR4/MyD88/Traf6 Pathway

As indicated by PPI analysis, TLR4 is one of the hub genes, which may have a strong association with METH-induced hepatotoxicity. As shown in **Figure 8**, protein levels of some key factors in the TLR4/MyD88-dependent signaling axis, including TLR4, MyD88, and Traf6, were upregulated in the METH-treated group, and antibiotic pretreatment effectively inhibited upregulation, while control and antibiotic groups showed no difference.

DISCUSSION

It has been confirmed that METH induces hepatotoxicity in humans, rats, and cells (Dias Da Silva et al., 2013; Zhao et al., 2020; Zhang et al., 2021). Consistent with findings, this research demonstrated that the escalating dose/multiple binge METH model could also lead to hepatotoxicity in mice, indicated by histopathological examination and ALT and AST activities. The histopathology visually showed METH-induced hepatotoxicity, including nuclear pyknosis and cytoplasmic vacuolation. ALT and AST activity levels in serum are biomarkers for evaluating liver function. After METH injection, these markers increased, suggesting that METH resulted in liver dysfunction. Collectively, antibiotic pretreatment improved abnormalities alteration above, demonstrating that antibiotics can protect the liver from METH damage.

Oxidative stress is characterized by imbalanced generation of reactive oxygen species (ROS) and activity of antioxidant defenses (Bresciani et al., 2015; Arefin et al., 2020) and is known to be

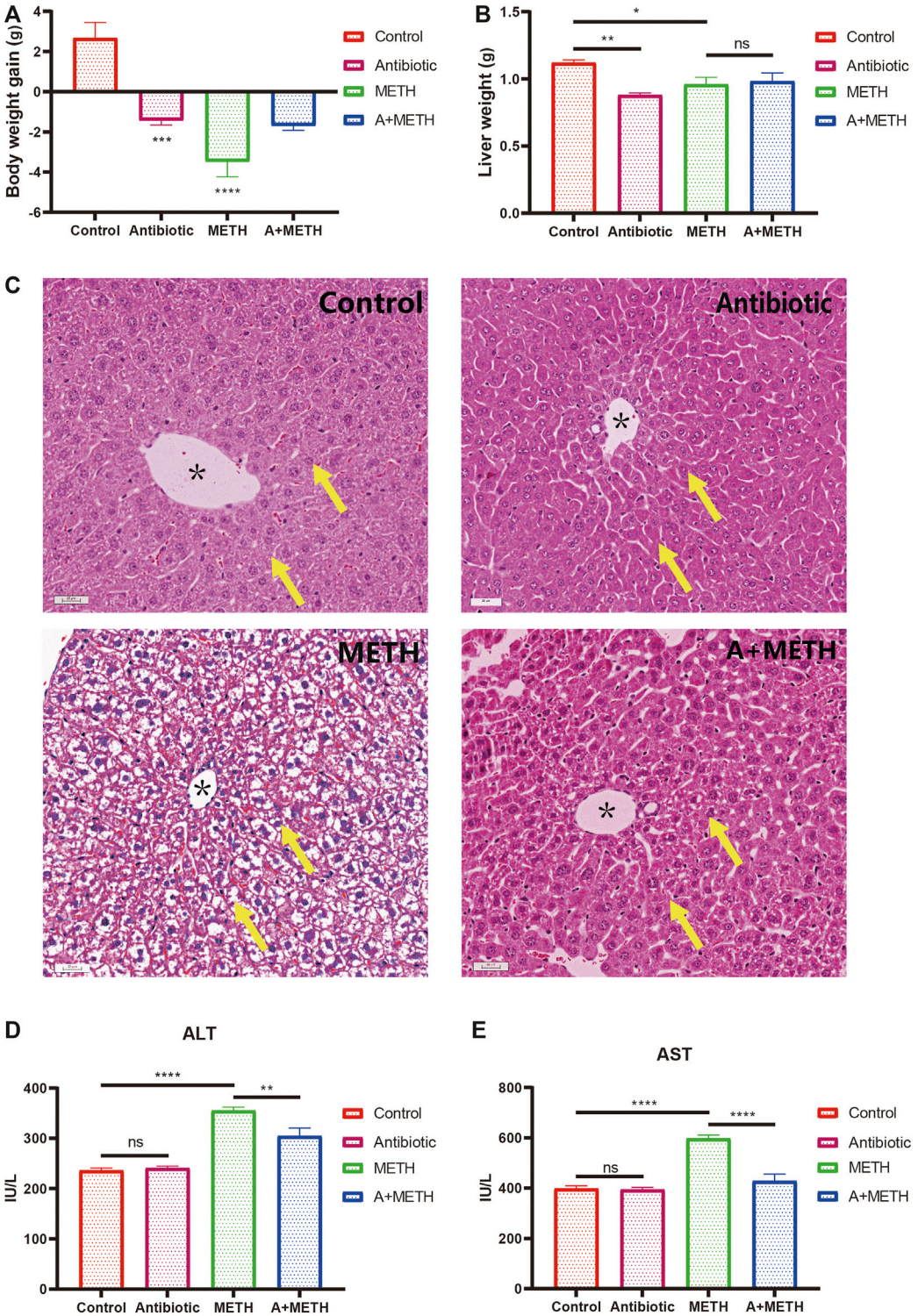

FIGURE 1 | Changes in body weight **(A)** and liver weight **(B)** of mice compared with the control group. Histopathological assessment of METH liver injury **(C)**. The yellow arrows point to the nucleus and cytoplasm; * indicates the central vein; bar = 20 μm, 20×. METH significantly enhanced serum ALT **(D)** and AST **(E)** activities relative to the control group. The increasing level was attenuated in the A + METH (antibiotic + METH) group. *$p < 0.05$; **$p < 0.01$; ***$p < 0.001$; ns, statistically non-significant.

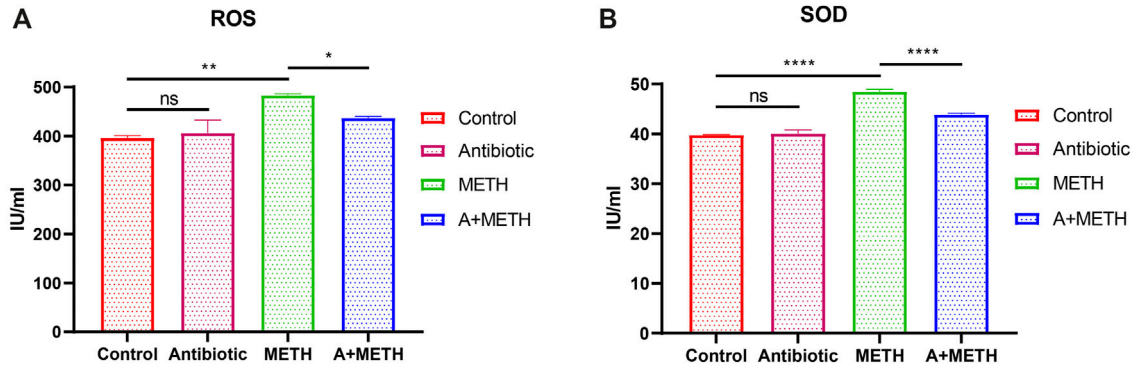

FIGURE 2 | Analyses of ROS and SOD activities. The treatment with METH significantly increased ROS **(A)** and SOD **(B)** activities, which significantly repressed with antibiotic pretreatment. Antibiotics alone did not change compared to the control group. *$p < 0.05$; **$p < 0.01$; ***$p < 0.001$; ns, statistically non-significant.

related to pathologies of some diseases, such as atherosclerosis (Kattoor et al., 2017), Alzheimer's disease (Chen and Zhong, 2014), and tumorigenesis (Gorrini et al., 2013). Oxidative stress is now recognized as a contributing factor in pathogenesis of various liver diseases. Alcoholic liver disease (ALD), non-alcoholic fatty liver disease (NAFLD), hepatic encephalopathy (HE), hepatic fibrosis, and hepatitis C virus (HCV) are undoubtedly linked to ROS overproduction and existence of oxidative stress within hepatocytes (Cichoż-Lach, 2014). Superoxide dismutase (SOD) is an important superoxide and free radical scavenger that controls the levels of all kinds of ROS and reactive nitrogen species (Halliwell and Gutteridge, 1984; Wang et al., 2018). SOD levels in serum and liver tissues are significantly increased in acute liver failure patients than in healthy controls, which may be an adaptive response to limit ROS harmful effects (Tian et al., 2018). Consistent with previous studies (Xie et al., 2018a; Zhang et al., 2018), this study reported that ROS and SOD levels were increased after METH treatment. Poorly absorbed antibiotics in drinking water were reported to reverse age-related arterial dysfunction, inflammation, and oxidative stress in mice by inhibiting intestinal flora (Brunt et al., 2019). The generation of ROS may be related to the gut microbiota (Jones and Neish, 2017), and gut microbiota–derived short-chain fatty acids (SCFAs) affect mitochondrial function and reduce ROS production (Mottawea et al., 2016; Luca et al., 2019). The present study also proved that antibiotic pretreatment could prevent METH-induced oxidative stress by inhibiting the increase of ROS and SOD, which may be the potential mechanism.

RNA-seq was also used to further investigate the underlying mechanism of protective effect of antibiotics against METH-induced hepatotoxicity. Hundreds of DEGs have been detected by sequencing, and we screened out some of the hub genes for subsequent verification; meanwhile, subsequent GO and KEGG analyses were performed based on these DEGs. The AMPK signaling pathway was reported to reverse steatosis and inflammation in non-alcoholic fatty liver disease (NAFLD) (Li et al., 2019). The PPAR signaling pathway plays an important role in attenuating liver fibrosis (Panebianco et al., 2017) and hepatic lipoinflammation (Ishtiaq et al., 2019). This research and our previous studies about METH-induced hepatotoxicity in rats (Koriem and Soliman, 2014; Wang et al., 2017) indicated that AMPK and PPAR signaling pathways were enriched in KEGG analysis, highlighting their possible significant correlation with METH-induced hepatotoxicity, though further research is required.

Toll-like receptors (TLRs) hold a fundamental function in regulating innate and adaptive immune response, pathogen recognition, and inflammatory responses (Lai et al., 2015; Xie et al., 2018b). TLR4 can recruit the adaptor proteins (such as MyD88), bind to Traf6, and eventually result in inflammation (Xie et al., 2018b). Interestingly, RNA-seq data suggested that TLR4 is one of the hub genes. The western blot results showed that TLR4/MyD88/Traf6 was elevated after METH treatment, suggesting that METH treatment induced liver inflammation, and antibiotics pretreatment can reverse this elevation. Moreover, excessive ROS production caused tissue damage and accelerated release and development of inflammation via activating the TLR4/MyD88/Traf6 pathway (Gong et al., 2019; Zhou et al., 2020). The above results indicated that antibiotic preconditioning exerts protection against METH-induced hepatotoxicity by inhibiting the TLR4/MyD88/Traf6 pathway.

There is growing evidence showing that alterations in the gut microbiome are linked to pathogenesis and advancement of liver diseases named the "gut–liver axis" (Ma et al., 2017; Milosevic et al., 2019; Albillos et al., 2020; Jones and Neish, 2021). A recent report revealed that intestinal dysbacteriosis might directly cause liver toxicity through the portal vein or destruction of the intestinal barrier, leading to increased bacterial translocation and inflammation (Acharya and Bajaj, 2021). Recent reports have shown that antibiotics positively affect liver injury caused by intestinal bacteria overgrowth, confirming the relationship between intestinal microbiota and liver diseases (Sajjad et al., 2005; Wu et al., 2008). Our previous studies have shown that, after METH treatment, intestinal probiotics were decreased and opportunistic pathogens were increased (Chen et al., 2021). Notably, antibiotics used in this study have been proven to affect clearing intestinal flora (Rakoff-Nahoum et al., 2004; Carvalho et al., 2012). Overall, our analysis reveals a novel

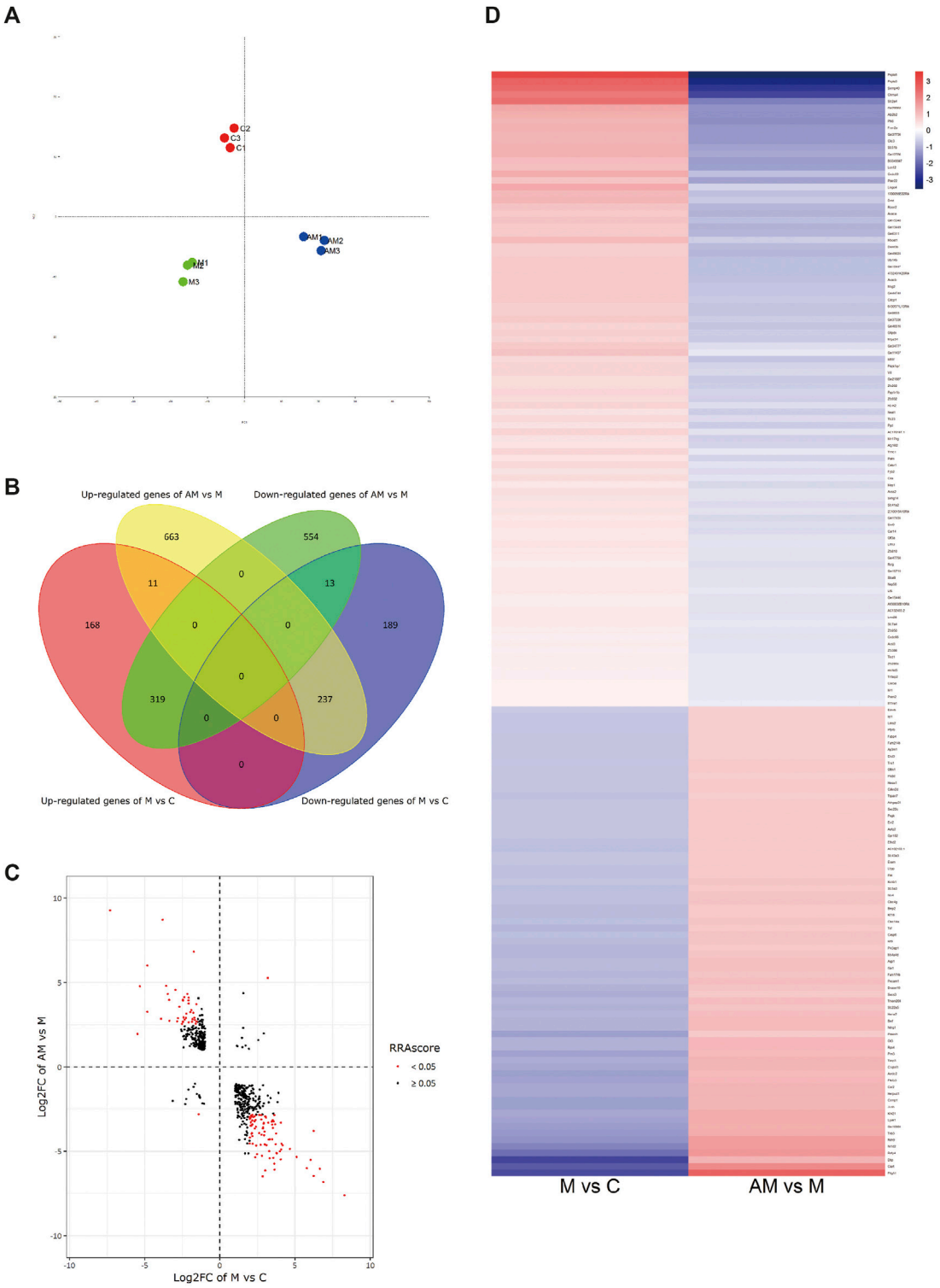

FIGURE 3 | (A) Principal correlation analysis. **(B)** Venn diagram of DEGs. **(C)** Volcano plot diagram: the first and third quadrants show the genes both up- and downregulated in both METH and antibiotic-pretreated groups, the second quadrant shows the genes downregulated in the METH group but upregulated in the AM group, and the fourth quadrant shows the genes upregulated in the METH group but downregulated in the AM group. **(D)** Heatmap diagram of DEG analysis among groups. The blue color represents downregulation, while red represents upregulation. C, control group; M, METH group; AM, antibiotic + METH group.

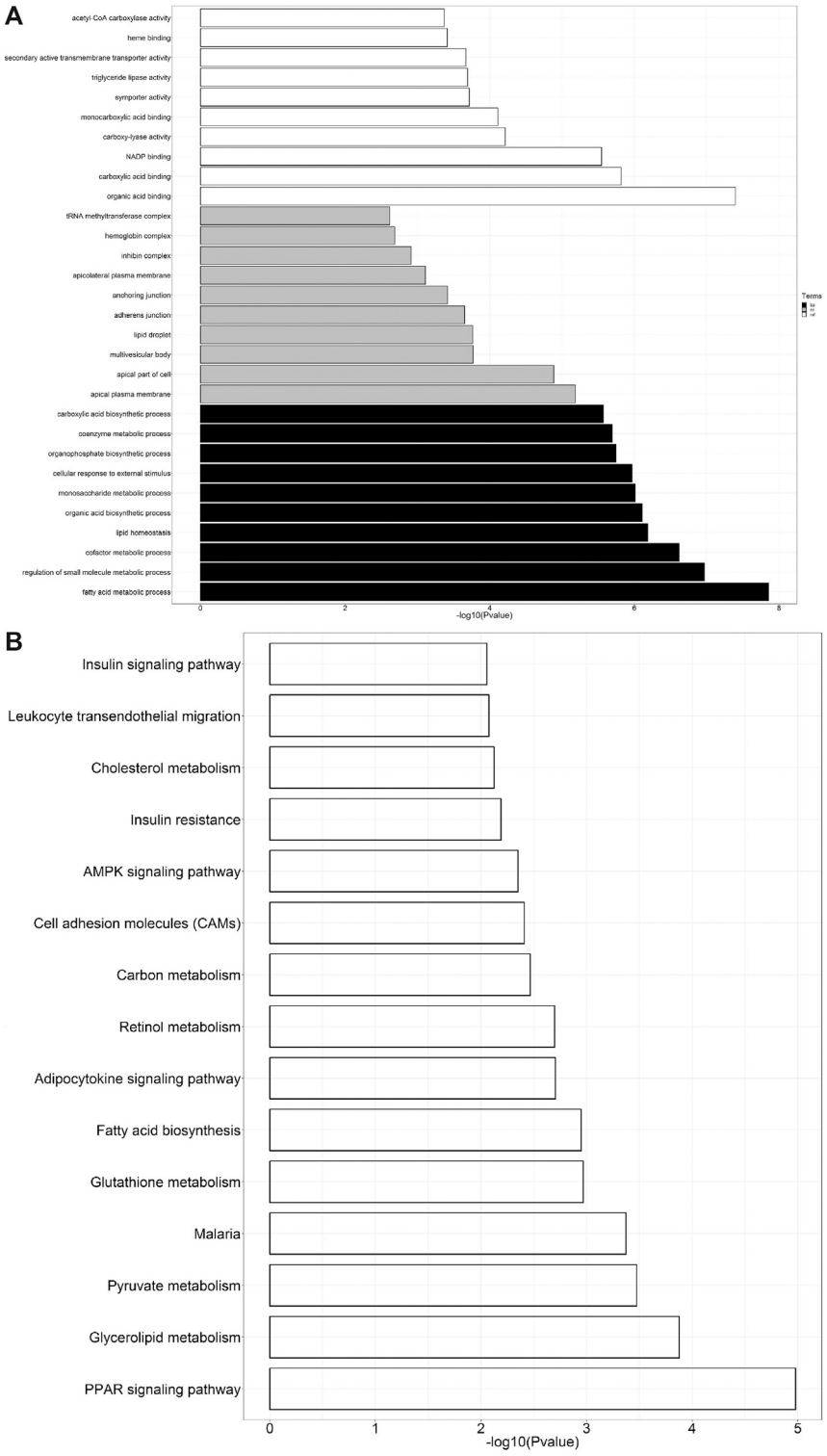

FIGURE 4 | (A) GO analysis of DEGs. The black bars represent biological processes (bp), gray represents cellular components (cc), and white represents molecular functions (mf). **(B)** KEGG pathway enrichment analysis of DEGs.

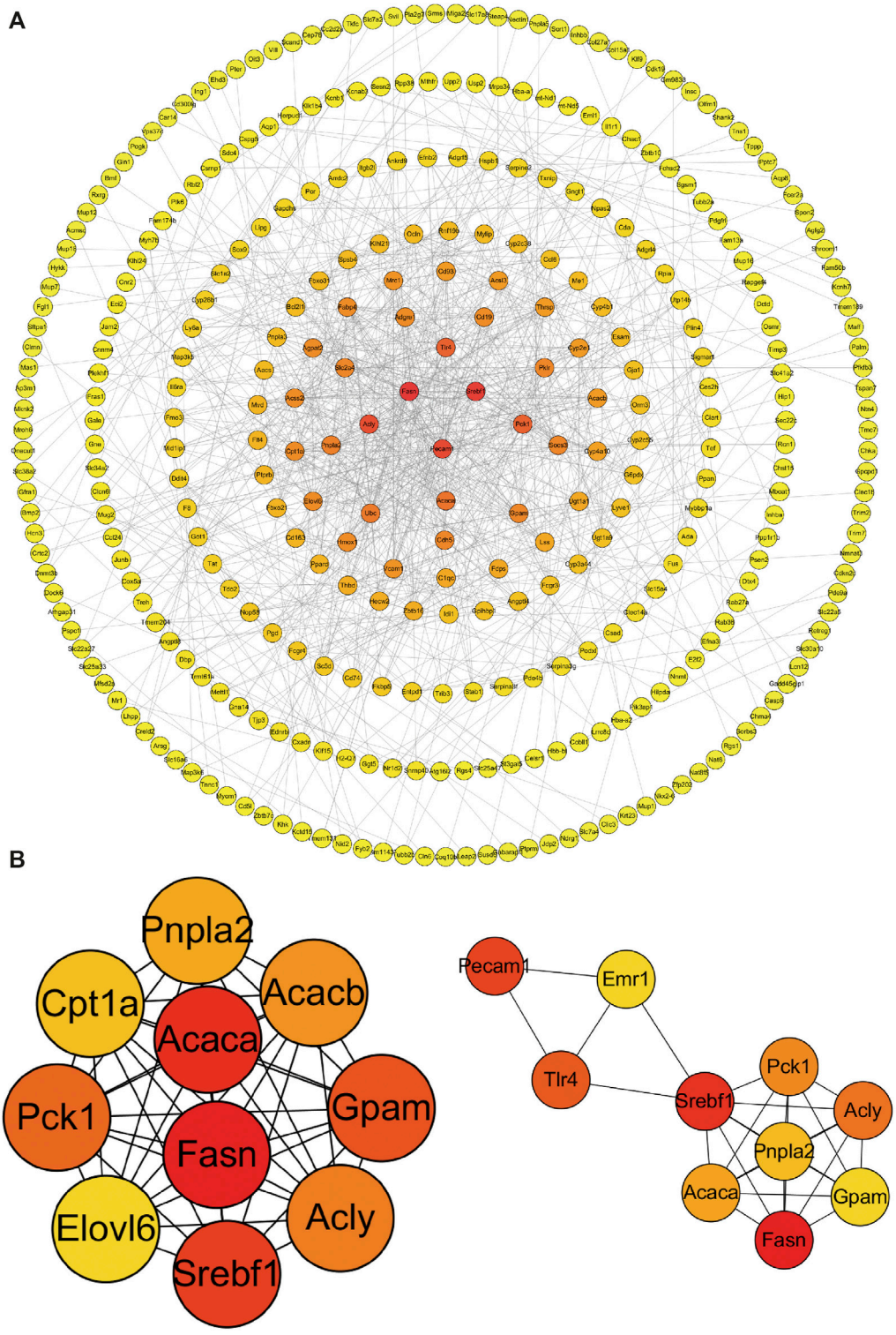

FIGURE 5 | PPI network **(A)** and hub genes **(B)** of all DEGs identified among the three groups. Red balls show the hub genes. PPI, protein–protein interaction.

perspective that METH can induce hepatotoxicity in mice, and the gut–liver axis may mediate the protective impact of antibiotic pretreatment.

Some limitations are found in this study. First, RNA-seq was not performed in the antibiotic group based on histopathology results, serological indexes, and oxidative stress. Antibiotics alone

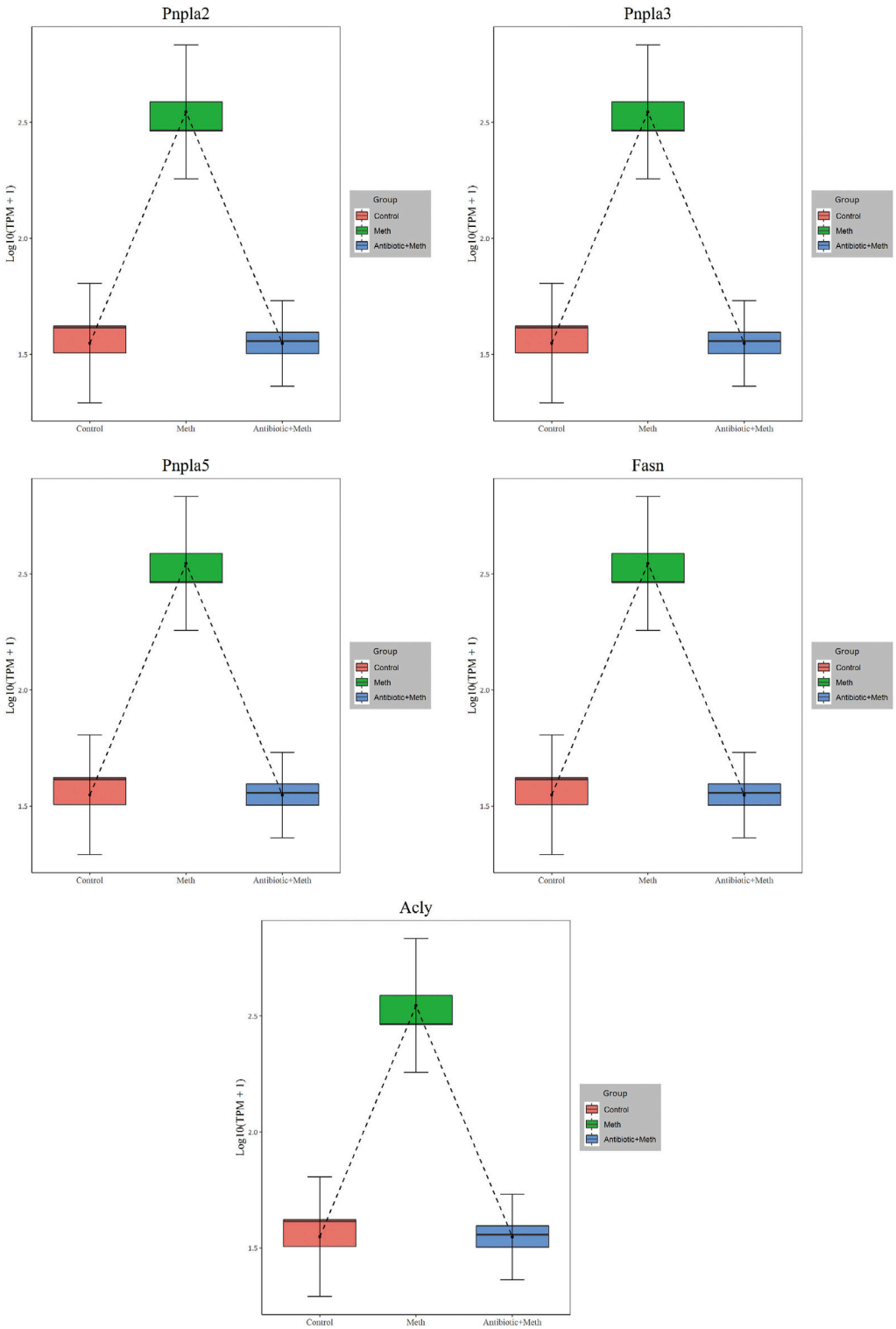

FIGURE 6 | Expression of hub genes in RNA-seq.

cannot cause liver damage. Subsequently, we verified RNA-seq results by RT-qPCR, and the gene changes after antibiotic treatment were consistent with those in the control group. Second, intestinal flora data lacked in this study, but antibiotics' effect on intestinal flora clearance has been confirmed. Finally, it has not been verified whether a

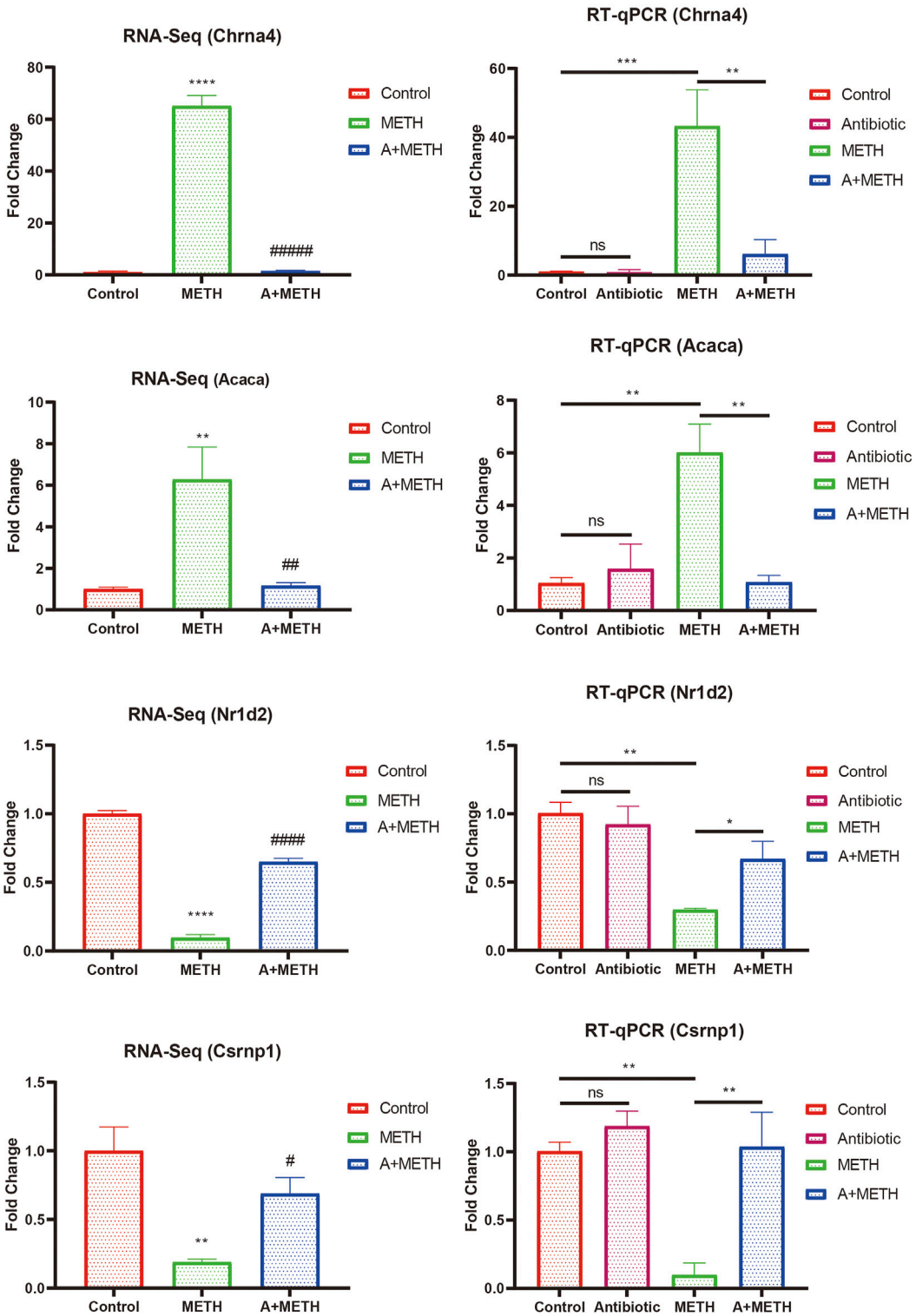

FIGURE 7 | Consistency of RNA-seq and RT-qPCR results. RT-qPCR results of selected DEGs (Chrna4, Acaca, Nr1d2, and Csrnp1) were consistent with those of RNA-seq. RNA-seq: *$p < 0.05$, **$p < 0.01$, ***$p < 0.001$, significantly different compared to the control group; #$p < 0.05$, ##$p < 0.01$, ###$p < 0.001$, significantly different compared to the METH group. RT-qPCR: *$p < 0.05$, **$p < 0.01$, ***$p < 0.001$, ns, statistically non-significant.

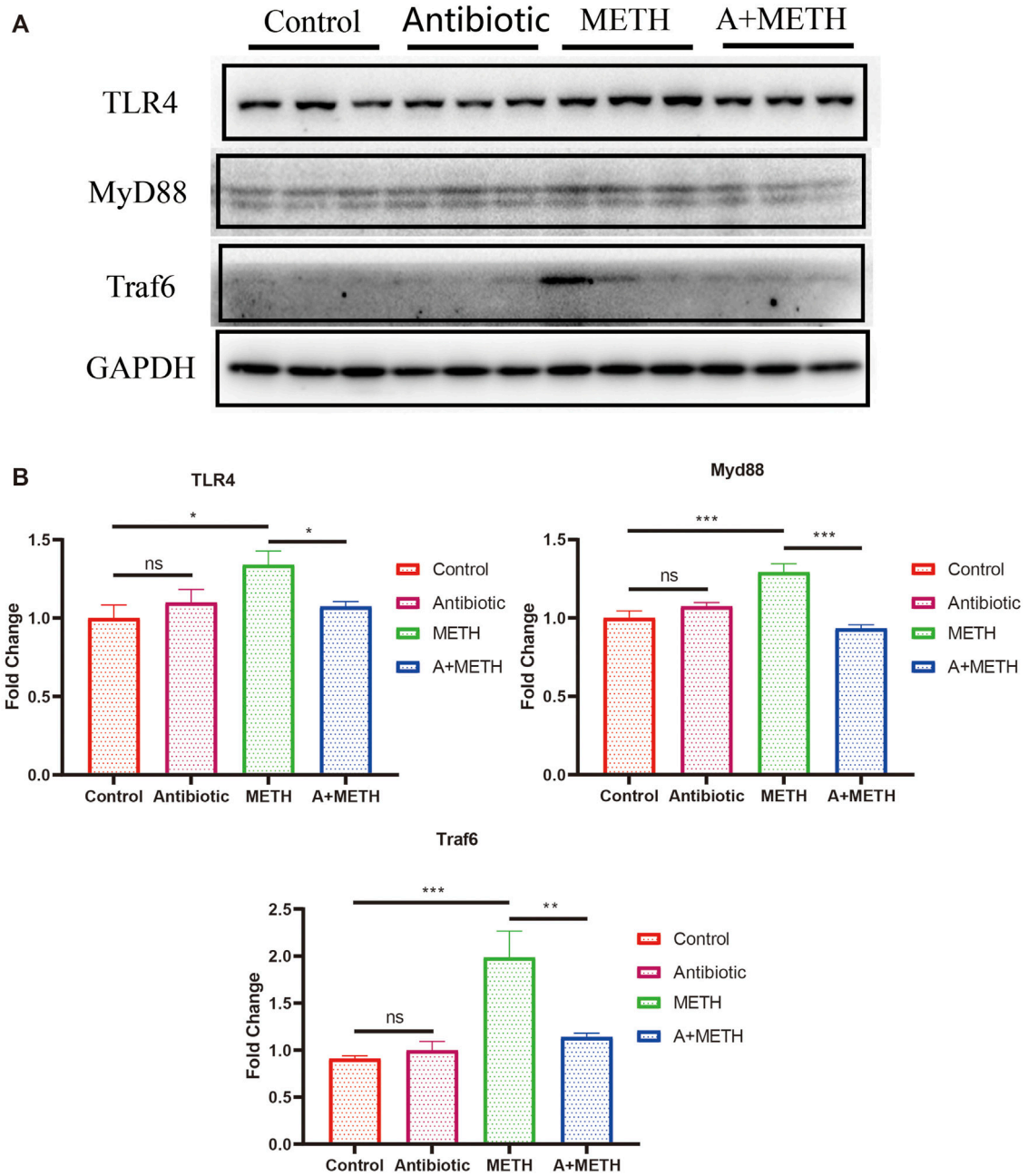

FIGURE 8 | (A) Western blots showing the expression of TLR4, MyD88, and Traf6 proteins in the mice liver. **(B)** The bar chart presents the statistical analysis of TLR4, MyD88, and Traf6 protein expressions. *$p < 0.05$; **$p < 0.01$; ***$p < 0.001$; ns, statistically non-significant.

correlation is found between METH-induced liver damage and intestinal flora. In combination with our previous study and the present study, further research is required to verify the interaction mechanism among intestinal microbiota, nervous system, and liver.

In conclusion, we demonstrated that METH exposure could lead to abnormal pathological and serological changes and activation of oxidative stress and TLR4/MyD88/Traf6 pathway. Gut microbiome clearance by antibiotics alleviated above METH-induced changes. The RNA-seq results provide a possible clue for the basic pathway and antibiotic mechanisms in response to METH. Notably, we first proposed the relationship between METH-induced hepatotoxicity and gut microbiota (**Figure 9**). Therefore, intestinal microbiota may be a potential therapy for

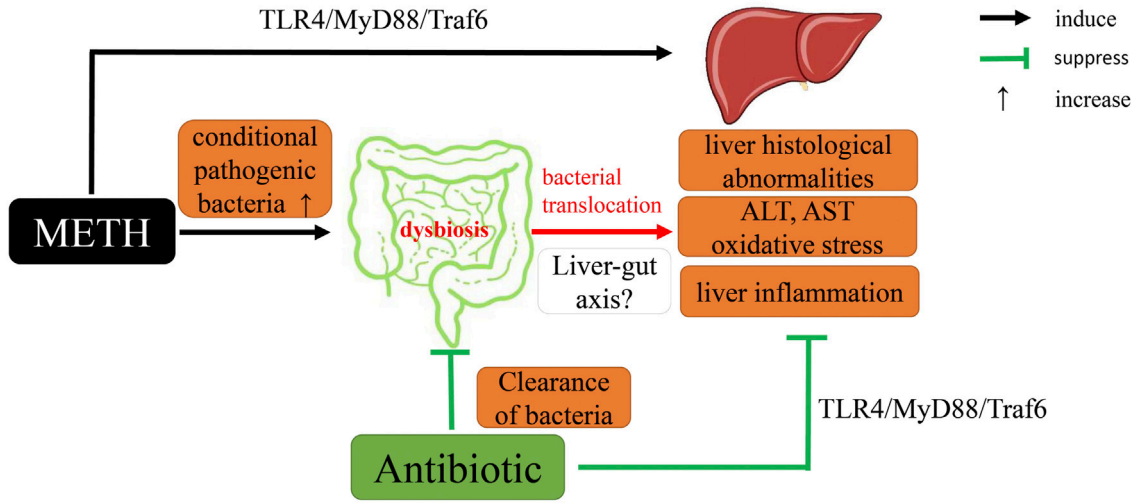

FIGURE 9 | A proposed mechanistic diagram of antibiotic protective action on METH-induced liver hepatotoxicity in this study.

METH-induced hepatotoxicity, though further research is needed to unveil the detailed mechanism.

DATA AVAILABILITY STATEMENT

The datasets presented in this study can be found in online repositories. The names of the repository/repositories and accession number(s) can be found below: NCBI SRA BioProject, accession no. PRJNA741711.

ETHICS STATEMENT

The animal study was reviewed and approved by the National Institutes of Health Guide for the Care and Use of Laboratory Animals of Southern Medical University (Ethical Committee Approval Code: L2018123).

AUTHOR CONTRIBUTIONS

L-JC, J-TH, MP and J-LL performed the experiments. L-JC, J-TH and MP analyzed the date, prepared the figures and/or tables and authored the original draft. J-LL and K-KZ wrote sections of the manuscript. J-HL, L-BW and L-LX organized the database. Y-KC and Q-YZ performed the statistical analysis. D-RL, J-TX and X-LX conceived and designed the experiments and authored or reviewed drafts of the paper. L-JC, J-TH, MP, D-RL, J-TX and X-LX approved the final draft.

FUNDING

This work was supported by the Guangdong Basic and Applied Basic Research Foundation (Grant Nos. 2020A1515010370 and 2018A0303130267).

REFERENCES

Acharya, C., and Bajaj, J. S. (2021). Chronic Liver Diseases and the Microbiome-Translating Our Knowledge of Gut Microbiota to Management of Chronic Liver Disease. *Gastroenterology* 160 (2021), 556–572. doi:10.1053/j.gastro.2020.10.056

Albhaisi, S. A. M., Bajaj, J. S., and Sanyal, A. J. (2020). Role of Gut Microbiota in Liver Disease. *Am. J. Physiol. Gastrointest. Liver Physiol.* 318, G84–G98. doi:10.1152/ajpgi.00118.2019

Albillos, A., de Gottardi, A., and Rescigno, M. (2020). The Gut-Liver axis in Liver Disease: Pathophysiological Basis for Therapy. *J. Hepatol.* 72, 558–577. doi:10.1016/j.jhep.2019.10.003

Albillos, A. (2003). Increased Lipopolysaccharide Binding Protein in Cirrhotic Patients with Marked Immune and Hemodynamic Derangement. *Hepatology* 37, 208–217. doi:10.1053/jhep.2003.50038

Arefin, S., Buchanan, S., Hobson, S., Steinmetz, J., Alsalhi, S., Shiels, P. G., et al. (2020). Nrf2 in Early Vascular Ageing: Calcification, Senescence and Therapy. *Clin. Chim. Acta* 505, 108–118. doi:10.1016/j.cca.2020.02.026

Bajaj, J. S., Barbara, G., DuPont, H. L., Mearin, F., Gasbarrini, A., and Tack, J. (2018). New Concepts on Intestinal Microbiota and the Role of the Non-absorbable Antibiotics with Special Reference to Rifaximin in Digestive Diseases. *Dig. Liver Dis.* 50, 741–749. doi:10.1016/j.dld.2018.04.020

Berg, R. D., and Garlington, A. W. (1979). Translocation of Certain Indigenous Bacteria from the Gastrointestinal Tract to the Mesenteric Lymph Nodes and Other Organs in a Gnotobiotic Mouse Model. *Infect. Immun.* 23, 403–411. doi:10.1128/IAI.23.2.403-411.1979

Bresciani, G., da Cruz, I. B. M., and González-Gallego, J. (2015). Manganese Superoxide Dismutase and Oxidative Stress Modulation. *Adv. Clin. Chem.*, 68: 87–130. doi:10.1016/bs.acc.2014.11.001

Brunt, V. E., Gioscia-Ryan, R. A., Richey, J. J., Zigler, M. C., Cuevas, L. M., Gonzalez, A., et al. (2019). Suppression of the Gut Microbiome Ameliorates Age-related Arterial Dysfunction and Oxidative Stress in Mice. *J. Physiol.* 597, 2361–2378. doi:10.1113/JP277336

Carvalho, B. M., Guadagnini, D., Tsukumo, D. M. L., Schenka, A. A., Latuf-Filho, P., Vassallo, J., et al. (2012). Modulation of Gut Microbiota by Antibiotics Improves Insulin Signalling in High-Fat Fed Mice. *Diabetologia* 55, 2823–2834. doi:10.1007/s00125-012-2648-4

Chen, L.-J., Zhi, X., Zhang, K.-K., Wang, L.-B., Li, J.-H., Liu, J.-L., et al. (2021). Escalating Dose-Multiple Binge Methamphetamine Treatment Elicits Neurotoxicity, Altering Gut Microbiota and Fecal Metabolites in Mice. *Food Chem. Toxicol.* 148, 111946. doi:10.1016/j.fct.2020.111946

Chen, Z., and Zhong, C. (2014). Oxidative Stress in Alzheimer's Disease. *Neurosci. Bull.* 30, 271–281. doi:10.1007/s12264-013-1423-y

Cichoż-Lach, H. (2014). Oxidative Stress as a Crucial Factor in Liver Diseases. *Wjg* 20, 8082. doi:10.3748/wjg.v20.i25.8082

Dias Da Silva, D., Carmo, H., Lynch, A., and Silva, E. (2013). An Insight into the Hepatocellular Death Induced by Amphetamines, Individually and in Combination: the Involvement of Necrosis and Apoptosis. *Arch. Toxicol.* 87, 2165–2185. doi:10.1007/s00204-013-1082-9

Eskandari, M. R., Rahmati, M., Khajeamiri, A. R., Kobarfard, F., Noubarani, M., and Heidari, H. (2014). A New Approach on Methamphetamine-Induced Hepatotoxicity: Involvement of Mitochondrial Dysfunction. *Xenobiotica* 44, 70–76. doi:10.3109/00498254.2013.807958

Fei, H., Chen, S., and Xu, C. (2020). RNA-sequencing and Microarray Data Mining Revealing: the Aberrantly Expressed mRNAs Were Related with a Poor Outcome in the Triple Negative Breast Cancer Patients. *Ann. Transl Med.* 8, 363. doi:10.21037/atm.2020.02.51

Gong, T., Jiang, W., Gao, Z., Chen, Y., and Gao, S. (2019). Dibromoacetic Acid Induced Hepatotoxicity in Mice through Oxidative Stress and Toll-like Receptor 4 Signaling Pathway Activation. *Oxid. Med. Cell Longevity* 2019, 1–10. doi:10.1155/2019/5637235

Gorrini, C., Harris, I. S., and Mak, T. W. (2013). Modulation of Oxidative Stress as an Anticancer Strategy. *Nat. Rev. Drug Discov.* 12, 931–947. doi:10.1038/nrd4002

Gregory, J. C., Buffa, J. A., Org, E., Wang, Z., Levison, B. S., Zhu, W., et al. (2015). Transmission of Atherosclerosis Susceptibility with Gut Microbial Transplantation. *J. Biol. Chem.* 290, 5647–5660. doi:10.1074/jbc.M114.618249

Halliwell, B., and Gutteridge, J. M. C. (1984). Oxygen Toxicity, Oxygen Radicals, Transition Metals and Disease. *Biochem. J.* 219, 1–14. doi:10.1042/bj2190001

Hashimoto, K., Ishima, T., Fujita, Y., and Zhang, L. (2013). [Antibiotic Drug Minocycline: a Potential Therapeutic Drug for Methamphetamine-Related Disorders], *Nihon Arukoru Yakubutsu Igakkai Zasshi*, 48, 118–125.

Hashimoto, K. (2008). Minocycline as a Therapeutic Drug for Methamphetamine Use Disorders. *Nihon Shinkei Seishin Yakurigaku Zasshi*, 28, 19–22.

Hu, J., Luo, H., Wang, J., Tang, W., Lu, J., Wu, S., et al. (2017).Enteric Dysbiosis-Linked Gut Barrier Disruption Triggers Early Renal Injury Induced by Chronic High Salt Feeding in Mice. *Exp. Mol. Med.*, 49, e370. doi:10.1038/emm.2017.122

Ishtiaq, S. M., Rashid, H., Hussain, Z., and Arshad, M. I. (2019). Adiponectin and PPAR: a Setup for Intricate Crosstalk between Obesity and Non-alcoholic Fatty Liver Disease. *Rev. Endocr. Metab. Dis.*, 253–261. doi:10.1007/s11154-019-09510-2

Jones, R. M., and Neish, A. S. (2021). Gut Microbiota in Intestinal and Liver Disease. *Annu. Rev. Pathol. Mech. Dis.* 16, 251–275. doi:10.1146/annurev-pathol-030320-095722

Jones, R. M., and Neish, A. S. (2017). Redox Signaling Mediated by the Gut Microbiota. *Free Radic. Biol. Med.* 105, 41–47. doi:10.1016/j.freeradbiomed.2016.10.495

Kim, D., Langmead, B., and Salzberg, S. L. (2015). HISAT: a Fast Spliced Aligner with Low Memory Requirements. *Nat. Methods* 12, 357–360. doi:10.1038/nmeth.3317

Koriem, K. M. M., and Soliman, R. E. (2014). Chlorogenic and Caftaric Acids in Liver Toxicity and Oxidative Stress Induced by Methamphetamine. *J. Toxicol.* 2014, 1–10. doi:10.1155/2014/583494

Lai, L., Chen, Y., Tian, X., Li, X., Zhang, X., Lei, J., et al. (2015). Artesunate Alleviates Hepatic Fibrosis Induced by Multiple Pathogenic Factors and Inflammation through the Inhibition of LPS/TLR4/NF-κB Signaling Pathway in Rats. *Eur. J. Pharmacol.* 765, 234–241. doi:10.1016/j.ejphar.2015.08.040

Halpin, L. E., Gunning, W. T., and Yamamoto, B. K. (2013). Methamphetamine Causes Acute Hyperthermia-dependent Liver Damage. *Pharmacol. res. perspect.* 1:e00008. doi:10.1002/prp2.8

Li, C.-X., Gao, J.-G., Wan, X.-Y., Chen, Y., Xu, C.-F., Feng, Z.-M., et al. (2019). Allyl Isothiocyanate Ameliorates Lipid Accumulation and Inflammation in Nonalcoholic Fatty Liver Disease via the Sirt1/AMPK and NF-Kb Signaling Pathways. *Wjg* 25, 5120–5133. doi:10.3748/wjg.v25.i34.5120

Liu, Y., Hao, B., Shi, Y., Xue, L., Wang, X., Chen, Y., et al. (2017). Violent Offences of Methamphetamine Users and Dilemmas of Forensic Psychiatric Assessment, *Forensic Sci. Res.*, 2. 11–17. doi:10.1080/20961790.2017.1287155

Luca, M., Di Mauro, M., Di Mauro, M., and Luca, A. (2019). Gut Microbiota in Alzheimer's Disease, Depression, and Type 2 Diabetes Mellitus: The Role of Oxidative Stress. *Oxidative Med. Cell Longev.* 2019, 1–10. doi:10.1155/2019/4730539

Ma, J., Zhou, Q., and Li, H. (2017). Gut Microbiota and Nonalcoholic Fatty Liver Disease: Insights on Mechanisms and Therapy. *Nutrients* 9, 1124. doi:10.3390/nu9101124

Mendoza, Y. P., Rodrigues, S. G., Bosch, J., and Berzigotti, A. (2020). Effect of Poorly Absorbable Antibiotics on Hepatic Venous Pressure Gradient in Cirrhosis: A Systematic Review and Meta-Analysis. *Dig. Liver Dis.* 52, 958–965. doi:10.1016/j.dld.2020.06.048

Meng, X., Li, S., Li, Y., Gan, R.-Y., and Li, H.-B. (2018). Gut Microbiota's Relationship with Liver Disease and Role in Hepatoprotection by Dietary Natural Products and Probiotics. *Nutrients* 10, 1457. doi:10.3390/nu10101457

Milosevic, I., Vujovic, A., Barac, A., Djelic, M., Korac, M., Radovanovic Spurnic, A., et al. (2019). Gut-Liver Axis, Gut Microbiota, and its Modulation in the Management of Liver Diseases: A Review of the Literature. *Ijms* 20, 395. doi:10.3390/ijms20020395

Moratalla, R., Khairnar, A., Simola, N., Granado, N., García-Montes, J. R., Porceddu, P. F., et al. (2017). Amphetamine-related Drugs Neurotoxicity in Humans and in Experimental Animals: Main Mechanisms. *Prog. Neurobiol.* 155, 149–170. doi:10.1016/j.pneurobio.2015.09.011

Mottawea, W., Chiang, C.-K., Mühlbauer, M., Starr, A. E., Butcher, J., Abujamel, T., et al. (2016). Altered Intestinal Microbiota-Host Mitochondria Crosstalk in New Onset Crohn's Disease. *Nat. Commun.* 7:13419. doi:10.1038/ncomms13419

Mu, C., and Zhu, W. (2019). Antibiotic Effects on Gut Microbiota, Metabolism, and beyond. *Appl. Microbiol. Biotechnol.* 103, 9277–9285. doi:10.1007/s00253-019-10165-x

Panebianco, C., Oben, J. A., Vinciguerra, M., and Pazienza, V. (2017). Senescence in Hepatic Stellate Cells as a Mechanism of Liver Fibrosis Reversal: a Putative Synergy between Retinoic Acid and PPAR-Gamma Signalings. *Clin. Exp. Med.* 17, 269–280. doi:10.1007/s10238-016-0438-x

Pertea, M., Pertea, G. M., Antonescu, C. M., Chang, T.-C., Mendell, J. T., and Salzberg, S. L. (2015). StringTie Enables Improved Reconstruction of a Transcriptome from RNA-Seq Reads. *Nat. Biotechnol.* 33, 290–295. doi:10.1038/nbt.3122

Kattoor, A. J., Pothineni, N. V. K., Palagiri, D., and Mehta, J. L. (2017). Oxidative Stress in Atherosclerosis. *Curr. Atheroscler. Rep.* 19, 42. doi:10.1007/s11883-017-0678-6

Qu, D., Zhang, K., Chen, L., Wang, Q., and Wang, H. (2020). RNA-sequencing Analysis of the Effect of Luteolin on Methamphetamine-Induced Hepatotoxicity in Rats: a Preliminary Study. *PeerJ* 8, e8529. doi:10.7717/peerj.8529

Rakoff-Nahoum, S., Paglino, J., Eslami-Varzaneh, F., Edberg, S., and Medzhitov, R. (2004). Recognition of Commensal Microflora by Toll-like Receptors Is Required for Intestinal Homeostasis. *Cell* 118, 229–241. doi:10.1016/j.cell.2004.07.002

Sajjad, A., Mottershead, M., Syn, W. K., Jones, R., Smith, S., and Nwokolo, C. U. (2005). Ciprofloxacin Suppresses Bacterial Overgrowth, Increases Fasting Insulin but Does Not Correct Low Acylated Ghrelin Concentration in Non-alcoholic Steatohepatitis. *Aliment. Pharmacol. Ther.* 22, 291–299. doi:10.1111/j.1365-2036.2005.02562.x

Tian, Z., Chen, Y., Yao, N., Hu, C., Wu, Y., Guo, D., et al. (2018). Role of Mitophagy Regulation by ROS in Hepatic Stellate Cells during Acute Liver Failure. *Am. J. Physiol.-Gastrointest. Liver Physiol.* 315, G374–G384. doi:10.1152/ajpgi.00032.2018

Tripathi, A., Debelius, J., Brenner, D. A., Karin, M., Loomba, R., Schnabl, B., et al. (2018). The Gut-Liver axis and the Intersection with the Microbiome. *Nat. Rev. Gastroenterol. Hepatol.* 15, 397–411. doi:10.1038/s41575-018-0011-z

Wang, Q., Wei, L.-W., Xiao, H.-Q., Xue, Y., Du, S.-H., Liu, Y.-G., et al. (2017). Methamphetamine Induces Hepatotoxicity via Inhibiting Cell Division, Arresting Cell Cycle and Activating Apoptosis: *In Vivo* and *In Vitro* Studies. *Food Chem. Toxicol.* 105, 61–72. doi:10.1016/j.fct.2017.03.030

Wang, Y., Branicky, R., Noë, A., and Hekimi, S. (2018). Superoxide Dismutases: Dual Roles in Controlling ROS Damage and Regulating ROS Signaling. *J. Cel Biol.* 217, 1915–1928. doi:10.1083/jcb.201708007

Wu, W.-C., Zhao, W., and Li, S. (2008). Small Intestinal Bacteria Overgrowth Decreases Small Intestinal Motility in the NASH Rats, *World J. Gastroenterol.*, 14. 313–317. doi:10.3748/wjg.14.313

Xie, C., Mao, X., Huang, J., Ding, Y., Wu, J., Dong, S., et al. (2011). KOBAS 2.0: a Web Server for Annotation and Identification of Enriched Pathways and Diseases. *Nucleic Acids Res.* 39, W316–W322. doi:10.1093/nar/gkr483

Xie, X.-L., He, J.-T., Wang, Z.-T., Xiao, H.-Q., Zhou, W.-T., Du, S.-H., et al. (2018). Lactulose Attenuates METH-Induced Neurotoxicity by Alleviating the Impaired Autophagy, Stabilizing the Perturbed Antioxidant System and Suppressing Apoptosis in Rat Striatum. *Toxicol. Lett.* 289, 107–113. doi:10.1016/j.toxlet.2018.03.015

Xie, X.-L., Zhou, W.-T., Zhang, K.-K., Chen, L.-J., and Wang, Q. (2018). METH-induced Neurotoxicity Is Alleviated by Lactulose Pretreatment through Suppressing Oxidative Stress and Neuroinflammation in Rat Striatum. *Front. Neurosci.* 12:802. doi:10.3389/fnins.2018.00802

Xie, X.-L., Zhou, W.-T., Zhang, K.-K., Yuan, Y., Qiu, E.-M., Shen, Y.-W., et al. (2019). PCB52 Induces Hepatotoxicity in Male Offspring through Aggravating Loss of Clearance Capacity and Activating the Apoptosis: Sex-Biased Effects on Rats. *Chemosphere*. 227, 389–400. doi:10.1016/j.chemosphere.2019.04.077

Xu, B., Ye, Y., and Liao, L. (2019). Rapid and Simple Analysis of Amphetamine-type Illegal Drugs Using Excitation-Emission Matrix Fluorescence Coupled with Parallel Factor Analysis, *Forensic Sci. Res.*, 4. 179–187. doi:10.1080/20961790.2017.1349600

Xu, F., and Liu, L. (2019). Simultaneous Determination of Free Methamphetamine, Pethidine, Ketamine and Tramadol in Urine by Dispersive Liquid-Liquid Microextraction Combined with GC-MS. *Forensic Sci. Res.*, 4. 188–194. doi:10.1080/20961790.2017.1377386

Yang, X., Wang, Y., Li, Q., Zhong, Y., Chen, L., Du, Y., et al. (2018). The Main Molecular Mechanisms Underlying Methamphetamine- Induced Neurotoxicity and Implications for Pharmacological Treatment. *Front. Mol. Neurosci.* 11, 186. doi:10.3389/fnmol.2018.00186

Zhang, K.-K., Wang, H., Qu, D., Chen, L.-J., Wang, L.-B., Li, J.-H., et al. (2021). Luteolin Alleviates Methamphetamine-Induced Hepatotoxicity by Suppressing the P53 Pathway-Mediated Apoptosis, Autophagy, and Inflammation in Rats. *Front. Pharmacol.* 12:641917. doi:10.3389/fphar.2021.641917

Zhang, K., Zhang, Q., Jiang, H., Du, J., Zhou, C., Yu, S., et al. (2018). Impact of Aerobic Exercise on Cognitive Impairment and Oxidative Stress Markers in Methamphetamine-dependent Patients. *Psychiatry Res.* 266, 328–333. doi:10.1016/j.psychres.2018.03.032

Zhang, Z., Gong, Q., Feng, X., Zhang, D., and Quan, L. (2017). Astrocytic Clasmatodendrosis in the Cerebral Cortex of Methamphetamine Abusers, *Forensic Sci. Res.*, 2, 139–144. doi:10.1080/20961790.2017.1280890

Zhao, T., Zhai, C., Song, H., Wu, Y., Ge, C., Zhang, Y., et al. (2020). Methamphetamine-Induced Cognitive Deficits and Psychiatric Symptoms Are Associated with Serum Markers of Liver Damage. *Neurotox. Res.* 37, 67–76. doi:10.1007/s12640-019-00115-w

Zhou, W.-T., Wang, L.-B., Yu, H., Zhang, K.-K., Chen, L.-J., Wang, Q., et al. (2020). N-acetylcysteine Alleviates PCB52-Induced Hepatotoxicity by Repressing Oxidative Stress and Inflammatory Responses. *PeerJ (San Francisco, CA)* 8, e9720. doi:10.7717/peerj.9720

Conflict of Interest: The authors declare that the research was conducted in the absence of any commercial or financial relationships that could be construed as a potential conflict of interest.

Publisher's Note: All claims expressed in this article are solely those of the authors and do not necessarily represent those of their affiliated organizations, or those of the publisher, the editors and the reviewers. Any product that may be evaluated in this article, or claim that may be made by its manufacturer, is not guaranteed or endorsed by the publisher.

frontiers in Neuroscience

MINI REVIEW
published: 06 August 2021
doi: 10.3389/fnins.2021.717956

The Mechanisms and Boundary Conditions of Drug Memory Reconsolidation

*Liangpei Chen[1], He Yan[1], Yufang Wang[1], Ziping He[2], Qihao Leng[2], Shihao Huang[3], Feilong Wu[3], Xiangyang Feng[4] and Jie Yan[1,4]**

[1] Department of Forensic Science, School of Basic Medical Science, Central South University, Changsha, China, [2] Xiangya School of Medicine, Central South University, Changsha, China, [3] Key Laboratory of Molecular Epidemiology of Hunan Province, School of Medicine, Hunan Normal University, Changsha, China, [4] Department of Forensic Science, School of Basic Medical Science, Xinjiang Medical University, Urumqi, China

Drug addiction can be seen as a disorder of maladaptive learning characterized by relapse. Therefore, disrupting drug-related memories could be an approach to improving therapies for addiction. Pioneering studies over the last two decades have revealed that consolidated memories are not static, but can be reconsolidated after retrieval, thereby providing candidate pathways for the treatment of addiction. The limbic–corticostriatal system is known to play a vital role in encoding the drug memory engram. Specific structures within this system contribute differently to the process of memory reconsolidation, making it a potential target for preventing relapse. In addition, as molecular processes are also active during memory reconsolidation, amnestic agents can be used to attenuate drug memory. In this review, we focus primarily on the brain structures involved in storing the drug memory engram, as well as the molecular processes involved in drug memory reconsolidation. Notably, we describe reports regarding boundary conditions constraining the therapeutic potential of memory reconsolidation. Furthermore, we discuss the principles that could be employed to modify stored memories. Finally, we emphasize the challenge of reconsolidation-based strategies, but end with an optimistic view on the development of reconsolidation theory for drug relapse prevention.

Keywords: drug memory, addiction, reconsolidation, limbic–corticostriatal system, boundary condition

OPEN ACCESS

Edited by:
Qi Wang,
Southern Medical University, China

Reviewed by:
Jie Zhu,
Xi'an Jiaotong University, China
Jingsong Yuan,
Columbia University, United States

****Correspondence:***
Jie Yan
wills212156@csu.edu.cn

Specialty section:
This article was submitted to Neuropharmacology, a section of the journal Frontiers in Neuroscience

Received: *31 May 2021*
Accepted: *20 July 2021*
Published: *06 August 2021*

Citation:
Chen L, Yan H, Wang Y, He Z, Leng Q, Huang S, Wu F, Feng X and Yan J (2021) The Mechanisms and Boundary Conditions of Drug Memory Reconsolidation. Front. Neurosci. 15:717956. doi: 10.3389/fnins.2021.717956

INTRODUCTION

Memory in drug addiction is usually abnormal and is considered to reflect a learning disorder (Phelps and Hofmann, 2019). The central goal of addiction treatments is to prevent relapse and compulsive drug-seeking behavior. Drug-associated memories, therefore, provide an effective treatment target to reduce relapse (Lee et al., 2017). Generally, drug memory can be viewed as a kind of associative memory that combines a conditioned stimulus (CS) with a rewarding drug stimulus [the unconditioned stimulus (US)] (Xue et al., 2012). Researchers have made substantial progress in reducing negative effects related to drugs by disrupting associative memory. One of the factors contributing to this advance is the significant development of the theory of memory reconsolidation. Although early studies indicated that consolidated memory may be

diminished after retrieval (Misanin et al., 1968; Przybyslawski and Sara, 1997), the mechanism underlying reconsolidation was not well understood. In 2000, Nader et al. (2000b) found that previously consolidated memories can be labile after retrieval, and that the synthesis of new proteins is necessary for long-term storage—a process they putatively termed reconsolidation. Initial research into reconsolidation mainly focused on fear memory, but because of the promising clinical therapeutic potential of this theory, later studies expanded the research to investigate drug memories with encouraging success (Lee et al., 2005; Xue et al., 2012). Editing well-established memories provides a means by which detrimental memories driving relapse can be disrupted (Xue et al., 2012, 2017b). Meanwhile, studies using a large variety of amnestic agents have contributed to elucidating neural circuits involved in memory updating. Here, we focus on reviewing the limbic–corticostriatal circuits recruited during reconsolidation, in addition to several molecular processes that may serve as potent targets to disrupt reconsolidation (see **Figure 1**). In addition, we discuss the boundary conditions that limit reconsolidation-based strategies.

STRUCTURES IN THE BRAIN RELATED TO RECONSOLIDATION

Several brain regions interact to form CS–US associative memories, thereby directing reward-seeking behaviors. Limbic-corticostriatal circuitry, including the amygdala, hippocampus, striatum, and prefrontal cortex, are required to form associative memories between stimuli and rewards. The underlying molecular mechanisms contributing to CS–US association memories in these brain areas and circuits are listed in **Table 1**.

Amygdala Is Required for Memory Retrieval

The amygdala is a brain structure that plays a critical role in emotion and motivation (Blundell et al., 2001) and that is actively involved in processing rewarding environmental stimuli (Janak and Tye, 2015). In terms of the subregions of the amygdala, the basolateral amygdala (BLA) is a key brain structure involved in CS-induced memory reconsolidation (Higginbotham et al., 2021a,b). BLA neurons store the associative emotional learning engrams that are recruited during retrieval (Pignatelli et al., 2019). BLA neurons receive dopaminergic input from the ventral tegmental area (VTA), and project to the nucleus accumbens (NAc) via glutamatergic neurons, contributing to the process underlying the incubation of craving (Lüscher, 2016). Remarkably, the central nucleus of the amygdala (CeA) and the BLA play different roles in memory reconsolidation (Kruzich and See, 2001). For example, Jian et al. (2014) found that CS-induced reconsolidation of morphine and cocaine memories in rats could be disrupted by selectively inhibiting the dephosphorylation of the eukaryotic initiation factor 2 α-subunit (eIF2α) in the BLA but not in the CeA. However, the CeA may play an essential role in US-induced drug memory reconsolidation. In another study, researchers found that US-induced but not CS-induced cocaine memory reconsolidation required β1-adrenergic signaling and *de novo* protein synthesis in the CeA, indicating that the CeA may be required for US retrieval but not CS retrieval (Zhu et al., 2018).

Hippocampus Is Required for the Storage of Drug-Paired Context

The hippocampus is known to organize episodic memory and is required for the formation of Pavlovian conditioned associations (also known as classical conditioning), as measured by conditioned place preference (CPP) (Taubenfeld et al., 2010; Liu et al., 2018). In terms of operant drug-seeking behavior, the hippocampus seems to be less directly required, as the cue or tone represents much less of a spatial object (Fuchs et al., 2005). Besides, the hippocampus does not appear to encode the memory trace of the conditioning context alone, as microinjections of the protein synthesis inhibitor anisomycin into the dorsal hippocampus (DH) do not disrupt cocaine memory reconsolidation (Ramirez et al., 2009). In contrast, contralateral BLA microinjections of the protein synthesis inhibitor baclofen/muscimol disrupt cocaine memory reconsolidation, suggesting that interaction between the DH and BLA is involved in editing the context–drug engram (Wells et al., 2011). Moreover, using optogenetic techniques, researchers found that the dorsal CA1 (dCA1) subregion of the hippocampus directly projects to the NAc, indicating that the spatial memory trace facilitates effective appetitive behavior via a limbic–motor interface (Trouche et al., 2019). Taken together, these studies demonstrate that the hippocampus is required for reward-motivated behavior and that it does not mediate reconsolidation alone.

Striatum Drives Cue–Reward Learning

The striatum is necessary for learning that actions result in reward and for executing actions. In rodents, the striatum is typically divided into three main subregions: dorsolateral striatum (DLS), dorsomedial striatum (DMS), and ventral striatum (VS) (Cox and Witten, 2019). The DLS plays a vital role in stimulus–response association, which is necessary for the formation of skills and for habituation (Barnes et al., 2005; O'Hare et al., 2016). In contrast, the DMS is involved in goal-directed behaviors that depend on response–outcome associations (Yin et al., 2005). In fact, there is a shift of action transitions from goal-directed to habitual after overtraining (Thorn et al., 2010). Both DLS and DMS are recruited in the process of drug-seeking and consumption, which rely on instrumental learning. Early studies proved that instrumental learning does not require protein synthesis-dependent memory reconsolidation (Hernandez and Kelley, 2004; Brown et al., 2008). However, recently it has been revealed that instrumental memories for drug addiction (e.g., to cocaine or nicotine) may go through reconsolidation (Exton-McGuinness et al., 2014, 2019; Piva et al., 2020), providing a new perspective on how to reduce drug abuse behaviors. With regard to the VS, its primary function can be attributed to its major component, the NAc, which is essential for the formation of stimulus–outcome associations in Pavlovian learning (Milton and Everitt, 2012). The NAc receives dopaminergic neuronal input from the VTA, which plays a key

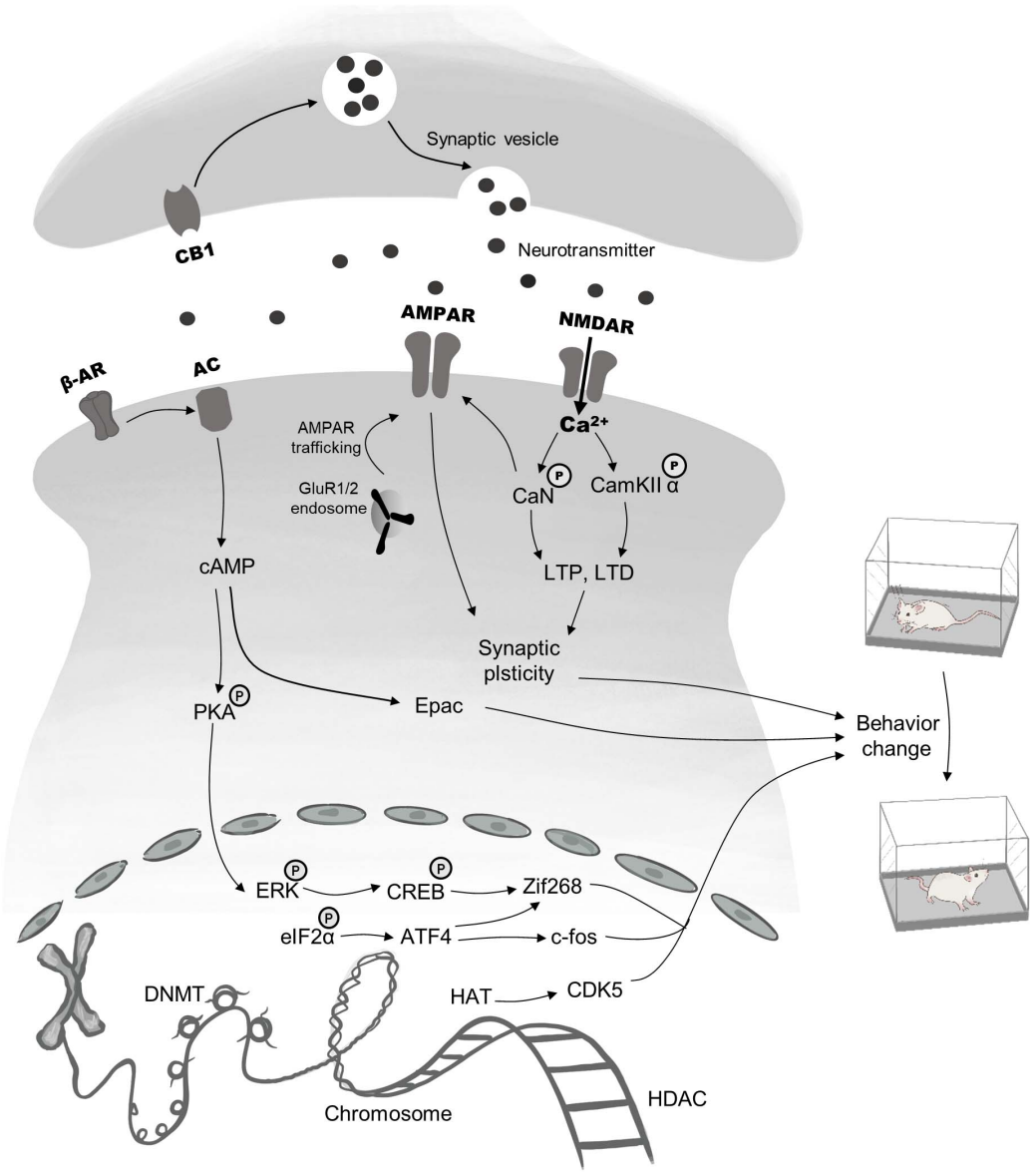

FIGURE 1 | Brief description of pharmacological targets and signaling cascades recruited in reconsolidation. The process of drug memory reconsolidation requires a complicated regulatory network, including epigenetic mechanisms, gene transcription, and activation of membrane receptors, all of which are responsible for behavior changes. Targets for epigenetic modifications mainly lie in the HAT, the HDAC, the DNMT. Besides, the phosphorylation and dephosphorylation of ERK and eIF2α within the nucleus regulate the expression of immediate early genes, such as CREB, Zif 268, and c-fos, thus ultimately lead to changes in addiction behaviors. Finally, pre-and postsynaptic membrane receptors including AMPAR, NMDAR, β-AR, and CB1 have been proved to be effective targets. Main downstream mechanisms contain the second messenger (cAMP)-mediated pathway, AMPAR & NMDAR regulated synaptic plasticity and neurotransmitter transport.

role in processing reward stimuli (Nutt et al., 2015). In addition, glutamatergic neurons in the BLA, prefrontal cortex (PFC), and ventral hippocampus also project to the NAc, contributing to its crucial role in drug-evoked synaptic plasticity (Lüscher, 2016).

Prefrontal Cortex Modulates Reward Circuits

Drug addiction was initially thought to be caused by the dysfunction of subcortical reward circuits. However, accumulating evidence indicates that the PFC is recruited during drug addiction via regulation of limbic reward regions (Goldstein and Volkow, 2011). The PFC is necessary for action selection and decision making based on the value of goals (Hyman et al., 2006; Szczepanski and Knight, 2014). Research has shown that associative learning during cocaine abuse induces plasticity in medial prefrontal cortex (mPFC) neurons to alter the reward system (Porter and Sepulveda-Orengo, 2020). Furthermore, the removal of perineuronal nets, which play an essential role in neural plasticity, from GABAergic

TABLE 1 | Summary of experiments addressing mechanisms of Pavlovian memory reconsolidation.

Brain area	Behavioral paradigm	Species	Drug	Target	Treatment	Effect	References
LA	SA	Rat	Cocaine	CaN	CGA	Disruption	Rich et al., 2020
LA	SA	Rat	Cocaine	Histone deacetylase	Inhibit (trichostatn A)	Enhance	Monsey et al., 2019
BLA	SA	Rat	Cocaine	DNA methyltransferase	Inhibit (5-azacytidine)	Disruption	Shi et al., 2015
BLA	CPP, SA	Rat	Morphine Heroin	eIF2α	Sal003	Disruption	Jian et al., 2014
BLA	SA	Rat	Cocaine	PKA	Rp-cAMPS,	Disruption	Arguello et al., 2014
BLA	SA	Rat	Cocaine	Epac	8-CPT	Disruption	Wan et al., 2014
BLA	SA	Rat	Cocaine	CaMKIIα	KN-93 or KN-62	Disruption	Rich et al., 2016
BLA	SA	Rat	Cocaine	Zif268	ASO	Disruption	Lee et al., 2005, 2006
BLA	SA	Rat	Cocaine	ERK	U0126	Disruption	Wells et al., 2013
BLA	CPP	Rat	Cocaine	CDK5	beta-butyrolactone	Disruption	Li et al., 2010
BLA	SA	Rat	Cocaine	NMDAR	D-APV	Disruption	Milton et al., 2008
BLA	CPP	Rat	Cocaine	β-AR	propranolol	Disruption	Otis et al., 2013
BLA	CPP	Rat	Morphine	GRs	GR agonist	Disruption	Wang et al., 2008
BLA	SA	Rat	Cocaine	NMDAR	D-APV	Disruption	Milton et al., 2008
BLA	CPP	Rat	Morphine	β-AR	Propranolol	No effect	Wu et al., 2014
BLA	CPP	Rat	Morphine	Protein synthesis	Anisomycin	No effect	Yim et al., 2006
BLA	SA	Rat	Cocaine	CaMKII	KN-93	No effect	Arguello et al., 2014
CeA	CPP	Mice	Cocaine	β2-AR	ICI 118, 551	No effect	Zhu et al., 2018
CeA	SA	Rat	Alcohol	mTORC1	Rapamycin	Disruption	Barak et al., 2013
CeA	CPP	Rat	Cocaine	CDK5	beta-butyrolactone	No effect	Li et al., 2010
DH	CPP	Mice	Cocaine	DNA demethylation	Knockdown (Tet3)	Disruption	Liu et al., 2018
NAc	SA	Rat	Cocaine	DNA methyltransferase	Inhabit (RG108)	Disruption	Massart et al., 2015
NAc	SA	Rat	Cocaine	DNA methyltransferase	Enhance (S-adenosylmethionine)	Disruption	Massart et al., 2015
NAc core	CPP, SA	Rat	Cocaine	calpain	calpain inhibitor	Disruption	Liang et al., 2017
NAc	SA	Rat	Cocaine	ERK	U0126	No effect	Wells et al., 2013
mPFC	CPP	Rat	Cocaine	PNNs	Ch-ABC	Disruption	Slaker et al., 2015
PL-mPFC	CPP	Rat	Cocaine	β-AR	Propranolol, nadolol	Disruption	Otis et al., 2013
system	CPP	Rat	Morphine	GR	stress	Disruption	Wang et al., 2008
system	SA	Rat	Cocaine	Histone acetyltransferase	Inhibit (garcinol)	Disruption	Dunbar and Taylor, 2017
system	SA	Rat	Cocaine	mTOR	rapamycin	Disruption	Zhang et al., 2021
system	SA	Rat	Cocaine	CB1R	AM251	Disruption	Higginbotham et al., 2021b
system	CPP	Rat	Heroin	β-AR	propranolol	Disruption	Chen et al., 2021

AM251, CB1R antagonist; anisomycin, protein synthesis inhibitor; ASO, anti-sense oligodeoxynucleotides; beta-butyrolactone, CDK5 inhibitor; β-AR, β-adrenergic receptor; BLA, basolateral amygdala; CaMKII, calcium-calmodulin-dependent kinase II; CaN, calcineurin; CB1R, cannabinoid type 1 receptor; CDK5, neuronal protein kinase cyclin-dependent kinase 5; CeA, central amygdala; CGA, chlorogenic acid; Ch-ABC, chondroitinase-ABC; CPP, conditioned place preference; D-APV, D(−)-2-amino-5-phosphonopentanoic acid (NMDAR antagonist); DH, dorsal hippocampus; 8-CPT, 8-(4-chlorophenylthio)-2′-O-methyladenosine-3′, 5′-cyclic monophosphate; Epac, (Exchange Protein Activated by cAMP)-specific agonist; eIF2α, eukaryotic initiation factor 2α; Epac, exchange protein activated by cAMP; ERK, extracellular signal-regulated kinase; garcinol, histone acetyltransferase inhibitor; GR, glucocorticoid; stress, 5-min forced swim in ice-cold water; ICI-118,551, a β2-AR selective antagonist; KN-93 and KN-62, CaMKII inhibitors; LA, lateral amygdala; mTORC1, mammalian target of rapamycin complex 1; NAc, nucleus accumbens; NMDAR, N-methyl-D-aspartate receptor; PKA, protein kinase A; PNNs, perineuronal nets; propranolol, non-specific β-AR inhibitor; rapamycin, mTORC1 inhibitor; Rp-cAMPS, Rp-adenosine 3′,5′-cyclic monophosphorothioate triethylammonium salt (PKA inhibitor); Sal003, a selective inhibitor of eIF2α dephosphorylation; Tet3, ten-eleven translocation methylcytosine dioxygenase 3; RG108, DNA methyltransferase inhibitor; SA, self-administration; S-adenosylmethionine, methyl donor; U0126, ERK inhibitor; Zif268, immediate-early gene, also known as EGR1, NGFI-A, and Krox24.

interneurons modulating the activity of pyramidal neurons in the PFC impaired the reconsolidation of a cocaine CPP (Slaker et al., 2015), suggesting that the PFC is required for drug memory reconsolidation. In another study, β-adrenergic receptor (β-AR) blockade in the prelimbic medial prefrontal cortex (PL-mPFC) persistently reduced the expression of a cocaine CPP memory when administered before, but not after, cocaine memory retrieval (Otis et al., 2013). This indicates that blockade of the β-ARs disrupted the retrieval, but not the reconsolidation, of cocaine CPP memory. These studies illustrate the sophisticated role played by the PFC in the process of memory reconsolidation.

There are limitations in the conclusions that can be drawn from circuit-based studies targeting specific brain regions using lesion or inactivation, as these methods may disrupt neural communication between structures. The mechanisms underlying reconsolidation remain to be further clarified considering the neuronal projections within the limbic–corticostriatal system. With the advance of neuronal manipulation techniques, such as the newly developed wireless optogenetic technique

(Yang et al., 2021), we are optimistic that these limitations can be addressed in future work.

POTENTIAL TARGETS FOR RELAPSE PREVENTION

While the brain areas required for associating environmental cues with drug stimuli have been well established, the underlying mechanisms of memory destabilization and re-stabilization at the molecular and synaptic levels are poorly understood. Here, we focus on reviewing novel potent targets for modulating drug memory reconsolidation.

Function of Epigenetic Mechanisms in Preventing Drug Relapse

Accumulating evidence indicates that epigenetic regulation plays a critical role in the process of drug-induced neuronal plasticity (Renthal and Nestler, 2008; Werner et al., 2021), which can involve long-lasting changes in gene expression and ultimately result in behavioral changes (Feng and Nestler, 2013). Here, we focus on the use of DNA demethylation and histone deacetylation during memory destabilization and their impact on relapse prevention.

DNA methylation in the VTA has been shown to play a role in associative memory combining environmental cues with drug reward (Day et al., 2013). Although DNA methylation was initially perceived as a stable process that cannot be rapidly modulated, subsequent studies have demonstrated that this is not the case (Miller et al., 2010; Zipperly et al., 2021). In the brain, DNA undergoes rapid methylation and demethylation, which is necessary for memory formation and synaptic plasticity (Feng et al., 2010; Miller et al., 2010; Day et al., 2013). This provides an avenue for disrupting drug memory during the reconsolidation window. For example, knockdown of the ten-eleven translocation 3 (TET3) gene of methylcytosine dioxygenase in pyramidal neurons of the DH was found to decrease the activation of pyramidal neurons, thus leading to the impairment of Pavlovian CPP memory reconsolidation (Liu et al., 2018). A putative explanation is that DNA demethylation promotes the binding of transcription factors (Miller et al., 2010; Jarome and Lubin, 2014), which in turn regulate the synthesis of new proteins necessary for memory updating. In another study, using a cocaine operant self-administration (SA) model, Massart et al. (2015) found that incubated cue-induced cocaine-seeking behavior was significantly reduced if the DNA methyltransferase (DNMT) inhibitor (RG108) was delivered intra-NAc on abstinence day 29 and immediately before the extinction test on day 30. This phenomenon could be reversed by the methyl donor S-adenosylmethionine (Massart et al., 2015), indicating that DNMT is a core target for relapse prevention. These results suggest that the signal cascade induced by memory reactivation opened a temporal window during which drug-related memories could be disrupted. In this study, the DNMT inhibitor RG108 was initially delivered one day before CS exposure and again immediately before CS presentation. In contrast, intra-BLA injection of the DNMT inhibitor 5-azacytidine (5-AZA) immediately after CS exposure, but not after a 6-h delay, disrupted cocaine memory reconsolidation (Shi et al., 2015). These two experiments reported similar results in spite of differences in the drug intervention times used, suggesting a complex mechanism underlying reconsolidation that will require more results to further clarify.

Experiments targeting the downstream gene, protein of the CDK5 (cyclin-dependent kinase 5), also found lower expression of the incubation of cocaine craving (Massart et al., 2015). Moreover, in another study, targeting protein kinase CDK5 in the BLA (but not CeA) immediately after memory reactivation, but not after a 6-h delay, abolished a cocaine CPP (Li et al., 2010). These studies suggest that DNA methylation is a core target for preventing relapse, and that protein expression, but not transcription, must be targeted within a specific reconsolidation time window (Nader et al., 2000a; Sorg et al., 2015).

Acetylation and deacetylation of chromatin is another signaling pathway involved in regulating the formation of drug context-associated memories contributing to addiction-like behaviors (Rogge et al., 2013; Bender and Torregrossa, 2020; Campbell et al., 2021). These processes are regulated by two kinds of functionally similar enzymes. Histone acetyltransferases (HATs) facilitate transcription (Korzus et al., 2004; Kouzarides, 2007; Barrett et al., 2011), while histone deacetylases (HDACs) repress transcription (Kumar et al., 2005; Kouzarides, 2007). Both HATs and HDACs are involved in long-term memory formation, and are necessary for Pavlovian cocaine memory consolidation (Malvaez et al., 2011; Taniguchi et al., 2012; Rogge et al., 2013). For example, mice showed significantly improved CPP acquisition after homozygous HDAC3 deletions, due to increased gene expression of c-Fos and nuclear receptor subfamily 4 group A member 2 (Nr4a2) (Rogge et al., 2013). As histone acetylation is required for drug-induced neuroplasticity, later studies have demonstrated that HATs and HDACs are actively involved in drug memory reconsolidation. For example, cue-induced cocaine reinstatement could be enhanced by infusion of trichostatin A (an HDAC inhibitor) into lateral amygdala (LA), and was disrupted by the amnestic agent garcinol (Monsey et al., 2019). These results suggest that changes in histone acetylation are required for memory reconsolidation specifically in the LA, and that targeting HDACs is a possible way to disrupt reconsolidation.

As epigenetic changes affect the initial stage of protein synthesis upstream of transcription, epigenetic manipulation often leads to non-specific consequences. To improve the therapeutic potential of the targeting epigenetic processes, downstream targets and their roles in drug relapse should be identified by future research.

Autophagy Is a Potent Target for Modifying Drug Memory

Autophagy is an essential pathway for maintaining proteostasis and plays a critical role in neuroplasticity (Liang, 2019). However, direct evidence of autophagy in drug memory consolidation and reconsolidation is rarely reported, although several studies

have indicated that autophagy is involved in fear memory consolidation and reconsolidation. For example, one study found that autophagy is recruited in auditory fear memory consolidation by regulating inhibitory neurotransmission via GABA(A)R-associated protein (GABARAP) and its interaction with the GABA(A)R γ2 subunit (Li et al., 2019). Moreover, fear memory reactivation could be prevented by inhibiting synaptic protein degradation (Lee et al., 2008). This effect could be reversed by autophagy-induced synaptic α-amino-3-hydroxy-5-methyl-4-isoxazolepropionic acid receptor (AMPAR) endocytosis (Shehata et al., 2018), suggesting that autophagy may participate in memory reconsolidation via synaptic protein degradation. These reports reveal that the GABAR and AMPAR are potent targets for modulating memory consolidation and reconsolidation. A few studies have also reported that autophagy is required during the degradation of endocytosed GABARs in Caenorhabditis elegans (Rowland et al., 2006) and the degradation of AMPARs in hippocampal neurons (Shehata et al., 2012). As both the GABAR and AMPAR are required for learning and memory (Luo et al., 2015; Roth et al., 2020; Davenport et al., 2021), this presents an ideal opportunity to verify whether autophagy is involved in drug memory consolidation and reconsolidation. However, one pitfall of this approach may be that, as implied in the study (Shehata et al., 2018), autophagy does not directly disrupt reconsolidation, but rather helps to enhance memory destabilization, thus leading to changes in reconsolidation-resistant memories.

Beta-Adrenergic Signaling Is a Promising Safe Target for Preventing Relapse

Two potential explanations for the limited efficacy of reconsolidation-based pharmacological therapy in preventing relapse are the adverse effects of the amnestic agents administered and the huge surgical trauma involved in targeting specific brain areas. However, these challenges can be addressed by using an amnestic agent with little toxicity that can be delivered in a safe way. Propranolol, a non-specific β-AR blocker, has been reported to be a promising candidate for preventing nicotine, heroin, and cocaine relapse in the clinic (Zhao et al., 2011; Saladin et al., 2013; Xue et al., 2017b; Chen et al., 2021). Furthermore, propranolol has been shown to cross the blood–brain barrier and target β-ARs in the amygdala to modulate drug memory reconsolidation (Otis et al., 2015; Zhu et al., 2018). Propranolol has few side effects and has proved powerful in reducing drug craving. Traditionally, to reduce relapse, the association between drug-paired cues and drug reward is targeted to affect CS-induced reconsolidation. However, the application of this approach may be limited as environmental cues are diverse and the extinguished response to cues may be reinstated with the passage of time (Luo et al., 2015). Nevertheless, the limitations of targeting CS-induced reconsolidation could be addressed by also targeting US-induced reconsolidation (Luo et al., 2015). Propranolol is capable of disrupting US-induced reconsolidation via beta-adrenergic signaling (Xue et al., 2017a,b; Deng et al., 2020), making this signaling pathway a promising target for the prevention of relapse.

Editing Drug Memory at the Synaptic Level

Synaptic plasticity plays an essential role in neuroadaptations caused by drug addiction and the subsequent maladaptive learning (Kauer and Malenka, 2007). Drug abuse induces changes in synaptic strength, known as synaptic plasticity, to support the formation of associative memories between environment cues and drug reward. Technological advances in experimental methods have allowed precise observation of the process of reconsolidation. For example, one study observed that recognizing training contexts more precisely and more effectively during fear memory retrieval required transiently increased excitation of engram cells (neuroplasticity) (Pignatelli et al., 2019), indicating the dynamic nature of synapses during reconsolidation. Furthermore, in a SA model, researchers found that cocaine memory retrieval promoted the re-maturation of matured silent synapses during the destabilization window (Wright et al., 2020). Blocking silent synapse re-maturation in the NAc during this window gave rise to reduced cocaine-seeking behavior after cue exposure, suggesting that synaptic plasticity is required for memory reconsolidation. Intriguingly, independent of memory retrieval, Young et al. (2016) found that context-induced drug-seeking was disrupted by preventing synaptic actin polymerization in methamphetamine (METH) addiction. In addition, BLA spine dynamics have been shown to contribute to the formation and disruption of METH-associated memory (Young et al., 2020). As the impairment of METH-associated memories was independent of memory reactivation, this approach provides a novel way to edit drug memory outside of the reconsolidation window. These studies reveal the dynamic nature of synaptic plasticity in reconsolidation-dependent, as well as reconsolidation-independent, memory editing.

BOUNDARY CONDITIONS FOR MEMORY RECONSOLIDATION

Boundaries for Memory Reactivation and Updating

Although drug-paired cues provide effective targets for editing addiction memory, there are several problems that limit reconsolidation-based therapy. Firstly, memory reactivation may be limited due to the requirements for specific retrieval conditions (e.g., context, schedule, or duration of retrieval) or memory features (e.g., age or strength) (Lee, 2009; Lee et al., 2017; Piva et al., 2019). In addition, to promote memory destabilization, a prediction error is usually required (Exton-McGuinness et al., 2015; Sinclair and Barense, 2019). Among people with drug addictions, inter-individual differences may be a boundary condition for the prediction error; this can be attributed to individual drug use histories and incentive value to cues (Kuijer et al., 2020). It would be a significant advance if future research was successful in identifying the biomarkers of drug memory destabilization (Wang et al., 2020). Secondly, CS-induced memory reconsolidation only helps to target specific drug-paired cues (Xue et al., 2012). Although US-induced

reconsolidation seems to be a more effective target for preventing relapse (Luo et al., 2015; Dunbar and Taylor, 2017; Xue et al., 2017b), there may be ethical barriers to evoking drug memories using low-dose drug priming in the clinic. Lastly, memory updates may be ineffective in people with drug addictions who also suffer from psychiatric disorders. For instance, in a clinical study, compared with control subjects, patients diagnosed with schizophrenia displayed significant impairment of CS-induced recall of an extinguished memory (Holt et al., 2009).

Boundaries for Reconsolidation-Based Therapy

Reconsolidation-based therapy has not been appreciably improved by neuroscientific research. One boundary limiting this is that mechanistic studies using rodent models do not combine volitional social factors (Heilig et al., 2016). Recently, Venniro et al. (2018, 2019) and Venniro and Shaham (2020) introduced social context into the classic SA model, demonstrating that operant social interaction could prevent drug addiction, broadening the horizon of relapse prevention. To prevent relapse, methodological innovation is needed in order to provide new ways to understand addiction and to control drug abuse.

CONCLUSION

Over the last two decades, reconsolidation theory has progressed from a topic of debate to a basis for clinical therapy. Fundamental research in rodents has revealed the brain regions and molecular processes recruited during reconsolidation. However, boundary conditions limiting progress in memory destabilization and clinical translation remain a challenge for neurobiologists. Meanwhile, reports implying that drug memories can be modified without memory reactivation could provide a promising supplementary approach to reconsolidation-based therapy (Young et al., 2016, 2020). With the development of novel techniques and the accumulation of scientific evidence, we keep an open mind with regard to the potential role of reconsolidation theory in drug relapse prevention.

AUTHOR CONTRIBUTIONS

LC developed the manuscript, corrected the style, reviewed and edited the manuscript, and discussed the central ideas of it. HY, YW, XF, SH, and FW developed the manuscript and discussed the central ideas of it. ZH and QL designed the graph and reviewed and edited the manuscript. JY developed the manuscript, proposed the central idea of it, reviewed and edited the manuscript, and acquired funding. All authors contributed to the article and approved the submitted version.

FUNDING

This work was supported in by National Natural Science Foundation of China (Nos. 81772024 and 82060339) and the Fundamental Research Funds for the Central Universities of Central South University (No. 2021zzts0939).

REFERENCES

Arguello, A. A., Hodges, M. A., Wells, A. M., Lara, H. III., Xie, X., and Fuchs, R. A. (2014). Involvement of amygdalar protein kinase A, but not calcium/calmodulin-dependent protein kinase II, in the reconsolidation of cocaine-related contextual memories in rats. *Psychopharmacology (Berl)* 231, 55–65. doi: 10.1007/s00213-013-3203-9

Barak, S., Liu, F., Hamida, S. B., Yowell, Q. V., Neasta, J., Kharazia, V., et al. (2013). Disruption of alcohol-related memories by mTORC1 inhibition prevents relapse. *Nat. Neurosci.* 16, 1111–1117. doi: 10.1038/nn.3439

Barnes, T. D., Kubota, Y., Hu, D., Jin, D. Z., and Graybiel, A. M. (2005). Activity of striatal neurons reflects dynamic encoding and recoding of procedural memories. *Nature* 437, 1158–1161. doi: 10.1038/nature04053

Barrett, R. M., Malvaez, M., Kramar, E., Matheos, D. P., Arrizon, A., Cabrera, S. M., et al. (2011). Hippocampal focal knockout of CBP affects specific histone modifications, long-term potentiation, and long-term memory. *Neuropsychopharmacology* 36, 1545–1556. doi: 10.1038/npp.2011.61

Bender, B. N., and Torregrossa, M. M. (2020). Molecular and circuit mechanisms regulating cocaine memory. *Cell. Mol. Life Sci.* 77, 3745–3768. doi: 10.1007/s00018-020-03498-8

Blundell, P., Hall, G., and Killcross, S. (2001). Lesions of the basolateral amygdala disrupt selective aspects of reinforcer representation in rats. *J. Neurosci.* 21, 9018–9026. doi: 10.1523/jneurosci.21-22-09018.2001

Brown, T. E., Lee, B. R., and Sorg, B. A. (2008). The NMDA antagonist MK-801 disrupts reconsolidation of a cocaine-associated memory for conditioned place preference but not for self-administration in rats. *Learn. Mem.* 15, 857–865. doi: 10.1101/lm.1152808

Campbell, R. R., Kramár, E. A., Pham, L., Beardwood, J. H., Augustynski, A. S., López, A. J., et al. (2021). HDAC3 Activity within the Nucleus Accumbens Regulates Cocaine-Induced Plasticity and Behavior in a Cell-Type-Specific Manner. *J. Neurosci.* 41, 2814–2827. doi: 10.1523/jneurosci.2829-20.2021

Chen, L., Huang, S., Yang, C., Wu, F., Zheng, Q., Yan, H., et al. (2021). Blockade of β-Adrenergic Receptors by Propranolol Disrupts Reconsolidation of Drug Memory and Attenuates Heroin Seeking. *Front. Pharmacol.* 12:686845. doi: 10.3389/fphar.2021.686845

Cox, J., and Witten, I. B. (2019). Striatal circuits for reward learning and decision-making. *Nat. Rev. Neurosci.* 20, 482–494. doi: 10.1038/s41583-019-0189-2

Davenport, C. M., Rajappa, R., Katchan, L., Taylor, C. R., Tsai, M. C., Smith, C. M., et al. (2021). Relocation of an Extrasynaptic GABA(A) Receptor to Inhibitory Synapses Freezes Excitatory Synaptic Strength and Preserves Memory. *Neuron* 109, 123–134.e4.

Day, J. J., Childs, D., Guzman-Karlsson, M. C., Kibe, M., Moulden, J., Song, E., et al. (2013). DNA methylation regulates associative reward learning. *Nat. Neurosci.* 16, 1445–1452. doi: 10.1038/nn.3504

Deng, J., Shi, L., Yuan, K., Yao, P., Chen, S., Que, J., et al. (2020). Propranolol-induced inhibition of unconditioned stimulus-reactivated fear memory prevents the return of fear in humans. *Transl. Psychiatry* 10:345.

Dunbar, A. B., and Taylor, J. R. (2017). Garcinol Blocks the Reconsolidation of Multiple Cocaine-Paired Cues after a Single Cocaine-Reactivation Session. *Neuropsychopharmacology* 42, 1884–1892. doi: 10.1038/npp.2017.27

Exton-McGuinness, M. T., Lee, J. L., and Reichelt, A. C. (2015). Updating memories–the role of prediction errors in memory reconsolidation. *Behav. Brain Res.* 278, 375–384. doi: 10.1016/j.bbr.2014.10.011

Exton-McGuinness, M. T., Patton, R. C., Sacco, L. B., and Lee, J. L. (2014). Reconsolidation of a well-learned instrumental memory. *Learn. Mem.* 21, 468–477. doi: 10.1101/lm.035543.114

Exton-McGuinness, M. T. J., Drame, M. L., Flavell, C. R., and Lee, J. L. C. (2019). On the Resistance to Relapse to Cocaine-Seeking Following Impairment of

Instrumental Cocaine Memory Reconsolidation. *Front. Behav. Neurosci.* 13:242. doi: 10.3389/fnbeh.2019.00242

Feng, J., and Nestler, E. J. (2013). Epigenetic mechanisms of drug addiction. *Curr. Opin. Neurobiol.* 23, 521–528. doi: 10.1016/j.conb.2013.01.001

Feng, J., Zhou, Y., Campbell, S. L., Le, T., Li, E., Sweatt, J. D., et al. (2010). Dnmt1 and Dnmt3a maintain DNA methylation and regulate synaptic function in adult forebrain neurons. *Nat. Neurosci.* 13, 423–430. doi: 10.1038/nn.2514

Fuchs, R. A., Evans, K. A., Ledford, C. C., Parker, M. P., Case, J. M., Mehta, R. H., et al. (2005). The role of the dorsomedial prefrontal cortex, basolateral amygdala, and dorsal hippocampus in contextual reinstatement of cocaine seeking in rats. *Neuropsychopharmacology* 30, 296–309. doi: 10.1038/sj.npp.1300579

Goldstein, R. Z., and Volkow, N. D. (2011). Dysfunction of the prefrontal cortex in addiction: neuroimaging findings and clinical implications. *Nat. Rev. Neurosci.* 12, 652–669. doi: 10.1038/nrn3119

Heilig, M., Epstein, D. H., Nader, M. A., and Shaham, Y. (2016). Time to connect: bringing social context into addiction neuroscience. *Nat. Rev. Neurosci.* 17, 592–599. doi: 10.1038/nrn.2016.67

Hernandez, P. J., and Kelley, A. E. (2004). Long-term memory for instrumental responses does not undergo protein synthesis-dependent reconsolidation upon retrieval. *Learn. Mem.* 11, 748–754. doi: 10.1101/lm.84904

Higginbotham, J. A., Jones, N. M., Wang, R., Christian, R. J., Ritchie, J. L., Mclaughlin, R. J., et al. (2021a). Basolateral amygdala CB1 receptors gate HPA axis activation and context-cocaine memory strength during reconsolidation. *Neuropsychopharmacology* 46, 1554–1564. doi: 10.1038/s41386-020-00919-x

Higginbotham, J. A., Wang, R., Richardson, B. D., Shiina, H., Tan, S. M., Presker, M. A., et al. (2021b). CB1 Receptor Signaling Modulates Amygdalar Plasticity during Context-Cocaine Memory Reconsolidation to Promote Subsequent Cocaine Seeking. *J. Neurosci.* 41, 613–629. doi: 10.1523/jneurosci.1390-20.2020

Holt, D. J., Lebron-Milad, K., Milad, M. R., Rauch, S. L., Pitman, R. K., Orr, S. P., et al. (2009). Extinction memory is impaired in schizophrenia. *Biol. Psychiatry* 65, 455–463.

Hyman, S. E., Malenka, R. C., and Nestler, E. J. (2006). Neural mechanisms of addiction: the role of reward-related learning and memory. *Annu. Rev. Neurosci.* 29, 565–598. doi: 10.1146/annurev.neuro.29.051605.113009

Janak, P. H., and Tye, K. M. (2015). From circuits to behaviour in the amygdala. *Nature* 517, 284–292. doi: 10.1038/nature14188

Jarome, T. J., and Lubin, F. D. (2014). Epigenetic mechanisms of memory formation and reconsolidation. *Neurobiol. Learn. Mem.* 115, 116–127. doi: 10.1016/j.nlm.2014.08.002

Jian, M., Luo, Y. X., Xue, Y. X., Han, Y., Shi, H. S., Liu, J. F., et al. (2014). eIF2α dephosphorylation in basolateral amygdala mediates reconsolidation of drug memory. *J. Neurosci.* 34, 10010–10021. doi: 10.1523/jneurosci.0934-14.2014

Kauer, J. A., and Malenka, R. C. (2007). Synaptic plasticity and addiction. *Nat. Rev. Neurosci.* 8, 844–858.

Korzus, E., Rosenfeld, M. G., and Mayford, M. (2004). CBP histone acetyltransferase activity is a critical component of memory consolidation. *Neuron* 42, 961–972. doi: 10.1016/j.neuron.2004.06.002

Kouzarides, T. (2007). Chromatin modifications and their function. *Cell* 128, 693–705. doi: 10.1016/j.cell.2007.02.005

Kruzich, P. J., and See, R. E. (2001). Differential contributions of the basolateral and central amygdala in the acquisition and expression of conditioned relapse to cocaine-seeking behavior. *J. Neurosci.* 21:RC155.

Kuijer, E. J., Ferragud, A., and Milton, A. L. (2020). Retrieval-Extinction and Relapse Prevention: rewriting Maladaptive Drug Memories? *Front. Behav. Neurosci.* 14:23. doi: 10.3389/fnbeh.2020.00023

Kumar, A., Choi, K. H., Renthal, W., Tsankova, N. M., Theobald, D. E., Truong, H. T., et al. (2005). Chromatin remodeling is a key mechanism underlying cocaine-induced plasticity in striatum. *Neuron* 48, 303–314. doi: 10.1016/j.neuron.2005.09.023

Lee, J. L., Di Ciano, P., Thomas, K. L., and Everitt, B. J. (2005). Disrupting reconsolidation of drug memories reduces cocaine-seeking behavior. *Neuron* 47, 795–801. doi: 10.1016/j.neuron.2005.08.007

Lee, J. L., Milton, A. L., and Everitt, B. J. (2006). Cue-induced cocaine seeking and relapse are reduced by disruption of drug memory reconsolidation. *J. Neurosci.* 26, 5881–5887. doi: 10.1523/jneurosci.0323-06.2006

Lee, J. L. C. (2009). Reconsolidation: maintaining memory relevance. *Trends Neurosci.* 32, 413–420. doi: 10.1016/j.tins.2009.05.002

Lee, J. L. C., Nader, K., and Schiller, D. (2017). An Update on Memory Reconsolidation Updating. *Trends Cogn. Sci.* 21, 531–545. doi: 10.1016/j.tics.2017.04.006

Lee, S. H., Choi, J. H., Lee, N., Lee, H. R., Kim, J. I., Yu, N. K., et al. (2008). Synaptic protein degradation underlies destabilization of retrieved fear memory. *Science* 319, 1253–1256. doi: 10.1126/science.1150541

Li, F. Q., Xue, Y. X., Wang, J. S., Fang, Q., Li, Y. Q., Zhu, W. L., et al. (2010). Basolateral amygdala cdk5 activity mediates consolidation and reconsolidation of memories for cocaine cues. *J. Neurosci.* 30, 10351–10359. doi: 10.1523/jneurosci.2112-10.2010

Li, K., Chen, H. S., Li, D., Li, H. H., Wang, J., Jia, L., et al. (2019). SAR405, a Highly Specific VPS34 Inhibitor, Disrupts Auditory Fear Memory Consolidation of Mice via Facilitation of Inhibitory Neurotransmission in Basolateral Amygdala. *Biol. Psychiatry* 85, 214–225. doi: 10.1016/j.biopsych.2018.07.026

Liang, J., Li, J.-L., Han, Y., Luo, Y.-X., Xue, Y.-X., Zhang, Y., et al. (2017). Calpain-GRIP Signaling in Nucleus Accumbens Core Mediates the Reconsolidation of Drug Reward Memory. *J. Neurosci.* 37, 8938–8951. doi: 10.1523/jneurosci.0703-17.2017

Liang, Y. (2019). Emerging Concepts and Functions of Autophagy as a Regulator of Synaptic Components and Plasticity. *Cells* 8:34. doi: 10.3390/cells8010034

Liu, C., Sun, X., Wang, Z., Le, Q., Liu, P., Jiang, C., et al. (2018). Retrieval-Induced Upregulation of Tet3 in Pyramidal Neurons of the Dorsal Hippocampus Mediates Cocaine-Associated Memory Reconsolidation. *Int. J. Neuropsychopharmacol.* 21, 255–266. doi: 10.1093/ijnp/pyx099

Luo, Y.-X., Xue, Y.-X., Liu, J.-F., Shi, H.-S., Jian, M., Han, Y., et al. (2015). A novel UCS memory retrieval-extinction procedure to inhibit relapse to drug seeking. *Nat. Commun.* 6, 7675–7675.

Lüscher, C. (2016). The Emergence of a Circuit Model for Addiction. *Annu. Rev. Neurosci.* 39, 257–276. doi: 10.1146/annurev-neuro-070815-013920

Malvaez, M., Mhillaj, E., Matheos, D. P., Palmery, M., and Wood, M. A. (2011). CBP in the nucleus accumbens regulates cocaine-induced histone acetylation and is critical for cocaine-associated behaviors. *J. Neurosci.* 31, 16941–16948. doi: 10.1523/jneurosci.2747-11.2011

Massart, R., Barnea, R., Dikshtein, Y., Suderman, M., Meir, O., Hallett, M., et al. (2015). Role of DNA Methylation in the Nucleus Accumbens in Incubation of Cocaine Craving. *J. Neurosci.* 35, 8042–8058. doi: 10.1523/jneurosci.3053-14.2015

Miller, C. A., Gavin, C. F., White, J. A., Parrish, R. R., Honasoge, A., Yancey, C. R., et al. (2010). Cortical DNA methylation maintains remote memory. *Nat. Neurosci.* 13, 664–666. doi: 10.1038/nn.2560

Milton, A. L., and Everitt, B. J. (2012). The persistence of maladaptive memory: addiction, drug memories and anti-relapse treatments. *Neurosci. Biobehav. Rev.* 36, 1119–1139. doi: 10.1016/j.neubiorev.2012.01.002

Milton, A. L., Lee, J. L., Butler, V. J., Gardner, R., and Everitt, B. J. (2008). Intra-amygdala and systemic antagonism of NMDA receptors prevents the reconsolidation of drug-associated memory and impairs subsequently both novel and previously acquired drug-seeking behaviors. *J. Neurosci.* 28, 8230–8237. doi: 10.1523/jneurosci.1723-08.2008

Misanin, J. R., Miller, R. R., and Lewis, D. J. (1968). Retrograde amnesia produced by electroconvulsive shock after reactivation of a consolidated memory trace. *Science* 160, 554–555. doi: 10.1126/science.160.3827.554

Monsey, M. S., Ruiz, S. G., and Taylor, J. R. (2019). Regulation of Garcinol on Histone Acetylation in the Amygdala and on the Reconsolidation of a Cocaine-Associated Memory. *Front. Behav. Neurosci.* 13:281. doi: 10.3389/fnbeh.2019.00281

Nader, K., Schafe, G. E., and Le Doux, J. E. (2000a). Fear memories require protein synthesis in the amygdala for reconsolidation after retrieval. *Nature* 406, 722–726. doi: 10.1038/35021052

Nader, K., Schafe, G. E., and LeDoux, J. E. (2000b). The labile nature of consolidation theory. *Nat. Rev. Neurosci.* 1, 216–219. doi: 10.1038/35044580

Nutt, D. J., Lingford-Hughes, A., Erritzoe, D., and Stokes, P. R. (2015). The dopamine theory of addiction: 40 years of highs and lows. *Nat. Rev. Neurosci.* 16, 305–312. doi: 10.1038/nrn3939

O'Hare, J. K., Ade, K. K., Sukharnikova, T., Van Hooser, S. D., Palmeri, M. L., Yin, H. H., et al. (2016). Pathway-Specific Striatal Substrates for Habitual Behavior. *Neuron* 89, 472–479. doi: 10.1016/j.neuron.2015.12.032

Otis, J. M., Dashew, K. B., and Mueller, D. (2013). Neurobiological Dissociation of Retrieval and Reconsolidation of Cocaine-Associated Memory. *J. Neurosci.* 33, 1271–1281. doi: 10.1523/jneurosci.3463-12.2013

Otis, J. M., Werner, C. T., and Mueller, D. (2015). Noradrenergic regulation of fear and drug-associated memory reconsolidation. *Neuropsychopharmacology* 40, 793–803. doi: 10.1038/npp.2014.243

Phelps, E. A., and Hofmann, S. G. (2019). Memory editing from science fiction to clinical practice. *Nature* 572, 43–50. doi: 10.1038/s41586-019-1433-7

Pignatelli, M., Ryan, T. J., Roy, D. S., Lovett, C., Smith, L. M., Muralidhar, S., et al. (2019). Engram Cell Excitability State Determines the Efficacy of Memory Retrieval. *Neuron* 101, 274–284.e5.

Piva, A., Gerace, E., Di Chio, M., Padovani, L., Paolone, G., Pellegrini-Giampietro, D. E., et al. (2019). Reconsolidation of sucrose instrumental memory in rats: The role of retrieval context. *Brain Res.* 1714, 193–201. doi: 10.1016/j.brainres.2019.03.006

Piva, A., Pintori, N., Padovani, L., and Chiamulera, C. (2020). Protocols for instrumental memory reconsolidation in rodents: a methodological review. *J. Neurosci. Methods* 342:108766. doi: 10.1016/j.jneumeth.2020.108766

Porter, J. T., and Sepulveda-Orengo, M. T. (2020). Learning-induced intrinsic and synaptic plasticity in the rodent medial prefrontal cortex. *Neurobiol. Learn. Mem.* 169, 107117–107117. doi: 10.1016/j.nlm.2019.107117

Przybyslawski, J., and Sara, S. J. (1997). Reconsolidation of memory after its reactivation. *Behav. Brain Res.* 84, 241–246. doi: 10.1016/s0166-4328(96)00153-2

Ramirez, D. R., Bell, G. H., Lasseter, H. C., Xie, X., Traina, S. A., and Fuchs, R. A. (2009). Dorsal hippocampal regulation of memory reconsolidation processes that facilitate drug context-induced cocaine-seeking behavior in rats. *Eur. J. Neurosci.* 30, 901–912. doi: 10.1111/j.1460-9568.2009.06889.x

Renthal, W., and Nestler, E. J. (2008). Epigenetic mechanisms in drug addiction. *Trends Mol. Med.* 14, 341–350. doi: 10.1016/j.molmed.2008.06.004

Rich, M. T., Abbott, T. B., Chung, L., Gulcicek, E. E., Stone, K. L., Colangelo, C. M., et al. (2016). Phosphoproteomic Analysis Reveals a Novel Mechanism of CaMKIIα Regulation Inversely Induced by Cocaine Memory Extinction versus Reconsolidation. *J. Neurosci.* 36, 7613–7627. doi: 10.1523/jneurosci.1108-16.2016

Rich, M. T., Huang, Y. H., and Torregrossa, M. M. (2020). Calcineurin Promotes Neuroplastic Changes in the Amygdala Associated with Weakened Cocaine-Cue Memories. *J. Neurosci.* 40, 1344–1354. doi: 10.1523/jneurosci.0453-19.2019

Rogge, G. A., Singh, H., Dang, R., and Wood, M. A. (2013). HDAC3 is a negative regulator of cocaine-context-associated memory formation. *J. Neurosci.* 33, 6623–6632. doi: 10.1523/jneurosci.4472-12.2013

Roth, R. H., Cudmore, R. H., Tan, H. L., Hong, I., Zhang, Y., and Huganir, R. L. (2020). Cortical Synaptic AMPA Receptor Plasticity during Motor Learning. *Neuron* 105, 895–908.e5.

Rowland, A. M., Richmond, J. E., Olsen, J. G., Hall, D. H., and Bamber, B. A. (2006). Presynaptic terminals independently regulate synaptic clustering and autophagy of GABAA receptors in Caenorhabditis elegans. *J. Neurosci.* 26, 1711–1720. doi: 10.1523/jneurosci.2279-05.2006

Saladin, M. E., Gray, K. M., Mcrae-Clark, A. L., Larowe, S. D., Yeatts, S. D., Baker, N. L., et al. (2013). A double blind, placebo-controlled study of the effects of post-retrieval propranolol on reconsolidation of memory for craving and cue reactivity in cocaine dependent humans. *Psychopharmacology (Berl)* 226, 721–737. doi: 10.1007/s00213-013-3039-3

Shehata, M., Abdou, K., Choko, K., Matsuo, M., Nishizono, H., and Inokuchi, K. (2018). Autophagy Enhances Memory Erasure through Synaptic Destabilization. *J. Neurosci.* 38, 3809–3822. doi: 10.1523/jneurosci.3505-17.2018

Shehata, M., Matsumura, H., Okubo-Suzuki, R., Ohkawa, N., and Inokuchi, K. (2012). Neuronal stimulation induces autophagy in hippocampal neurons that is involved in AMPA receptor degradation after chemical long-term depression. *J. Neurosci.* 32, 10413–10422. doi: 10.1523/jneurosci.4533-11.2012

Shi, H. S., Luo, Y. X., Yin, X., Wu, H. H., Xue, G., Geng, X. H., et al. (2015). Reconsolidation of a cocaine associated memory requires DNA methyltransferase activity in the basolateral amygdala. *Sci. Rep.* 5:13327.

Sinclair, A. H., and Barense, M. D. (2019). Prediction Error and Memory Reactivation: how Incomplete Reminders Drive Reconsolidation. *Trends Neurosci.* 42, 727–739. doi: 10.1016/j.tins.2019.08.007

Slaker, M., Churchill, L., Todd, R. P., Blacktop, J. M., Zuloaga, D. G., Raber, J., et al. (2015). Removal of perineuronal nets in the medial prefrontal cortex impairs the acquisition and reconsolidation of a cocaine-induced conditioned place preference memory. *J. Neurosci.* 35, 4190–4202. doi: 10.1523/jneurosci.3592-14.2015

Sorg, B. A., Todd, R. P., Slaker, M., and Churchill, L. (2015). Anisomycin in the medial prefrontal cortex reduces reconsolidation of cocaine-associated memories in the rat self-administration model. *Neuropharmacology* 92, 25–33. doi: 10.1016/j.neuropharm.2014.12.029

Szczepanski, S. M., and Knight, R. T. (2014). Insights into human behavior from lesions to the prefrontal cortex. *Neuron* 83, 1002–1018. doi: 10.1016/j.neuron.2014.08.011

Taniguchi, M., Carreira, M. B., Smith, L. N., Zirlin, B. C., Neve, R. L., and Cowan, C. W. (2012). Histone deacetylase 5 limits cocaine reward through cAMP-induced nuclear import. *Neuron* 73, 108–120. doi: 10.1016/j.neuron.2011.10.032

Taubenfeld, S. M., Muravieva, E. V., Garcia-Osta, A., and Alberini, C. M. (2010). Disrupting the memory of places induced by drugs of abuse weakens motivational withdrawal in a context-dependent manner. *Proc. Natl. Acad. Sci. U. S. A.* 107, 12345–12350. doi: 10.1073/pnas.1003152107

Thorn, C. A., Atallah, H., Howe, M., and Graybiel, A. M. (2010). Differential dynamics of activity changes in dorsolateral and dorsomedial striatal loops during learning. *Neuron* 66, 781–795. doi: 10.1016/j.neuron.2010.04.036

Trouche, S., Koren, V., Doig, N. M., Ellender, T. J., El-Gaby, M., Lopes-Dos-Santos, V., et al. (2019). A Hippocampus-Accumbens Tripartite Neuronal Motif Guides Appetitive Memory in Space. *Cell* 176, 1393–1406.e16.

Venniro, M., Russell, T. I., Zhang, M., and Shaham, Y. (2019). Operant Social Reward Decreases Incubation of Heroin Craving in Male and Female Rats. *Biol. Psychiatry* 86, 848–856. doi: 10.1016/j.biopsych.2019.05.018

Venniro, M., and Shaham, Y. (2020). An operant social self-administration and choice model in rats. *Nat. Protoc.* 15, 1542–1559. doi: 10.1038/s41596-020-0296-6

Venniro, M., Zhang, M., Caprioli, D., Hoots, J. K., Golden, S. A., Heins, C., et al. (2018). Volitional social interaction prevents drug addiction in rat models. *Nat. Neurosci.* 21, 1520–1529. doi: 10.1038/s41593-018-0246-6

Wan, X., Torregrossa, M. M., Sanchez, H., Nairn, A. C., and Taylor, J. R. (2014). Activation of exchange protein activated by cAMP in the rat basolateral amygdala impairs reconsolidation of a memory associated with self-administered cocaine. *PLoS One* 9:e107359. doi: 10.1371/journal.pone.0107359

Wang, X.-Y., Zhao, M., Ghitza, U. E., Li, Y.-Q., and Lu, L. (2008). Stress Impairs Reconsolidation of Drug Memory via Glucocorticoid Receptors in the Basolateral Amygdala. *J. Neurosci.* 28, 5602–5610. doi: 10.1523/jneurosci.0750-08.2008

Wang, Z., Jin, T., Le, Q., Liu, C., Wang, X., Wang, F., et al. (2020). Retrieval-Driven Hippocampal NPTX2 Plasticity Facilitates the Extinction of Cocaine-Associated Context Memory. *Biol. Psychiatry* 87, 979–991. doi: 10.1016/j.biopsych.2019.10.009

Wells, A. M., Arguello, A. A., Xie, X., Blanton, M. A., Lasseter, H. C., Reittinger, A. M., et al. (2013). Extracellular signal-regulated kinase in the basolateral amygdala, but not the nucleus accumbens core, is critical for context-response-cocaine memory reconsolidation in rats. *Neuropsychopharmacology* 38, 753–762. doi: 10.1038/npp.2012.238

Wells, A. M., Lasseter, H. C., Xie, X., Cowhey, K. E., Reittinger, A. M., and Fuchs, R. A. (2011). Interaction between the basolateral amygdala and dorsal hippocampus is critical for cocaine memory reconsolidation and subsequent drug context-induced cocaine-seeking behavior in rats. *Learn. Mem.* 18, 693–702. doi: 10.1101/lm.2273111

Werner, C. T., Altshuler, R. D., Shaham, Y., and Li, X. (2021). Epigenetic Mechanisms in Drug Relapse. *Biol. Psychiatry* 89, 331–338. doi: 10.1016/j.biopsych.2020.08.005

Wright, W. J., Graziane, N. M., Neumann, P. A., Hamilton, P. J., Cates, H. M., Fuerst, L., et al. (2020). Silent synapses dictate cocaine memory destabilization and reconsolidation. *Nat. Neurosci.* 23, 32–46. doi: 10.1038/s41593-019-0537-6

Wu, Y., Li, Y., Yang, X., and Sui, N. (2014). Differential effect of beta-adrenergic receptor antagonism in basolateral amygdala on reconsolidation of aversive and appetitive memories associated with morphine in rats. *Addict Biol.* 19, 5–15. doi: 10.1111/j.1369-1600.2012.00443.x

Xue, Y. X., Chen, Y. Y., Zhang, L. B., Zhang, L. Q., Huang, G. D., Sun, S. C., et al. (2017a). Selective Inhibition of Amygdala Neuronal Ensembles Encoding Nicotine-Associated Memories Inhibits Nicotine Preference and Relapse. *Biol. Psychiatry* 82, 781–793. doi: 10.1016/j.biopsych.2017.04.017

Xue, Y. X., Deng, J. H., Chen, Y. Y., Zhang, L. B., Wu, P., Huang, G. D., et al. (2017b). Effect of Selective Inhibition of Reactivated Nicotine-Associated Memories With Propranolol on Nicotine Craving. *JAMA Psychiatry* 74, 224–232. doi: 10.1001/jamapsychiatry.2016.3907

Xue, Y. X., Luo, Y. X., Wu, P., Shi, H. S., Xue, L. F., Chen, C., et al. (2012). A memory retrieval-extinction procedure to prevent drug craving and relapse. *Science* 336, 241–245. doi: 10.1126/science.1215070

Yang, Y., Wu, M., Vázquez-Guardado, A., Wegener, A. J., Grajales-Reyes, J. G., Deng, Y., et al. (2021). Wireless multilateral devices for optogenetic studies of individual and social behaviors. *Nat. Neurosci.* 24, 1035–1045. doi: 10.1038/s41593-021-00849-x

Yim, A. J., Moraes, C. R., Ferreira, T. L., and Oliveira, M. G. (2006). Protein synthesis inhibition in the basolateral amygdala following retrieval does not impair expression of morphine-associated conditioned place preference. *Behav. Brain Res.* 171, 162–169. doi: 10.1016/j.bbr.2006.03.031

Yin, H. H., Ostlund, S. B., Knowlton, B. J., and Balleine, B. W. (2005). The role of the dorsomedial striatum in instrumental conditioning. *Eur. J. Neurosci.* 22, 513–523. doi: 10.1111/j.1460-9568.2005.04218.x

Young, E. J., Blouin, A. M., Briggs, S. B., Sillivan, S. E., Lin, L., Cameron, M. D., et al. (2016). Nonmuscle myosin IIB as a therapeutic target for the prevention of relapse to methamphetamine use. *Mol. Psychiatry* 21, 615–623. doi: 10.1038/mp.2015.103

Young, E. J., Lin, H., Kamenecka, T. M., Rumbaugh, G., and Miller, C. A. (2020). Methamphetamine Learning Induces Persistent and Selective Nonmuscle Myosin II-Dependent Spine Motility in the Basolateral Amygdala. *J. Neurosci.* 40, 2695–2707. doi: 10.1523/jneurosci.2182-19.2020

Zhang, F., Huang, S., Bu, H., Zhou, Y., Chen, L., Kang, Z., et al. (2021). Disrupting Reconsolidation by Systemic Inhibition of mTOR Kinase via Rapamycin Reduces Cocaine-Seeking Behavior. *Front. Pharmacol.* 12:652865. doi: 10.3389/fphar.2021.652865

Zhao, L. Y., Sun, L. L., Shi, J., Li, P., Zhang, Y., and Lu, L. (2011). Effects of β-adrenergic receptor blockade on drug-related memory reconsolidation in abstinent heroin addicts. *Drug Alcohol Depend.* 118, 224–229. doi: 10.1016/j.drugalcdep.2011.03.025

Zhu, H., Zhou, Y., Liu, Z., Chen, X., Li, Y., Liu, X., et al. (2018). β1-Adrenoceptor in the Central Amygdala Is Required for Unconditioned Stimulus-Induced Drug Memory Reconsolidation. *Int. J. Neuropsychopharmacol.* 21, 267–280. doi: 10.1093/ijnp/pyx104

Zipperly, M. E., Sultan, F. A., Graham, G.-E., Brane, A. C., Simpkins, N. A., Carullo, N. V. N., et al. (2021). Regulation of dopamine-dependent transcription and cocaine action by Gadd45b. *Neuropsychopharmacology* 46, 709–720. doi: 10.1038/s41386-020-00828-z

Conflict of Interest: The authors declare that the research was conducted in the absence of any commercial or financial relationships that could be construed as a potential conflict of interest.

Publisher's Note: All claims expressed in this article are solely those of the authors and do not necessarily represent those of their affiliated organizations, or those of the publisher, the editors and the reviewers. Any product that may be evaluated in this article, or claim that may be made by its manufacturer, is not guaranteed or endorsed by the publisher.

frontiers in Pharmacology

ORIGINAL RESEARCH
published: 13 August 2021
doi: 10.3389/fphar.2021.708034

Potential Ago2/miR-3068-5p Cascades in the Nucleus Accumbens Contribute to Methamphetamine-Induced Locomotor Sensitization of Mice

Dan Liu[1,2,3], Min Liang[1,2], Li Zhu[1,2], Ting-ting Zhou[1,2], Yu Wang[1,2], Rui Wang[1,2], Fei-fei Wu[1,2], Eyleen L. K. Goh[4,5] and Teng Chen[1,2]**

[1]College of Forensic Medicine, Xi'an Jiaotong University Health Science Center, Xi'an, China, [2]The Key Laboratory of Health Ministry for Forensic Science, Xi'an Jiaotong University, Xi'an, China, [3]Guangdong Provincial Key Laboratory of Brain Connectome and Behavior, CAS Key Laboratory of Brain Connectome and Manipulation, The Brain Cognition and Brain Disease Institute, Shenzhen-Hong Kong Institute of Brain Science-Shenzhen Fundamental Research Institutions, Shenzhen Institute of Advanced Technology, Chinese Academy of Sciences, Shenzhen, China, [4]Department of Research, National Neuroscience Institute, Singapore, Singapore, [5]Neuroscience and Mental Health Faculty, Lee Kong China School of Medicine, Nanyang Technological University, Singapore, Singapore

OPEN ACCESS

Edited by:
Qi Wang,
Southern Medical University, China

Reviewed by:
Jing Han,
Shaanxi Normal University, China
Yan-Xue Xue,
Peking University, China
Tengfei Ma,
Nanjing Medical University, China

***Correspondence:**
Teng Chen
chenteng@xjtu.edu.cn
Eyleen L. K. Goh
eyleen.gohlk@ntu.edu.sg

Specialty section:
This article was submitted to Neuropharmacology, a section of the journal Frontiers in Pharmacology

Received: *11 May 2021*
Accepted: *12 July 2021*
Published: *13 August 2021*

Citation:
Liu D, Liang M, Zhu L, Zhou T, Wang Y, Wang R, Wu F, Goh ELK and Chen T (2021) Potential Ago2/miR-3068-5p Cascades in the Nucleus Accumbens Contribute to Methamphetamine-Induced Locomotor Sensitization of Mice. Front. Pharmacol. 12:708034. doi: 10.3389/fphar.2021.708034

Dysregulation of microRNA (miRNA) biogenesis is involved in drug addiction. Argonaute2 (Ago2), a specific splicing protein involved in the generation of miRNA, was found to be dysregulated in the nucleus accumbens (NAc) of methamphetamine (METH)-sensitized mice in our previous study. Here, we determined whether Ago2 in the NAc regulates METH sensitization in mice and identified Ago2-dependent miRNAs involved in this process. We found a gradual reduction in Ago2 expression in the NAc following repeated METH use. METH-induced hyperlocomotor activity in mice was strengthened by knocking down NAc neuronal levels of Ago2 but reduced by overexpressing Ago2 in NAc neurons. Surprisingly, miR-3068-5p was upregulated following overexpression of Ago2 and downregulated by silencing Ago2 in the NAc. Knocking down miR-3068-5p, serving as an Ago2-dependent miRNA, strengthened the METH sensitization responses in mice. These findings demonstrated that dysregulated Ago2 in neurons in the NAc is capable of regulating METH sensitization and suggested a potential role of Ago2-dependent miR-3068-5p in METH sensitization.

Keywords: Ago2, Grin1, locomotor sensitization, methamphetamine, miR-3068-5p

INTRODUCTION

Methamphetamine (METH) is a widely abused psychoanaleptic that induces cognitive impairment or psychotic episodes in mammals (Ikeda et al., 2013; Zhong et al., 2016; Greening et al., 2019) and may cause a large number of serious social criminal issues. METH is a functional dopamine agonist that induces locomotor sensitization by producing dysfunctional mesolimbic dopaminergic systems, including the nucleus accumbens (NAc) (Buchanan et al., 2010; Mizoguchi and Yamada, 2019). Locomotor sensitization, which reflects motivation and psychosis (Chen et al., 2014), heightens the sensitivity of behavioral effects in response to repeated intermittent psychostimulant exposure to the same or lower dose (Robinson and Becker, 1986). This locomotor sensitization in response to METH

is long-lasting, indicating that alterations in molecule and gene expression occur in relevant brain regions, such as the NAc (Nestler and Malenka, 2004; Jayanthi et al., 2014). Sustained effort has been devoted to determining the mechanisms of METH-induced locomotor sensitization (METH sensitization) to find a more precise target to cure METH addiction.

MicroRNAs (miRNAs) are among the multiple factors underlying the dynamic adjustment of gene expression at the posttranscriptional level (Fabian et al., 2010; Störchel et al., 2015). miRNAs represent an important class of noncoding RNAs that can inhibit mRNA translation and accelerate their decay by binding to their 3′-untranslated regions (3′ UTR) (Bartel, 2004). In mammals, the primary transcripts of miRNAs undergo endonucleolytic processing by Drosha/Dgcr8 in the nucleus to generate precursors of miRNAs (pre-miRNAs), which are then exported to the cytoplasm to be spliced into approximately 22-nucleotide (nt) mature miRNAs by Dicer1 (Chendrimada et al., 2005). Then, the miRNAs are loaded into the RNA-induced silencing complex (RISC) by association with the Argonaute2 (Ago2) protein, which is responsible for silencing target mRNAs by mRNA degradation or repressing translation (Chendrimada et al., 2005). miRNAs are capable of regulating neuronal development, spine morphogenesis, and synaptic function (Fabian et al., 2010; Störchel et al., 2015). Thus, it is not surprising that dysregulation of miRNAs and their biogenesis is involved in several neurological and neuropsychiatric diseases, such as ALS and drug addiction (Schaefer et al., 2010; Emde et al., 2015; Störchel et al., 2015). Therefore, miRNAs function in different areas and cell types of the brain as members of physiological and disease states, and they could potentially be used as medicines because of their selectivity and small size, allowing them to penetrate the blood-brain barrier.

The Ago2 protein is essential for miRNA-mediated gene silencing and has endonuclease activity for splicing pre-miRNA to miRNA (Ha and Kim, 2014). Furthermore, the splicing function of Ago2 is selective, and only a fraction of miRNAs can be spliced by Ago2. For example, maturation of miR-451, which is important for erythropoiesis, requires Ago2 but not Dicer1 (Cheloufi et al., 2010). The roles of Ago2 in mouse brain development, neurodegenerative diseases, dendritic spine plasticity, and addiction have been studied (Juvvuna et al., 2012; Garcia-Perez et al., 2013; Pircs et al., 2018; Rajgor et al., 2018; Liu et al., 2019). Ago2 deficiency in dopamine 2 receptor (DRD2)- expressing neurons reduced the motivation for cocaine self-administration in mice by dysregulating miRNAs (Schaefer et al., 2010; Shekar et al., 2011). Overexpression or enhanced activity of Ago2 elicited specific changes in miRNAs and mRNAs and showed a strong relationship with high-risk myeloma (Zhou et al., 2010; Hagiwara et al., 2012; Zhang et al., 2013). In our previous study, we found a set of downregulated miRNAs and decreased levels of Ago2 in response to METH (Liu et al., 2019). Therefore, a better understanding of how Ago2 regulates METH sensitization and identifying Ago-dependent miRNAs in METH sensitization would provide new insights into METH addiction.

Here, we found that Ago2 was downregulated progressively in the NAc of mice following METH administration. Adeno-associated virus (AAV)-mediated neuron-specific overexpression of Ago2 (AAV-SYN-Ago2) in the NAc attenuated METH sensitization (20%), while knocking down the NAc neuronal levels of Ago2 (AAV-SYN-shAgo2) enhanced the effect of METH. We further identified an Ago2-dependent miRNA, miR-3068-5p, that was upregulated or downregulated when Ago2 was overexpressed or knocked down in the NAc, respectively. Consistent with this, AAV-mediated neuron-specific knockdown of miR-3068-5p also enhanced METH sensitization and caused induction of *Grin1*, an N-methyl-D-aspartate receptor (NMDAR) subunit that plays a role in the plasticity of synapses (Chiu et al., 2018). Our results demonstrated that neuron-specific expression of Ago2 in the NAc plays a role in regulating METH sensitization. We further identified Ago2-dependent miR-3068-5p as part of a potential mechanistic cascade regulating METH sensitization.

MATERIALS AND METHODS

Animals

Eight-to-ten-week-old wild-type C57BL/6J mice (Beijing Vital River Laboratory Animal Technology, Beijing, China) weighing 25–30 g were used in this research. Mice were housed four per cage in a temperature-controlled (21–25°C) and humidity-controlled (40–60%) room with a 12 h light/dark cycle (lights on from 7:00 to 19:00) and ad libitum access to chow and water. All behavioral tests were conducted during the light cycle. Mice were habituated to these housing conditions for 7 days and handled daily before starting the experiments. Animal procedures were conducted in accordance with the United Kingdom Animals (Scientific Procedures) Act and Institutional Animal Care Committee at Xi'an Jiaotong University.

Drugs

METH hydrochloride (National Institute for the Control of Pharmaceutical and Biological Products, Beijing, China) was dissolved in 0.9% physiological saline to a concentration of 0.2 mg/ml for injections. The dose of METH used here was 2 mg/kg, which was injected intraperitoneally (i.p.) at a volume of 10 ml/kg.

Adeno-Associated Virus

Neural AAV expressing synapsin-1 (SYN) specific promoters was supplied by OBiO Technology (Shanghai, China). AAV-SYN-Ago2 was used to mediate overexpression of Ago2 (NM_153178); AAV-SYN-shAgo2 was used to mediate shRNA expression to interfere with Ago2; AAV-SYN-spmiR-3068-5p was used to mediate "miRNA sponge" expression to inhibit miR-3068-5p; AAV-SYN-spmiR-30a-5p was used to mediate "miRNA sponge" expression to inhibit miR-30a-5p. The final preparation was titrated by quantitative real-time PCR (qPCR), and all titers of the viral vector were over 2.5E+12 vg/ml. AAV was expressed for 4 weeks, and a behavioral test was performed.

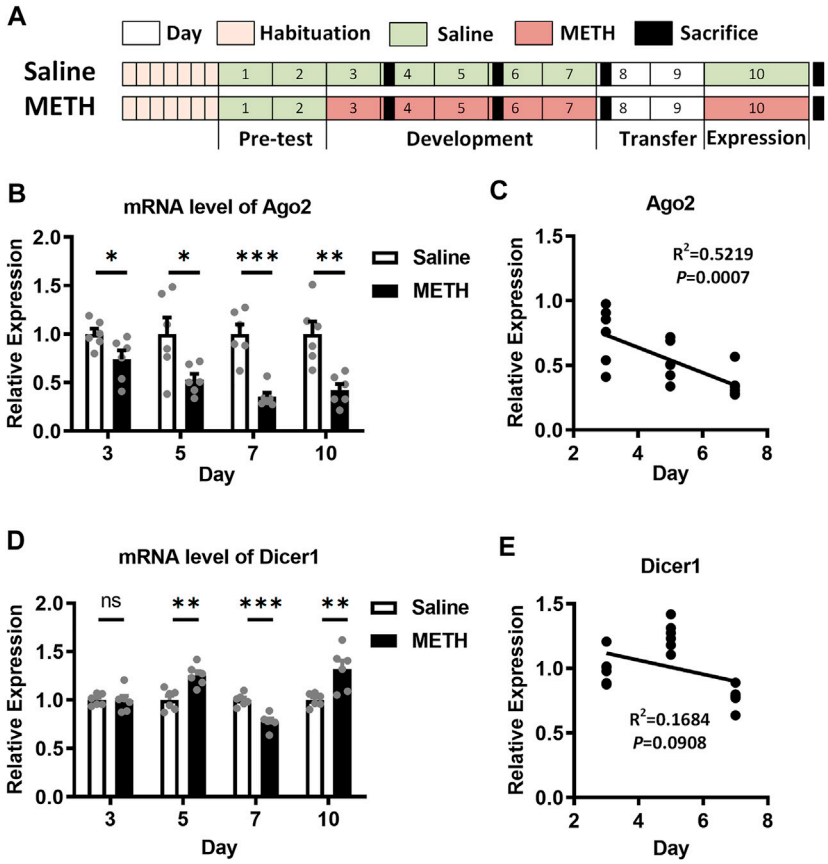

FIGURE 1 | Expression of Ago2 and Dicer1 in the NAc of METH-sensitized mice. **(A)** Illustrations showing the schedule and procedure of the METH sensitization model. **(B)** Differential expression of Ago2 mRNA in the NAc of mice in response to METH. **(C)** Pearson's correlation analyses between Ago2 expression and days in the development phase of METH sensitization. **(D)** Differential expression of Dicer1 mRNA in the NAc of mice in response to METH. **(E)** Pearson's correlation analyses between Dicer1 expression and days in the development phase of METH sensitization. Student's *t*-test: $^{*}p < 0.05$, $^{**}p < 0.01$, and $^{***}p < 0.001$ compared with the saline group. The data are presented as the mean ± SEM, $n = 6$. NAc, nucleus accumbens; METH sensitization, METH-induced locomotor sensitization.

Stereotaxic Surgery

Mice were anesthetized using isoflurane and positioned onto a stereotaxic apparatus (RWD, Shenzhen, China). AAVs were injected bilaterally into the NAc (0.4–0.6 μl per side, 0.2 μl/min, AP: +0.16 cm from bregma, ML: ± 0.26 cm from the midline, and DV: −0.48 cm from the skull at 20° angle) (Franklin and Paxinos, 2001; Aguilar-Valles et al., 2014) with a Hamilton microsyringe (Hamilton 1700 series, Nevada, United States) and an automated injection pump (RWD, Shenzhen, China). After the infusion was completed, the microsyringe was left in place for 6 min to allow for diffusion of AAV complexes. Mice were housed with free access to food and water and given standard care. Four weeks after AAV microinjection, the targeted sites were verified by examining GFP *via* fluorescence microscopy (Leica DM3000, Oskar, Germany), and the up- or downregulation of each molecule was detected by qPCR or Western blot (WB).

Locomotor Activity Test

METH-induced locomotor sensitization was quantified using an open-field (OF) test (**Figure 1A** (Liu et al., 2019)). After 7 days of habituation, the experiments were initiated with 2 days of saline injection (days 1–2, pretest). Mice were then randomly allocated into the saline or METH treatment groups. The METH or saline group was treated with METH or saline for 5 consecutive days (day 3–7, the development phase). Subsequently, the same doses of the METH or saline challenge injections (day 10, the expression phase) were given after an injection-free interval of 2 days (days 8–9, the transfer phase). Horizontal locomotor activities were recorded in metal test chambers (43 cm × 43 cm × 43 cm) and analyzed for 60 min after injection using a smart video tracking system (version 2.5; PanLab Technology for Bioresearch, Barcelona, Spain).

Tissue Preparation

Mice were sacrificed 24 h after the last injection, and their brains were rapidly removed. The NAc (+ 1.70 mm from bregma (Franklin and Paxinos, 2001), including the core and shell, was identified based on structure and landmarks under a dissecting microscope and was separated bilaterally. The whole NAc was then immediately frozen in liquid nitrogen.

TABLE 1 | qPCR primers.

Gene	Forward (5′-3′)	Reverse (5′-3′)
Gapdh	TGTGTCCGTCGTGGATCTGA	TTGCTGTTGAAGTCGCAGGAG
Dicer1	GAATTGCTCGAGATGGAACCAGA	AGCTCCGGCCAACACCTTTA
Ago2	ACATTCCCGCAGGCACAA	GTCATCCCAAAGCACGTGGTAG
Grin1	GGCTGACTACCCGAATGTCCA	TGTAGACGCGCATCATCTCAAAC
Gabbr1	ACGTCACCTCGGAAGGTTG	CACAGGCAGGAAATTGATGGC
Msfd2a	AACAAGCTTTGCTATGCAGTTGGAG	GCTAATGCAGAAGCCCACCAG
Agt	GGGTCAGTACAGACAGCACCCTA	CGGAGATCATGGGCACAGAC
App	TTCTGGGCTGACAAACATCAAGAC	GGTGATGACAATCACGGTTGCTA

For RNA extraction, total RNA was isolated by the miRNeasy Mini Kit (217004, Qiagen, United States). The RNA concentration and quality were determined with a NanoDrop spectrophotometer (Thermo Scientific, United States). For miRNA reverse transcription, 380 ng of total RNA per sample was reverse-transcribed to 10 μl of cDNA with the Mir-X™ miRNA First-Strand Synthesis Kit (Takara Biomedical Technology, Beijing, China) at 37°C for 60 min and 85°C for 5 s. cDNA samples were stored at −80°C for further use. For mRNA, 500 ng of total RNA was reverse-transcribed into 10 μl of cDNA with Prime Script ™ RT Master Mix (Takara Biomedical Technology, Beijing, China) by incubating at 37°C for 15 min, 85°C for 5 s, and 4°C for 5 min.

For protein extraction, NAc tissues were homogenized in RIPA (HEART WB009, Xi'an, China) lysis buffer with proteinase and a phosphatase inhibitor (Roche, Shanghai, China). After 60 min of incubation on ice, the homogenates were centrifuged at 12,000 ×g for 5 min at 4°C. The supernatants were collected, and the protein concentrations were measured using the Bradford BCA protein assay (Applygen Technologies Inc. P1511, Beijing, China). Protein homogenates were stored at −80°C for further use.

Quantitative Real-Time Reverse Transcription PCR

qPCR for miRNA detection was performed with SYBR Premix Ex Taq II (Takara Biomedical Technology, Beijing) using a Bio-Rad iQ5 detection instrument (Bio-Rad, United States) under the following conditions: 95°C for 30 s, followed by 40 cycles of 95°C for 10 s and 62°C for 60 s. *U6* snRNA was used as an endogenous control for detecting miRNAs, and *Gapdh* was the endogenous control for measuring protein-coding gene expression. The relative expression levels were determined using the $2^{-\triangle\triangle Ct}$ method (Schmittgen and Livak, 2008). miRNAs were then ligated to 3′ adaptors and reverse-transcribed to cDNAs in step extraction. A uni-miR qPCR primer (Takara Biomedical Technology, Beijing) was used as the reverse primer, and the mature miRNA sequences were used as forward primers. The sequences of the primer pairs for protein-coding genes are shown in **Table 1**.

Western Blot

Protein homogenates were prepared with 5× protein loading buffer (HEART R0891, Xi'an, China) and denatured at 95°C for 5 min. Fifteen micrograms of protein per sample was resolved on a precast 10% (w/v) SDS-PAGE gel and transferred onto a polyvinylidene fluoride (PVDF) membrane (Millipore IPVH00010, Bedford, MA, United States). Blots were blocked with 5% (w/v) nonfat milk solution (in Tris-buffered saline with 0.1% Tween-20 (TBST)) and then incubated overnight at 4°C in primary antibody solutions (Anti-Ago2, Abcam, ab186733, diluted 1:2000). Membranes were then washed with TBST and probed with the appropriate horseradish peroxidase-conjugated secondary antibodies (1:2000) for 1 h at room temperature. Membranes were visualized using an enhanced chemiluminescence detection kit (Solarbio PE0010, Beijing, China) and quantified with ImageLab 1.46 (BioRad, United States).

Ingenuity Pathway Analysis Bioinformatics Analysis

Ingenuity Pathway Analysis (IPA) software (version 2019 summer) (Ingenuity Systems, Redwood City, CA, United States; apps.ingenuity.com) was used to characterize the molecular function and regulatory mechanism together with the differentially expressed mRNAs that were identified previously by Zhu et al. with miR-3068-5p target genes predicted by TargetScan (http://www.targetscan.org/vert_71/). Annotation of biological diseases and functions and identification of interaction networks were conducted.

Dual-Luciferase Reporter Assay

The 3′UTR of *Grin1* (*Grin1* 3′UTR (Wt)) was cloned into the pMIR vector with the firefly luciferase coding region (OBiO Technology, Shanghai, China). The *Grin1* 3′UTR (Mu) was derived from the *Grin1* 3′UTR (Wt) by mutating the miR-3068-5p seed site. 293T cells were inoculated into 96-well plates. The luciferase reporter vector DNA and mimic-miR-3068-5p (OBiO Technology, Shanghai, China) were cotransfected into 293T cells. The relative luciferase activity of 293T cells was assayed by the Dual-Luciferase® Reporter Assay (Spark 10M, TECAN). pRL-CMV containing Renilla luciferase was cotransfected with the 3′UTR of *Grin1* for data normalization, and the data are expressed as Luc/R-luc.

Statistical Analysis

Statistical analyses were performed using SPSS 18.0 or Prism 6. For the OF test, mixed-measures ANOVA and then multiple

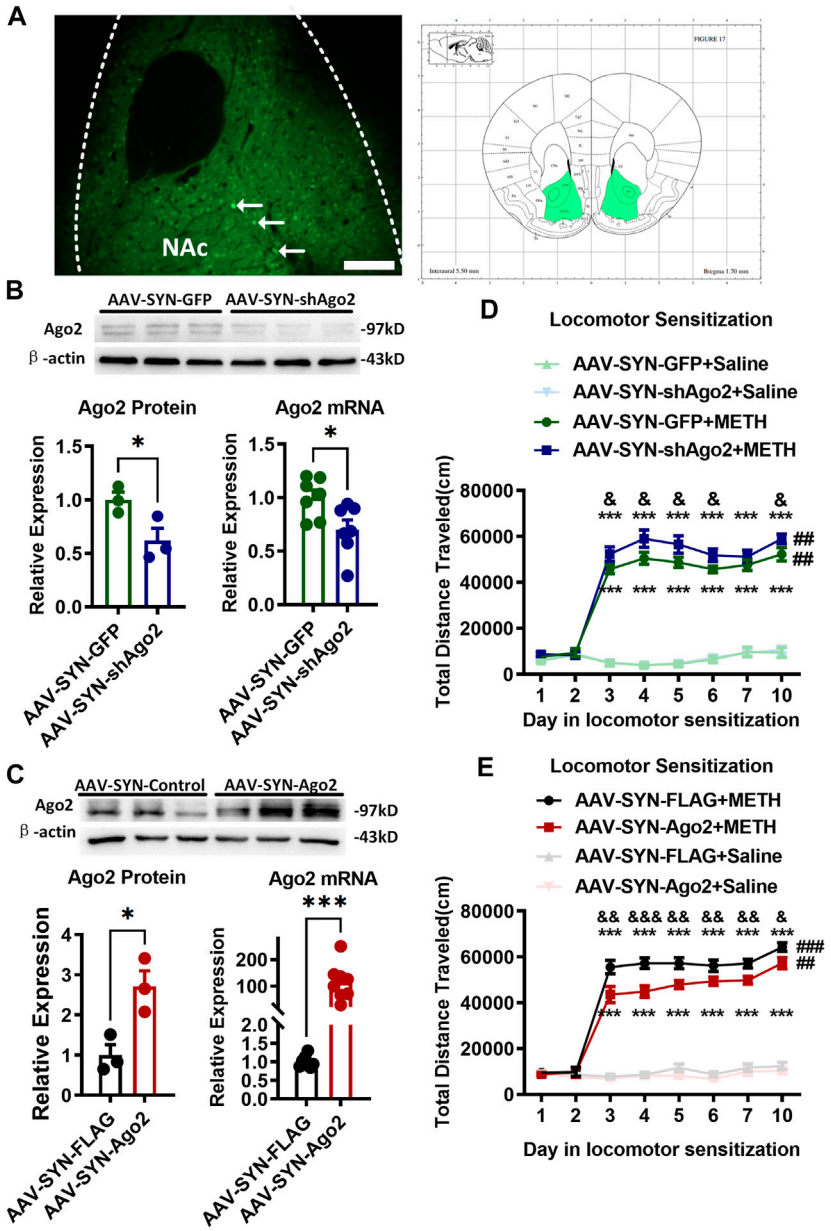

FIGURE 2 | Regulation of Ago2 in NAc neurons affected METH sensitization. **(A)** Fluorescence image showing the location of AAV expression and bilateral NAc (Franklin and Paxinos, 2001) of mouse neurons (arrows). Scale bar, 100 μm. **(B)** Injection of AAV-SYN-shAgo2 into the NAc of mice effectively reduced Ago2 protein and mRNA levels. **(C)** Injection of AAV-SYN-Ago2 into the NAc of mice increased Ago2 protein and mRNA levels. Student's *t*-test showed ***$p < 0.001$ compared to the virus control group. The data are presented as the mean ± SEM, $n = 3$–7. **(D)** Ago2 downregulation in NAc neurons enhanced METH sensitization. **(E)** Ago2 overexpression in NAc neurons attenuated METH sensitization. Mixed-measures ANOVA showed the following: *$p < 0.05$, ***$p < 0.001$, vs. the corresponding saline groups; &$p < 0.05$, &&$p < 0.01$, vs. AAV-SYN-GFP+METH or AAV-SYN-FLAG+METH; ##$p < 0.01$, compared to the locomotor activities recorded on day 3 within the same group. The data were presented as the mean ± SEM, $n = 8$–12. NAc, nucleus accumbens; METH sensitization, METH-induced locomotor sensitization.

comparisons tests were performed to determine significance for the 8 days of the OF test, with days as the within-subject variable and treatments (AAV and METH) as the between-subject factor. qPCR data were standardized by the $2^{-\triangle\triangle Ct}$ method with *Gapdh/U6*, and Student's *t*-test or two-way ANOVA (Tukey's multiple comparisons test) was used to analyze the expression changes. For Western blots, data normalized to β-actin were analyzed by Student's *t*-test. The data are expressed as mean ± SEM. *p*-values < 0.05 were defined as significant.

RESULTS

Progressive Downregulation of Argonaute2 in Response to Methamphetamine

In our previous study, both the Ago2 mRNA and protein were found to be downregulated in the NAc of METH-sensitized mice (Liu et al., 2019). To further investigate the role of Ago2 in METH sensitization, we measured Ago2 mRNA expression in the NAc of mice during the development and expression phases of METH sensitization. Ago2 in METH-treated mice showed progressively downregulated expression, where 26% ($t_{(10)} = 2.427$, $^{*}p < 0.05$), 47% ($t_{(10)} = 2.587$, $^{*}p < 0.05$), 65% ($t_{(10)} = 5.900$, $^{***}p < 0.001$), and 58% ($t_{(10)} = 4.054$, $^{**}p < 0.01$) decreases relative to the control were detected 24 h after injection at days 3, 5, 7, and 10 (**Figure 1B**). Furthermore, the mRNA level of Ago2 was significantly negatively correlated ($F_{(1, 16)} = 17.46$, $^{*}p < 0.05$) with the day of the development phase of METH sensitization (**Figure 1C**). Another miRNA biogenesis enzyme, Dicer1, also showed stochastic changes during the timeline of our model (**Figure 1D**). However, there was no correlation ($F_{(1, 16)} = 3.239$, $p > 0.05$) between the mRNA level of Dicer1 and the development phase of METH sensitization (**Figure 1E**).

Methamphetamine Sensitization Can Be Regulated by Argonaute2 in Nucleus Accumbens Neurons

Next, we elucidated whether dysregulation of Ago2 could modulate METH sensitization in mice. Neural-specific AAVs were constructed to over express (AAV-SYN-Ago2) or knockdown (AAV-SYN-shAgo2) Ago2 in neurons and were bilaterally microinjected into the NAc. Neural-specific GFP expression detected in the NAc indicated localized microinjection sites (**Figure 2A**). The expression of Ago2 in NAc neurons was detected to verify efficient overexpression or downregulation upon microinjection of the respective AAV constructs. The levels of the Ago2 protein ($t_{(4)} = 2.786$, $^{*}p < 0.05$) and mRNA ($t_{(12)} = 2.637$, $^{*}p < 0.05$) were significantly lower in the NAc of AAV-SYN-shAgo2 mice than in those of AAV-SYN-GFP mice (**Figure 2B**). Mice microinjected with AAV-SYN-Ago2 showed significant overexpression of the Ago2 protein ($t_{(4)} = 3.675$, $^{*}p < 0.05$) and mRNA ($t_{(14)} = 4.799$, $^{***}p < 0.001$) in the NAc (**Figure 2C**).

After Ago2 knockdown (**Figure 2D**), all mice showed no significant differences in locomotor activities during the pretest (days 1–2). Mixed-measures ANOVA by Bonferroni's *post hoc* tests revealed the main effects of AAV ($F_{(1,28)} = 4.101$, $p = 0.052$), METH ($F_{(1,28)} = 681.223$, $p < 0.001$) and day ($F_{(7,22)} = 106.364$, $p < 0.001$) and the interactions of AAV ×day ($F_{(7,22)} = 1.603$, $p = 0.187$), METH ×day ($F_{(7,22)} = 99.744$, $p < 0.001$) and AAV ×METH ×day ($F_{(7,22)} = 0.592$, $p = 0.756$) following Ago2 knockdown. The locomotor sensitization test showed that METH still induced a strong increase in locomotion when METH-treated groups and their corresponding saline-treated groups were compared, regardless of Ago2 knockdown (**Figure 2D** $F_{(1, 28)} = 681.233$, $^{***}p < 0.001$). Significant METH sensitization was also observed on the challenge day (day 10) compared to day 3 in the same group ($^{\#\#}p < 0.01$). There was no difference between day 7 and day 3 ($p = 0.176$) or day 5 ($p = 0.659$) in the development phase of the AAV-SYN-GFP+METH group. The AAV-SYN-shAgo2+METH group displayed higher locomotor activity than that in the AAV-SYN-GFP+METH group from day 3 to day 6 ($F_{(1, 28)} = 5.793$, $\&p < 0.05$) and even at day 10 ($F_{(1, 28)} = 4.578$, $\&p < 0.05$). There was no significant difference between the AAV-SYN-shAgo2+Saline and AAV-SYN-GFP +Saline groups (day 10, $p = 0.689$).

When Ago2 was overexpressed (**Figure 2E**), mixed-measures ANOVA by Bonferroni's *post hoc* tests revealed the effects of AAV ($F_{(1,44)} = 11.054$, $p < 0.01$), METH ($F_{(1,44)} = 693.148$, $p < 0.001$), and day ($F_{(7,38)} = 129.799$, $p < 0.001$), as well as the interactions of AAV ×day ($F_{(7,38)} = 2.247$, $p = 0.051$), METH ×day ($F_{(7,38)} = 119.364$, $p < 0.001$) and AAV ×METH ×day ($F_{(7,38)} = 1.929$, $p = 0.092$). The locomotor sensitization test showed that METH induced a strong increase in locomotion when the METH-treated groups and their corresponding saline-treated groups were compared, regardless of Ago2 overexpression ($F_{(1, 44)} = 693.148$, $^{***}p < 0.001$). Significant METH sensitization was also observed on the challenge day (day 10) compared to day 3 in the same group ($^{\#\#\#}p < 0.001$). There was no difference between day 7 and day 3 ($p = 0.129$) or day 5 ($p = 0.974$) in the development phase of the AAV-SYN-FLAG+METH group. As expected, locomotion performed by the mice in AAV-SYN-AGO2+METH group was significantly decreased on each METH injection day (day 3, $F_{(1, 44)} = 12.886$, $\&\&p < 0.01$) compared to that in the AAV-SYN-FLAG+METH group (**Figure 2E**). There was also no significant difference between the AAV-SYN-Ago2+Saline and AAV-SYN-FLAG + Saline groups (day 10, $p = 0.414$).

miR-3068-5p Is an Argonaute2-Dependent miRNA in the Nucleus Accumbens and Can Disrupt Methamphetamine Sensitization

Considering the miRNA biogenesis role of Ago2, we further verified the Ago2-dependent miRNAs and whether these miRNAs regulated METH sensitization. We detected miRNA expression in the NAc when Ago2 was overexpressed or silenced. Ago2-dependent miRNAs (Schaefer et al., 2010) and miRNAs that were downregulated upon METH treatment (Liu et al., 2019) were selected and verified by qPCR. Interestingly, miR-3068-5p ($t_{(14)} = 3.755$, $^{**}p < 0.01$) and miR-30a-5p ($t_{(14)} = 2.253$, $^{*}p < 0.05$) were found to be enriched by neuronal Ago2 overexpression in the NAc of mice (**Figure 3A**). However, we found that three miRNAs (miR-124-3p, miR-33-5p, and miR-376a-3p) were downregulated and 18 miRNAs were unchanged following neuronal Ago2 overexpression (**Figure 3C**). Surprisingly, miR-3068-5p was the only significantly depleted miRNA ($t_{(14)} = 3.117$, $^{**}p < 0.01$) in the NAc following neuronal Ago2 knockdown (**Figure 3B**). miR-33-5p ($t_{(14)} = 3.894$, $^{**}p < 0.01$) and miR-376a-3p ($t_{(14)} = 2.203$, $^{*}p < 0.05$) were upregulated in the AAV-SYN-shAgo2 group (**Figure 3B**), and miR-124-3p and miR-30a-5p were unchanged between the AAV-SYN-GFP and AAV-SYN-shAgo2 groups (**Figure 3B**). These results indicated that miR-3068-5p may be an Ago2-dependent miRNA in neurons in the NAc.

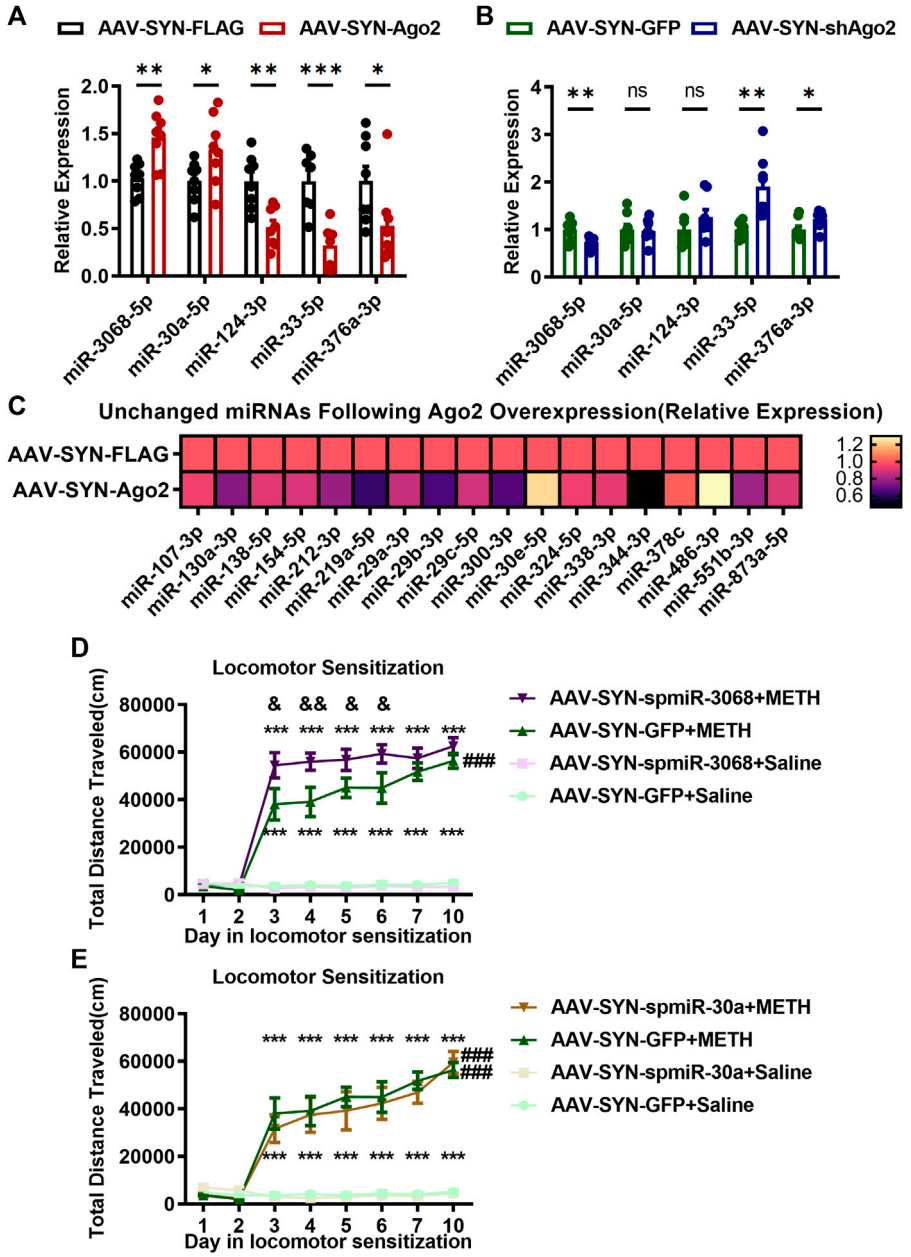

FIGURE 3 | miR-3068-5p was found to be an Ago2-dependent miRNA in the NAc of mice **(A, C)**. Changes in miRNA expression following Ago2 overexpression in the NAc of mice. Student's *t*-test: *$p < 0.05$, **$p < 0.01$, and ***$p < 0.001$ compared with the AAV-SYN-FLAG group. The data are presented as the mean ± SEM, $n = 8$. **(B)** Changes in miRNA expression in the NAc of mice in the AAV-SYN-shAgo2 group. Student's *t*-test: *$p < 0.05$ and **$p < 0.01$ compared with the AAV-SYN-GFP group. Data are presented as the mean ± SEM, $n = 8$. **(D)** miR-3068-5p interference in NAc neurons strengthens METH sensitization. **(E)** No change in METH sensitization after miR-30a-5p interference in NAc neurons. Mixed-measures ANOVA: ***$p < 0.001$, vs. the corresponding saline groups; &$p < 0.05$, &&$p < 0.01$, AAV-SYN-spmiR-3068-5p+METH vs. AAV-SYN-GFP+METH; ###$p < 0.001$, compared to the locomotor activities recorded on day 3 within the same group. The data are presented as the mean ± SEM, $n = 8$. NAc, nucleus accumbens; METH sensitization, METH-induced locomotor sensitization.

Therefore, we investigated whether miR-3068-5p also contributes to METH sensitization by intervening with the expression of miR-3068-5p in NAc neurons. A neuron-specific AAV-mediated sponge sequence expression vector for miR-3068-5p (AAV-SYN-spmiR-3068-5p) and the corresponding control vector AAV-SYN-GFP were constructed and microinjected bilaterally into the NAc. The locomotion of mice in response to METH was measured (**Figure 3D**). Mixed-measures ANOVA by Bonferroni's *post hoc* tests revealed the effects of AAV ($F_{(1,28)} = 4.218$, $p < 0.05$), METH ($F_{(1,28)} = 291.487$, $p < 0.001$), and day

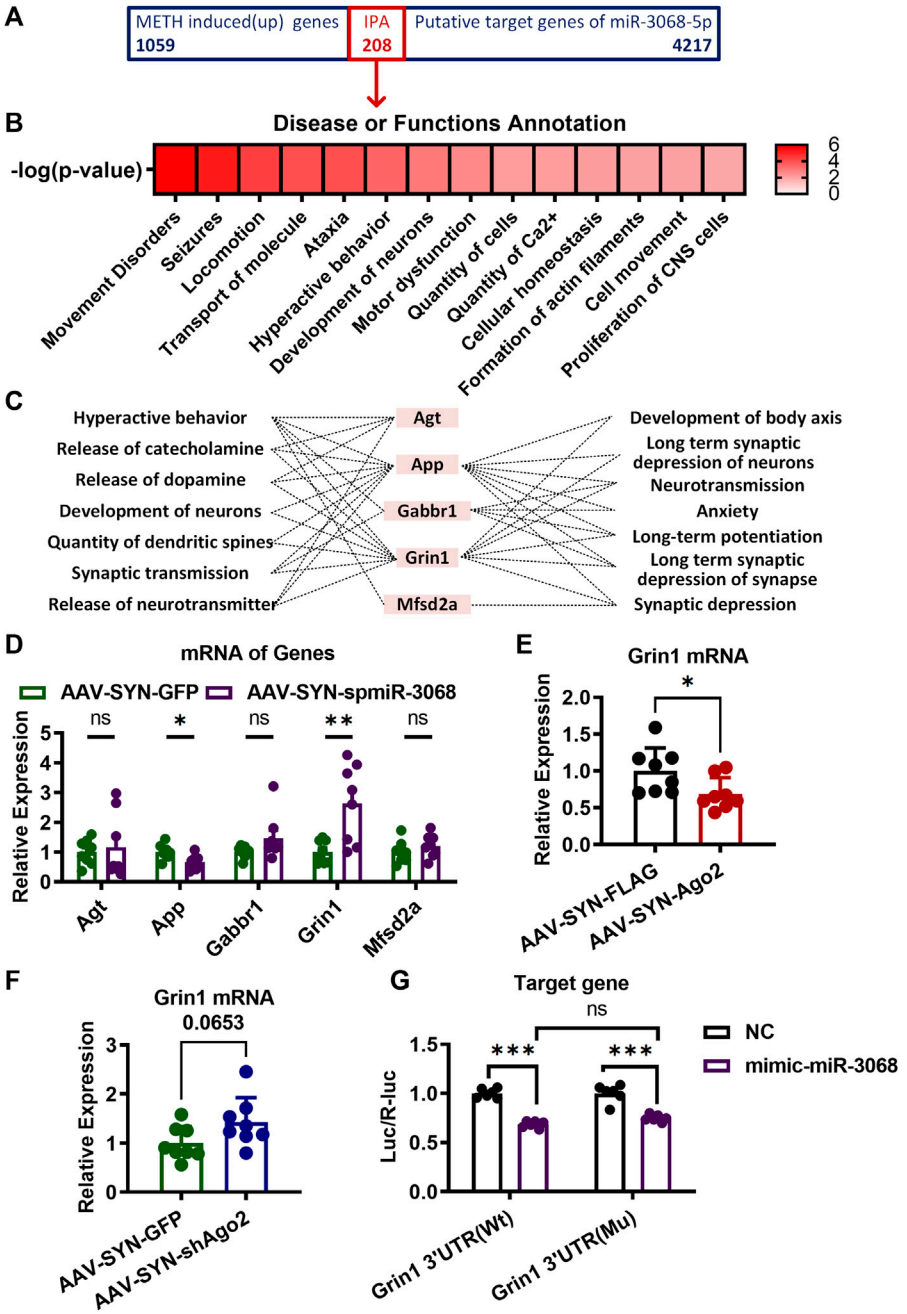

FIGURE 4 | Target genes of miR-3068-5p in NAc of mice involving in METH sensitization. **(A)** A total of 208 overlapping genes between the METH-induced genes in our previous study (https://www.ebi.ac.uk/arrayexpress/, E-MTAB-2843) and the predicted target genes of miR-3068-5p were identified and subjected to IPA analysis. **(B)** Identification of the main neurological dysfunctions of the 208 genes identified from **(A)**. **(C)** IPA analysis identified five overlapping genes from **(A)** relevant to hyperactive behavior, release of catecholamine, release of dopamine, development of neurons, quantity of dendritic spines, synaptic transmission, release of neurotransmitters, development of the body axis, long-term synaptic depression of neurons, neurotransmission, anxiety, long-term potentiation, long-term synaptic depression of synapses, and synaptic depression. **(D)** mRNA expression of the five predicted target genes of miR-3068-5p relevant to locomotion following miR-3068-5p sponging in the NAc of METH-sensitized mice. **(E, F)** Graphs show the expression of *Grin1* mRNA upon overexpression **(E)** or knockdown **(F)** of Ago2. Student's *t*-test: $^{*}p < 0.05$ and $^{**}p < 0.01$ compared to the AAV control group. The data are presented as the mean ± SEM, $n = 6–8$. **(G)** Graphs showing the dual-luciferase activities upon transfection of *Grin1* Wt or mutant (Mu) expression conducted alone (NC) or by cotransfection with mimic-miR-3068-5p. Two-way ANOVA: $^{***}p < 0.001$ compared to the corresponding NC group. The data are presented as the mean ± SEM, $n = 6$. NAc, nucleus accumbens; METH sensitization, METH-induced locomotor sensitization; IPA, Ingenuity Pathway Analysis.

($F_{(7,22)}$ = 73.642, $p < 0.001$), as well as the interactions of AAV ×day ($F_{(7,22)}$ = 3.663, $p < 0.01$), METH ×day ($F_{(7,22)}$ = 75.459, $p < 0.001$), and AAV ×METH ×day ($F_{(7,22)}$ = 1.756, $p = 0.147$). METH still induced a strong increase in locomotion when the METH-treated groups and their corresponding saline-treated groups were compared, regardless of miR-3068-5p inhibition. There was a difference between day 7 and day 3 ($p = 0.472$) or day 5 ($p = 0.767$) in the development phase of the AAV-SYN-spmiR-3068 + METH group, while in the AAV-SYN-GFP+METH group, increased locomotor activity was observed on day 7 compared to day 3 ($p < 0.01$) and day 5 ($p < 0.01$). Significant METH sensitization was observed on the challenge day (day 10) compared to day 3 in the AAV-SYN-GFP group (###$p < 0.001$).

However, miR-3068-5p inhibited METH sensitization on day 10, as observed when day 10 and day 3 in the AAV-SYN-spmiR-3068-5p +METH group were compared (**Figure 3D**, $p = 0.065$). Interestingly, the AAV-SYN-spmiR-3068-5p +METH group exhibited significant hyperlocomotor activity from day 3 ($F_{(1, 28)}$ = 7.501, &$p < 0.05$) to day 6 ($F_{(1, 28)}$ = 7.141, &$p < 0.05$) compared with the AAV-SYN-GFP +METH group. We also investigated whether miR-30a-5p plays a role in METH sensitization. However, intervening with AAV-SYN-spmiR-30a-5p expression did not change METH sensitization in mice (**Figure 3E**).

miR-3068-5p Regulated Methamphetamine Sensitization by Targeting *Grin1*

Considering the downregulation of miR-3068-5p in response to METH in our previous study (Liu et al., 2019), we speculated that the potential target genes of miR-3068-5p would be upregulated in response to METH. Therefore, comparisons were made between the predicted targets of miR-3068-5p and mRNAs that were upregulated in the NAc of METH-treated mice in our previous study (https://www.ebi.ac.uk/arrayexpress/, E-MTAB-2843), and 208 transcripts were identified as METH-responsive putative targets for miR-3068-5p. These potential targets were further analyzed by IPA to verify their functional characteristics (**Figure 4A**). Disease and functional annotations classified these targets into several functions, such as hyperactive behavior, release of catecholamine, release of dopamine, development of neurons, quantity of dendritic spines, synaptic transmission, release of neurotransmitters, development of the body axis, long-term synaptic depression of neurons, neurotransmission, anxiety, long-term potentiation, long-term synaptic depression of synapses, and synaptic depression (**Figure 4B**). Five genes (*Agt, App, Gabbr1, Grin1*, and *Mfsd2a*) were found to be significantly enriched in pathways involved in the regulation of synaptic plasticity, morphology, and development (**Figure 4C**). We measured the relative expression of *Agt, App, Gabbr1, Grin1*, and *Mfsd2a* in the NAc of AAV-SYN-spmiR-3068-5p mice but did not detect any changes in the expression of *Agt*, *Gabbr1*, or *Mfsd2a* (**Figure 4D**). Moreover, a significant reduction in *App* was observed in the NAc of mice with AAV-SYN-spmiR-3068-5p microinjection. Only *Grin1* showed significant upregulation ($t_{(14)}$ = 3.408, **$p < 0.01$) when the expression of miR-3068-5p was disrupted by AAV-SYN-spmiR-3068-5p. We further found that *Grin1* was downregulated ($t_{(14)}$ = 2.306, *$p < 0.05$) in the NAc when Ago2 was overexpressed (**Figure 4E**) and showed an upregulation trend ($t_{(14)}$ = 1.999, $p = 0.065$, **Figure 4F**) in the NAc when Ago2 expression was disrupted (**Figure 4F**). As such, we used a Dual-Luciferase Reporter assay to further verify whether miR-3068-5p could target *Grin1* expression. As shown in **Figure 4G**, cotransfection of the *Grin1* 3′UTR (Wt) and mimic-miR-3068-5p resulted in a significant decrease ($t_{(1, 20)}$ = 9.632, ***$p < 0.001$) in the ratio of the dual-luciferase activities in 293T cells, indicating that miR-3068-5p could indeed inhibit *Grin1* expression. However, this decreased ratio of the dual-luciferase activities in cells was not rescued with *Grin1* 3′UTR (Mu) and mimic-miR-3068-5p cotransfection. The *Grin1* 3′UTR (Mu) alone showed a comparable ratio of the dual-luciferase activities as the *Grin1* 3′UTR (Wt). These data suggest the presence of other atypical binding sites of miR-3068-5p on *Grin1* or other mechanisms in addition to direct targeting of the expression of *Grin1*.

DISCUSSION

Argonaute2 in the Nucleus Accumbens Is Important for the Development of Methamphetamine Addiction

Here, we found that Ago2 was progressively downregulated in the NAc of mice during METH sensitization development. We further identified that overexpressing or silencing neural Ago2 could attenuate or enhance METH sensitization, respectively, and especially affect locomotion after the first injection of METH, indicating that Ago2 can regulate the acute response to METH. Evidence has shown that Ago2 is involved in the regulation of neural plasticity. It was reported that Ago2 overexpression can rescue the loss of miRNA activity and decrease dendrite complexity (Störchel et al., 2015). In addition, Ago2 was also found to be involved in changes in NMDAR-modulated dendritic spine morphology (Rajgor et al., 2018). Neddens found that acute METH injection into reared gerbils restrained the development of adult dopamine fiber density in the NAc (Neddens et al., 2002). In our previous study, repeated METH injections led to an increase in synaptic density on medium spiny neurons (MSNs) in the NAc (Zhu et al., 2012). Here, we found repeated METH treatment significantly downregulated Ago2 expression in the NAc of mice and METH-induced sensitization was attenuated when Ago2 was overexpressed in NAc neurons. It is reasonable to assume that Ago2 overexpression attenuated METH sensitization through decreasing synaptic density in the NAc. Thus, further studies are warranted to address whether Ago2 modulates METH addiction by regulating neural transmission in the NAc.

METH is a psychostimulant that induces a hyperlocomotion response by persistently activating dopaminergic transmission in the NAc (Lominac et al., 2014). Kelly et al. (2008) have reported a significant reduction in METH locomotor sensitization of the amplitude and duration in DRD2-deficient mice, regardless of whether they received METH for the first time or after several prior exposures. In addition,

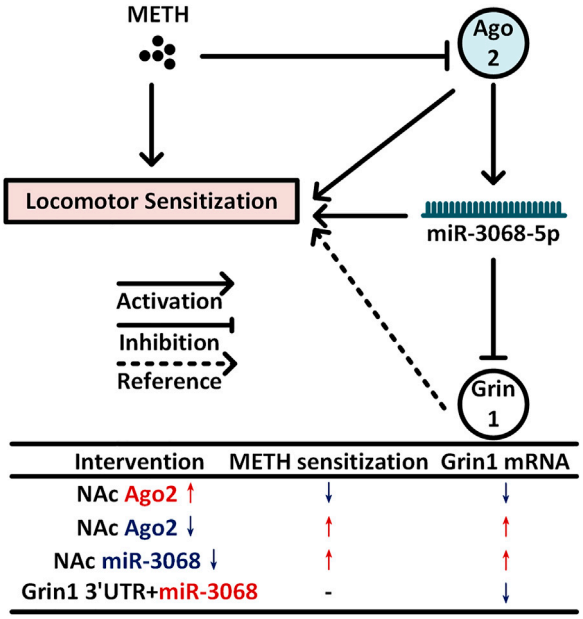

FIGURE 5 | Model for NAc neural Ago2/miR-3068-5p cascades in regulating METH sensitization. METH induces progressive downregulation of Ago2 in the NAc. Downregulation of Ago2 may cause a significant decrease in miR-3068-5p in the NAc and then contribute to METH sensitization. *Grin1*, encoding a critical subunit of NMDAR (Beutler et al., 2011), is a potential downstream gene of miR-3068-5p and may be involved in these effects.

Schaefer et al. found that deficiency of Ago2 in DRD2-expressing neurons can result in the downregulation of a subset of miRNAs that may be involved in cocaine motivation (Schaefer et al., 2010). Based on these studies, we speculated that Ago2 expressed in the NAc may be a downstream molecule of DRD2 in response to METH. Since dopamine DRD1- and DRD2-expressing MSNs are the main NAc neurons and play essential roles in drug reward (Lobo et al., 2010) and given that we verified the function of Ago2 expressed in neurons of the NAc in general without separating different dopamine receptor-expressing neurons, the behavioral phenotype that we observed in our study could be a net effect modulated by both types of neurons. Nevertheless, the observed role of Ago2 in cocaine addiction and METH sensitization indicated that Ago2 may play an important role in regulating drug addiction with a neural type-specific pattern.

miR-3068-5p Could Be a Neural Argonaute2-Dependent Reduced by Methamphetamine (NADRM) miRNA in the Nucleus Accumbens of Mice

Although Dicer1 cleaves miRNA from its precursor to mature form (Knight and Bass, 2001), Ago2 was also found to play a slicer endonuclease role, deficiency of which impaired miRNA biogenesis from precursors to miRNAs and caused a reduction in the expression of miRNAs, such as miR-451 (Cheloufi et al., 2010; Yang et al., 2010). Overexpression or enhanced activity of Ago2 elicited specific changes in miRNAs and mRNAs and had a strong relationship with high-risk myeloma (Zhou et al., 2010; Hagiwara et al., 2012; Zhang et al., 2013). In our previous study (Liu et al., 2019), we found that several METH-reduced miRNAs may be Ago2-dependent. Thus, we determined whether any Ago2-dependent miRNA regulates METH sensitization. Interestingly, we found increased and decreased expression of miR-3068-5p upon overexpression and knockdown of Ago2 in NAc neurons, respectively. miR-3068-5p was one of the potential Ago2-dependent miRNAs found in our previous study (Liu et al., 2019), the downregulated expression of which paralleled the downregulated Ago2 expression, suggesting an involvement of this miRNA in METH sensitization. As expected, decreasing the expression of miR-3068-5p in NAc neurons also enhanced the development of METH sensitization, similar to the behavioral changes mediated by inhibiting Ago2 expression. Although miR-30a-5p was enriched following overexpression of Ago2 in NAc neurons, it was not depleted when Ago2 was downregulated in NAc neurons and did not exhibit any effects on METH sensitization. Collectively, these results suggested that miR-3068-5p could be neural Ago2-dependent reduced by METH (NADRM) miRNA in the NAc of mice. Decreased expression of miR-3068-5p may contribute to METH sensitization.

In the current study, we also observed different alteration patterns of miRNAs upon changes in Ago2 expression. For example, the levels of miR-33-5p and miR-376a-3p were both decreased and increased upon bidirectional regulation of Ago2 expression. There was also a set of miRNAs that were not changed following Ago2 overexpression or knockdown. This phenomenon may be due to the selectivity of Ago2 splicing and other indirect or unknown functions of Ago2 (Yang et al., 2010). Moreover, Ago2 is expressed and functions not only in nerve cells but also in gliocytes (He et al., 2012; Chaudhuri et al., 2018). In addition, reported evidence showed that the PAZ domain of Ago2 was capable of shortening mature miRNA (Juvvuna et al., 2012), which likely explains the opposite expression changes of miR-33-5p and miR-376a-3p following Ago2 regulation.

However, Ago2 is not only involved in specific miRNA biogenesis but also a key component of the RISC involved in miRNA- or siRNA-mediated target mRNA degradation. Thus, the potentially universal effect of Ago2 silencing on mRNA function should be considered. We speculated that the downregulation of Ago2 may induce the hypofunction of RISC and disinhibition of RNAi, which may result in considerable upregulation of mRNA expression. However, in our previous study, mRNAs were greatly downregulated by METH (Zhu et al., 2016). Since mRNA can also be regulated by other transcription factors, the universal changes in mRNA function were neutralized by multiple factors as a complex consequence of the response to METH sensitization. Nevertheless, our study showed that differential expression of Ago2 in the NAc could modulate METH sensitization by regulating miR-3068-5p biogenesis, indicating that Ago2, which plays an important role in miRNA generation and execution of miRNA-mediated gene silencing, is involved in the regulation of METH addiction.

Grin1 May Be Involved in the Effects of Argonaute2/miR-3068-5p on Methamphetamine Sensitization

To identify the potential targets of miR-3068-5p in regulating METH sensitization, we predicted the target genes of miR-3068-5p and compared them to the previously identified upregulated genes in the NAc of METH-sensitized mice since miR-3068-5p was downregulated in the NAc of mice in response to METH. We focused on the genes with functions relevant to synaptic plasticity and morphology by IPA, and *Grin1* was the only gene that was upregulated when miR-3068-5p was downregulated by AAV-SYN-spmiR-3068-5p. *Grin1* encodes N-methyl-D-aspartate receptor (NMDAR) subunit 1 (NR1), which is essential to the formation of functioning NMDARs. Specifically, removing NMDAR signaling from DRD1-expressing MSNs could prevent amphetamine sensitization, and this attenuation of sensitization could be rescued by virus-mediated restoration of NR1 (encoded by *Grin1*) in DRD1-expressing neurons in the NAc, demonstrating the requirement of *Grin1* in NAc MSNs for amphetamine sensitization (Beutler et al., 2011). Here, we found that decreasing miR-3068-5p levels in the NAc could enhance METH sensitization and increase *Grin1* expression. More importantly, *Grin1* was downregulated following Ago2 overexpression and showed an upregulation trend when Ago2 was knocked down. These results further indicated that the effects of Ago2/miR-3068-5p on METH sensitization may occur via regulation of *Grin1* in NAc neurons (**Figure 5**).

CONCLUSION AND LIMITATIONS

In summary, we found that Ago2 was downregulated progressively in the NAc of mice during METH sensitization, and METH sensitization could be attenuated or enhanced by overexpression or knockdown of Ago2 in NAc neurons. Furthermore, miR-3068-5p is considered an NADRM miRNA, and neural Ago2/miR-3068-5p cascades are important for METH sensitization. Downregulation of miR-3068-5p in NAc neurons increased locomotor activity during the development of METH sensitization. This functional role of Ago2/miR-3068-5p is likely to occur through the regulation of *Grin1* in neurons within the NAc (Beutler et al., 2011) (**Figure 5**).

However, there were also some limitations of this study. First, since the trace of mice in the OF test in the corner partially reflected anxiety behavior, Ago2 overexpression did not change the central area traveled time or distance on the first day when the mice were put into the OF box. Apparently, there was no effect of Ago2 on anxiety-like behavior in this model, but other anxiety tests should be performed in future studies. Second, although Ago2, as a key molecule in RNAi, was found to be widely expressed throughout the brain, there was no evidence showing the expression pattern of miR-3068 in the brain regions. For now, it cannot be determined if the role of Ago2/miR-3068-5p is NAc-specific. In addition, because of the different upstream receptors of Ago2 and different target genes of miR-3068, Ago2/miR-3068-5p may display specific functions in specific neural types, which are needed for further research. Finally, different functions of the NAc core and shell have been reported, but, here, we did not determine the different roles of Ago2/miR-3068 in the NAc core or shell. Considering that Ago2 can modulate the expression of miRNAs in a cell-specific type, the role of Ago2/miR-3068 in the NAc subregion may be different and should be investigated with a deep understanding of neural types, such as DRD1- and DRD2-expressing neurons.

DATA AVAILABILITY STATEMENT

The original contributions presented in the study are included in the article/**Supplementary Material**; further inquiries can be directed to the corresponding authors.

ETHICS STATEMENT

The animal study was reviewed and approved by the Institutional Animal Care Committee at Xi'an Jiaotong University.

AUTHOR CONTRIBUTIONS

TC and EG initiated the project; TC, DL, and LZ designed the experiments; DL and ML carried out the microinjection of AAV and METH exposure experiment; RW and FW performed the PCR experiments; TZ and ML performed the Western blot experiments; ML, YW, and DL performed the computational analyses and experimental analyses; DL wrote the manuscript; LZ and EG provided critical revision of the manuscript for intellectual content. All of the authors critically reviewed the content and approved the final version of the manuscript for publication. TC and EG should be considered joint corresponding authors.

FUNDING

This work was supported by grants from the National Natural Science Foundation of China given to TC (Grant no. 81772034) and LZ (Grant no. 81701870); the Natural Science Foundation of Shaanxi Province to LZ (2020JQ-081); the Ministry of Education (MOE) Tier 3 grant to EG (Grant no. MOE2017-T3-1-002).

ACKNOWLEDGMENTS

The authors wish to thank Jia-qi Li, Hang Su, Tong Ni, and Nan Dong for participating in stimulating discussions and providing animal care.

SUPPLEMENTARY MATERIAL

The Supplementary Material for this article can be found online at: https://www.frontiersin.org/articles/10.3389/fphar.2021.708034/full#supplementary-material

REFERENCES

Aguilar-Valles, A., Vaissière, T., Griggs, E. M., Mikaelsson, M. A., Takács, I. F., Young, E. J., et al. (2014). Methamphetamine-associated Memory Is Regulated by a Writer and an Eraser of Permissive Histone Methylation. *Biol. Psychiatry* 76 (1), 57–65. doi:10.1016/j.biopsych.2013.09.014

Bartel, D. P. (2004). MicroRNAs. *Cell* 116 (2), 281–297. doi:10.1016/s0092-8674(04)00045-5

Beutler, L. R., Wanat, M. J., Quintana, A., Sanz, E., Bamford, N. S., Zweifel, L. S., et al. (2011). Balanced NMDA Receptor Activity in Dopamine D1 Receptor (D1R)- and D2R-Expressing Medium Spiny Neurons Is Required for Amphetamine Sensitization. *Proc. Natl. Acad. Sci.* 108 (10), 4206–4211. doi:10.1073/pnas.1101424108

Buchanan, J. B., Sparkman, N. L., and Johnson, R. W. (2010). Methamphetamine Sensitization Attenuates the Febrile and Neuroinflammatory Response to a Subsequent Peripheral Immune Stimulus. *Brain Behav. Immun.* 24 (3), 502–511. doi:10.1016/j.bbi.2009.12.008

Chaudhuri, A. D., Dastgheyb, R. M., Yoo, S.-W., Trout, A., Talbot Jr, C. C., Hao, H., et al. (2018). TNFα and IL-1β Modify the miRNA Cargo of Astrocyte Shed Extracellular Vesicles to Regulate Neurotrophic Signaling in Neurons. *Cell Death Dis.* 9 (3), 363. doi:10.1038/s41419-018-0369-4

Cheloufi, S., Dos Santos, C. O., Chong, M. M. W., and Hannon, G. J. (2010). A Dicer-independent miRNA Biogenesis Pathway that Requires Ago Catalysis. *Nature* 465 (7298), 584–589. doi:10.1038/nature09092

Chen, Y.-W., Kao, H.-Y., Min, M.-Y., and Lai, W.-S. (2014). A Sex- and Region-Specific Role of Akt1 in the Modulation of Methamphetamine-Induced Hyperlocomotion and Striatal Neuronal Activity: Implications in Schizophrenia and Methamphetamine-Induced Psychosis. *Schizophr. Bull.* 40 (2), 388–398. doi:10.1093/schbul/sbt031

Chendrimada, T. P., Gregory, R. I., Kumaraswamy, E., Norman, J., Cooch, N., Nishikura, K., et al. (2005). TRBP Recruits the Dicer Complex to Ago2 for microRNA Processing and Gene Silencing. *Nature* 436 (7051), 740–744. doi:10.1038/nature03868

Chiu, C. Q., Martenson, J. S., Yamazaki, M., Natsume, R., Sakimura, K., Tomita, S., et al. (2018). Input-Specific NMDAR-Dependent Potentiation of Dendritic GABAergic Inhibition. *Neuron* 97 (2), 368–377. doi:10.1016/j.neuron.2017.12.032

Emde, A., Eitan, C., Liou, L. L., Libby, R. T., Rivkin, N., Magen, I., et al. (2015). Dysregulated Mi RNA Biogenesis Downstream of Cellular Stress and ALS -causing Mutations: a New Mechanism for ALS. *EMBO J.* 34 (21), 2633–2651. doi:10.15252/embj.201490493

Fabian, M. R., Sonenberg, N., and Filipowicz, W. (2010). Regulation of mRNA Translation and Stability by microRNAs. *Annu. Rev. Biochem.* 79, 351–379. doi:10.1146/annurev-biochem-060308-103103

Franklin, K., and Paxinos, G. (2001). *The Mouse Brain in Stereotaxic Coordinates*. San Diego, CA: Academic Press.

García-Pérez, D., Sáez-Belmonte, F., Laorden, M., Núñez, C., and Milanés, M. (2013). Morphine Administration Modulates Expression of Argonaute 2 and Dopamine-Related Transcription Factors Involved in Midbrain Dopaminergic Neurons Function. *Br. J. Pharmacol.* 168 (8), 1889–1901. doi:10.1111/bph.12083

Greening, D. W., Notaras, M., Chen, M., Xu, R., Smith, J. D., Cheng, L., et al. (2019). Chronic Methamphetamine Interacts with BDNF Val66Met to Remodel Psychosis Pathways in the Mesocorticolimbic Proteome. *Mol. Psychiatry*. doi:10.1038/s41380-019-0617-8

Ha, M., and Kim, V. N. (2014). Regulation of microRNA Biogenesis. *Nat. Rev. Mol. Cel Biol.* 15 (8), 509–524. doi:10.1038/nrm3838

Hagiwara, K., Kosaka, N., Yoshioka, Y., Takahashi, R.-u., Takeshita, F., and Ochiya, T. (2012). Stilbene Derivatives Promote Ago2-dependent Tumour-Suppressive microRNA Activity. *Sci. Rep.* 2, 314. doi:10.1038/srep00314

He, M., Liu, Y., Wang, X., Zhang, M. Q., Hannon, G. J., and Huang, Z. J. (2012). Cell-type-based Analysis of microRNA Profiles in the Mouse Brain. *Neuron* 73 (1), 35–48. doi:10.1016/j.neuron.2011.11.010

Ikeda, M., Okahisa, Y., Aleksic, B., Won, M., Kondo, N., Naruse, N., et al. (2013). Evidence for Shared Genetic Risk between Methamphetamine-Induced Psychosis and Schizophrenia. *Neuropsychopharmacol* 38 (10), 1864–1870. doi:10.1038/npp.2013.94

Jayanthi, S., Mccoy, M. T., Chen, B., Britt, J. P., Kourrich, S., Yau, H.-J., et al. (2014). Methamphetamine Downregulates Striatal Glutamate Receptors via Diverse Epigenetic Mechanisms. *Biol. Psychiatry* 76 (1), 47–56. doi:10.1016/j.biopsych.2013.09.034

Juvvuna, P. K., Khandelia, P., Lee, L. M., and Makeyev, E. V. (2012). Argonaute Identity Defines the Length of Mature Mammalian microRNAs. *Nucleic Acids Res.* 40 (14), 6808–6820. doi:10.1093/nar/gks293

Kelly, M. A., Low, M. J., Rubinstein, M., and Phillips, T. J. (2008). Role of Dopamine D1-like Receptors in Methamphetamine Locomotor Responses of D2 Receptor Knockout Mice. *Genes Brain Behav.* 7 (5), 568–577. doi:10.1111/j.1601-183X.2008.00392.x

Knight, S. W., and Bass, B. L. (2001). A Role for the RNase III Enzyme DCR-1 in RNA Interference and Germ Line Development in Caenorhabditis elegans. *Science* 293 (5538), 2269–2271. doi:10.1126/science.1062039

Liu, D., Zhu, L., Ni, T., Guan, F. L., Chen, Y. J., Ma, D. L., et al. (2019). Ago2 and Dicer1 Are Involved in METH-induced Locomotor Sensitization in Mice via Biogenesis of miRNA. *Addict. Biol.* 24 (3), 498–508. doi:10.1111/adb.12616

Lobo, M. K., Covington, H. E., Chaudhury, D., Friedman, A. K., Sun, H., Damez-Werno, D., et al. (2010). Cell Type-specific Loss of BDNF Signaling Mimics Optogenetic Control of Cocaine Reward. *Science* 330 (6002), 385–390. doi:10.1126/science.1188472

Lominac, K. D., Mckenna, C. L., Schwartz, L. M., Ruiz, P. N., Wroten, M. G., Miller, B. W., et al. (2014). Mesocorticolimbic Monoamine Correlates of Methamphetamine Sensitization and Motivation. *Front. Syst. Neurosci.* 8, 70. doi:10.3389/fnsys.2014.00070

Mizoguchi, H., and Yamada, K. (2019). Methamphetamine Use Causes Cognitive Impairment and Altered Decision-Making. *Neurochem. Int.* 124, 106–113. doi:10.1016/j.neuint.2018.12.019

Neddens, J., Lesting, J., Dawirs, R. R., and Teuchert-Noodt, G. (2002). An Early Methamphetamine challenge Suppresses the Maturation of Dopamine Fibres in the Nucleus Accumbens of Gerbils: on the Significance of Rearing Conditions. *J. Neural Transm.* 109 (2), 141–155. doi:10.1007/s007020200010

Nestler, E. J., and Malenka, R. C. (2004). The Addicted Brain. *Sci. Am.* 290 (3), 78–85. doi:10.1038/scientificamerican0304-78

Pircs, K., Petri, R., Madsen, S., Brattås, P. L., Vuono, R., Ottosson, D. R., et al. (2018). Huntingtin Aggregation Impairs Autophagy, Leading to Argonaute-2 Accumulation and Global MicroRNA Dysregulation. *Cel Rep.* 24 (6), 1397–1406. doi:10.1016/j.celrep.2018.07.017

Rajgor, D., Sanderson, T. M., Amici, M., Collingridge, G. L., and Hanley, J. G. (2018). NMDAR -dependent Argonaute 2 Phosphorylation Regulates Mi RNA Activity and Dendritic Spine Plasticity. *EMBO J.* 37 (11). doi:10.15252/embj.201797943

Robinson, T. E., and Becker, J. B. (1986). Enduring Changes in Brain and Behavior Produced by Chronic Amphetamine Administration: a Review and Evaluation of Animal Models of Amphetamine Psychosis. *Brain Res. Rev.* 11 (2), 157–198. doi:10.1016/s0006-8993(86)80193-710.1016/0165-0173(86)90002-0

Schaefer, A., Im, H.-I., Venø, M. T., Fowler, C. D., Min, A., Intrator, A., et al. (2010). Argonaute 2 in Dopamine 2 Receptor-Expressing Neurons Regulates Cocaine Addiction. *J. Exp. Med.* 207 (9), 1843–1851. doi:10.1084/jem.20100451

Schmittgen, T. D., and Livak, K. J. (2008). Analyzing Real-Time PCR Data by the Comparative CT Method. *Nat. Protoc.* 3 (6), 1101–1108. doi:10.1038/nprot.2008.73

Shekar, P. C., Naim, A., Sarathi, D. P., and Kumar, S. (2011). Argonaute-2-null Embryonic Stem Cells Are Retarded in Self-Renewal and Differentiation. *J. Biosci.* 36 (4), 649–657. doi:10.1007/s12038-011-9094-1

Störchel, P. H., Thümmler, J., Siegel, G., Aksoy-Aksel, A., Zampa, F., Sumer, S., et al. (2015). A Large-scale Functional Screen Identifies N Ova1 and N Coa3 as Regulators of Neuronal Mi RNA Function. *EMBO J.* 34 (17), 2237–2254. doi:10.15252/embj.201490643

Yang, J.-S., Maurin, T., Robine, N., Rasmussen, K. D., Jeffrey, K. L., Chandwani, R., et al. (2010). Conserved Vertebrate Mir-451 Provides a Platform for Dicer-independent, Ago2-Mediated microRNA Biogenesis. *Proc. Natl. Acad. Sci.* 107 (34), 15163–15168. doi:10.1073/pnas.1006432107

Zhang, X., Graves, P., and Zeng, Y. (2013). Overexpression of Human Argonaute2 Inhibits Cell and Tumor Growth. *Biochim. Biophys. Acta Gen. Subj.* 1830 (3), 2553–2561. doi:10.1016/j.bbagen.2012.11.013

Zhong, N., Jiang, H., Du, J., Zhao, Y., Sun, H., Xu, D., et al. (2016). The Cognitive Impairments and Psychological Wellbeing of Methamphetamine Dependent Patients Compared with Health Controls. *Prog. Neuro. Psychopharmacol. Biol. Psychiatry* 69, 31–37. doi:10.1016/j.pnpbp.2016.04.005

Zhou, Y., Chen, L., Barlogie, B., Stephens, O., Wu, X., Williams, D. R., et al. (2010). High-risk Myeloma Is Associated with Global Elevation of miRNAs and

Overexpression ofEIF2C2/AGO2. *Proc. Natl. Acad. Sci. USA* 107 (17), 7904–7909. doi:10.1073/pnas.0908441107

Zhu, J., Chen, Y., Zhao, N., Cao, G., Dang, Y., Han, W., et al. (2012). Distinct Roles of Dopamine D3 Receptors in Modulating Methamphetamine-Induced Behavioral Sensitization and Ultrastructural Plasticity in the Shell of the Nucleus Accumbens. *J. Neurosci. Res.* 90 (4), 895–904. doi:10.1002/jnr.22821

Zhu, L., Li, J., Dong, N., Guan, F., Liu, Y., Ma, D., et al. (2016). mRNA Changes in Nucleus Accumbens Related to Methamphetamine Addiction in Mice. *Sci. Rep.* 6, 36993. doi:10.1038/srep36993

Conflict of Interest: The authors declare that the research was conducted in the absence of any commercial or financial relationships that could be construed as a potential conflict of interest.

Publisher's Note: All claims expressed in this article are solely those of the authors and do not necessarily represent those of their affiliated organizations, or those of the publisher, the editors and the reviewers. Any product that may be evaluated in this article, or claim that may be made by its manufacturer, is not guaranteed or endorsed by the publisher.

frontiers in Pharmacology

ORIGINAL RESEARCH
published: 04 October 2021
doi: 10.3389/fphar.2021.750397

Social Interaction With Relapsed Partner Facilitates Cocaine Relapse in Rats

Shiqiu Meng[1†], Wei Yan[2†], Xiaoxing Liu[2†], Yimiao Gong[2], Shanshan Tian[2], Ping Wu[1], Yan Sun[1], Jie Shi[1], Lin Lu[1,2], Kai Yuan[2] and Yanxue Xue[1,3]**

[1]National Institute on Drug Dependence and Beijing Key Laboratory of Drug Dependence, Peking University, Beijing, China , [2]NHC Key Laboratory of Mental Health (Peking University), National Clinical Research Center for Mental Disorders (Peking University Sixth Hospital), Peking University Sixth Hospital, Peking University Institute of Mental Health, Beijing, China, [3]Chinese Institute for Brain Research, Beijing, China

Social factors strongly contribute to drug use and relapse, and epidemiological studies have found that members of peer groups influence each other to use drugs. However, previous animal models mostly failed to incorporate social factors and demonstrate the effects of social partners on drug addiction and relapse. In the present study, we investigated the transfer of relapse to cocaine seeking between drug-addicted partners in rats. Male Sprague–Dawley rats were pair-housed and subjected to training and extinction of cocaine self-administration and conditioned place preference (CPP). 24 h after extinction test, the targeted rats interacted with a cocaine-primed (relapsed) partner or stranger, or saline-injected (unrelapsed) partner for 30 min, after which the targeted rats were tested for drug seeking behavior. We found that social interaction with a relapsed partner increased drug seeking behavior in cocaine self-administration and CPP models in rats, while social interaction with an unrelapsed partner or relapsed stranger had no effect on cocaine seeking. Moreover, the effect of social interaction on cocaine seeking could last for at least 1 day. Our findings demonstrate a facilitation effect of relapsed social partners on drug relapse in rats and provide a novel animal model for social transfer of drug relapse.

Keywords: social interaction, cocaine, relapse, peer influence, addiction, animal model

OPEN ACCESS

Edited by:
Qi Wang,
Southern Medical University, China

Reviewed by:
Qiu Pingming,
Southern Medical University, China
Rui Zhao,
China Medical University, China

****Correspondence:***
Yanxue Xue
yanxuexue@bjmu.edu.cn
Kai Yuan
yuankai@pku.edu.cn

†These authors have contributed equally to this work

Specialty section:
This article was submitted to Neuropharmacology, a section of the journal Frontiers in Pharmacology

Received: *30 July 2021*
Accepted: *31 August 2021*
Published: *04 October 2021*

Citation:
Meng S, Yan W, Liu X, Gong Y, Tian S, Wu P, Sun Y, Shi J, Lu L, Yuan K and Xue Y (2021) Social Interaction With Relapsed Partner Facilitates Cocaine Relapse in Rats. Front. Pharmacol. 12:750397. doi: 10.3389/fphar.2021.750397

INTRODUCTION

Drug addiction is a chronic recurrent disease bringing heavy burden to individuals, families, and society (Volkow and Boyle, 2018), and is characterized by high rates of relapse even after treatment (Sinha, 2011). Social and environmental factors are acknowledged as determinants of drug use and relapse, and among various factors, social partners may be critical (Bahr et al., 2005; Simons-Morton and Chen, 2006). Epidemiological investigations have demonstrated that people easily become addicts if their friends are addicted to drugs (Walden et al., 2004; Bahr et al., 2005; Simons-Morton and Chen, 2006). Some clinical research indicates that social interaction with alcohol-addicted partners not only accelerated acquisition of addiction, but also enhanced alcohol tolerance (Caudill and Marlatt, 1975; Lied and Marlatt, 1979; Caudill and Kong, 2001; Larsen et al., 2010; Kirkpatrick and de Wit, 2013), demonstrating that social interaction with addicted partners may play a facilitation effect on addiction. Having drug-using friends has also been found to increase risks of heroin relapse in patients under methadone maintenance treatment (Li et al., 2012). On the contrary, joining recovery communities like Alcoholics Anonymous (Kelly et al., 2012; Frings et al.,

2021) and interacting with non-addicted peers to change their social network (Bathish et al., 2017) promotes recovery from addiction. However, due to ethical reasons, human studies on impact of social partners on illicit drug addiction are limited.

Animal models are critical to reveal the neural mechanisms of drug addiction and help clinicians to develop potential treatments, whereas only a few studies have incorporated social factors and demonstrated the effects of social partners on drug addiction. For example, Smith et al. (2015) have found that self-administration behavior of rats is promoted when they are reared with a partner and both trained with cocaine self-administration, while the addictive behavior decreases when the partners have no access to cocaine. Compared with peers who did not experience cocaine self-administration training, rats showed more preference to partners with whom they were trained for self-administration together (Smith and Pitts, 2014), especially those who took similar drugs (Smith et al., 2015). Similar results were also found in the conditioned place preference (CPP) model (Larsen et al., 2010; Koordeman et al., 2011). The above findings suggest that social interaction with addicted partners affects the acquisition and maintenance of addiction. However, the impact of social partners on addiction relapse needs further study.

Numerous studies have demonstrated that after abstinence or extinction, drug craving can still be triggered once the animals are exposed to drug or drug-related cues (e.g., sound and light) (Davachi, 2006; Brandon et al., 2007; Goldfarb and Sinha, 2018). Thus, we speculate that drug craving may also be prompted by social interaction with relapsed partners. In the present study, we established an animal model of social transfer of relapse and investigated the effect of social interaction on cocaine seeking behavior after extinction.

MATERIALS AND METHODS

Experimental Design

Experiment 1: Effects of social interaction with relapsed partner. Rats were pair-housed and subjected to 10 days cocaine self-administration training, followed by extinction. 24 h after extinction test, one of the two rats (relapsed partner) was primed with cocaine (10 mg/kg, i.p.), and subjected to 1 h reinstatement test. Next, the relapsed partner was put back to their homecage, and interacted with the other rat (targeted rat) for 30 min. Then the targeted rat was immediately subjected to 1 h reinstatement test.

Experiment 2: Effects of social interaction with unrelapsed partner. Rats were pair-housed and subjected to cocaine self-administration training and extinction. 24 h after extinction test, one of the two rats (unrelapsed partner) was injected with saline (1 ml/kg, i.p.), and subjected to reinstatement test. Next, the unrelapsed partner was put back to their homecage, and interacted with the other rat (targeted rat) for 30 min. Then the targeted rat was subjected to reinstatement test immediately.

Experiment 3: Effects of social interaction with relapsed partner for different time. Rats were pair-housed and subjected to cocaine self-administration training and extinction. 24 h after extinction test, one of the two rats (relapsed partner) was primed with cocaine (10 mg/kg, i.p.), and subjected to reinstatement test. Next, the other rat (targeted rat) interacted with the relapsed partner in their homecage for 0, 10, 30, or 60 min, followed by reinstatement test immediately.

Experiment 4: The maintenance of facilitation effect after 30 min social interaction with the relapsed partner. Rats were pair-housed and subjected to cocaine self-administration training and extinction. 24 h after extinction test, one of the two rats (relapsed partner) was primed with cocaine (10 mg/kg, i.p.), and subjected to reinstatement test. Next, the other rat (targeted rat) interacted with the relapsed partner in their homecage for 30 min, and subjected to reinstatement test immediately (0 min), or 1–7 days later.

Experiment 5: Effects of social interaction with relapsed stranger. Rats were pair-housed and subjected to cocaine self-administration training and extinction. 24 h after extinction test, a rat kept in another cage (relapsed stranger) was injected with a single dose of cocaine (10 mg/kg, i.p.) and subjected to reinstatement test. Then the relapsed stranger was put into the homecage of the targeted rat (its partner was removed from the cage) for 30 min social interaction, and the targeted rat was subjected to reinstatement test immediately.

Experiment 6: Effects of social interaction on relapse to cocaine-induced CPP. Rats were pair-housed and subjected to the baseline test. After CPP training and extinction, the rats were subjected to the extinction test. 24 h later, the targeted rats interacted with relapsed partners, unrelapsed partners, or relapsed strangers for 30 min in homecages, and then were subjected to reinstatement test immediately.

Subjects

We used adult male Sprague–Dawley (SD) rats (280–300 g upon arrival) purchased from Vital River Laboratories. The rats were pair-housed in an animal facility with appropriate temperature (22 ± 2°C) and humidity (50 ± 10%), as well as freely accessible water and food. The lighting time was controlled, under a 12 h light/dark circle. All behavioral experiments were performed under the dark circle and in accordance with the National Institutes of Health Guide for the Care and Use of Laboratory Animals, and approved by the Biomedical Ethics Committee for Animal Use and Protection of Peking University.

Surgery

Rats were under anesthetic through pentobarbital sodium (20 mg/ml, 60 mg/kg, i.p.) and received catheters insertion into the right jugular vein with the tip reaching the opening of right atrium. After the surgery, rats were recovered for 7 days with penicillin administration (resolved in 0.2% heparin sodium) every day, preventing infection and cannula blocking.

Intravenous Cocaine Self-Administration Training

Cocaine-HCl was purchased from the Qinghai Pharmaceutical Factory and resolved in 0.9% saline (5 mg/ml).

The training procedure was based on our previous studies (Xue et al., 2012; Luo et al., 2015). The chambers (AniLab Software and Instruments) were equipped with two nosepoke holes 9 cm above the underside, one was active-nosepoke hole and the other was inactive-nosepoke hole. The two rats in each cage were trained at the same time in different chambers for fixed ratio 1 (FR1) cocaine self-administration training for 10 days during three 1 h sessions per day with 5 min intervals. Every session started from the illumination of a house light. Poking to the active-nosepoke hole led to a cocaine infusion (0.75 mg/kg), accompanied with a 5 s tone-light cue, while poking to the inactive-nosepoke hole did not result in cocaine infusion or tone-light cue. There was a 40 s time-out phase between each infusion, after which the house light would turn on again. The number and time of active nosepokes, inactive nosepokes, and infusions were recorded. To prevent rats administrating overdose of cocaine, the number of infusions was limited to 20 times in each session. After training, the rats were returned to their homecages.

Extinction of Self-Administration

The two rats in each cage were subjected to extinction at the same time in different chambers. During the extinction sessions, the conditions were the same as those during the self-administration training. But there was no cocaine infusion after rats poked the active-nosepoke hole. At the end of extinction every day, they were put back in their homecages. The extinction was performed until the number of active-nosepokes decreased to below 20% of the mean nosepokes during the last 3 days of self-administration training for at least two consecutive days. 24 h later, the rats were subjected to test for drug seeking (extinction test).

Training of Cocaine-Induced CPP

The procedure was based on our previous studies (Xue et al., 2012). Three-chamber apparatuses were used, and time the rats spent in each chamber was recorded. The two rats in each cage were trained at the same time in different apparatuses. For the baseline test (day 1), there were no partitions among the chambers. Rats were put into the middle chamber and allowed to move freely for 15 min. Rats that presented a preference for one of the boxes (resistance time >540 s) were ruled out. Then the rats were trained for cocaine-induced CPP for 8 days. Rats received intraperitoneal cocaine (10 mg/kg, day 2/4/6/8) or saline (1 ml/kg, day 3/5/7/9) injections alternatively and were confined to the conditioning chambers for 45 min after injection. The rats were returned to their homecages after training every day. 24 h after the last-day training (day 10), drug seeking test (training test) was performed.

Extinction of Cocaine-Induced CPP

The two rats in each cage were subjected to extinction at the same time in different chambers. The conditions for extinction were the same as training except that no injections were given. At the end of extinction every day, they were put back in their homecages. After 8 days of extinction, rats were subjected to drug seeking test (extinction test).

Drug Priming

For cocaine priming or saline injection, the rats were intraperitoneally injected with 10 mg/kg cocaine or 1 ml/kg saline, and then they were delivered to drug seeking test (reinstatement test).

Social Interaction

To investigate the effect of social interaction with a relapsed partner, one rat in each cage was intraperitoneally injected with cocaine (10 mg/kg), and tested for drug seeking. Next, it was put back to its homecage as a relapsed partner, and interacted with the other rat (targeted rat) for 0, 10, 30, or 60 min.

To test the effect of social interaction with an unrelapsed partner, saline (1 ml/kg) was intraperitoneally injected to one rat in each cage, and then drug seeking was tested. Then it was put back to its homecage as an unrelapsed partner, and interacted with the other rat (targeted rat) for 30 min.

To investigate the effect of social interaction with a relapsed stranger, one rat in each cage was intraperitoneally injected with cocaine (10 mg/kg) and tested for drug seeking. Then it was put back to another cage as a relapsed stranger, and interacted with the rat (targeted rat) in this cage for 30 min. The partner of the targeted rat was removed from their homecage in advance.

After social interaction, the targeted rats were subjected to drug seeking test (reinstatement test).

Drug Seeking Test

The conditions during the drug seeking tests in the self-administration model were the same as those during the extinction sessions, and the tests lasted for 1 h.

The conditions during the drug seeking tests in the CPP model were the same as those during the baseline test, and the tests lasted for 15 min. The time spent in the cocaine-paired chamber minus the time spent in the saline-paired chamber was calculated as the CPP score.

Statistical Analysis

All of the statistical analyses were performed using SPSS 20.0 software (SPSS, Chicago, IL, United States). The data were expressed as mean ± SEM, and analyzed by repeated measures analysis of variance (ANOVA) with appropriate within-group factors for each experiment (see Results), followed by least significant difference (LSD) post hoc tests in Experiment 6. Values of $p < 0.05$ were considered statistically significant.

RESULTS

Social Interaction With Relapsed Partner Triggered Relapse to Cocaine Seeking

First, we investigated the effect of social interaction on cocaine seeking behavior in the self-administration model. We first

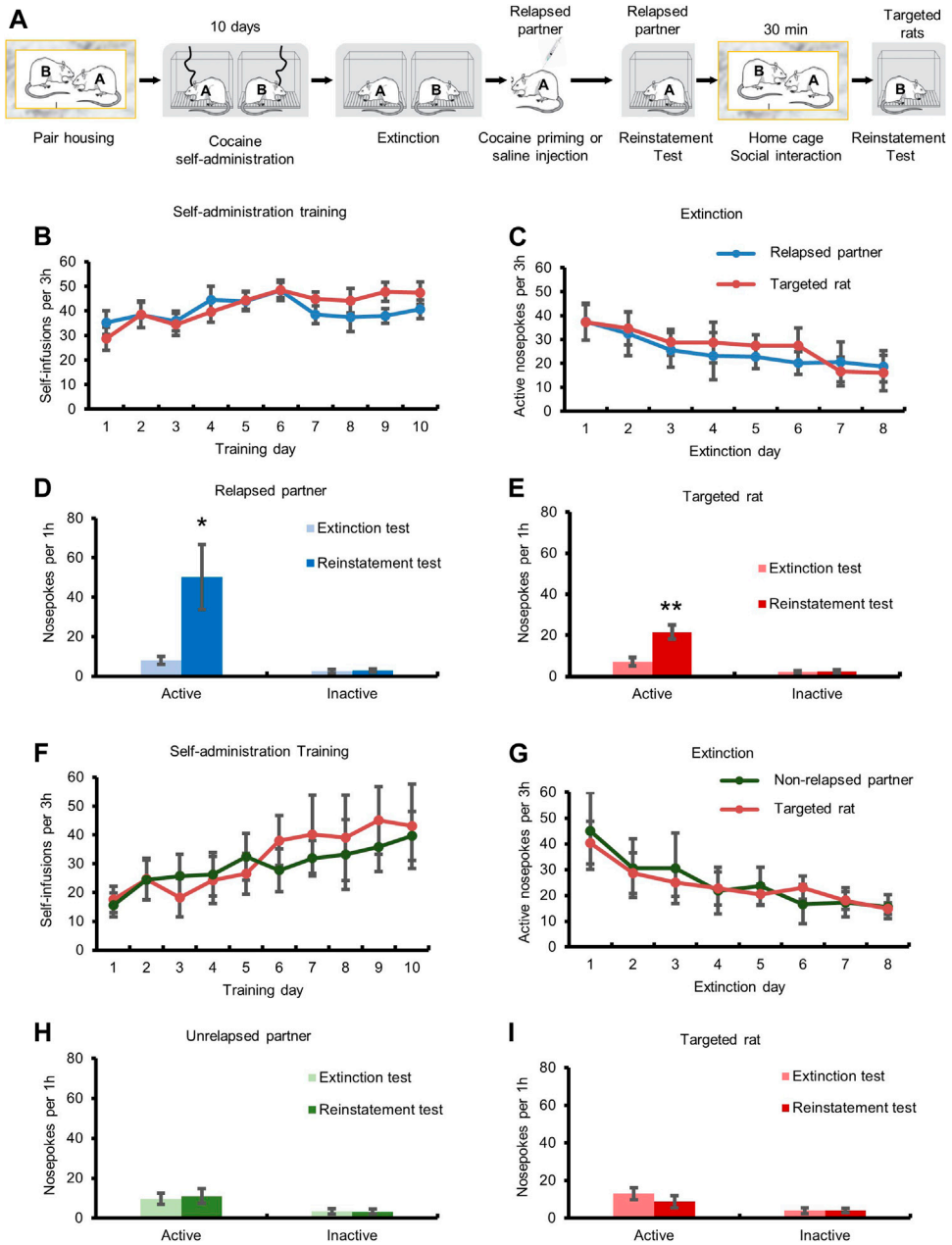

FIGURE 1 | Social interaction with relapsed partner induced relapse to cocaine seeking behavior. **(A)** Experimental timeline. **(B,F)** Targeted rats and partners acquired cocaine self-administration training. **(C,G)** Drug-seeking behavior of targeted rats and partners was extinguished. **(D)** Cocaine injection triggered drug seeking behavior. **(E)** Drug-seeking behavior of targeted rats was increased after social interaction with relapsed partner (Data are shown as mean ± SEM. $^{**}p < 0.01$, compared with extinction test. $n = 11$). **(H)** Saline injection had no effect on drug seeking behavior. **(I)** Drug-seeking behavior of targeted rats had no change after social interaction with unrelapsed partner (Data are shown as mean ± SEM. $n = 7$).

explored whether social interaction with a relapsed partner would induce relapse (**Figures 1A–C**). The repeated measures ANOVA with the within-subjects factors (extinction test and reinstatement test) showed that cocaine injection increased the number of active-nosepokes ($F_{1,10} = 6.670$, $p < 0.05$), and had no effect on the number of inactive-nosepokes ($p > 0.05$) in the reinstatement test, indicating that cocaine priming induced reinstatement of drug seeking (**Figure 1D**). In the targeted rats group, the repeated measures ANOVA of nosepokes with the within-subjects factors (extinction test and reinstatement test) revealed that the number of active-nosepokes was increased after social interaction with relapsed partner ($F_{1,10} = 17.862$, $p < 0.01$), and inactive-nosepokes had no change ($p > 0.05$) in the reinstatement test, suggesting that social interaction with relapsed partner resulted in relapse of cocaine seeking (**Figure 1E**).

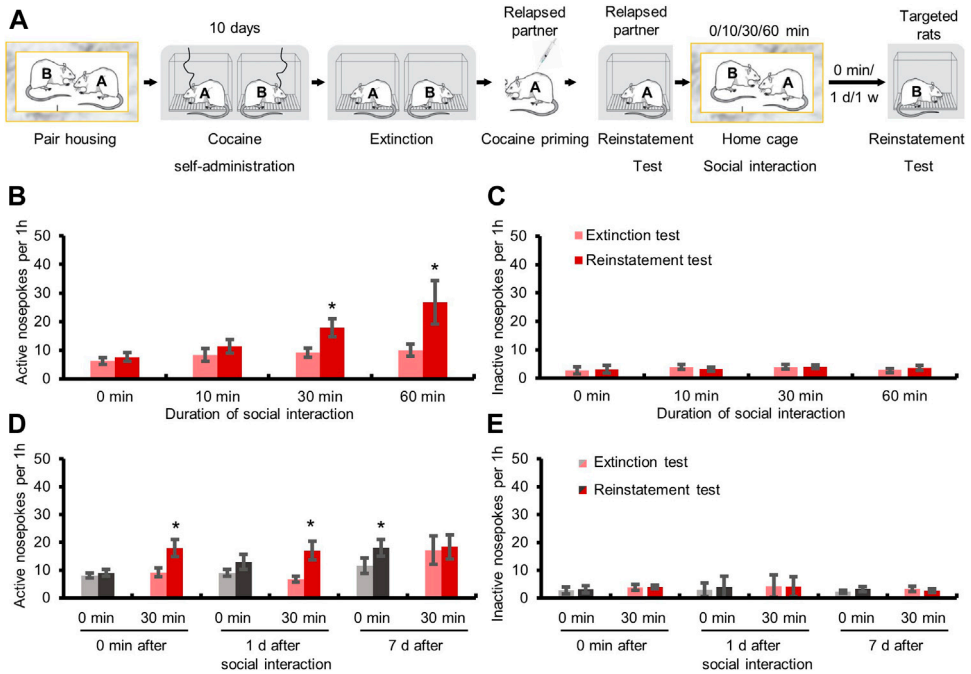

FIGURE 2 | Social interaction with relapsed partners for over 30 min triggered relapse to drug-seeking behavior and this effect lasted for at least 1 day. **(A)** Experimental timeline. **(B)** Active nosepokes were enhanced after social interaction with relapsed partner for 30 or 60 min. **(C)** Inactive nosepokes had no change after social interaction (Data are shown as mean ± SEM. *$p < 0.05$, compared with extinction test. $n = 7$–9). **(D)** Active nosepokes were increased immediately or 1 day after 30 min social interaction with relapsed partner. **(E)** Inactive nosepokes had no change after social interaction (Data are shown as mean ± SEM. *$p < 0.05$, compared with extinction test. $n = 6$–9).

We also assessed the effect of social interaction with an unrelapsed partner on cocaine seeking (**Figures 1A,F,G**). The repeated measures ANOVA showed that the number of active-nosepokes had no significant change ($p > 0.05$) after saline injection in the reinstatement test, indicating that saline injection did not induce cocaine relapse (**Figure 1H**). The repeated measures ANOVA of the number of active-nosepokes of the targeted rats showed no significant change (both $p > 0.05$) after social interaction with unrelapsed partner, indicating that social interaction with unrelapsed partner did not induce relapse of cocaine seeking.

We next explored the effect of different interaction time on the relapse to cocaine seeking, and targeted rats interacted with relapsed partner for 0, 10, 30, or 60 min (**Figure 2A**). The repeated measures ANOVA showed that the numbers of active-nosepokes of the targeted rats were elevated after 30 min ($F_{1,7} = 9.171$, $p < 0.05$) and 60 min ($F_{1,6} = 7.088$, $p < 0.05$) social interaction with the relapsed partner, but not after 0 min (no social interaction) or 10 min social interaction (**Figure 2B**, both $p > 0.05$). The above findings indicated that social interaction required a certain amount of time (no less than 30 min) to produce the facilitation effect on relapse.

Then we further tested how long the facilitation effect of social interaction with relapsed partner on relapse could last (**Figure 2A**). The repeated measures ANOVA showed that the targeted rats had a higher number of active-nosepokes when tested immediately ($F_{1,7} = 9.171$, $p < 0.05$), or 1 day ($F_{1,5} = 13.164$, $p < 0.05$), but not 7 days ($p > 0.05$), after 30 min social interaction with relapsed partners, while no significant change was found when the targeted rats which did not interact with relapsed partners were tested immediately or 1 day later (both $p > 0.05$). Interestingly, when tested 7 days later, the number of active-nosepokes of the targeted rats that did not experience social interaction was increased during the drug seeking test ($F_{1,6} = 6.161$, $p < 0.05$), possibly resulting from spontaneous recovery of drug seeking (**Figure 2D**). These results demonstrated that the effect of social interaction on cocaine seeking lasted for at least 1 day.

Social Interaction With Relapsed Strangers did not Induce Relapse to Cocaine Seeking

Next, we investigated whether social interaction with relapsed strangers could also induce cocaine relapse (**Figures 3A–C**). The repeated measures ANOVA with within-subject factors (extinction test and reinstatement test) showed that the numbers of active-nosepokes of the strangers were elevated after cocaine injection (**Figure 3D**, $F_{1,8} = 13.857$, $p < 0.05$). No significant change was found in the numbers of active-nosepokes of the targeted rats after social interaction with relapsed strangers (**Figure 3E**, $p > 0.05$). The above findings indicated that transfer of cocaine relapse occurred during social interaction with relapsed partner rather than relapsed stranger.

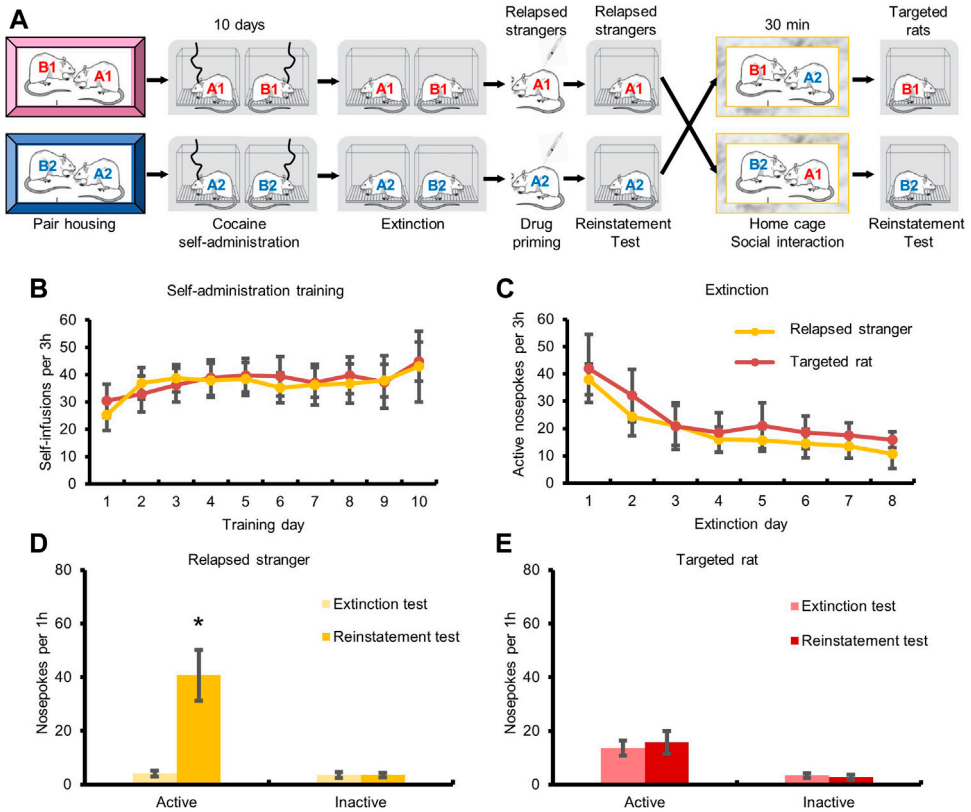

FIGURE 3 | Social interaction with relapsed strangers had no effect on drug-seeking behavior. **(A)** Experimental timeline. **(B)** Targeted rats and strangers acquired cocaine self-administration training. **(C)** Drug-seeking behavior of targeted rats and strangers was extinguished. **(D)** Cocaine injection triggered drug-seeking behavior. **(E)** Drug-seeking behavior of targeted rats had no change after social interaction with relapsed stranger (Data are shown as mean ± SEM. *$p < 0.05$, compared with extinction test. $n = 9$).

Social Interaction With Relapsed Partners Promoted Relapse to Cocaine-Induced CPP

Finally, we validated the facilitation effect of social interaction on cocaine relapse through the cocaine-induced conditioned place preference (CPP) model, which is also a widely used animal model to study drug addiction (**Figure 4A**). The repeated measures ANOVA of CPP scores of relapsed partners with within-subjects factors (baseline test, training test, extinction test, and reinstatement test), showed a significant main effect (**Figure 4B**, $F_{3,15} = 4.665$, $p < 0.05$). Post hoc tests revealed significant differences between baseline test and training test ($p < 0.05$), training test and extinction test ($p < 0.01$), or extinction test and reinstatement test ($p < 0.05$). Meanwhile, the repeated measures ANOVA of CPP scores of the targeted rats with within-subjects factors (baseline test, training test, extinction test, and reinstatement test), showed a significant main effect (**Figure 4B**, $F_{3,15} = 14.166$, $p < 0.01$). Post hoc tests revealed significant differences between baseline test and training test ($p < 0.01$), training test and extinction test ($p < 0.01$), or extinction test and reinstatement test ($p < 0.05$). The above results suggested that social interaction with relapsed partners promoted the transfer of cocaine relapse. But if the targeted rats did not interact with relapsed partners, no difference was found between the extinction test and reinstatement test (**Figure 4C**, $p > 0.05$).

For the unrelapsed partners, the repeated measures ANOVA of CPP scores showed a significant main effect (**Figure 4D**, $F_{3,15} = 3.785$, $p < 0.05$). Post hoc tests revealed significant differences between the baseline test and training test ($p < 0.01$), or training test and extinction test ($p < 0.05$), but no difference between the extinction test and reinstatement test ($p > 0.05$). The repeated measures ANOVA of the CPP scores of targeted rats which interacted with unrelapsed partners revealed a significant main effect (**Figure 4D**, $F_{3,15} = 9.560$, $p < 0.01$). Post hoc tests revealed significant differences between baseline test and training test ($p < 0.05$), or training test and extinction test ($p < 0.01$). No change was found between the extinction test and reinstatement test ($p > 0.05$), demonstrating that social interaction with unrelapsed partners had no effect on the transfer of cocaine relapse.

A significant main effect was shown for the CPP scores of the relapsed strangers by repeated measures ANOVA (**Figure 4E**, $F_{3,18} = 14.296$, $p < 0.01$), and post hoc tests revealed significant differences between baseline test and training test ($p < 0.01$), training test and extinction test ($p < 0.01$), or extinction test and reinstatement test ($p < 0.05$). Meanwhile, the repeated measures

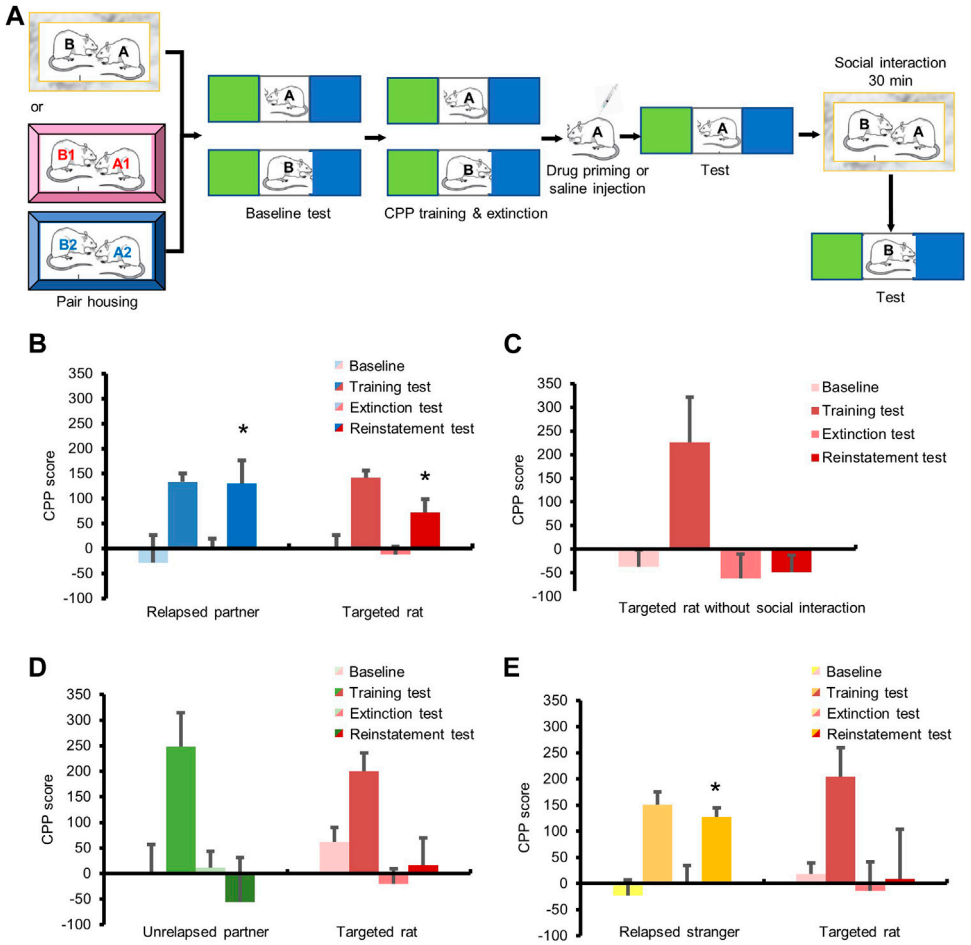

FIGURE 4 | Social interaction with relapsed partners triggered relapse in cocaine CPP model. **(A)** Experimental timeline. **(B–E)** All rats obtained cocaine CPP training and extinction. **(B)** Cocaine injection triggered relapse of the partners, and social interaction with relapsed partner enhanced drug seeking of targeted rats. **(C)** No social interaction had no influence on relapse of targeted rats. **(D)** Social interaction with unrelapsed partner had no effect on relapse of targeted rats. **(E)** Social interaction with relapsed stranger had no effect on relapse of targeted rats. (Data are shown as mean ± SEM. *$p < 0.05$, compared with extinction test. $n = 6–7$).

ANOVA of CPP scores of the targeted rats interacting with relapsed strangers showed a significant main effect (**Figure 4E**, $F_{3,18} = 4.050$, $p < 0.05$). Post hoc revealed significant differences between baseline test and training test ($p < 0.01$), or training test and extinction test ($p < 0.05$), while no change was found between the extinction test and reinstatement test ($p > 0.05$), indicating that social interaction with relapsed strangers did not affect cocaine seeking.

DISCUSSION

In the present study, we proposed a novel animal model to explore the effects of social partners on relapse, and investigated the social transfer of drug relapse based on two classic behavioral paradigms, cocaine self-administration and CPP. We found that social interaction with relapsed (cocaine-primed) partners for at least 30 min induced relapse to cocaine seeking behavior, and the effect lasted for over 24 h. In contrast, neither social interaction with relapsed strangers nor with unrelapsed partners had a facilitation effect on cocaine relapse.

Social experiences are important influential factors for drug addiction and relapse (Heilig et al., 2016). In previous studies, many animal models of addiction relapse have been established and validated that drug priming, drug-related cues or context, and stress can induce reinstatement/relapse after extinction (Pohorecky, 2008; Neisewander et al., 2012; Heilig et al., 2016). However, only a few models incorporated social factors, and there remain debates about the role of social factors in relapse. Ribeiro Do Couto et al. (2009) found that social isolation before CPP training or exposure to social defeat stress before cocaine priming promoted relapse to cocaine-induced CPP, whereas exposure to a non-addicted female mouse or brief social interaction with a non-addicted and non-aggressive male mouse before cocaine priming could reduce relapse (Ribeiro Do Couto et al., 2009). Venniro et al. (2018) built a model of choice between drugs and social interaction, and found that access to social interaction with

non-addicted rats, as a social reward, could prevent methamphetamine self-administration and relapse. While some studies demonstrated that social interaction with addicted peers promoted the possibility of addiction (Doty and de Wit, 1995; Kirkpatrick and de Wit, 2013), other studies reported the inhibitory effects of social factors on addiction (Deatherage, 1972; Weisinger et al., 1989). For example, compared with rats kept in pairs, rats kept solely got more morphine in the social environment (Alexander et al., 1981; Raz and Berger, 2010). If these isolated rats were allowed to interact with other non-addicted peers before the test, the preference for morphine was also attenuated (Hadaway et al., 1979; Raz and Berger, 2010). Based on the findings above, we speculated that social interaction with non-addicted or unrelapsed peers may prevent relapse, while interaction with addicted or relapsed peers may facilitate relapse. We found that interaction with relapsed partner, but not unrelapsed partner, after extinction promoted cocaine seeking. The present study provides a perspective that relapsed and unrelapsed partners produce different effects on relapse. Our results and previous findings confirmed the social-learning theory (Peitz et al., 2013) which demonstrates that partners of a group affect the behavior of other members.

However, the role of social interaction on addiction and relapse is complex and the state of partners is not the only determining factor. Some research revealed that interaction with non-addicted partners produced a dose-response effect (Wolffgramm, 1990; Wolffgramm and Heyne, 1991). Compared with isolated rats, rats that interacted with members of peer group partly (there was a segregation network between them) was prevented from alcohol seeking, while rats that interacted with partners completely (there was no segregation network between them) presented increased alcohol intake (Wolffgramm, 1990), suggesting there was a dose-effect relationship between interaction degree and alcohol intake. Moreover, the gender of partners also has an effect. A study using prairie voles found that male prairie voles which were pair-housed with other male ones showed more preference to alcohol (Anacker et al., 2011), whereas alcohol preference of those kept with female prairie voles had no change (Hostetler et al., 2012). The above findings reveal that the effect of social interaction on addiction and relapse depends on not only whether the partners got addicted or relapsed but also the interaction degree and gender of partners. Thus, further studies are needed to investigate the effect of social interaction at different degrees or in different communicating ways (i.e., olfactory, auditory, visual, or tactile communication), or with peers having different genders on drug relapse.

Previous research has showed various brain regions responsible for social interaction and provides an insight into the "social brain" (Insel and Fernald, 2004). It includes the brain areas activated during the social cognition tasks, like the regions for social identification, environmental assessment, social motivation, and behavior execution. Both human and animal studies verified the critical effect of the medial prefrontal cortex (mPFC), hippocampus, amygdala, and thalamus on social interaction (Kas et al., 2014), and meanwhile, these brain areas also contribute to cocaine addiction and relapse (Brandon et al., 2007). Notably, EI Rawas et al. (2012) found that similar brain regions were activated by cocaine-induced CPP and social interaction-induced CPP, including prelimbic, infralimbic, orbitofrontal, and cingulate cortex, as well as striatum, central and basolateral amygdala, and ventral tegmental areas, which had been proved to be associated with cocaine conditioned stimuli and social interaction (Thomas et al., 2003; Salchner et al., 2004; Miller and Marshall, 2005). Inhibiting protein synthesis in the mPFC (Marcondes et al., 2020), hippocampus (Garrido Zinn et al., 2016), or amygdala (Gur et al., 2014; Garrido Zinn et al., 2016) impaired the discrimination ability between familiar peers and strangers, suggesting that social interaction with relapsed partners instead of strangers possibly activated these brain regions and retrieved seeking for cocaine. This may be why only interaction with relapsed partners instead of strangers can induce cocaine relapse. Besides, the mirror neuron system is the hub for understanding other's emotions, intentions, and actions (Rizzolatti et al., 1999; Rizzolatti and Craighero, 2004; Molenberghs et al., 2009). Mirror neurons are widely distributed in the inferior frontal gyrus, primary somatosensory cortex, supplementary motor area, and other cortex (Molenberghs et al., 2009), and a study recruiting patients with lesions in the lateral prefrontal cortex showed deficits in understanding other's emotion, indicating mirror neurons also exist in the prefrontal cortex (Perry et al., 2017). Therefore, mirror neurons in the prefrontal cortex may play an important role in the social transfer of drug relapse, which needs further investigation.

There are some limitations in our work. First, we established a novel model for the transfer of relapse between partners, but it remains unclear whether it is applicable in other drugs like heroin and nicotine. Furthermore, social interaction may produce similar effects in other disorders such as depression and post-traumatic stress disorder, which also needs further investigation. Second, we did not investigate the neural mechanisms underlying the effects of social interaction on relapse. Future studies need to be conducted to explore how the information is transmitted from the relapsed partners to the targeted rats, and how the brain areas mediating social information processing activate the ones required for addiction and relapse.

In conclusion, we introduced a novel animal model for the social transfer of drug relapse, and found that cocaine relapse could be induced by social interaction with relapsed partner, but not unrelapsed partner or relapsed stranger. Our findings suggest the importance of living in drug-free communities and keeping away from relapsed partners for abstinent drug users, and emphasize the necessity of paying attention to social interaction factors when formulating prevention and treatment strategies for relapse.

DATA AVAILABILITY STATEMENT

The raw data supporting the conclusion of this article will be made available by the authors, without undue reservation.

ETHICS STATEMENT

The animal study was reviewed and approved by the Biomedical Ethics Committee for Animal Use and Protection of Peking University.

AUTHOR CONTRIBUTIONS

SM, LL, and YX designed the study. SM, KY, and XL performed the experiments, analyzed the data, and prepared the first draft of the manuscript. WY, KY, YG, ST, YX, PW, YS, JS, and LL revised the manuscript. All the authors have read and approved the final version of the manuscript.

FUNDING

This work was supported in part by the National Natural Science Foundation of China (Nos. 81901352, 81821092, 81871046, 31800897, 82001404 and 81722018) and Clinic Medicine + X Fund of PKUHSC (No. PKU2020LCXQ016).

REFERENCES

Alexander, B. K., Beyerstein, B. L., Hadaway, P. F., and Coambs, R. B. (1981). Effect of Early and Later colony Housing on Oral Ingestion of Morphine in Rats. *Pharmacol. Biochem. Behav.* 15 (4), 571–576. doi:10.1016/0091-3057(81)90211-2

Anacker, A. M., Loftis, J. M., Kaur, S., and Ryabinin, A. E. (2011). Prairie Voles as a Novel Model of Socially Facilitated Excessive Drinking. *Addict. Biol.* 16 (1), 92–107. doi:10.1111/j.1369-1600.2010.00234.x

Bahr, S. J., Hoffmann, J. P., and Yang, X. (2005). Parental and Peer Influences on the Risk of Adolescent Drug Use. *J. Prim. Prev.* 26 (6), 529–551. doi:10.1007/s10935-005-0014-8

Bathish, R., Best, D., Savic, M., Beckwith, M., Mackenzie, J., and Lubman, D. I. (2017). "Is it Me or Should My Friends Take the Credit?" the Role of Social Networks and Social Identity in Recovery from Addiction. *J. Appl. Soc. Psychol.* 47 (1), 35–46. doi:10.1111/jasp.12420

Brandon, T. H., Vidrine, J. I., and Litvin, E. B. (2007). Relapse and Relapse Prevention. *Annu. Rev. Clin. Psychol.* 3, 257–284. doi:10.1146/annurev.clinpsy.3.022806.091455

Caudill, B. D., and Kong, F. H. (2001). Social Approval and Facilitation in Predicting Modeling Effects in Alcohol Consumption. *J. Subst. Abuse* 13 (4), 425–441. doi:10.1016/s0899-3289(01)00099-2

Caudill, B. D., and Marlatt, G. A. (1975). Modeling Influences in Social Drinking: an Experimental Analogue. *J. Consult Clin. Psychol.* 43 (3), 405–415. doi:10.1037/h0076689

Davachi, L. (2006). Item, Context and Relational Episodic Encoding in Humans. *Curr. Opin. Neurobiol.* 16 (6), 693–700. doi:10.1016/j.conb.2006.10.012

Deatherage, G. (1972). Effects of Housing Density on Alcohol Intake in the Rat. *Physiol. Behav.* 9 (1), 55–57. doi:10.1016/0031-9384(72)90264-8

Doty, P., and de Wit, H. (1995). Effect of Setting on the Reinforcing and Subjective Effects of Ethanol in Social Drinkers. *Psychopharmacology (Berl)* 118 (1), 19–27. doi:10.1007/BF02245245

Frings, D., Wood, K. V., and Albery, I. P. (2021). New Converts and Seasoned Campaigners: the Role of Social Identity at Different Stages in the Addiction Recovery Journey. *Drugs Educ. Prev. Pol.*, 1–8. doi:10.1080/09687637.2021.1914551

Garrido Zinn, C., Clairis, N., Silva Cavalcante, L. E., Furini, C. R., de Carvalho Myskiw, J., and Izquierdo, I. (2016). Major Neurotransmitter Systems in Dorsal hippocampus and Basolateral Amygdala Control Social Recognition Memory. *Proc. Natl. Acad. Sci. U S A.* 113 (33), E4914–E4919. doi:10.1073/pnas.1609883113

Goldfarb, E. V., and Sinha, R. (2018). Drug-induced Glucocorticoids and Memory for Substance Use. *Trends Neurosci.* 41 (11), 853–868. doi:10.1016/j.tins.2018.08.005

Gur, R., Tendler, A., and Wagner, S. (2014). Long-term Social Recognition Memory Is Mediated by Oxytocin-dependent Synaptic Plasticity in the Medial Amygdala. *Biol. Psychiatry* 76 (5), 377–386. doi:10.1016/j.biopsych.2014.03.022

Hadaway, P. F., Alexander, B. K., Coambs, R. B., and Beyerstein, B. (1979). The Effect of Housing and Gender on Preference for Morphine-Sucrose Solutions in Rats. *Psychopharmacology (Berl)* 66 (1), 87–91. doi:10.1007/BF00431995

Heilig, M., Epstein, D. H., Nader, M. A., and Shaham, Y. (2016). Time to Connect: Bringing Social Context into Addiction Neuroscience. *Nat. Rev. Neurosci.* 17 (9), 592–599. doi:10.1038/nrn.2016.67

Hostetler, C. M., Anacker, A. M., Loftis, J. M., and Ryabinin, A. E. (2012). Social Housing and Alcohol Drinking in Male-Female Pairs of Prairie Voles (Microtus Ochrogaster). *Psychopharmacology (Berl)* 224 (1), 121–132. doi:10.1007/s00213-012-2836-4

Insel, T. R., and Fernald, R. D. (2004). How the Brain Processes Social Information: Searching for the Social Brain. *Annu. Rev. Neurosci.* 27, 697–722. doi:10.1146/annurev.neuro.27.070203.144148

Kas, M. J., Modi, M. E., Saxe, M. D., and Smith, D. G. (2014). Advancing the Discovery of Medications for Autism Spectrum Disorder Using New Technologies to Reveal Social Brain Circuitry in Rodents. *Psychopharmacology (Berl)* 231 (6), 1147–1165. doi:10.1007/s00213-014-3464-y

Kelly, J. F., Hoeppner, B., Stout, R. L., and Pagano, M. (2012). Determining the Relative Importance of the Mechanisms of Behavior Change within Alcoholics Anonymous: a Multiple Mediator Analysis. *Addiction* 107 (2), 289–299. doi:10.1111/j.1360-0443.2011.03593.x

Kirkpatrick, M. G., and de Wit, H. (2013). In the Company of Others: Social Factors Alter Acute Alcohol Effects. *Psychopharmacology (Berl)* 230 (2), 215–226. doi:10.1007/s00213-013-3147-0

Koordeman, R., Kuntsche, E., Anschutz, D. J., van Baaren, R. B., and Engels, R. C. (2011). Do we Act upon what We See? Direct Effects of Alcohol Cues in Movies on Young Adult's Alcohol Drinking. *Alcohol Alcohol* 46 (4), 393–398. doi:10.1093/alcalc/agr028

Larsen, H., Engels, R. C., Souren, P. M., Granic, I., and Overbeek, G. (2010). Peer Influence in a Micro-perspective: Imitation of Alcoholic and Non-alcoholic Beverages. *Addict. Behav.* 35 (1), 49–52. doi:10.1016/j.addbeh.2009.08.002

Li, L., Lin, C., Wan, D., Zhang, L., and Lai, W. (2012). Concurrent Heroin Use Among Methadone Maintenance Clients in China. *Addict. Behav.* 37 (3), 264–268. doi:10.1016/j.addbeh.2011.11.004

Lied, E. R., and Marlatt, G. A. (1979). Modeling as a Determinant of Alcohol Consumption: Effect of Subject Sex and Prior Drinking History. *Addict. Behav.* 4 (1), 47–54. doi:10.1016/0306-4603(79)90020-0

Luo, Y. X., Xue, Y. X., Liu, J. F., Shi, H. S., Jian, M., Han, Y., et al. (2015). A Novel UCS Memory Retrieval-Extinction Procedure to Inhibit Relapse to Drug Seeking. *Nat. Commun.* 6, 7675. doi:10.1038/ncomms8675

Marcondes, L. A., Nachtigall, E. G., Zanluchi, A., de Carvalho Myskiw, J., Izquierdo, I., and Furini, C. R. G. (2020). Involvement of Medial Prefrontal Cortex NMDA and AMPA/kainate Glutamate Receptors in Social Recognition Memory Consolidation. *Neurobiol. Learn. Mem.* 168, 107153. doi:10.1016/j.nlm.2019.107153

Miller, C. A., and Marshall, J. F. (2005). Altered Fos Expression in Neural Pathways Underlying Cue-Elicited Drug Seeking in the Rat. *Eur. J. Neurosci.* 21 (5), 1385–1393. doi:10.1111/j.1460-9568.2005.03974.x

Molenberghs, P., Cunnington, R., and Mattingley, J. B. (2009). Is the Mirror Neuron System Involved in Imitation? A Short Review and Meta-Analysis. *Neurosci. Biobehav Rev.* 33 (7), 975–980. doi:10.1016/j.neubiorev.2009.03.010

Neisewander, J. L., Peartree, N. A., and Pentkowski, N. S. (2012). Emotional Valence and Context of Social Influences on Drug Abuse-Related Behavior in Animal Models of Social Stress and Prosocial Interaction. *Psychopharmacology (Berl)* 224 (1), 33–56. doi:10.1007/s00213-012-2853-3

Peitz, G. W., Strickland, J. C., Pitts, E. G., Foley, M., Tonidandel, S., and Smith, M. A. (2013). Peer Influences on Drug Self-Administration: an Econometric Analysis in Socially Housed Rats. *Behav. Pharmacol.* 24 (2), 114–123. doi:10.1097/FBP.0b013e32835f1719

Perry, A., Saunders, S. N., Stiso, J., Dewar, C., Lubell, J., Meling, T. R., et al. (2017). Effects of Prefrontal Cortex Damage on Emotion Understanding: EEG and Behavioural Evidence. *Brain* 140 (4), 1086–1099. doi:10.1093/brain/awx031

Pohorecky, L. A. (2008). Psychosocial Stress and Chronic Ethanol Ingestion in Male Rats: Effects on Elevated Plus Maze Behavior and Ultrasonic Vocalizations. *Physiol. Behav.* 94 (3), 432–447. doi:10.1016/j.physbeh.2008.02.010

Raz, S., and Berger, B. D. (2010). Social Isolation Increases Morphine Intake: Behavioral and Psychopharmacological Aspects. *Behav. Pharmacol.* 21 (1), 39–46. doi:10.1097/FBP.0b013e32833470bd

Ribeiro Do Couto, B., Aguilar, M. A., Lluch, J., Rodríguez-Arias, M., and Miñarro, J. (2009). Social Experiences Affect Reinstatement of Cocaine-Induced Place Preference in Mice. *Psychopharmacology (Berl)* 207 (3), 485–498. doi:10.1007/s00213-009-1678-1

Rizzolatti, G., and Craighero, L. (2004). The Mirror-Neuron System. *Annu. Rev. Neurosci.* 27, 169–192. doi:10.1146/annurev.neuro.27.070203.144230

Rizzolatti, G., Fadiga, L., Fogassi, L., and Gallese, V. (1999). Resonance Behaviors and Mirror Neurons. *Arch. Ital. Biol.* 137 (2-3), 85–100. doi:10.4449/aib.v137i2.575

Salchner, P., Lubec, G., and Singewald, N. (2004). Decreased Social Interaction in Aged Rats May Not Reflect Changes in Anxiety-Related Behaviour. *Behav. Brain Res.* 151 (1-2), 1–8. doi:10.1016/j.bbr.2003.07.002

Simons-Morton, B., and Chen, R. S. (2006). Over Time Relationships between Early Adolescent and Peer Substance Use. *Addict. Behav.* 31 (7), 1211–1223. doi:10.1016/j.addbeh.2005.09.006

Sinha, R. (2011). New Findings on Biological Factors Predicting Addiction Relapse Vulnerability. *Curr. Psychiatry Rep.* 13 (5), 398–405. doi:10.1007/s11920-011-0224-0

Smith, M. A., and Pitts, E. G. (2014). Social Preference and Drug Self-Administration: a Preclinical Model of Social Choice within Peer Groups. *Drug Alcohol Depend* 135, 140–145. doi:10.1016/j.drugalcdep.2013.12.001

Smith, M. A., Strickland, J. C., Bills, S. E., and Lacy, R. T. (2015). The Effects of a Shared History of Drug Exposure on Social Choice. *Behav. Pharmacol.* 26 (7 Spec No), 631–635. doi:10.1097/FBP.0000000000000139

Thomas, K. L., Arroyo, M., and Everitt, B. J. (2003). Induction of the Learning and Plasticity-Associated Gene Zif268 Following Exposure to a Discrete Cocaine-Associated Stimulus. *Eur. J. Neurosci.* 17 (9), 1964–1972. doi:10.1046/j.1460-9568.2003.02617.x

Venniro, M., Zhang, M., Caprioli, D., Hoots, J. K., Golden, S. A., Heins, C., et al. (2018). Volitional Social Interaction Prevents Drug Addiction in Rat Models. *Nat. Neurosci.* 21 (11), 1520–1529. doi:10.1038/s41593-018-0246-6

Volkow, N. D., and Boyle, M. (2018). Neuroscience of Addiction: Relevance to Prevention and Treatment. *Am. J. Psychiatry* 175 (8), 729–740. doi:10.1176/appi.ajp.2018.17101174

Walden, B., McGue, M., Lacono, W. G., Burt, S. A., and Elkins, I. (2004). Identifying Shared Environmental Contributions to Early Substance Use: the Respective Roles of Peers and Parents. *J. Abnorm Psychol.* 113 (3), 440–450. doi:10.1037/0021-843X.113.3.440

Weisinger, R. S., Denton, D. A., and Osborne, P. G. (1989). Voluntary Ethanol Intake of Individually- or Pair-Housed Rats: Effect of ACTH or Dexamethasone Treatment. *Pharmacol. Biochem. Behav.* 33 (2), 335–341. doi:10.1016/0091-3057(89)90510-8

Wolffgramm, J. (1990). Free Choice Ethanol Intake of Laboratory Rats under Different Social Conditions. *Psychopharmacology (Berl)* 101 (2), 233–239. doi:10.1007/BF02244132

Wolffgramm, J., and Heyne, A. (1991). Social Behavior, Dominance, and Social Deprivation of Rats Determine Drug Choice. *Pharmacol. Biochem. Behav.* 38 (2), 389–399. doi:10.1016/0091-3057(91)90297-f

Xue, Y. X., Luo, Y. X., Wu, P., Shi, H. S., Xue, L. F., Chen, C., et al. (2012). A Memory Retrieval-Extinction Procedure to Prevent Drug Craving and Relapse. *Science* 336 (6078), 241–245. doi:10.1126/science.1215070

Conflict of Interest: The authors declare that the research was conducted in the absence of any commercial or financial relationships that could be construed as a potential conflict of interest.

Publisher's Note: All claims expressed in this article are solely those of the authors and do not necessarily represent those of their affiliated organizations, or those of the publisher, the editors and the reviewers. Any product that may be evaluated in this article, or claim that may be made by its manufacturer, is not guaranteed or endorsed by the publisher.

frontiers in Pharmacology

ORIGINAL RESEARCH
published: 29 October 2021
doi: 10.3389/fphar.2021.756822

Krill Oil Alleviated Methamphetamine-Induced Memory Impairment *via* the MAPK Signaling Pathway and Dopaminergic Synapse Pathway

Qin Ru[1], *Xiang Tian*[1], *Qi Xiong*[1], *Congyue Xu*[1], *Lin Chen*[2]* *and Yuxiang Wu*[2]*

[1]*Wuhan Institutes of Biomedical Sciences, School of Medicine, Jianghan University, Wuhan, China,* [2]*Department of Health and Physical Education, Jianghan University, Wuhan, China*

OPEN ACCESS

Edited by:
Qi Wang,
Southern Medical University, China

Reviewed by:
Hongying Du,
Huazhong Agricultural University, China
Weibing Xie,
Southern Medical University, China

***Correspondence:**
Yuxiang Wu
yxwu@jhun.edu.cn
Lin Chen
hdycl@126.com

Specialty section:
This article was submitted to Neuropharmacology, a section of the journal Frontiers in Pharmacology

Received: *11 August 2021*
Accepted: *15 September 2021*
Published: *29 October 2021*

Citation:
Ru Q, Tian X, Xiong Q, Xu C, Chen L and Wu Y (2021) Krill Oil Alleviated Methamphetamine-Induced Memory Impairment via the MAPK Signaling Pathway and Dopaminergic Synapse Pathway. Front. Pharmacol. 12:756822. doi: 10.3389/fphar.2021.756822

Methamphetamine (METH) abuse exerts severe harmful effects in multiple organs, especially the brain, and can induce cognitive dysfunction and memory deficits in humans. Krill oil is rich in polyunsaturated fatty acids, while its effect on METH-induced cognitive impairment and mental disorders, and the underlying mechanism remain unknown. The aim of the present study was to investigate the protective effect of krill oil on METH-induced memory deficits and to explore the molecular mechanisms by using an integrated strategy of bioinformatics analysis and experimental verification. METH-exposed mice were treated with or without krill oil. Learning and memory functions were evaluated by the Morris water maze. The drug–component–target network was constructed in combination with network pharmacology. The predicted hub genes and pathways were validated by the Western blot technique. With krill oil treatment, memory impairment induced by METH was significantly improved. 210 predicted targets constituted the drug–compound–target network by network pharmacology analysis. 20 hub genes such as DRD2, MAPK3, CREB, BDNF, and caspase-3 were filtered out as the underlying mechanisms of krill oil on improving memory deficits induced by METH. The KEGG pathway and GO enrichment analyses showed that the MAPK signaling pathway, cAMP signaling pathway, and dopaminergic synapse pathway were involved in the neuroprotective effects of krill oil. In the hippocampus, DRD2, cleaved caspase-3, and γ-H2AX expression levels were significantly increased in the METH group but decreased in the krill oil–treated group. Meanwhile, krill oil enhanced the expressions of p-PKA, p-ERK1/2, and p-CREB. Our findings suggested that krill oil improved METH-induced memory deficits, and this effect may occur *via* the MAPK signaling pathway and dopaminergic synapse pathways. The combination of network pharmacology approaches with experimental validation may offer a useful tool to characterize the molecular mechanism of multicomponent complexes.

Keywords: krill oil, methamphetamine, memory deficits, network pharmacology, hippocampus

INTRODUCTION

As one of the most commonly abused psychostimulants in the world (Siefried et al., 2020), methamphetamine (METH) abuse results in various severe complications systemically affecting multiple organs, especially the brain (Casaletto et al., 2015; Huang et al., 2019). METH addiction can induce neurodegenerative changes in the hippocampus and frontal cortex, which are all related to long-term cognitive dysfunction and memory deficits in humans (Casaletto et al., 2015; Chen et al., 2015; Wang et al., 2018). Long-term METH addiction reduces the abusers' awareness of memory impairment, and overestimation of memory further exacerbates their executive dysfunction (Casaletto et al., 2015). It is important to note that neurocognitive deficits did not just occur in people who are currently abusing METH but has also been found in those who have stopped taking METH for an extended period of time (Cherner et al., 2010; Silva et al., 2014). In line with these clinical investigations, several studies in animal models also have documented that repeated METH administration could essentially affect different brain areas including the frontal cortex and hippocampus, which are all associated with cognitive and memory function (Fan et al., 2020; Golsorkhdan et al., 2020; Lwin et al., 2020; Veschsanit et al., 2021). However, the potential mechanism of cognitive dysfunction induced by METH is unclear. A deep understanding of its mechanism may provide more valuable ideas for the treatment of METH addiction and its induced mental disorders.

Krill oil is extracted from the Antarctic microcrustacean *Euphausia superba*, and is a rich source of astaxanthin, and (n-3)/polyunsaturated fatty acids (PUFAs), including eicosapentaenoic acid (EPA) and docosahexaenoic acid (DHA) (Alvarez-Ricartes et al., 2018). Due to the high presence of astaxanthin, EPA, and DHA, krill oil has been reported to have positive effects on cardiovascular disease, insulin resistance, lipid and glucose metabolism, and neurocognitive impairment in various animal experiments (Cheong et al., 2017; Sun et al., 2017; Tome-Carneiro et al., 2018). As a food supplement, krill oil has great bioavailability (Sun et al., 2017) and has become popular with some pilot trials and randomized controlled trials indicating healthy benefits. For instance, krill oil could reduce the plasma triacylglycerol level and improves the related lipoprotein particle concentration, fatty acid composition, and redox status in healthy young adults (Berge et al., 2015). Krill oil could modestly improve cardiovascular risk in patients with type 2 diabetes, and krill oil supplementation may lead to a small but significant increase in the mean omega-3 index (Lobraico et al., 2015; van der Wurff et al., 2019; van der Wurff et al., 2020). Krill oil could also activate cognitive function in the elderly and is more effective than sardine oil in the working memory task (Konagai et al., 2013). However, despite the several studies conducted to show the beneficial effects of krill oil on neurocognitive function, the precise mechanism of krill oil on neurocognitive dysfunction in the central nervous system has rarely been reported.

Our previously published study showed that krill oil alleviated oxidative stress and apoptosis induced by METH *in vitro* (Xiong et al., 2018). Therefore, the aim of the present study was to evaluate the protective potential of krill oil in mice subjected to chronic METH exposure *in vivo*. Network pharmacology is an excellent approach for the study of multicomponent compounds through multi-target and multi-pathway therapeutic mechanisms. Therefore, after the behavioral test, network pharmacological tools and resources were used to screen the potential targets and pathways of major active components of krill oil and to reveal their mechanism of action in the treatment of METH-induced memory impairment. In addition, experiments were also conducted to validate the potential underlying mechanism of krill oil on METH-induced memory impairment, as predicted by the network pharmacology approach.

MATERIALS AND METHODS

Reagents

METH (98%) was offered by the Hubei Public Security Bureau. Krill oil was provided by the Aker BioMarine Antarctic Company (Norway). Antibodies against protein kinase A (PKA), phosphorylated protein kinase A (p-PKA), cAMP-response element-binding protein (CREB), phosphorylated CREB (p-CREB), extracellular regulated protein kinase 1/2 (ERK1/2), and phosphorylated ERK1/2 (p-ERK1/2) were bought from Cell Signaling Technology (Danvers, United States). Antibodies against the dopamine D1 receptor (DRD1), dopamine D2 receptor (DRD2), dopamine transporter (DAT), and cleaved caspase-3 were obtained from Absin Bioscience Co., Ltd. (Shanghai, China). Antibodies against GAPDH, horseradish peroxides (HRP)-conjugated goat anti-rabbit antibody and HRP-conjugated goat anti-mouse antibody, protein extraction buffer, protease inhibitors, and phosphatase inhibitors were obtained from Wuhan Boster Biological Technology Co., Ltd. (Wuhan, China). Antibodies against the brain-derived neurotrophic factor (BDNF) were purchased from Santa Cruz Biotechnology (Santa Cruz, United States). All other reagents used were of analytical grade.

Animal Treatment

C57BL/6 mice (male, 8 weeks) were provided by Beijing Vital River Laboratory Animal Technology Co., Ltd. Mice were housed five per cage in a 12-h light–dark cycle and a temperature-controlled environment. All animal experiment procedures were approved by the Ethics Committee of Jianghan University. Specifically, mice were divided randomly into the control group, METH group, krill oil-L group and krill oil-H group, and the experimental procedure is detailed in **Figure 1A**. Before administration, krill oil was dissolved in ethanol and then diluted with saline, and METH was dissolved in saline at a concentration of 10 mg/ml. For the first 2 weeks, mice in the krill oil-L group and krill oil-H group were intragastrically administrated with 10 mg/kg and 100 mg/kg krill oil every day, respectively, and mice in the control group and METH group were intragastrically administrated with vehicle. At the third week, 1 hour after intragastric administration, mice in the METH, krill oil-L group, and krill oil-H group were intraperitoneally injected with 10 mg/kg METH, and mice in

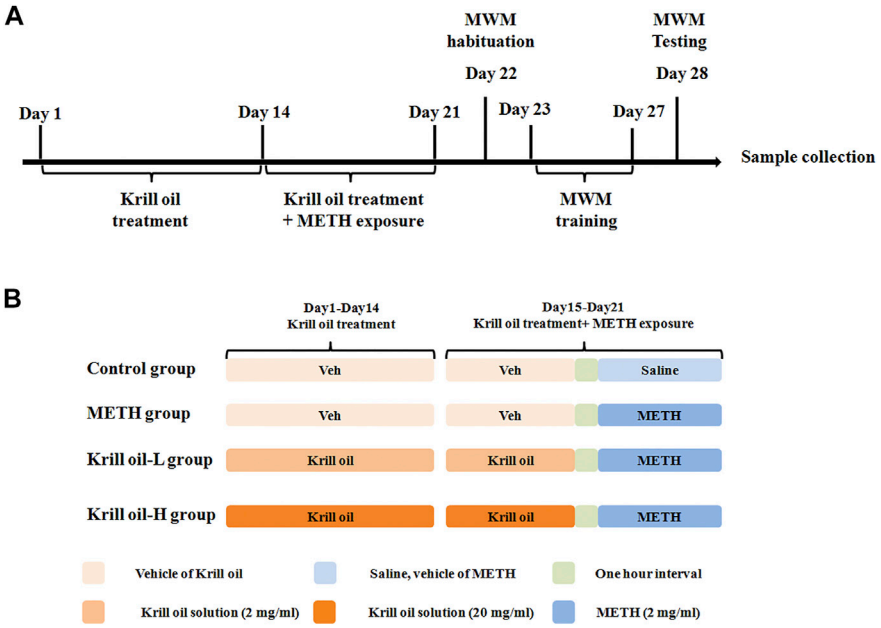

FIGURE 1 | Experimental procedure of krill oil–ameliorated memory deficits induced by METH. **(A)** For the first 3 weeks, mice were administrated with different doses of krill oil with or without METH. After that, the behavioral tests and Western blotting experiments were performed. **(B)** Drug treatment of the animal experiment. For the first 2 weeks, mice were intragastrically administrated with different doses of krill oil or vehicle. At the third week, 1 h after the intragastric administration, mice were intraperitoneally injected with METH or saline.

the control group were intraperitoneally injected with saline. Behavioral experiments, sample collection, and the Western blot test were performed as follows (**Figure 1**).

Morris Water Maze Task

Memory training on the hidden platform of the Morris water maze was used to measure the associative, spatial memory of mice as a previous report. Briefly, water (23 ± 2°C) was added into a circular pool (21 cm in deep and 120 cm in diameter). A circular hidden platform was placed in the center of the target quadrant and submerged 1.5 cm below the water surface. XR-XM101 software was used to automatically measure the animal escape latency, swimming speed, and the amount of time spent in the target quadrant (Shanghai Xinruan Information Technology Co., Ltd.). Mice underwent four trials each day during the training phase, and the starting position of each trial was different. Mice have a maximum of 60 s in each trial to find the platform, and mice were allowed to stay on the platform for 15 s after boarding the platform. If the mice cannot find the platform within 60 s, it was guided to the platform to rest for 15 s. The time interval between trials was 30 min. Mice were dried with a towel, placed in a cage with a heating lamp, and then returned to their home cage after the last trial. The training phase lasted for 5 days. To test the spatial memory ability of mice, a 60-s free swimming test without a platform was performed on the sixth day.

Network Pharmacology Analysis

The potential protein targets of krill oil, related genes of METH, and related genes of memory deficits were collected from the GeneCards database (https://www.genecards.org/). Then, the protein targets of krill oil were mapped with related genes of METH and related genes of memory impairment on the Bioinformatics and Evolutionary Genomics website (http://bioinformatics.psb.ugent.be/webtools/Venn/). To further characterize the molecular mechanism of krill oil on METH-induced memory deficits, the compound–target networks were generated using Cytoscape 3.8.0. In these graphical networks, the compounds and proteins were expressed as nodes, whereas the compound–target interactions were expressed as edges.

The gene ontology (GO) analyses and KEGG pathway analyses were conducted using the functional annotation tool of DAVID Bioinformatics Resources 6.7 (http://david.abcc.ncifcrf.gov/). Terms with thresholds of counts ≥ 10 and p values ≤ 0.05 were chosen in functional annotation clustering. Related target proteins of krill oil on METH-induced memory deficits were analyzed by online STRING 11.0 (https://string-db.org/) to construct a protein–protein interaction (PPI) network. The network was visualized with Cytoscape (v3.1.2) and CytoHubba, a plug-in in Cytoscape, to filter the modules from the PPI network and to obtain the most important hub genes based on the degree score.

Western Blotting Analysis

Hippocampi were isolated, lysed, and centrifuged for 15 min (4°C) at 12,000 g . After the detection of concentration, the supernatants were mixed with a loading buffer and denatured for 5 min. Protein samples were separated using a gel electrophoresis system and transferred to the polyethylene difluoride membranes. After blocking for 1 h in 5% non-fat

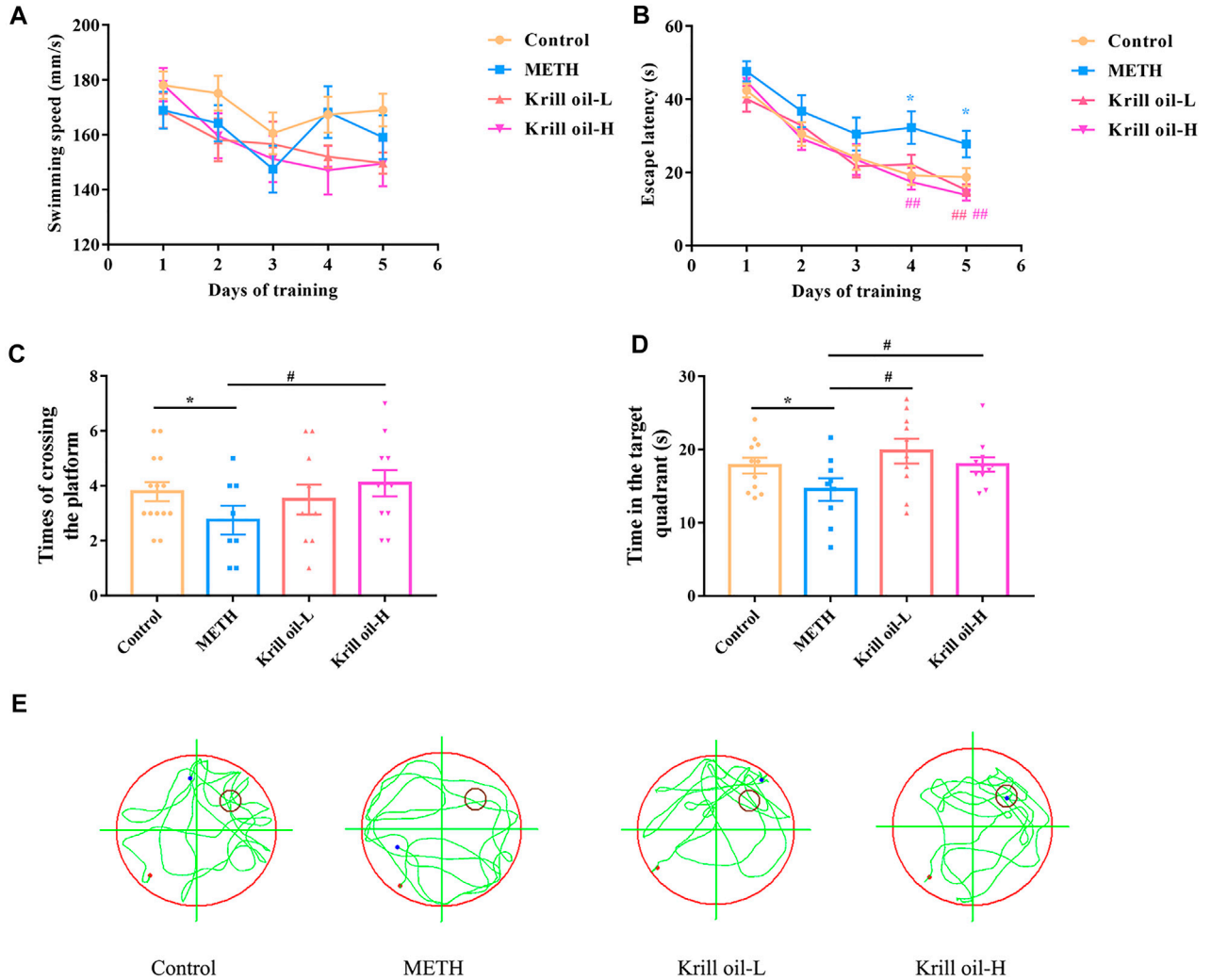

FIGURE 2 | Krill oil–ameliorated impairment of spatial learning and memory induced by METH in the MWM task. **(A)** Swimming speed of each group during the training session. The Morris water maze test was conducted to evaluate spatial learning and memory function. **(B)** Acquisition of spatial memory in mice. The escape latency during the training phase was shown. **(C)** Retention of spatial memory in mice. Times of crossing the platform of mice were shown. **(D)** Retention of spatial memory in mice. The time in the target quadrant of mice was shown. **(E)** Representative swimming trajectories of Morris water maze testing. $n = 10$ for each group, and data were presented by means ± SEM, $^{*}p < 0.05$, $^{**}p < 0.01$ compared to the control group, and $\#p < 0.05$, $\#\#p < 0.01$ compared to the METH group.

milk, the membranes were incubated with the primary antibody and then with the HRP secondary antibody. Enhanced chemiluminescence (Thermo Fisher, United States) was used to observe the bands using a chemiluminescence detector (Gene Corporation, Hong Kong). The intensity of each band was determined quantitatively by ImageJ and calibrated by the corresponding internal reference protein, and the results were shown as normalized for the control group.

Statistical Analysis

Data were expressed as the mean ± standard error (SEM). All results were analyzed using SPSS 23.0 software. Results of the swimming speed and escape latency during the training phase of MWM were analyzed by one-way ANOVA with repeated measures. Other data used one-way ANOVA and Tukey's HSD *post hoc* test. A p value less than 0.05 was considered statistically significant.

RESULTS

Krill Oil Ameliorated the Impairment of Spatial Learning and Memory Induced by METH in MWM Task

The Morris water maze test was used to determine whether krill oil alleviated METH-induced spatial learning and memory impairment. As shown in **Figure 2**, the locomotor activity of mice was not influenced by METH or krill oil treatment since the swimming speed did not differ among the groups (**Figure 2A**).

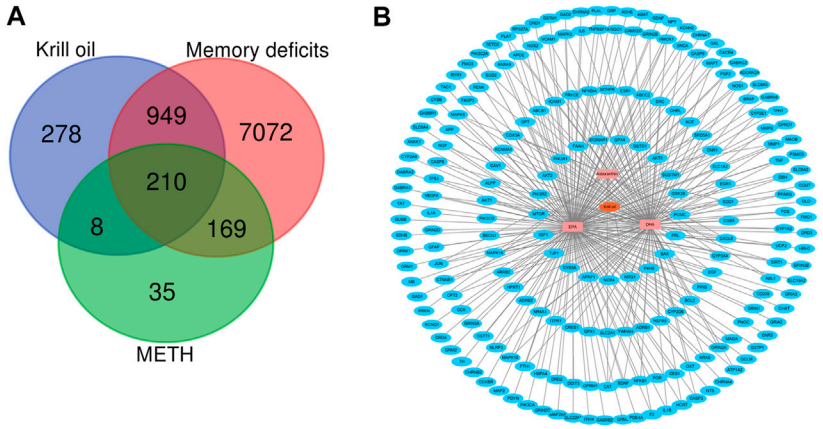

FIGURE 3 | Compound–target network for krill oil on METH-induced memory deficits. **(A)** Venn plot for the possible targets of main compounds of krill oil and related genes of METH and memory deficits. **(B)** Network of active compounds and the possible targets for krill oil on METH-induced memory deficits. The orange polygon represented krill oil. The pink squares represented active compounds of krill oil and the blue circle represented potential protein targets. The edges represent the interactions between them.

Mice in the METH group had a higher escape latency than those in the control group on day 4 and day 5 of the training phase (**Figure 2B**), suggesting that repeated METH exposure triggered a decline in the spatial learning ability of mice ($p < 0.05$). Moreover, compared with the METH group, 10 mg/kg krill oil treatment greatly reduced the increase of learning latency in mice induced by METH on day 5 ($p < 0.01$), and mice pretreated with 100 mg/kg of krill oil performed significantly better than those that received METH alone on day 4 and day 5 ($p < 0.01$), suggesting that learning deficits were improved following krill oil treatment. In the testing section, results revealed significant differences among group effects (**Figures 2C,D**, $p < 0.05$). Mice in the METH group had worse performance in the parameter of times of crossing the platform and time in the quadrant of the platform than those of the control group ($p < 0.05$). Treatment with krill oil (10 or 100 mg/kg), however, remarkably increased the times of crossing the platform and the time in the quadrant of the platform ($p < 0.05$). The swimming trajectory further confirmed that the krill oil–treated mice stayed in the target quadrant longer than the METH group (**Figure 2E**). Taken together, these findings demonstrated that krill oil improved METH-induced cognitive deficits of spatial learning and memory.

Target Identification of Krill Oil on METH-Induced Memory Deficits

Krill oil from *Euphausia superba* (Antarctic krill), an Antarctic marine species, is rich in EPA, DHA, and astaxanthin. Among the three main bioactive components of krill oil, 1,846 protein targets were retrieved from the GeneCards database. The detailed information is shown in **Supplementary Table S1**. After eliminating the overlaps, 1,445 protein targets were obtained for further analyses. 8400 memory deficit–related genes and 422 METH-related genes were collected from the GeneCards database. The detailed information is shown in **Supplementary Tables S2, and S3**. Then, these protein targets of krill oil were mapped with related genes of METH and memory impairment on the Bioinformatics and Evolutionary Genomics website. As a result, 210 targets of krill oil were associated with METH-induced memory impairment, and the detailed information of the 210 targets is shown in **Supplementary Table S4** and **Figure 3A**. Among the 210 target genes, 116 were target genes for DHA, 174 were target genes for EPA, and 16 were target genes for astaxanthin. The detailed information is shown in **Supplementary Table S5** and **Supplementary Figure S1**.

As krill oil may exhibit multiple pharmacological activities *via* multiple targets, it was constructive to investigate the underlying mechanisms of krill oil on complex diseases by network analysis. In the current study, the compound–target network of krill oil on METH-induced memory deficits was constructed with Cytoscape 3.8.1 software (**Figure 3B**). Among these potential protein targets, there were 12 high-degree targets associated with multiple compounds (**Supplementary Figure S1**), namely, NFKBIA, COX5A, MAPK14, HMOX1, NOS2, MAPK8, JUN, CAT, MMP1, CYP3A4, CXCL8, and SOD1. These high-degree protein targets in the network may account for the essential protective effects of krill oil on METH-induced memory impairment.

GO and Pathway Enrichment Analyses

To identify the biological characteristics of putative targets of krill oil on METH-induced memory impairment in detail, the GO and KEGG pathway enrichment analyses of involved targets were conducted *via* the functional annotation tool of DAVID Bioinformatics Resources 6.8. There were 78 biological processes (BP), 46 cellular components (CC), and 23 molecular function (MF) terms in total, which met the requirements of counts ≥ 10 and p values ≤ 0.05. The detailed GO information is shown in **Supplementary Table S6**. The top 15 significantly enriched terms in BP, CC, and MF categories are shown in **Figure 4A**, which indicated that krill oil may improve METH-induced memory impairment *via* regulation of the neuron apoptotic

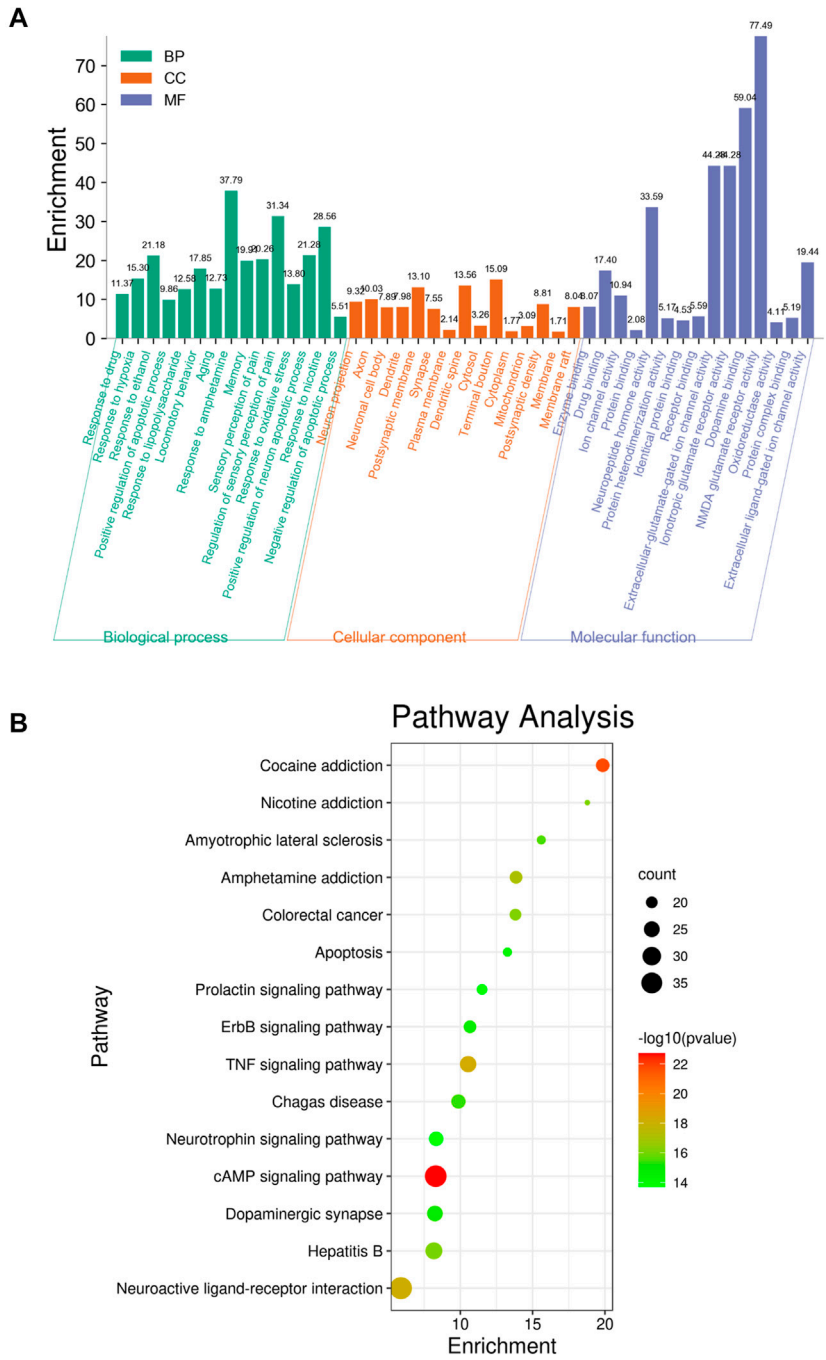

FIGURE 4 | Top 15 significantly enriched terms gene ontology **(A)** and pathway enrichment **(B)** analyses of potential target genes of krill oil on METH-induced memory deficits.

process, response to oxidative stress, response to hypoxia, dopamine binding, NMDA glutamate receptor activity, and oxidoreductase activity. To explore the underlying involved pathways of krill oil on METH-induced memory impairment, a KEGG pathway analysis of involved targets was conducted. The detailed pathway information of krill oil on METH-induced memory impairment is shown in **Supplementary Table S7**. There were 94 pathways that met the requirements of counts ≥ 10 and p values ≤ 0.05. The top 15 significantly enriched pathways are shown in **Figure 4B**. The pathways in neuroactive ligand–receptor interaction exhibited the largest number of involved targets (38 counts).

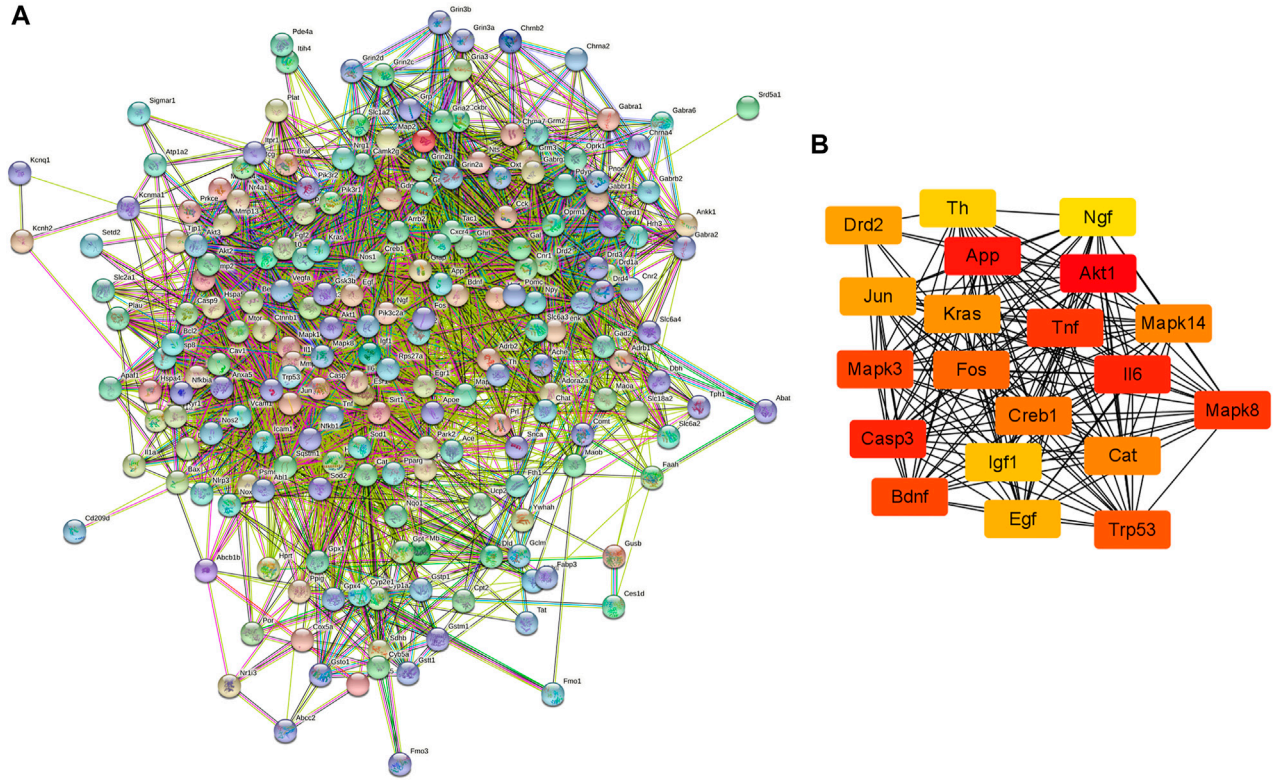

FIGURE 5 | PPI network of the potential target genes and hub genes screen. **(A)** The PPI network of the potential target genes was constructed using STRING. **(B)** The most significant hub genes were obtained from the PPI network using Cytoscape and CytoHubba.

Screen of Hub Genes

The PPI network of possible target genes involved in the protective effect of krill oil on METH-induced memory impairment was constructed using STRING (**Figure 5A**).

There were 205 nodes and 3,388 edges, and the average node degree was 33.1. The average local clustering coefficient was 0.565, and the *p* value of PPI enrichment was less than 1.0e-16. To obtain the hub genes in the PPI network, these node pairs were entered into Cytoscape software. The scores of nodes were calculated by CytoHubba, and the top 20 hub genes are shown in **Figure 5B**, and the hub gene symbols, full names, and functions are shown in **Table 1**. The pathway enrichment analyses of hub genes were conducted *via* DAVID Bioinformatics Resources 6.8. There were 54 pathways that met the requirements of count ≥ 5 and *p* values ≤ 0.05. The detailed pathway information of hub genes is shown in **Supplementary Table S8**. The top 25 significantly enriched pathways are shown in **Figure 6A** and **Table 2**. The compound–hub gene–pathway network of krill oil on METH-induced memory deficits was constructed with Cytoscape 3.8.1 software (**Figure 6B**).

The pathways in the MAPK signaling pathway exhibited the largest number of involved targets (13 counts). Among the 20 hub genes, 17 were target genes for DHA, 17 were target genes for EPA, and 4 were target genes for astaxanthin. The detailed information is shown in **Supplementary Table S9** and **Supplementary Figure S2**.

Expression Levels of Hub Genes in the Hippocampus of Mice

Network pharmacology analysis predicted that the molecular targets highly associated with the common signaling pathways including the MAPK signaling pathway, dopaminergic synapse, and cAMP signaling pathway may be related to the neuroprotective effect of krill oil on METH-induced memory impairment in regulating neuron functions and apoptosis. We further validated the expressions of the potential hub genes identified *via* network pharmacology. As shown in **Figures 7A and B**, compared with the control group, the expression of DRD2 in the hippocampus of mice in the METH group was greatly increased and the expression of DAT was decreased, and 100 mg/kg krill oil treatment significantly decreased the expression of DRD2 and increased the expression of DAT, while 10 mg/kg krill oil treatment significantly decreased the expression of DRD2. There was no significant difference of the expression of DRD1 among different groups. Likewise, METH treatment led to apparent repression of p-PKA, p-ERK1/2, p-CREB, and BDNF (**Figures 7A,C–F**), and 10 and 100 mg/kg krill oil treatment significantly increased the expression of

TABLE 1 | Detail information of hub genes involved in the neuroprotective effect of krill oil on METH-induced memory impairment.

Hub gene symbol	Full names	Functions	Degree
AKT1	RAC-alpha serine/threonine-protein kinase	Regulates many processes including metabolism, proliferation, cell survival, growth, and angiogenesis	117
APP	Amyloid-beta precursor protein	A cell surface receptor and performs physiological functions on the surface of neurons relevant to neurite growth, neuronal adhesion, and axonogenesis	95
IL6	Interleukin-6	A cytokine with a wide variety of biological functions in immunity, tissue regeneration, and metabolism	92
CASP3	Caspase-3	Involved in the activation cascade of caspases responsible for apoptosis execution	92
MAPK8	Mitogen-activated protein kinase 8	Serine/threonine-protein kinase involved in various processes such as cell proliferation, differentiation, migration, transformation, and programmed cell death	91
TNF	Tumor necrosis factor	It is a cytokine and mainly secreted by macrophages. It can induce cell death of certain tumor cell lines and bind to TNFRSF1A/TNFR1 and TNFRSF1B/TNFBR	91
BDNF	Brain-derived neurotrophic factor	Promotes the survival and differentiation of selected neuronal populations of the peripheral and central nervous systems during development	90
MAPK3	Mitogen-activated protein kinase 3	MAPK1/ERK2 and MAPK3/ERK1 are the 2 MAPKs which play an important role in the MAPK/ERK cascade and act as essential components of the MAP kinase signal transduction pathway	90
TRP53	Cellular tumor antigen p53	Acts as a tumor suppressor in many tumor types, induces growth arrest, or apoptosis depending on the physiological circumstances and the cell type	87
FOS	Proto-oncogene c-Fos	A nuclear phosphoprotein which forms a tight but non-covalently linked complex with the JUN/AP-1 transcription factor	83
CREB1	Cyclic AMP-responsive element-binding protein 1	Phosphorylation-dependent transcription factor that stimulates transcription upon binding to the DNA cAMP response element (CRE), a sequence present in many viral and cellular promoters	80
CAT	Catalase	Occurs in almost all aerobically respiring organisms and serves to protect cells from the toxic effects of hydrogen peroxide	79
MAPK14	Mitogen-activated protein kinase 14	MAPK14 is one of the four p38 MAPKs which play an important role in the cascades of cellular responses evoked by extracellular stimuli such as pro-inflammatory cytokines or physical stress leading to direct activation of transcription factors	79
KRAS	GTPase KRas	Ras proteins bind GDP/GTP and possess intrinsic GTPase activity and play an important role in the regulation of cell proliferation	74
DRD2	D(2) dopamine receptor	Dopamine receptor whose activity is mediated by G proteins which inhibit adenylyl cyclase	72
JUN	Transcription factor AP-1	A transcription factor that recognizes and binds to the enhancer heptamer motif 5′-TGA[CG]TCA-3'	72
EGF	Pro-epidermal growth factor	EGF stimulates the growth of various epidermal and epithelial tissues *in vivo* and *in vitro* and of some fibroblasts in the cell culture	71
IGF1	Insulin-like growth factor I	The insulin-like growth factor is structurally and functionally related to insulin but have a much higher growth-promoting activity	70
TH	Tyrosine 3-monooxygenase	Plays an important role in the physiology of adrenergic neurons	69
NGF	Beta-nerve growth factor	Nerve growth factor is important for the development and maintenance of the sympathetic and sensory nervous systems	67

p-PKA, p-ERK1/2, p-CREB, and BDNF. There were no significant differences of the expression of PKA, ERK1/2, and CREB among different groups. Moreover, METH treatment led to apparent enrichment of cleaved caspase-3 (**Figures 7A,F**), and 10 and 100 mg/kg krill oil treatment significantly reduced the expression of cleaved caspase-3. These results validated that krill oil may regulate the neuron functions and apoptosis mainly through the MAPK signaling pathway, cAMP signaling pathway, and dopaminergic synapse pathway.

DISCUSSION

Krill oil, extracted from small Antarctic krill, has been reported to have health benefits, including improved memory impairment, systemic inflammation, glucose metabolism, and hepatic steatosis (Kwantes and Grundmann 2015; Sistilli et al., 2021; Zhou et al., 2021). This study aimed to assess the ability of krill oil supplementation to affect memory dysfunction induced by METH in mice and figure out the possible mechanism. In the present study, we found that krill oil enhanced the neurocognitive functions of METH-treated mice, and targets like DRD2, MAPK, CREB, CASP3, and BDNF, and some signaling pathways such as the MAPK signaling pathway, PI3K-Akt signaling pathway, AMPK signaling pathway, neurotrophin signaling pathway, and cAMP signaling pathway were filtered out as the underlying mechanisms of krill on improving memory deficits induced by METH. To our best knowledge, it is the first time that integrating system pharmacology and bioinformatics analysis have been used to predict mechanisms of krill oil in the treatment of central nervous system injury.

Multiple METH exposures can result in neurodegenerative changes, including long-term cognitive dysfunction, memory deficits, and depression in humans and animal models (Ru et al., 2019; Zeng et al., 2021). The data from the literature revealed that krill oil supplementation in the diet could suppress neuroinflammation, oxidative stress, and improve the

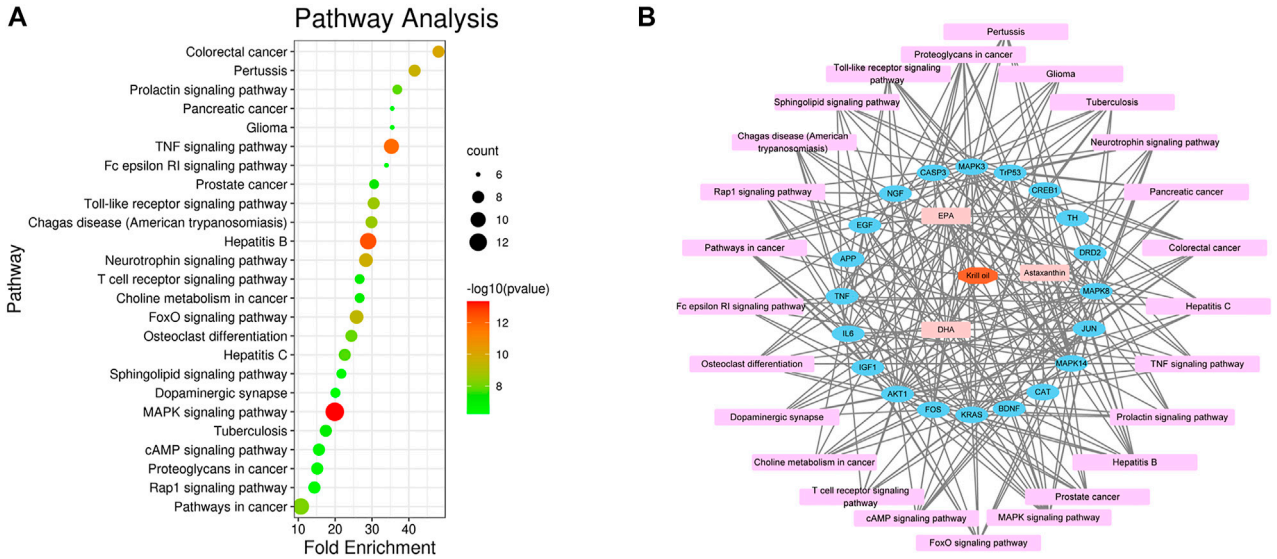

FIGURE 6 | Pathway enrichment and network analyses of hub genes. **(A)** The top 25 significantly enriched pathways of hub genes. **(B)** The compound–target–pathway network for krill oil on METH-induced memory deficits. The orange polygon represented krill oil. The pink squares represented active compounds of krill oil and the blue circle represented potential hub genes. The mauve squares represented pathways. The edges represent the interactions between them.

TABLE 2 | Top 25 significantly enriched pathways of hub genes.

Number	Pathway	Genes
1	MAPK signaling pathway	JUN, BDNF, EGF, FOS, NGF, MAPK14, TNF, MAPK8, TRP53, CASP3, AKT1, KRAS, and MAPK3
2	Hepatitis B	IL6, MAPK8, JUN, CREB1, TRP53, CASP3, AKT1, KRAS, FOS, TNF, and MAPK3
3	TNF signaling pathway	IL6, MAPK8, JUN, CREB1, CASP3, AKT1, FOS, MAPK14, TNF, and MAPK3
4	Colorectal cancer	MAPK8, JUN, TRP53, CASP3, AKT1, KRAS, FOS, and MAPK3
5	Neurotrophin signaling pathway	MAPK8, JUN, BDNF, TRP53, AKT1, KRAS, MAPK14, NGF, and MAPK3
6	Pertussis	IL6, MAPK8, JUN, CASP3, FOS, MAPK14, TNF, and MAPK3
7	FoxO signaling pathway	IL6, MAPK8, EGF, CAT, AKT1, KRAS, IGF1, MAPK14, and MAPK3
8	Toll-like receptor signaling pathway	IL6, MAPK8, JUN, AKT1, FOS, MAPK14, TNF, and MAPK3
9	Chagas disease (American trypanosomiasis)	IL6, MAPK8, JUN, AKT1, FOS, MAPK14, TNF, and MAPK3
10	Pathways in cancer	IL6, MAPK8, JUN, EGF, TRP53, CASP3, AKT1, KRAS, IGF1, FOS, and MAPK3
11	Osteoclast differentiation	MAPK8, JUN, CREB1, AKT1, FOS, MAPK14, TNF, and MAPK3
12	Prolactin signaling pathway	MAPK8, TH, AKT1, KRAS, FOS, MAPK14, and MAPK3
13	Hepatitis C	MAPK8, EGF, TRP53, AKT1, KRAS, MAPK14, TNF, and MAPK3
14	Prostate cancer	CREB1, EGF, TRP53, AKT1, KRAS, IGF1, and MAPK3
15	Choline metabolism in cancer	MAPK8, JUN, EGF, AKT1, KRAS, FOS, and MAPK3
16	T-cell receptor signaling pathway	JUN, AKT1, KRAS, FOS, MAPK14, TNF, and MAPK3
17	Tuberculosis	IL6, MAPK8, CREB1, CASP3, AKT1, MAPK14, TNF, and MAPK3
18	cAMP signaling pathway	MAPK8, JUN, CREB1, BDNF, AKT1, FOS, DRD2, and MAPK3
19	Proteoglycans in cancer	TRP53, CASP3, AKT1, KRAS, IGF1, MAPK14, TNF, and MAPK3
20	Sphingolipid signaling pathway	MAPK8, TRP53, AKT1, KRAS, MAPK14, TNF, and MAPK3
21	Pancreatic cancer	MAPK8, EGF, TRP53, AKT1, KRAS, and MAPK3
22	Glioma	EGF, TRP53, AKT1, KRAS, IGF1, and MAPK3
23	Rap1 signaling pathway	EGF, AKT1, KRAS, IGF1, MAPK14, NGF, DRD2, and MAPK3
24	Fc epsilon RI signaling pathway	MAPK8, AKT1, KRAS, MAPK14, TNF, and MAPK3
25	Dopaminergic synapse	MAPK8, CREB1, TH, AKT1, FOS, MAPK14, and DRD2

lipopolysaccharide-induced cognitive impairment (Polotow et al., 2015; Choi et al., 2017). In this study, we investigated the effect of krill oil on METH-induced memory impairment and discovered the possible molecular mechanism. The MWM task was used to investigate the ability of mice to learn locations and perform spatial memory recall through escape latency and measuring times to cross the platform in the water maze. The results of the MWM task showed that METH-treated mice learned more slowly than mice in the control group during the training period, and 10 mg/kg krill oil pretreatment significantly reduced escape

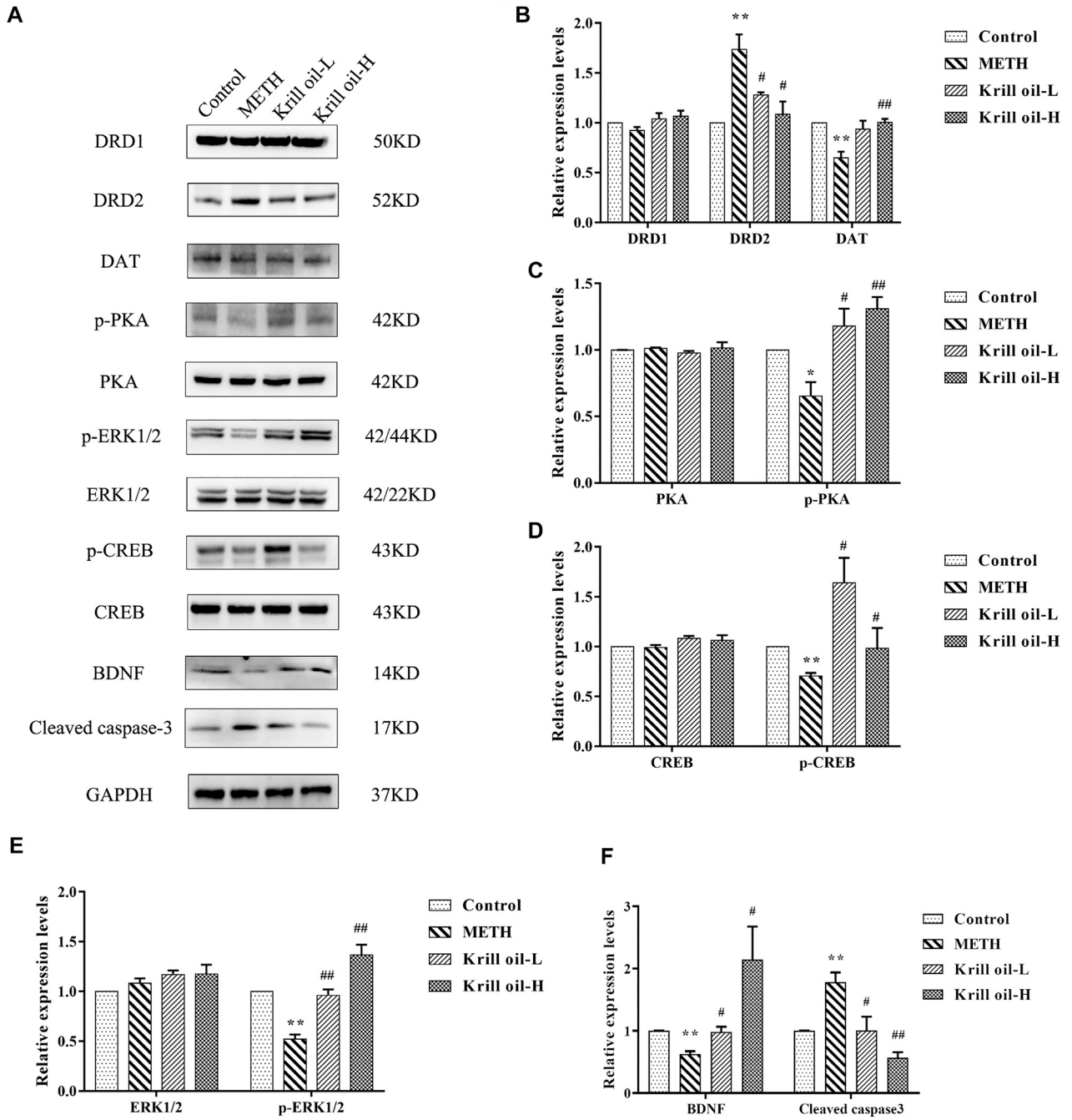

FIGURE 7 | Relative expressions of related proteins in the hippocampus of mice treated with METH and/or krill oil. **(A)** Representative images of DRD1, DRD2, DAT, p-PKA, PKA, p-ERK1/2, ERK1/2, p-CREB, CREB, BDNF, and cleaved caspase-3. **(B)** Statistical results of DRD1, DRD2, and the DAT protein. **(C)** Statistical results of the p-PKA and PKA protein. **(D)** Statistical results of the p-CREB and CREB protein. **(E)** Statistical results of the p-ERK1/2 and ERK1/2 protein. **(F)** Statistical results of the mature BDNF protein and cleaved caspase-3. Data were presented as means ± SEM. $^{*}p < 0.05$, $^{**}p < 0.01$ compared to the control group, $\#p < 0.05$, $\#\#p < 0.01$ compared to the METH group.

latency on day 5 of the training phase, while 100 mg/kg krill oil pretreatment significantly reduced escape latency on days 4 and 5. For testing the maintenance of memory, the times of crossing the platform and the time spent in the target quadrant in the METH group were significantly decreased, and 10 mg/kg krill oil–treated mice spent much more time in the target quadrant zone than METH-treated mice, while mice in the 100 mg/kg krill oil group had more probability of crossing the platform and target quadrant time. Thus, pretreatment with krill oil could improve neurocognitive functions and alleviate the impairment of learning

and memory caused by METH, and the protective effect of krill oil may be improved by increasing the dose within the dose range of 10–100 mg/kg.

Krill oil consists of multiple components, so it is difficult to determine the molecular mechanisms with traditional technology. Network pharmacology methods provide an effective tool for investigating multicomponents and exploring the mechanisms (Zhou et al., 2021). To determine the molecular mechanisms of krill oil on METH-induced memory impairment, network pharmacology approaches were used in this study. We selected DHA, EPA, and astaxanthin, which were present in high contents in krill oil, as the main active compounds, and the GeneCards database was used to identify the potential targets of krill oil, memory deficits, or METH. After the evaluation of the primary network nodes and potential targets, 210 targets were identified in the drug–compound–target network, which indicated that krill oil had multi-targets that were involved in the regulation of multiple signaling pathways. With the use of the CytoHubba and MCODE analysis, 20 genes were identified as hub genes. From the integrated hub target prediction and pathway analysis, krill oil may exert its neuroprotective effects on METH-induced memory deficits *via* the regulation of neuron functions and apoptosis, which was characterized as the important mechanism of memory impairment (Muhammad et al., 2019; Skelly et al., 2019).

As predicted by network pharmacology methods, CASP3, BDNF, MAPK3, CREB1, and DRD2 were the hub genes in krill oil to alleviate METH-induced memory impairment. KEGG signaling pathway enrichment analyses showed that krill oil may exert therapeutic effects on memory deficits primarily by regulating neuron and cell apoptosis *via* the MAPK signaling pathway, dopaminergic synapse, and cAMP signaling pathway. To further validate the postulation, we investigated the expression levels of main hub genes. Dopamine neurotransmission is critical for the physiological activity of the brain, including spatial learning and psychiatric disorders (Kempadoo et al., 2016). Because of its structural similarity to dopamine, METH could act on the dopamine transporter (DAT) in the presynaptic membrane, which inhibits dopamine reuptake and increases the dopamine level in the synaptic cleft, thereby causing overactivation of dopamine receptors in the postsynaptic membrane and excitatory oxidative damage to postsynaptic neurons (Ares-Santos et al., 2013; Yu et al., 2015). There are five types of dopamine receptors grouped into two major subclasses: DRD1-like, including DRD1 and D1RD5, and DRD2-like, including DRD2, DRD3, and DRD4, which often interact to regulate neurotransmission (Sun et al., 2017). Repeated METH exposure could increase the protein expression of DRD2 in the hippocampus area and reduce the protein expression of DAT (Zhou et al., 2019), and pretreatment with DRD2 antagonist sulpiride attenuated the effects of METH on egocentric and spatial learning and memory (Gutierrez et al., 2019). DAT-KO rats demonstrated deficits in sensorimotor gating and working memory tests (Leo et al., 2018). In line with the literature, our results showed that the expressions of DRD2 receptors in the hippocampus were greatly increased, while the levels of DAT were reduced after repeated METH exposure. Meanwhile, 100 mg/kg krill oil pretreatment significantly decreased the expressions of DRD2 and increased the expressions of DAT. The expression levels of DRD1, which was not a hub gene, did not change among groups. These results confirmed the results predicted by network pharmacology and validated the role of the dopaminergic synapse pathway in the improvement of METH-induced memory impairment by krill oil.

MAP kinases (MAPK), also known as extracellular signal-regulated kinases (ERK), are involved in a variety of biochemical processes such as cell proliferation and differentiation. MAPK3/ERK1 is one of the important members of the MAP kinase family. The cAMP-response element binding protein (CREB), which has been reported to be involved in the learning and memory deficits, is the target of ERK1/2, and protein kinase A (PKA) also can mediate the increase in ERK1/2 phosphorylation (Lyu et al., 2020; Mu et al., 2020). Therefore, after METH exposure, the expressions of p-PKA, p-ERK1/2, and p-CREB were significantly reduced. When mice were pretreated with 10 and 100 mg/kg krill oil, the increased expression of p-PKA, p-ERK1/2, and p-CREB may partially contribute to its improved effects of memory impairment. The brain-derived neurotrophic factor (BDNF) is a key factor of synaptic transmission and plays an important role in supporting neuronal survival, regulating synaptogenesis and contributing to the formation of memory (Leal et al., 2014). As a transcription factor, CREB regulates the transcription of BDNF, especially the activation of BDNF promoters I and IV (Esvald et al., 2020). From the experimental validation, our results showed that METH may decrease BDNF mostly by lowering the phosphorylated CREB protein. Krill oil may raise the levels of BDNF by activating the ERK1/2/CREB signaling pathway. Taken together, our findings suggested that krill oil may improve METH-induced memory deficits mainly *via* the regulation of neuron functions and apoptosis through the MAPK, dopaminergic synapse, and cAMP signaling pathway.

Hub gene caspase-3 is a key cysteine protease protein and acts as one of the executioner caspases (caspase-3, -6, and -7) that carry out the demolition phase of apoptosis (Boice and Bouchier-Hayes 2020). Cleaved caspase-3 can cleave structural and functional proteins in cells and induce cell apoptosis (Jiang et al., 2020). METH induced increase in the expression of cleaved caspase-3 in the hippocampus, which was involved in METH-induced neurotoxicity as well as spatial learning and memory impairments (Wen et al., 2019). Our previous data showed that krill oil could inhibit the METH-induced increase of cleaved caspase-3 *in vitro* (Xiong et al., 2018). Caspase-3 was one of the predicted hub gene; herein, we investigated the expression of cleaved caspase-3. Results showed that the expressions of cleaved caspase-3 were significantly increased after METH exposure, and pretreatment with both 10 and 100 mg/kg krill oil reduced the increasing expression of

cleaved caspase-3, which may partially contribute to its improved effects of memory impairment.

CONCLUSION

In summary, the neuroprotective effect of krill oil on METH-induced memory impairment and the underlying pharmacological mechanism were investigated with the combination of network pharmacology prediction analysis and experimental validation. These results of the behavioral test showed that krill oil can improve memory deficits caused by METH exposure. Network pharmacology analysis demonstrated that krill oil may modulate function and apoptosis of neurons mainly *via* the regulation of the MAPK, cAMP, and dopaminergic synapse signaling pathway, which was verified by further experiment. Further experimental and clinical research trials of krill oil supplementation in METH abusers may help and support the identification of the potential therapeutic effects of krill oil on METH-induced cognitive and psychiatric disorders.

DATA AVAILABILITY STATEMENT

The original contributions presented in the study are included in the article/**Supplementary Material**; further inquiries can be directed to the corresponding authors.

ETHICS STATEMENT

The animal study was reviewed and approved by the Ethics Committee of Jianghan University.

AUTHOR CONTRIBUTIONS

QR, LC, XT, and YW designed the study. QR, XT, and QX performed the experiments. QR, LC, and YW analyzed the data and prepared the manuscript together. All the authors have read and approved the final version of the manuscript.

FUNDING

This study was supported by the National Natural Science Foundation of China (Grant Nos. 81971775 to LC and 82071970 to YW), the Wuhan Municipal Science and Technology Bureau (Grant No. 2019020701011499), and Science and Technology Innovation Project of Jianghan University (Grant No. 2021kjzx008).

SUPPLEMENTARY MATERIAL

The Supplementary Material for this article can be found online at: https://www.frontiersin.org/articles/10.3389/fphar.2021.756822/full#supplementary-material

REFERENCES

Alvarez-Ricartes, N., Oliveros-Matus, P., Mendoza, C., Perez-Urrutia, N., Echeverria, F., Iarkov, A., et al. (2018). Intranasal Cotinine Plus Krill Oil Facilitates Fear Extinction, Decreases Depressive-Like Behavior, and Increases Hippocampal Calcineurin A Levels in Mice. *Mol. Neurobiol.* 55, 7949–7960. doi:10.1007/s12035-018-0916-0

Ares-Santos, S., Granado, N., and Moratalla, R. (2013). The role of dopamine receptors in the neurotoxicity of methamphetamine. *J. Intern. Med.* 273, 437–453. doi:10.1111/joim.12049

Berge, R. K., Ramsvik, M. S., Bohov, P., Svardal, A., Nordrehaug, J. E., Rostrup, E., et al. (2015). Krill oil reduces plasma triacylglycerol level and improves related lipoprotein particle concentration, fatty acid composition and redox status in healthy young adults - a pilot study. *Lipids Health Dis.* 14, 163. doi:10.1186/s12944-015-0162-7

Boice, A., and Bouchier-Hayes, L. (2020). Targeting apoptotic caspases in cancer. *Biochim. Biophys. Acta Mol. Cel Res* 1867, 118688. doi:10.1016/j.bbamcr.2020.118688

Casaletto, K. B., Obermeit, L., Morgan, E. E., Weber, E., Franklin, D. R., Grant, I., et al. (2015). Depression and executive dysfunction contribute to a metamemory deficit among individuals with methamphetamine use disorders. *Addict. Behav.* 40, 45–50. doi:10.1016/j.addbeh.2014.08.007

Chen, C. K., Lin, S. K., Chen, Y. C., Huang, M. C., Chen, T. T., Ree, S. C., et al. (2015). Persistence of psychotic symptoms as an indicator of cognitive impairment in methamphetamine users. *Drug Alcohol Depend* 148, 158–164. doi:10.1016/j.drugalcdep.2014.12.035

Cheong, L. Z., Sun, T., Li, Y., Zhou, J., Lu, C., Li, Y., et al. (2017). Dietary krill oil enhances neurocognitive functions and modulates proteomic changes in brain tissues of d-galactose induced aging mice. *Food Funct.* 8, 2038–2045. doi:10.1039/c6fo01848c

Cherner, M., Suarez, P., Casey, C., Deiss, R., Letendre, S., Marcotte, T., et al. (2010). Methamphetamine use parameters do not predict neuropsychological impairment in currently abstinent dependent adults. *Drug Alcohol Depend* 106, 154–163. doi:10.1016/j.drugalcdep.2009.08.010

Choi, J. Y., Jang, J. S., Son, D. J., Im, H. S., Kim, J. Y., Park, J. E., et al. (2017). Antarctic Krill Oil Diet Protects against Lipopolysaccharide-Induced Oxidative Stress, Neuroinflammation and Cognitive Impairment. *Int. J. Mol. Sci.* 18. doi:10.3390/ijms18122554

Esvald, E. E., Tuvikene, J., Sirp, A., Patil, S., Bramham, C. R., and Timmusk, T. (2020). CREB Family Transcription Factors Are Major Mediators of BDNF Transcriptional Autoregulation in Cortical Neurons. *J. Neurosci.* 40, 1405–1426. doi:10.1523/JNEUROSCI.0367-19.2019

Fan, X. Y., Yang, J. Y., Dong, Y. X., Hou, Y., Liu, S., and Wu, C. F. (2020). Oxytocin inhibits methamphetamine-associated learning and memory alterations by regulating DNA methylation at the Synaptophysin promoter. *Addict. Biol.* 25, e12697. doi:10.1111/adb.12697

Golsorkhdan, S. A., Boroujeni, M. E., Aliaghaei, A., Abdollahifar, M. A., Ramezanpour, A., Nejatbakhsh, R., et al. (2020). Methamphetamine administration impairs behavior, memory and underlying signaling pathways in the hippocampus. *Behav. Brain Res.* 379, 112300. doi:10.1016/j.bbr.2019.112300

Gutierrez, A., Regan, S. L., Hoover, C. S., Williams, M. T., and Vorhees, C. V. (2019). Effects of intrastriatal dopamine D1 or D2 antagonists on methamphetamine-induced egocentric and allocentric learning and memory deficits in Sprague-Dawley rats. *Psychopharmacology (Berl)* 236, 2243–2258. doi:10.1007/s00213-019-05221-3

Huang, J., Zheng, Y., Gao, D., Hu, M., and Yuan, T. (2019). Effects of Exercise on Depression, Anxiety, Cognitive Control, Craving, Physical Fitness and Quality of Life in Methamphetamine-dependent Patients. *Front. Psychiatry* 10, 999. doi:10.3389/fpsyt.2019.00999

Jiang, M., Qi, L., Li, L., and Li, Y. (2020). The caspase-3/GSDME signal pathway as a switch between apoptosis and pyroptosis in cancer. *Cell Death Discov* 6, 112. doi:10.1038/s41420-020-00349-0

Kempadoo, K. A., Mosharov, E. V., Choi, S. J., Sulzer, D., and Kandel, E. R. (2016). Dopamine release from the locus coeruleus to the dorsal hippocampus

promotes spatial learning and memory. *Proc. Natl. Acad. Sci. U S A.* 113, 14835–14840. doi:10.1073/pnas.1616515114

Konagai, C., Yanagimoto, K., Hayamizu, K., Han, L., Tsuji, T., and Koga, Y. (2013). Effects of krill oil containing n-3 polyunsaturated fatty acids in phospholipid form on human brain function: a randomized controlled trial in healthy elderly volunteers. *Clin. Interv. Aging* 8, 1247–1257. doi:10.2147/CIA.S50349

Kwantes, J. M., and Grundmann, O. (2015). A brief review of krill oil history, research, and the commercial market. *J. Diet. Suppl.* 12, 23–35. doi:10.3109/19390211.2014.902000

Leal, G., Comprido, D., and Duarte, C. B. (2014). BDNF-induced local protein synthesis and synaptic plasticity. *Neuropharmacology* 76 Pt C, 639–656. doi:10.1016/j.neuropharm.2013.04.005

Leo, D., Sukhanov, I., Zoratto, F., Illiano, P., Caffino, L., Sanna, F., et al. (2018). Pronounced Hyperactivity, Cognitive Dysfunctions, and BDNF Dysregulation in Dopamine Transporter Knock-out Rats. *J. Neurosci.* 38, 1959–1972. doi:10.1523/JNEUROSCI.1931-17.2018

Lobraico, J. M., DiLello, L. C., Butler, A. D., Cordisco, M. E., Petrini, J. R., and Ahmadi, R. (2015). Effects of krill oil on endothelial function and other cardiovascular risk factors in participants with type 2 diabetes, a randomized controlled trial. *BMJ Open Diabetes Res. Care* 3, e000107. doi:10.1136/bmjdrc-2015-000107

Lwin, T., Yang, J. L., Ngampramuan, S., Viwatpinyo, K., Chancharoen, P., Veschsanit, N., et al. (2020). Melatonin ameliorates methamphetamine-induced cognitive impairments by inhibiting neuroinflammation via suppression of the TLR4/MyD88/NFκB signaling pathway in the mouse hippocampus. *Prog. Neuropsychopharmacol. Biol. Psychiatry* 110109, 110109. doi:10.1016/j.pnpbp.2020.110109

Lyu, Y., Ren, X. K., Zhang, H. F., Tian, F. J., Mu, J. B., and Zheng, J. P. (2020). Sub-chronic administration of benzo[a]pyrene disrupts hippocampal long-term potentiation via inhibiting CaMK II/PKC/PKA-ERK-CREB signaling in rats. *Environ. Toxicol.* 35, 961–970. doi:10.1002/tox.22932

Mu, J., Wang, R., Li, G., Li, B., and Wang, Z. (2020). Midazolam accelerates memory deterioration and neuron apoptosis of Alzheimer's disease model rats via PKA-ERK-CREB signaling pathway. *Panminerva Med.*, 4. doi:10.23736/S0031-0808.20.03994-4

Muhammad, T., Ikram, M., Ullah, R., Rehman, S. U., and Kim, M. O. (2019). Hesperetin, a Citrus Flavonoid, Attenuates LPS-Induced Neuroinflammation, Apoptosis and Memory Impairments by Modulating TLR4/NF-κB Signaling. *Nutrients*, 11. doi:10.3390/nu11030648

Polotow, T. G., Poppe, S. C., Vardaris, C. V., Ganini, D., Guariroba, M., Mattei, R., et al. (2015). Redox Status and Neuro Inflammation Indexes in Cerebellum and Motor Cortex of Wistar Rats Supplemented with Natural Sources of Omega-3 Fatty Acids and Astaxanthin: Fish Oil, Krill Oil, and Algal Biomass. *Mar. Drugs* 13, 6117–6137. doi:10.3390/md13106117

Ru, Q., Xiong, Q., Zhou, M., Chen, L., Tian, X., Xiao, H., et al. (2019). Withdrawal from chronic treatment with methamphetamine induces anxiety and depression-like behavior in mice. *Psychiatry Res.* 271, 476–483. doi:10.1016/j.psychres.2018.11.072

Siefried, K. J., Acheson, L. S., Lintzeris, N., and Ezard, N. (2020). Pharmacological Treatment of Methamphetamine/Amphetamine Dependence: A Systematic Review. *CNS drugs* 34, 337–365. doi:10.1007/s40263-020-00711-x

Silva, C. D., Neves, A. F., Dias, A. I., Freitas, H. J., Mendes, S. M., Pita, I., et al. (2014). A single neurotoxic dose of methamphetamine induces a long-lasting depressive-like behaviour in mice. *Neurotox Res.* 25, 295–304. doi:10.1007/s12640-013-9423-2

Sistilli, G., Kalendova, V., Cajka, T., Irodenko, I., Bardova, K., Oseeva, M., et al. (2021). Krill Oil Supplementation Reduces Exacerbated Hepatic Steatosis Induced by Thermoneutral Housing in Mice with Diet-Induced Obesity. *Nutrients* 13. doi:10.3390/nu13020437

Skelly, D. T., Griffin, É. W., Murray, C. L., Harney, S., O'Boyle, C., Hennessy, E., et al. (2019). Acute transient cognitive dysfunction and acute brain injury induced by systemic inflammation occur by dissociable IL-1-dependent mechanisms. *Mol. Psychiatry* 24, 1533–1548. doi:10.1038/s41380-018-0075-8

Sun, D., Zhang, L., Chen, H., Feng, R., Cao, P., and Liu, Y. (2017). Effects of Antarctic krill oil on lipid and glucose metabolism in C57BL/6J mice fed with high fat diet. *Lipids Health Dis.* 16, 218. doi:10.1186/s12944-017-0601-8

Sun, X., Luquet, S., and Small, D. M. (2017). DRD2: Bridging the Genome and Ingestive Behavior. *Trends Cogn. Sci.* 21, 372–384. doi:10.1016/j.tics.2017.03.004

Tomé-Carneiro, J., Carmen Crespo, M., Burgos-Ramos, E., Tomas-Zapico, C., García-Serrano, A., Castro-Gómez, P., et al. (2018). Buttermilk and Krill Oil Phospholipids Improve Hippocampal Insulin Resistance and Synaptic Signaling in Aged Rats. *Mol. Neurobiol.* 55, 7285–7296. doi:10.1007/s12035-018-0934-y

van der Wurff, I. S. M., von Schacky, C., Bergeland, T., Leontjevas, R., Zeegers, M. P., Jolles, J., et al. (2019). Effect of 1 Year Krill Oil Supplementation on Cognitive Achievement of Dutch Adolescents: A Double-Blind Randomized Controlled Trial. *Nutrients* 11. doi:10.3390/nu11061230

van der Wurff, I. S. M., von Schacky, C., Bergeland, T., Leontjevas, R., Zeegers, M. P., Kirschner, P. A., et al. (2020). Effect of one year krill oil supplementation on depressive symptoms and self-esteem of Dutch adolescents: A randomized controlled trial. *Prostaglandins Leukot. Essent. Fatty Acids* 163, 102208. doi:10.1016/j.plefa.2020.102208

Veschsanit, N., Yang, J. L., Ngampramuan, S., Viwatpinyo, K., Pinyomahakul, J., Lwin, T., et al. (2021). Melatonin reverts methamphetamine-induced learning and memory impairments and hippocampal alterations in mice. *Life Sci.* 265, 118844. doi:10.1016/j.lfs.2020.118844

Wang, L. J., Chen, C. K., Lin, S. K., Chen, Y. C., Xu, K., and Huang, M. C. (2018). Cognitive profile of ketamine-dependent patients compared with methamphetamine-dependent patients and healthy controls. *Psychopharmacology (Berl)* 235, 2113–2121. doi:10.1007/s00213-018-4910-z

Wen, D., Hui, R., Wang, J., Shen, X., Xie, B., Gong, M., et al. (2019). Effects of Molecular Hydrogen on Methamphetamine-Induced Neurotoxicity and Spatial Memory Impairment. *Front. Pharmacol.* 10, 823. doi:10.3389/fphar.2019.00823

Xiong, Q., Ru, Q., Tian, X., Zhou, M., Chen, L., Li, Y., et al. (2018). Krill oil protects PC12 cells against methamphetamine-induced neurotoxicity by inhibiting apoptotic response and oxidative stress. *Nutr. Res.* 58, 84–94. doi:10.1016/j.nutres.2018.07.006

Yu, S., Zhu, L., Shen, Q., Bai, X., and Di, X. (2015). Recent advances in methamphetamine neurotoxicity mechanisms and its molecular pathophysiology. *Behav. Neurol.* 2015, 103969. doi:10.1155/2015/103969

Zeng, Q., Xiong, Q., Zhou, M., Tian, X., Yue, K., Li, Y., et al. (2021). Resveratrol attenuates methamphetamine-induced memory impairment via inhibition of oxidative stress and apoptosis in mice. *J. Food Biochem.* 45, e13622. doi:10.1111/jfbc.13622

Zhou, L., Wu, X., Yang, F., Zhang, M., Huang, R., and Liu, J. (2021). Characterization of Molecular Species and Anti-inflammatory Activity of Purified Phospholipids from Antarctic Krill Oil. *Mar. Drugs* 19, 124. doi:10.3390/md19030124

Zhou, M., Gong, X., Ru, Q., Xiong, Q., Chen, L., Si, Y., et al. (2019). The Neuroprotective Effect of L-Stepholidine on Methamphetamine-Induced Memory Deficits in Mice. *Neurotox Res.* 36, 376–386. doi:10.1007/s12640-019-00069-z

Zhou, Y., Wu, R., Cai, F. F., Zhou, W. J., Lu, Y. Y., Zhang, H., et al. (2021). Xiaoyaosan decoction alleviated rat liver fibrosis via the TGFβ/Smad and Akt/FoxO3 signaling pathways based on network pharmacology analysis. *J. Ethnopharmacol* 264, 113021. doi:10.1016/j.jep.2020.113021

Conflict of Interest: The authors declare that the research study was conducted in the absence of any commercial or financial relationships that could be construed as a potential conflict of interest.

Publisher's Note: All claims expressed in this article are solely those of the authors and do not necessarily represent those of their affiliated organizations, or those of the publisher, the editors, and the reviewers. Any product that may be evaluated in this article, or claim that may be made by its manufacturer, is not guaranteed or endorsed by the publisher.

Advantages of publishing in Frontiers

OPEN ACCESS
Articles are free to read for greatest visibility and readership

FAST PUBLICATION
Around 90 days from submission to decision

HIGH QUALITY PEER-REVIEW
Rigorous, collaborative, and constructive peer-review

TRANSPARENT PEER-REVIEW
Editors and reviewers acknowledged by name on published articles

Frontiers
Avenue du Tribunal-Fédéral 34
1005 Lausanne | Switzerland

Visit us: www.frontiersin.org
Contact us: frontiersin.org/about/contact

REPRODUCIBILITY OF RESEARCH
Support open data and methods to enhance research reproducibility

DIGITAL PUBLISHING
Articles designed for optimal readership across devices

FOLLOW US
@frontiersin

IMPACT METRICS
Advanced article metrics track visibility across digital media

EXTENSIVE PROMOTION
Marketing and promotion of impactful research

LOOP RESEARCH NETWORK
Our network increases your article's readership